

3 1761 11554962 8





Digitized by the Internet Archive
in 2022 with funding from
University of Toronto

<https://archive.org/details/31761115549628>

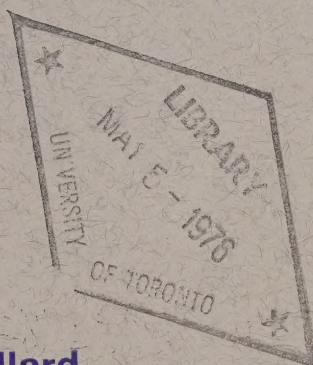
CAI EP 321

-76R05

(5)

THE TIDES IN THE FRASER ESTUARY

by



Alard Ages and Anne Woollard

Canada

INSTITUTE OF OCEAN SCIENCES, PATRICIA BAY
Victoria, B.C.



For additional copies or further information, please write to:

Environment Canada

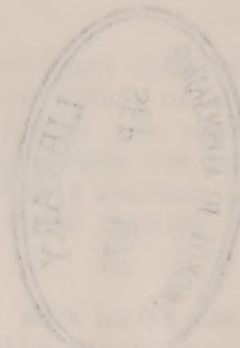
Institute of Ocean Sciences, Patricia Bay

512 - 1230 Government Street

Victoria, B.C.

V8W 1Y4

Pacific Marine Science Report 76-5



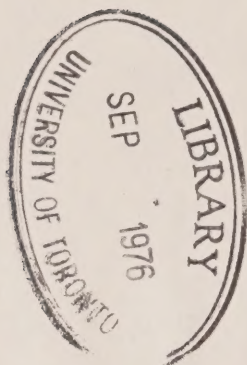
THE TIDES IN THE FRASER ESTUARY

by

Alard Ages and Anne Woollard

Institute of Ocean Sciences, Patricia Bay
Victoria, B.C.

January, 1976



This is a manuscript which has received only limited circulation. On citing this report in a bibliography, the title should be followed by the words "UNPUBLISHED MANUSCRIPT" which is in accordance with accepted bibliographic custom.

ABSTRACT

The interaction between the tides in the Strait of Georgia and the discharge of the Fraser River is examined by a one-dimensional numerical model of the Fraser estuary. The model computes water surface elevations between the head of the tide water at Chilliwack and the mouth of the Fraser, including all four delta arms and Pitt Lake.

After a brief description of the conventional computation method, the report covers some practical aspects in the development of a tidal model, such as the field work preceding the model's calibration, the schematization, the effect of inaccuracies in the boundary conditions upon the computed water levels, and other sources of error. A relationship between the high and low waters in the navigable part of the river and those outside the mouth is examined for a variety of discharges.

Other uses of the model are discussed, such as an estimate of energy dissipation, and the effect of proposed hydraulic structures upon the tides in the estuary.

ACKNOWLEDGEMENTS

The field work to collect the necessary tidal data for the model's calibration was carried out jointly by Water Survey of Canada in Vancouver, and the Tides and Currents Section of the Canadian Hydrographic Service in Victoria. Several staff members of both organizations participated in the data acquisition, and in particular, we acknowledge the generous help of Jack Wallace, Dick Brawn and Margaret Key of Water Survey, and of Syd Wigen, Willie Rapatz and Bob Brown of Tides and Currents.

We would like to thank Sus Tabata, Rick Thomson and John Garrett of Offshore Oceanography, and Pat Crean and Falconer Henry of Numerical Modelling for their helpful discussions and constructive criticism. We are also indebted to Dave Prandle of the Institute of Coastal Oceanography at Liverpool, and Norm Crookshank of the National Research Council at Ottawa for their expert advice in the initial development of the model.

Finally, we appreciate the assistance of Anne Harrison who drew the sketches, Lynne Egan who typed the report, and Sharon Thomson who did the proof-reading.

TABLE OF CONTENTS

	<u>Page</u>
Abstract	i
Acknowledgements	iii
Table of Contents	v
List of Figures	vii
Introduction	1
The Fraser	3
The Tides in the Strait of Georgia	11
Tidal Computations	13
Assumptions	19
Schematization	21
Stability and the Time Step	23
Boundary Conditions	25
Initial Conditions	29
Field Observations	31
Calibration	35
Results	39
Other Applications	77
The Accuracy of the Model	81
Remarks	93
Terminology	97
References	99

LIST OF FIGURES

<u>Figure</u>		<u>Page</u>
1	The Fraser River basin	2
2	Profile of the Fraser River	3
3	Hydrograph for Fraser River at Hope, 1972	4
4	The lower Fraser River	5
5	Approximate boundaries of salinity wedge at low and high discharges	6
6	Schematization of sections	14
7	Smoothing of cross-sectional areas	15
8	Computer scheme	17
9	Schematization at Deas Island	20
10	Schematization at Douglas Island	20
11	Induced instability (New Westminster)	23
12	Upstream boundary conditions	26
13	Downstream boundaries	27
14	Night levelling at Sandheads	32
15	Pressure unit of North Arm tide gauge	33
16	Distribution of friction coefficients	38
17	Model-predicted correspondence between highs and lows at Point Atkinson and New Westminster (heights: data points) . . .	42
18	Model-predicted correspondence between highs and lows at Point Atkinson and New Westminster (time lags: data points)	43
19	Model-predicted correspondence between highs and lows at Point Atkinson and New Westminster (heights: best-fit curves)	44
20	Model-predicted correspondence between highs and lows at Point Atkinson and New Westminster (time lags: best-fit curve) . . .	45
21	Model-predicted correspondence between highs and lows at Point Atkinson and Steveston (heights)	46
22	Model-predicted correspondence between highs and lows at Point Atkinson and Steveston (time lags)	47

<u>Figure</u>		<u>Page</u>
23	Model-predicted correspondence between highs and lows at Point Atkinson and Deas Island (heights)	48
24	Model-predicted correspondence between highs and lows at Point Atkinson and Deas Island (time lags)	49
25	Model-predicted correspondence between highs and lows at Point Atkinson and Middle Arm (heights)	50
26	Model-predicted correspondence between highs and lows at Point Atkinson and Middle Arm (time lags)	51
27	Model-predicted correspondence between highs and lows at Point Atkinson and Fraser Street (heights)	52
28	Model-predicted correspondence between highs and lows at Point Atkinson and Fraser Street (time lags)	53
29	Model-predicted correspondence between highs and lows at Point Atkinson and Port Mann (heights)	54
30	Model-predicted correspondence between highs and lows at Point Atkinson and Port Mann (time lags)	55
31	Model-predicted correspondence between highs and lows at Point Atkinson and Port Coquitlam (heights)	56
32	Model-predicted correspondence between highs and lows at Point Atkinson and Port Coquitlam (time lags)	57
33	Model-predicted correspondence between highs and lows at Point Atkinson and Mission (heights)	58
34	Model-predicted correspondence between highs and lows at Point Atkinson and Mission (time lags)	59
35	Actual correspondence between highs and lows at Point Atkinson and New Westminster 1970-73. $Q_{HOPE} = 25,000$ cfs (heights) . .	60
36	Actual correspondence between highs and lows at Point Atkinson and New Westminster 1970-73. $Q_{HOPE} = 50,000$ cfs (heights) . .	61
37	Actual correspondence between highs and lows at Point Atkinson and New Westminster 1970-73. $Q_{HOPE} = 100,000$ cfs (heights) . .	62
38	Actual correspondence between highs and lows at Point Atkinson and New Westminster 1970-73. $Q_{HOPE} = 150,000$ cfs (heights) . .	63
39	Actual correspondence between highs and lows at Point Atkinson and New Westminster 1970-73. $Q_{HOPE} = 200,000$ cfs (heights) . .	64

<u>Figure</u>		<u>Page</u>
40	Actual correspondence between highs and lows at Point Atkinson and New Westminster 1970-73. $Q_{HOPE} = 250,000$ cfs (heights) . . .	65
41	Actual correspondence between highs and lows at Point Atkinson and New Westminster 1970-73. $Q_{HOPE} = 300,000$ cfs (heights) . .	66
42	Actual correspondence between highs and lows at Point Atkinson and New Westminster 1970-73 (heights: best-fit curves)	67
43	Actual correspondence between highs and lows at Point Atkinson and New Westminster 1970-73. $Q_{HOPE} = 25,000 - 100,000$ cfs (time lags)	68
44	Actual correspondence between highs and lows at Point Atkinson and New Westminster 1970-73. $Q_{HOPE} = 150,000 - 200,000$ cfs (time lags)	69
45	Actual correspondence between highs and lows at Point Atkinson and New Westminster 1970-73. $Q_{HOPE} = 250,000 - 300,000$ cfs (time lags)	70
46	Actual correspondence between highs and lows at Point Atkinson and New Westminster 1970-73 (time lags: best-fit curve)	71
47	Progression of a tidal wave in the Fraser River	73
48	Model-produced profiles of Fraser River (non-freshet)	74
49	Model-produced profiles of Fraser River (freshet)	75
50	Proposed Boundary Bay diversion canal	79
51	Model-predicted velocities in Pitt Lake	80
52	Comparison of model-predicted and observed extrema at New Westminster 1970-73 (height errors)	82
53	Comparison of model-predicted and observed extrema at New Westminster 1970-73 (time errors)	83
54	Effect of errors in upstream boundary conditions (discharges) upon model-predicted heights	84
55	Comparison over 56 days of observed extrema at Point Atkinson with those obtained by Harmonic Method	86
56	Comparison over 56 days of observed extrema at Point Atkinson with those listed in tide tables	87
57	Comparison of tide table and observed higher high and lower low waters at Point Atkinson 1970-73	88

<u>Figure</u>		<u>Page</u>
58	Effect of errors in downstream boundary conditions (tidal heights) upon model-predicted heights	90
59	Flowchart	95

INTRODUCTION

This report discusses a method to compute tidal heights in the Fraser estuary from the upstream discharges and the tides in the Strait of Georgia outside the delta. The method is based on a conventional one-dimensional numerical model, which was developed to improve tidal height predictions in the navigable portion of the Fraser River. Water surface elevations and velocities are computed every $2\frac{1}{2}$ minutes at two-mile intervals. A graphical relationship is subsequently established between maximum and minimum tidal heights at selected points along the river, and corresponding extrema outside the mouth.

The model was calibrated with 15 tide gauges. Although the calculated and observed water levels show good agreement in height and phase at all stations, the accuracy of the model's flow computations cannot be established until more velocity measurements have been made.

Rather than restricting itself to a discussion of the numerical technique followed, the report covers several phases in the development of a hydrodynamic model, i.e. the field measurements, the schematization, the calibration, and an error analysis. The model's accuracy is tested by comparing the computed heights and times of maximum and minimum tides at New Westminster with the observed values over a four-year period.

Some other practical applications of the model are mentioned, such as an assessment of the energy dissipated by friction in the tidal portion of the river.

NOTE: Because of its engineering applications and the nature of the data input, this report generally uses British units. Where necessary, the MKS values are given in parentheses.

FIG. 1

THE FRASER RIVER BASIN



THE FRASER

The Fraser River, one of the major rivers in North America, drains about 90,000 square miles of British Columbia (one quarter of the province) before entering the Strait of Georgia (Figure 1).

The source of the river is near Jasper at the Alberta border, 850 miles from the mouth, with an elevation of 6,000 feet above mean sea level. The river descends rapidly to an elevation of 2,400 feet in the first 80 miles, then flows at moderate slopes through plateau country and canyons. At Hope, about 100 miles east of the mouth, the Fraser reaches an alluvial valley, widens and flattens out to a mature stream, and, at low discharges, begins to "feel" the tidal influence near Chilliwack, 60 river miles from the mouth. Below New Westminster, the river divides into four distributaries - Main Arm, North Arm, Middle Arm, and Canoe Pass.

The profile in Figure 2 shows the Fraser water surface and mean discharges (1).

Fig.2 PROFILE OF THE FRASER RIVER

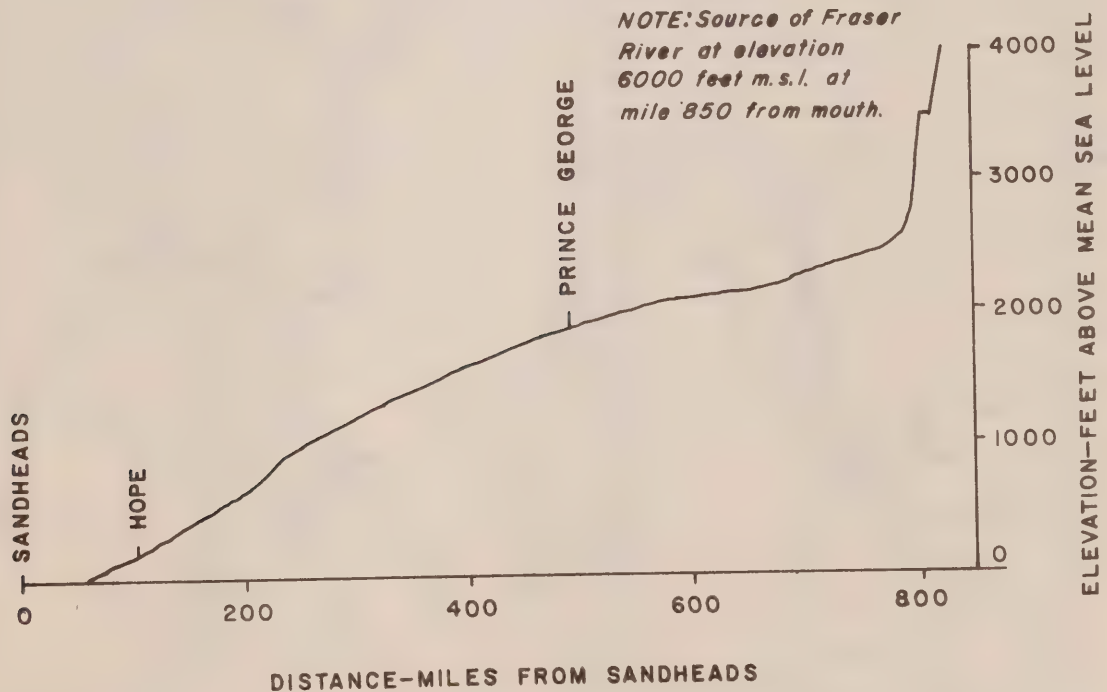
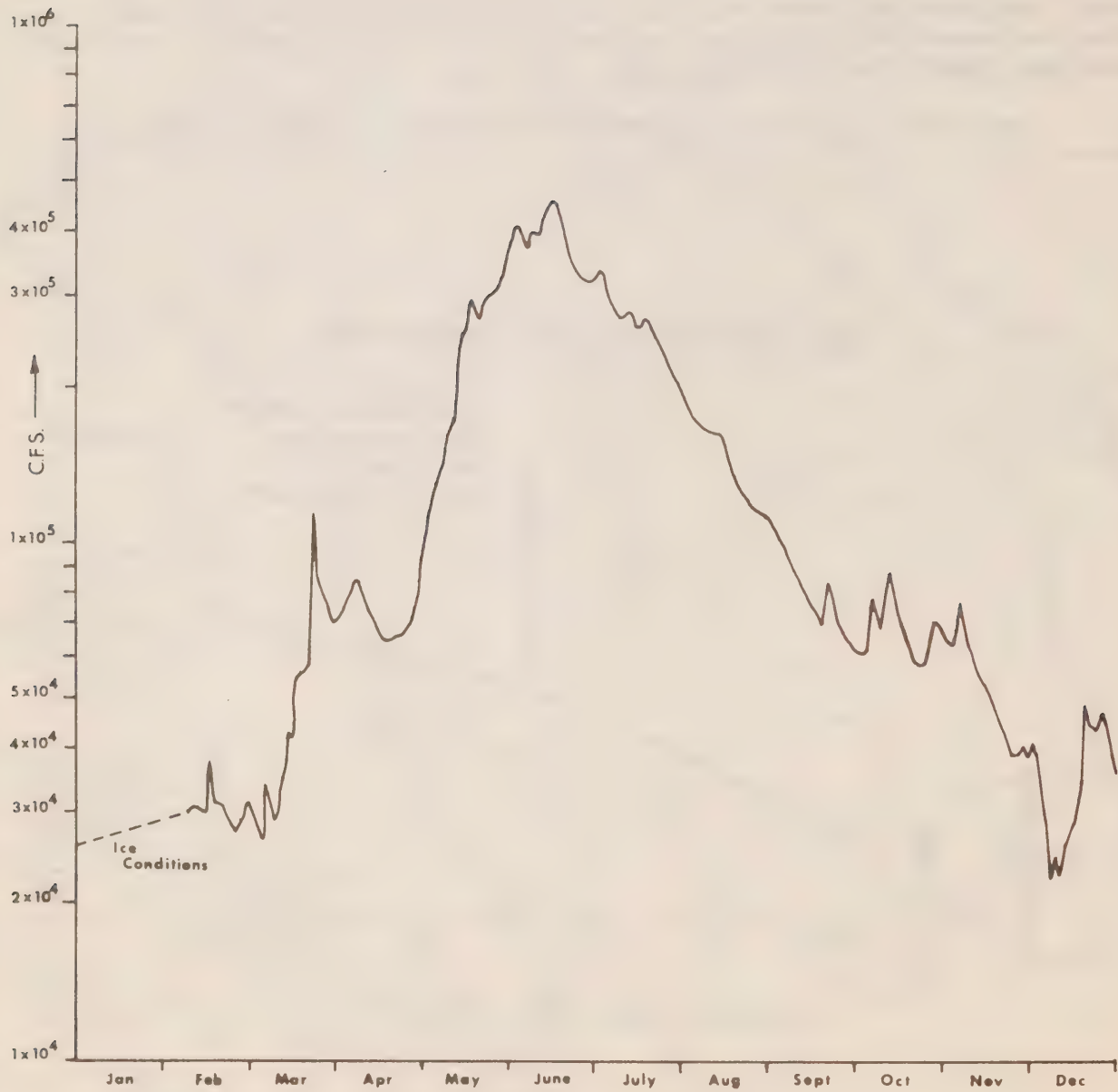


Fig.3 HYDROGRAPH FOR FRASER RIVER
AT HOPE 1972



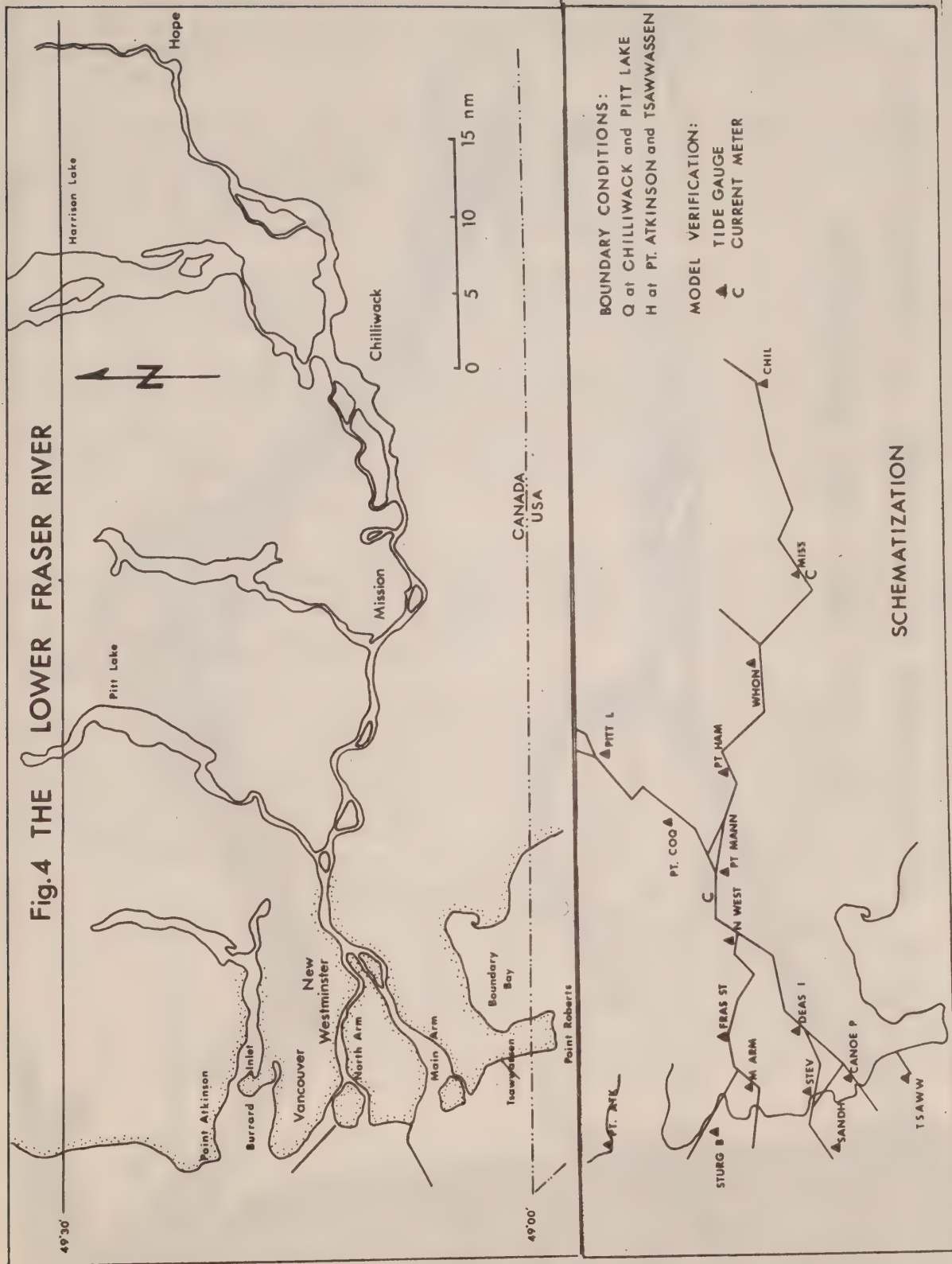
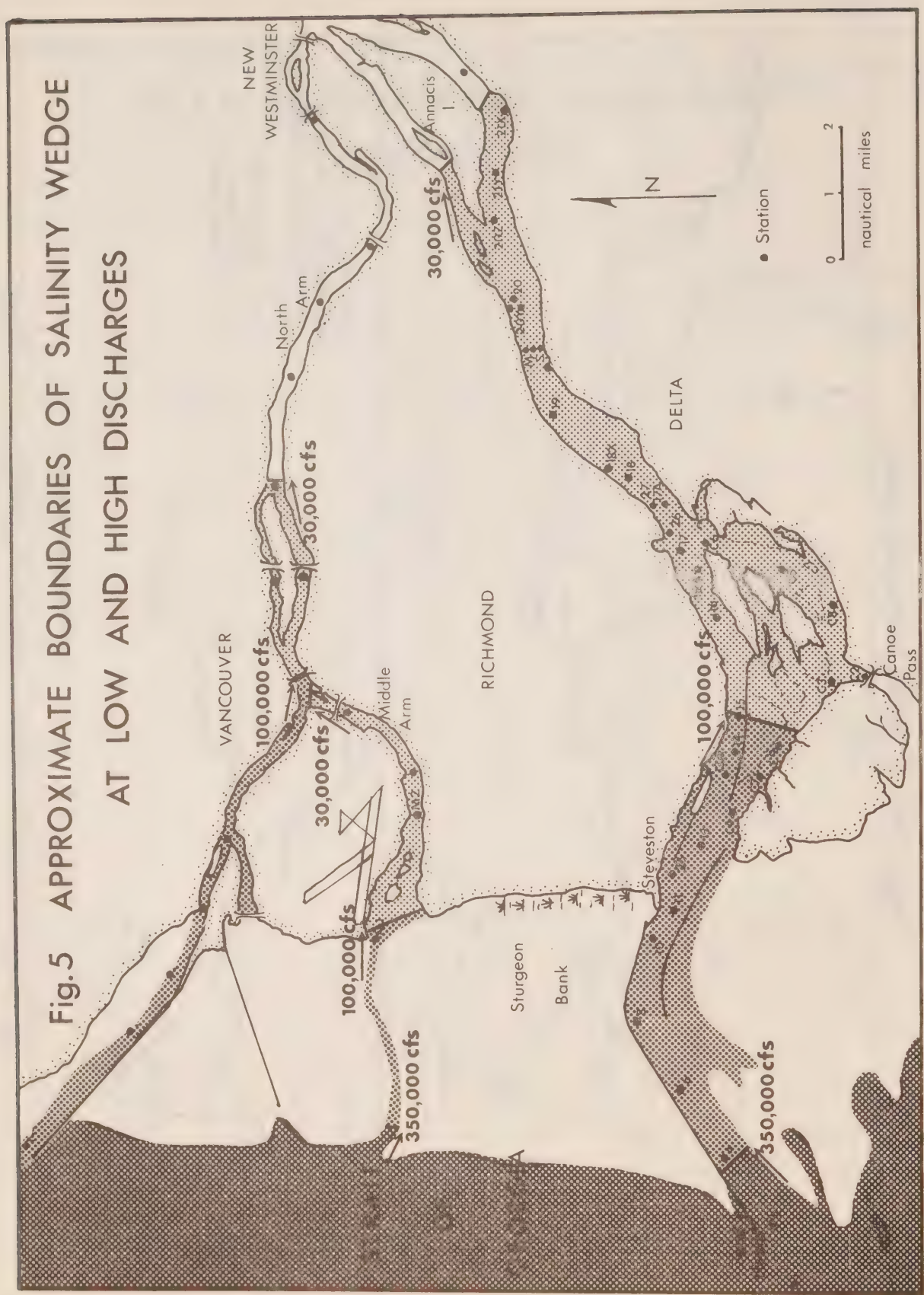


Fig.5 APPROXIMATE BOUNDARIES OF SALINITY WEDGE
AT LOW AND HIGH DISCHARGES



Snow forms about two-thirds of the precipitation in the drainage basin. The snow starts to melt in April, increasing the run-off to a maximum in late May or early June. This run-off has been measured since 1912 at Hope, a gauging station at the head of the Lower Fraser Valley, well upstream of the tidal influence.

The mean daily discharge measured at Hope varies between 20,000 cfs ($600 \text{ m}^3/\text{sec}$) in the winter and 310,000 cfs ($8800 \text{ m}^3/\text{sec}$) in the summer, averaged over 44 years (1912-1956). A peak flow of 536,000 cfs ($15,200 \text{ m}^3/\text{sec}$) was recorded on May 31, 1948, when 55,000 acres in the Lower Fraser Valley were flooded. Figure 3 shows a typical hydrograph (1972).

The tide in the Strait of Georgia propagates to Chilliwack in the winter, during periods of low discharges (non-freshet), and to Mission in the summer during the freshet. The tide also propagates into Pitt Lake, with ranges of more than three feet. Water levels are recorded continuously by several gauges throughout the Valley (see Figure 4), and currents are measured with non-directional meters at Mission and Port Mann. Although the tidal records show a periodic rise and fall of the water level as far upstream as Chilliwack, actual flow reversals due to the flooding tide do not occur above Mission. During a strong freshet, the flow is outward all the way to the mouth, at all stages of the tide.

The upper limit of the salinity wedge has been observed as far upstream as Annacis Island at low discharges of 30,000 cfs (2) (see Figure 5). At average discharges (100,000 cfs or $2800 \text{ m}^3/\text{sec}$), the salinity wedge reaches the proximity of the Deas Island tunnel in the Main Arm, and the Oak Street Bridge in the shallower North Arm.

The mean annual total sediment load of the Fraser at Hope has been estimated at 25,000,000 tons (3), which is the sum of suspended load (including wash load and saltation load) and bed load. At New Westminster, the laboratory of the Sediment Survey of Water Survey of Canada has been analyzing sediment samples collected at Hope, Agassiz, Mission, and Port Mann since approximately 1965. Of the sediment load transported by the Fraser, only a small percentage has been found to be bed load; for instance, the total sediment load measured at Port Mann in 1966 was about 22,000,000 tons, of which 20,000,000 tons was suspended load and 2,000,000 tons bed load. However, it is the movement of the bed load which may alter the configuration of the river bed in the delta and affect the accuracy of model-predictions. During freshets, large bed waves migrate slowly downstream and continually change the cross-sectional areas. These bed waves can be measured by echo sounders. During the 1950 freshet, a bed wave with a height of 15 feet from trough to crest was followed downstream from the Deas Island tunnel. The wave was 500 feet long, and moved downstream at a rate of 250 feet per day (4).

Along the western delta front, there appears to be a sediment movement in a net northerly direction, with the principal deposition taking place off the main channel. Recent measurements (5) indicate an advancement of the delta front of up to 60 feet per year just south of Sandheads.

During periods of high discharge, the harbour of New Westminster (the only freshwater port in Western Canada) is subject to heavy siltation. At New Westminster, the river trifurcates into the North Arm, Annacis Channel and

Annieville Channel, with a consequent decrease in flow and increase in sedimentation in the Main Arm immediately below New Westminster. The Department of Public Works carries out an annual dredging program between the port of New Westminster and the mouth of the Fraser River, 21 miles downstream. Four million tons of bed load (the equivalent of three million cubic yards) are dredged annually from the entire estuary between New Westminster and the Strait of Georgia, 80-90% being from the Main Arm (6). To alleviate shoaling in the navigable part of the Fraser, a series of training walls was recently constructed to increase the river's sediment-carrying capacity in certain critical areas. This project, generally known as the Trifurcation Scheme (7), was designed and tested during the 1950's in a hydraulic movable-bed model at the University of British Columbia (horizontal scale 1:600). The Trifurcation Scheme, completed in 1973, was one of the major contributing factors in the increase in the Fraser River's annual gross shipping tonnage (8) from 4,868,248 tons in 1973 to 5,631,937 tons in 1974 (9).

At present, the maximum permissible draught for deep sea vessels entering the port of New Westminster is 32 feet on a 12 foot tide (10). To accommodate large container ships and bulk carriers, dredging operations are being considered to increase the permissible draught to 40 feet.

The North Arm is navigable by ships with a 12 foot draught.

While the primary purpose of the hydraulic model at UBC was to investigate methods to improve the regulation of the navigable channels in the Fraser, a second hydraulic model (fixed-bed, horizontal scale 1:1440), built shortly afterwards by the National Research Council at Ottawa, studied the flood danger in the Lower Fraser Valley. An intriguing feature of this NRC model was a proposal to construct a diversion canal from Annacis Island to Boundary Bay, which would reduce the flood water levels noticeably (11). This scheme and other related proposals were verified at NRC by a numerical model (12). Both hydraulic models have since been discontinued. In recent years, Western Canada Hydraulic Laboratories Ltd. at Port Coquitlam constructed a third model similar to the UBC model but on a larger horizontal scale of 1:480. All three physical models extended from the Strait of Georgia to a point beyond Chilliwack, the upper limit of tidal influence.

The possibility of regulating the Fraser River by dams, both to control floods and to generate power, has been studied in detail during the past two decades, but has met with stiff opposition from fisheries interests and environmental groups. The Fraser is the largest salmon-producing river in North America, and has created a multi-million dollar protein food industry. At present, no device exists which can pass migrating salmon safely either way over a high dam such as the proposed Moran Dam (Figure 1).

Although the demand for hydro-electric power in the Lower Mainland rises with increasing population and industry, the construction of a major dam in the Fraser would have to be a compromise among several interests. This project would require a joint study which has yet to be undertaken.

A dam would, of course, have a significant effect upon the tidal characteristics of the delta; it would smooth out seasonal fluctuations in the tides and currents and related phenomena such as sedimentation and the boundaries of the salinity wedge.

The reduction in maximum river heights and currents due to the decrease in discharge from freshet to regulated flow would, however, be partly compensated for by the tides: the tidal wave would penetrate further upstream, raising the high water levels and also adding to peak flows at ebb, due to storage of the preceding flood tides.

THE TIDES IN THE STRAIT OF GEORGIA

The tides in the Strait of Georgia at the mouth of the Fraser River are mixed, mainly semi-diurnal, as demonstrated by the ratio of the sum of the diurnal constituents ($K_1 + O_1$) to that of the semi-diurnal constituents ($M_2 + S_2$) (13): this ratio is 1.16 for Point Atkinson, a principal reference port in the strait located on the north side of Burrard Inlet, about 12 nautical miles north of the entrance to the main channel of the Fraser Delta (see Figure 13). The Point Atkinson gauge has been in operation since 1914, and its recorded or predicted tides form one of the boundary conditions of the numerical model discussed later. A second gauge, operating since 1967, and also used for a boundary condition, is located at Tsawwassen, nine nautical miles south of the entrance to the main channel (see Figure 13). Its records show a $(K_1 + O_1)/(M_2 + S_2)$ ratio of 1.27.

The tidal range for large tides is 16.2 feet (4.9 m) at Point Atkinson, and 15.4 feet (4.7 m) at Tsawwassen.

At the mouth of the Main Arm of the Fraser, the sea water level is slightly raised by the river outflow. A tide gauge operating at Sandheads from March to September 1969 recorded water levels with monthly averages 0.6 feet higher than those at Tsawwassen during the freshet, and 0.3 feet higher at very low discharges. It is interesting to note that oceanographic records (14) of a station two nautical miles west of Sandheads, at high discharges show geopotential anomalies about five dynamic centimetres (0.17 feet) higher than those observed outside the main river plume, all dynamic heights being referred to a depth of no motion of 328 feet (100 m). There was much less consistency at very low discharges.

TIDAL COMPUTATIONS

The tidal computations extend from the head of the tide water at Chilliwack to the mouth of the Fraser (Figure 4), including all four delta arms and Pitt Lake. The one-dimensional model used for these computations is based on the shallow-water wave equations (15) and has been described in detail in a previous publication (16). It will be discussed only briefly here.

The one-dimensional partial differential equations of continuity and motion can be written in the form

$$\text{(CONTINUITY)} \quad \frac{\partial Q}{\partial x} + W \frac{\partial h}{\partial t} = 0,$$

where Q is the discharge in the x -direction (downstream) in feet³/sec, W is the width of the water surface in feet, h is the elevation of the water surface in feet above geodetic datum, and x and t are the variables for distance and time, respectively;

$$\text{(MOTION)} \quad \frac{\partial u}{\partial t} + u \frac{\partial u}{\partial x} = -g \frac{\partial h}{\partial x} - g \frac{u|u|}{C^2 d},$$

where u is the water velocity in the x -direction in feet/sec, g is the acceleration of gravity in feet/sec², d is the elevation of the water surface above the river bottom in feet, and C is the friction coefficient in feet^{1/2}/sec. Considering u to be the average velocity over the river cross-section A (in feet²), and expressing the equation of motion in terms of the discharge Q (in feet³/sec), we may write

$$\text{(MOTION)} \quad \frac{1}{A} \frac{\partial Q}{\partial t} - \frac{Q}{A^2} \frac{\partial A}{\partial t} + \frac{Q}{A} \left\{ \frac{1}{A} \frac{\partial Q}{\partial x} - \frac{Q}{A^2} \frac{\partial A}{\partial x} \right\} = -g \frac{\partial h}{\partial x} - g \frac{Q|Q|}{A^2 C^2 d}.$$

After some additional minor modifications, both the Equation of Continuity and the Equation of Motion can be written in finite difference form ($\Delta x, \Delta t$), and solved at the intersections of a space-time grid, with the river discharge at one end of the model and the tides at the other (seaward) end as boundary conditions.

To express the equations in finite-difference form, the first derivatives are approximated by central differences (17), e.g.

$$\frac{\partial h}{\partial x} = \frac{H_{m+1}^k - H_{m-1}^k}{2\Delta x}$$

where k and m indicate time and distance steps, respectively.

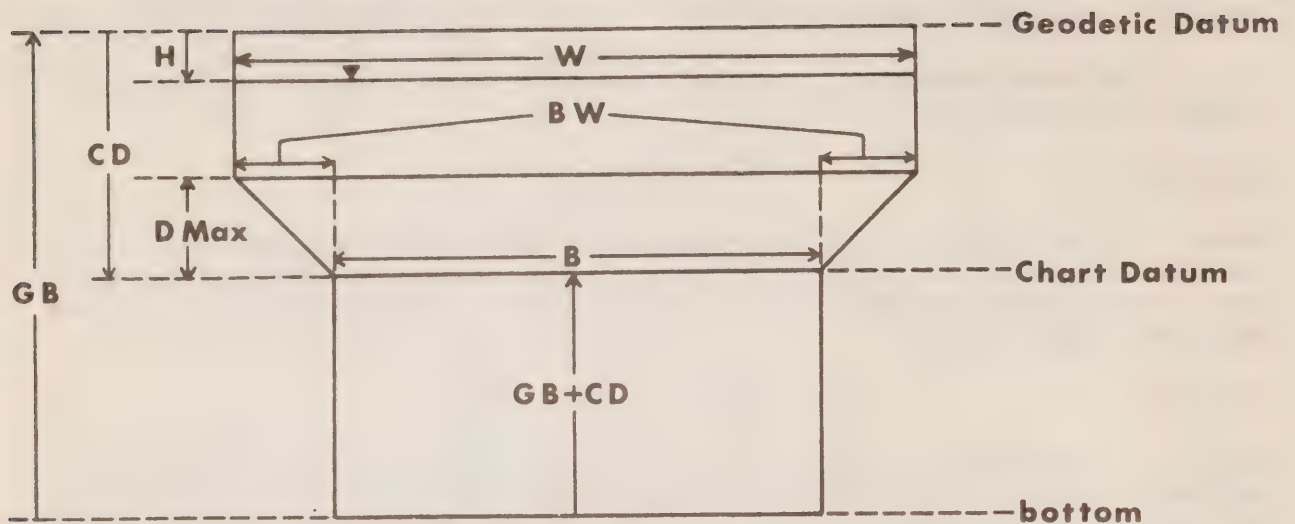
The term $\partial Q / \partial x$ may be inaccurate in finite-difference form because of the relatively long length (Δx) of the sections of the Fraser model, and is therefore replaced by $-W \partial h / \partial t$ (from continuity).

Putting $\partial A / \partial t = \partial A / \partial h \cdot \partial h / \partial t$, we can rewrite the equation of motion as

$$\frac{1}{gA} \frac{\partial Q}{\partial t} - \left(\frac{\partial A}{\partial h} + W \right) \frac{Q}{gA^2} \frac{\partial h}{\partial t} - \frac{Q^2}{gA^3} \frac{\partial A}{\partial x} = - \frac{\partial h}{\partial x} - \frac{Q|Q|}{C^2 A^2 d}.$$

The term $\partial A / \partial h$ is approximated by the width of the conveyance channel, B in Figure 6, while W also includes shoals.

Fig.6 SCHEMATIZATION OF SECTIONS



B - Mean width of a section at Chart Datum (fixed)

W - Mean width at time t (variable)

BW - Bank width (fixed)

GB - Geodetic Datum wrt bottom (fixed)

CD - Chart Datum wrt Geodetic Datum (fixed)

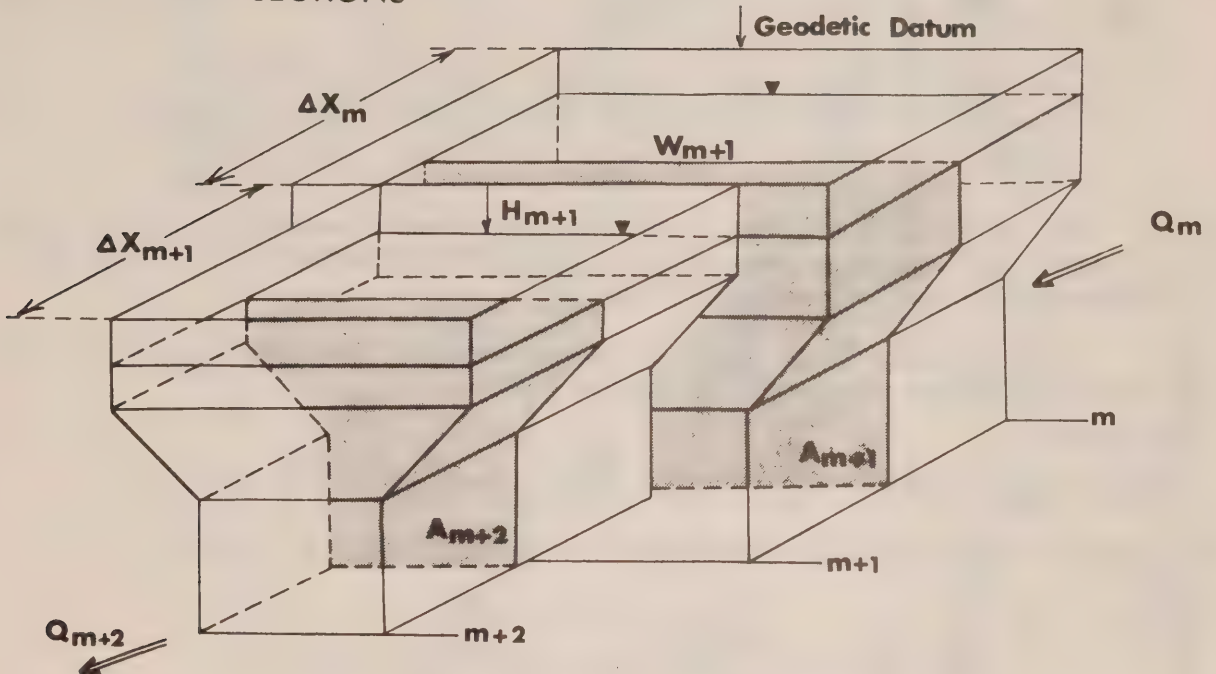
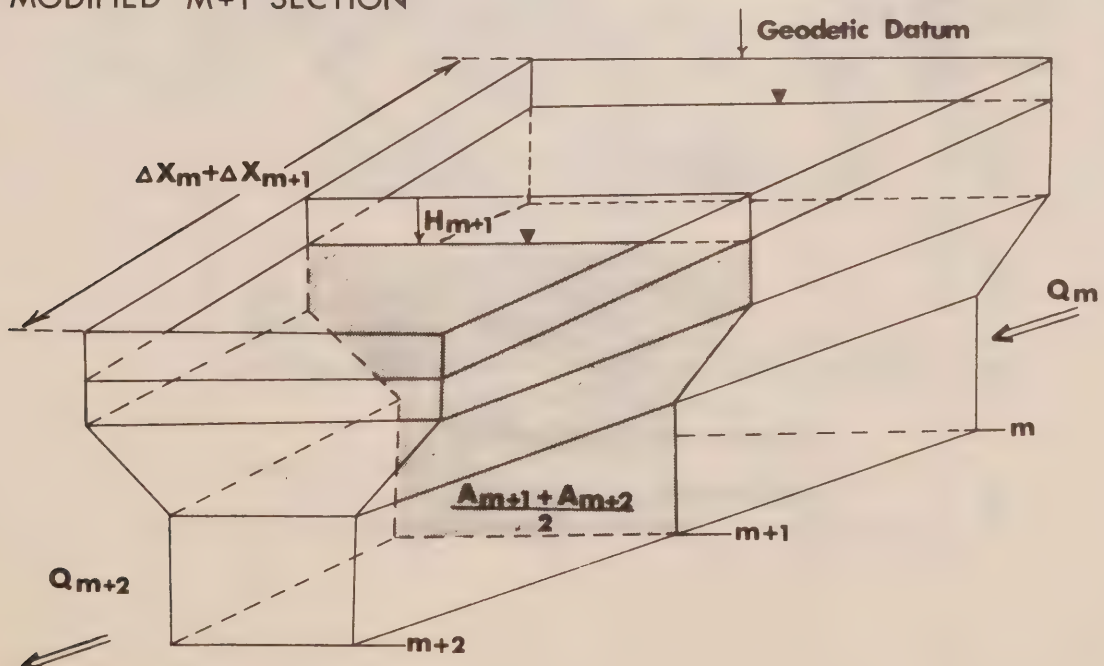
$DMax$ - Maximum bank height (fixed)

H - Water level wrt Geodetic Datum (variable; negative in figure)

$GB + CD$ - Chart Datum wrt bottom (fixed), obtained from hydrographic charts

Fig.7 SMOOTHING OF CROSS-SECTIONAL AREAS

SCHEMATIZED SECTIONS

MODIFIED $M+1$ SECTION

With these modifications, the equations of continuity and motion are respectively expressed as follows:

$$\begin{aligned} & \frac{Q_{m+2}^{k-1} - Q_m^{k-1}}{\Delta x_m + \Delta x_{m+1}} + W_{m+1}^{k-1} \cdot \frac{H_{m+1}^k - H_{m+1}^{k-2}}{2\Delta t} = 0. \\ & \frac{1}{gA_m^k} \cdot \frac{Q_m^{k+1} - Q_m^{k-1}}{2\Delta t} - (B + W)_m^k \frac{Q_m^{k+1}}{g(A_m^k)^2} \cdot \frac{(H_{m+1}^k + H_{m-1}^k) - (H_{m+1}^{k-2} + H_{m-1}^{k-2})}{4\Delta t} \\ & - \frac{Q_m^{k-1} Q_m^{k+1}}{g(A_m^k)^3} \cdot \left(\frac{A_{m+1}^k - A_{m-1}^k}{\Delta x_m + \Delta x_{m-1}} \right) = - \frac{H_{m+1}^k - H_{m-1}^k}{\Delta x_m + \Delta x_{m-1}} - \frac{Q_m^{k+1} |Q_m^{k-1}|}{(C_m)^2 (A_m^k)^2 D_m^k}. \end{aligned}$$

The subscript m for the friction coefficient C enables the program to vary C with each section. The product $Q_m^{k+1} Q_m^{k-1}$ linearizes Q^2 , because Q_m^{k-1} is obtained from the previous time step ($k-1$).

In their final form, when the model's matrix has been compressed and the rows relabelled, the equations are as follows:

(CONTINUITY)

$$H_{m+1}^{n+1} = H_{m+1}^n - \{4\Delta t \cdot (Q_{m+2}^n - Q_m^n)\} \cdot \{(W_{m+1}^n + W_{m+2}^n) \cdot (\Delta x_m + \Delta x_{m+1})\}^{-1}.$$

The term $1/2 (W_{m+1} + W_{m+2})$ represents the width at section line $m+1$ in Figure 7.

(MOTION)

$$\begin{aligned} Q_m^{n+1} = & \left\{ \frac{\Delta x_m + \Delta x_{m-1}}{g \cdot \Delta t \cdot (A_m^{n+1} + A_{m+1}^{n+1})} Q_m^n - (H_{m+1}^{n+1} - H_{m-1}^{n+1}) \right\} \\ & \cdot \left\{ \frac{\Delta x_m + \Delta x_{m-1}}{g \cdot \Delta t \cdot (A_m^{n+1} + A_{m+1}^{n+1})} + \frac{(\Delta x_m + \Delta x_{m-1}) \cdot |Q_m^n|}{C_m^2 \cdot \left(\frac{A_m^{n+1} + A_{m+1}^{n+1}}{2} \right)^2 \cdot \left(GB_m + \frac{H_{m+1}^{n+1} + H_{m-1}^{n+1}}{2} \right)} \right. \\ & - \frac{Q_m^n \cdot \{(A_{m+1}^{n+1} + A_{m+2}^{n+1}) - (A_m^{n+1} + A_{m-1}^{n+1})\}}{g \frac{(A_m^{n+1} + A_{m+1}^{n+1})^3}{4}} \\ & - \frac{(\Delta x_m + \Delta x_{m-1}) \cdot (B_m^{n+1} + W_m^{n+1} + B_{m+1}^{n+1} + W_{m+1}^{n+1})}{8g \cdot \Delta t \cdot \left(\frac{A_m^{n+1} + A_{m+1}^{n+1}}{2} \right)^2} \\ & \left. \cdot \left[(H_{m+1}^{n+1} + H_{m-1}^{n+1}) - (H_{m+1}^n + H_{m-1}^n) \right] \right\}^{-1}. \end{aligned}$$

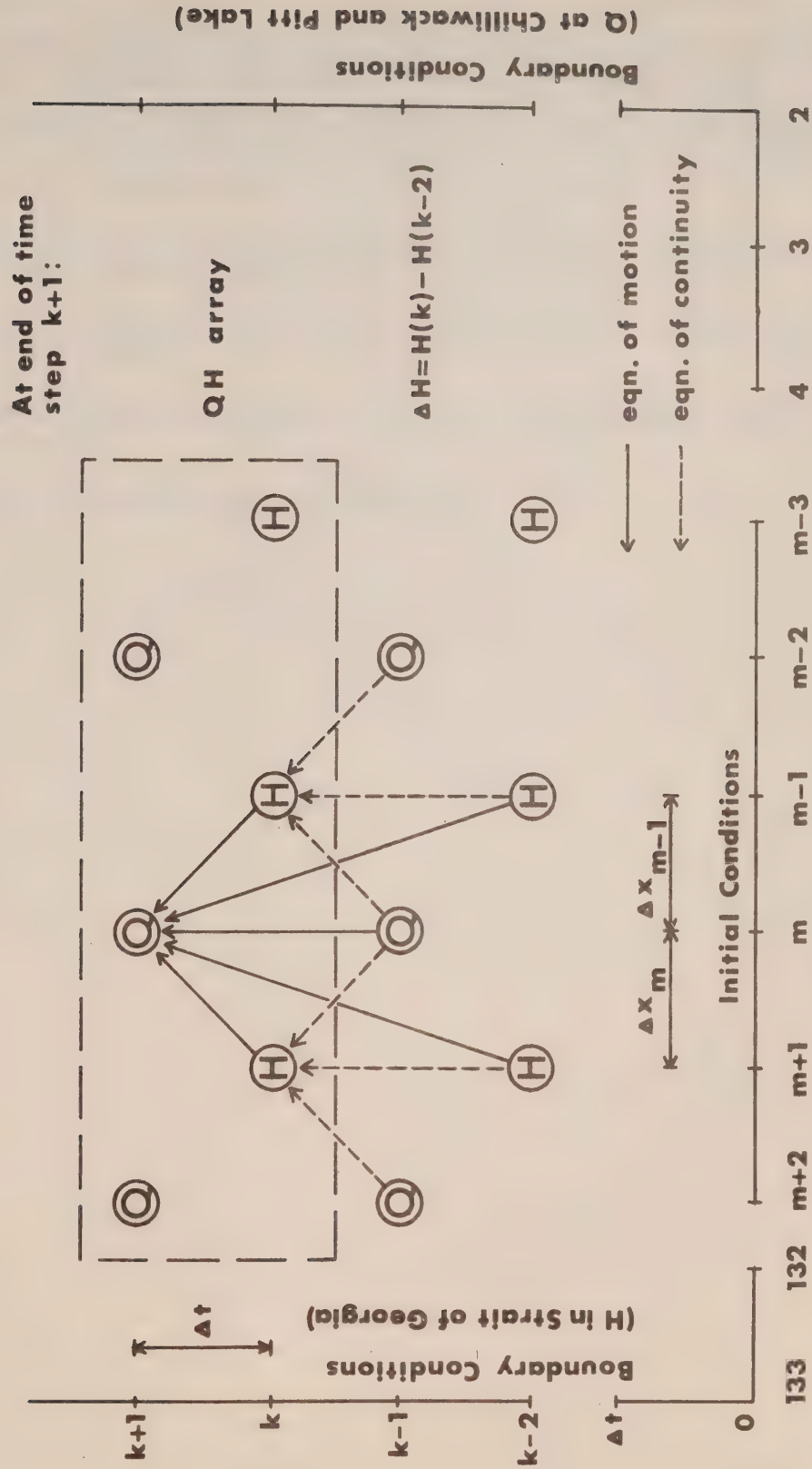


Fig.8 COMPUTER SCHEME

As the computation scheme in Figure 8 illustrates, the tidal heights H are computed at the odd-numbered sections in the x -direction (starting at the river mouth with the observed tidal heights as the downstream boundary conditions) and the discharges Q at the even-numbered sections (starting at Chilliwack and Pitt Lake with the observed discharges as the upstream boundary conditions).

ASSUMPTIONS

The tidal computations assume one-dimensional, vertically integrated flow throughout the delta.

The downstream boundary conditions at the mouth of the Fraser are assumed to be truly represented by the vertical tides at Point Atkinson and Tsawwassen (with minor adjustments for river discharge).

Except for the tidal interaction with Pitt Lake, tributary inflow between Chilliwack and the mouth of the Fraser has been omitted.

The effects of wind, barometric pressure and centrifugal forces in river bends are ignored.

Changes in cross-sectional areas due to sedimentation (bed waves, etc.) have been neglected.

Salinity intrusion has been neglected.

Fig.9 SCHEMATIZATION AT DEAS ISLAND

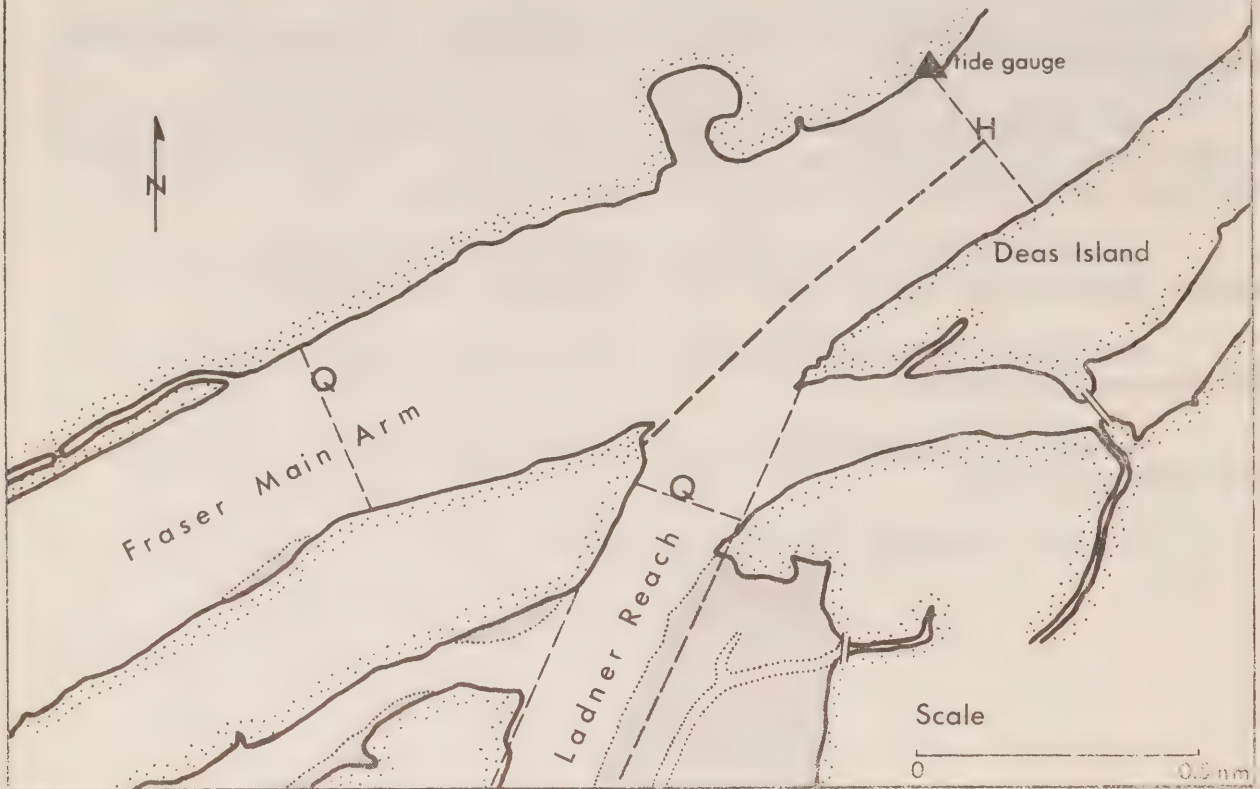
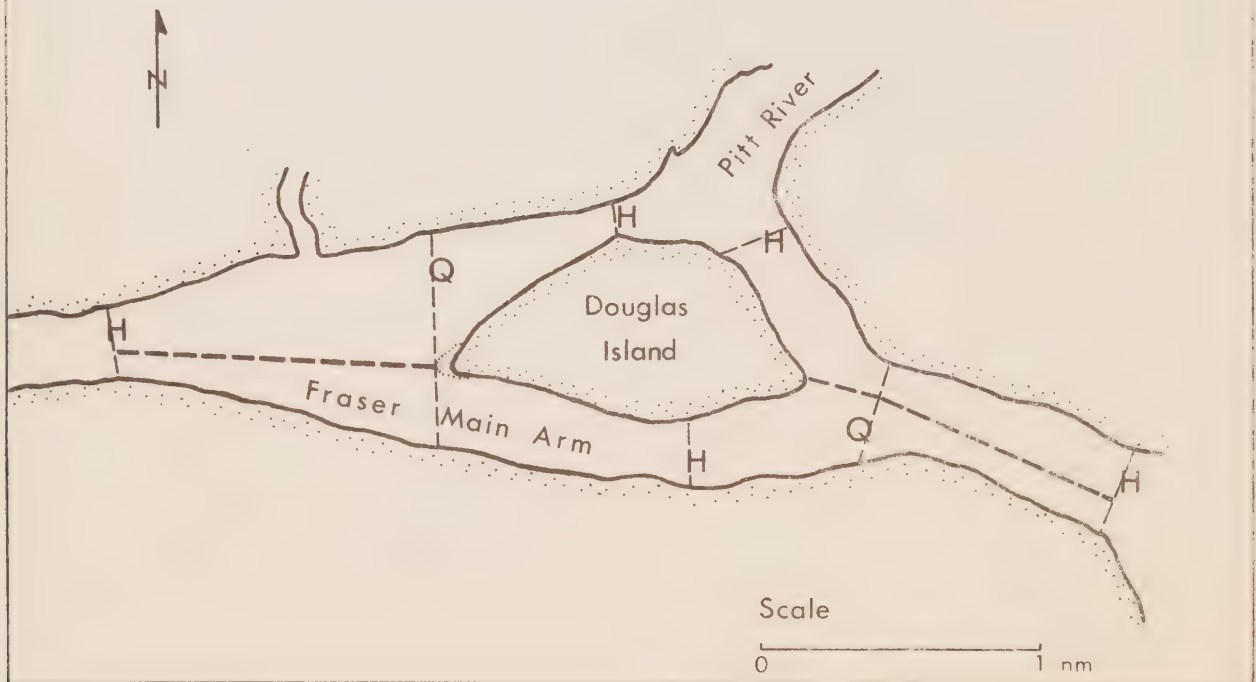


Fig.10 SCHEMATIZATION AT DOUGLAS ISLAND



SCHEMATIZATION

The river and its tributaries were divided into segments, about 6000 feet long. The depth of each segment with respect to the chart datum was obtained from a fieldsheet by overlaying the soundings with a transparent grid, and tabulating the average sounding per square. The sum of these average soundings was divided by the total number of squares to find the representative depth. The width was determined by division of the surface area (the total number of squares multiplied by the area per square) by the length of the segment. Since geodetic datum was used as a reference level for tidal heights, the depths were adjusted accordingly. Geodetic datum was selected as a reference level because it remains the same throughout the model, while chart datum is raised at regular intervals in an upstream direction.

To avoid abrupt changes in cross-sectional areas, the dimensions were smoothed out as in Figure 7.

The values B, BW, DMAX, CD and GB (see Figure 6) were taken from the charts, and are part of the data input.

To facilitate calibration, the segments were arranged so that the H-sections as sketched in Figure 8 would coincide with the locations of the tide gauges. Another criterion for the schematization was that a common H-section should be assigned to each river arm at a bifurcation or confluence (rather than a Q section and an uncertain flow distribution). If this arrangement was not feasible, the division was extended upstream (bifurcation) or downstream (confluence) to the nearest H-section by a hypothetical training wall (see Figures 9 and 10).

At Douglas Island, where Pitt River enters the Fraser, both confluences and bifurcations occur (see Figure 10). In addition to the usual modifications in the calculations arising from these conditions, the configuration of the schematized flow made it necessary to perform the calculations in one reach in a direction opposite to those in an adjoining arm.

STABILITY AND THE TIME STEP

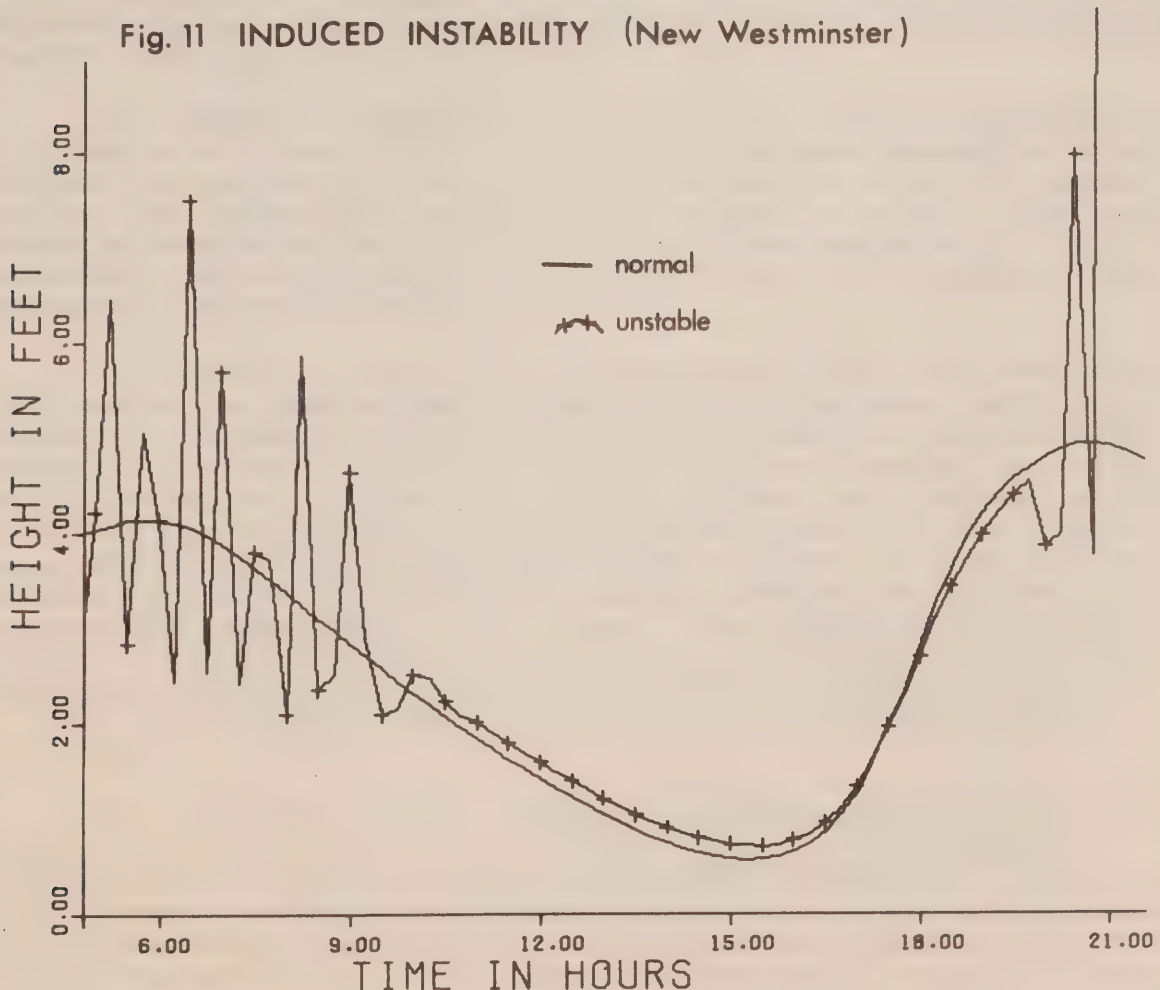
Stability is essential in an explicit scheme to prevent the progressive amplification of numerical errors introduced by finite-difference approximations to differential equations. The accepted criterion for the unconditional stability of a one-dimensional explicit scheme is

$$\frac{\Delta x}{\Delta t} > c ;$$

where c is the velocity of propagation of a tidal wave. ($c = \sqrt{gh}$, where h is the maximum water depth in the system.)

In the Fraser model, the (minimum) section length Δx had been determined by the schematization (as 3700 feet). Therefore, the time step Δt was adjusted in order to attain stability in the calculations. Although the model was unstable for a time step of 112.5 seconds, it appeared to be stable with $\Delta t = 75$ seconds. A subsequent run of the model with $\Delta t = 37.5$ seconds produced the same values for the predicted heights, confirming that stability had been reached. Therefore, a time step of 75 seconds was selected for the model.

Fig. 11 INDUCED INSTABILITY (New Westminster)



To investigate the importance of the section lengths in establishing stability, the lengths of several sections near New Westminster were reduced to 1600 feet from about 6000 feet. Figure 11 shows the predicted heights at New Westminster for both the normal and modified schemes. Although the calculations for the modified scheme are unstable and fluctuate rapidly at 5 hrs, the predicted heights return to normal when the water depth decreases to within stability bounds. However, when the critical depth is exceeded (i.e. when the stability criterion is no longer satisfied) at 20 hrs, the calculated heights oscillate wildly outside the range of the normal computations.

BOUNDARY CONDITIONS

The model's *upstream* boundary conditions are the steady-state river discharges Q at points outside the tidal influence in the Fraser and Pitt Rivers:

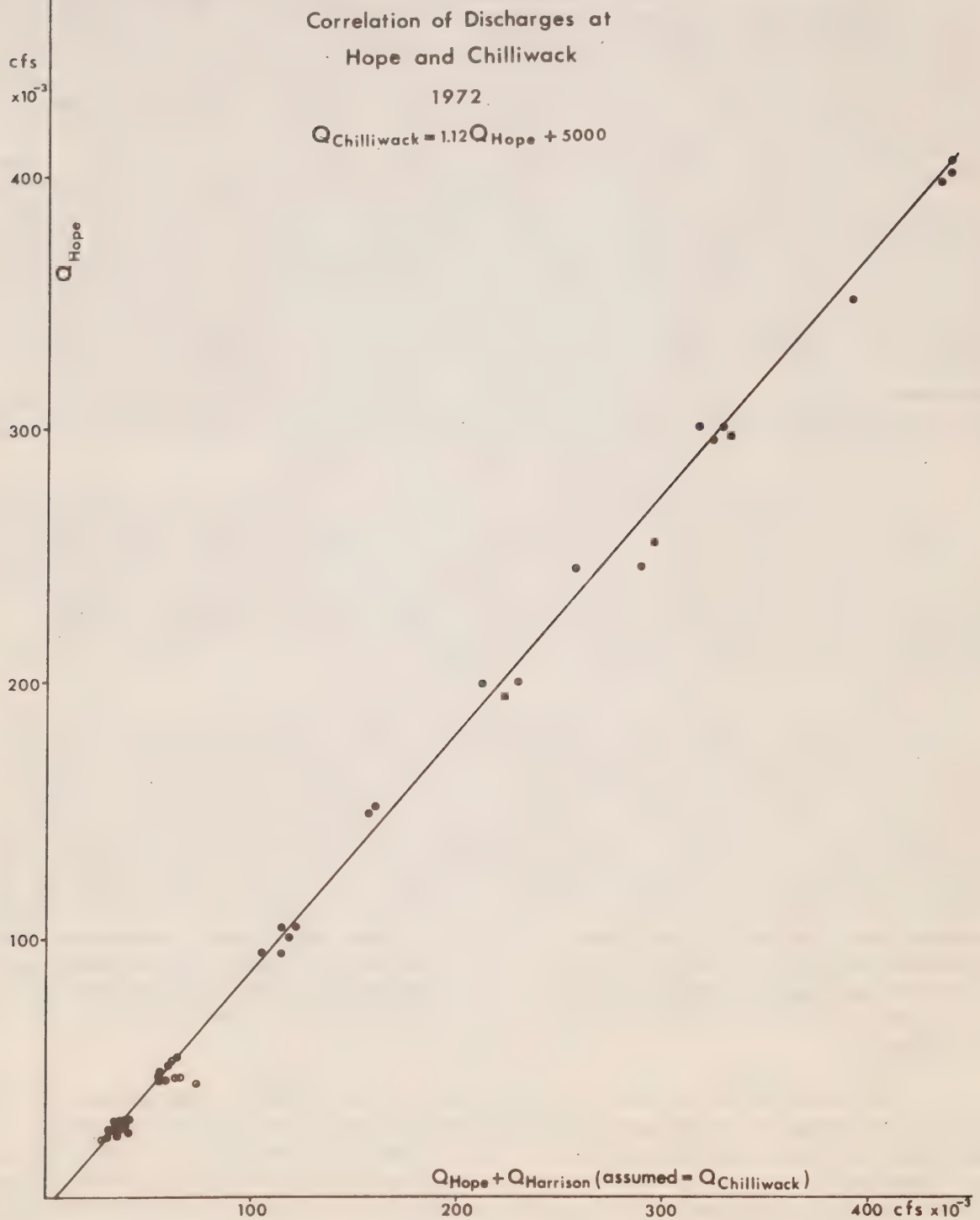
For the Fraser River, the limit of the tidal influence was considered to be at Chilliwack, the location of the first upstream river gauge without daily fluctuations in its records of water surface elevations. River discharges are not measured at Chilliwack, and the model's eastern input is based on the discharge of the Fraser at Hope, 30 miles upstream from Chilliwack, and of the Harrison River at Harrison Hot Springs. Between Hope and Chilliwack, the Harrison River is the only tributary with a significant discharge. The records of the gauges at Hope and at Harrison Hot Springs were compiled from the 1969-72 surface water records of Water Survey of Canada (18), and their sums plotted against the corresponding discharges at Hope. Although the data for all four years showed the same linear relationship, the 1972 data were the most useful because of their large range, and were used to determine the model input at Chilliwack (Figure 12). The sum of the discharges at Hope and at Harrison Hot Springs was assumed to be a reasonable estimate for the discharge at Chilliwack, and a linear approximation to the data points gave the relationship $Q_{\text{CHILL}} = 1.12 Q_{\text{HOPE}} + 5000$ cfs. The x-intercept of 5000 cfs might be considered to be the outflow of the Harrison River in the hypothetical case that the discharge of the Fraser at Hope becomes zero.

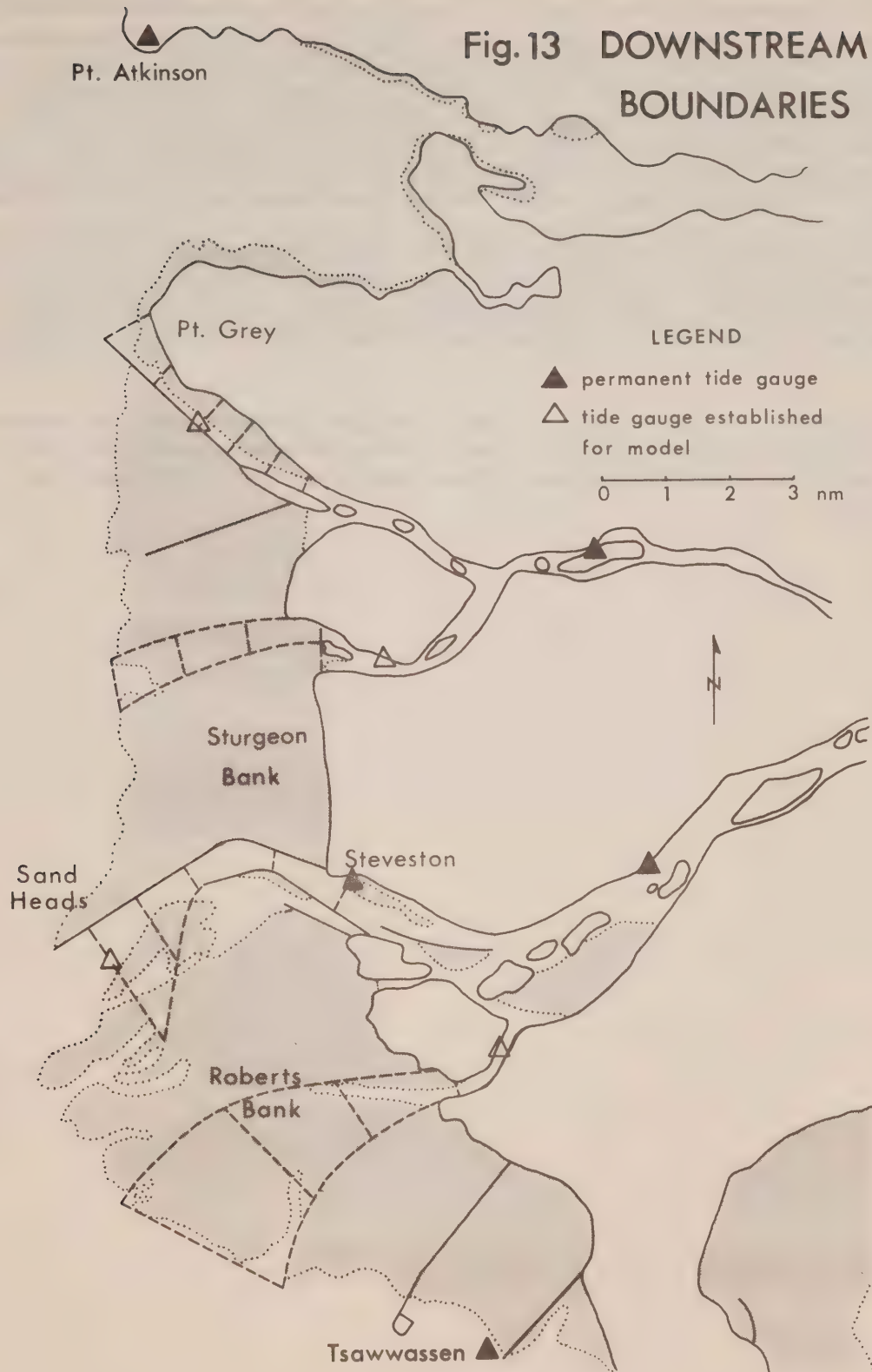
The predicted discharges at Chilliwack (i.e. values obtained using the relationship in Figure 12) were compared with discharges measured at Mission (15 miles downstream from Chilliwack) for four periods during the freshet, when the tidal effect upon the flow at Mission would be minimal. The observed discharges were an average of 4.5% higher than predicted which might be accounted for by local run-off and tributary inflow (e.g. Chilliwack River) between the two stations during the freshet.

A considerable part of the tide propagates through Pitt River into Pitt Lake and this system therefore was included in the model, with the discharge Q at the head of Pitt Lake as a boundary condition. Records of discharges into the head of Pitt Lake were not available; however, one estimate of 4000 cfs was obtained from Water Survey of Canada for a discharge at Hope of 150,000 cfs. To arrive at an approximate relationship between Q_{PITT} and Q_{HOPE} , the available discharge records of other rivers with their sources in the same area as the Pitt River (i.e. Mamquam, Cheakamus and Lillooet) were compared with those of the Fraser at Hope. These comparisons suggested the existence of a linear relationship. A similar relationship was assumed to exist between Q_{HOPE} and Q_{PITT} ; thus for a discharge at Hope of 400,000 cfs ($11,300 \text{ m}^3/\text{sec}$), the model input at the head of Pitt Lake was 10,000 cfs ($300 \text{ m}^3/\text{sec}$).

The *downstream* boundary conditions are the tides in the Strait of Georgia. Initially, they were derived from records of tide gauges established in the four distributaries, as illustrated in Figure 13. These gauges were operated by the Tides and Currents Section of the Canadian Hydrographic Service for several months during the pre-freshet and freshet periods of 1969. However, the gauges were temporary, their purpose being to provide boundary conditions for the strictly one-dimensional portion of the estuary during the

Fig.12 UPSTREAM BOUNDARY CONDITIONS





preliminary calibration. When the friction coefficients had been established, the model was extended to the Strait of Georgia and the boundary conditions transferred to the permanent tide gauges at Point Atkinson and Tsawwassen. The mean sea levels obtained from the Sandheads gauge during the freshet and non-freshet were compared with those of Point Atkinson and Tsawwassen for the same periods. The resulting small corrections (between 0.3 and 0.6 feet) were then applied to the records of Point Atkinson and Tsawwassen to obtain respectively the boundary conditions at North Arm and Middle Arm; and Main Arm and Canoe Pass. In essence, these height corrections accounted for the slight rise in water level along the outer edge of the delta, due to the fresh water outflow. The outermost sections of the river arms in the model were subsequently gradually widened to allow the main channel to expand laterally into the Strait of Georgia. This simplification, although less realistic than a two-dimensional scheme of the approaches to the Fraser, proved to be quite satisfactory.

The model's final version is run with the slightly modified observed or predicted tides at Point Atkinson and Tsawwassen downstream; and the measured or anticipated discharges at Hope (adjusted for Chilliwack) and Pitt Lake upstream.

INITIAL CONDITIONS

For calibration of the model, the initial conditions used at the odd-numbered (H) sections were the water surface elevations obtained from tide gauges along the river, interpolated linearly for sections without gauges. The discharge used at the even-numbered (Q) sections was the measured discharge at Hope (adjusted for Chilliwack) assumed to be uniform initially, and distributed among the four arms in proportion to the cross-sectional areas.

When no actual records are available, the initial conditions estimated for an average discharge are used. To avoid errors in the predictions due to inaccurate initial conditions, in other words, to allow the model to "settle down", the program is normally run for one complete tidal cycle prior to its required output.

FIELD OBSERVATIONS

Between Chilliwack and Steveston, eleven float gauges are operated by Water Survey of Canada. Their records were used to calibrate the model. To provide the calibration with accurate height and phase data, the heights and times of the gauge records were checked at intervals of a few days whenever feasible. Water Survey also modified some of the chart driving mechanisms when there appeared to be a need for higher resolution in the recorded tide curves. In addition to the river gauges, four pressure gauges were installed by the Tides and Currents Section in the four distributaries (Figure 4). They were levelled in to the nearest geodetic bench marks.

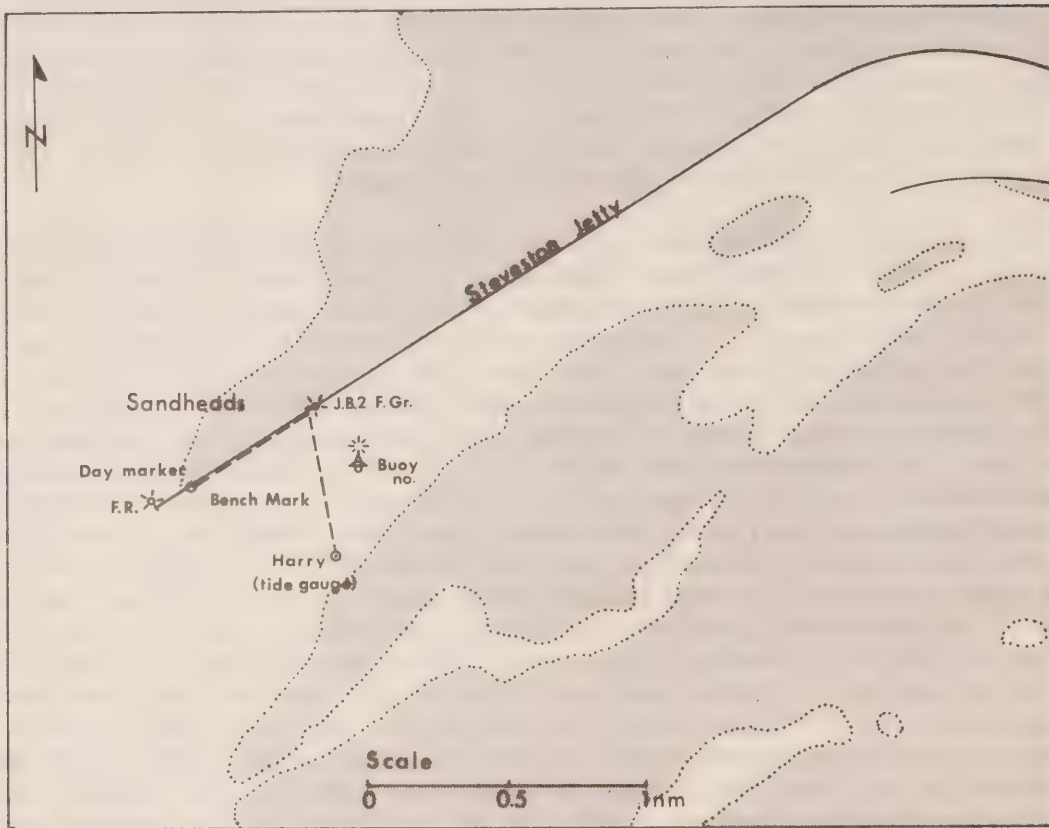
As Figure 13 illustrates, the location of the gauge at Sandheads made conventional levelling over land impossible. It had been decided not to build the gauge on the Steveston Jetty because of the very strong river velocities nearby, which would result in variable pressure heads in the tidal records. Therefore, the pressure gauge was built on a pile just outside the main river flow. The nearest bench mark had been established earlier by the Geodetic Survey of Canada on the Steveston Jetty, 3000 feet away across the mouth of the Main Arm. A preliminary test with a red laser to level across the water was unsatisfactory mainly because of the difficulty in designing an instrument which could project a perfectly horizontal beam over 3000 feet, even without considering terrestrial refraction and the curvature of the earth. An alternative method was finally found which, after some further tests and refinements, will be described in detail in a separate paper. Briefly, the procedure was as follows: Rather than a laser beam directed at a levelling rod from a large distance, a pen-light held against the rod at night provided a very bright and well defined point, no larger than the smallest division (0.01 ft) on a standard survey rod. Installed in a target, this pen-light was slowly moved up and down the rod by the rod man, and followed through the level telescope by the observer. As soon as the light point crossed the horizontal crosshair of the telescope, the observer instructed the rod man by radio to read the rod. A series of observations was made, with the target moving in opposite directions an equal number of times, to cancel out errors due to human response. Similar sightings were subsequently taken on a rod on the other survey mark and the means of both sets of sightings computed to obtain the difference in elevations between the reference points.

The effect of the earth's curvature and refraction is quite significant for distances over 1000 feet. The amount varies as the square of the distance and is roughly 0.18 feet for 3000 feet. It is therefore important that the foresight and backsight are exactly equal, which cancels this error as well as the instrument's collimation error.

Before attempting to level across the Fraser in this fashion, tests were carried out with an automatic level along a one mile stretch of beach near Victoria. An error of 0.02 feet was found over this distance; in other words, the method was of second order precision, a result which was confirmed by field tests at a later date.

The 3000 foot long sights to the bench mark and tide gauge were taken during a cool September night, shortly after midnight in excellent visibility. The observer's position on the jetty was located by marking off equal backsights and foresights on the chart.

Fig.14 NIGHT LEVELLING AT SANDHEADS



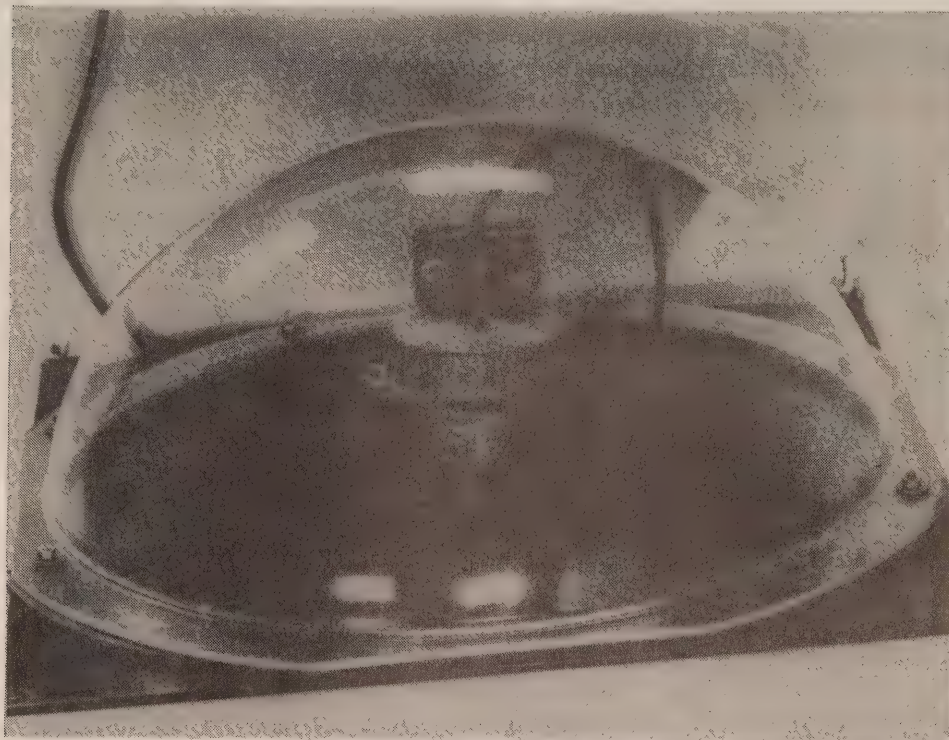
To ensure that both sightings would be taken over water and would presumably be equally affected by refraction, they were taken at high tide when almost the entire jetty between the observer and the bench mark was flooded.

The two sets of sightings were completed within an hour; the instrument used was a Zeiss N12. As Figure 14 shows, only one set-up was possible for this particular problem; therefore, the results could be verified only by repeated observations. If we assume second order levelling, the error in the observed Sandheads tides used for the model would not have exceeded 0.02 feet.

The gauges at Middle Arm and Canoe Passage were established in more convenient sites. However, the gauge in North Arm also required some improvisation. The recorder was put on a pile on the North Arm Jetty, but the pressure unit had to be placed on the river bed. To prevent the diaphragm from becoming clogged up by sand, it was built in an eight inch high plastic dome, weighted by 1/4 inch steel plate, and raised about one inch above the plate. Small 1/16 inch holes in the top of the dome exposed the diaphragm to the ambient water pressure. Although this design kept the pressure unit free from sand for several months and also provided it with a stable base (and consequently the tidal records with a constant reference level), it had an

important disadvantage: it measured the total pressure, whereas the static pressure was required for the boundary condition.

Fig. 15 PRESSURE UNIT OF NORTH ARM TIDE GAUGE



The dynamic pressure (about $\frac{3}{2} \rho U^2$, where U is the water velocity above the dome) at the top of the dome would cause significant errors in the tide gauge records during the freshet. Therefore, it was necessary to place the pressure unit of the gauge near the shore in slower moving water. However, in this location, anchored log booms would press the unit deeper into the sand at very low tides, thus changing the reference level of the records. Despite frequent surveillance with a launch stationed in Richmond, several days of records were lost due to log booms.

The pressure gauges were set for salt water at a specific gravity of 1.025. Such a gauge, operating in ten feet of fresh water, would record 9.75, i.e. 0.25 feet too low, a significant discrepancy for the boundary conditions. To examine the density distribution in the water column above the gauge, several salinity measurements were taken with a Beckman portable RS 5-3 salinometer within a few feet of the gauge positions. These measurements indicated that during the freshet the salt water intrusion at all four sites was negligible. Since the initial calibration was carried out during the freshet, we assumed that the records of all four temporary delta gauges contained negative errors varying from zero feet at low tide to -0.2 feet at high tide. However, frequent comparisons in the field with tide staffs, particularly at the important Sandheads and North Arm gauges, made it possible to adjust the field data to compensate for this error.

In addition to spot measurements of salinities and temperatures near the sites of the tide gauges, a number of cruises were made in the delta to determine the limit of salt water intrusion, as it varies with tides and river discharge. These observations, which have been published as a data record (2), were reconnaissances.

The field program primarily considered the vertical tidal movement. A detailed study of currents and the behaviour of the salinity wedge was deferred to a later date, when we may have made sufficient progress in numerical techniques to develop a useful stratified model.

CALIBRATION

After the schematization of the river, and the development of the computer program, the model was calibrated.

The tidal curves produced by the model at the sites of the tide gauges along the river were compared with the curves recorded by the gauges. The friction coefficient C in the equation of motion was subsequently adjusted throughout the river until the model output finally agreed satisfactorily with the prototype data, a trial and error procedure analogous to the calibration of a physical model with friction elements.

The model was run with, as boundary conditions, the measured discharges at Hope (adjusted for Chilliwick), and the actual tides recorded by the temporary tide gauges at the entrances of the four distributaries. Three consecutive days, 16-18 July 1969, were selected for the first calibration. During this period, there was a spring tide in the Strait of Georgia, which provided a large tidal range (11 feet or 3.35 m); the discharge (150,000 cfs or 4200 m³/sec at Hope) was high enough to virtually eliminate salt water intrusion and its effect upon the consistency of the recorded tidal heights; the winds at Sandheads were light easterly, averaging six mph, so that the effect of wind upon the tides could be neglected; and finally, all tide gauges performed well during this period.

Both model-produced and observed heights were referred to geodetic datum for all locations.

To adjust the friction coefficients, the program was run about a dozen times until the model-produced and observed tide curves agreed within acceptable limits (in most cases 0.5 feet or 15 cm). The friction coefficients were assigned to blocks of segments rather than to individual segments, which would have been more representative of the prototype flow but would have involved a very large number of tests at an unwarranted cost.

After the schematization had been extended to the Strait of Georgia, and the boundary conditions transferred to the two permanent gauges at Point Atkinson and Tsawwassen (Figure 13), the model was verified by comparing the output with the gauge records for other dates in 1969 (freshet and non-freshet). The discrepancies were in the order of 0.5 to 1.0 feet in height and one-half to one hour in time.

The calibration was carried out for a relatively low freshet in 1969. The model's validity had yet to be established for an unusually high discharge, not only because of changes in the schematization of the cross-sectional areas due to flooding, but also because of a hydrodynamic consideration:

In the equation of motion:

$$\frac{\partial u}{\partial t} + u \frac{\partial u}{\partial x} = -g \frac{\partial h}{\partial x} - g \frac{|u|u}{C^2 d},$$

we can manipulate only the last term (the friction term) to align the tide curves produced by the model with the curves recorded by the gauges. We thus "tune" the model by adjusting the friction coefficient C .

The significance of the friction term increases as the square of the water velocity, i.e. with the discharge. Consequently, a model which has been calibrated at a discharge of 150,000 cfs, may not respond realistically to a discharge of 400,000 cfs, but would be valid for discharges below 150,000 cfs. The year 1969, with a peak discharge at Hope of less than 300,000 cfs, was obviously not a good year to calibrate the Fraser model.

It was not until 1972, with a peak discharge at Hope of 450,000 cfs (12,700 m³/sec) that this concept could be further examined.

The program was run and recalibrated for observed tides at Point Atkinson and Tsawwassen with a very high range of 15 feet, and for observed discharges at Hope increasing from 385,000 to 400,000 cfs.

As Table I illustrates, the original friction coefficients established for a discharge at Hope of 150,000 cfs induced large height discrepancies at extreme discharges. The program run with these same friction coefficients for a low discharge of 51,000 cfs produced minor discrepancies of the same order as for the calibration discharge of 150,000 cfs. However, the friction coefficients determined at a discharge of 398,000 cfs also apply well to the discharges of 150,000 cfs and 51,000 cfs. The table confirms the suggestion that the model's height predictions are reliable only for discharges at or below that for which it was calibrated (in our case, 398,000 cfs).

A similar comparison of time differences between model-produced and observed high and low waters (Table II) is much less conclusive because the exact times of high and low waters during a freshet are difficult to identify.

As mentioned earlier in this section, another potential weakness in the application of a river model at high discharges is the change in the schematization of cross-sections due to flooding. However, most of the abrupt changes in cross-sectional areas in the Fraser occur at low discharges, and can be schematized from detailed charts. The crest of the dykes along the Fraser is set at two feet above the highest known water level (i.e. the 1894 flood). We may therefore assume that the river flow will be contained by the dykes, and that the schematized cross-sections are not altered by flooding.

Figure 16 shows the distribution of the friction coefficients resulting from the final calibration at 398,000 cfs (11,300 m³/sec).

The friction coefficients determined at 150,000 cfs are also shown to illustrate the importance of the discharge when calibrating the model.

MODEL CALIBRATION AT HIGH AND EXTREME DISCHARGES

TABLE I: HEIGHT ERRORS IN FEET
(PREDICTED - OBSERVED)

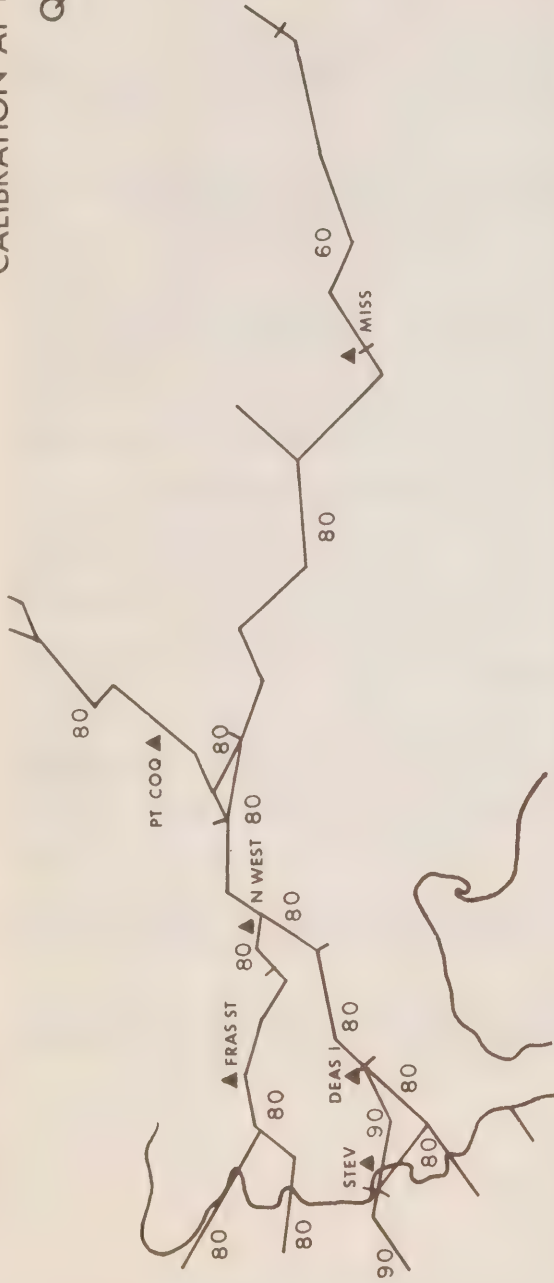
Q _{HOPE} used for calibration (cfs)	TIDE	LOCATION:					
		MISSION	PT. COQ.	N. WEST.	FRAS. ST.	DEAS	STEVESTON
		DATES RUN: Nov. 12-14/71 (Q _{HOPE} = 51,000 cfs)					
150,000	HI	- 0.9	- 0.3	- 0.6	- 0.1	- 0.5	- 0.3
	LO	- 0.7	- 0.3	+ 0.3	+ 0.2	- 0.5	+ 0.2
398,000	HI	- 0.9	- 0.3	- 0.5	- 0.1	- 0.3	- 0.1
	LO	- 0.9	- 0.3	+ 0.3	+ 0.2	+ 0.4	+ 0.4
		DATES RUN: June 11-13/72 (Q _{HOPE} = 398,000 cfs)					
150,000	HI	+ 1.8	+ 0.6	+ 0.3	- 0.2	- 0.2	+ 0.2
	LO	+ 1.9	+ 0.8	+ 1.8	+ 1.6	+ 1.6	+ 0.8
398,000	HI	+ 0.4	- 0.5	- 0.6	- 0.1	- 0.3	+ 0.1
	LO	+ 0.4	- 0.5	+ 0.6	+ 0.6	+ 0.2	+ 0.2
		DATES RUN: July 16-18/69 (Q _{HOPE} = 150,000 cfs)					
150,000	HI	0	- 0.1	- 0.3	- 0.2	- 0.4	- 0.2
	LO	- 0.3	- 0.4	- 0.2	+ 0.2	- 0.2	- 0.3

TABLE II: TIME ERRORS IN MINUTES
(PREDICTED - OBSERVED)

Q _{HOPE} used for calibration (cfs)	TIDE	LOCATION:					
		MISSION	PT. COQ.	N. WEST.	FRAS. ST.	DEAS	STEVESTON
		DATES RUN: Nov. 12-14/71 (Q _{HOPE} = 51,000 cfs)					
150,000	HI	- 30	0	+ 15	- 23	- 23	+ 8
	LO	- 23	- 8	- 8	0	+ 15	- 1
398,000	HI	- 30	+ 8	- 8	- 30	- 30	+ 8
	LO	- 23	- 15	+ 8	- 8	+ 15	- 1
		DATES RUN: June 11-13/72 (Q _{HOPE} = 398,000 cfs)					
150,000	HI	- 75	- 15	0	- 15	0	- 104
	LO	- 8	- 23	+ 30	+ 45	- 15	- 122
398,000	HI	- 105	- 38	- 15	- 15	- 8	- 3
	LO	0	- 23	+ 38	+ 30	- 23	- 23
		DATES RUN: July 16-18/69 (Q _{HOPE} = 150,000 cfs)					
150,000	HI	+ 68	- 8	+ 15	- 30	0	+ 11
	LO	- 45	- 15	- 23	- 15	- 30	- 19

CALIBRATION AT LOW FRESHET

$Q_{\text{Hope}} = 150,000 \text{ cfs}$



CALIBRATION AT HIGH FRESHET

$Q_{\text{Hope}} = 398,000 \text{ cfs}$

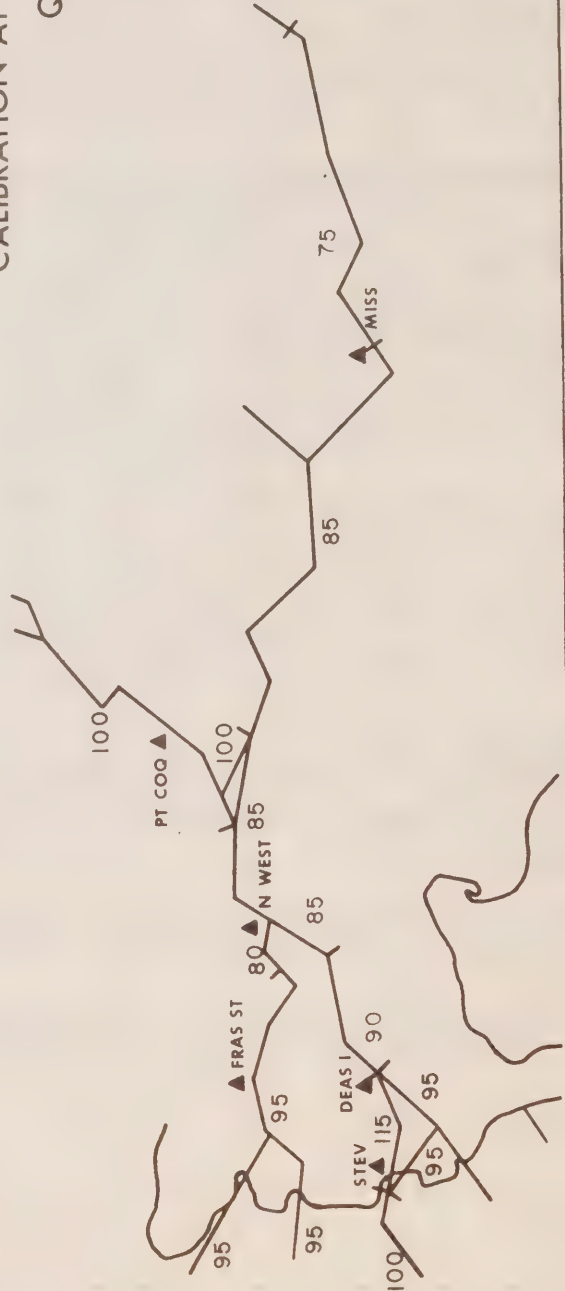


Fig.16 DISTRIBUTION OF FRICTION COEFFICIENTS

RESULTS

The principal objective of the Fraser model was to compute water surface elevations for the tidal portion of the river, as a function of the tides in the Strait of Georgia, and the river discharges. An obvious application is the prediction of heights and times of high and low waters in the navigable part of the river, by relating them to the corresponding high and low waters at Point Atkinson, and the discharges at Hope. The times and heights of maximum and minimum water levels at Point Atkinson are predictable and are tabulated in the Canadian Tide and Current Tables. Short-term discharge estimates can be made, based on measurements of the previous days and the weather forecast for the Hope area; the program can be adjusted easily in the case of unexpected changes.

The model was run for several tidal cycles with ranges between lower low and higher high waters varying from 8 to 16 feet observed at Point Atkinson and Tsawwassen during the following periods: June 25-July 2, 1969; August 28-September 4, 1969 and January 11-18, 1969; and for seven discharges at Hope between 25,000 and 300,000 cfs. Of course, very few of these discharges actually occurred during any of the eight-day periods. Eight locations along the Fraser were selected for tidal predictions: Steveston, Deas Island Tunnel, Middle Arm, Fraser Street Bridge, New Westminster, Port Mann, Port Coquitlam and Mission. Heights and time differences of a total of 42 predicted extrema per station per discharge were plotted against the heights of the corresponding extrema at Point Atkinson. Figures 17 and 18 are the height and time lag plots for New Westminster. Only the higher high and the lower low waters were considered, and the first day of each run was ignored. The least-squares best-fit curves of 2nd order ($y = ax^2 + bx + c$) were subsequently plotted for each case, Figures 19-34.

Since the daily higher high and lower low waters at Point Atkinson do not occur near geodetic datum (approximately mean sea level), the central, dashed portions of the curves are estimates. The curves are best-fit curves and do not necessarily represent the true hydrodynamic relationship between the river extrema and those at Point Atkinson.

If we could develop an expression for the water surface elevation H at an upstream point x , as a series of simple-harmonic functions of time, we could set $\partial H / \partial t = 0$ for maximum and minimum elevations, solve for t and H_{extrema} , and obtain an exact relationship between the extrema at any point x along the river and at Point Atkinson ($x = 0$). However, it is impossible to solve the equations of motion and continuity analytically, and therefore we have to content ourselves with a best-fit curve (an approximation) through data points obtained by a numerical method (another approximation).

The height prediction curves clearly reflect the interaction between tides and discharges: the spread of the curves for New Westminster (Figure 19) compared with that for Steveston (Figure 21) demonstrates the increasing contribution of the discharge to the rise and fall of the water surface elevation as we move upstream. The slope of each individual curve ($\partial H_{\text{ext Atkinson}} / \partial H_{\text{ext Fraser}}$) decreases as the height at Point Atkinson increases, indicating the decreasing influence of the discharge upon the local river heights as the tides in the Strait of Georgia become higher. The height prediction curve for Mission at 300,000 cfs (see Figure 33) is a straight vertical line showing

there is no noticeable tidal influence at Mission for that discharge, which would occur at the peak of an average freshet.

To verify these model-produced heights at New Westminster, similar computer plots were generated for four years of observed data (1970-1973). Figures 35-41 show the actual heights of the extrema at New Westminster corresponding to the higher high and lower low waters at Point Atkinson for various discharges. Figure 42 displays the least-squares best-fit curves of 2nd order for these plots, and supports the model results of Figure 19.

Unlike the height comparisons between Point Atkinson and the Fraser gauges, the best-fit curves for the predicted time differences were plotted without distinguishing among the discharges. As was mentioned in the section on calibration, the choice of the culmination points has much more influence upon the time differences than upon the heights.

In other words, if we slightly misjudge the exact location of a culmination point on the tide curve (in the prototype by visual inspection, in the model predictions by a programming technique), the time would be much more in error than the height. This would particularly be the case at an upstream station during the freshet, where at high tide the change in water surface elevation over several hours might be imperceptible.

Figure 18 illustrates the difficulty of determining a separate time lag curve for each discharge; the time differences of the predicted higher high and lower low waters at New Westminster are plotted against the observed higher highs and lower lows at Point Atkinson. Although there is a definite envelope of maxima and minima, the clustering of the data points, particularly at high waters, makes it impossible to establish a family of discharge curves. Therefore, a single least-squares best-fit curve of second order was calculated over all discharges for each upstream location (e.g. Figure 20 for New Westminster).

Time lags at New Westminster were plotted for four years (1970-1973) of observed data to check the model predictions. Figures 43, 44 and 45 represent the actual time lags between each higher high or lower low water at Point Atkinson and the corresponding high and low at New Westminster for several discharge ranges, and Figure 46 shows the overall best-fit curve. These actual data plots agree closely with the results of the model. For sea water levels at Point Atkinson below mean sea level (i.e. low waters), the time lag curves have a distinct negative slope, which reverses above mean sea level, but only slightly. This reversal is particularly evident at low discharges (Figure 43). The time lag curves for other locations along the river show a similar trend.

Although a detailed interpretation of the complex water motion in the delta is outside the scope of this report, some general comments on the shape of the time lag curves may be enlightening:

At any location x along the river, we may express the vertical displacement of one of the tidal components with respect to mean level as:

$$\eta_{xt} = Ae^{-\mu x} \cos(\omega t - \kappa x), \text{ where}$$

A = amplitude at the entrance of the river

ω = frequency of the component (i.e. $\frac{2\pi}{T}$, T = period)

κ = wave number (i.e. $\frac{2\pi}{L}$, L = wave length)

μ = damping modulus, normally evaluated from tidal records (19). This modulus accounts for tidal friction and, consequently, the decrease in amplitude with x .

At any location x ,

$$\frac{\partial \eta}{\partial t} = -A\omega e^{-\mu x} \sin(\omega t - \kappa x),$$

from which we deduce that the tide rises and falls faster at Sandheads ($x = 0$) than at New Westminster ($x = 18$ n.m.).

In an average water depth of about 30 feet, the tidal wave would travel from Sandheads to New Westminster in slightly less than one hour, if there was no friction. In that case, low water at New Westminster would occur approximately one hour after the corresponding low water at Sandheads. However, due to friction ($e^{-\mu x}$), the tide will fall more slowly at New Westminster than at Sandheads. One hour after low water at Sandheads, the tide at New Westminster will still be falling, and will continue to do so until the steady-state hydraulic grade line has been re-established. At this point, the tide at Sandheads has started to rise. (The hydraulic grade line between New Westminster and Sandheads is identical to the water surface, and has a steady-state drop of about five feet during the freshet, and of about 0.5 feet during non-freshet conditions, see Figures 48 and 49.) The lower the low water is at Sandheads, the longer it will take the tide at New Westminster to fall to the hydraulic grade line. Therefore, the time lags between low waters at Sandheads and New Westminster will increase with the displacement of the low waters at Sandheads from mean sea level.

Conversely, the tide also rises faster at Sandheads than at New Westminster. At a high tide in the Strait of Georgia, the gradient is close to zero and equilibrium between New Westminster and Sandheads is quickly attained. A very high tide at Sandheads reverses the gradient between Sandheads and New Westminster at low discharges; one hour after high tide at Sandheads, the tide at New Westminster will still be rising since equilibrium has not yet been reached. The higher the high tide is at Sandheads, the longer it will take the rising tide at New Westminster (and the falling tide at Sandheads) to reach equilibrium. Figure 43 indeed shows a trend for the time lags to increase with higher maxima at Sandheads. This trend is not so pronounced as for low waters because the (negative) gradient between New Westminster and Sandheads is much smaller at high tides than the (positive) gradient is at low tides (Figures 48 and 49).

The plotted time differences for high waters at New Westminster (model-predictions: Figure 18; observations: Figure 43) show irregularities at low discharges, which are too large to be caused by friction alone, or by the ambiguity of the location of the culmination point. The complex flow régime at the trifurcation may well be responsible for these isolated points.

Fig.17 MODEL-PREDICTED CORRESPONDENCE BETWEEN
HIGHS AND LOWS AT
POINT ATKINSON AND NEW WESTMINSTER

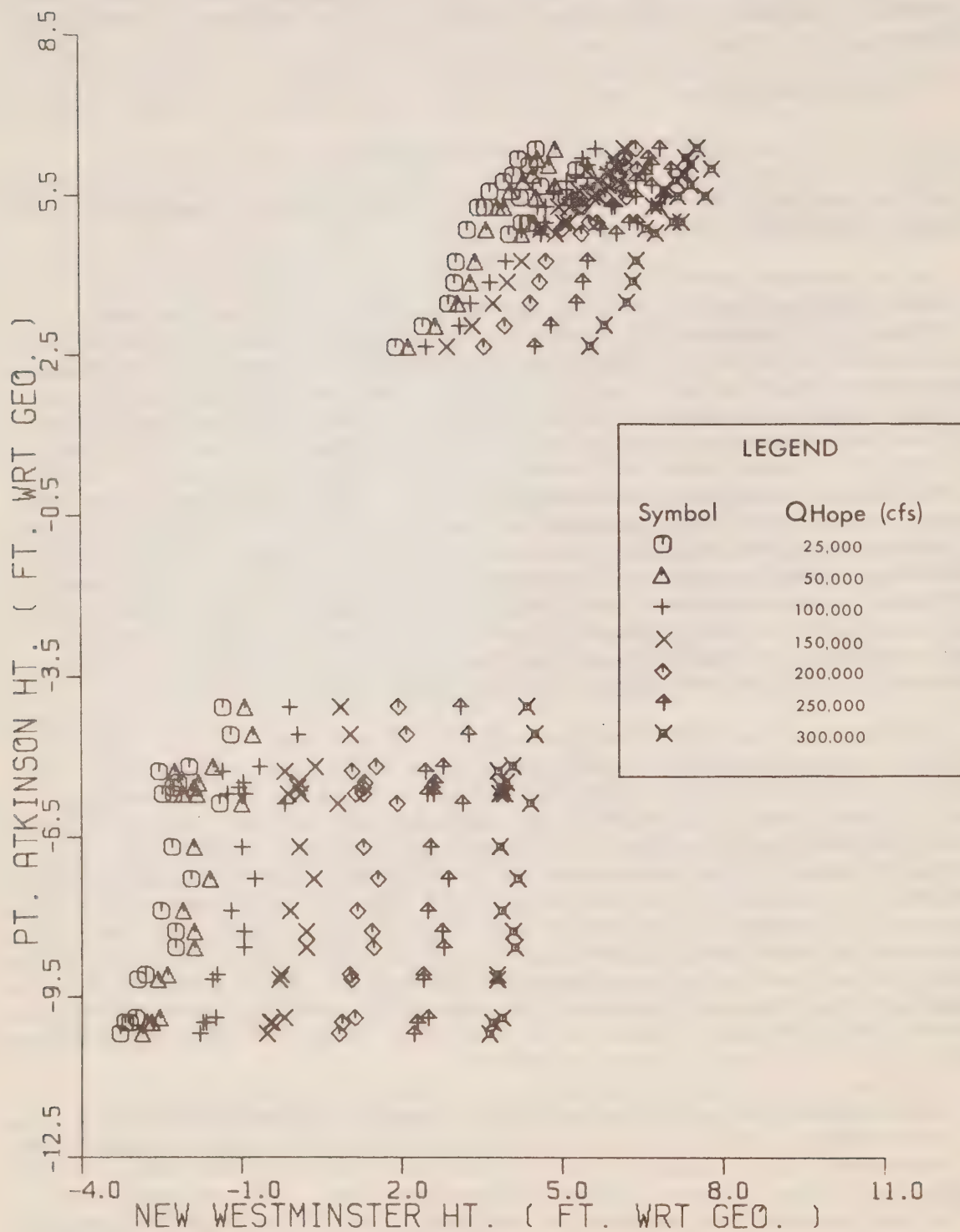


Fig.18 MODEL-PREDICTED CORRESPONDENCE BETWEEN
HIGHS AND LOWS AT
POINT ATKINSON AND NEW WESTMINSTER

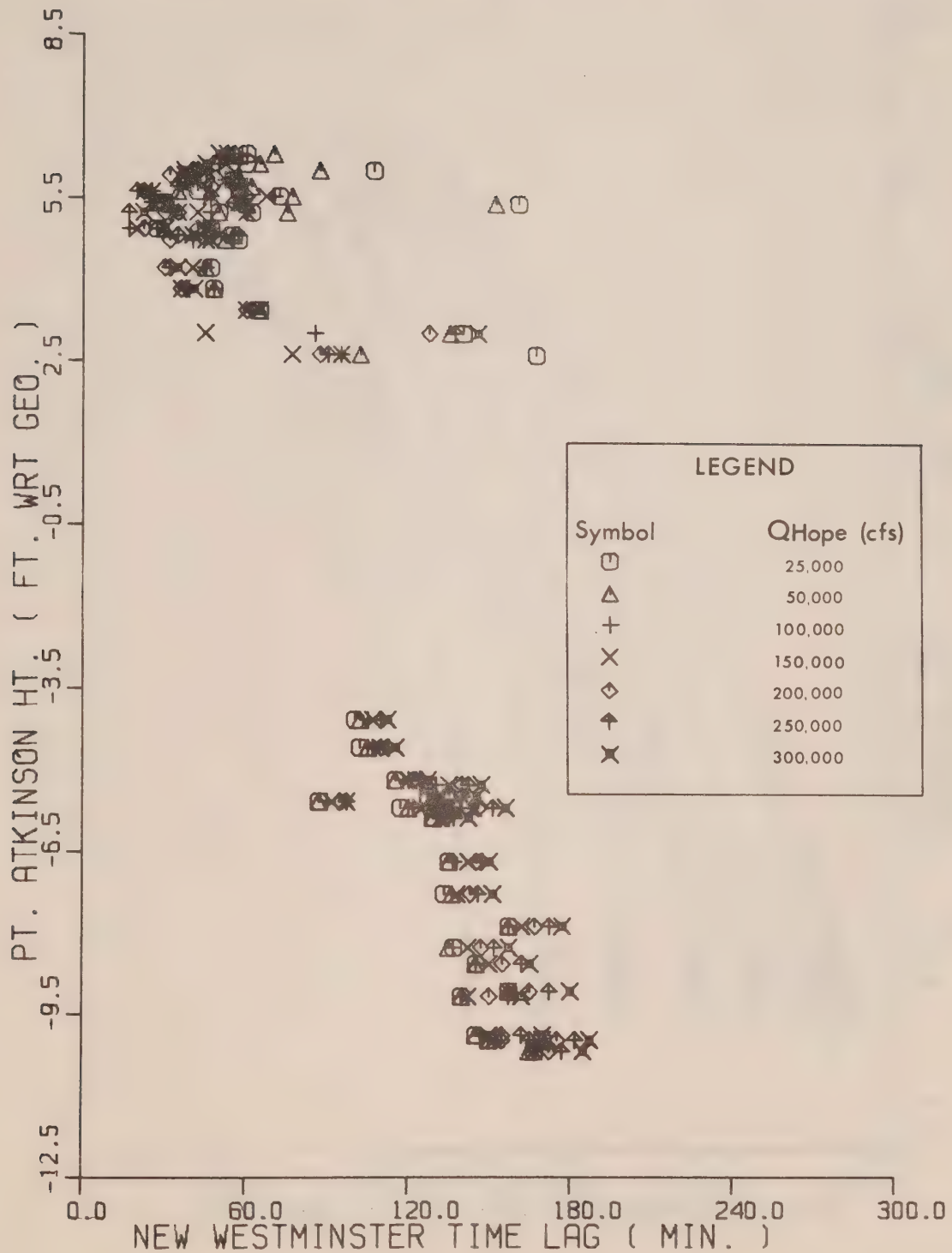


Fig.19 MODEL-PREDICTED CORRESPONDENCE BETWEEN
HIGHS AND LOWS AT
POINT ATKINSON AND NEW WESTMINSTER

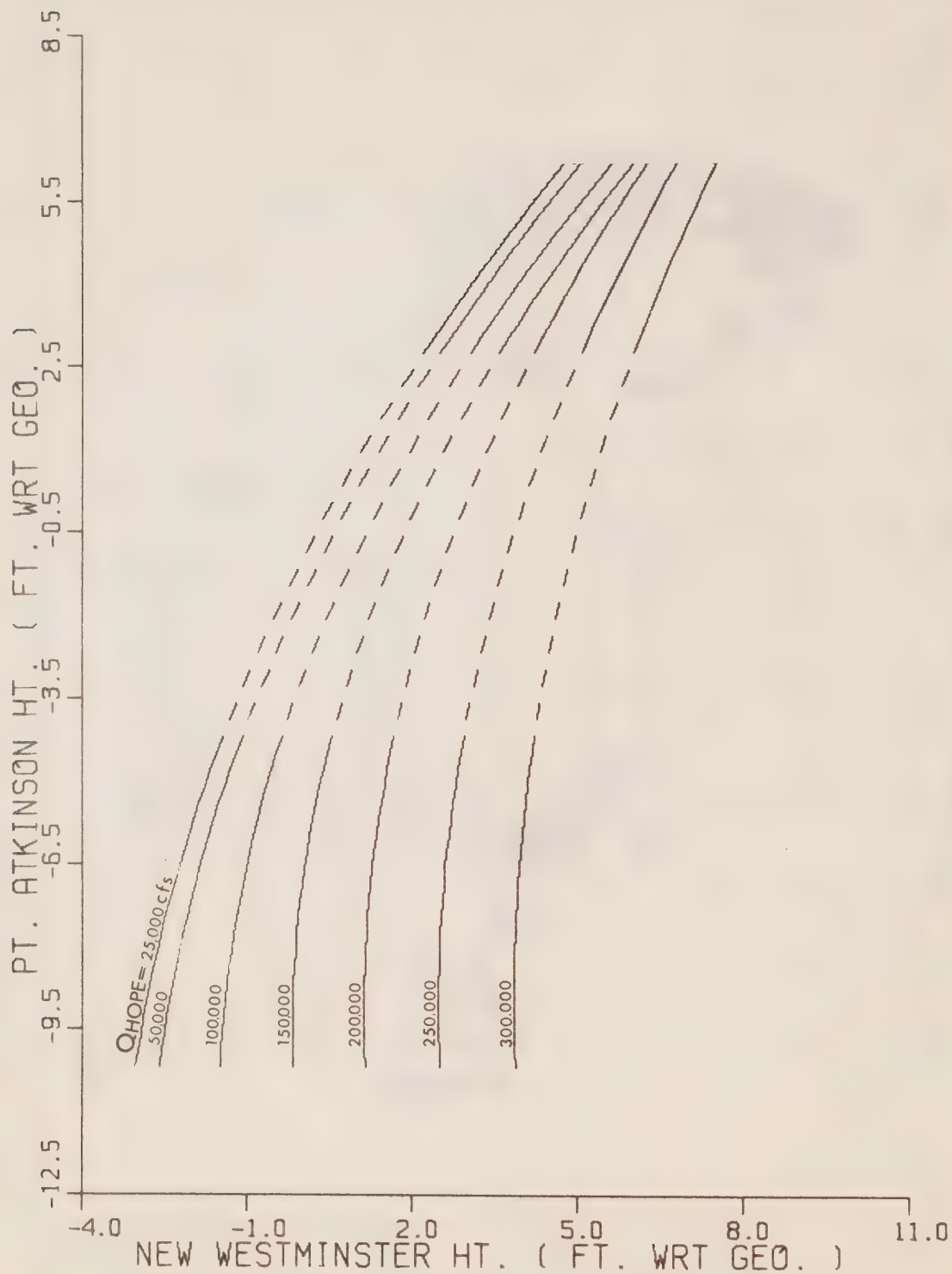


Fig.20 MODEL-PREDICTED CORRESPONDENCE BETWEEN
HIGHS AND LOWS AT
POINT ATKINSON AND NEW WESTMINSTER

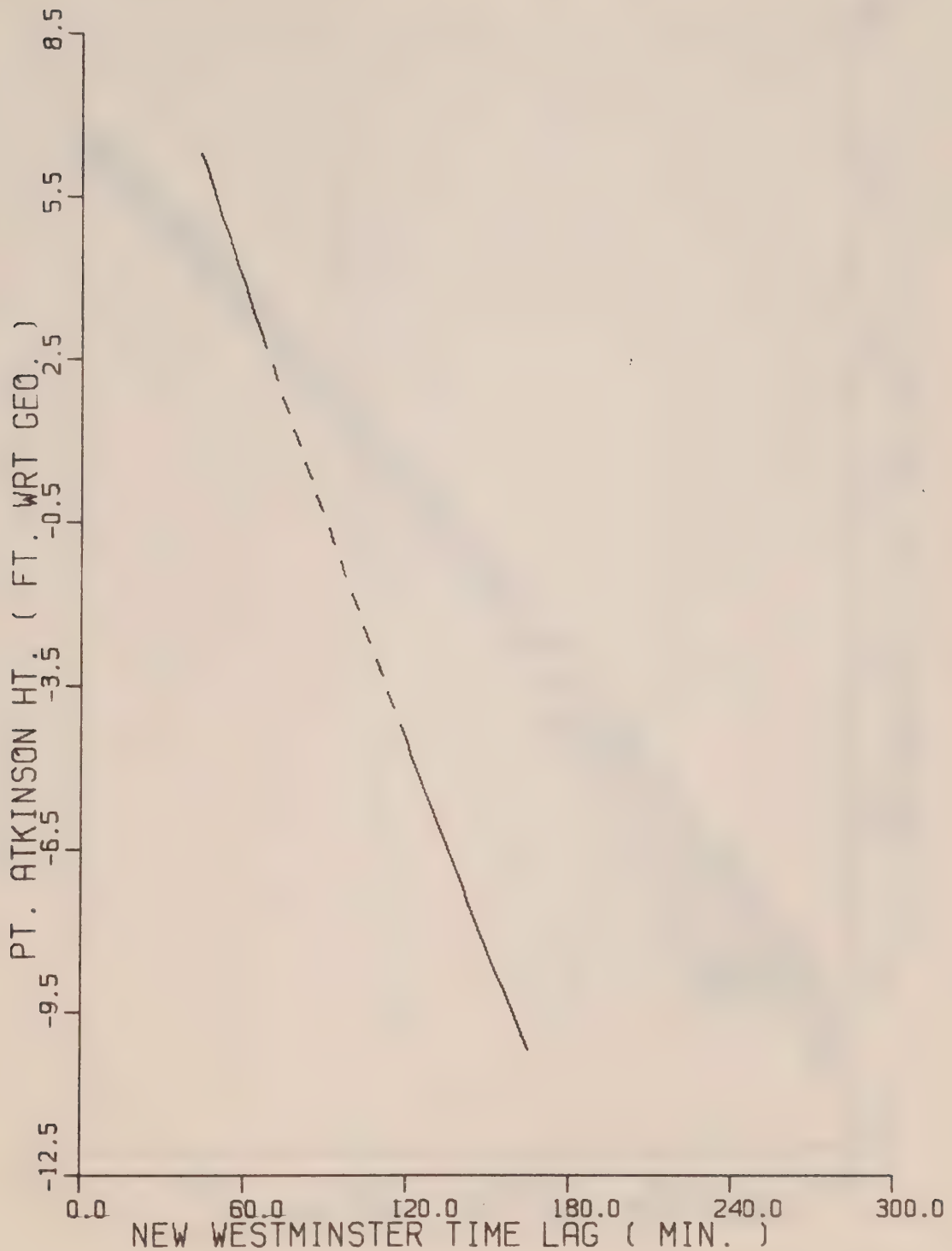


Fig. 21 MODEL-PREDICTED CORRESPONDENCE BETWEEN
HIGHS AND LOWS AT
POINT ATKINSON AND STEVESTON

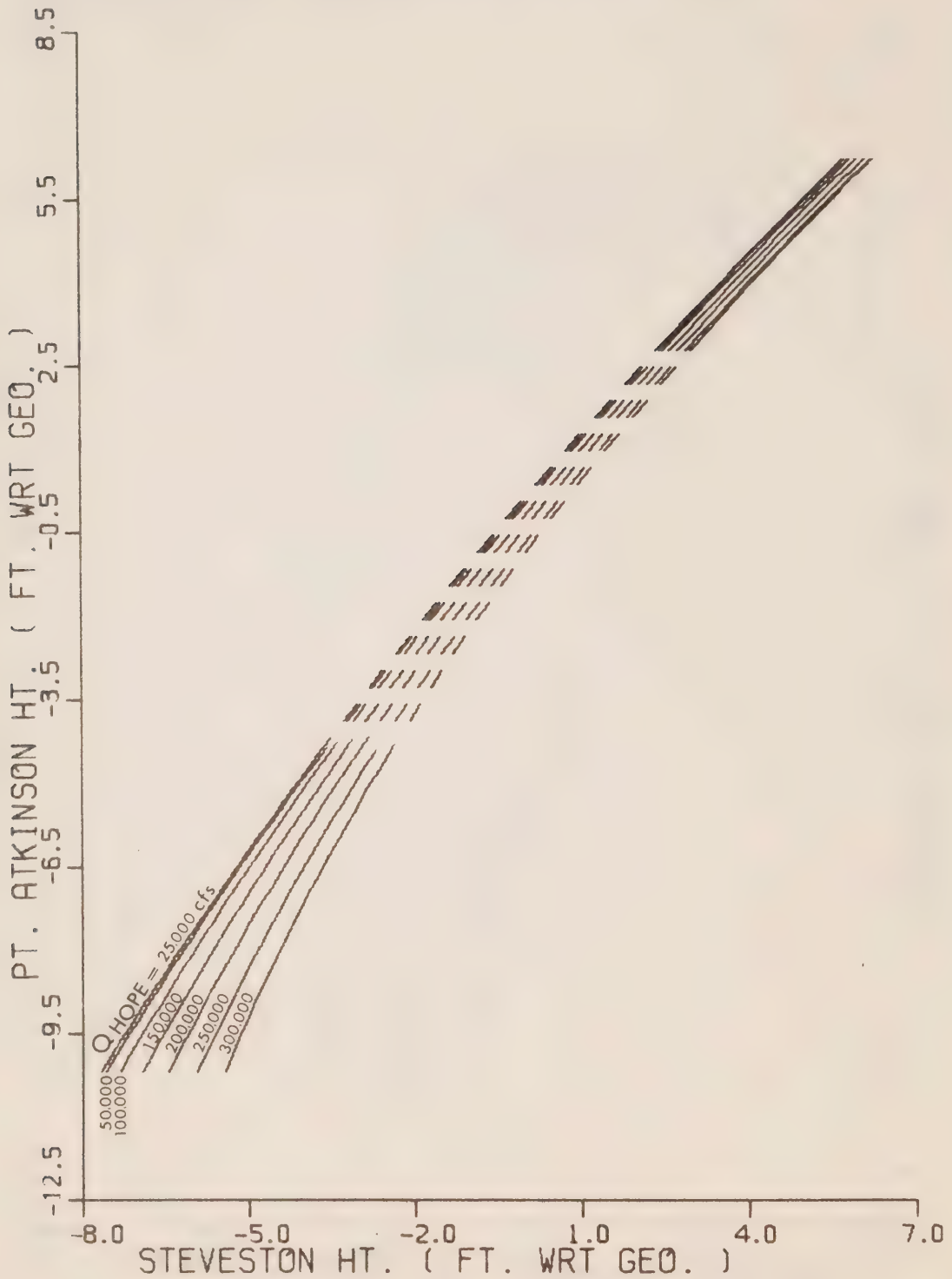


Fig.22 MODEL-PREDICTED CORRESPONDENCE BETWEEN
HIGHS AND LOWS AT
POINT ATKINSON AND STEVESTON

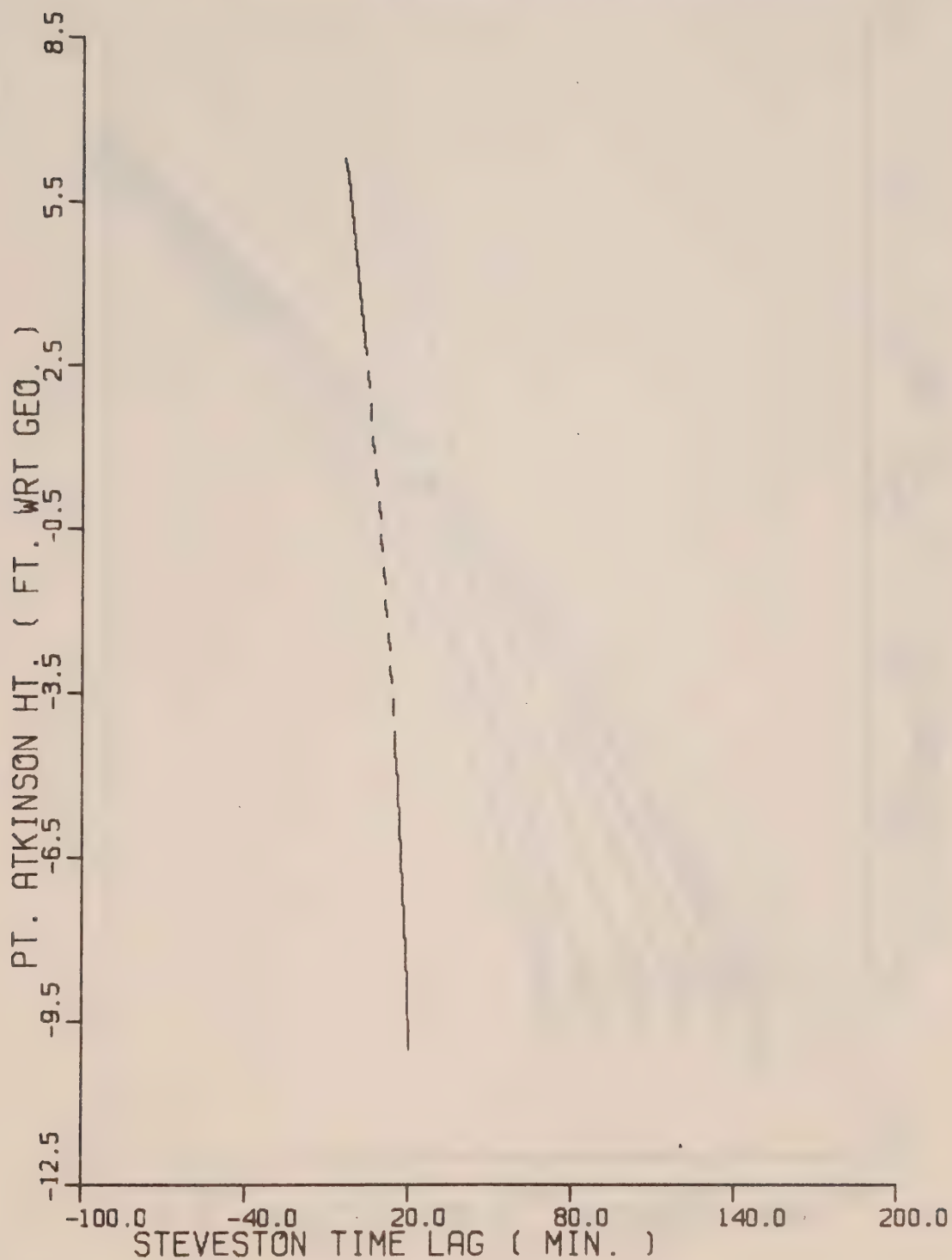


Fig. 23 MODEL-PREDICTED CORRESPONDENCE BETWEEN
HIGHS AND LOWS AT
POINT ATKINSON AND DEAS ISLAND

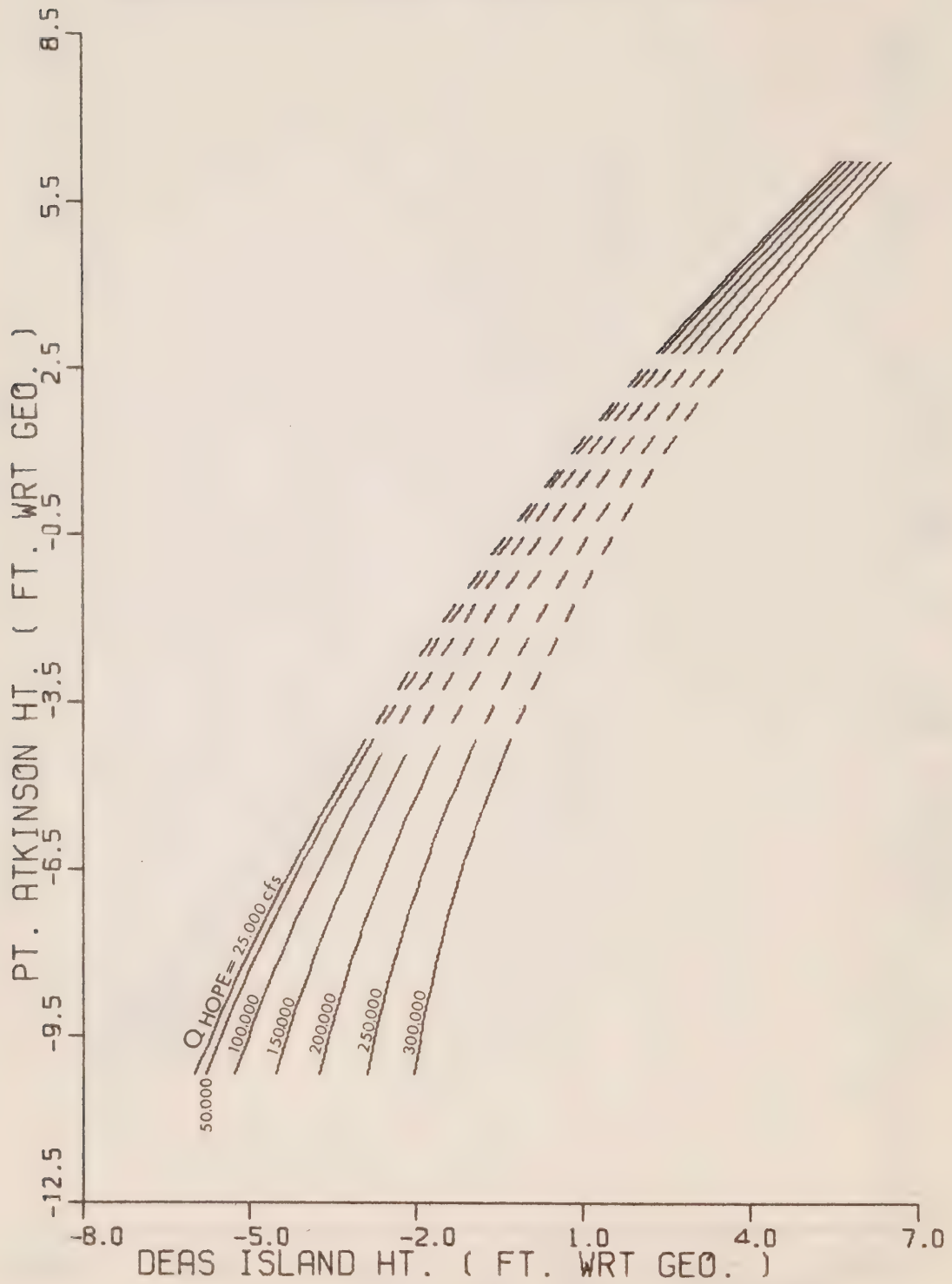


Fig.24 MODEL-PREDICTED CORRESPONDENCE BETWEEN
HIGHS AND LOWS AT
POINT ATKINSON AND DEAS ISLAND

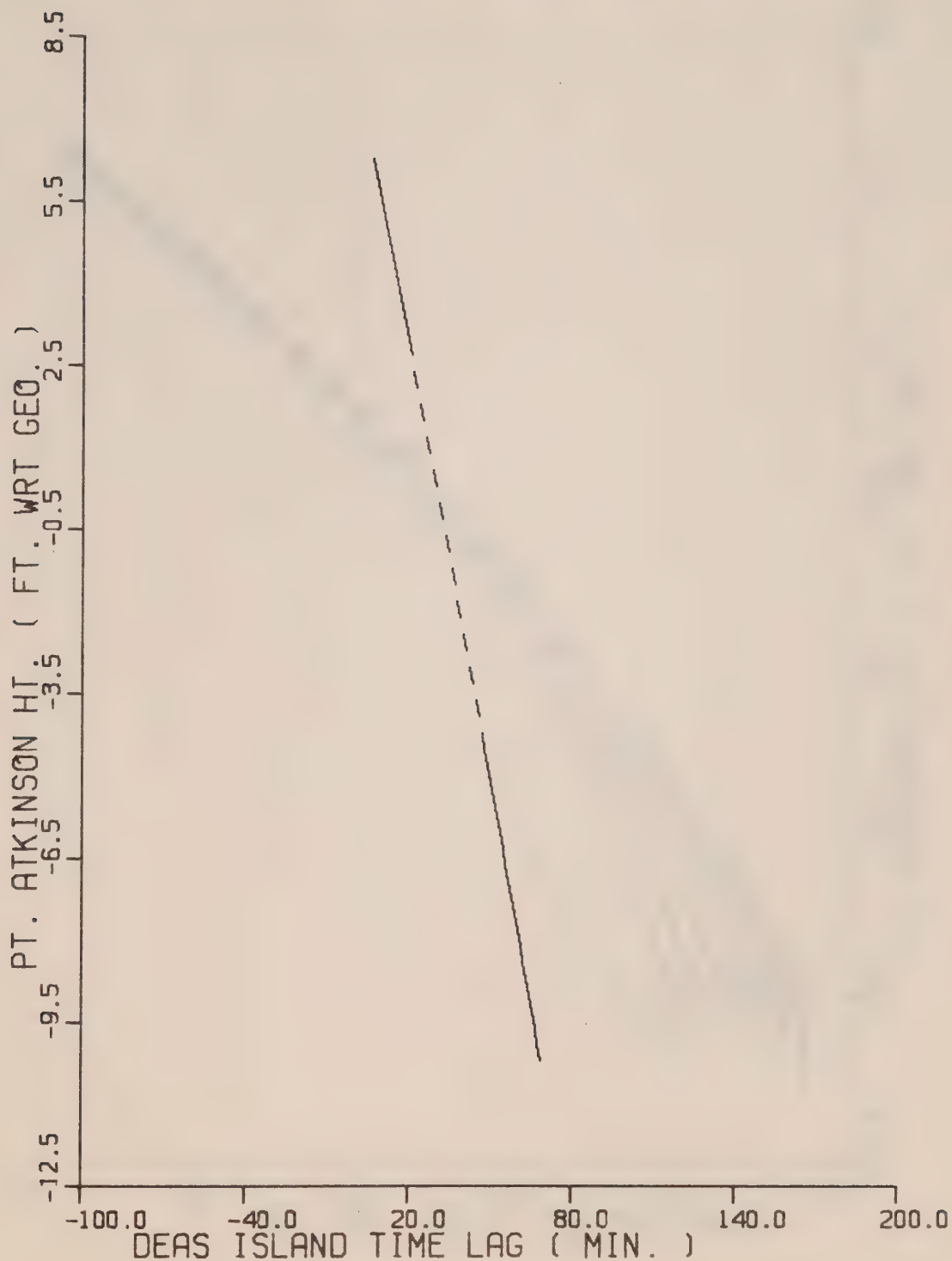


Fig.25 MODEL-PREDICTED CORRESPONDENCE BETWEEN
HIGHS AND LOWS AT
POINT ATKINSON AND MIDDLE ARM

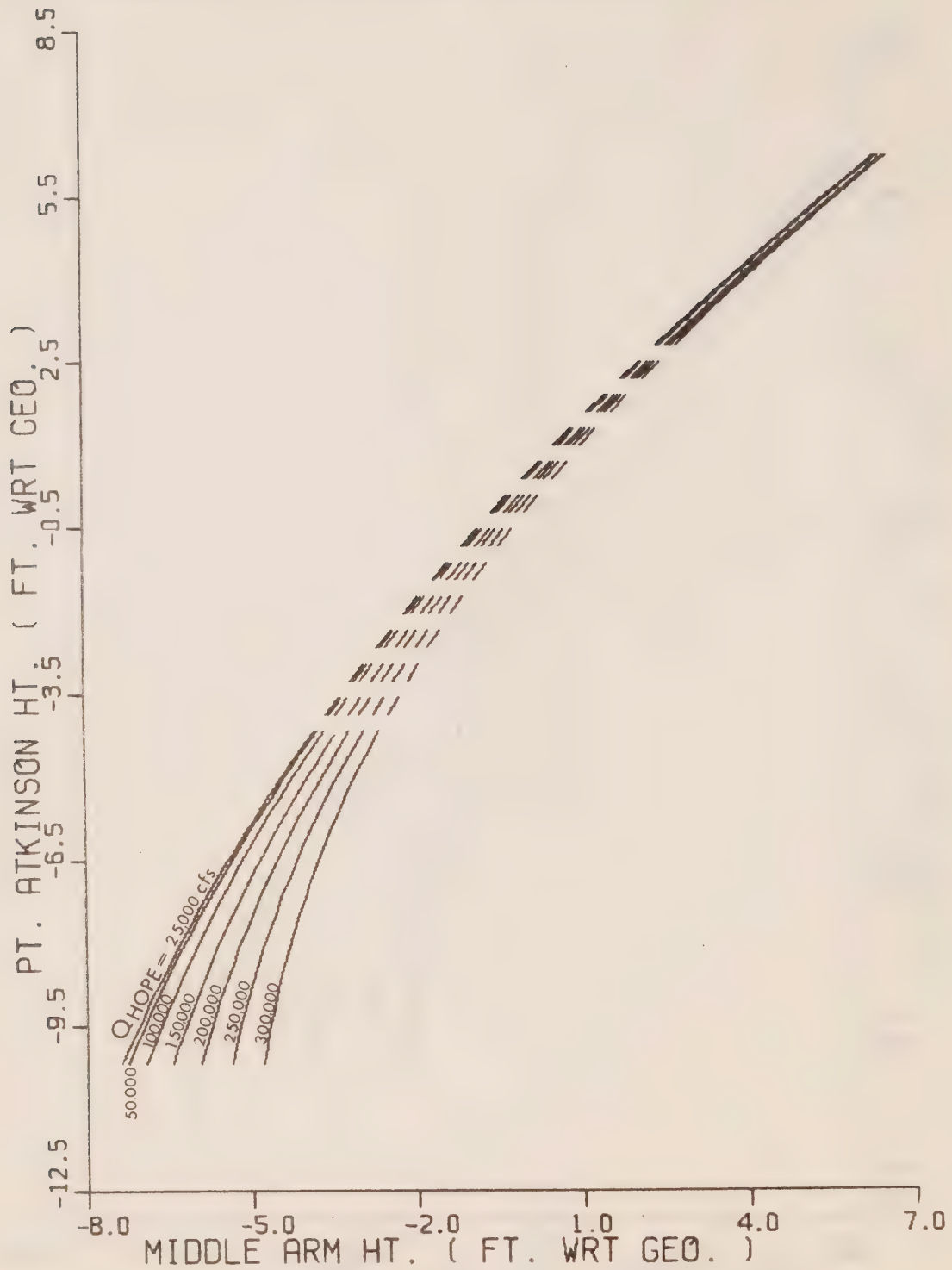


Fig. 26 MODEL-PREDICTED CORRESPONDENCE BETWEEN
HIGHS AND LOWS AT
POINT ATKINSON AND MIDDLE ARM

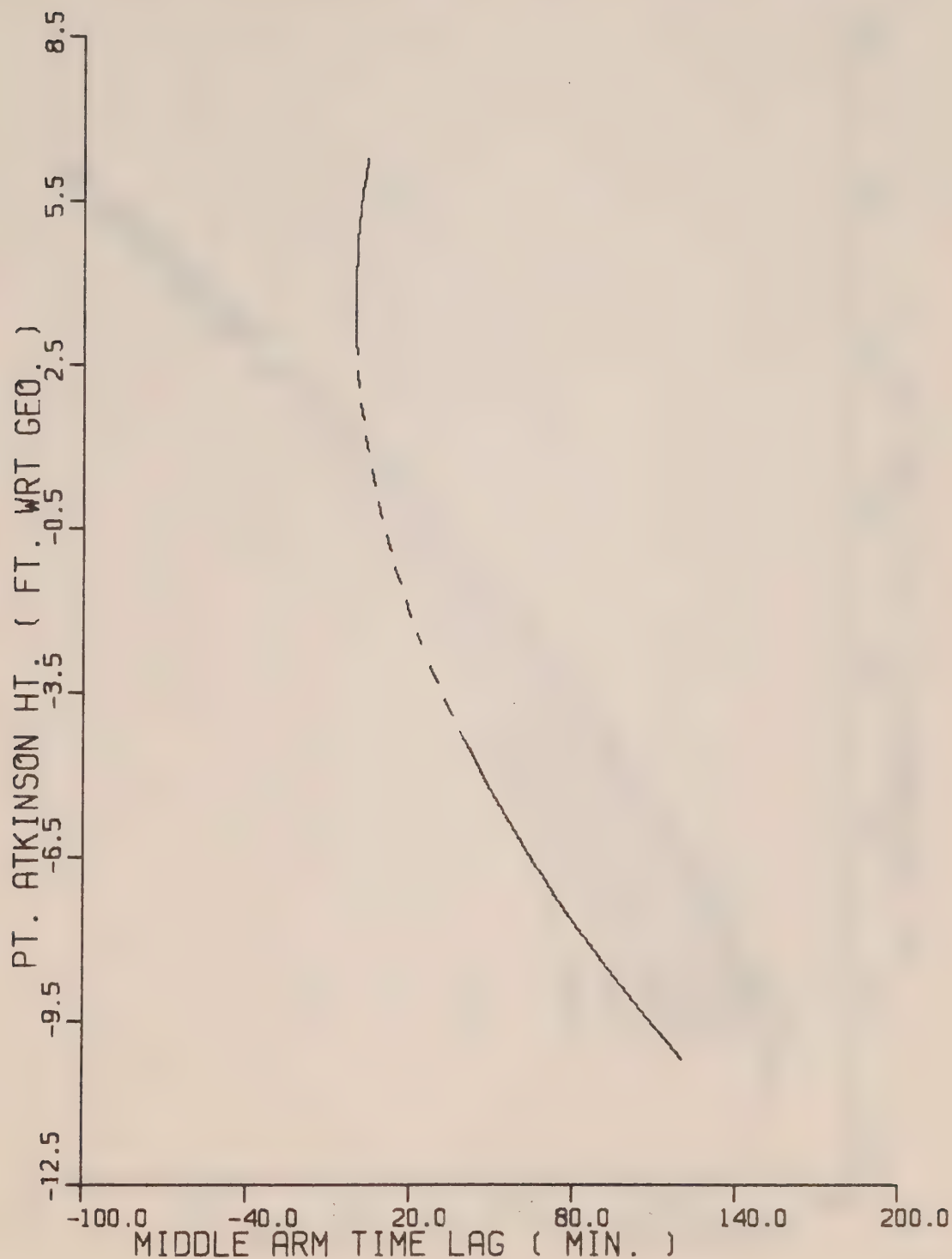


Fig. 27 MODEL-PREDICTED CORRESPONDENCE BETWEEN
HIGHS AND LOWS AT
POINT ATKINSON AND FRASER STREET

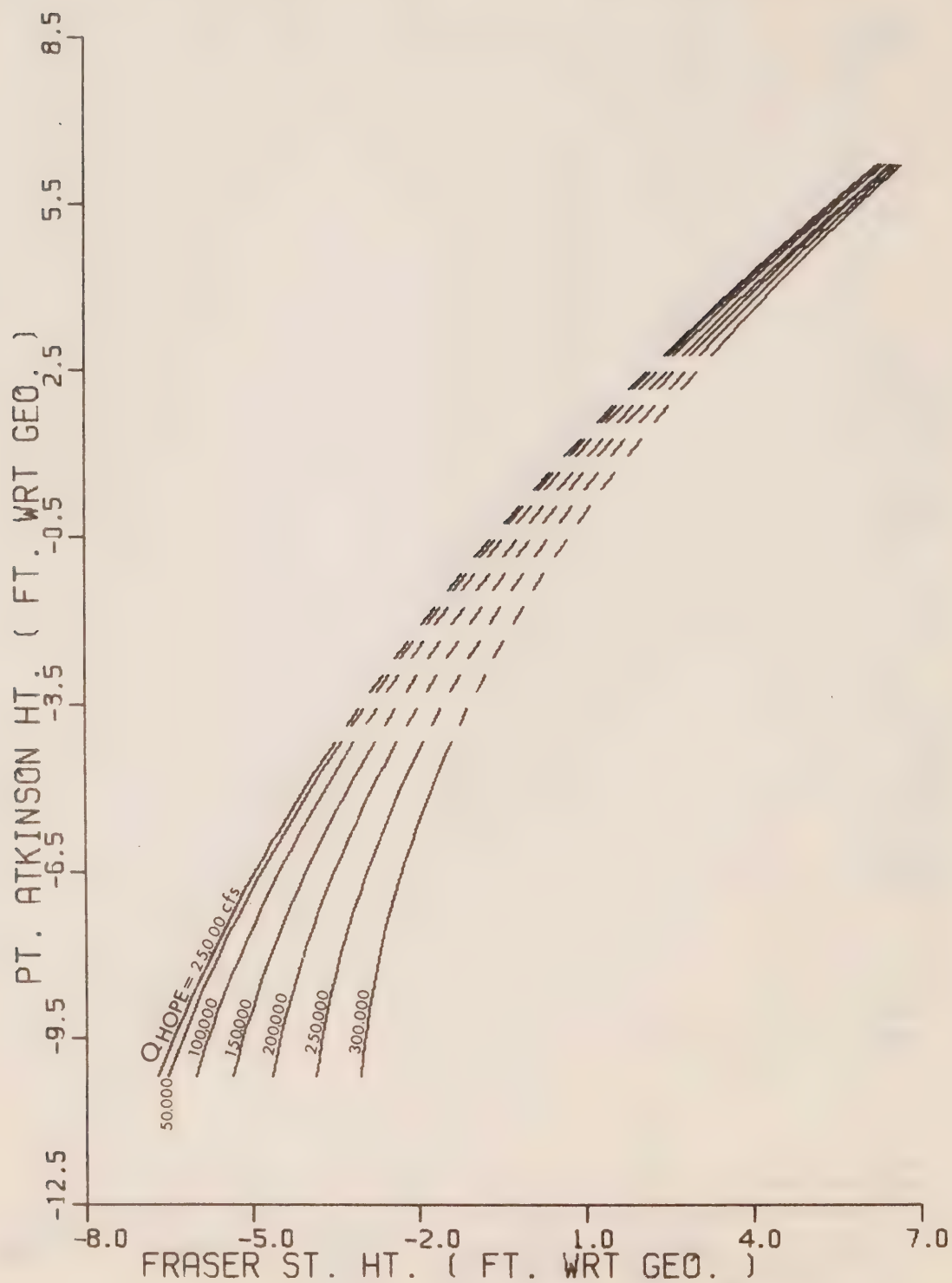


Fig. 28 MODEL-PREDICTED CORRESPONDENCE BETWEEN
HIGHS AND LOWS AT
POINT ATKINSON AND FRASER STREET

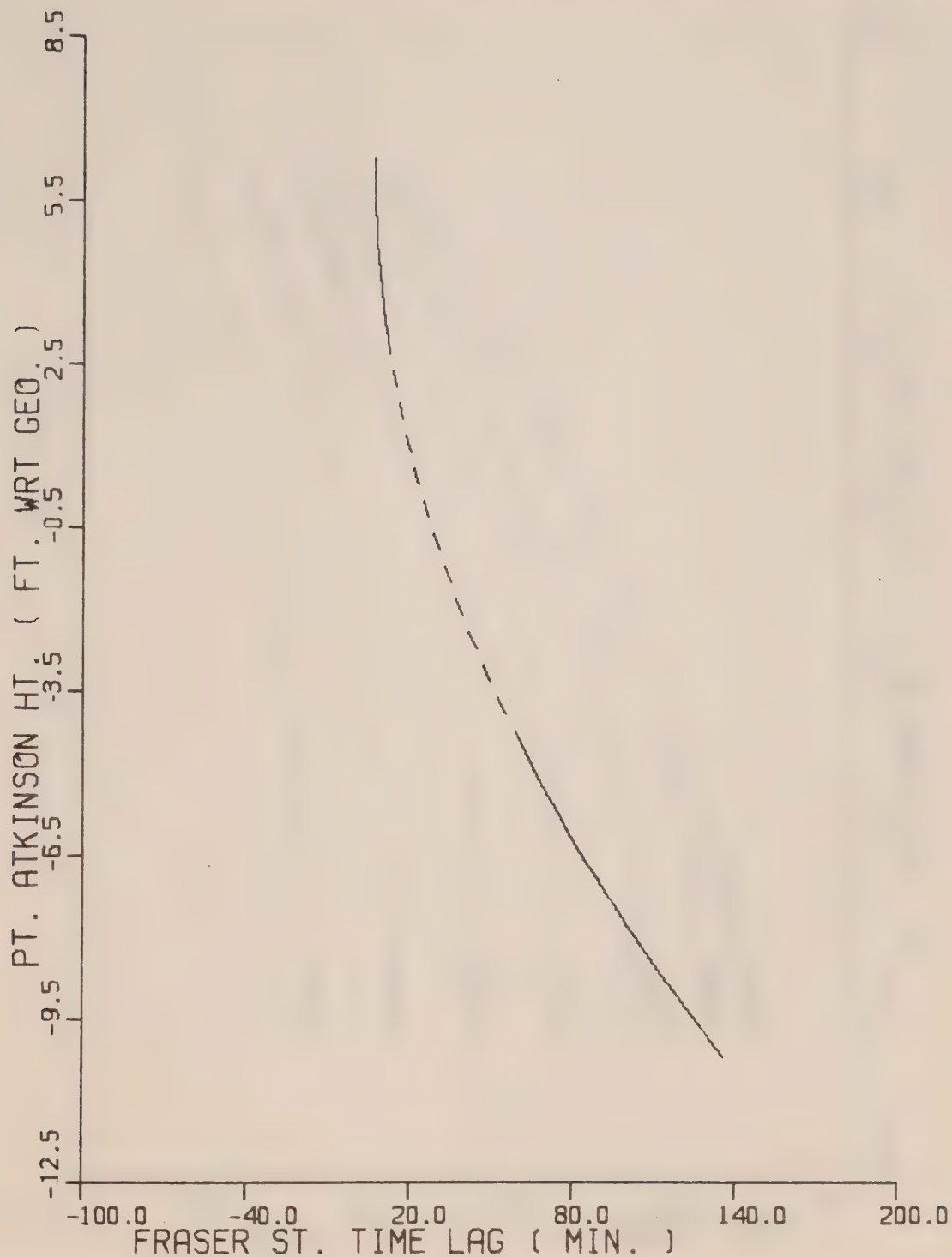


Fig. 29 MODEL-PREDICTED CORRESPONDENCE BETWEEN
HIGHS AND LOWS AT
POINT ATKINSON AND PORT MANN

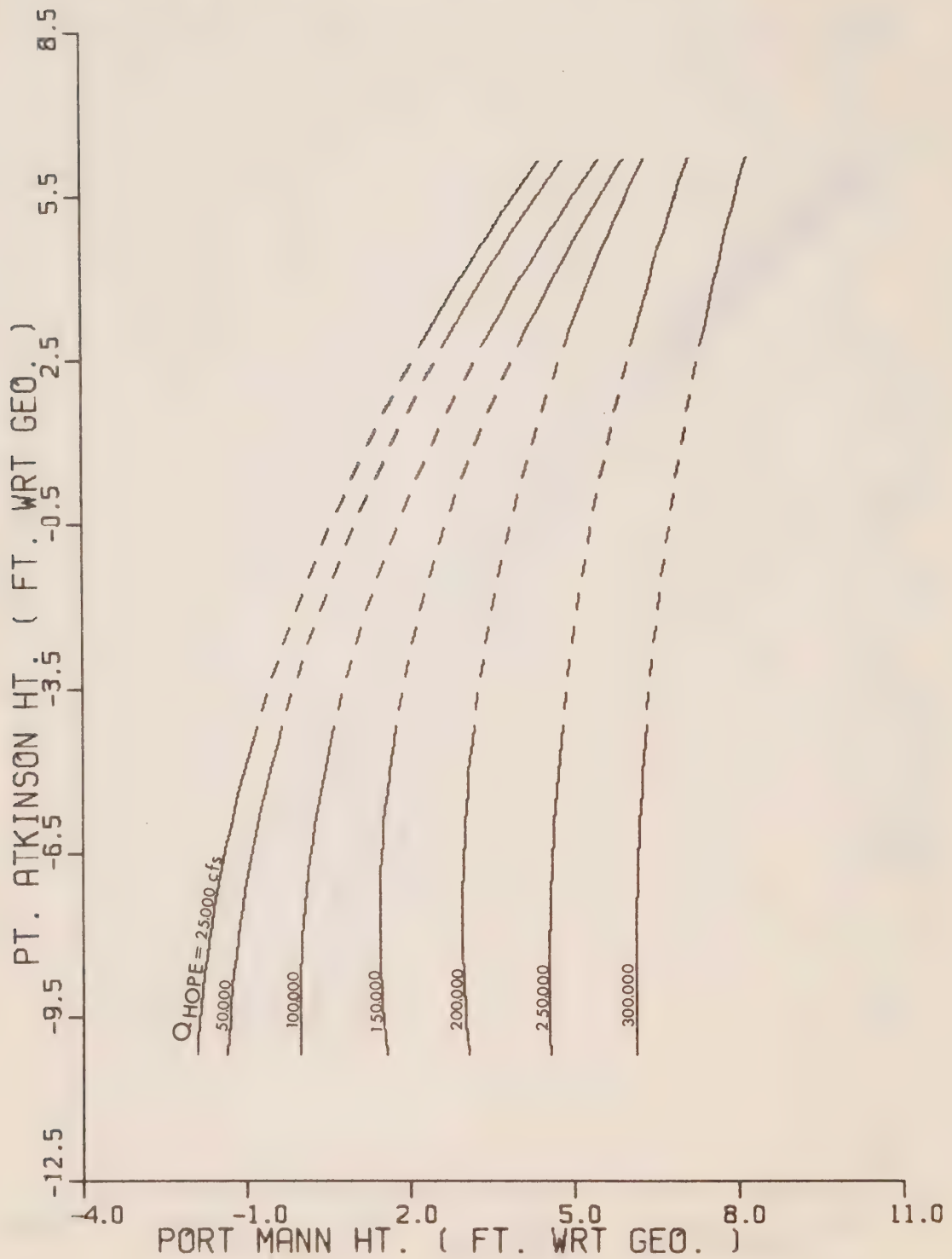


Fig.30 MODEL-PREDICTED CORRESPONDENCE BETWEEN
HIGHS AND LOWS AT
POINT ATKINSON AND PORT MANN

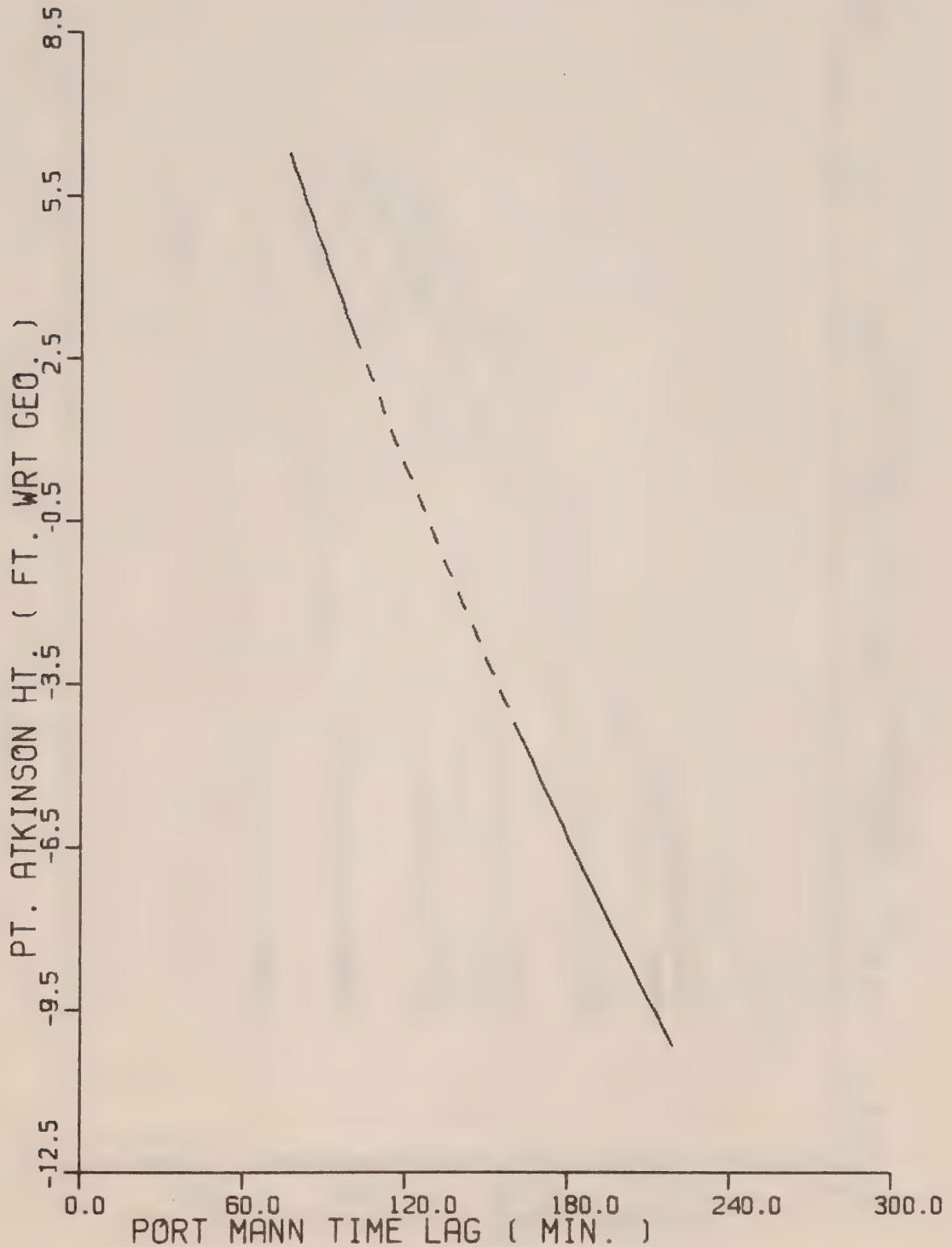


Fig.31 MODEL-PREDICTED CORRESPONDENCE BETWEEN
HIGHS AND LOWS AT
POINT ATKINSON AND PORT COQUITLAM

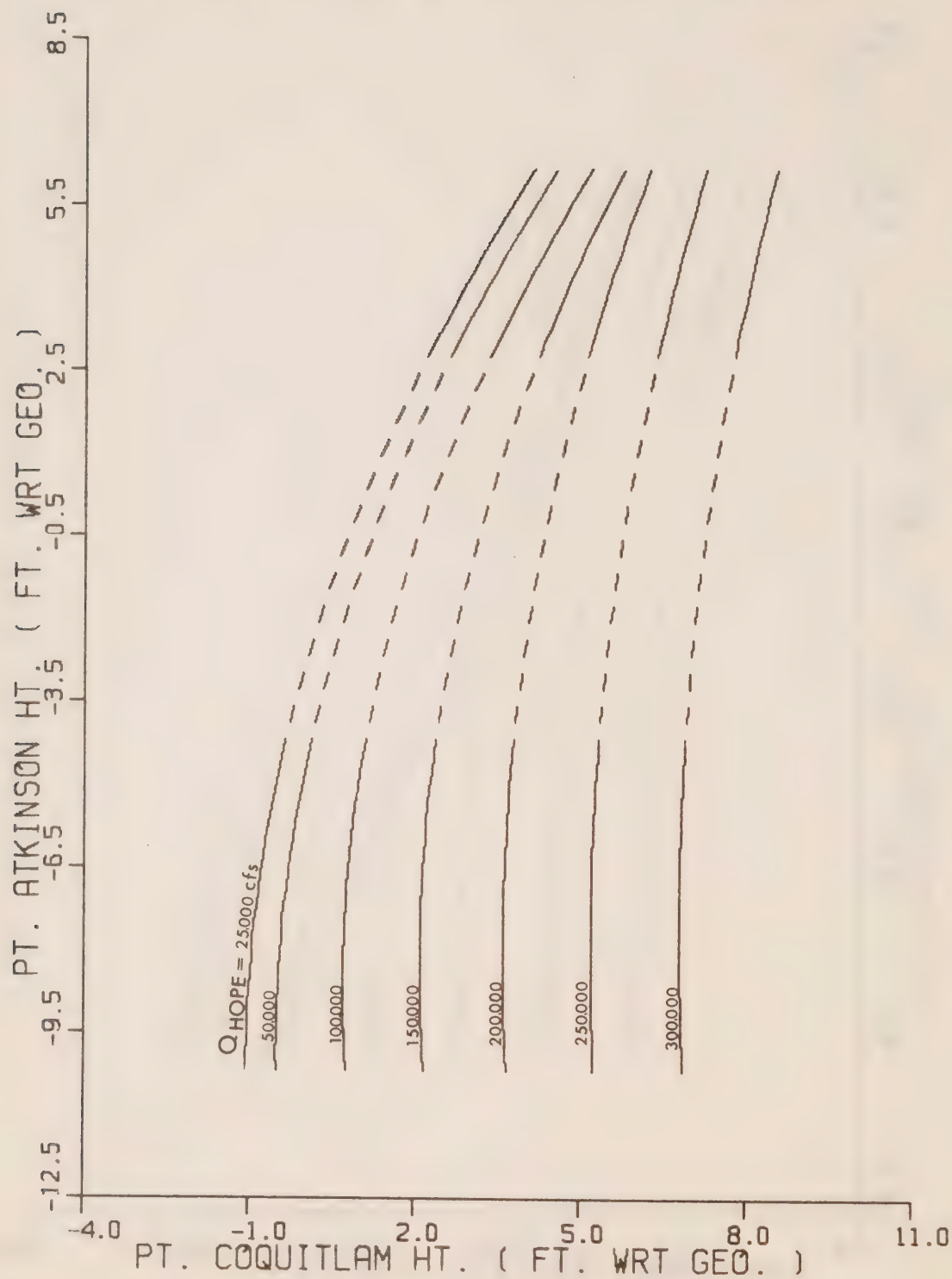


Fig.32 MODEL-PREDICTED CORRESPONDENCE BETWEEN
HIGHS AND LOWS AT
POINT ATKINSON AND PORT COQUITLAM

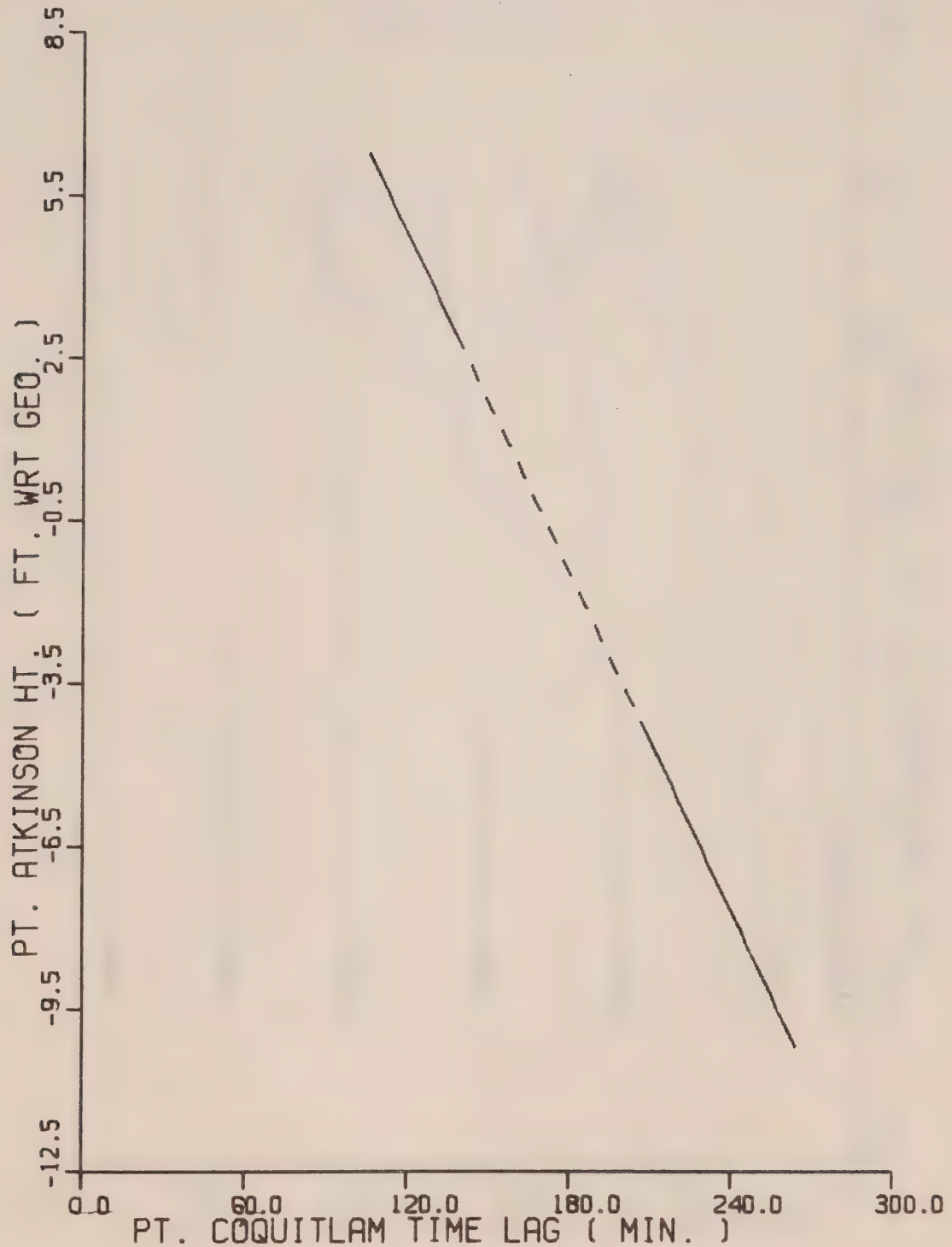


Fig. 33 MODEL-PREDICTED CORRESPONDENCE BETWEEN
HIGHS AND LOWS AT
POINT ATKINSON AND MISSION

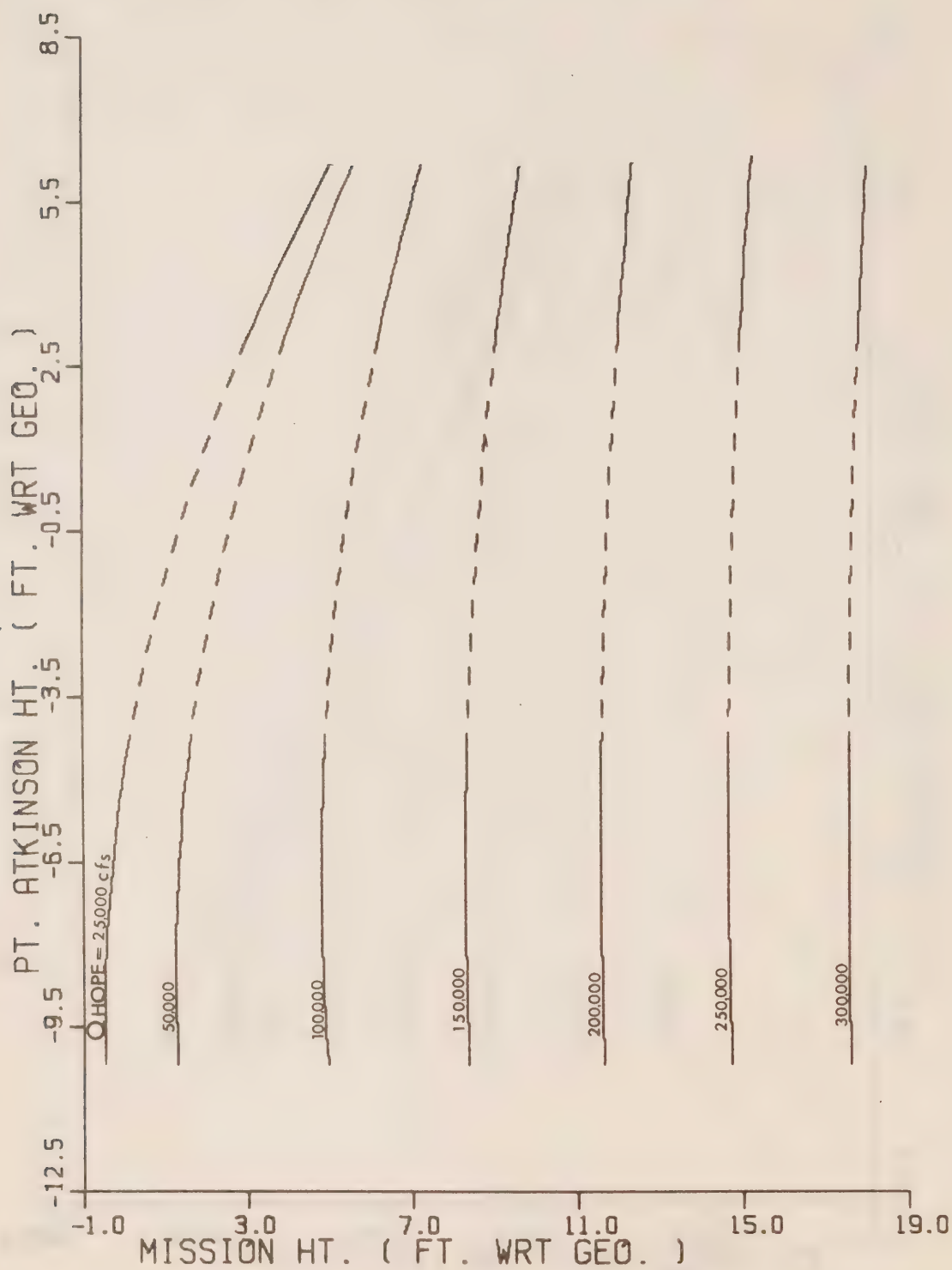


Fig. 34 MODEL-PREDICTED CORRESPONDENCE BETWEEN
HIGHS AND LOWS AT
POINT ATKINSON AND MISSION

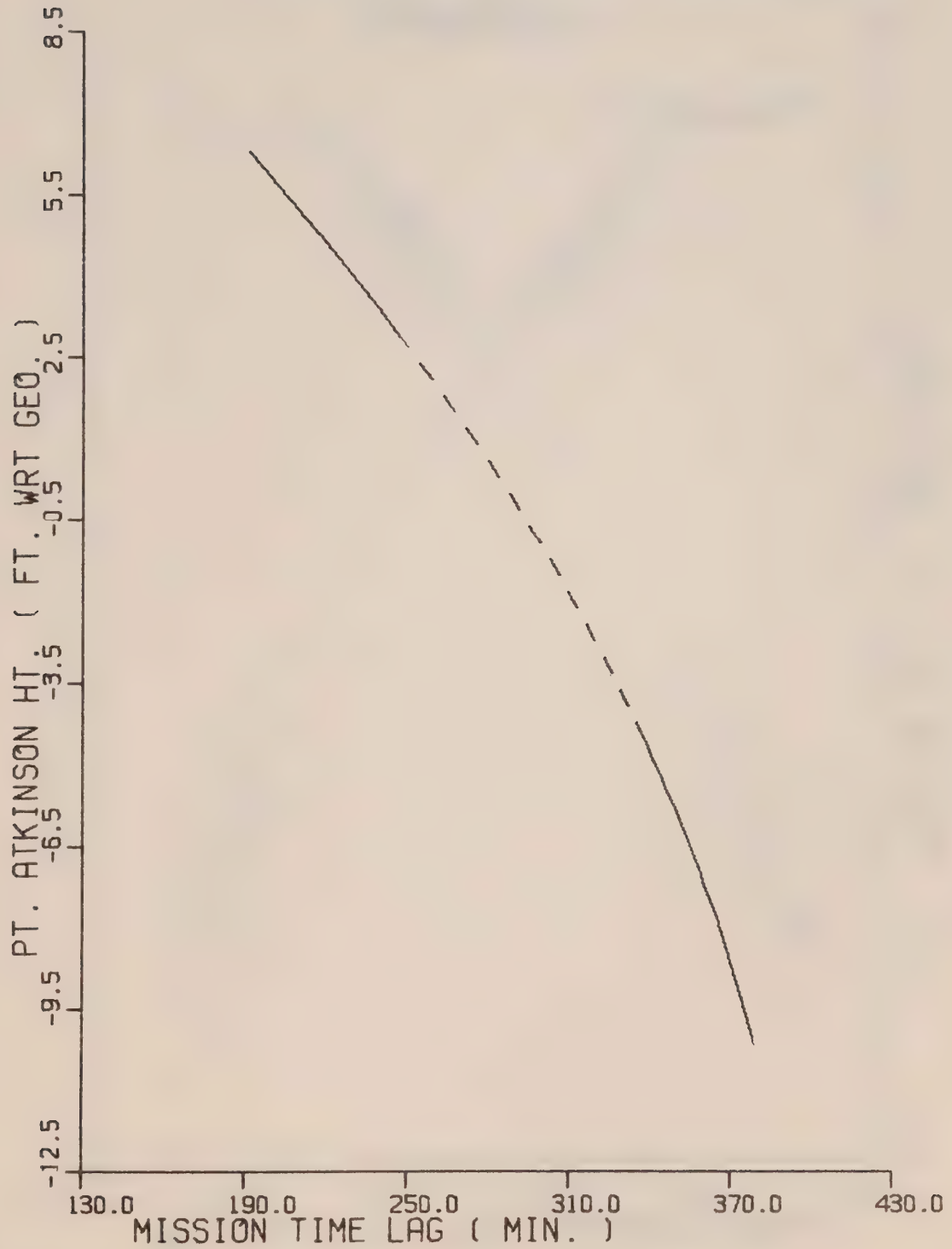


Fig. 35 ACTUAL CORRESPONDENCE BETWEEN
HIGHS AND LOWS AT
POINT ATKINSON AND NEW WESTMINSTER
1970-1973

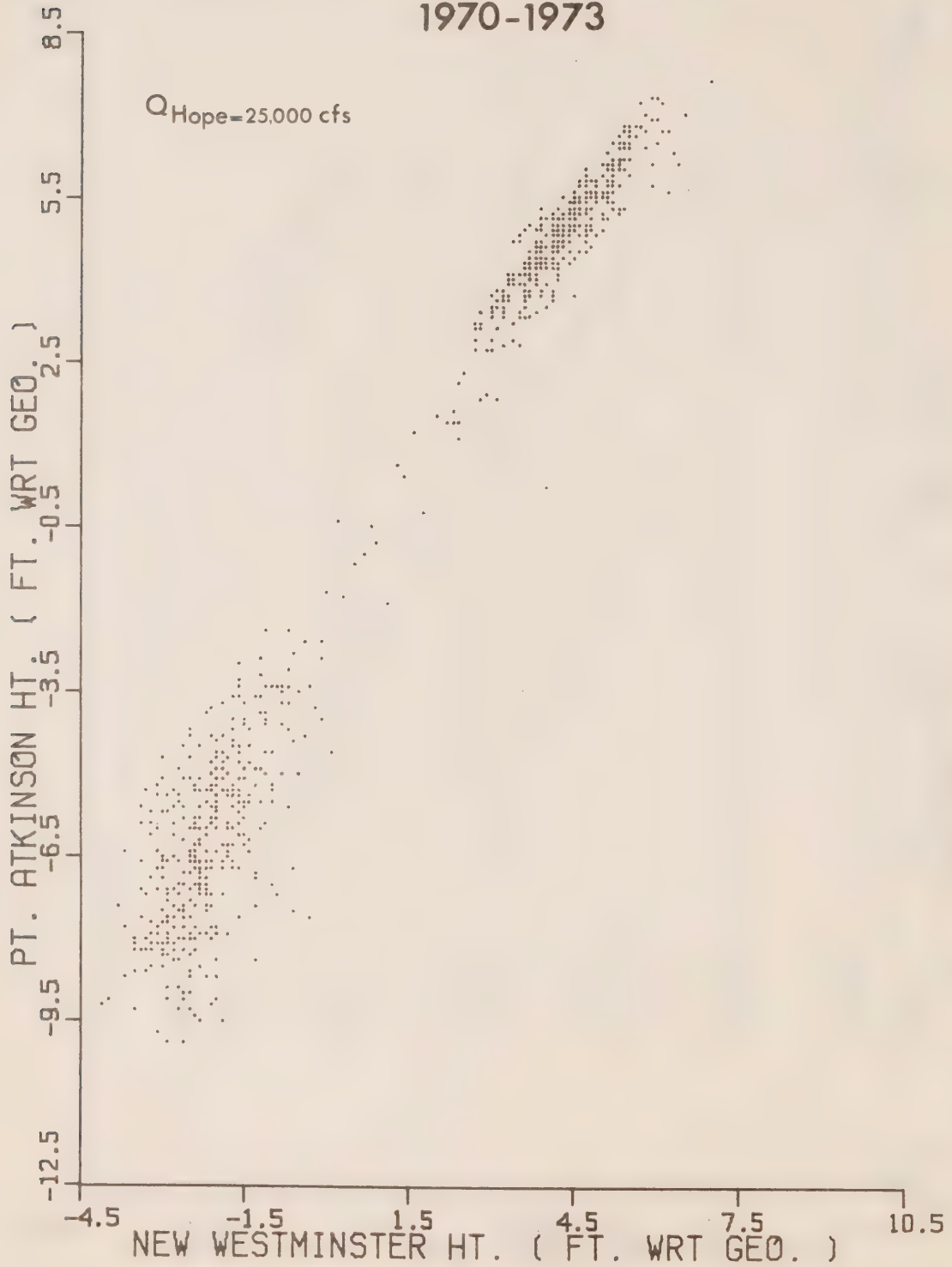


Fig.36 ACTUAL CORRESPONDENCE BETWEEN
HIGHS AND LOWS AT
POINT ATKINSON AND NEW WESTMINSTER

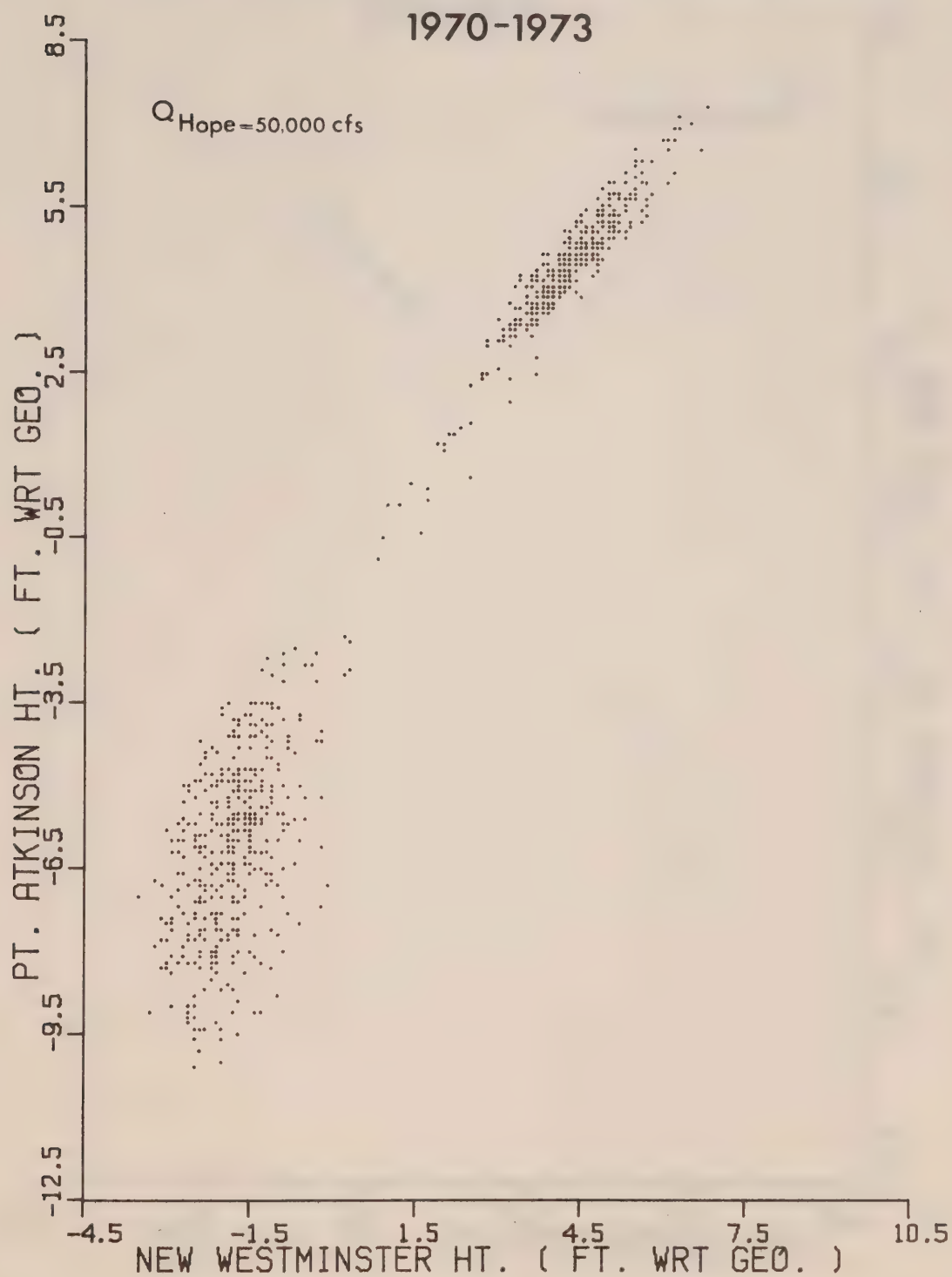


Fig.37 ACTUAL CORRESPONDENCE BETWEEN
HIGHS AND LOWS AT
POINT ATKINSON AND NEW WESTMINSTER
1970-1973

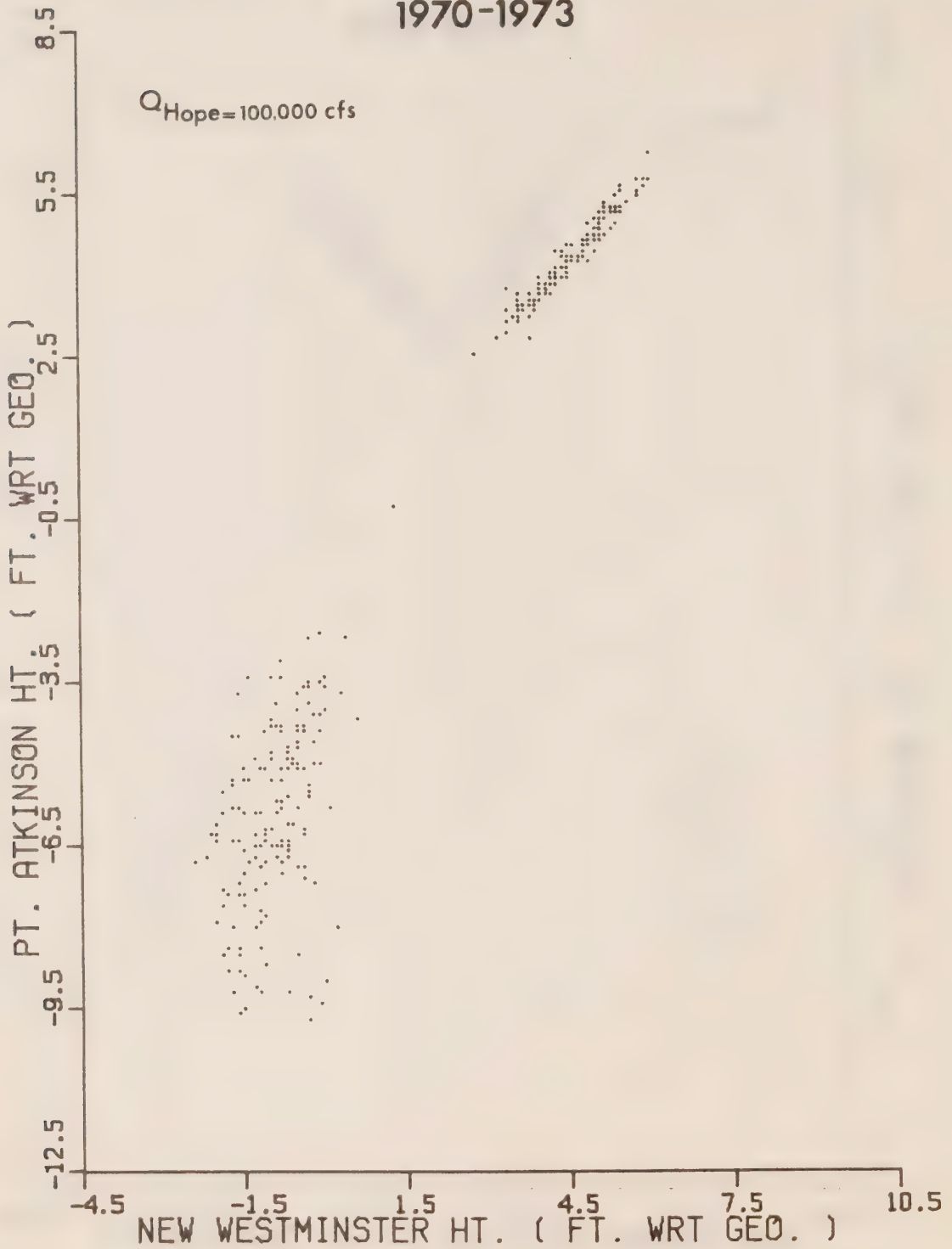


Fig. 38 ACTUAL CORRESPONDENCE BETWEEN
HIGHS AND LOWS AT
POINT ATKINSON AND NEW WESTMINSTER
1970-1973

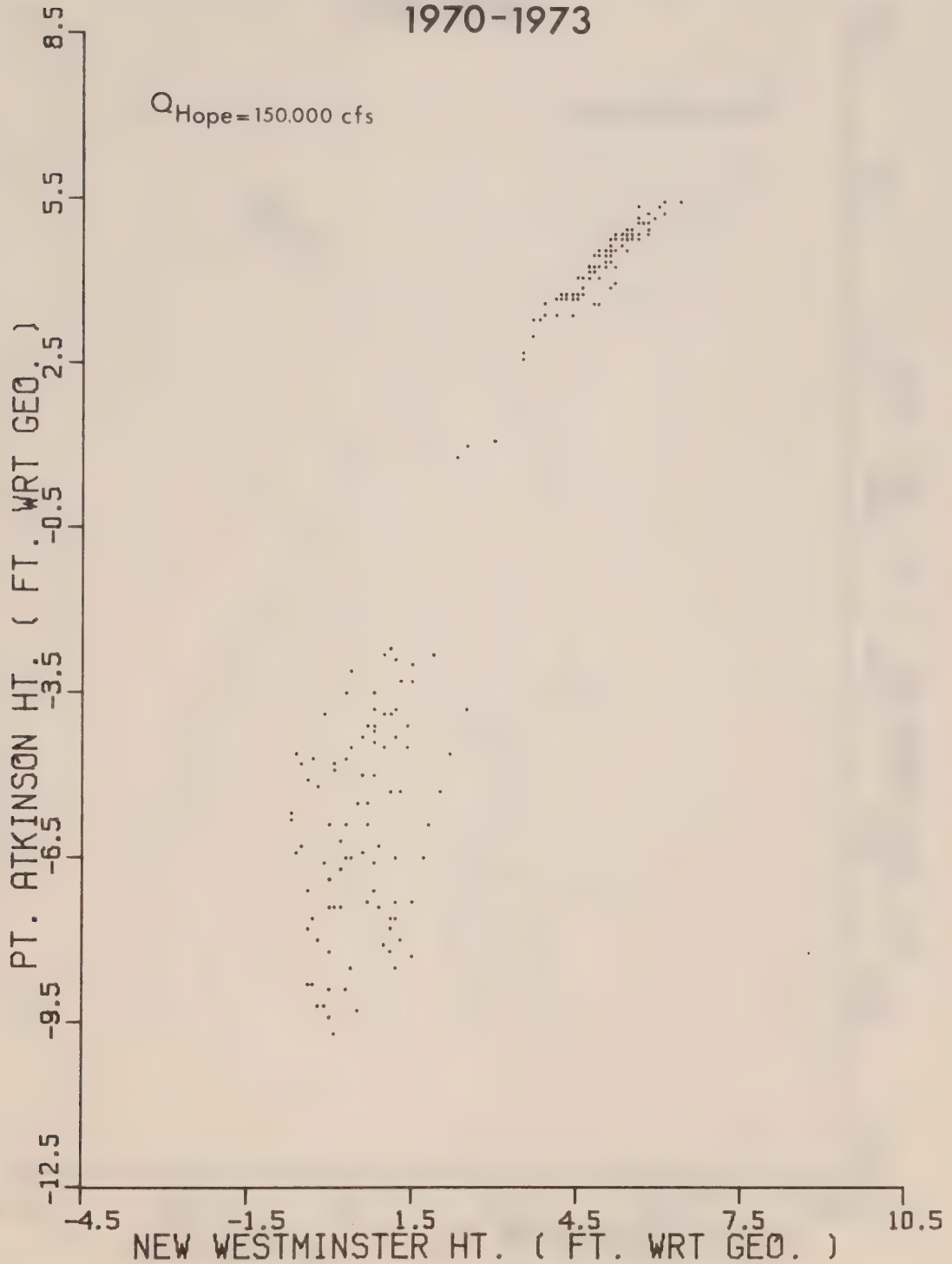


Fig.39 ACTUAL CORRESPONDENCE BETWEEN
HIGHS AND LOWS AT
POINT ATKINSON AND NEW WESTMINSTER
1970-1973



Fig.40 ACTUAL CORRESPONDENCE BETWEEN
HIGHS AND LOWS AT
POINT ATKINSON AND NEW WESTMINSTER
1970-1973

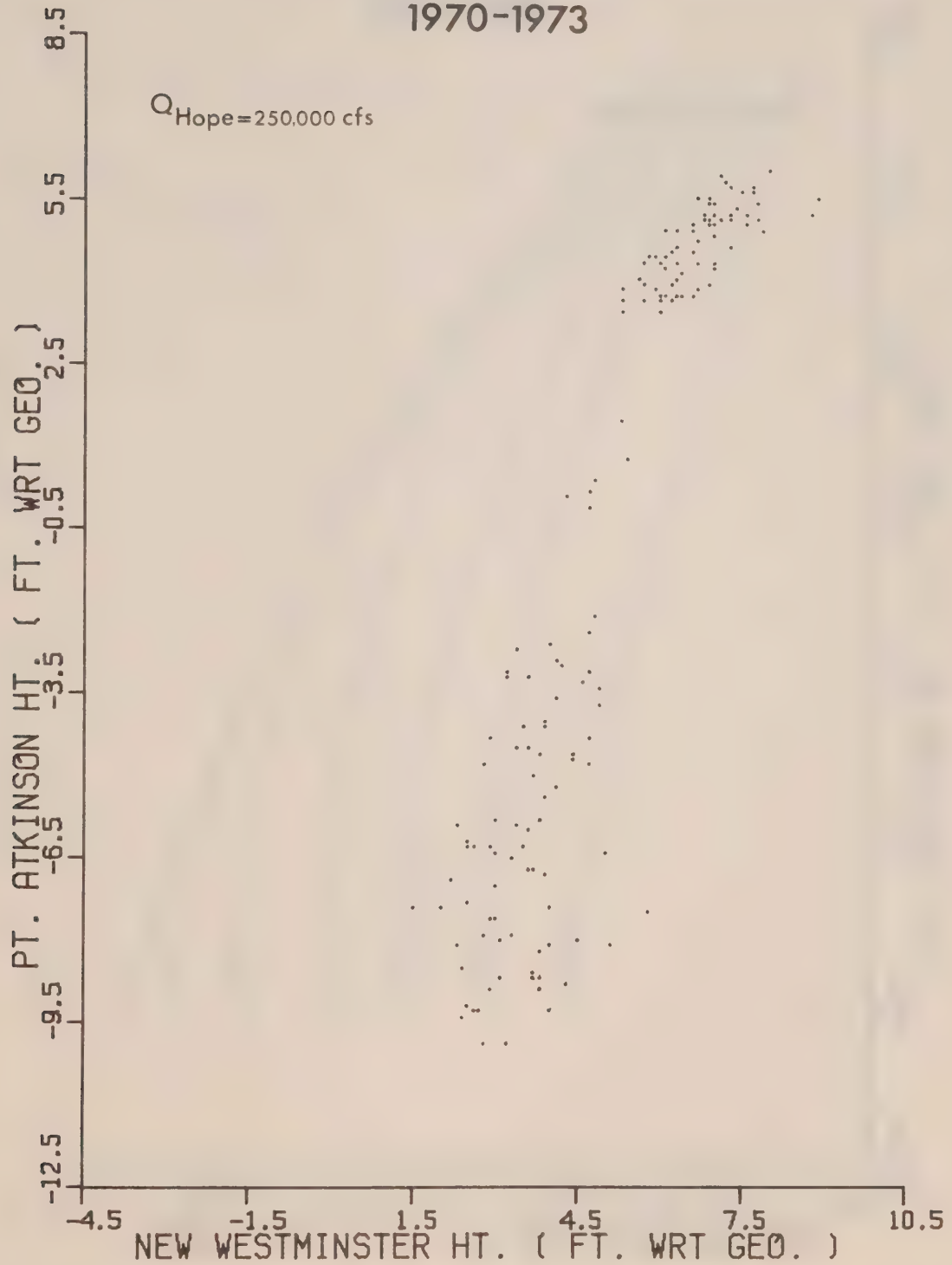


Fig. 41 ACTUAL CORRESPONDENCE BETWEEN
HIGHS AND LOWS AT
POINT ATKINSON AND NEW WESTMINSTER

1970-1973



Fig.42 ACTUAL CORRESPONDENCE BETWEEN
HIGHS AND LOWS AT
POINT ATKINSON AND NEW WESTMINSTER
1970-1973

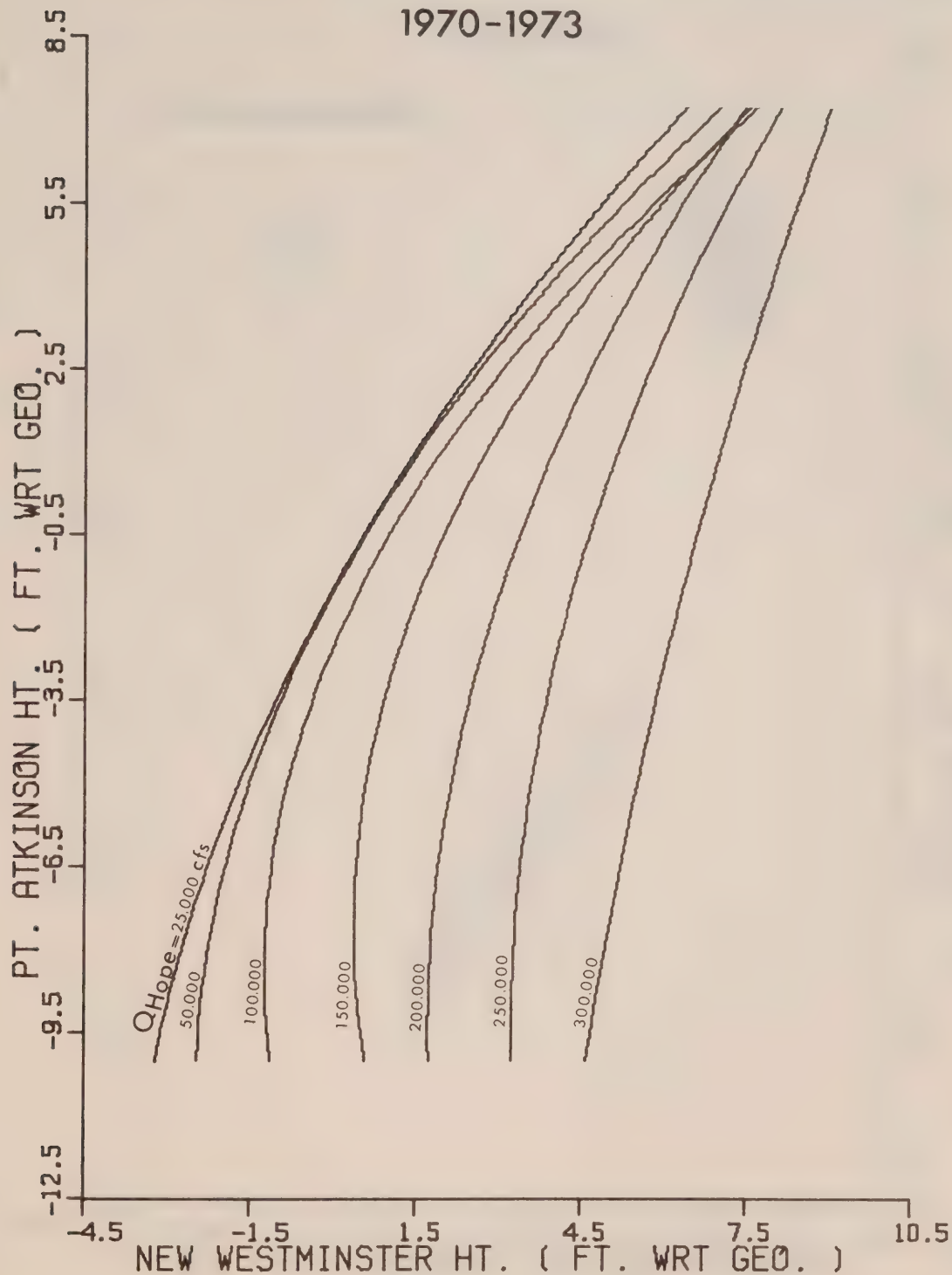


Fig.43 ACTUAL CORRESPONDENCE BETWEEN
HIGHS AND LOWS AT
POINT ATKINSON AND NEW WESTMINSTER
1970-1973

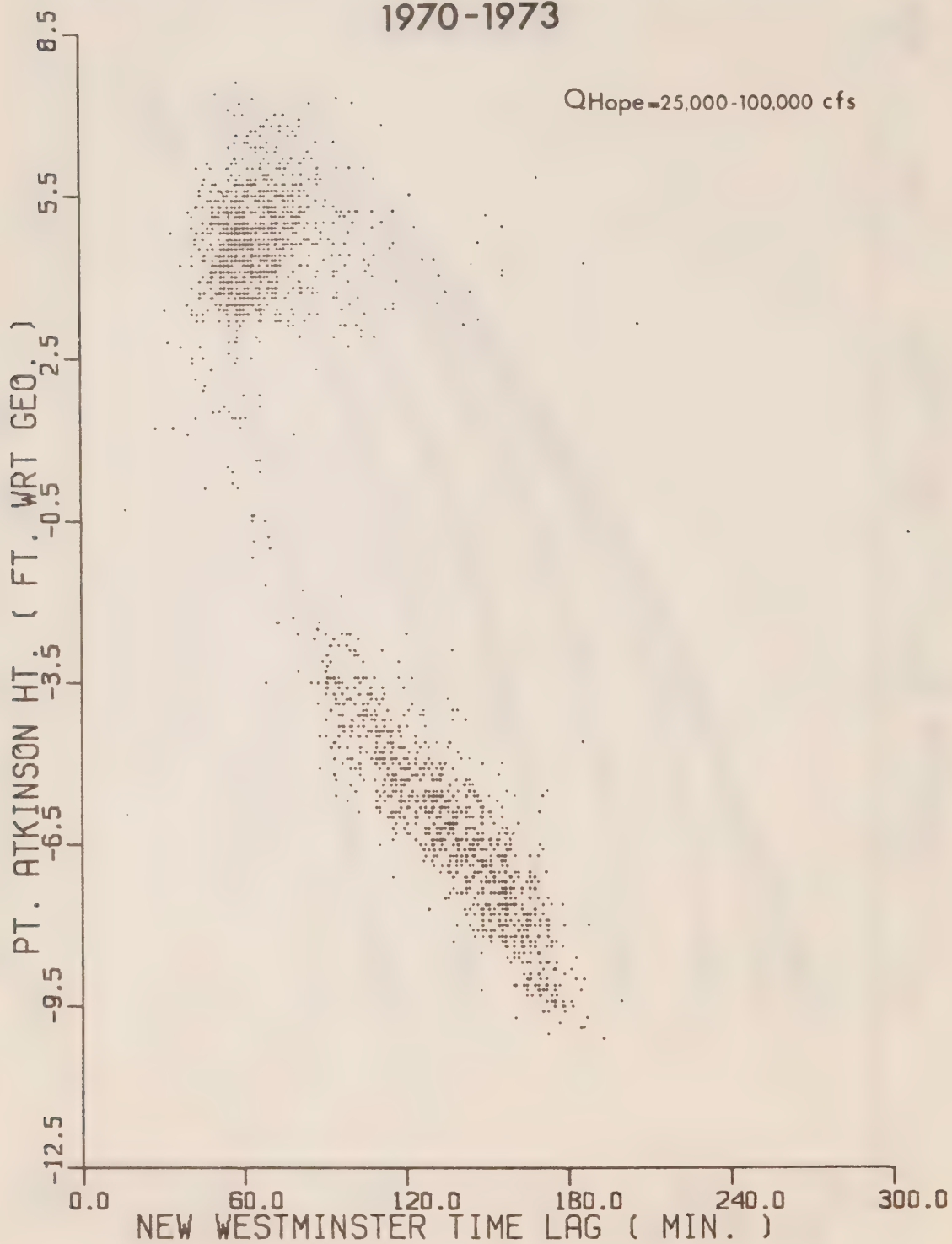


Fig.44 ACTUAL CORRESPONDENCE BETWEEN
HIGHS AND LOWS AT
POINT ATKINSON AND NEW WESTMINSTER
1970-1973

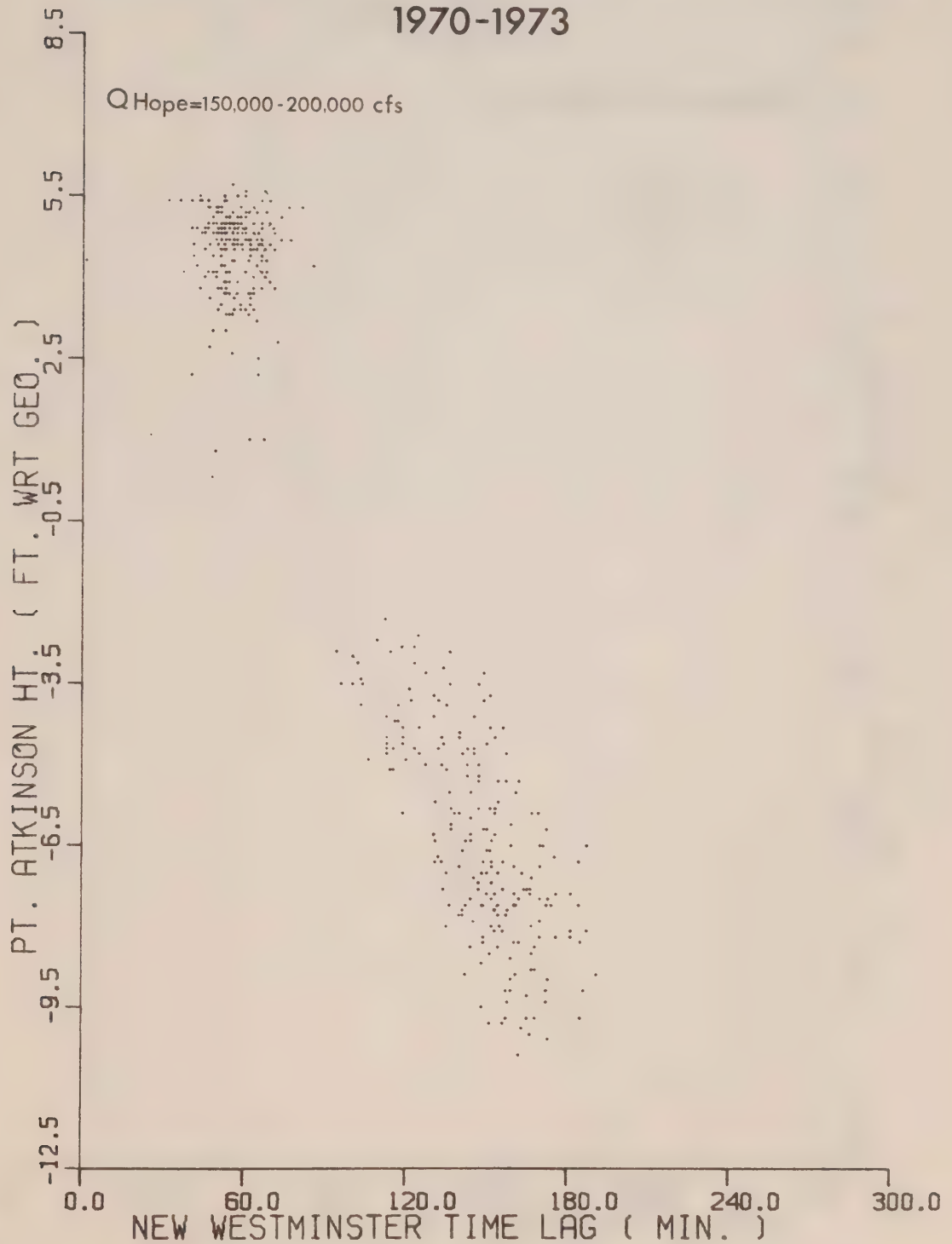


Fig.45 ACTUAL CORRESPONDENCE BETWEEN
HIGHS AND LOWS AT
POINT ATKINSON AND NEW WESTMINSTER
1970-1973

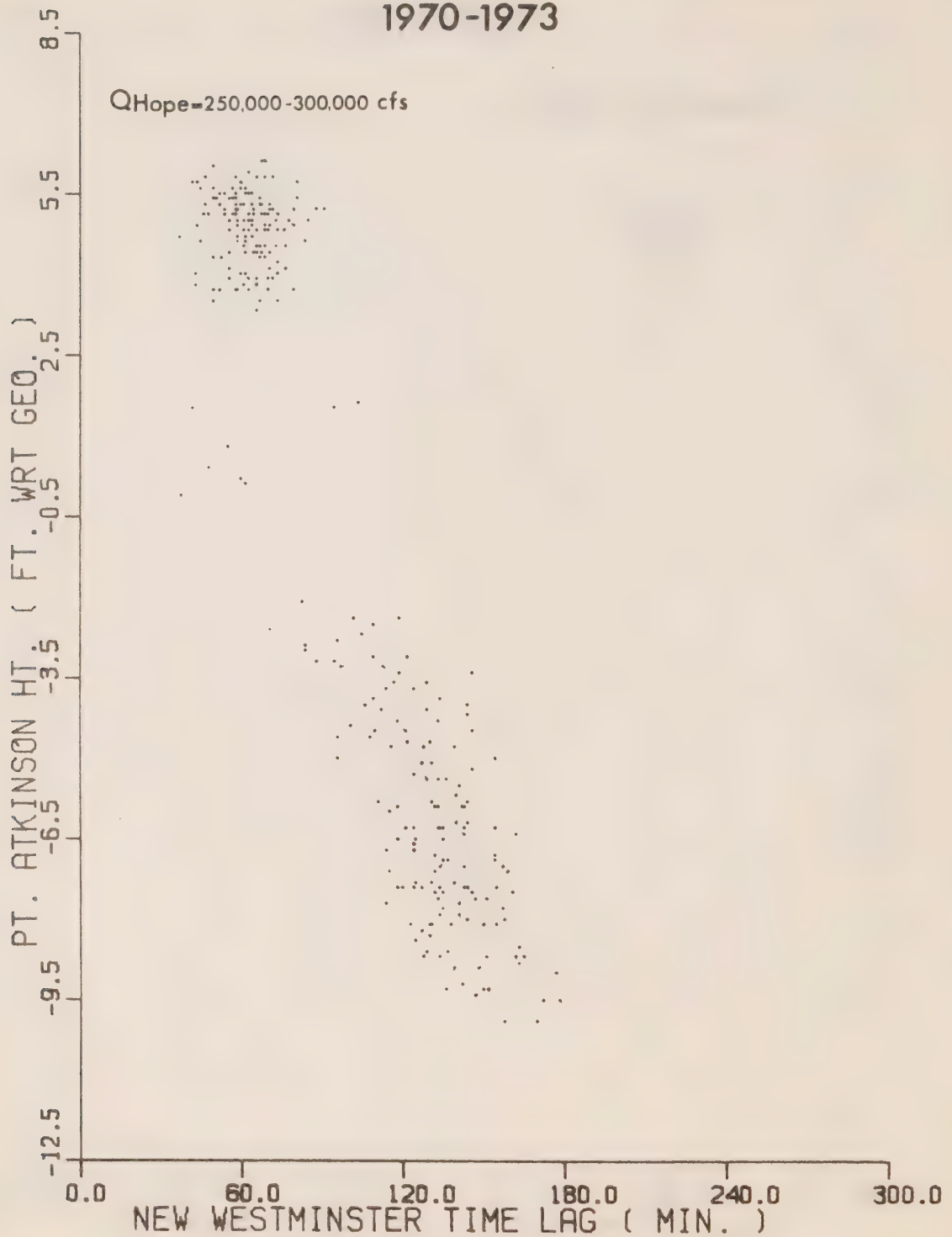
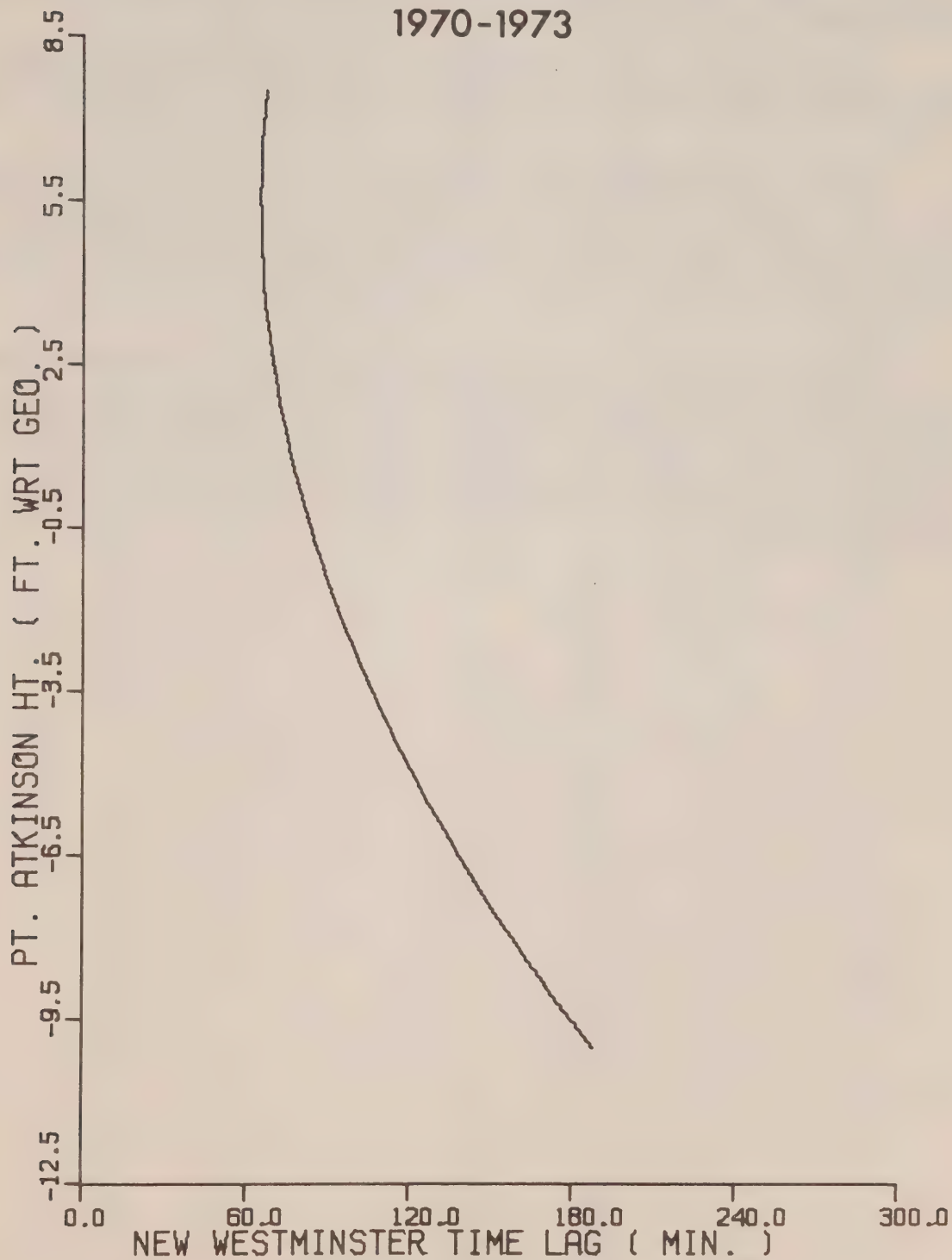


Fig.46 ACTUAL CORRESPONDENCE BETWEEN
HIGHS AND LOWS AT
POINT ATKINSON AND NEW WESTMINSTER
1970-1973



In general, we may conclude that the high waters at New Westminster occur about one hour later than those at Point Atkinson, the low waters about two hours later. This large discrepancy cannot be due to the difference in depth as is occasionally suggested in the literature. An upstream tidal range of six feet would hardly affect the propagation speed $c = \sqrt{gh}$ in an average minimum depth of 30 feet.

The prediction curves for Steveston, Deas Island and New Westminster were converted into tables for publication in the Canadian Tide and Current Tables for 1976.

Figure 47 illustrates the progression of a tidal wave in the Fraser River under freshet and non-freshet conditions, with typical changes in the range and shape of the tide curve along the river. Observed tidal curves for 24 hours are superimposed upon a "river flow only" curve which was produced by the model. Of course, a "river flow only" situation does not exist in the prototype.

Figures 48 and 49 show the model-produced maximum and minimum water levels generated by a spring tide for non-freshet and freshet conditions. The observed tides in the Strait of Georgia on June 28, 1969 were used as the downstream boundary conditions for both cases. The figures demonstrate how the point of convergence of the low water and high water lines, that is, the point where the daily tidal fluctuations cease to exist, moves westward as the discharge increases.

Fig. 47 PROGRESSION OF A TIDAL WAVE IN THE FRASER RIVER

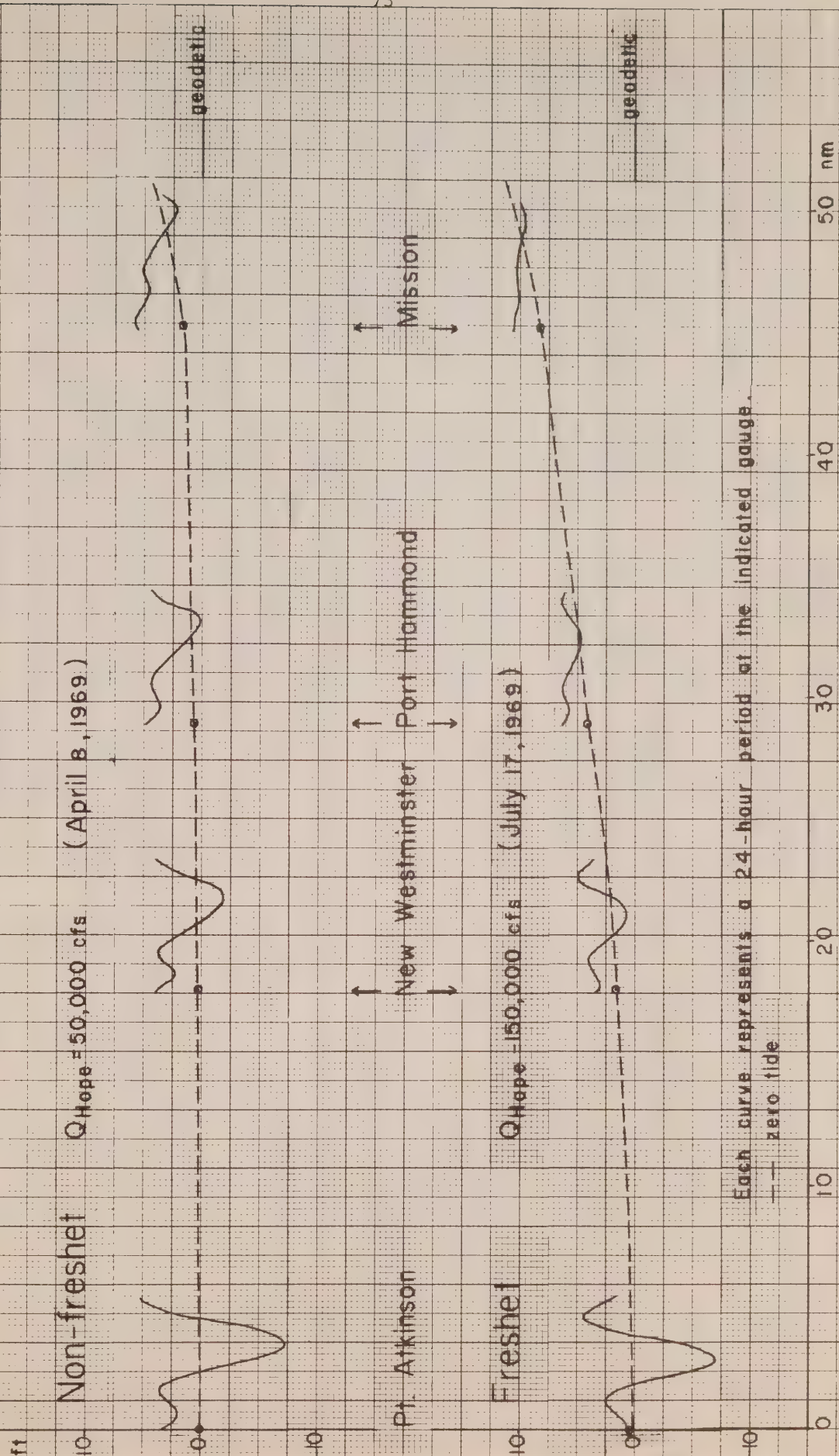


Fig 48 MODEL-PRODUCED PROFILES OF FRASER RIVER

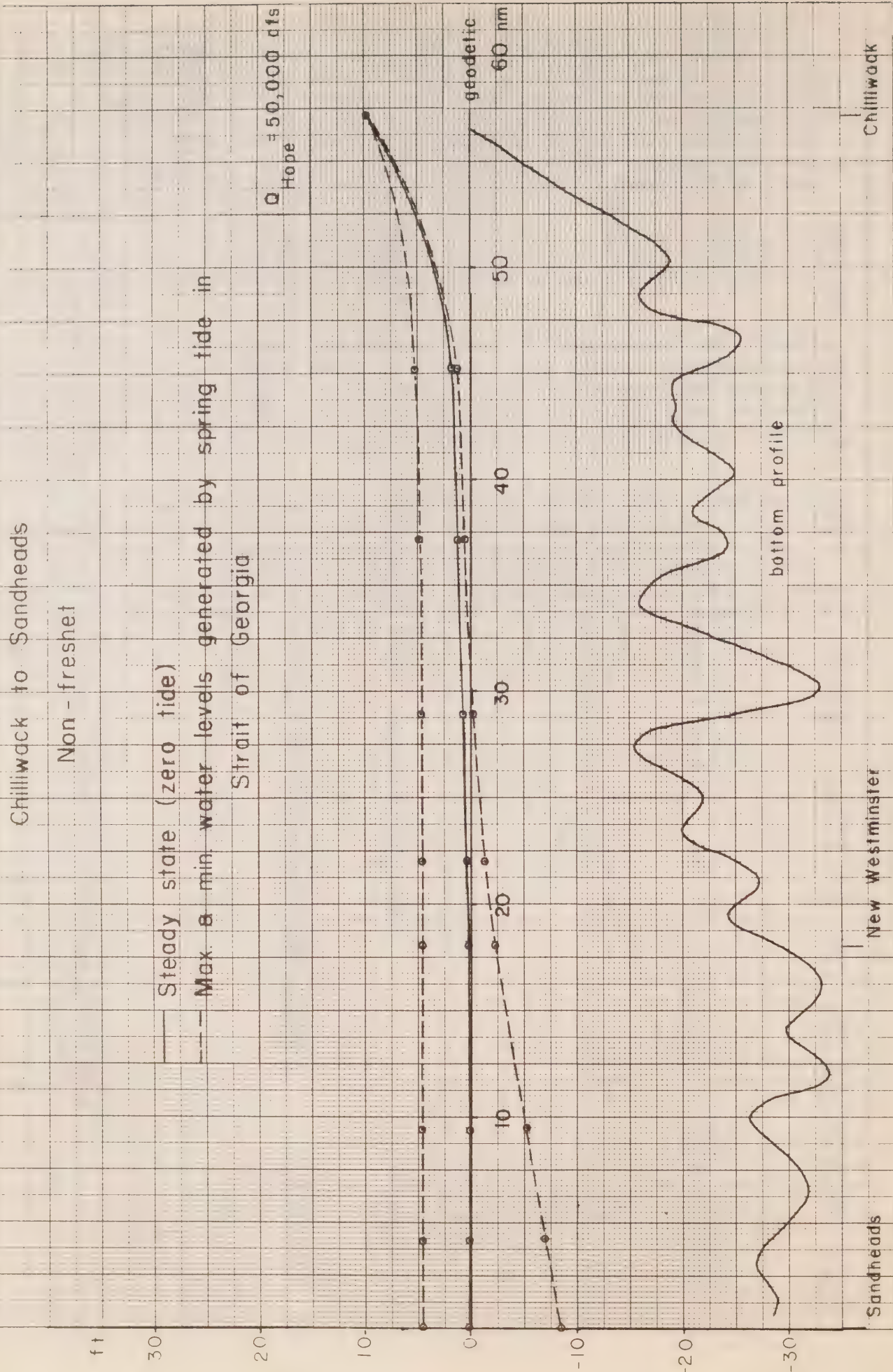


Fig 49 MODEL-PRODUCED PROFILES OF FRASER RIVER

Chilliwack to Sandheads

Freshet

— Steady state (zero tide)

— Max. & min. water levels generated by spring tide in

Straits of Georgia

$Q_{\text{Hope}} = 300,000 \text{ cfs}$

75

geodetic

60 nm

50

40

30

20

10

bottom profile

Sandheads

New Westminster

Chilliwack

ft

30

20

10

0

-10

-20

-30

OTHER APPLICATIONS

A. Energy Dissipation

Considering the area between high and low water lines in Figures 48 and 49 to be a measure of energy losses, most of the tidal energy at low discharges, and almost all of it at high discharges, is dissipated between Sandheads and New Westminster.

A more quantitative evaluation of these energy losses may be obtained from the model by isolating the friction term in the equation of motion:

$$\frac{\partial u}{\partial t} + u \frac{\partial u}{\partial x} = -g \frac{\partial h}{\partial x} - g \frac{|u|u}{C^2 d}.$$

All four terms in their original form are forces per unit mass; the term a $|u|u/C^2 d$ representing the friction. The work done by friction on one model segment per unit time would be $(g |u|u/C^2 d) (Q\rho) \Delta x$, where Q is the average volume of water passing through the segment per unit time, ρ is the density of the water, and Δx is the length of the segment. During the model's progress, this term is normally evaluated for two segments at a time, with Q ($= uA$) calculated at the centre section (see Figure 7). The sum of these friction terms for all segments of the schematized estuary over a complete tidal cycle would represent the energy dissipation due to friction during a tidal cycle, in foot-pounds or in ergs, i.e. in finite-difference form:

$$\text{Energy Dissipation} = \sum \sum \left(\frac{g \frac{Q}{A} \frac{Q}{A}}{C^2 d} \right) (Q\rho) \Delta x \Delta t$$

where X is the number of segments and T is the number of time steps.

The total energy dissipated between Chilliwack and the Fraser mouth (including all four distributaries) was thus computed and averaged over a tidal cycle for both freshet and non-freshet conditions.

For a discharge of 213,000 cfs at Hope (June 20, 1969), the total energy dissipated was found to be 3.17×10^8 foot-pounds/second (0.4298×10^{16} ergs/sec); for a discharge of 29,700 cfs (March 11, 1969), it was 0.47×10^8 foot-pounds/second (0.0637×10^{16} ergs/sec). Per unit surface area, these values were respectively 0.19 foot-pounds/foot²/second (2760 ergs/cm²/sec) and 0.04 foot-pounds/foot²/second (521 ergs/cm²/sec).

It would be useful to compare the average rate of energy dissipation obtained by this method, with the average rate of energy entering through the boundaries of the model. Generally, for a given time interval, the change in energy in the system should balance the sum of the work on the upstream and downstream boundaries, the work done by the friction, the work done by the wind and the work done by the atmospheric pressure. The effects of wind and atmospheric pressure have been ignored in the model. We assume the net change in energy over a complete tidal cycle to be zero.

G.I. Taylor (20) has developed an expression for the work done per second on the boundaries of a tidal basin.

The average rate at which work is done on one of the boundaries is, in general terms:

$$W_B = \int_0^S \frac{1}{2} \rho u^2 dt \{g (D + h)^2 + gh^2 - gD^2 + u^2 (D + h)\} ds$$

where D is the distance between the bottom and the datum (GB in the Fraser model, see Figure 6), h is the distance between the water level and the datum (H in the Fraser model), and S is the surface width (W in the Fraser model). For each computer time step, W_B can be evaluated at each of the six boundaries of the model. The resulting values are summed over all boundaries over a complete tidal cycle, and the average rate determined.

Applying Taylor's expression for W_B to the same tidal cycles used for the energy dissipation, the energy input into the system was calculated to be 4.93×10^8 foot-pounds/second (0.6683×10^{16} ergs/sec) for $Q_{HOPE} = 213,000$ cfs and 0.70×10^8 foot-pounds/second (0.0951×10^{16} ergs/sec) for $Q_{HOPE} = 29,700$ cfs.

In his paper on the tidal friction in the Irish Sea, Taylor used $k\rho u^3$ for the amount of energy dissipated/cm²/second, and obtained a value of 0.089 foot-pounds/foot²/second (1300 ergs/cm²/sec) for a spring tide in the Irish Sea. In this expression, u is the water velocity, and k is the friction coefficient calculated by Bazin's formula $k = 0.0013 (1 + M/\sqrt{R})$. M is determined by the nature of the bottom, and R, the hydraulic radius, may be assumed to be equal to the depth in the case of a stream which is very broad compared with its depth. Bazin's M varies from 0.1 for smooth surfaces to 3.2 for rough channels. In the case of the Irish Sea, with a depth of 80 metres, the choice of M is not significant. Using M = 0.85 for a "clean stony bottom", Taylor calculated a value for k of 0.002, observing that this value was very nearly the same as the one obtained for large rivers. However, a value of M = 0.85 appears to be quite low for the Fraser, where bed waves, anchored log booms and training walls would indicate a value of 3.17 (suggested by Bazin for exceptionally rough channels with weeds and boulders). For R = 10 metres, we may put k = 0.0026. Obtaining the average value of u over a complete tidal cycle from the model for all segments, the energy dissipation for a freshet of 213,000 cfs was calculated to be 0.115 foot-pounds/foot²/second (1680 ergs/cm²/sec), and it was 0.012 foot-pounds/foot²/second (179 ergs/cm²/sec) for a low discharge of 29,700 cfs. Both values are well below those determined by the method using the friction term, and compared poorly with the calculated energy input; however, they are based on much broader assumptions than the previous method.

B. Hydraulic Structures

As we mentioned in the first section, a proposal to construct a diversion canal from Annacis Island to Boundary Bay was examined in 1966 by the National Research Council at Ottawa in a hydraulic and a numerical model (11,12). The canal was intended to alleviate the flood danger of the Lower Fraser River at very high freshets, by diverting about half of the water from the Main Arm. The proposed (but not accepted) canal was 5.3 miles long, 1000 feet wide and had a depth of about 35 feet below geodetic datum. For a catastrophic discharge of 536,000 cfs at Hope, the NRC models predicted decreases in high water levels varying from 0.5 feet at Steveston to 3.5 feet at New

Westminster. Similar results were obtained from the numerical model presented in this report. The canal between Annacis Island and Boundary Bay was schematized in 10 sections, with a depth (GB) of 35.14 feet, and the tides at Tsawwassen as a boundary condition. Only a few program modifications were needed to include the canal in the model, a distinct advantage of a numerical approach. However, numerical methods have not yet been developed to simulate the important scouring effects created by the very high velocities expected at the northern entrance of the canal. A moveable-bed hydraulic model might be more suitable in this respect.

Fig. 50 PROPOSED BOUNDARY BAY DIVERSION CANAL



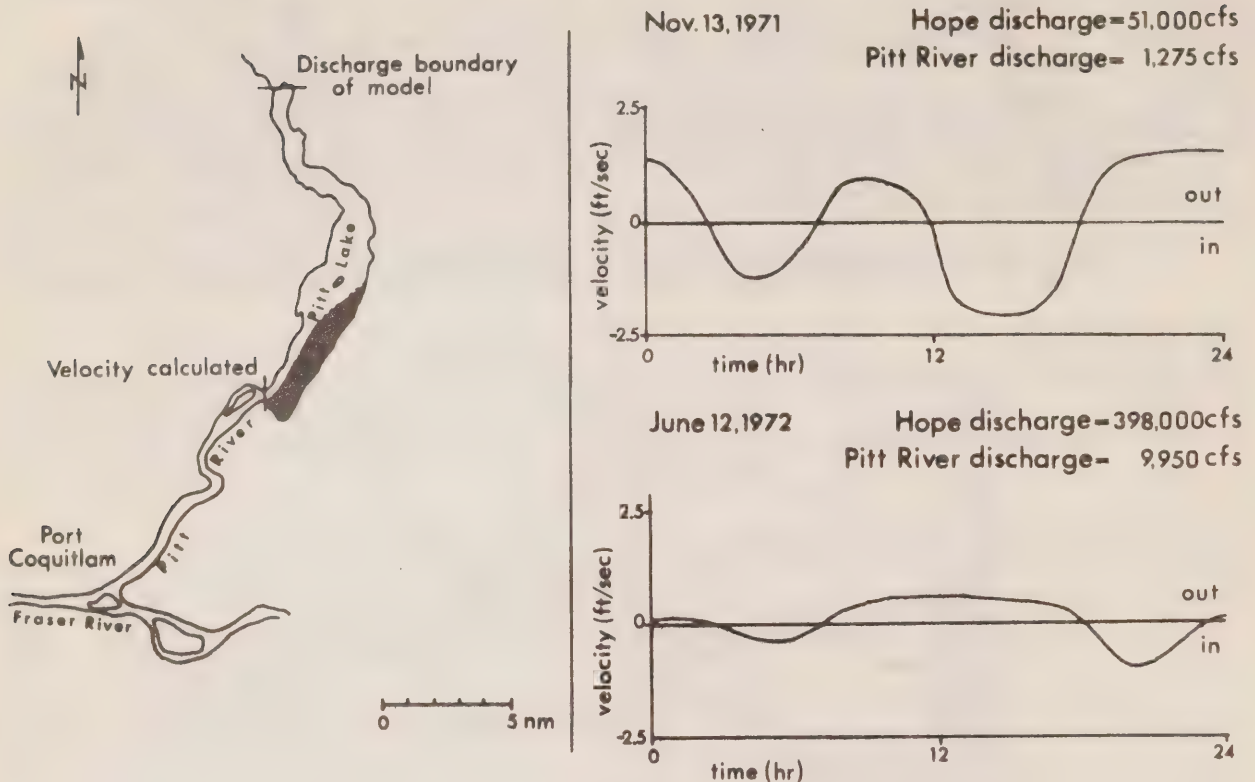
Other proposed hydraulic structures such as the Moran Dam (Figure 1) could be considered in the model simply by adjusting the upstream boundary condition at Chilliwack for the regulated discharge.

C. Sedimentation of Pitt Lake

The rather unusual "negative" delta formation near the southern entrance to Pitt Lake was examined briefly by running the model for two discharges and plotting the calculated river velocities for a 24 hour period as shown in Figure 51.

In both cases, the inward flow is of shorter duration but has a higher maximum than the outward flow. The important factor in this sedimentation process seems to be the magnitude rather than the duration of the current. The inward flow with its higher peak velocity is capable of carrying into the lake sediment particles which are too heavy to be carried out by the weaker outward flow, even though the outflow is of longer duration. Hence, a net inward movement of sediment occurs.

Fig. 51 MODEL-PREDICTED VELOCITIES IN PITT LAKE



D. Movement of Salinity Wedge

During an incoming tide on August 23, 1971, a field study of the behaviour of the salinity wedge in the Main Arm near Steveston measured the speed of the salinity wedge at 1.1 knots. The discharge at Hope for that date was 103,000 cfs. The speed of the wedge was determined by noting the times when the first traces of salinity ($S = 1\text{‰}$) appeared at two points along the centre line of the river, 1.6 nautical miles apart.

The model-produced water velocity based on the actual boundary conditions was 0.4 knots in the upstream direction, much less than that of the salinity wedge. However, this velocity was averaged over a cross-section and would be much lower than that in the central part of the river.

THE ACCURACY OF THE MODEL

A valuable feature of the Fraser model was the large number of data available to test the accuracy of the predictions.

Figures 52 and 53 compare four years of observed daily higher high and lower low waters at New Westminster with the model-produced values, both for height and time. The model-produced values were computed from the equations of the best-fit curves (Figures 19-34).

The histograms for the height errors show that about 76% of the computed water surface elevations are too low (67% within one foot). This trend is an advantage since the model's principal purpose is to predict tidal heights for shipping, and an underestimated depth is a desirable safety precaution.

Most (92%) of the computed times of high and low waters were in error by less than 30 minutes.

The model was assumed to be calibrated only after a large number of repetitions with a variety of friction coefficients, which were assigned to blocks of segments. To refine the model further, in other words to simulate nature more closely, friction coefficients would have to be assigned to each segment individually, requiring a much larger number of computer runs. This procedure would be extremely costly and might only be warranted if the other parameters used in the model were exact. Unfortunately, the essential parameters, the boundary conditions, are still beset by imperfections in our measuring techniques and instrumentation.

The field data for the upstream boundary condition at Chilliwack are the discharge records of the Fraser River at Hope, computed from point measurements with a non-directional Price current meter. At very high discharges in excess of 350,000 cfs, the current can be measured only near the surface, because the 300 lb current meter is swept away by the current (in the order of 17 feet per second) as soon as it enters the water. A multiplication factor is used to convert the measured surface velocity to mean velocity, which is then multiplied by the cross-sectional area (calculated from depth soundings at low flow) to obtain the discharge (21).

The discharge data derived by this technique may be in error at high discharges, because it is difficult to estimate an accurate multiplication factor by extrapolation from low-flow measurements, and it is virtually impossible to verify this factor.

Figure 54 examines the influence of a 5% error in discharge measurements of 398,000 cfs at Hope (June 12, 1972) on the tidal heights at Mission and Deas Island. At this high discharge, the resulting change at Mission is about one foot, at Deas Island 0.2 feet. At low discharges, these changes are considerably reduced.

Although no discharge records exist for the head of Pitt Lake, and hence the boundary condition at that location is an estimate, the flow is small relative to the discharge of the Fraser; any errors introduced into the system by this approximation can be ignored.

Fig. 52 COMPARISON OF MODEL-PREDICTED AND
OBSERVED EXTREMA AT NEW WESTMINSTER
1970 - 1973 (Error = predicted - observed)

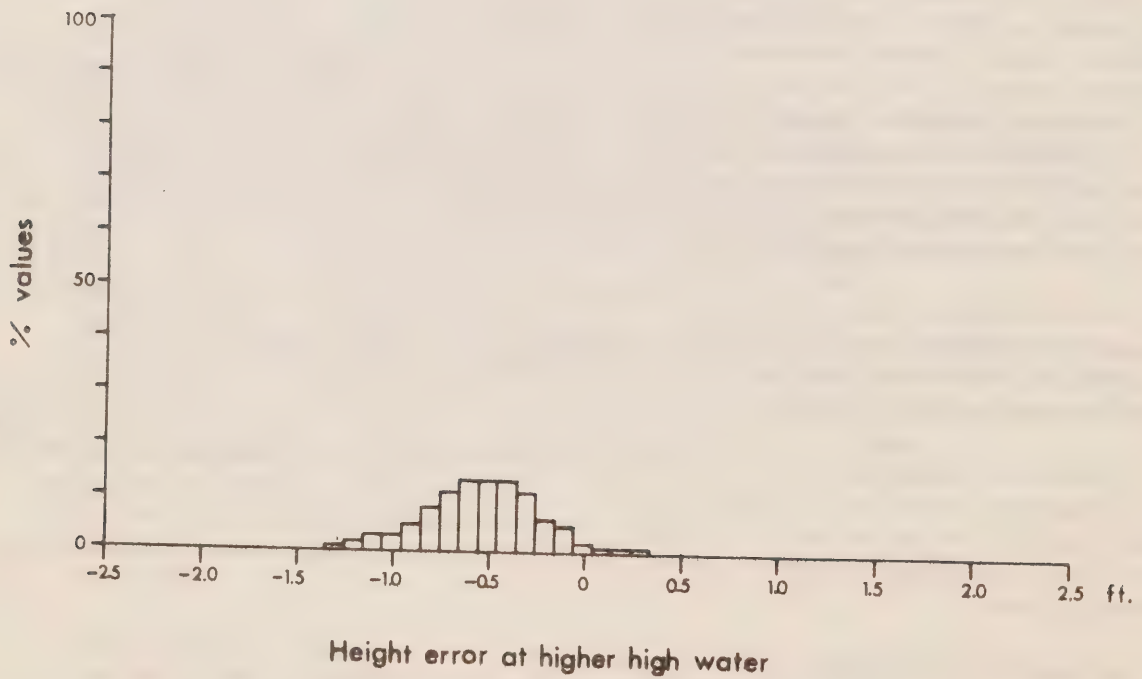
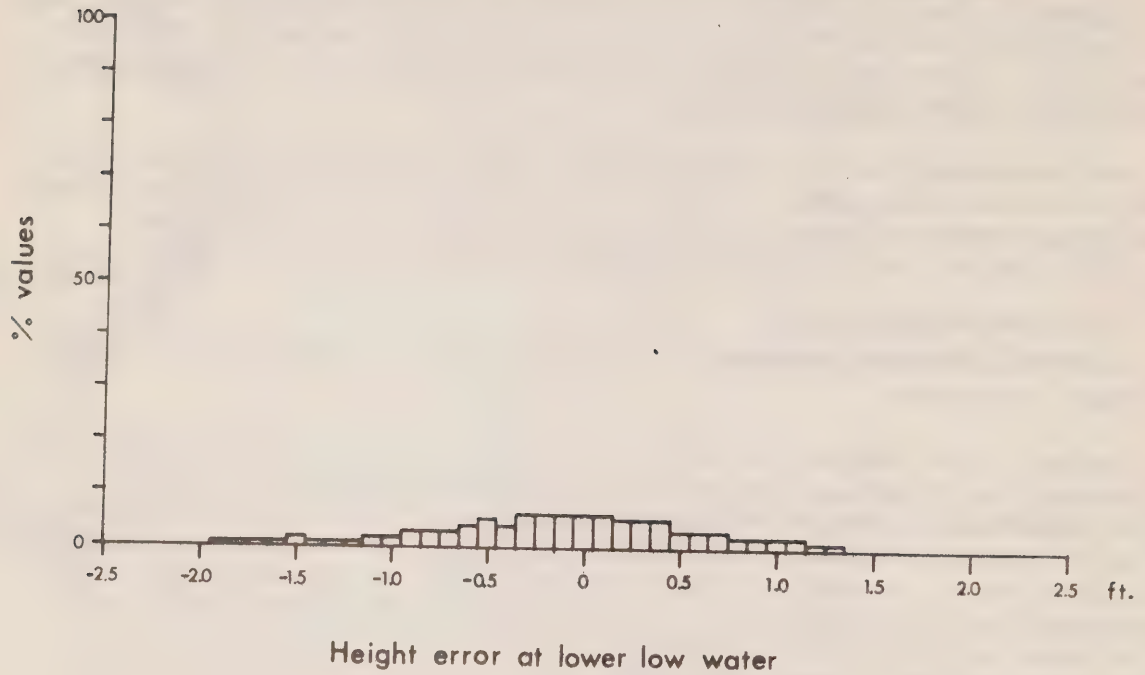


Fig.53 COMPARISON OF MODEL-PREDICTED AND OBSERVED EXTREMA AT NEW WESTMINSTER

1970-1973 (Error=predicted-observed)

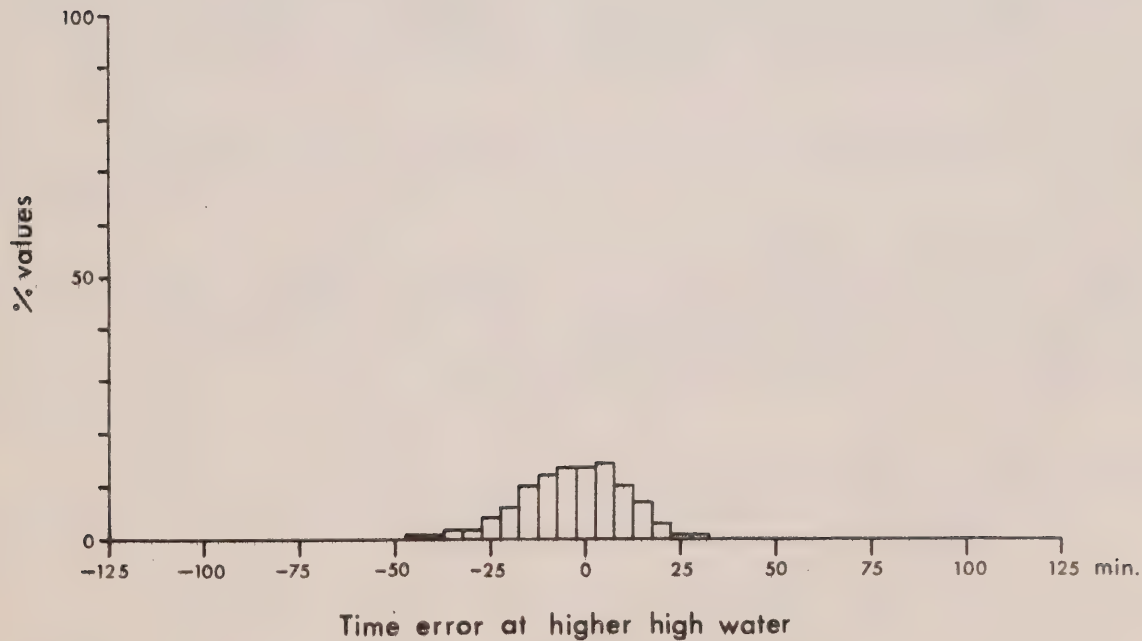
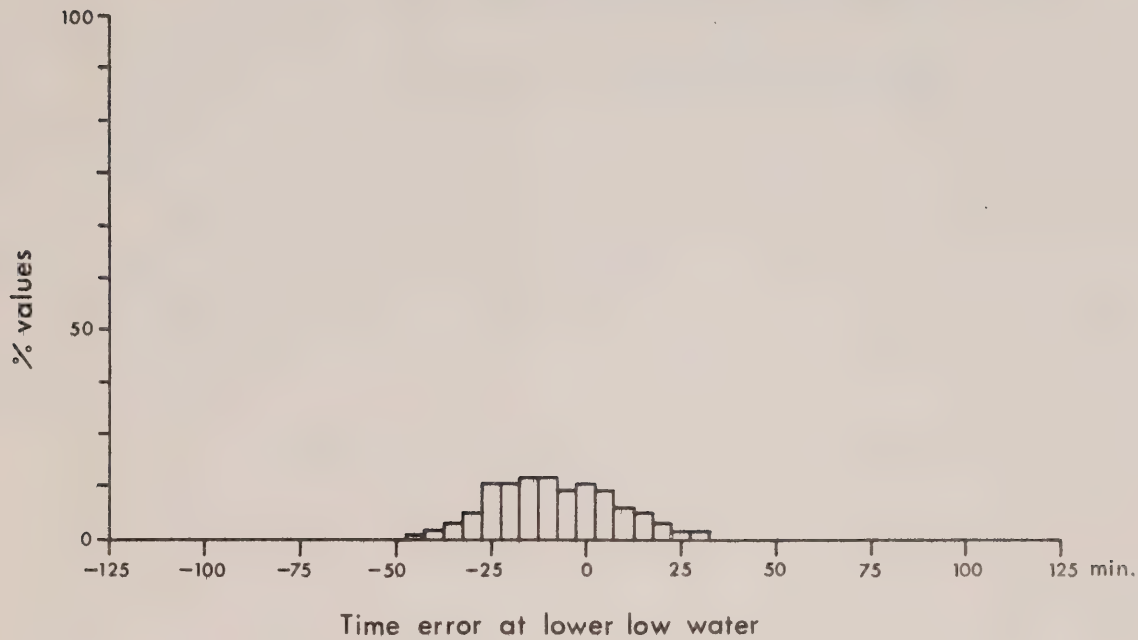
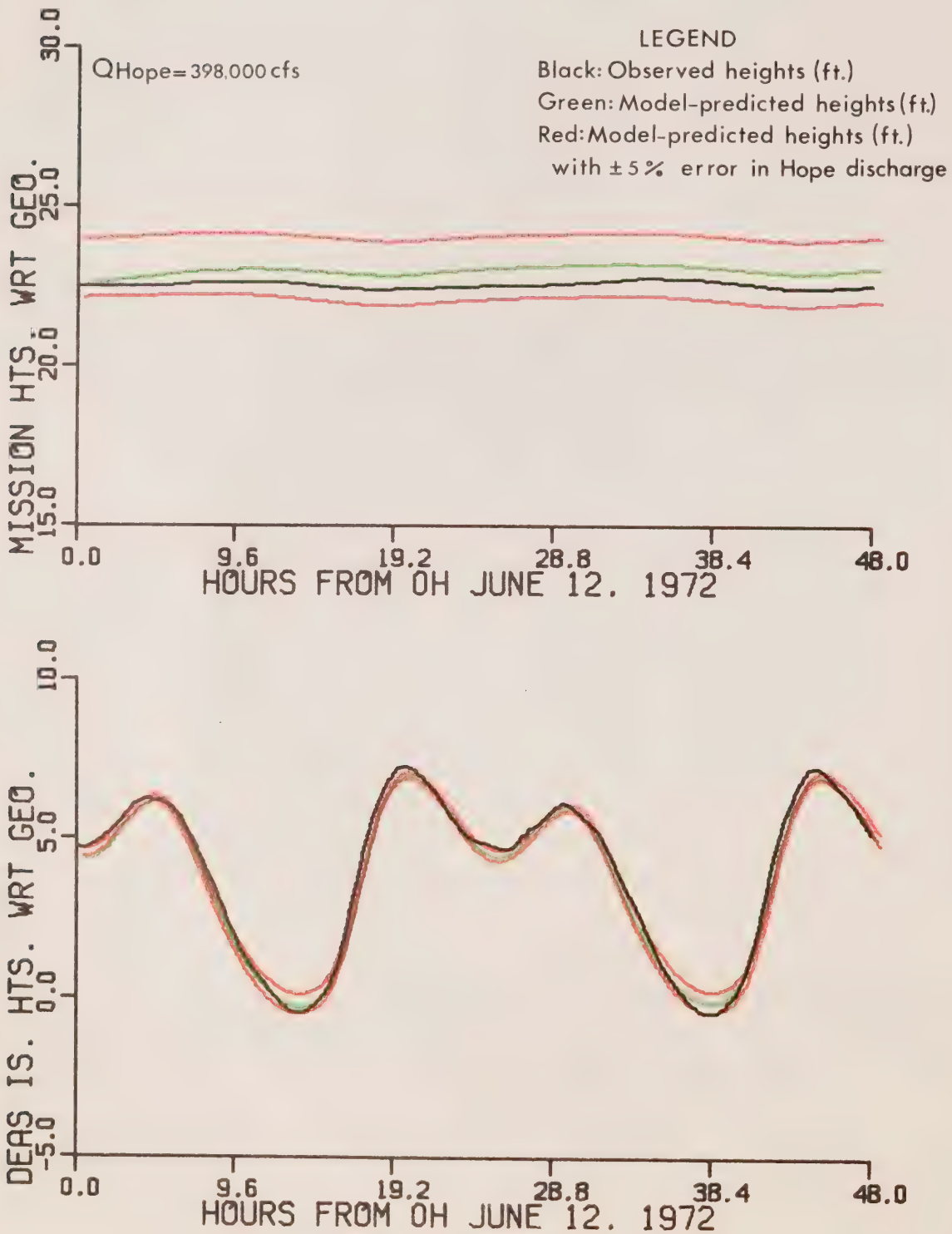


Fig.54 EFFECT OF ERRORS IN UPSTREAM BOUNDARY
CONDITIONS (DISCHARGES)
UPON MODEL-PREDICTED HEIGHTS



The observed and predicted tidal heights at Point Atkinson and Tsawwassen form the model's downstream input. The observed heights are used for calibrating the model (and for "hindcasting"). They are measured by float gauges, and the recorded values are verified once every two days using a steel tape and a staff with a precision of 0.01 feet. The resulting tide graphs are digitized at hourly intervals, with a precision of 0.01 feet (the thickness of the pen line). The data required for the model are then interpolated to 15 minute intervals using Fourier Series, and subsequently interpolated linearly to 150 second intervals (two time steps). When the Point Atkinson and Tsawwassen tides are used as boundary conditions at the mouth of the Fraser, a small height correction is applied to account for the fresh water outflow (see page 28). This correction was obtained from a comparison between mean sea levels at Point Atkinson, Tsawwassen and Sandheads over a relatively short period (April-September, 1969). The lack of sufficient data makes it difficult to estimate the precision of this correction, but, on the basis of the available values, it seems reasonable to assume an error not exceeding 0.1 feet. Neglecting possible flaws in the interpolation technique, we conclude that a total error in the order of 0.1 feet is accumulated in the processing of observed data.

The predicted heights do not consider the influence of barometric pressure, wind, density, etc. and therefore should be examined more critically:

The Point Atkinson and Tsawwassen tidal predictions for the Fraser model are obtained by a harmonic method using 50 constituents. The computer program used for this method is a simplified version of the program developed by the Marine Environmental Data Service for the Canadian Tide Tables. These two programs were found to be of similar accuracy when their computed maxima and minima were compared with actual data over a total of 56 days of selected spring and neap tides (217 values). This comparison is illustrated by the histograms for Point Atkinson in Figures 55 and 56 (the Tsawwassen histograms are similar, and therefore are not shown).

Although the purpose of these histograms was to confirm the adequacy of a simplified program, they also indicated significant errors in the height predictions of both programs.

To examine the error distribution more closely, a much larger sample was considered. Figure 57 compares four years (1970-1973) of predicted (from the Tide Tables) and observed higher high and lower low waters at Point Atkinson. Of the predicted heights, 24% were in error by more than 0.5 feet. However, the times agreed surprisingly well: 80% of the predicted times were within ten minutes of the observed values.

The 24% probability that the boundary conditions are in error by more than 0.5 feet, seriously weakens the model's predictive capability, particularly as the calibration itself only aims at an accuracy of 0.5 feet.

It has been suggested (21) that many of the anomalies in the tidal predictions at Point Atkinson, and other stations in the general vicinity of the Strait of Georgia, are caused by atmospheric pressure fields. Until a method is developed which reproduces these anomalies, the tidal predictions in the Fraser cannot be expected to be more accurate than 0.5 feet, regardless of the level of calibration.

Fig.55 COMPARISON OVER 56 DAYS OF OBSERVED
EXTREMA AT POINT ATKINSON WITH THOSE
OBTAINED BY HARMONIC METHOD

(Error=predicted-observed)

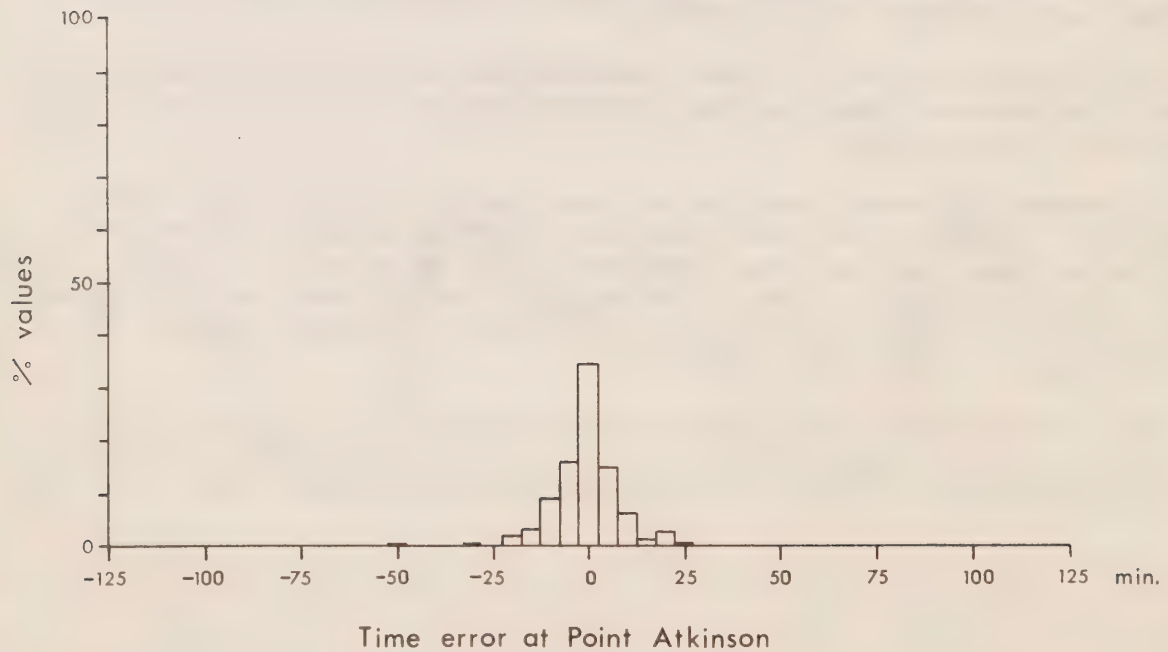
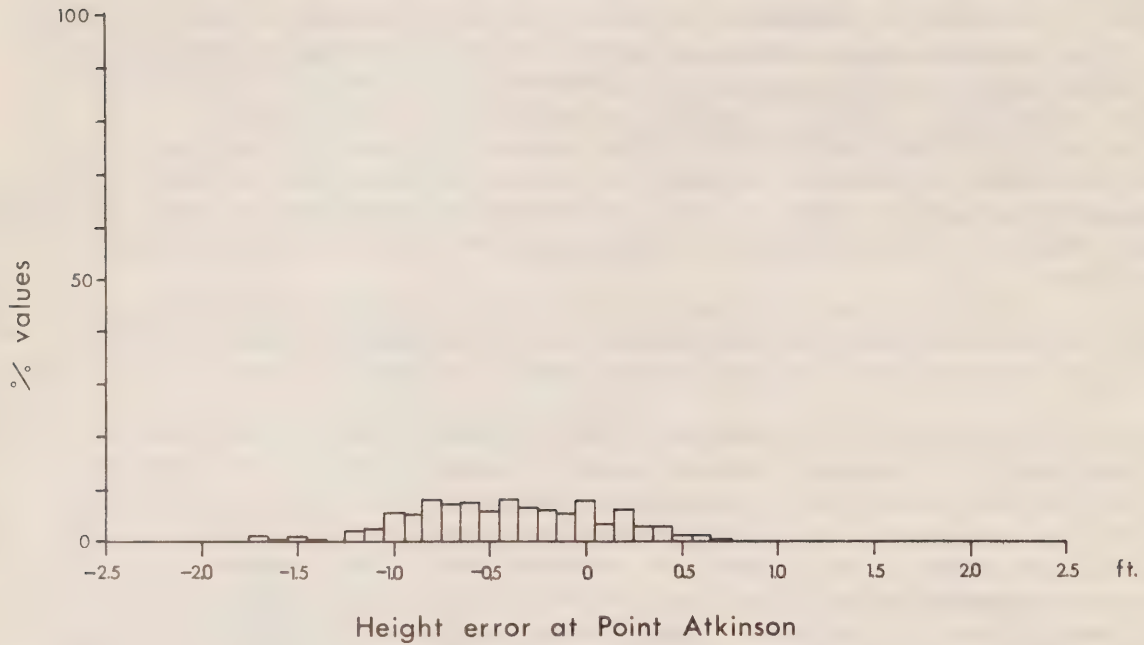


**Fig. 56 COMPARISON OVER 56 DAYS OF OBSERVED
EXTREMA AT POINT ATKINSON WITH THOSE
LISTED IN TIDE TABLES**

(Error=predicted-observed)

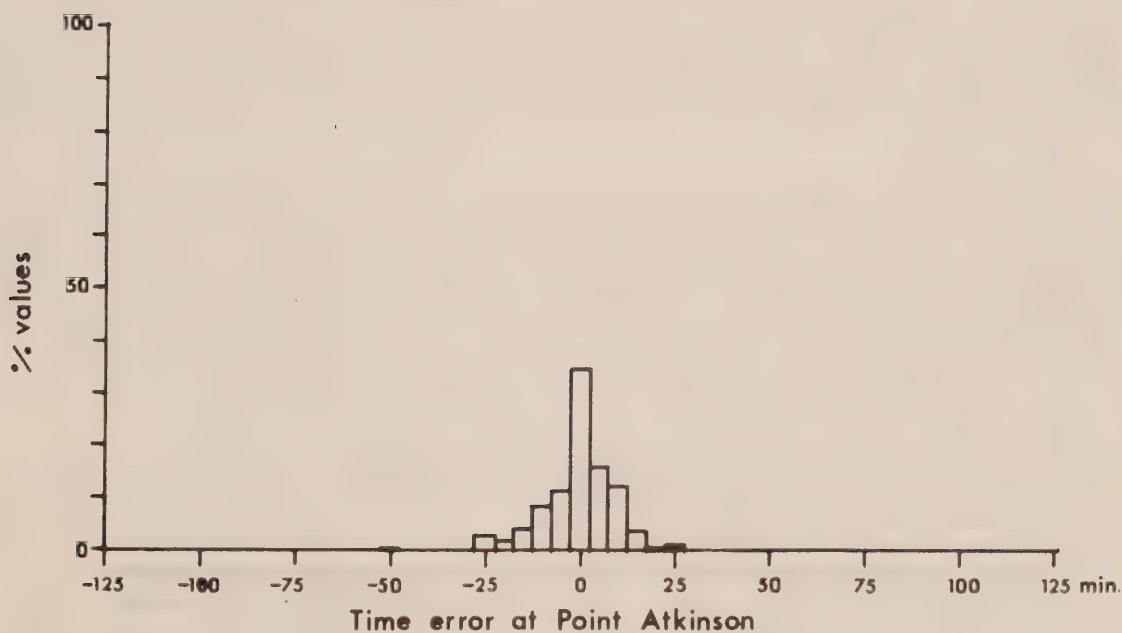
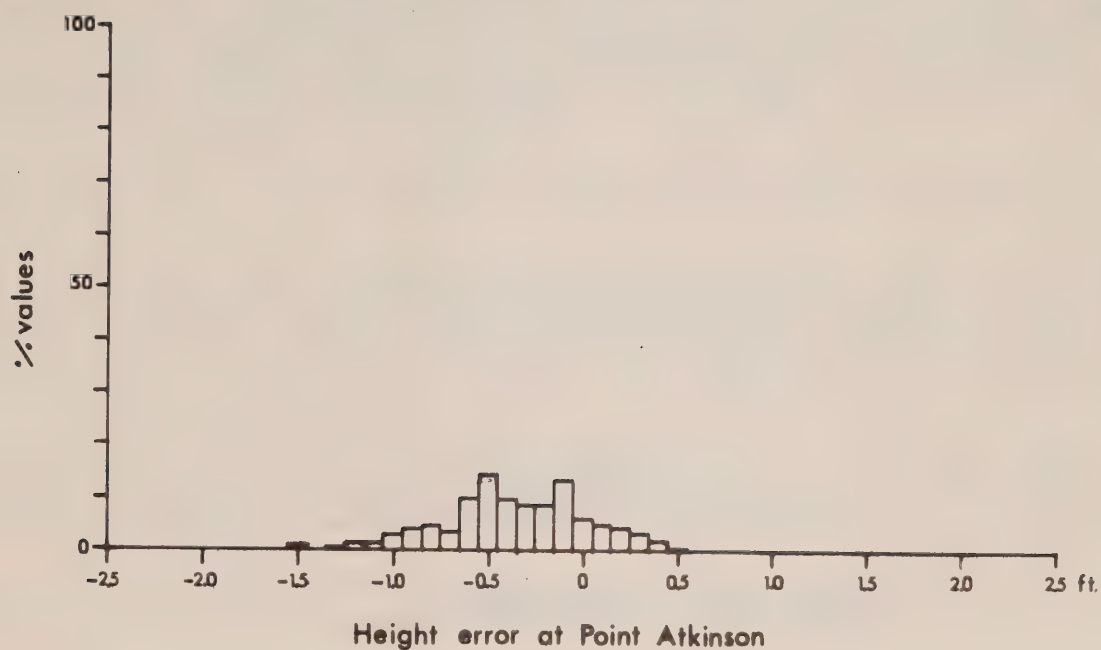
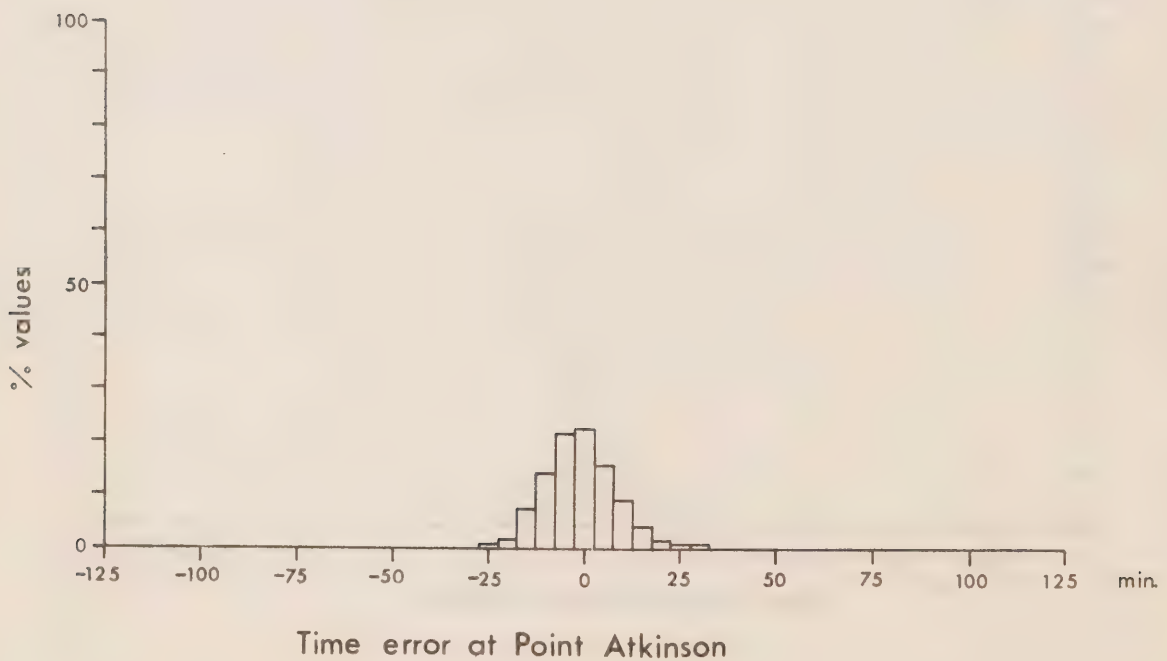
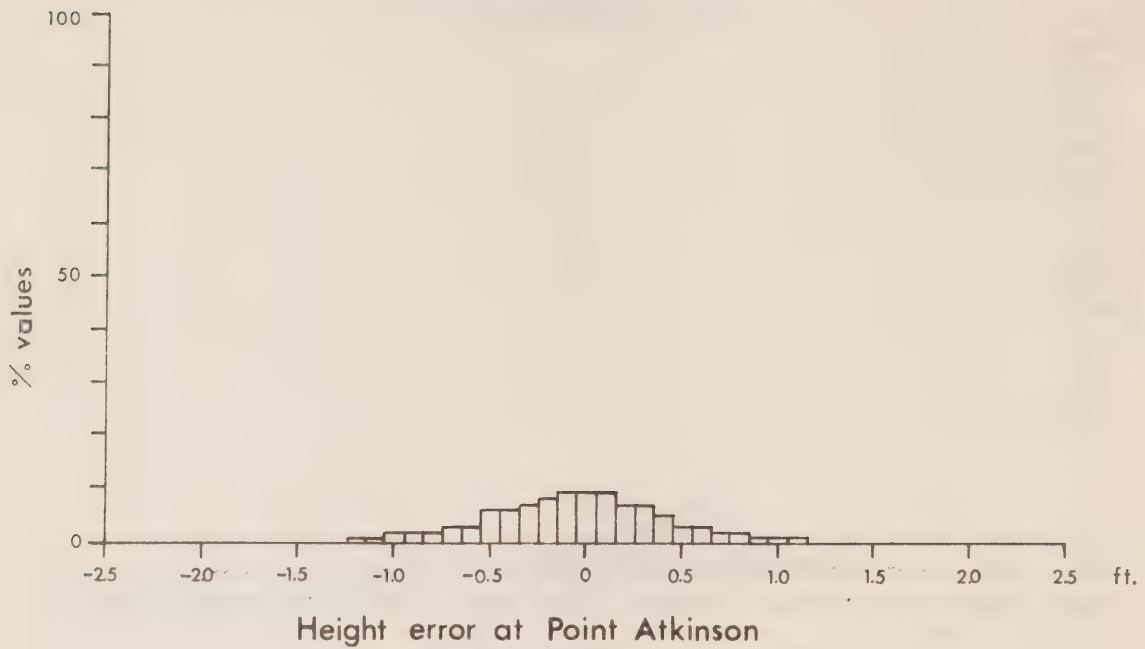


Fig.57 COMPARISON OF TIDE TABLE AND OBSERVED
HIGHER HIGH AND LOWER LOW WATERS AT
POINT ATKINSON 1970-1973 (Error = predicted - observed)



The effect of an error in height of 0.5 feet in the downstream boundary conditions upon the predicted water surface elevations at Deas Island and Mission is illustrated in Figure 58. A discharge of 51,000 cfs (November 13, 1971) was chosen because the tidal influence at Mission is more pronounced at low discharges.

It is interesting to note that the actual tide (used for the model-predictions in Figure 58) at Point Atkinson on November 13, 1971 was an average of 0.5 feet higher than predicted. The barometric pressure at Vancouver at 1000 hrs PST on this date was 1009.9 mb, 15.7 mb below the average annual pressure, and corresponding to a rise in sea water level of about 15 cm, or 0.5 feet above normal. (Figure 58 indicates the change in predicted levels that would result from such an error.)

Another possible source of errors is the assumption that the flow is homogeneous.

The model was calibrated for freshet conditions, because the model's behaviour is then more sensitive to adjustments of the friction coefficients. Moreover, as Figure 5 shows, even a low freshet tends to keep the salinity wedge outside the delta, thus confirming the supposition of homogeneous flow.

Comparisons between predicted and observed water levels at New Westminster at low discharges suggest that the effect of the saline wedge upon the river heights is negligible, although the exact relationship would be the concern of a two-layer model.

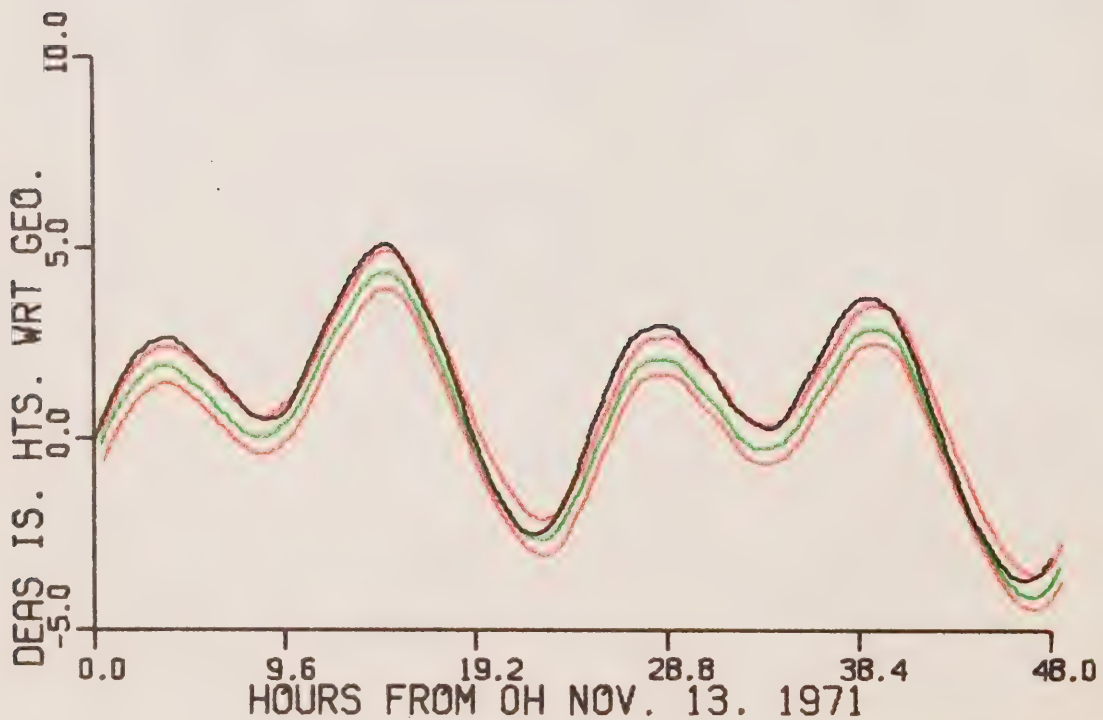
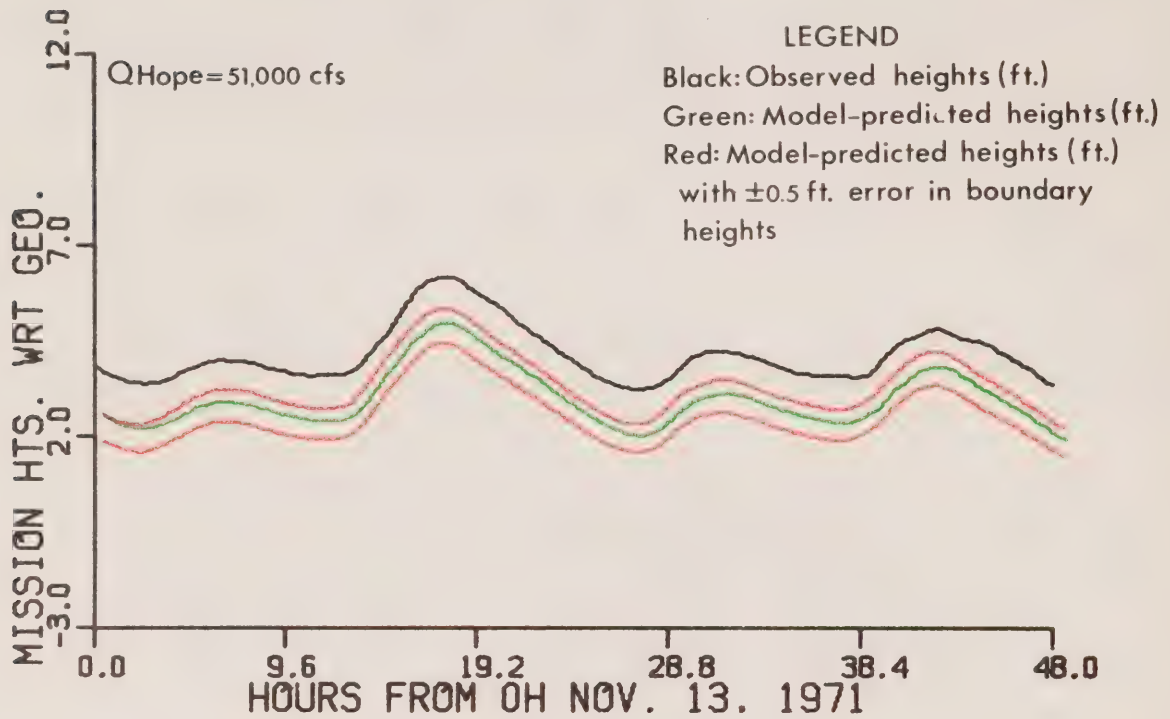
In the schematization, certain simplifications were made which were examined more closely upon the completion of the model:

Local run-off, being difficult to assess, was neglected. To determine the consequences of this omission, a flash flood of two days' duration and a peak flow of 800 cfs was introduced into the model at Mission. With a discharge at Hope of 39,000 cfs, the maximum resulting change in the predicted river elevations was only 0.03 feet.

Annacis Channel, a four mile long arm west of New Westminster, was omitted from the schematization because no soundings were shown on the chart, and the channel is bypassed by the main flow, due to a causeway. Inclusion of Annacis Channel (conservatively estimating the depth as 15 feet) produced a discrepancy at New Westminster of -0.06 feet at high tide, and -0.23 feet at low tide, for a freshet discharge of 213,000 cfs at Hope; and of + 0.03 feet and -0.08 feet respectively for a discharge of 30,000 cfs.

The schematization was based on nautical charts which show soundings for normal conditions. However, the model was calibrated for freshet conditions, when the cross-sectional area of the Fraser River channel undergoes changes due to sedimentation. To determine the error in the schematization due to sedimentation, the amount of bed-load dredged annually from the delta (i.e. the amount of sediment deposited during the freshet) was compared with the river volume of the delta at zero tide and a discharge at Hope of 150,000 cfs. The average annual amount dredged between New Westminster and the Strait of Georgia (over all four distributaries) was calculated by the Department of Public Works to be about 4×10^6 tons, or 10^8 ft³ of bed load. With a river

Fig.58 EFFECT OF ERRORS IN DOWNSTREAM BOUNDARY
CONDITIONS (TIDAL HEIGHTS)
UPON MODEL-PREDICTED HEIGHTS



volume between New Westminster and Georgia Strait of $120 \times 10^8 \text{ ft}^3$, the percentage error in the schematization due to neglecting sedimentation is 0.8%. This percentage is only an overall figure and does not account for local sedimentation (bed waves) which would affect the schematization considerably but which would be difficult to estimate.

REMARKSProgram Notes

For more efficient use of computer storage space, the matrix of the traditional "leap-frog" scheme shown in Figure 8 was not stored in full by the program. Instead, at the end of the calculations for the time step $k + 1$, $H(k, m)$ and $Q(k + 1, m)$ are retained in the $QH(m)$ array, and the value of $H(k, m) - H(k - 2, m)$ is retained in the $\Delta H(m)$ array, for all appropriate m . These are the only variables which are necessary for calculations at the next time step. Any values which are required for subsequent analysis can be stored elsewhere for later reference. Thus, the 2-dimensional array $QH(n, m)$ can be replaced by the two 1-dimensional arrays $QH(m)$ and $\Delta H(m)$, drastically reducing the amount of storage space required since these arrays are independent of the simulation time.

The program was written in Fortran and requires 20 K (20,000) words of storage for execution. Fast Fourier Transform routines were used for the interpolation of tidal data. The program was executed on the Univac 1108 operated by Computer Sciences Canada, Ltd. at Calgary, Alberta. Input/output was performed on both a conversational teletype terminal and a batch terminal interfaced with a card reader and a line printer. Plotting instructions were written on magnetic tape by various routines developed on the IBM 370/168 at the University of British Columbia in Vancouver. The plots were subsequently produced on a local Calcomp 563 plotter interfaced with a Hewlett-Packard 2114A mini-computer.

For an average run of three days simulated time, with height predictions printed out at fifteen minute intervals for six locations, the model requires about 70 seconds of CPU (Central Processing Unit) time.

Least-Squares Polynomial Approximation

Given $(n + 1)$ pairs of values $(x_0, y_0), (x_1, y_1), \dots, (x_n, y_n)$, where only the y -values are experimentally produced, we require a polynomial y of degree m

$$y = a_0 + a_1x + \dots + a_mx^m$$

which fits the given points as well as possible. When $m < n$, the coefficients a_0, a_1, \dots, a_m are determined by minimizing

$$S = \sum_{j=0}^n (a_0 + a_1x_j + \dots + a_mx_j^m - y_j)^2.$$

Fourier Series Interpolation

Fourier series were used to interpolate tidal heights for the model boundary conditions from hourly intervals to 15 minute intervals. The two subroutines used were written by J.R. Wilson of the Institute of Oceanography at the University of British Columbia. For the given data points, the first call to the subroutines performs a Fourier analysis, calculating the coefficients of the Fourier series. The second reference to the subroutines

applies a Fourier synthesis to these coefficients, producing data points at the required intervals.

Harmonic Method of Tidal Prediction

The tidal predictions for Point Atkinson and Tsawwassen follow the "Manual of Harmonic Analysis and Prediction of Tides" of the U.S. Coast and Geodetic Survey, using the general equation

$$h = H_0 + \sum fH \cos [at + \text{Greenwich } (V_0 + u) - g]$$

where

h = height of tide at time t ;

H_0 = mean height of water level above datum;

H = mean amplitude of constituent;

f = factor for reducing mean amplitude H to year of prediction;

a = speed of constituent

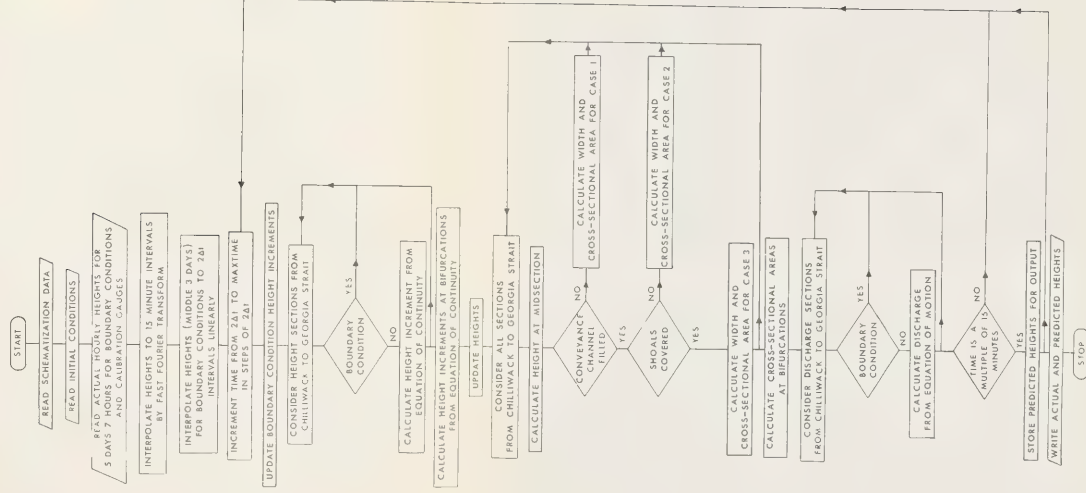
Greenwich $(V_0 + u)$ = value of equilibrium argument at Greenwich when $t = 0$;

g = modified epoch (or phase lag) of constituent.

A total of 50 constituents were used for the prediction of tidal heights for boundary conditions in the model. This total included 23 shallow water constituents.

The amplitude and modified epoch for each constituent vary with location, and were obtained from "Harmonic Constants and Associated Data for Canadian Tidal Waters", Tides and Water Levels, D.O.E. The speed (or frequency) of each constituent is listed in Appendix 2 of "The Analysis of Tides" by Gabriel Godin. The factor and equilibrium argument vary with the date and were calculated by program ASTRO, developed by Godin. The program uses Doodson numbers which are given in Appendix 1 of "The Analysis of Tides". Various other ratios required as data have also been developed by Godin from the information given in the appendices to his book.

Fig. 59 FLOWCHART



TERMINOLOGY

Since several disciplines are involved in the project, some definitions of the terms used in this report may be informative.

Barotropic:

the density does not vary along isobaric surfaces in the estuary; more specifically, a barotropic model of an estuary ignores the salt wedge.

Bed load:

coarse material which rolls along the bottom of the river.

Bed wave:

sand dunes on the bed of the river which migrate slowly downstream.

Collimation error (vertical):

error in a surveyor's level due to the line of sight not being parallel to the bubble tube axis. This error is eliminated if the distances of backsight and foresight are equal.

Diurnal tide:

one complete tidal oscillation per day (one high, one low water).

Explicit scheme in a one-dimensional model:

during each computation, one unknown (Q or h) is calculated from a set of previously obtained values. The result is subsequently used to calculate the next Q or h in distance or time. (An implicit scheme computes all values of Q and h at time step $t + \Delta t$ from the known ones at step t , requiring a large number of simultaneous equations.)

Dynamic pressure head:

the velocity term $v^2/2g$ in Bernouilli's equation. A high local water velocity would "depress" the water surface at the tide gauge significantly, decreasing the static pressure head measured by the tide gauge. In such a case, the gauge readings do not truly represent the tidal heights in the general vicinity.

Geodetic datum:

based on mean sea level prior to 1929 and computed from gauge readings at Caulfeild Cove (Pt. Atkinson).

Geopotential anomaly:

defined as $\Delta D = \int_{p_1}^{p_2} \delta dp$, where δ is the specific volume anomaly (a function of temperature, salinity and pressure) and p_1, p_2 represent the isobaric surfaces. In the Strait of Georgia near the mouth of the Fraser, we put $\Delta D = \int_{328 \text{ ft}}^0 \delta dp$, assuming 328 feet, 100 metres (or about 100 decibars) as the depth of no motion. Different anomalies at two stations outside the mouth of the Fraser indicate a slope of the sea surface (0 decibars).

Freshet:

in this report, a freshet is defined as a discharge at Hope exceeding 100,000 cfs.

Harmonic analysis:

the observed tidal data are separated into a number of harmonic constituents. The analysis leads to amplitudes and phase relations, called harmonic constants, which subsequently are used for "harmonic prediction".

Hydraulic radius:

the cross-sectional area of the channel divided by the wetted perimeter (the portion of the perimeter where the wall is in contact with the fluid).

Hydrograph:

a graphical record of the daily discharge measurements.

Neap tide:

occurs shortly after a first or a third quarter of the moon and has the smallest range in half a lunar month.

Saltation load:

sediment which is transported by bouncing along the bed.

Semi-diurnal tide:

two complete tidal oscillations per day.

Spring tide:

occurs shortly after full or new moon and has the largest range in half a lunar month.

Suspended load:

sediment particles of a size comparable to those in the bed load, but which are kept in the flow area by turbulence, and occasionally fall to the bed.

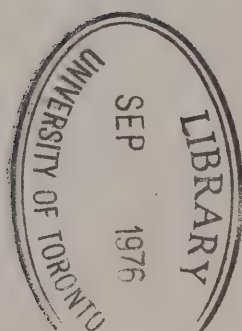
Wash load:

very fine particles which do not tend to settle out of suspension.

REFERENCES

1. Fraser River Board (1958). Report on flood control and hydro-electric power. Government of British Columbia, Victoria, B.C.
2. Hughes, G. and A. Ages (1975). Salinity and temperature measurements in the lower Fraser River. Pacific Marine Science Report 75-2, Institute of Ocean Sciences, Victoria, B.C.
3. Mathews, W.H. and F.P. Shepard (1962). Sedimentation of Fraser River Delta, British Columbia. Bull. Amer. Assoc. Petroleum Geologists 46: 1416-1443.
4. Pretious, E.S. (1969). The sediment load of the lower Fraser River. The University of British Columbia, Dept. Civil Engineering, Vancouver, B.C.
5. Luternauer, J.L. and J.W. Murray (1973). Sedimentation of the Western Delta-front of the Fraser River. Can. J. Earth Sci. 10(11): 1642-1663.
6. Pretious, E.S. (1972). Downstream sedimentation effects of dams on the Fraser River, B.C. The University of British Columbia, Dept. Civil Engineering, Vancouver, B.C.
7. Pretious, E.S. and E. Vollmer (1959). Final report on plans for reduction of shoaling and for improvement of the Fraser River at New Westminster, B.C. FRM 232, The University of British Columbia, Vancouver, B.C.
8. Fraser River Harbour Commission (1973). Sixth Annual Report, New Westminster, B.C.
9. Fraser River Harbour Commission (1974). Deep Sea Shipping Report, New Westminster, B.C. (December).
10. Kavanagh, Capt. J.W., Port Manager - personal communication.
11. Neu, H.J.A. (1966). Proposals for improving flood and navigation conditions in the lower Fraser River. Unpublished manuscript, National Research Council of Canada, Ottawa.
12. Crookshank, N. (1971). A one-dimensional model of the lower Fraser River. National Research Council of Canada, LTR-HY-14, Ottawa.
13. Defant, A. (1961). *Physical Oceanography*. Permagon Press, New York.
14. Crean, P.B. and A. Ages (1971). Oceanographic records from twelve cruises in the Strait of Georgia and Juan de Fuca Strait, 1968. Environment Canada, Marine Sciences Branch, Victoria, B.C.
15. Dronkers, J.J. (1964). *Tidal Computations*. North Holland Publishing Co., Amsterdam.

16. Ages, A. (1973). A numerical model of Victoria Harbour to predict tidal response to proposed hydraulic structures. Pacific Marine Science Report 73-3. Environment Canada, Marine Sciences Branch, Victoria, B.C.
17. Richtmyer, R.D. and K.W. Morton (1967). *Difference Methods for Initial-Value Problems*. Wiley, New York.
18. Water Survey of Canada (1969-1972). Surface water data, British Columbia. Environment Canada, Inland Waters Branch, Ottawa.
19. Ippen, A.T. (1966). *Estuary and Coastline Hydrodynamics*. McGraw-Hill, New York.
20. Taylor, G.I. (1919). Tidal friction in the Irish Sea. Proc. Roy. Soc. Vol. CCXX: 1-93.
21. Elchuck, D., Area Engineer, Water Survey of Canada, New Westminster, B.C. - personal communication.
22. Chang, P. (1976). Subsurface currents in the Strait of Georgia, west of Sturgeon Bank. MSc Thesis, Institute of Oceanography, The University of British Columbia, Vancouver, B.C.

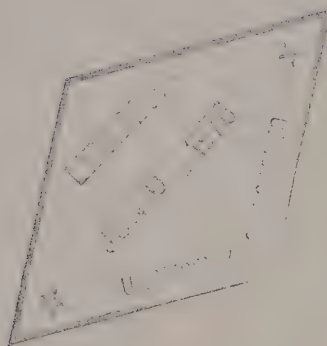


Government
Publications

CAI EP 321
-76R06

**OBSERVATIONS OF CURRENTS, BOTTOM PRESSURES AND
DENSITIES THROUGH A CROSS – SECTION OF
JUAN DE FUCA STRAIT**

by



D.B. Fissel and W.S. Huggett

**INSTITUTE OF OCEAN SCIENCES, PATRICIA BAY
Victoria, B.C.**



For additional copies or further information, please write to:

Environment Canada

Institute of Ocean Sciences, Patricia Bay

512 - 1230 Government Street

Victoria, B.C.

V8W 1Y4

Pacific Marine Science Report 76-6

OBSERVATIONS OF CURRENTS, BOTTOM PRESSURES AND
DENSITIES THROUGH A CROSS-SECTION OF
JUAN DE FUCA STRAIT

by

D.B. Fissel and W.S. Huggett

Institute of Ocean Sciences, Patricia Bay
Victoria, B.C.

March, 1976

This is a manuscript which has received only limited circulation. On citing this report in a bibliography, the title should be followed by the words "UNPUBLISHED MANUSCRIPT" which is in accordance with accepted bibliographic custom.

TABLE OF CONTENTS

	<u>Page</u>
1. Introduction-----	1
2. Observation Program-----	1
a. Currents and Bottom Pressures-----	1
b. STD Observations-----	2
c. Weather Data-----	2
3. Instrument Description-----	3
4. Data Processing-----	4
5. Current Meter Observations-----	5
a. Current Meter Depth-----	5
b. Currents-----	7
c. Temperature-----	9
d. Salinity-----	10
6. Bottom Pressures-----	10
7. Winds and Air Pressure-----	11
8. Water Properties-----	11
9. Summary-----	12
10. Acknowledgements-----	13
11. References-----	14

1. Introduction

Continuous records of currents, bottom pressures, winds and air pressure were obtained in Juan de Fuca Strait from late May to mid-July 1975. For two periods, at the beginning and midway through the observation program, measurements of salinity and temperature were obtained in the vicinity of the current meter locations.

The primary purpose of these measurements was to investigate the relationship between the currents flowing through the strait to the difference in bottom pressures across the strait. A close correspondence between these two quantities would provide a method for computing the currents from pressure measurements made on opposite sides of the strait. Computation of the currents could then be incorporated into an "on line" water level measurement system (Godin, 1975) to provide an instantaneous record of the velocities. The analysis of the data for this purpose is underway and the results will be presented in a later report.

Since Juan de Fuca Strait is an important waterway for commercial navigation, fisheries and recreational boating, the summary of the data presented here may be useful for future investigations or for solving oceanographic and coastal engineering problems related to the strait.

2. Observation Program

a. Currents and Bottom Pressures

The system used to differentiate between the various current meters and bottom pressure gauges was: - all current meter stations had a three number prefix starting with 13_, and the meters at each station had a three number code signifying their depth at that station. e.g. 136020 (the current meter at 20 m depth at station 136). All bottom pressure gauges were labelled TG followed by a number denoting the station (figure 1). At stations 130, 136 and 137 bottom pressure gauges were attached to the anchors at those stations, and were labelled TG6, TG8 and TG7 respectively.

The current meters and bottom pressure gauges were installed between May 26 and May 28, 1975 using the MV Pandora II and the CSS Richardson. Radar was used to fix the stations position in most cases with the exceptions of Stations TG1, TG3, TG4 and TG5, which were located by transits (Figure 1). In this study, all current meters and bottom pressure gauges were placed at one of two depths; approximately 20 m or 120 m below low water level.

Eight current meters and four bottom pressure gauges were used in a cross-sectional array between Sheringham Point and a point two miles west of Pillar Point (Figure 2). One current meter at 20 m depth and bottom pressure gauges at 20 m and 120 m were deployed in the vicinity of a shallow shelf off Jordan River (Stations 137 and TG2). Another bottom pressure gauge was

installed at approximately 20 m depth 4 miles west of Pillar Point on the south side of the strait (Station TG4) and the last off San Juan Point (Station TG5).

The mooring system used for Stations 130, 136 and 137 is illustrated in Figure 3. At Stations 131, 133 and 135 a second Aanderaa current meter and float were attached 100 m below the upper meter and no bottom pressure gauges were used. Recovery of the instruments was facilitated by acoustic releases triggered by a command from a shipboard transponder. The shallow-water TG stations consisted of a bottom pressure gauge mounted in a hole in a cement block anchor. An acoustic pinger, attached to the handle of each gauge allowed divers to locate and recover the instrument using a portable direction finder.

All but one station were recovered by personnel working off the CSS Richardson and the Canadian Hydrographic Service launch Brisk during the period July 10 to July 15, 1975. At Station 130 the acoustic release responded but failed to release. On August 13, divers working off the CSS Richardson attached a line with a surface float to the top of the mooring and the entire mooring was then pulled aboard the charter vessel Seatech II on August 16, 1975.

The names of the ships and personnel participating in the program are given in Table 1.

b. STD Observations

The measurements of salinity and temperature were made from the Pandora II during the periods of May 26-28, 1975 and June 14-15, 1975 using a Series 8700 Guildline Salinity Temperature Depth Recorder (STD). Surface and subsurface water samples were also collected and analyzed as a check on the STD measurements.

Five stations (shown in Figure 1) were occupied for STD measurements. From the May 26-28 period, a total of 26 STD casts were made at night and from the June 14-15 cruise, 43 STD casts were made sequentially at the cross-strait stations (S1, S2, S3, S4, S3, S2, S1, etc.) over a 25 hour tidal cycle. A summary of the times and locations of the STD casts is given in Table 2.

c. Weather Data

The only available meteorological measurements taken in this part of Juan de Fuca Strait are hourly wind measurements at the Sheringham Point Lightstation. A barograph and anemometer were borrowed from the Atmospheric Environment Service, Vancouver to provide additional data. The barograph was installed at the Sheringham Point Lightstation while the anemometer was installed at the U.S. Coast Guard's lightstation at Slip Point. The barograph operated from 1200 May 18 to 1100 July 28, 1975 (Pacific Standard Time) and the anemometer functioned from 1100 June 5 to 1300 July 24, 1975. The Sheringham Point wind data was

supplied by Victoria Marine Radio, Sooke, B.C., for the period 0000 May 26 to 2300 July 31, 1975.

3. Instrument Description

All current measurements were made with the Aanderaa Model 4 current meter, sampling at 15 minute intervals. These instruments measure currents ranging in speed from 1.5 to 250 cm/sec by counting the number of revolutions of a Savonius rotor. While the manufacturer does not specify the accuracy of speed measurements, comparisons with other current meters indicate generally good performance (Unesco, 1969; Ramster and Howarth, 1974). The direction measurements are specified to be accurate to ± 5 degrees and the compasses were calibrated before being used. All the current meters had the capability of measuring temperature (accurate to $\pm 0.1^{\circ}\text{C}$) and some were equipped to measure pressure (accurate to $\pm 1\%$ of range) and conductivity (no accuracy specified). The calibrations of temperature, conductivity and pressure are supplied by the manufacturer.

The bottom pressures were measured by using Aanderaa Model TG-2A water level gauges. The gauges were calibrated by the manufacturer, just before and just after the field work. For this study two different transducer ranges were available: 0-45 psi (0-31 dbar) used at Stations TG1, TG2 and TG3, or 0-400 psi (0-276 dbar) used at Stations TG4, TG5, TG6, TG7 and TG8. According to the manufacturer, these instruments have an accuracy of $\pm 0.01\%$ of full range and a resolution of 0.001% of full range. The accuracy of the 0-31 dbar and the 0-276 dbar gauges would then be 0.31 mbar and 2.8 mbar respectively. However, it should be noted that the accuracy of the calibration technique in use at Aanderaa Instruments at that time is estimated to be accurate only to about ± 2 mbar.

The data was recorded sequentially every 15 minutes and 30 minutes for the current meter and bottom pressure gauges respectively. The time was measured by a quartz crystal clock, whose average loss or gain was only 40 seconds, with the largest difference being 2 minutes. The current meter at 131020 (station #, nominal depth) was missing one record, which was apparently lost between the time the instrument was started and the time it was placed in the water. The bottom pressure gauge at Station TG2 was missing two readings, apparently lost between the time the gauge was removed from the water and the time the instrument was stopped. The gauge at Station TG8 had one duplicate reading missing at the beginning of the record. The bottom pressure gauges have selectable integration times and for this experiment a 15 minute integration time was used.

The Guildline STD measures temperature, conductivity and pressure, and computes the salinity from these measurements. The instrument has a specified accuracy of $\pm 0.04^{\circ}/\text{oo}$ for salinity $\pm 0.01^{\circ}\text{C}$ for temperature and ± 0.5 m for depth. A comparison of the salinities measured by the STD and those measured from samples gathered by bottles at depth, or bucket samples at the surface, show the STD to be reading high by $0.03^{\circ}/\text{oo}$ at the surface and $0.06^{\circ}/\text{oo}$ at 150 m depth. These

differences are consistent with similar comparisons made aboard the weather ship CCGS Quadra using the same STD unit. Salinities were corrected as follows: $S = S_{STD} - .0002 \cdot D(m) - .03(^{\circ}/_{\text{oo}})$.

A comparison of the temperatures determined from a reversing thermometer on the bottle attached immediately above the STD unit with those of the STD show a considerable amount of scatter ($\pm .06^{\circ}\text{C}$). The difference is at least partly attributable to the wire angle being increased as the ship makes leeway due to the wind and thus continuously reduces the depth from the time of reaching maximum depth to the triggering of the thermometer. This effect is greater for temperature than salinity, because in the deeper water the temperature gradients are larger than salinity gradients. Because of the larger amount of scatter, temperature corrections were based on the corrections determined from the Quadra cruise 75-002 to Ocean Weather Station P before the Juan de Fuca experiment.

4. Data Processing

The Aanderaa current meters and bottom gauges both record the data in digital form on 1/4" magnetic tapes. These tapes are translated onto a 9 track computer compatible tape, plotted and then examined for any missing or erroneous values. The incorrect values are summarized in Table 3. These values were usually replaced by means of linear interpolation but in a few cases, where a long sequence of data was found to be incorrect, the values were set to the mean value of that quantity.

The signal which consistently showed the most errors is the current direction, and these errors are easily located as single point spikes on the plots of the cross-strait component of the currents. These anomalous values occur usually during the times the current is turning from flood to ebb or ebb to flood, and fewer errors are found at 120 m depth than at 20 m depth. Such errors are probably the result of movement in the mooring induced by surface wave motions.

To determine the current speed, the difference in the number of rotations of the rotor between the present recording time and the previous recording time must be known. On the older model current meters (serial numbers 506, 507, 736, 838, 839) the number of rotor counts is recorded, while on the later models, the counter resets to zero each time. On the older models, because of a dead spot in the potentiometer driven by the rotor, spurious readings result when this dead spot is sampled. These latter readings account for almost all the erroneous current speed data with the exception of the data from the two current meters at Station 133.

Hereafter, individual current meters will be designated by a six digit number: the first three digits represent the station location and the last three digits are the nominal depth in metres.

The upper current meter at Station 133020 has a gap in the data from 0900 June 30 to 0030 July 1 (all times are Pacific Standard), apparently the result of a recording problem. The records of current

speed and direction were beyond recovery and were set to their mean values. However, the temperature data was recovered. The lower current meter recorded no speed data as the rotor was broken off, probably while the mooring was being lowered into position.

The pressure data recorded by the current meter at Station 136020 were obviously incorrect (apparent depths ranged from above surface to greater than 100 m) from 1315 June 2 to 0345 June 21. The entire pressure record at Station 135120 was faulty due to the pressure orifice being partially plugged.

The temperature data records had few errors (10 or less) except for the measurements at Station 136020. The instrument used here showed large fluctuations when compared with other instruments. The criteria used for rejecting single point spikes was 0.3°C or more, except at Station 136020 where only spikes greater than 0.7°C were removed.

From the corrected speed and direction data, the "up-strait" and "cross-strait" components of the currents were computed. The positive up-strait component is 112°T , and the positive cross-strait current is 022°T .

The wind and air pressure data records are very nearly complete. Only one wind measurement reading is missing from the hourly records at Sheringham Point, and two from those at Slip Point. The air pressure record at Sheringham Point is missing 36 readings. All missing readings were replaced by values determined through linear interpolation.

The bottom pressure data has few errors except for a gap in the data at Station TG6 where the instrument malfunctioned between 0030 June 30 and 1600 July 2. This data was replaced by the mean value.

The STD data in the form of analog temperature and salinity profiles on chart paper were machine digitized using a Hewlett Packard Model 9864A Digitizer. Any anomolous features in the profiles were not digitized. It is estimated that errors introduced from digitizing the data are less than 0.01°C and $0.01\text{ }^{\circ}/\text{oo}$ in the temperature and salinity respectively.

5. Current Meter Observations

a. Current Meter Depth

For each current meter that had a pressure sensor, the depth of the meter (Figure 4) was computed by taking one metre of water to be equivalent to 1.005 decibars (see Figure 4). The mean depths from the pressure records are noticeably different in some cases from the nominal depths calculated from the depth of water and the amount of wire used. Station 135020, for example was found to have a mean depth of 12.0 m versus a nominal depth of 20 m while 136020 had a mean depth of 29.4 m versus a nominal depth of 20 m.

The depths of the current meters were increased by the action of tidal currents pulling the moorings away from the longer moorings. The spring-neap tidal cycle is very conspicuous in the pressure records, since the drag on the moorings is approximately quadratic in the speed of the current and thus the smaller neap currents have less effect compared to the larger spring currents. At all stations the largest excursions in depth occurred around July 10. On that date at Stations 130, 131 and 135 the maximum deviation of the mooring from the vertical was 39° , and at Stations 136 and 137, the deviations were 28° and 26° respectively. At Station 133, since the depth is similar to that of 135, we can assume the responses of the moorings will also be similar.

The effect of the mooring tilt on the current measurements can be discussed only in qualitative terms. The current meters will not tilt as much as the moorings because of stabilizer fins attached to the direction vane which tend to keep the current meter aligned with the vertical. However, the spindle of the current meter is so designed that it can tilt only 30° with respect to the mooring, and the allowable tilt of the current meter is 10° before any changes in the response are noted. Therefore, the current meters should have remained within 10° of the vertical at the times of the strongest currents provided that the stabilizer fins were effective. Further investigation of this effect is needed, but it is beyond the scope of this study.

Another effect of the change in meter depth on the current measurements is that the measured currents will vary according to the vertical shear in the currents. A calculation for the 24 hour period on July 10 (which should be close to an extreme case) was made of the mean shear between currents at the top and bottom positions at Station 131. From the mean shear we can estimate the difference between the current at the actual depth and the nominal depth. A maximum difference of 18 cm/sec (at 0945 PST) was found in the 15 minute averaged current for the upper current meter (131020). The change in the daily mean up-strait (flood) current is 0.9 cm/sec. These results must be regarded as tentative as the actual shear may differ considerably from the mean shear, particularly in the near surface levels.

Moorings motions induced by wave action will cause increased variability in the direction measurements. Gould and Sambuco (1975) have shown at a mid-ocean location, that these mooring motions also result in artificially high current speeds when surface buoy moorings are used. However, the use of sub-surface moorings in this study should reduce errors of this type.

b. Currents

Time series of the currents are displayed in Figure 5 in the form of up-strait and cross-strait current components. Table 4 summarizes the basic data while joint frequency distributions of the speed and direction are presented in the Appendix. In discussing the currents it is useful to compute the power or auto-spectra of the time series, and from this determine the scales at which important motions occur. The spectral density estimates were calculated using the method of Jenkins and Watts (1968) from Fast Fourier Transform values computed from an algorithm devised by Singleton (1969). The spectra were all computed from a common 45 day (4320 data points) time series beginning 0000 PST May 28 and from which the mean and linear trends were removed. To improve the statistical reliability each estimate had 10 degrees of freedom and a band width of 0.111 cycles/day.

The character of the currents is examined by computing the rotary power spectra (Figures 6 a, b and c). The rotary spectrum shows the contributions to the variance from the two oppositely rotating vectors for each discrete frequency band (Pillsbury, 1972). As an aid to interpreting the rotary spectra, consider the following examples: If the clockwise part of the spectrum is zero and the anti-clockwise part is non zero, then the currents over that frequency band are circular, rotating anti-clockwise. If the clockwise and anti-clockwise spectral values are equal, the current motion is then linear (i.e. the rotating vector tip traces out a straight line).

The rotary spectra are dominated by peaks at the diurnal and semi-diurnal tidal frequencies with smaller peaks present at the higher tidal frequencies (around 3, 4, 5 and 6 cycles/day). Relatively high activity is found in the lower frequency bands centered at a frequency of 0.067 cycles/day corresponding to a period of 15 days. The spectral levels are generally lower over all frequencies at the deeper stations than at the near surface stations.

The clockwise and anti-clockwise spectral values are the same, within statistical limits, at the semi-diurnal and diurnal peaks and at the low frequency end of the spectrum. Thus at these frequencies, the motion is linear rather than rotary. At the higher frequency tidal peaks, there are more pronounced differences between the clockwise and anti-clockwise spectra, with the clockwise values being significantly larger. There is no evidence of a significant peak in the clockwise spectrum at the inertial frequency (1.46 cycles/day) at any of the stations.

In the following discussion we will present some features of the currents at tidal frequencies based on the results of the spectral analysis. A harmonic analysis, not reported here, is in agreement with the results of the spectral analysis.

The semi-diurnal and diurnal tidal peaks account for

86% of the total variance at the near surface stations and 94% of the total variance at the deeper levels. With two exceptions, the semi-diurnal spectral values are nearly twice as large as the diurnal values, corresponding to a ratio of the current amplitudes of 1.4. One exception occurs at Station 137020 where the strength of the diurnal peak is abnormally large in comparison with the other stations, and the other exception occurs at Station 136020 where the strength of the semi-diurnal peak is considerably smaller than at any other near surface location. No attempt will be made to explain these apparent anomalies other than to point out that both stations are located in places of atypical bathymetry; Station 137020 is immediately adjacent to a broad shallow shelf, and Station 136020 is located off a sharp rise to the southern side of the strait.

A comparison of the up-strait and cross-strait currents was made by computing their respective power spectra (Figure 7). At the diurnal and semi-diurnal tidal frequencies the spectral levels of the cross-strait currents are smaller than the up-strait levels by factors ranging from 12.5 to 300 (corresponding to ratios in the amplitude of the currents from 3.5 to 17). The spectral levels are also smaller near the sides of the strait where the frictional boundary influence is stronger. Similarly, a comparison of the spectral levels at the lowest frequencies shows that there is considerably less activity in the cross-strait component than the up-strait component. However, at higher frequencies (>3.0 cycles/day) the activity in the up-strait and cross-strait components is comparable. At these frequencies the horizontal scales of the motion are apparently small enough to be unaffected by the boundary influence.

The low frequency (or residual) currents are presented in more detail by computing the progressive vector diagrams (Figure 8). These diagrams show the characteristic net outflow in the near surface layer, which consists of lower density water from river discharges into Puget Sound and the Strait of Georgia, and a compensating net inflow in the deeper layer of denser open ocean water (Herlinveaux and Tully, 1961). There are significant variations in the residual current across the strait. In the deeper layer the data shows that the inflow is markedly stronger on the south side than on the north side, (see Table 4), and this is supported by earlier results obtained in 1973 (Huggett, 1976). In the near surface layer the data shows that the net outflow is also stronger on the south side of the strait, but the difference is not as marked. The net outflow is reduced at those stations near the sides of the strait (130020, 136020 and 137020).

At most stations the net flow is in a direction nearly parallel to the sides of the strait. However, at Station 133020, and to a lesser degree at Station 131020, the residual flow is more nearly westward (i.e. it has a negative cross-strait component) which may be a continuation of the westward currents

found in the vicinity of Race Rocks. Station 137020 shows a weak residual current moving outwards and towards the centre of the strait. Here the flood current tends to be parallel to the sides of the strait, but the ebb current has a distinct cross-strait component.

The residual flow (the remaining current after the diurnal and semi-diurnal tidal currents have been removed) shows very few reversals in direction. However, the flow is far from uniform, often stalling almost completely for several days at a time. In a few cases, especially when the flow is unusually weak or unusually strong, features seem to occur simultaneously in all near surface current records. For example, a strong outflow occurred on days July 2 to July 6, 1975 (183-187). More often there appears to be little correlation between the residual currents at each station. For example, on days May 30 to June 2, 1975 (150-153), a stronger than average outflow was present at Stations 135020 and 133020, but at Stations 130020, 131020 and 136020, the outflow was below average.

c. Temperature

All the current meters were equipped with temperature sensors, and the time series plots of the temperatures are shown in Figure 9. The temperature spectra (Figure 10) were computed using the same analysis techniques as those used for the current spectra (see Section 5b).

In the near surface layers the temperatures have an average value between 8.0° and 9.0°C , and the highest spectral levels were found in the lowest frequency band. These low frequency oscillations (period of about 15 days) have an amplitude of 0.2° to 0.35°C and are in phase at all the near surface stations. These oscillations may be a result of increased tidal mixing at times of spring currents, particularly in the passes and over the sills connecting Juan de Fuca Strait with the Strait of Georgia. The increased mixing raises the temperature of the water in the upper layers, through the mixing of warm surface waters downwards. The time delay of about 10 days between the maximum temperatures and currents is apparently the time of transit for the water to be carried by the net flow to the observation positions. As the distance between the stations of this study and mixing sites is about 55 nautical miles, the average drift speed is about 12 cm/sec.

At higher frequencies, the largest spectral peaks occur at the diurnal and semi-diurnal tidal frequencies probably the result of mooring motions and the horizontal advection of water of different temperatures by diurnal and semi-diurnal currents.

An anomalous feature occurs at Station 136020 where the semi-diurnal peak is considerably larger than at any other

station. There is no apparent reason for this.

The temperatures measured at the deeper stations have average values of 6.3° to 6.6°C. At these depths, the variation of all frequencies is much smaller. At Stations 131120 and 133120, the temperature record shows sudden increases of up to 0.5°C, which may be due to faulty instrument response on recording.

d. Salinity

Only one of the current meters (136020) was equipped with a conductivity sensor. Using Perkins and Walker algorithm (1972), the salinity was computed from the measured conductivity, temperature and pressure (Figure 11). While the accuracy is not specified for the conductivity measurements, the least count resolution is 0.08 mho/cm, corresponding to a salinity difference of 0.09‰ at a constant temperature of 8°C. A comparison of the salinity at Station 136020 with those recorded by the STD at Station S-4 at 29 m depth on July 14-15 gave differences of ± 0.29 ‰. Some of this difference may be attributed to the spatial variability in the salinity field.

The measurements showed that the salinity ranged from 30.5 to 33.4‰ with two notable exceptions. These exceptions occurred on July 12 and July 13 when the salinity abruptly dropped to 29.5‰. The salinity, like the temperature at 136020, showed a considerable semi-diurnal variation.

6. Bottom Pressures

The bottom pressures are shown in Figure 12 and their statistics are summarized in Table 5. Spectra were computed for each bottom pressure record (Figure 13) using 2058 samples beginning 0000 May 29. Each spectral estimate has 10 degrees of freedom and a band width of 0.117 cycles/day.

The bottom pressures are dominated by the diurnal and semi-diurnal tidal variations. While there is some tidal activity at higher frequency, the peaks near 3.0, 4.0, 5.0 and 6.0 cycles per day are three orders of magnitude smaller than the diurnal and semi-diurnal peaks. The lowest frequency (period of 14.3 days) spectral value shows some energy, typically in the order of $.006 \text{ (m/sec)}^2/\text{day}$ corresponding to an average range of 7.5 millibars.

The strengths of the diurnal and semi-diurnal tidal peaks vary with respect to both the up-strait and cross-strait positions (Figure 14). The diurnal spectral values increase as one proceeds up the strait. The diurnal range (computed as $2 \cdot (2 \cdot \phi \Delta f)^{1/2}$ where ϕ is the spectral estimate) increases from 1.09 dbar at Station TG5 to 1.28 dbar at Station TG2 to 1.31 dbar at Station TG1. In contrast, the amount of semi-diurnal activity decreases from 1.43 dbar at Station TG5 to 1.08

dbar at Station TG2 to 1.00 dbar at Station TG1. The cross-strait differences are smaller but a comparison of spectral levels shows that the range at both the semi-diurnal and diurnal tidal peaks is consistently larger on the south side of the strait. For example, the diurnal range is 0.06 dbar larger at Station TG3 than at Station TG2 and the corresponding difference in the semi-diurnal range is .016 dbar.

7. Winds and Air Pressure

The wind at Sheringham Point and Slip Point along with the air pressure at Sheringham Point are shown in Figure 15, and the basic statistics relating to these data are included in Table 5. Spectra of the winds and air pressure (Figure 16) were computed following the procedure discussed in Section 4. The spectra of the Sheringham Point winds and air pressures are computed from a 45 day record beginning 0000 May 28, 1975 while the Slip Point wind spectra are computed from a 30 day record beginning 1100 June 5, 1975.

The air pressure record is dominated by low frequency variations (periods greater than 3 days). At these lower frequencies, the spectral levels are comparable to those of the bottom pressures. However, the spectral values of the air pressure drop off very rapidly as the frequency increases. The air pressure spectrum reveals that small, but statistically significant, oscillations occur at 1.0 cycle/day and 2.0 cycles/day amounting to an average range of 1.2 mbar and 0.4 mbar, respectively.

The winds measured at the shore stations reflect the local character of the stations, and are not always representative of the winds over the open water of the strait. A comparison of the winds measured aboard the MV Pandora II from a mast approximately 15 m above sea level during June 14-15 with those taken at Sheringham Point and Slip Point shows the following discrepancies: at Sheringham Point the wind is more from the west (270°T) while in the open strait, the wind tends to be parallel to the shores (290°T). At Slip Point, the wind speed is reduced by a factor of 2 from that observed in mid-strait. Such discrepancies indicate the importance of taking wind measurements over the open water rather than relying on land based measurements.

The spectra of the wind show more activity at low frequencies ($f < 1.0$ cycle/day) and, compared to the spectra of the air pressure, there is appreciable activity over all frequencies. The up-strait wind component has spectral levels that are generally an order of magnitude larger than those of the cross-strait wind. A significant peak occurs at a period of one day with a strength of $14.7 \text{ (m/sec)}^2/\text{day}$ at Sheringham Point corresponding to an average daily range of 3.6 m/sec.

8. Water Properties

The water properties across the strait will be described from the STD casts taken on the cruises of May 26-28 and June 14-15. Densities are computed from the temperature, pressure and salinity measurements using Knudsen's formula (Fofonoff, 1962). From the computed values of the June 14-15 cruise, Figure 17 shows the average of the profiles taken

at Station S-2 of the three quantities, temperature, salinity and density (σ_t). The horizontal lines show the standard deviation of the readings at that depth. From this figure a pycnocline is discernible down to about 110 metres with well mixed water above the pycnocline and nearly uniform water below. A considerable amount of variability in the individual profiles was found within the pycnocline probably due to internal wave motions and horizontal advection by the tidal currents.

Figure 18 shows the variation in density across the strait computed from the average density profiles at each station. Through the pycnocline the isopycnals slope upwards to the south (i.e. the water becomes more dense across the strait from north to south for both cruises). The observations over the June 14-15 period were made during a complete 25-hour tidal cycle thereby eliminating any bias of the averages due to tidal advection. On the other hand, the May 26-28 observations were made in the evenings during the times of a weak ebb current.

9. Summary

A continuous time series of currents and bottom pressures was made through a cross-section of Juan de Fuca Strait from late May to mid-July 1975. To augment this data set, observations of winds, air pressure, water temperature and salinity were also taken.

Current measurements were taken at two levels at five stations across the strait, at depths of 20 m and 120 m. Current speeds up to 150 cm/sec were observed. The current was dominated by the semi-diurnal and diurnal tidal motions with the in-going tidal current being considerably stronger than the cross-strait current by a factor ranging from 3.5 to 17. A net outflow was found at the 20 m depth and a net inflow at the 120 m depth. Considerable variation in the residual current was found at the different stations across the strait.

A time series of the water temperature recorded by the current meters showed a 15 day oscillation of 0.2 to 0.35°C at the 20 m depth. This is attributed to the spring-neap cycle of the tidal mixing in the narrow passes connecting Juan de Fuca Strait with Strait of Georgia. There was a time difference of 10 days from the time of maximum current to the time of maximum temperature, which is approximately the time required for the mean flow to carry the warmer well-mixed water to the observed cross-section of the strait.

The bottom pressures are dominated by semi-diurnal and diurnal frequencies to a much greater extent than the currents. Some activity was found at periods of about 15 days with a range of 8 millibars, which is equivalent to a variation of 8 cm in the water level. The diurnal tidal range increases up the strait while the semi-diurnal tidal range decreases. The tidal range is somewhat larger on the south side of the strait than on the north side with the difference in range amounting to 6 millibars for the semi-diurnal tide and 1.6 mbar for the diurnal tide.

10. Acknowledgements

Many people contributed to this work, especially the scientific personnel involved in the field work (Table 1), and the officers and crews of the research vessels. We are grateful to the Atmospheric Environment Service, Pacific Region, Vancouver, and especially Messrs. Don Faulkner and Frank Buchinski of that agency for lending us weather recording instruments. We also acknowledge the cooperation and assistance given by 13th U.S. Coast Guard District in granting us permission to make use of the Slip Point Lightstation for wind observations and Mr. J. Bruton of the Sheringham Point Lightstation, Ministry of Transport, who kindly operated the barograph during the experiment. Also Mr. A. Douglas, Tidal and Current Survey, who provided much valuable advice and assistance in the processing of the data. We are grateful to Mr. Cor de Jong, Offshore Oceanographic Group, for assistance with the STD and we express our sincere gratitude to Dr. R.E. Thomson, Offshore Oceanographic Group for many helpful discussions and unfailing assistance throughout all phases of the study.

11. References

- Fofonoff, N.P., 1962: Physical properties of sea water. The Sea, Vol. 1 ed. M.N. Hill Interscience Publishers, New York, pp 3-28.
- Godin, G., 1975: An improved system for water level measurements. Environment Canada, Marine Environmental Data Service, Tech. Note No. 5, 23 p.
- Gould, W.J., and Sambuco, E., 1975: The effect of mooring types on measured values of ocean currents. Deep-Sea Res., 22, pp 55-62.
- Herlinveaux, R.H. and J.P. Tully, 1961: Some oceanographic features of Juan de Fuca Strait. J. Fis. Res. Bd. Canada, 18(6), pp 1027-1071.
- Huggett, W.S., 1976: Current measurements in Juan de Fuca Strait, 1973. Environment Canada, Canadian Hydrographic Service, Tech. Report in preparation.
- Jenkins, J.M. and D.G. Watts 1968: Spectral Analysis. Holden-Day, San Francisco, 325 p.
- Perkins, R.G., and E.R. Walker, 1972: Salinity calculations from in situ measurements. J. Geophys. Res. 77 (33): pp. 6618-6621.
- Pillsbury, R.D., 1972: A description of hydrography, winds and currents during upwelling season near Newport, Oregon. Ph.D. Thesis, Oregon State University. 163 p.
- Ramster, J.W. and M.J. Howarth, 1974: A detailed comparison of the data recorded by Aanderaa Model 4 and Plessey MO21 recording current meters moored in two shelf-sea locations, each with strong tidal currents. Deutsche Hydrographische Zeitschrift, 28(1): pp. 1-25.
- Singleton, R.C., 1969: An algorithm for computing the mixed radix Fast Fourier Transform. IEEE Transactions on Audio and Electroacoustics, 17(2), pp. 93-103.
- Unesco, 1969: An intercomparison of some current meters. Unesco technical papers in Marine Science No. 11, 70 p.

TABLE 1

Cruise No.	Date(s)	Ship(s) (Master)	Object of Cruise	Personnel
75-1	May 26-May 28	MV Pandora II (R. Dickenson)	To install moorings at Stations 130, 131, 133, 135, 136 and 137 plus STD Stations	S. Huggett D. Fissel F. Hermiston M. Woodward D. Smith*
		C.S.S. Richardson (M. Wheeler)	To install bottom pressure gauges at Stations at TG1 TG2, TG3, TG4, TG5	F. Stephenson
75-2	June 14-June 15	MV Pandora II (R. Dickenson)	STD Stations on cross-strait line	D. Fissel B. Grasty A. Wier W. Bennett
75-3	July 10-July 11	C.S.S. Richardson (M. Wheeler)	Recovered gauges at TG5 and TG2	D. Fissel N. Fujino R. Tamasi
	July 14-July 15	C.S.S. Richardson (M. Wheeler)	Recovered instruments and moorings at Stations 131, 133, 135, 136, 137	S. Huggett F. Hermiston F. Otu**
	July 14-July 15	Launch Brisk	Recovered gauges at TG1, TG3 and TG4	D. Fissel N. Fujino R. Tamasi
75-4	August 13	C.S.S. Richardson (M. Wheeler)	Attached line and surface float to the top of moor- ing 130	S. Huggett F. Hermiston M. Woodward J. Galloway

TABLE 1 (continued)

Cruise No.	Date(s)	Ship(s) (Master)	Object of Cruise	Personnel
75-4	August 16	Seatech II (J. Dobrocky)	Pulled up mooring at Station 130	M. Woodward D. Fissel

* Student, University of Washington, Seattle, Washington

** Visiting Hydrographer, Nigerian Ports Authority, Lagos, Nigeria

TABLE 2Times and Locations of STD CastsCruise 75-1

Times are given as hours: minutes/date of May 1975.
All times are Pacific Standard (PST).

	<u>S1</u>	<u>S2</u>	<u>Stations</u> <u>S3</u>	<u>S4</u>	<u>S5</u>
1.	20:25/26	20:51/26	22:00/26	22:55/26	19:35/26
2.	00:52/27	00:15/27	23:40/26	16:25/27	13:55/27
3.	14:30/27	15:10/27	15:40/27	21:30/27	
4.	18:02/27	17:36/27	17:00/27	01:23/27	
5.	19:50/27	20:31/27	20:57/27		
6.	23:26/27	22:35/27	22:06/27		
		00:05/28	00:42/28		

Cruise 75-2

Times are given as hours: minutes/date of June 1975.

	<u>S1</u>	<u>S2</u>	<u>Stations</u> <u>S3</u>	<u>S4</u>
1.	10:45/14	11:25/14	11:48/14	12:28/14
2.	14:37/14	13:57/14	13:20/14	16:21/14
3.	18:15/14	15:27/14	15:47/14	20:15/14
4.	22:08/14	17:33/14	17:00/14	00:11/15
5.	01:53/15	19:00/14	19:38/14	03:44/15
6.	05:23/15	21:30/14	20:46/14	06:59/15
7.	08:33/15	22:42/14	23:29/14	10:38/15
8.	12:22/15	1:17/14	0:44/15	
9.		2:29/15	3:05/15	
10.		4:42/15	4:14/15	
11.		5:49/15	6:28/15	
12.		8:05/15	7:30/15	
13.		9:32/15	10:08/15	
14.		11:48/15	11:07/15	

TABLE 3

Summary of Incorrect Time Series Data

A. Current Meter Data

Station (Station #, depth)	No. of Readings	T	C	P	θ	U
130020 Serial #1603	7871	10	N	0	33	0
131020 Serial #1606	4677	1	N	2	33	3
131120 Serial #1605	4677	0	N	0	27	0
133020 Serial #839	4598	5	N	N	274	252
133120 Serial #838	4598	3	N	N	*	*
135020 Serial #507	4617	3	N	0	59	52
135120 Serial #506	4617	3	N	*	27	41
136020 Serial #736	4718	32	0	1786	80	33
137020 Serial #1604	4682	0	N	0	31	0

N - not recorded
 * - missing entire time series
 T - temperature
 P - pressure
 C - conductivity
 θ - direction
 U - Speed

TABLE 3 (continued)B. Bottom Pressure, Wind and Air Pressure Data

Station Serial #	No. of Readings	No. of Incorrect Readings
TG1 #86	2387	3
TG2 #90	2204	0
TG3 #93	2310	2
TG4 #41	2312	13
TG5 #92	2101	2
TG6 #81	3800	143
TG7 #80	2341	0
TG8 #78	2358	1
Wind N	1608	1
Wind S	1176	2
Air Pressure	1704	36

TABLE 4. Statistics of data measured by moored current meters.
The sampling interval was 15 minutes.

	Temperature °C	Salinity ‰	Depth m	Speed cm/s	Up-Strait Current	Cross-Strait Current
Station 130020 - No. of Readings 7871 - Serial No. 1603						
First reading 1415 May 26 Last reading 1345 Aug. 16						
Mean	8.94	-	19.1	41.1	-9.8	1.4
Std. Dev.	0.57	-	3.4	28.0	47.6	10.4
Maximum	11.77	-	65.5	136.3	119.0	44.0
Minimum	7.59	-	15.1	2.8	-135.5	-46.8
Station 130020 - No. of Readings 4800 - Serial No. 1603						
First reading 1415 May 26 Last reading 1415 July 15						
Mean	8.70	-	19.4	41.4	-8.5	1.6
Std. Dev.	0.37	-	2.9	28.1	48.2	10.3
Maximum	10.53	-	38.3	136.2	118.1	33.3
Minimum	7.70	-	16.6	2.8	-135.5	-43.7
Station 131020 - No. of Readings 4677 - Serial No. 1606						
First reading 1845 May 26 Last reading 1130 July 14						
Mean	8.95	-	16.7	45.0	-14.0	-2.2
Std. Dev.	0.42	-	3.7	29.4	50.1	13.2
Maximum	10.51	-	40.8	153.1	118.5	61.0
Minimum	8.02	-	13.0	4.1	-150.7	-42.5

TABLE 4 (continued)

	Temperature °C	Salinity o/oo	Depth m	Speed cm/s	Up-Strait Current	Cross-Strait Current
Station 133020 - No. of Readings 4598 - Serial No. 839						
First reading 1930 May 27 Last reading 1645 July 14						
Mean	9.06	-	-	49.7	-22.3	-5.6
Std. Dev.	0.51	-	-	31.9	52.1	15.8
Maximum	10.97	-	-	152.5	109.0	74.3
Minimum	7.77	-	-	5.0	-151.8	-51.6
Station 135020 - No. of Readings 4617 - Serial No. 507						
First reading 1245 May 27 Last reading 1445 July 14						
Mean	8.83	-	11.9	48.6	-23.3	0.9
Std. Dev.	0.55	-	5.3	30.5	49.5	17.0
Maximum	10.56	-	47.3	150.5	107.9	59.6
Minimum	7.09	-	8.1	6.1	-149.6	-44.3
Station 136020 - No. of Readings 4718 - Serial No. 736						
First reading 0915 May 27 Last reading 1230 July 15						
Mean	8.14	32.39	29.2	36.4	-12.7	1.0
Std. Dev.	0.60	0.45	1.6	27.5	43.1	7.6
Maximum	10.53	33.42	40.2	145.0	101.4	29.5
Minimum	6.71	29.54	27.6	0.0	-143.5	-31.5

TABLE 4 (continued)

	Temperature °C	Salinity o/oo	Depth m	Speed cm/s	Up-Strait Current	Cross-Strait Current
Station 137020 - No. of Readings 4682 - Serial No. 1604						
	First reading 1645 May 26			Last reading 1130 July 14		
Mean	8.72	-	21.0	45.6	-4.7	-3.5
Std. Dev.	0.35	-	1.3	32.3	54.4	11.0
Maximum	10.56	-	29.3	148.8	128.0	33.3
Minimum	7.84	-	19.0	3.4	-146.9	-46.2
Station 131120 - No. of Readings 4677 - Serial No. 1605						
	First reading 1845 May 26			Last reading 1145 July 14		
Mean	6.44	-	119.6	37.7	5.9	-1.0
Std. Dev.	0.14	-	0.9	26.8	44.5	11.0
Maximum	7.48	-	126.5	122.1	120.9	36.8
Minimum	6.20	-	118.0	1.9	-107.5	-34.3
Station 133120 - No. of Readings 4596 - Serial No. 838						
	First reading 1930 May 27			Last reading 1645 July 14		
Mean	6.36	-	-	-	-	-
Std. Dev.	0.14	-	-	-	-	-
Maximum	7.05	-	-	-	-	-
Minimum	6.10	-	-	-	-	-

TABLE 4 (continued)

	Temperature °C	Salinity o/oo	Depth m	Speed cm/s	Up-Strait Current	Cross-Strait Current
Station 135120 - No. of Readings 4617 - Serial No. 506						
First reading 1245 May 27 Last reading 1445 July 14						
Mean	6.59	-	-	36.2	16.3	-1.0
Std. Dev.	0.15	-	-	26.4	40.8	8.2
Maximum	7.05	-	-	115.8	115.7	21.7
Minimum	6.20	-	-	0.0	-93.2	-31.6

TABLE 5. Statistics of bottom pressure, air pressure and wind data

Quantity	Starting Time	No. of Readings	Mean	Standard Deviation	Maximum	Minimum
TG1 Pressure	1500 May 26	2387	29.60	0.64	30.91	27.94
TG2 Pressure	1630 May 26	2199	28.90	0.65	30.24	27.23
TG3 Pressure	1030 May 27	2311	31.07	0.70	32.43	29.24
TG4 Pressure	0900 May 27	2312	28.76	0.70	30.10	26.90
TG5 Pressure	1230 May 28	2101	30.44	0.68	31.94	28.75
TG6 Pressure	1430 May 26	3800	128.06	0.62	129.37	126.24
TG6 Pressure	1430 May 26	2372	128.04	0.63	129.37	126.24
TG7 Pressure	1700 May 26	2341	130.89	0.65	132.20	129.16
TG8 Pressure	0930 May 27	2358	136.48	0.70	137.83	134.63
	Pressures in decibars.					
	Sampling rate - 30 min.					
Air Pressure	0000 May 26	1524	1017.6	15.0	1009.2	1029.6
	Sampling rate - 30 min.					
	Pressure in millibars.					
Sheringham Pt.						
Wind Speed	0000 May 26	1608	5.8	3.3	15.2	0.0
Up-Strait Wind	0000 May 26	1608	5.1	3.4	14.1	- 6.2
Cross-Strait Wind	0000 May 26	1608	2.1	1.5	6.4	- 7.5
	Sampling rate - 60 min.					
	Winds in m/sec.					
Slip Pt.						
Wind Speed	1100 June 5	1176	2.9	1.8	8.2	0.1
Up-Strait Wind	1100 June 5	1176	2.0	2.4	7.9	- 6.1
Cross-Strait Wind	1100 June 5	1176	0.1	1.4	6.3	- 5.2
	Sampling rate - 60 min.					
	Winds in m/sec.					

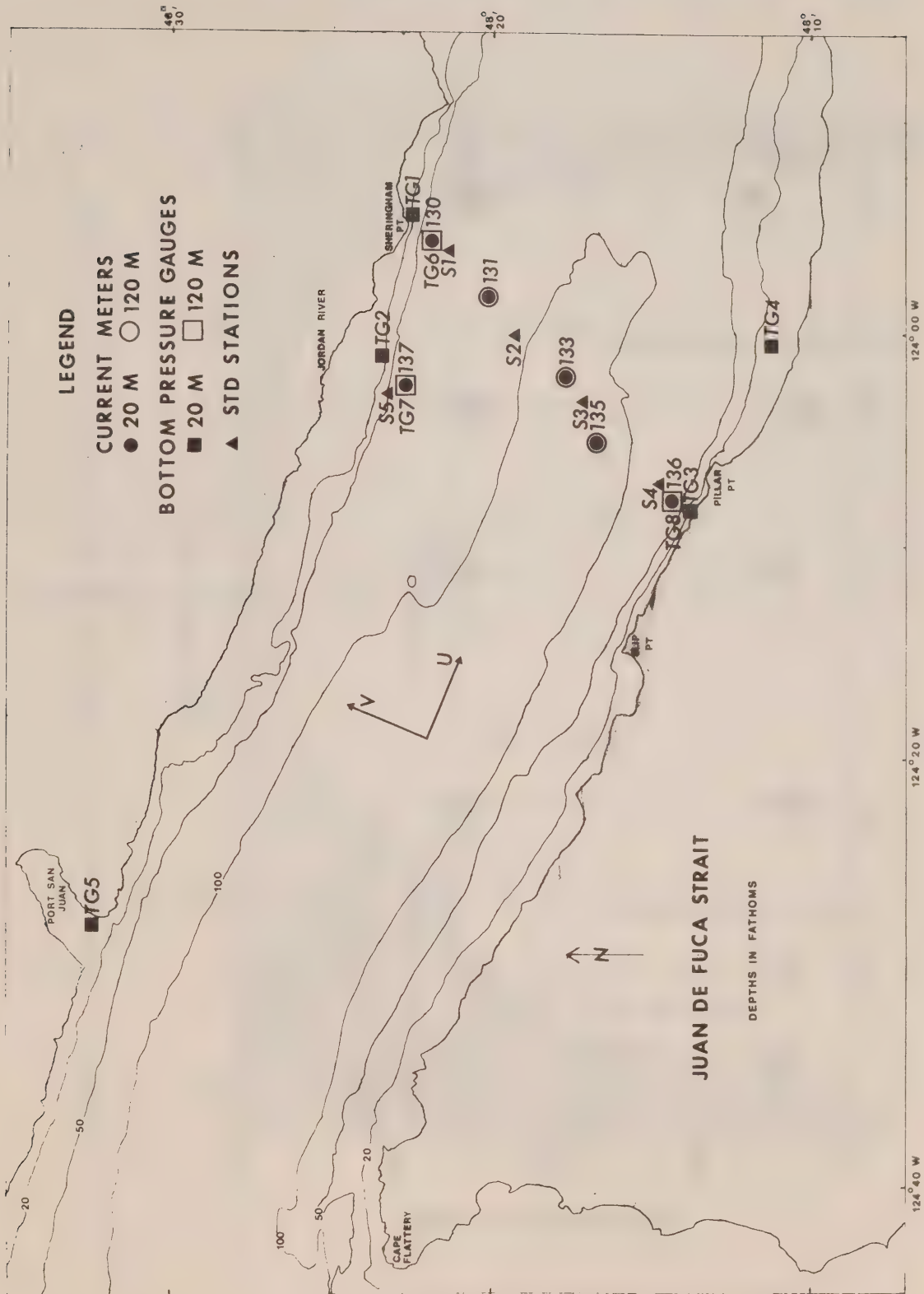


Figure 1: Location of stations in Juan de Fuca Strait.

SHERINGHAM PT. CANADA
PILLAR PT. U.S.

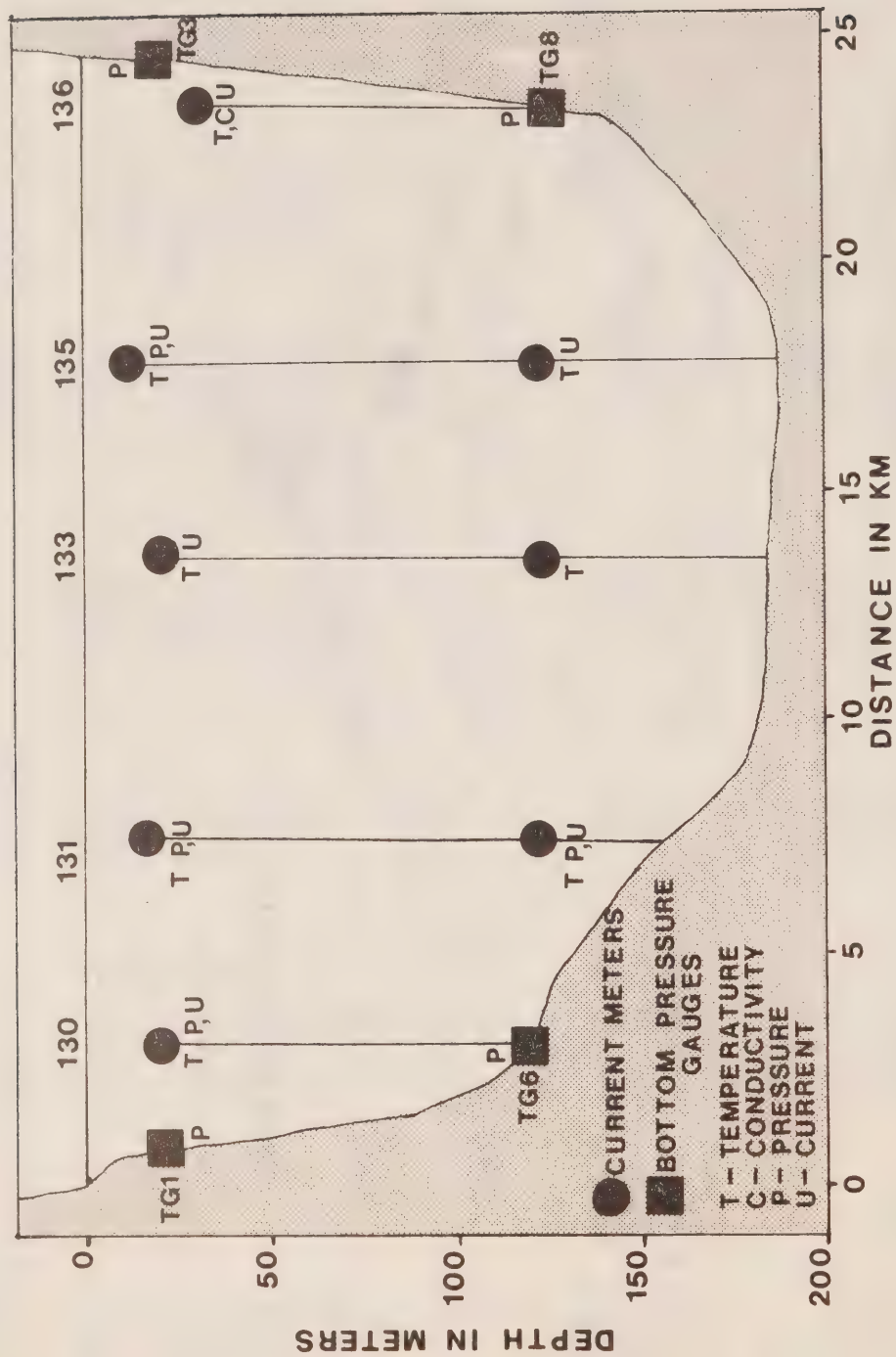
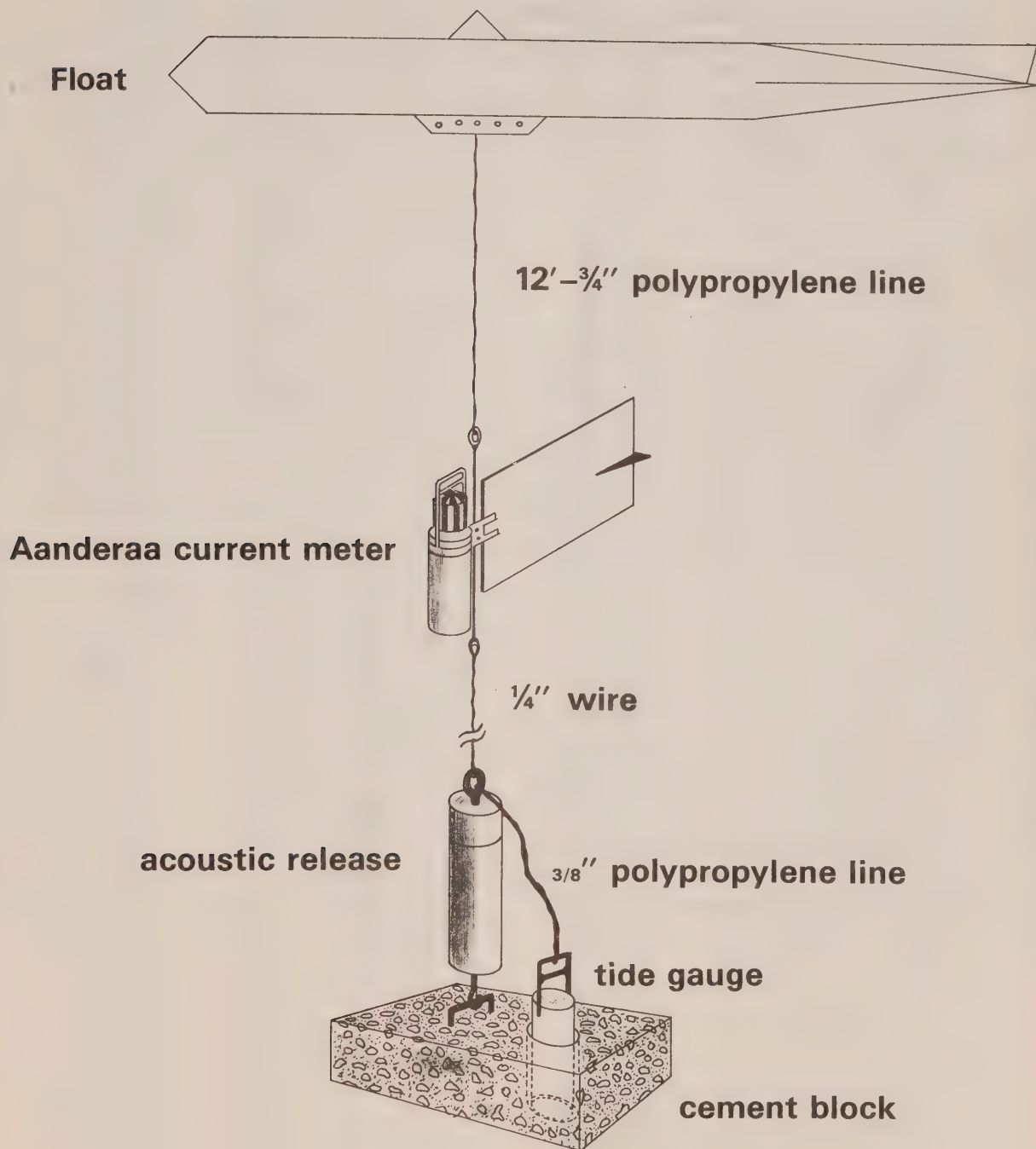


Figure 2: Cross-section along the line of stations 130, 131, 133, 135, 136, TG1, TG6, TG3 and TG8 between Sheringham Pt. and Pillar Pt.

FIGURE 3

ANCHORING SYSTEM USED IN JUAN DE FUCA STRAIT

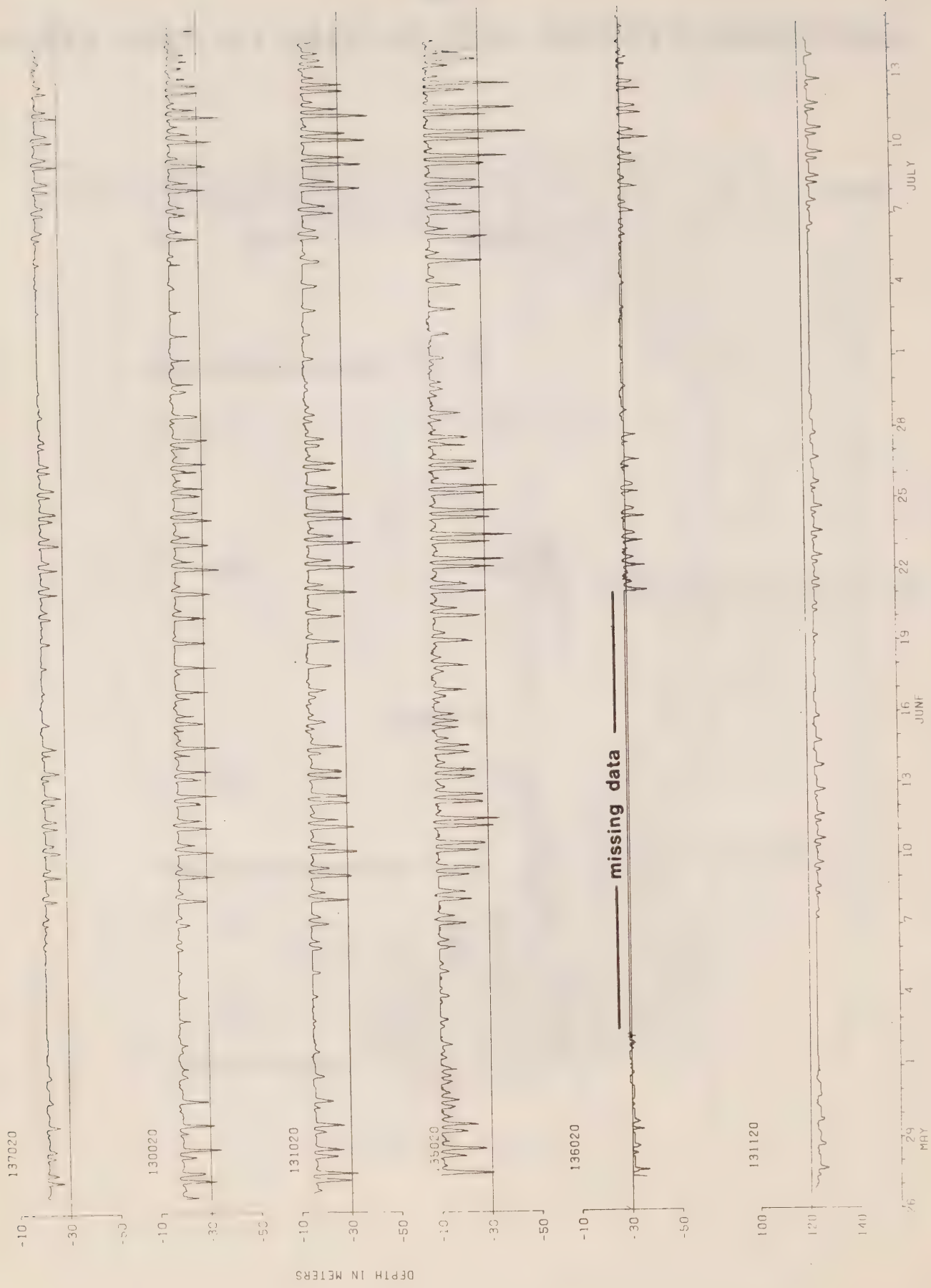


Figure 4: Depths of Current Meters.

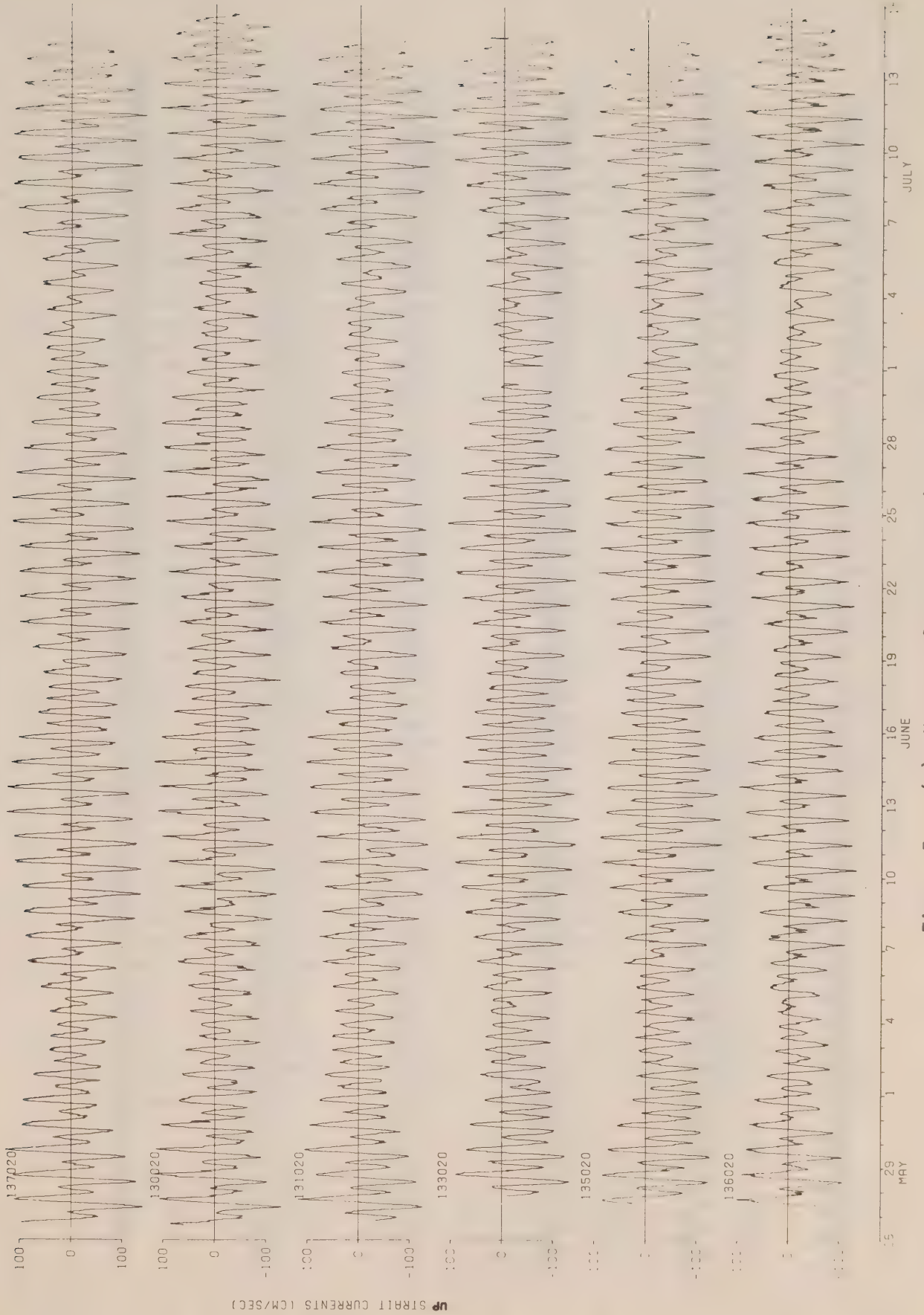


Figure 5: (a) Near surface up-strait currents.

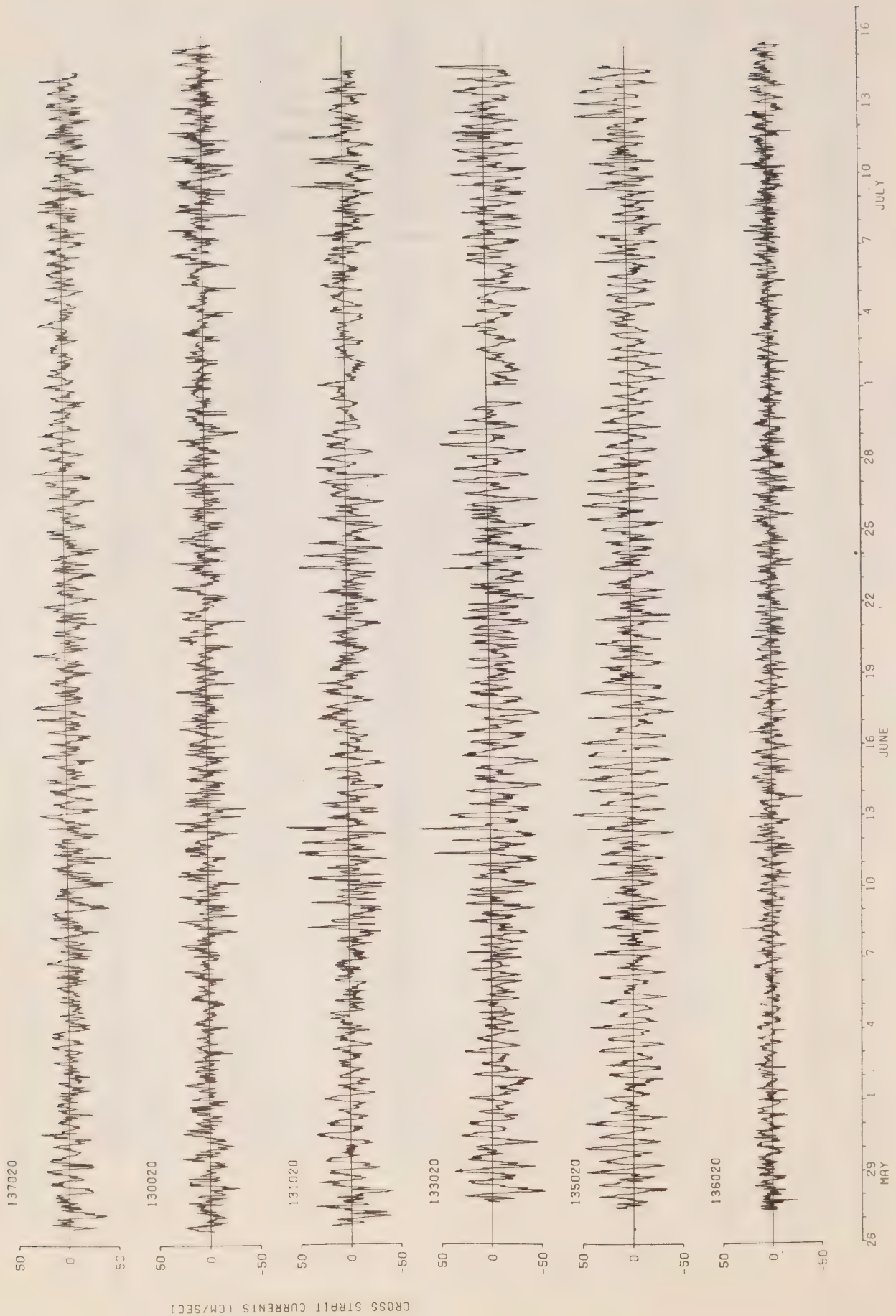


Figure 5: (b) Near surface cross-strait currents.

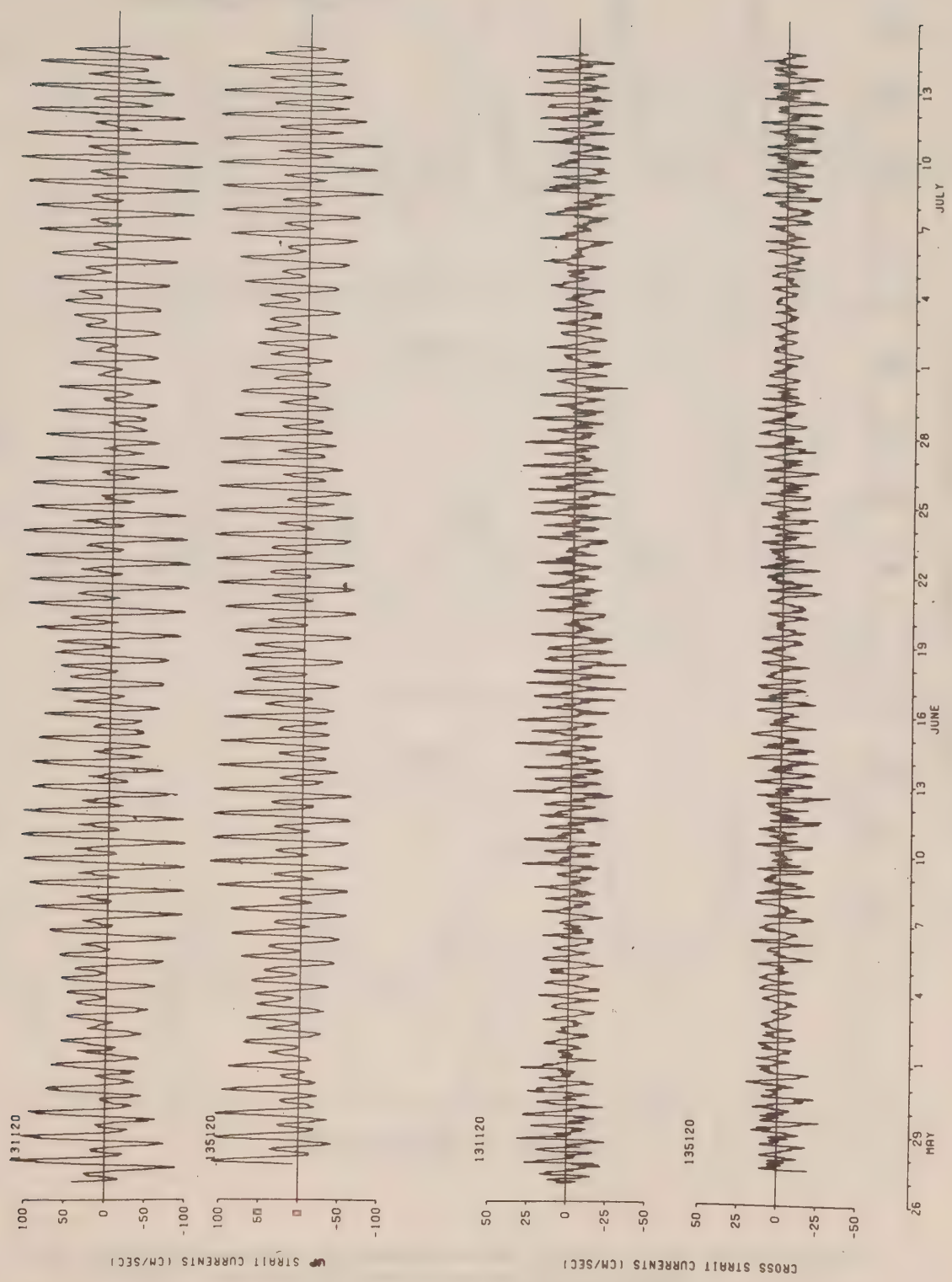


Figure 5: (c) 120 m currents

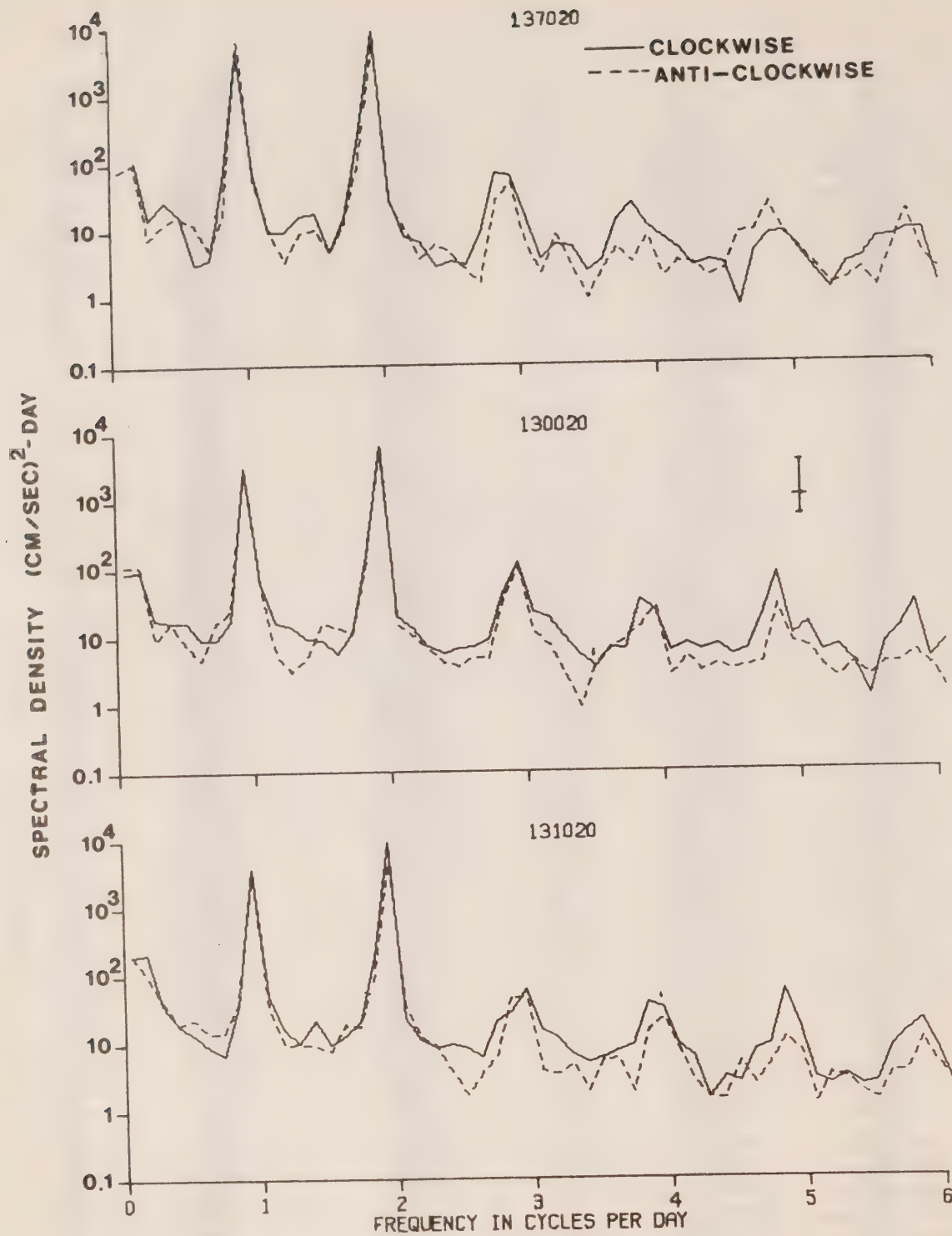


Figure 6: (a) Rotary spectra of the currents at stations 137020 and 131020. The error bars represent the 95% confidence interval and the band width.

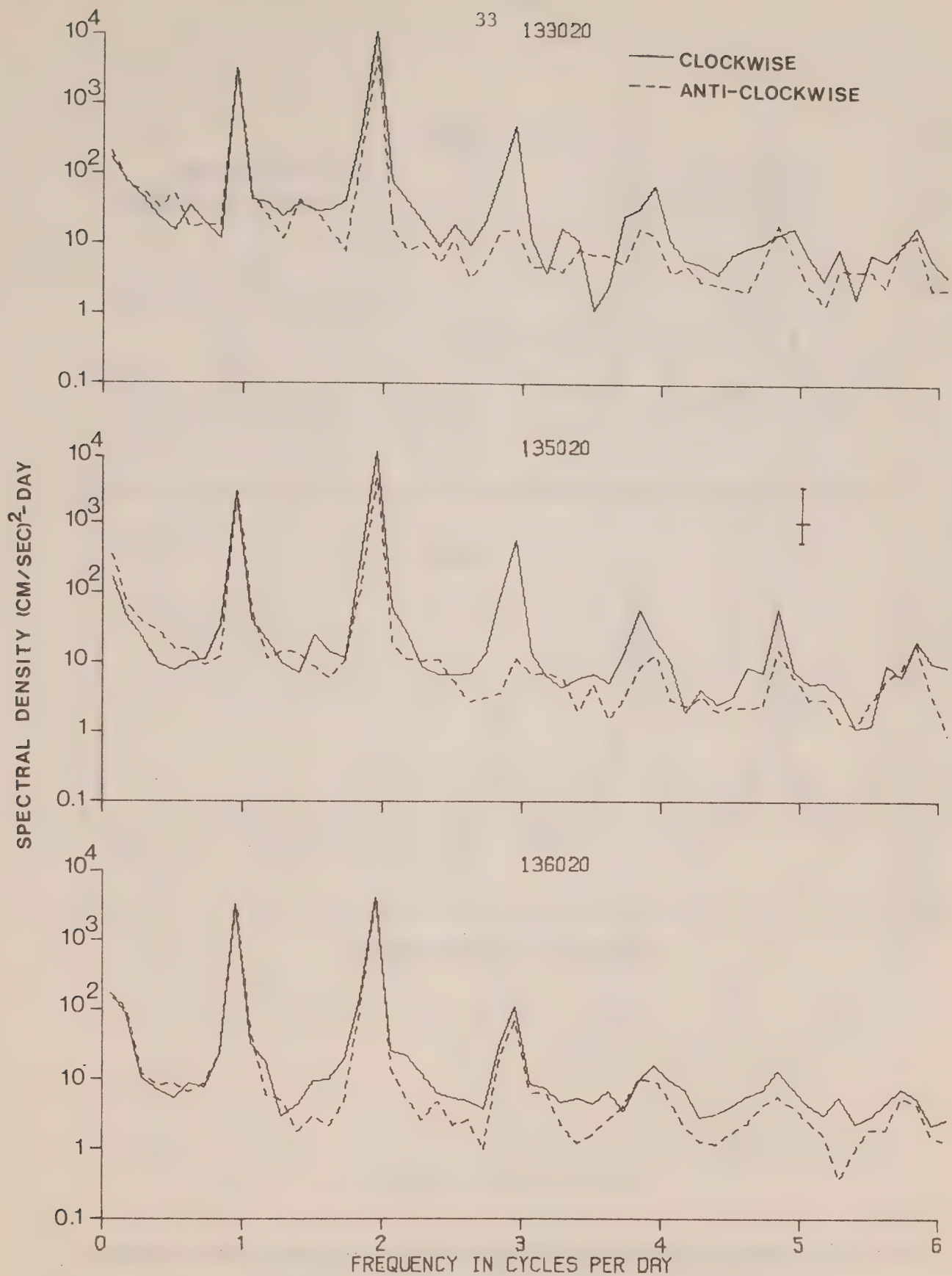


Figure 6 (b) Rotary spectra of the currents at stations 133020, 135020 and 136020.

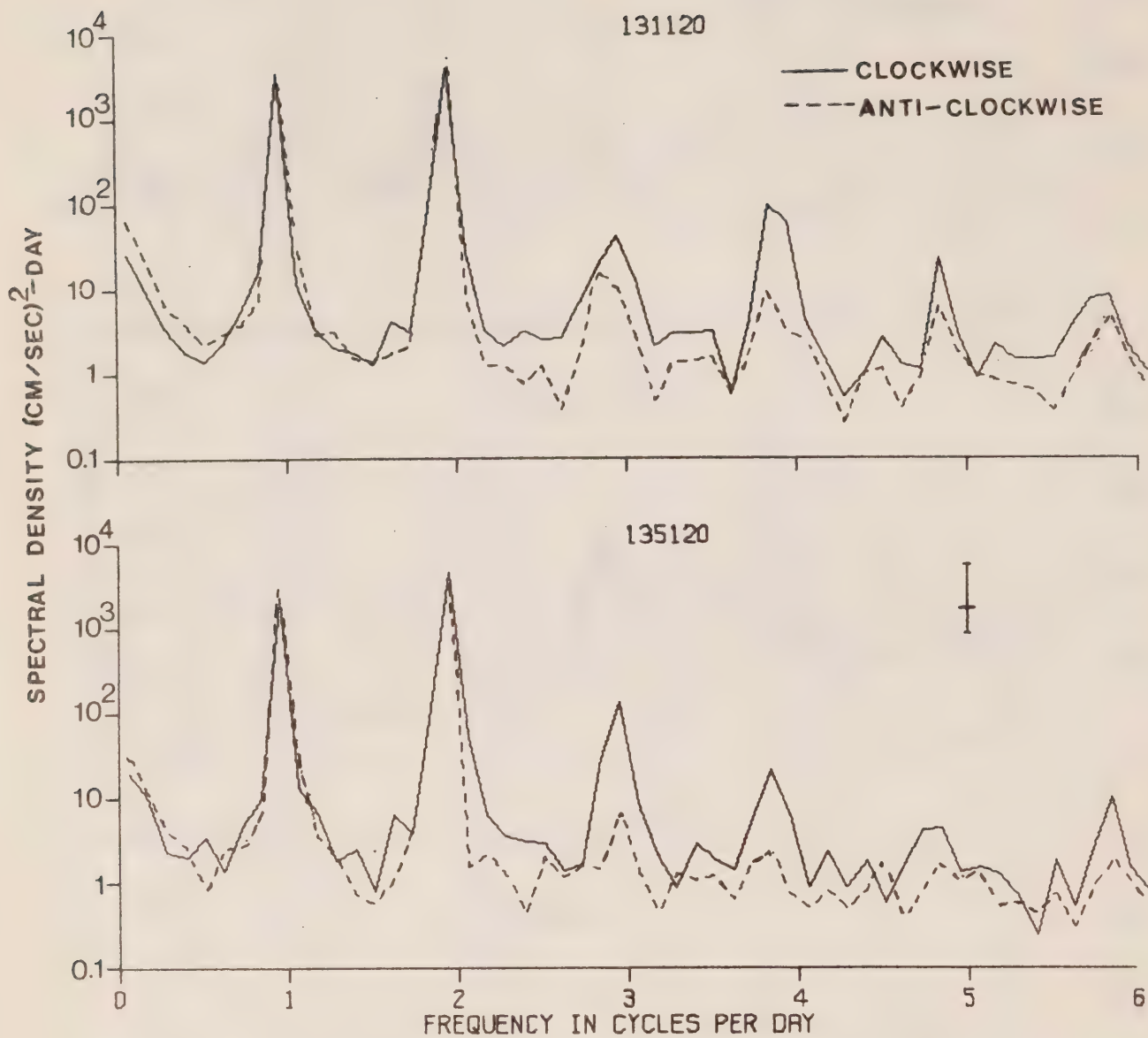


Figure 6 (c) Rotary spectra of the currents at stations 131120 and 135120.

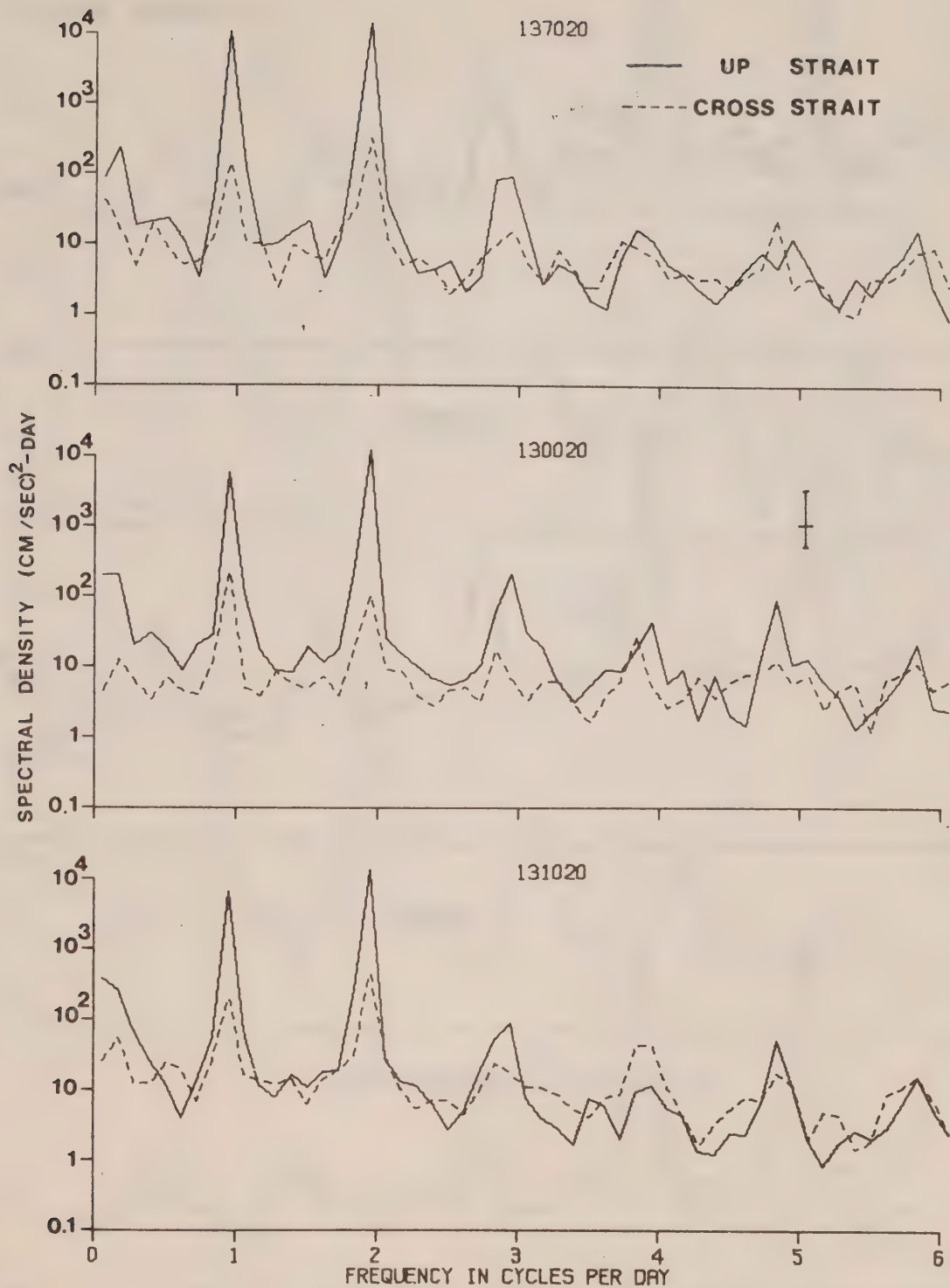


Figure 7: (a) Spectra of the up-strait and cross-strait current components at stations 137020, 130020 and 131020. The error bars represent the 95% confidence interval and the band width.

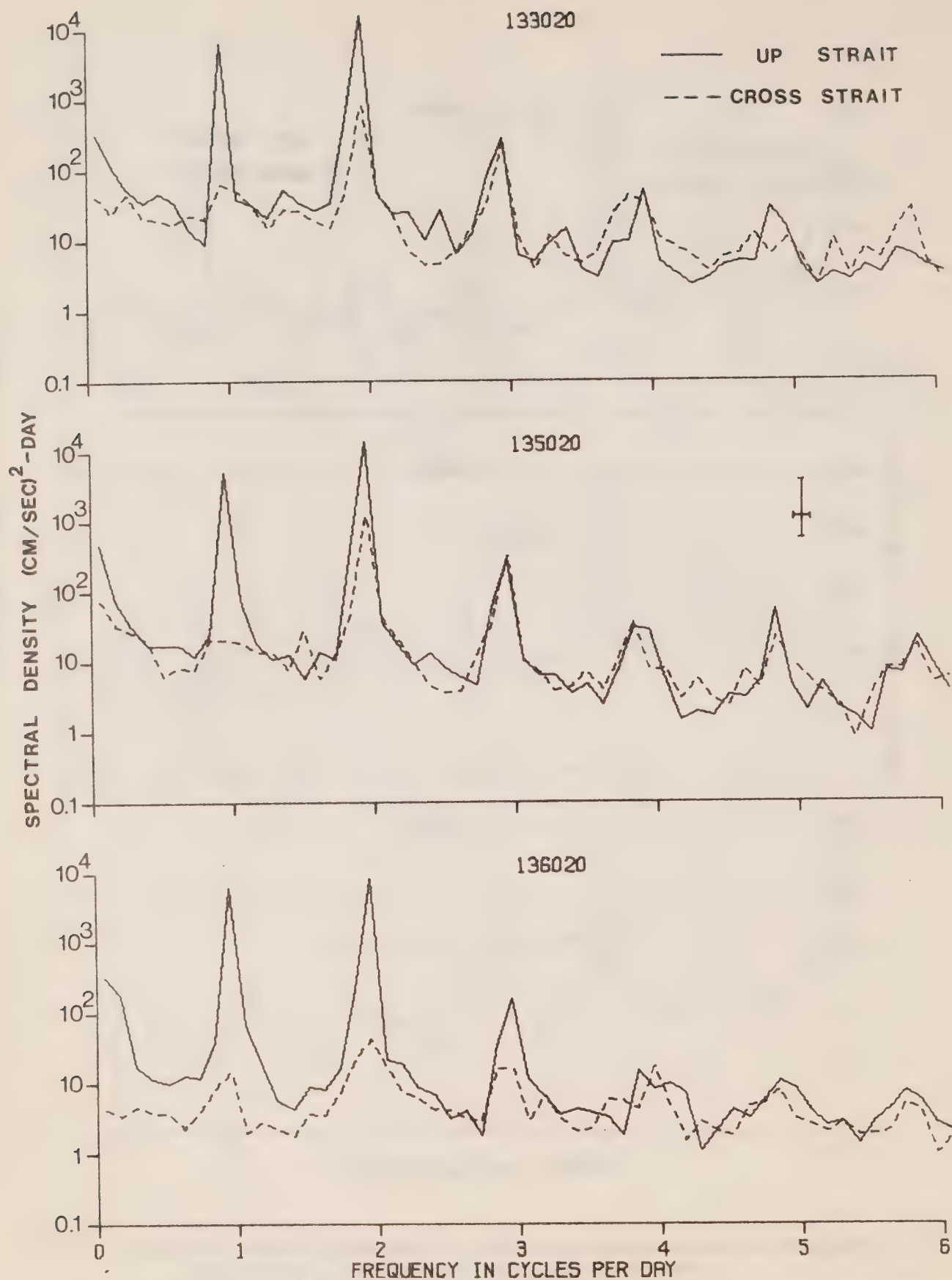


Figure 7: (b) Spectra of the up-strait and cross-strait current components at stations 133020, 135020 and 136020.

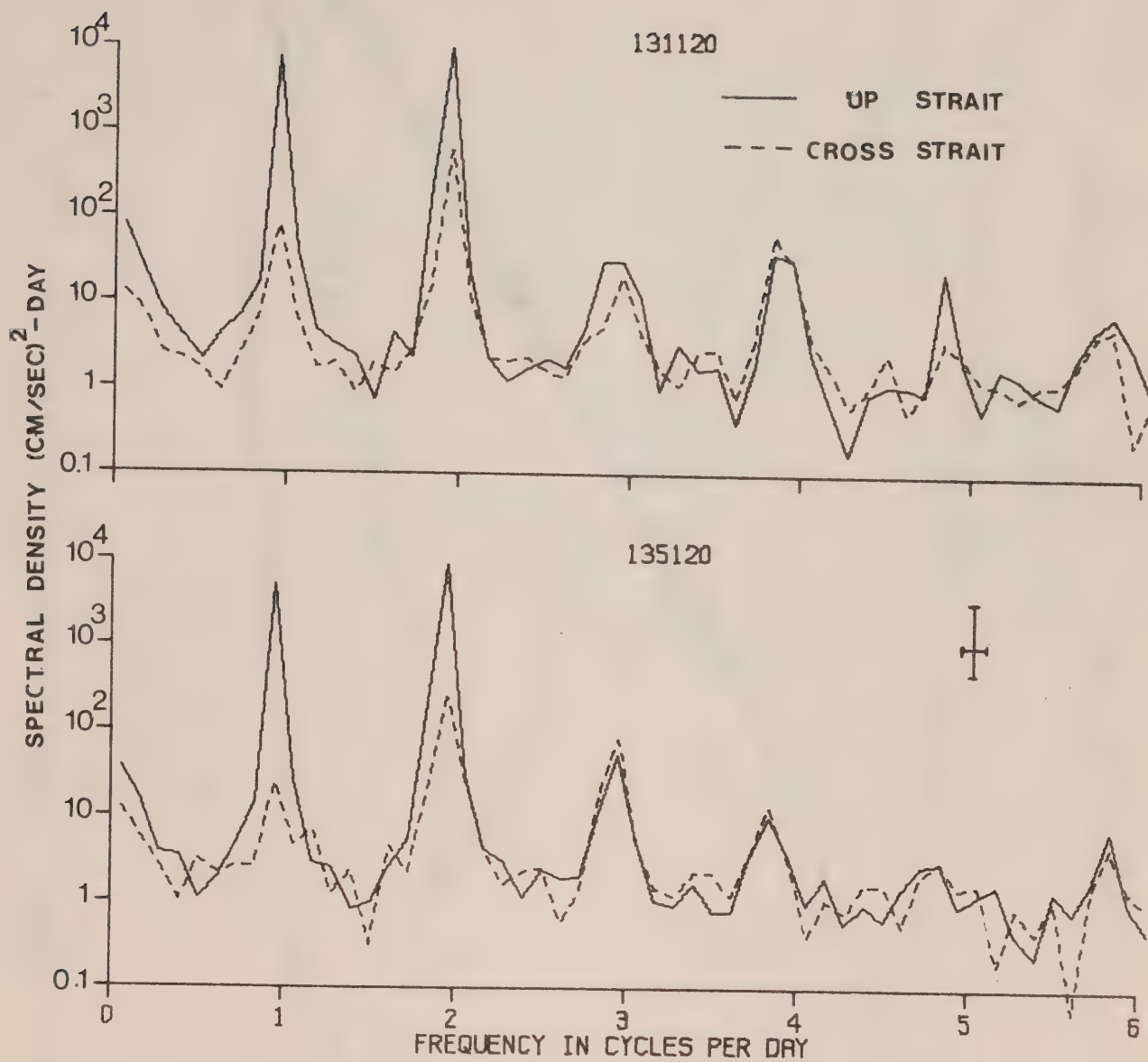


Figure 7: (c) Spectra of the up-strait and cross-strait current components at stations 131120 and 135120.

PROGRESSIVE VECTOR DIAGRAM

STATION OF OBSERVATION

NUMBER OF DAYS

NUMBER OF DAYS

NUMBER OF DAYS

NUMBER OF DAYS

NUMBER OF DAYS

NUMBER OF DAYS

NUMBER OF DAYS

NUMBER OF DAYS

NUMBER OF DAYS

NUMBER OF DAYS

NUMBER OF DAYS

NUMBER OF DAYS

NUMBER OF DAYS

NUMBER OF DAYS

NUMBER OF DAYS

NUMBER OF DAYS

NUMBER OF DAYS

NUMBER OF DAYS

NUMBER OF DAYS

NUMBER OF DAYS

NUMBER OF DAYS

NUMBER OF DAYS

NUMBER OF DAYS

NUMBER OF DAYS

NUMBER OF DAYS

NUMBER OF DAYS

NUMBER OF DAYS

NUMBER OF DAYS

NUMBER OF DAYS

NUMBER OF DAYS

NUMBER OF DAYS

NUMBER OF DAYS

NUMBER OF DAYS

NUMBER OF DAYS

NUMBER OF DAYS

NUMBER OF DAYS

NUMBER OF DAYS

NUMBER OF DAYS

NUMBER OF DAYS

NUMBER OF DAYS

NUMBER OF DAYS

NUMBER OF DAYS

NUMBER OF DAYS

NUMBER OF DAYS

NUMBER OF DAYS

NUMBER OF DAYS

NUMBER OF DAYS

NUMBER OF DAYS

NUMBER OF DAYS

NUMBER OF DAYS

NUMBER OF DAYS

NUMBER OF DAYS

NUMBER OF DAYS

NUMBER OF DAYS

NUMBER OF DAYS

NUMBER OF DAYS

NUMBER OF DAYS

NUMBER OF DAYS

NUMBER OF DAYS

NUMBER OF DAYS

NUMBER OF DAYS

NUMBER OF DAYS

NUMBER OF DAYS

NUMBER OF DAYS

NUMBER OF DAYS

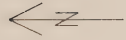
NUMBER OF DAYS



Figure 8: (a) Progressive vector diagram of currents at stations 130020, 131020 and 133020.

JUAN DE FUCA PROGRESSIVE VECTOR DIAGRAM

▲ START OF OBSERVATIONS
 □ 0000 NUMBERED DAYS
 ○ 0600 NUMBERED DAYS
 + SIX HOUR INTERVAL



STN DEPTH AREA JULIAN DATE NO DAYS
 133 20M 7000 147/75 48
 135
 136
 SCALE 10 KMS

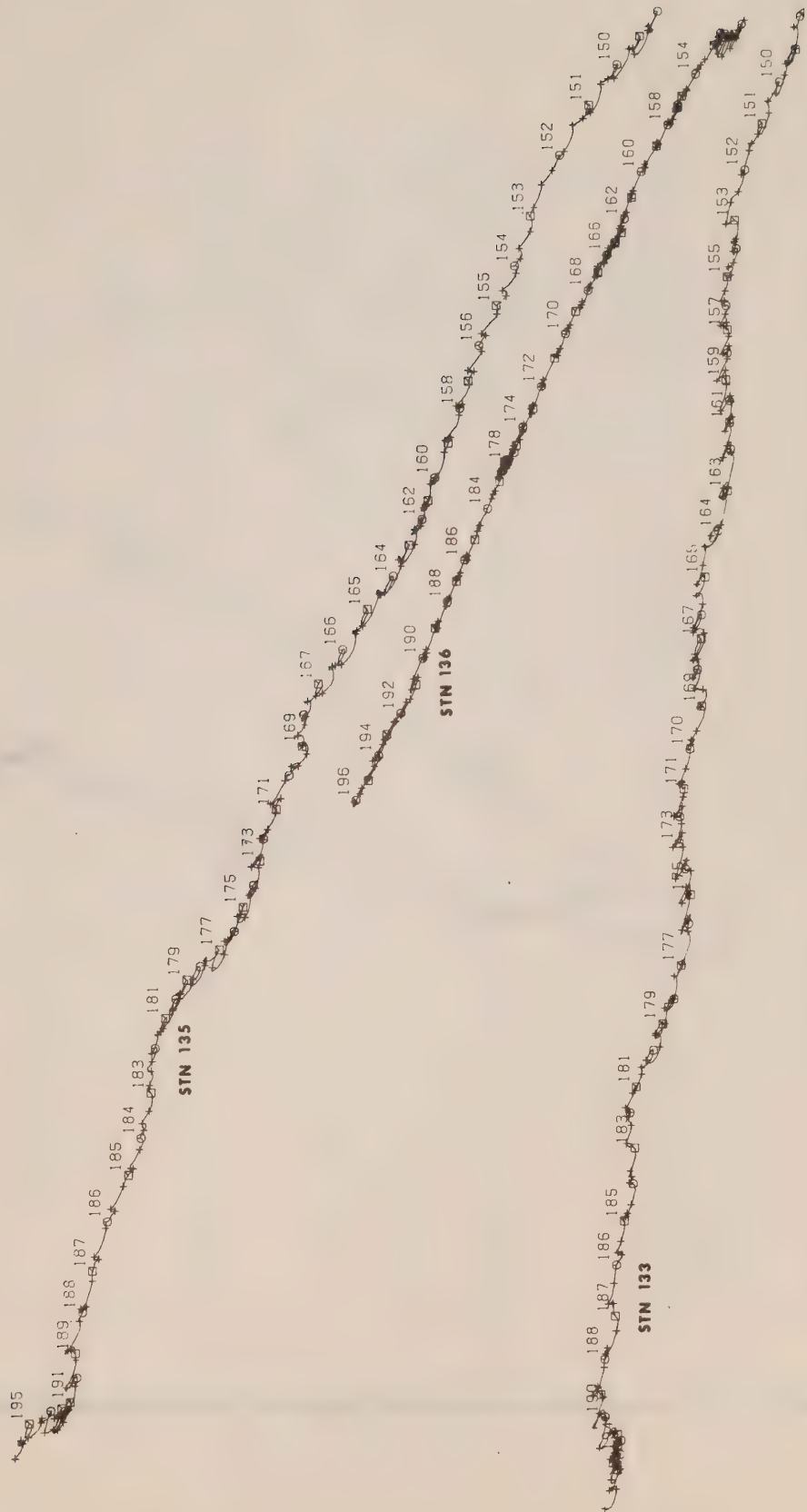


Figure 8: (b) Progressive vector diagram of currents at stations 133020, 135020 and 136020.

JUAN DE FUCA STRAIT PROGRESSIVE VECTOR DIAGRAM

△ START OF OBSERVATIONS
 □ ODD NUMBERED DAYS
 ○ EVEN NUMBERED DAYS
 + SIX HOUR INTERVAL

STN	DEPTH	AREA	JULIAN DATE	NO DAYS
137	020M	7000	146/75	48

SCALE ++++
 10 KMS



Figure 8: (c) Progressive vector diagram of currents at station 137020.

JUAN DE FUCA PROGRESSIVE VECTOR DIAGRAM

△ START OF OBSERVATIONS
 □ 000 NUMBERED DAYS
 ○ EVEN NUMBERED DAYS
 + SIX HOUR INTERVAL

STN	DEPTH	AREA	JULIAN DATE	NO DAYS
131	120M	7000	146/75	48

SCALE ---
 10 KMS

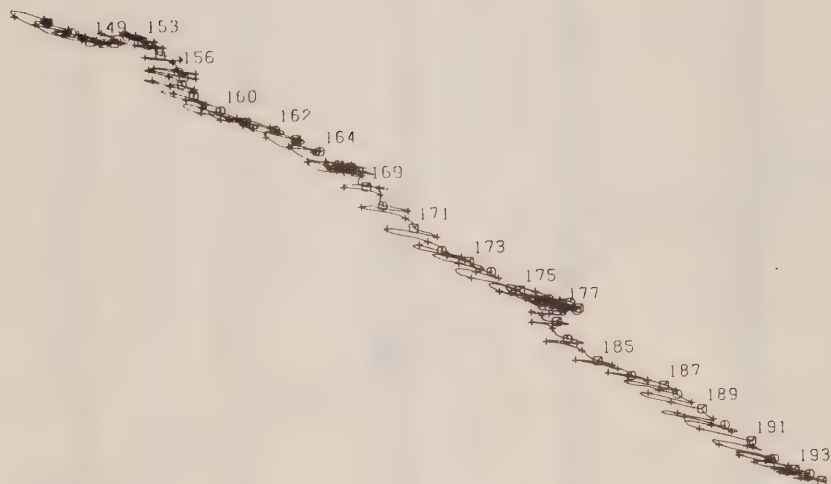


Figure 8: (d) Progressive vector diagram of currents at station 131120.

JUAN DE FUCA PROGRESSIVE VECTOR DIAGRAM

△ START OF OBSERVATIONS

□ 000 NUMBERED DAYS

○ EVEN NUMBERED DAYS

+ SIX HOUR INTERVAL

STN	DEPTH	AREA	JULIAN DATE	NO DAYS
135	120M	7000	147/75	48

SCALE 
10 KMS

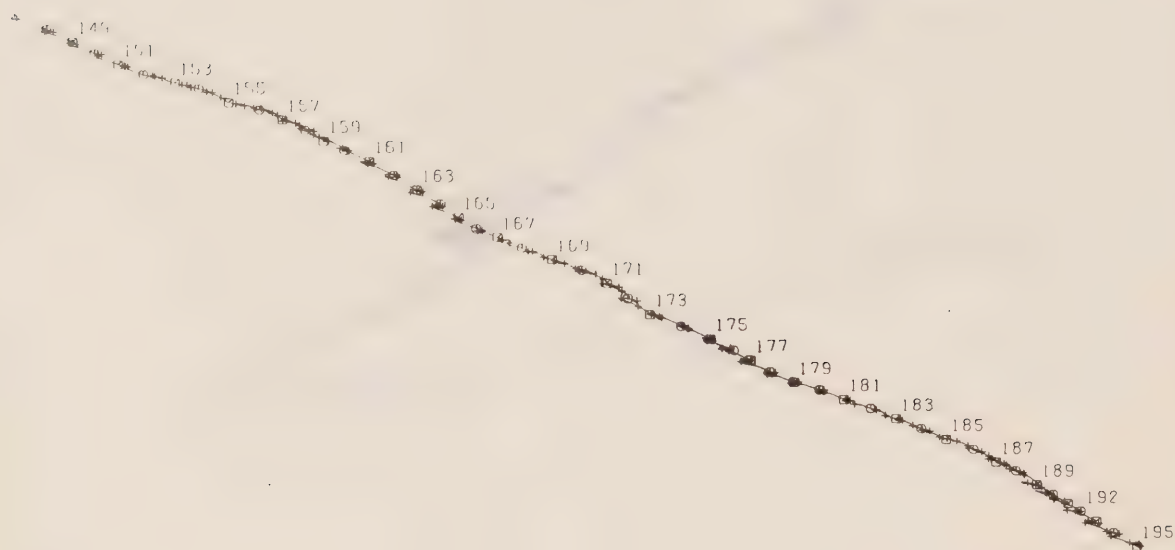
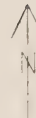


Figure 8: (e) Progressive vector diagram of currents at station 135120.

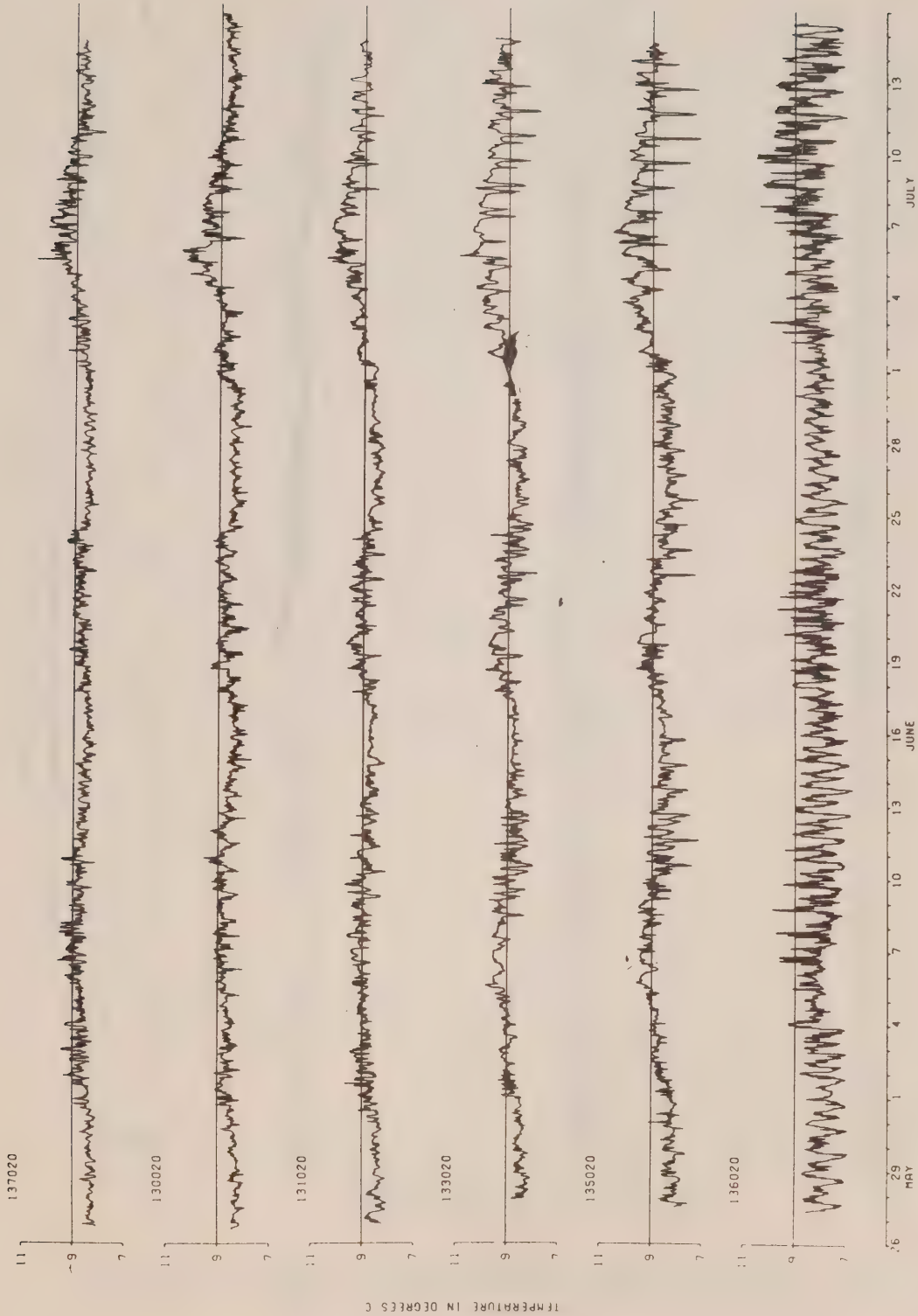


Figure 9: (a) Temperatures measured by near surface current meters.

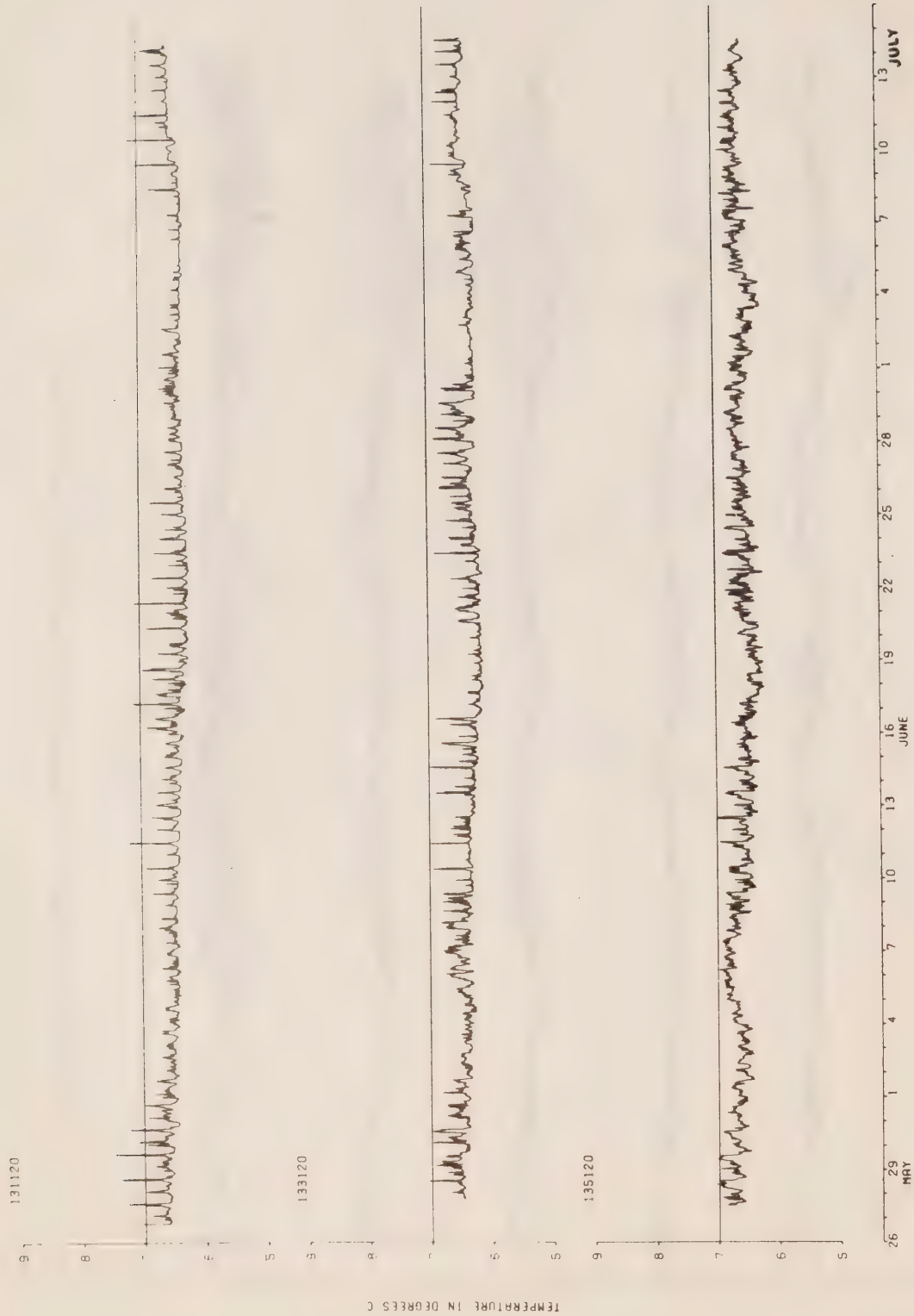


Figure 9: (b) Temperatures measured by deep current meters.

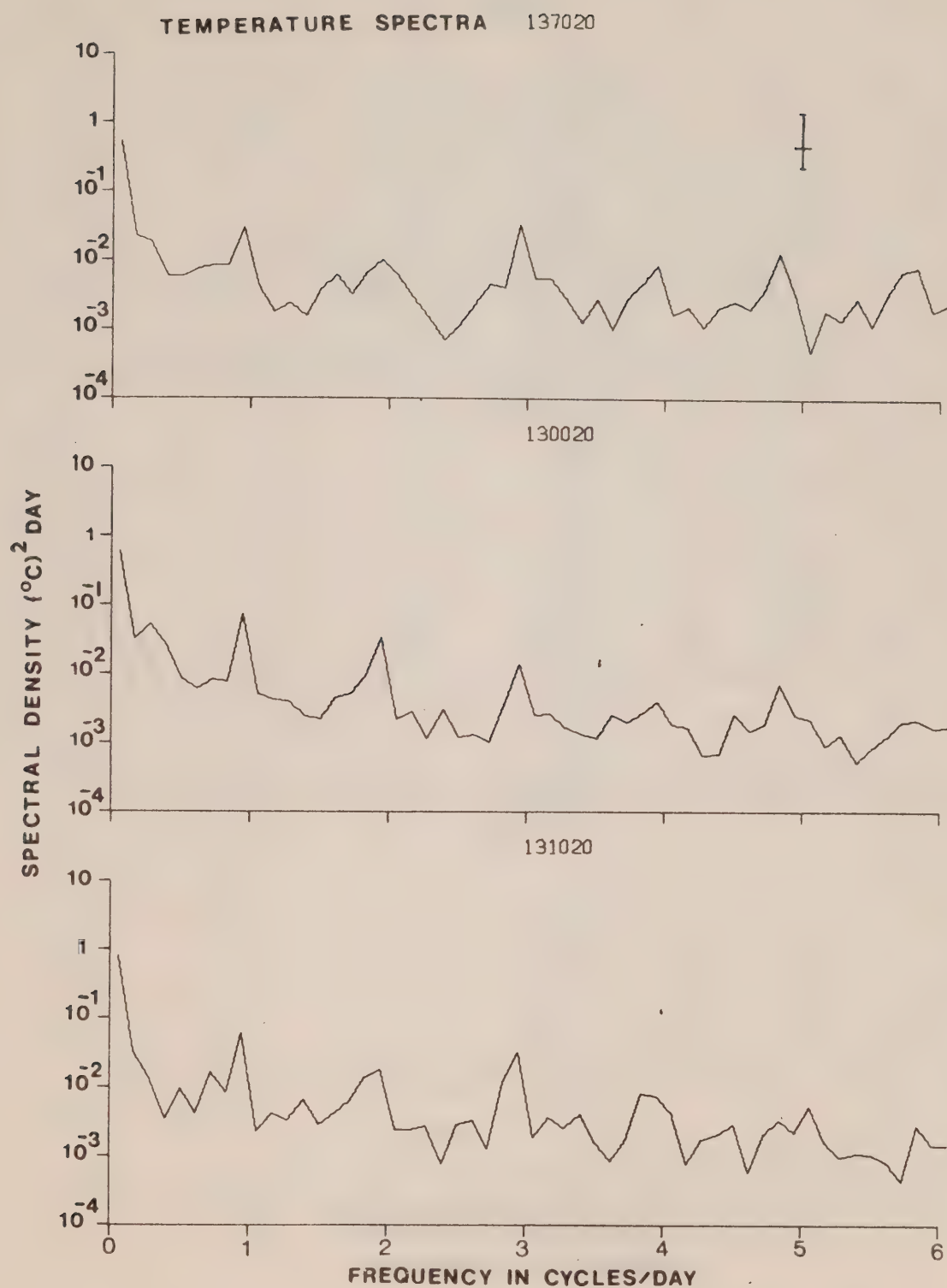


Figure 10: (a) Spectra of the temperatures at stations 137020, 130020 and 131020. The error bars represent the 95% confidence interval.

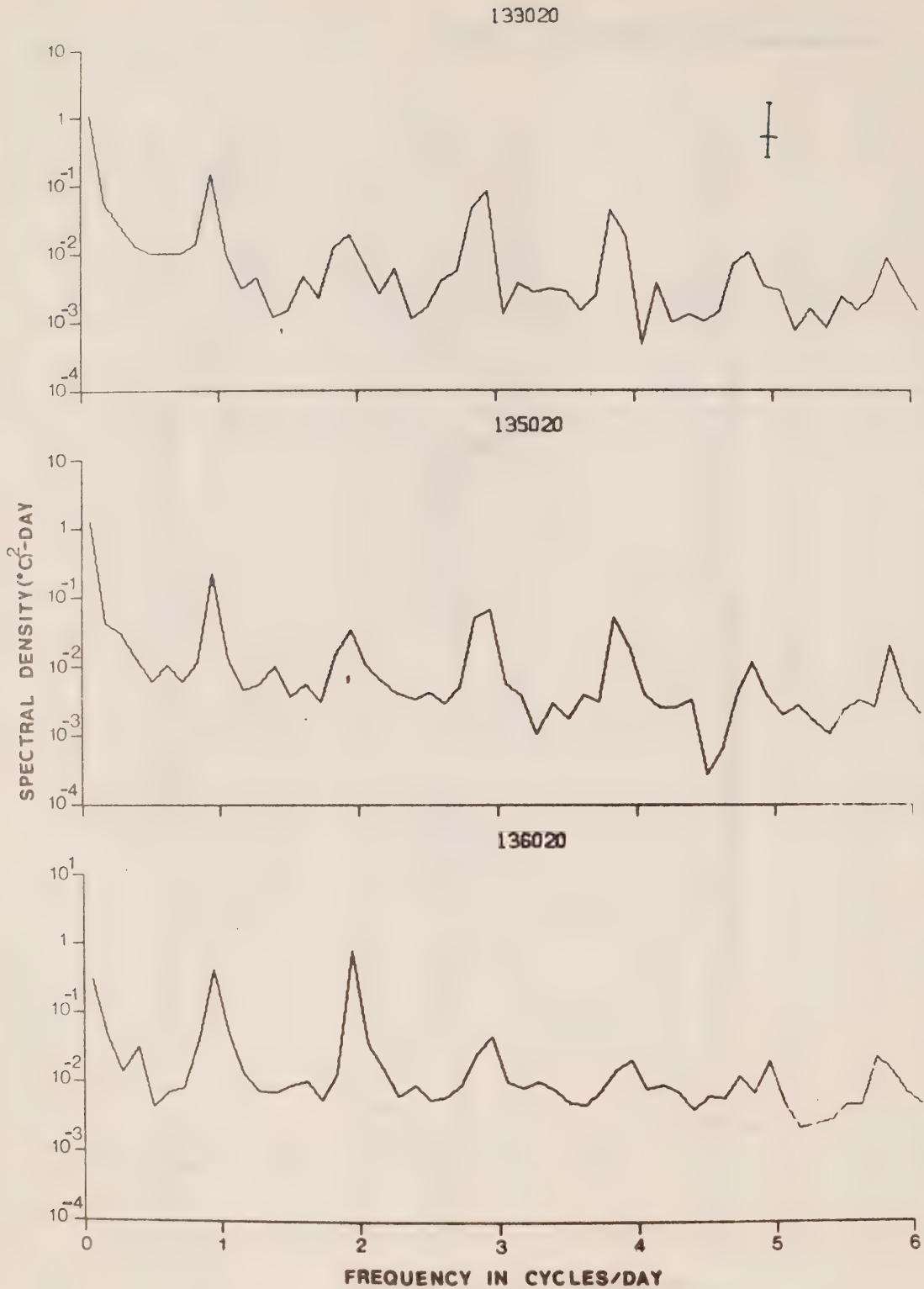


Figure 10: (b) Spectra of the temperatures at stations 133020, 135020 and 136020. The error bars represent the 95% confidence interval.

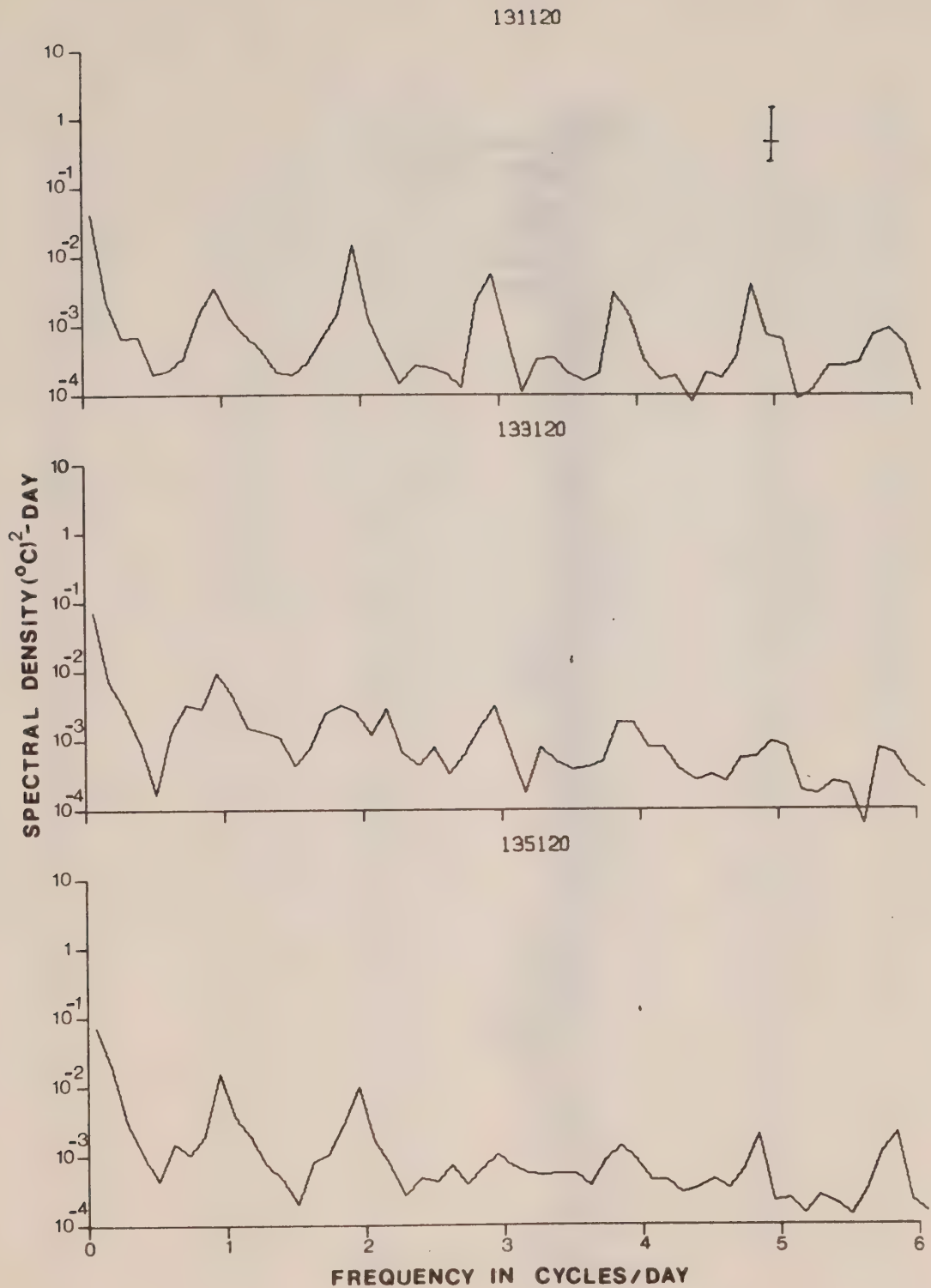


Figure 10: (c) Spectra of the temperatures at stations 131120, 133120 and 135120. The error bars represent the 95% confidence interval.

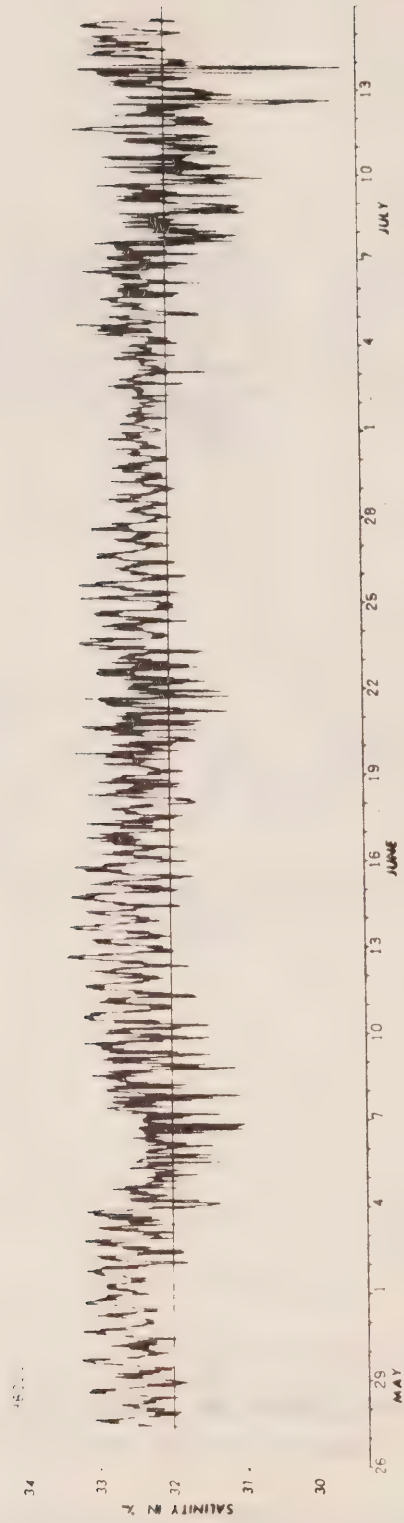


Figure 11: The salinity at station 136020.

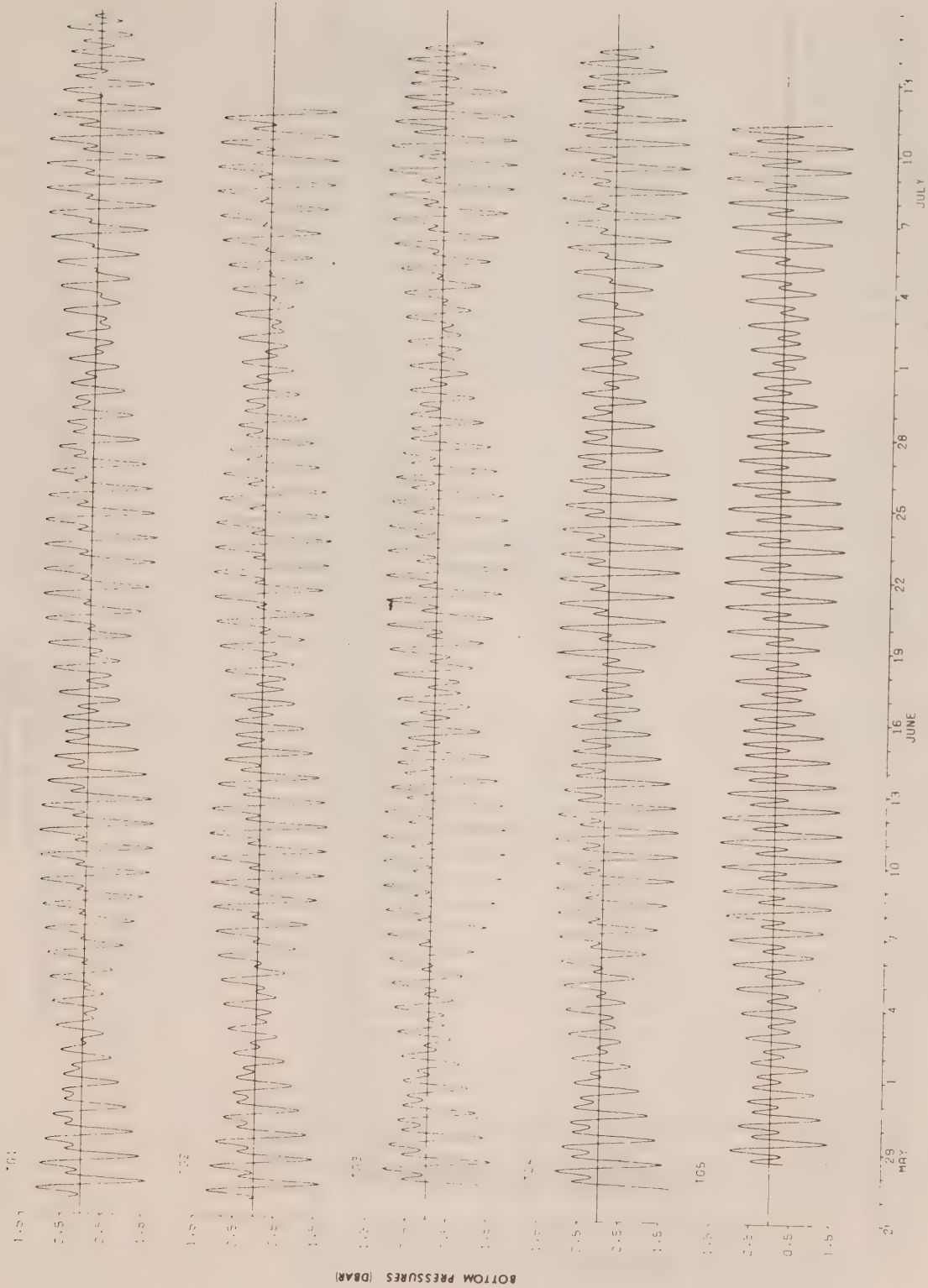


Figure 12: (a) The bottom pressure measured at those stations TG1, TG2, TG3, TG4 and TG5 with a nominal depth of 20 m, plotted about their mean values.

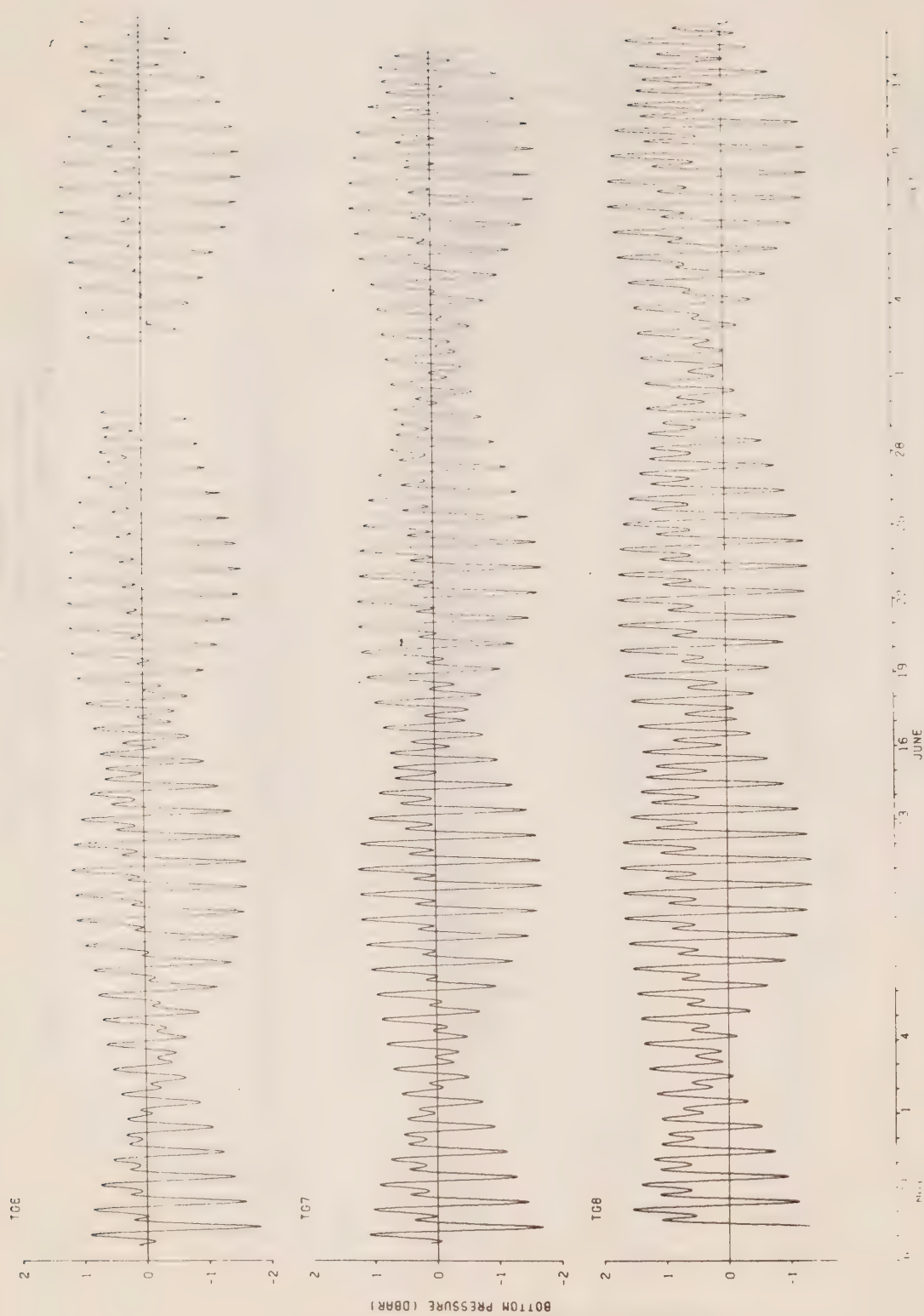


Figure 12: (b) The bottom pressure measured at those stations TC6, TC7 and TC8 with a nominal depth of 120 m, plotted about their mean values.

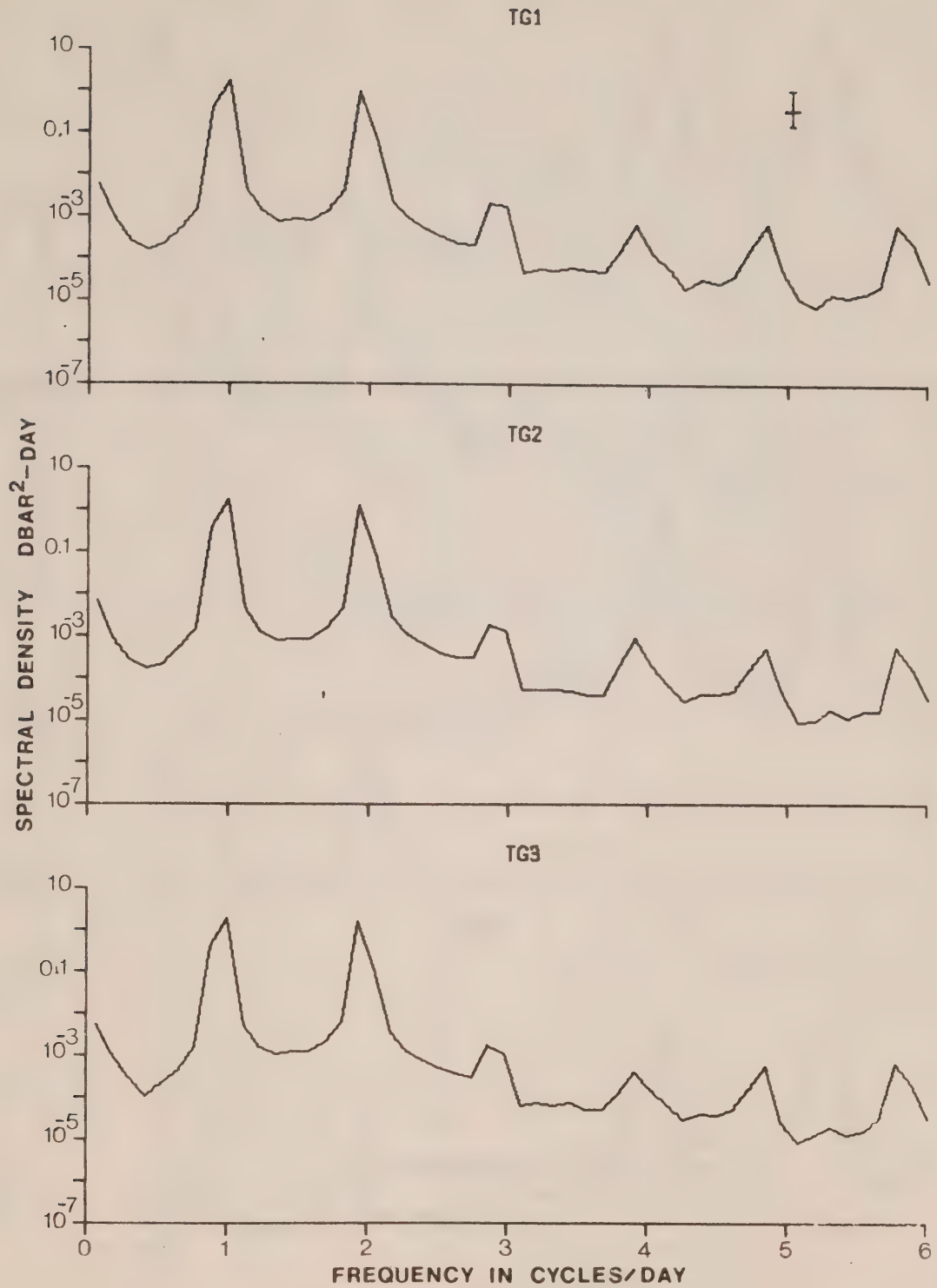
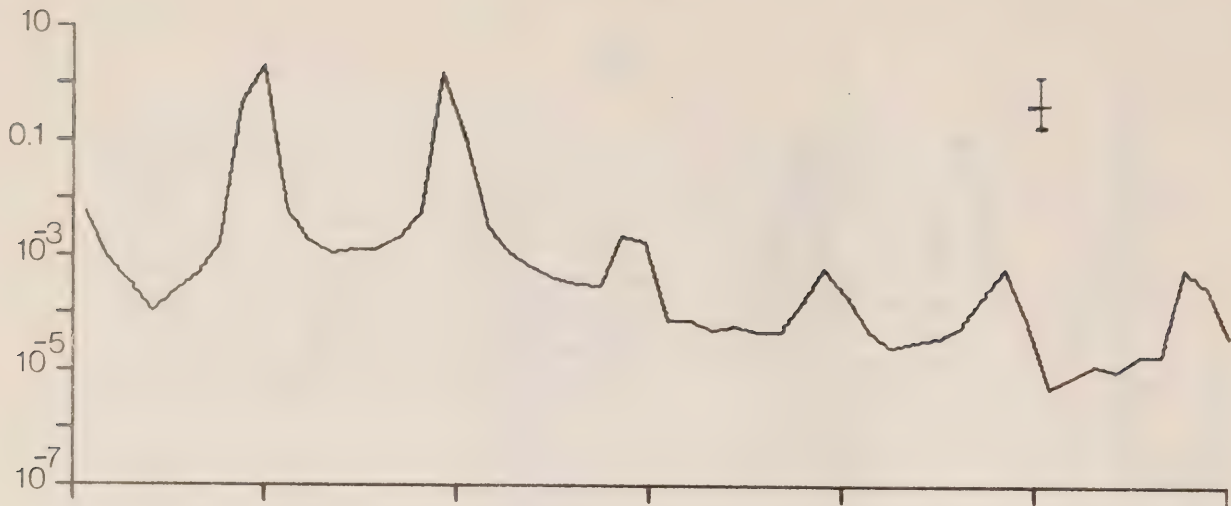
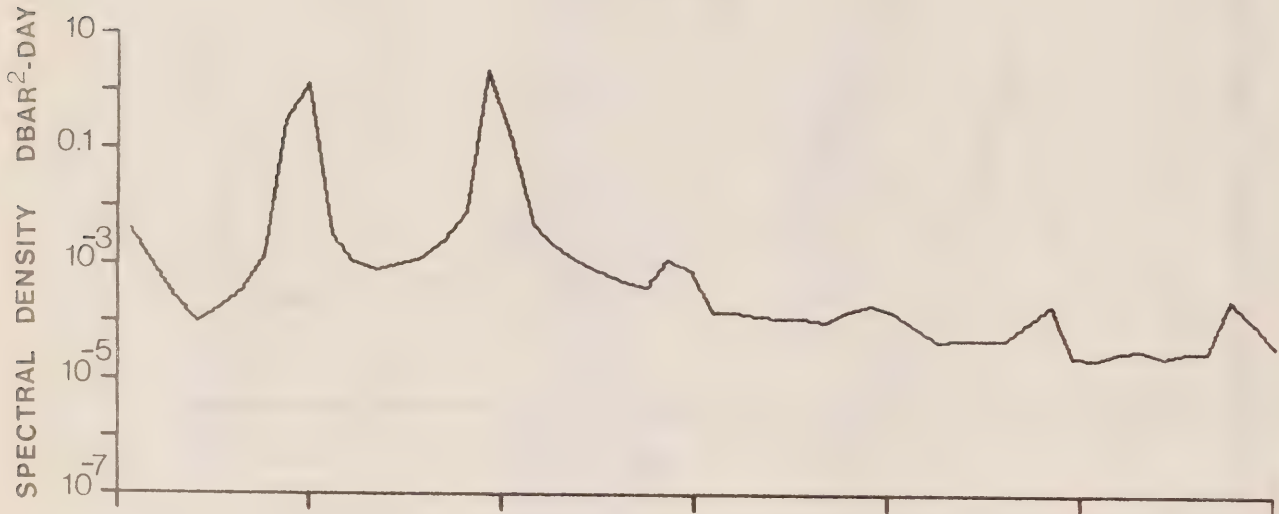


Figure 13: (a) Spectra of the bottom pressures at stations TG1, TG2 and TG3. The error bars represent the 95% confidence interval and the band width.

TG4



TG5



TG6

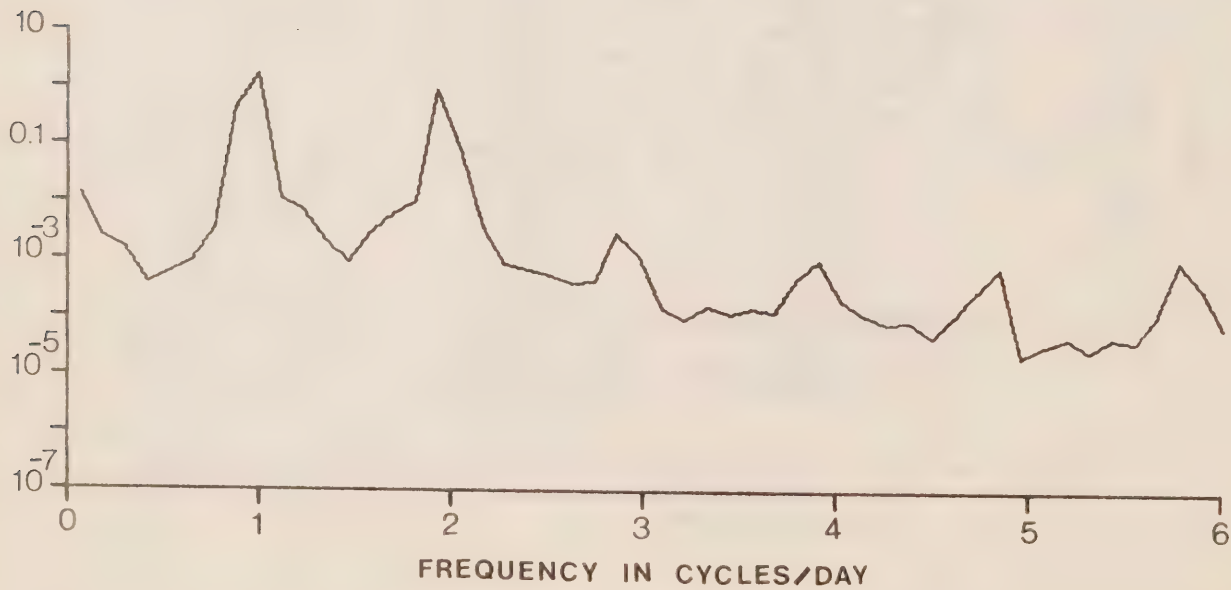


Figure 13: (b) Spectra of the bottom pressures at stations TG4, TG5 and TG6.

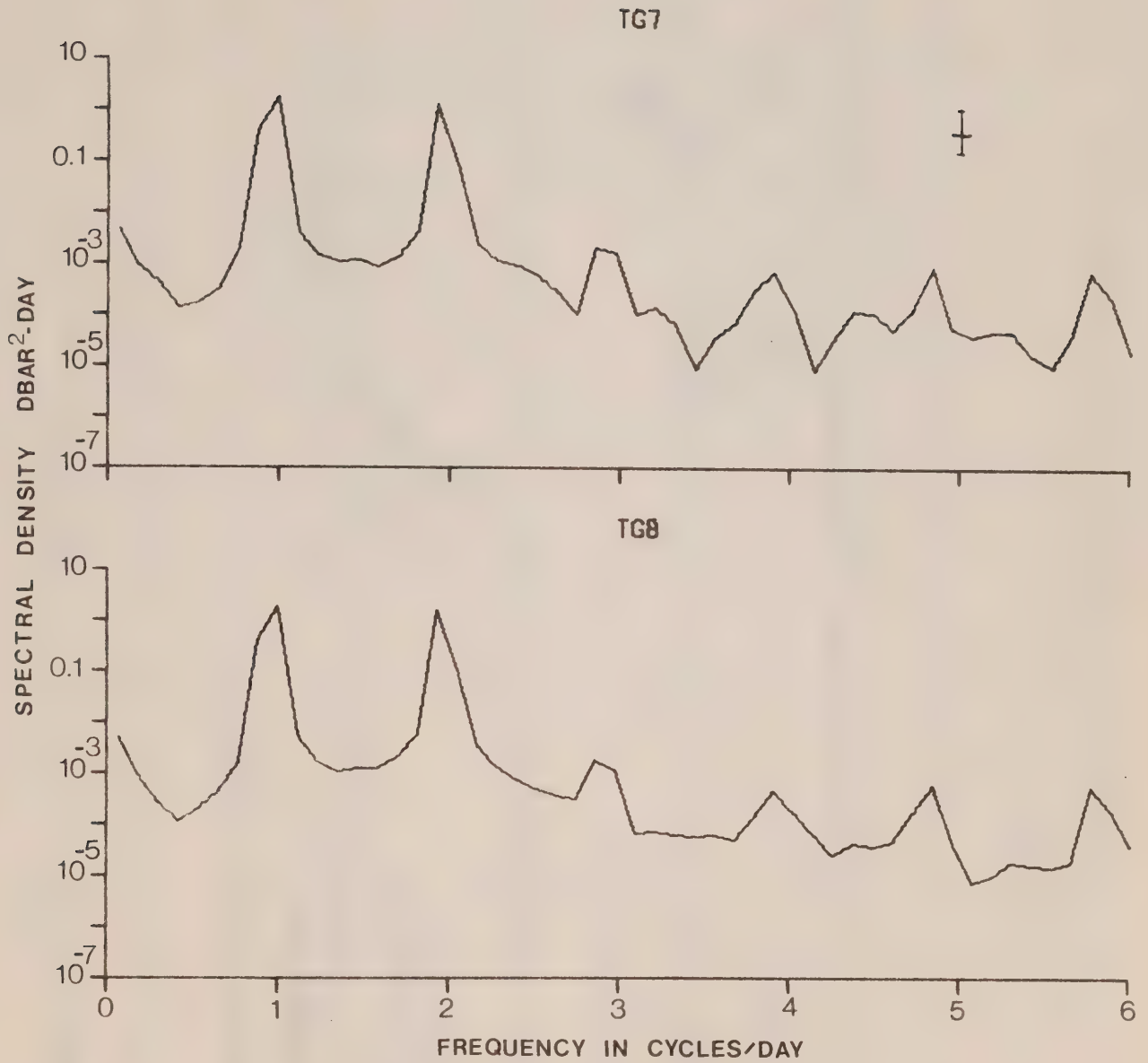


Figure 13: (c) Spectra of the bottom pressures at stations TG7 and TG8.

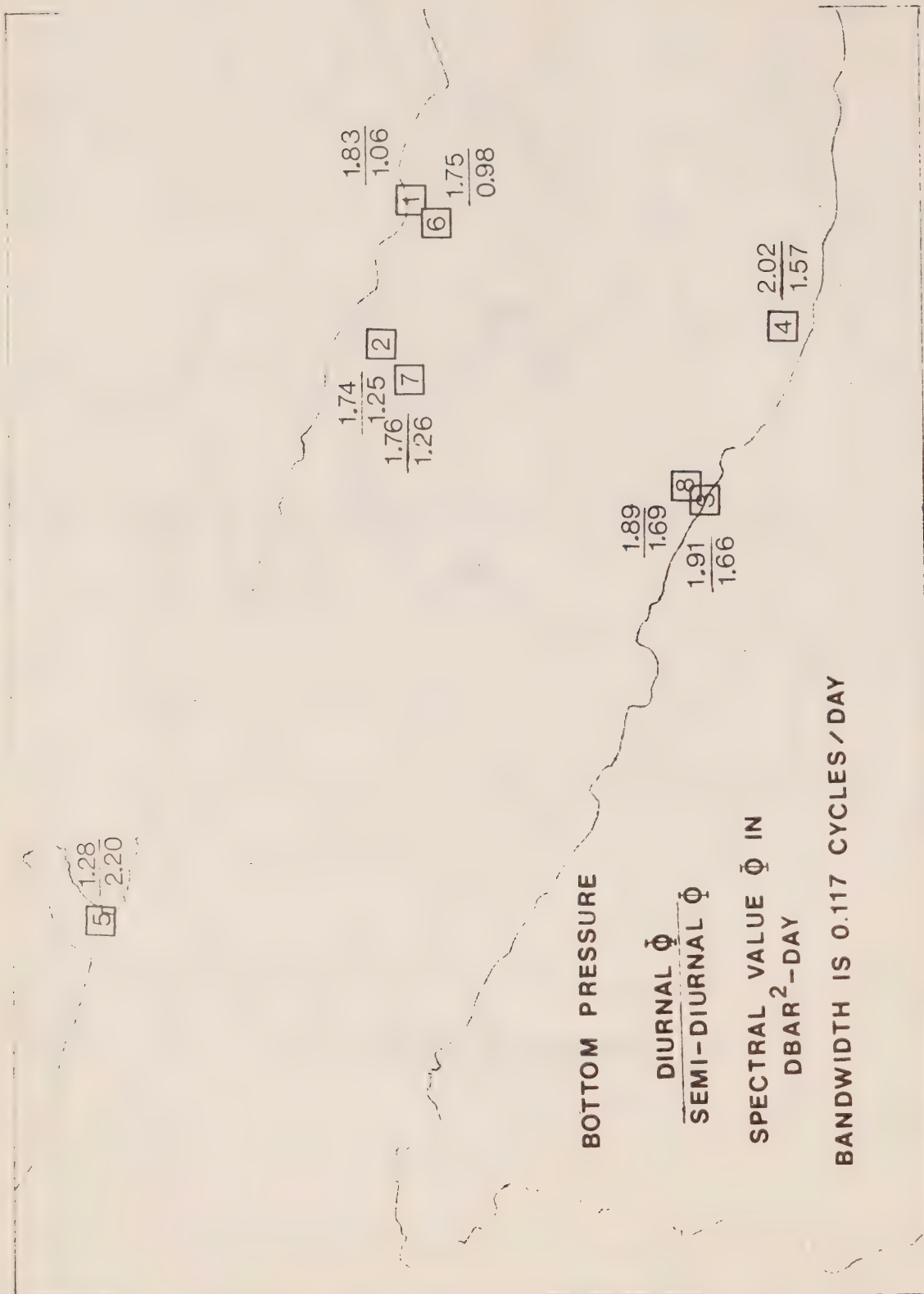


Figure 14: The ratio of the diurnal to semi-diurnal spectral density estimates for each bottom pressure gauge.

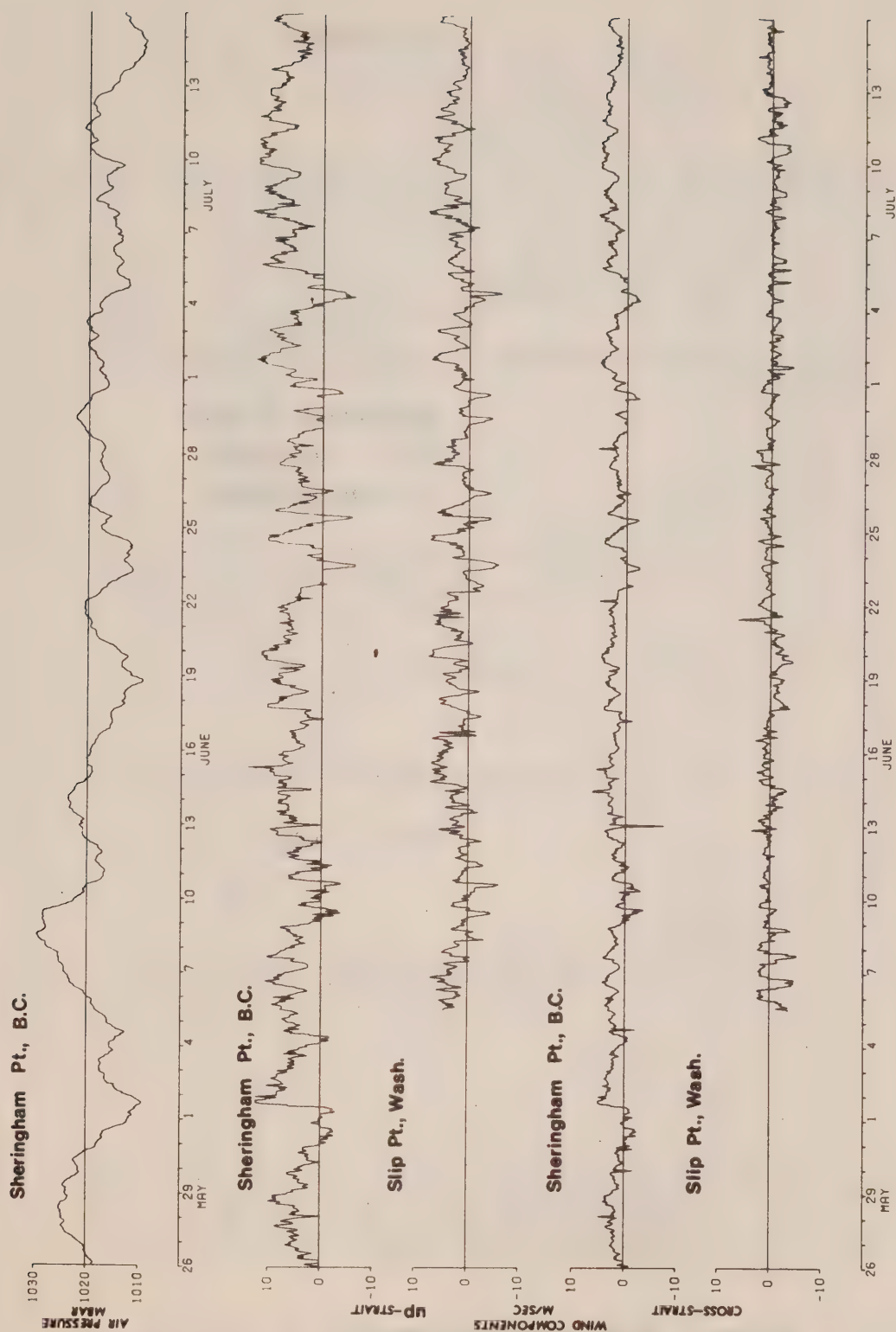


Figure 15: The air pressure measured at Sheringham Pt., B.C., and the wind components at Sheringham Pt., B.C., and Slip Pt., Wash.

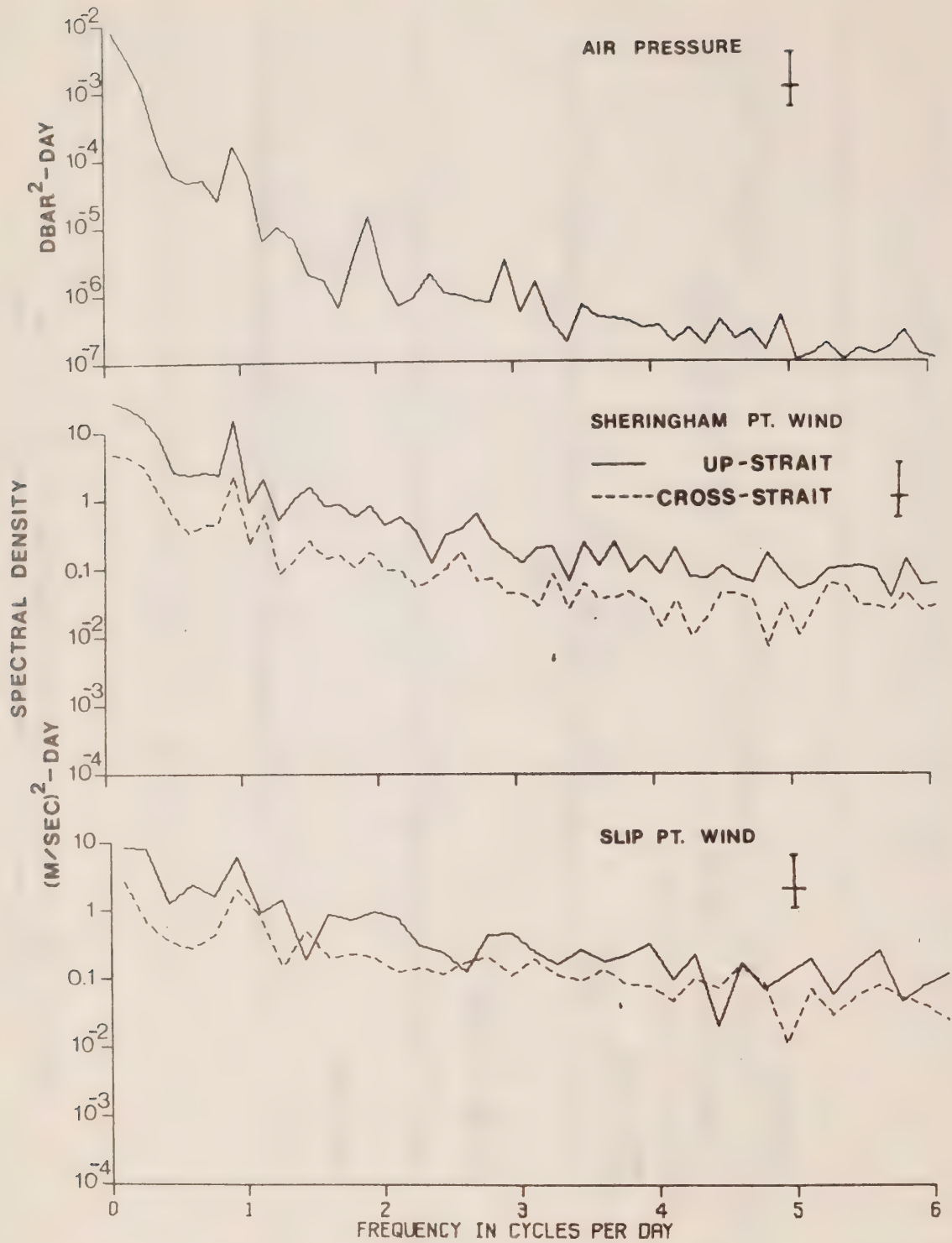


Figure 16: Spectra of the air pressure at Sheringham Pt., B.C., and spectra of both wind components at Sheringham Pt., B.C., and Slip Pt., Wash. The error bars represent the 95% confidence interval and the band width.

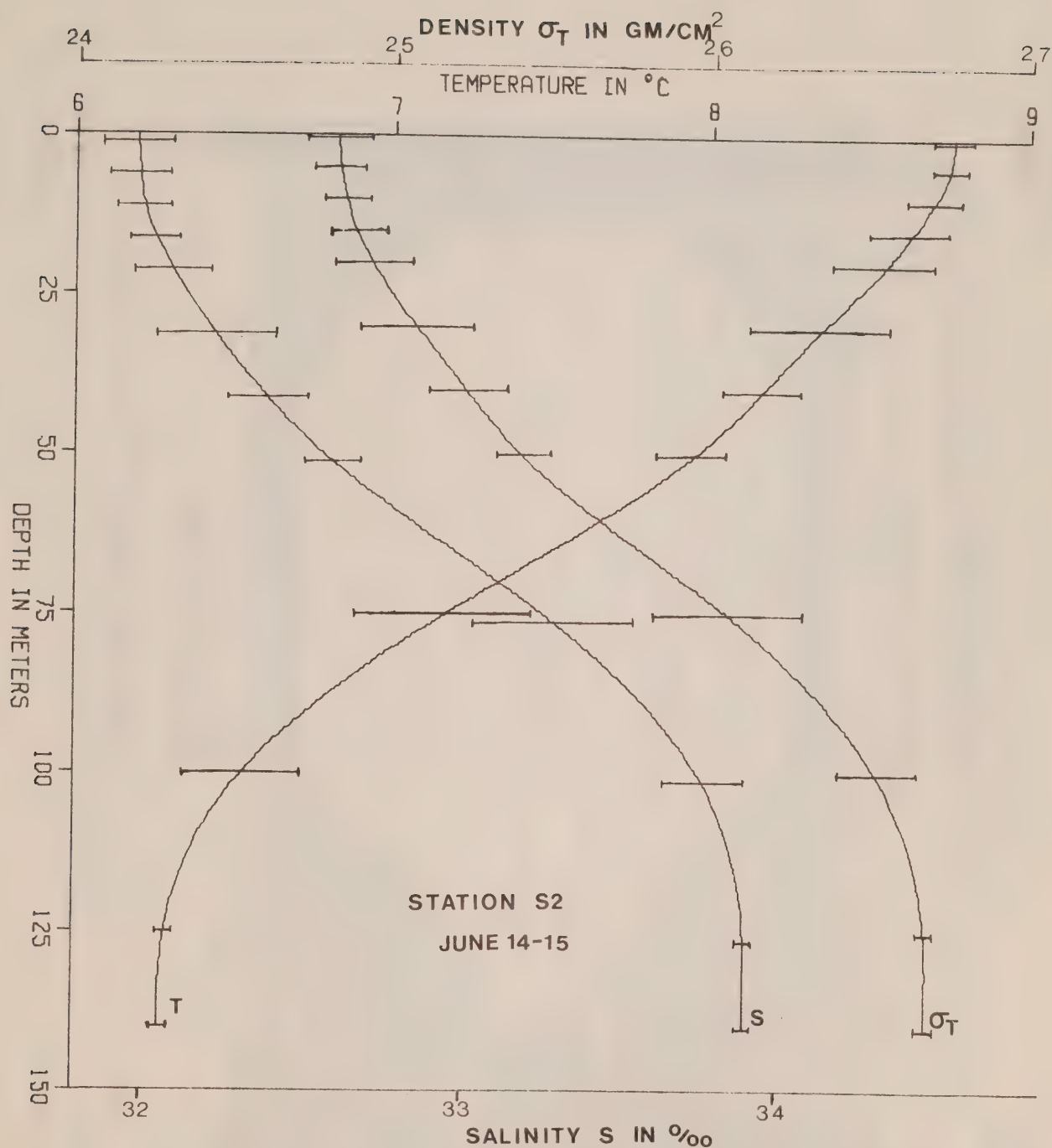


Figure 17: The average profiles of temperature, salinity and density (sigma-t) for station S2 from the cruise of June 14-15, 1975. The horizontal lines represent the standard deviation about the mean.

PILLAR PT.
U.S.A.

SHERINGHAM PT.
CANADA

MAY 26 28, 1975

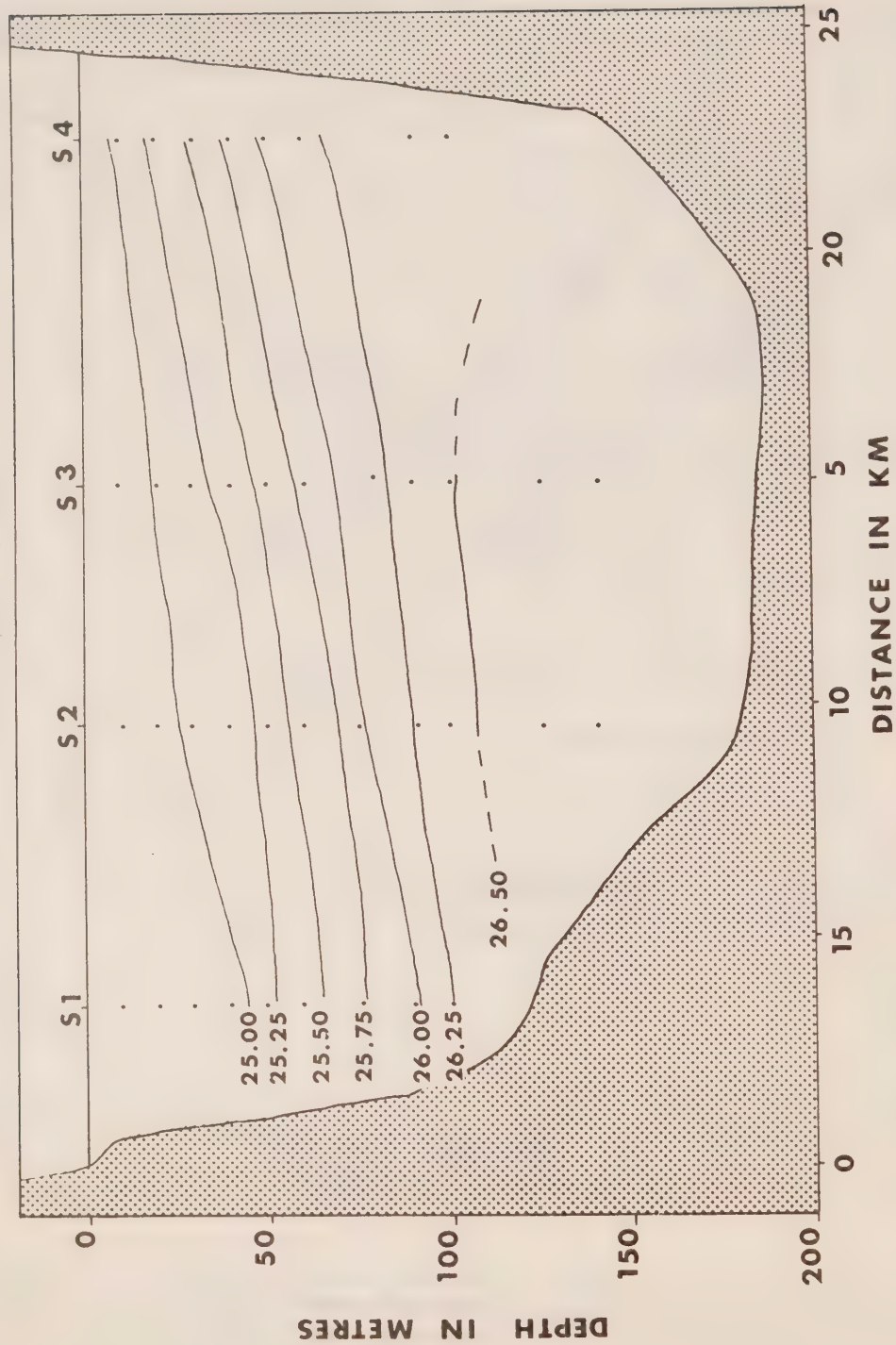


Figure 18: (a) The isopycnals through a cross-section of Juan de Fuca Strait as computed from the averaged density profiles of the May 26-28 cruise.

SHERINGHAM PT. CANADA
PILLAR PT. U.S.A.

JUNE 14-15, 1975

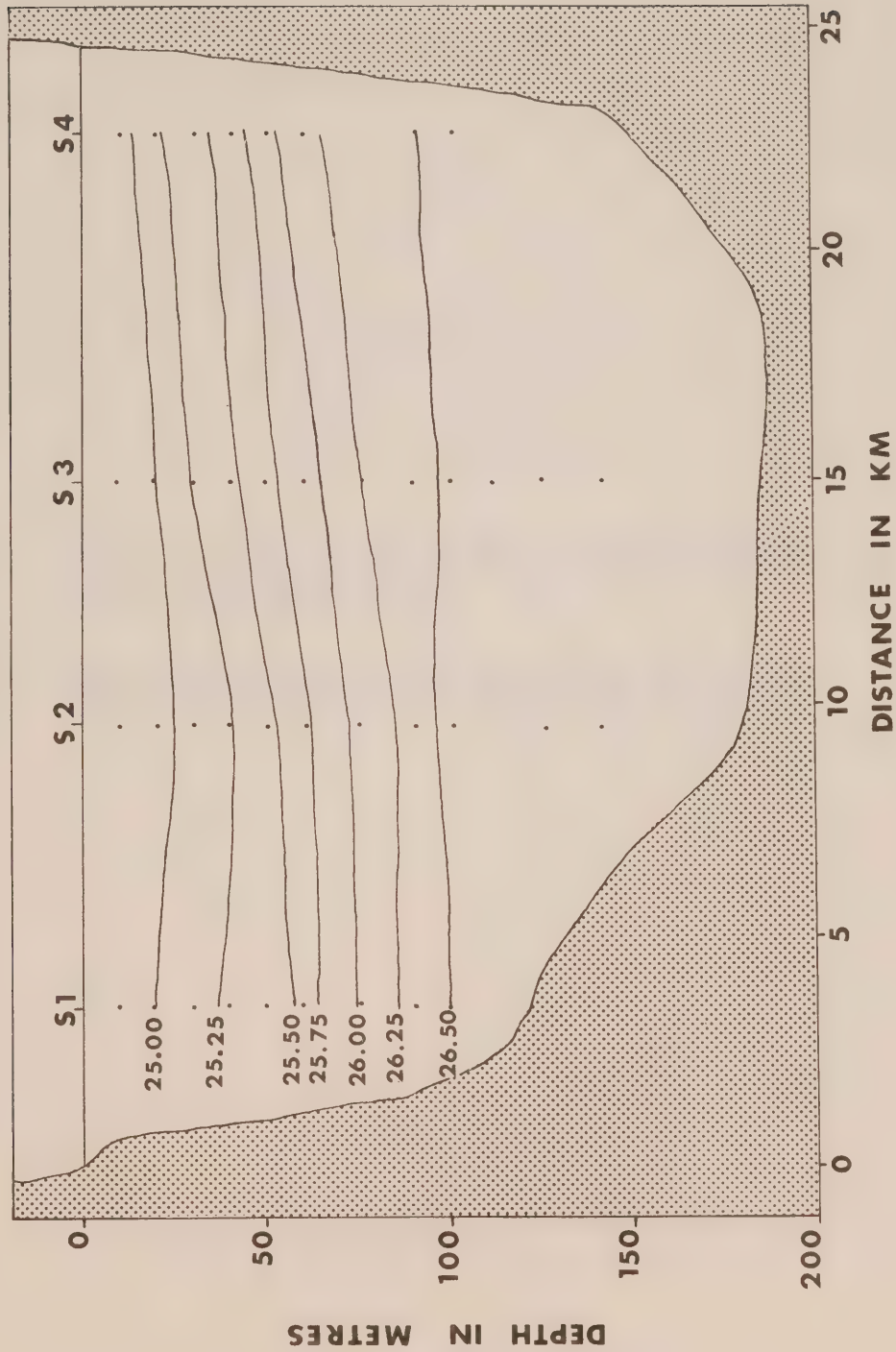


Figure 18: (b) The isopycnals through a cross-section of Juan de Fuca Strait as computed from the averaged density profiles of the June 14-15 cruise.

A P P E N D I X

Frequency distribution of speed and direction for each current meter record.

Note that for station 133 depth 20 m, the 72 zero speeds are fictitious and replace erroneous data.

STN 131 DEPTH 020 7000TC START OF RECORD 45 MN 18 HR 26 DY 05 MO 75 YR
 LENGTH OF RECORD= 49 DAYS
 RATE OF OBSER.= 4 PER HOUR

FREQUENCY DISTRIBUTION OF DIRECTION AND RATE CM/SEC

000 001 010 020 030 040 050 060 070 080 090 100 110 120 130 140 150 160 170 180 190 200 210 220 230 240
 TO

DIR	0-9	10-19	20-29	30-39	40-49	50-59	60-69	70-79	80-89	90-99	100-109	110-119	120-129	130-139	140-149	150-159	160-169	170-179	180-189	190-199	200-209	210-219	220-229	230-239	240-249
0-9	009	019	029	039	049	059	069	079	089	099	109	119	129	139	149	159	169	179	189	199	209	219	229	239	249
10-19	007	022	006	002	001																				
20-29	009	018	006	004	002																				
30-39	003	012	003	002	001																				
40-49	004	011	006	002	002	001																			
50-59	007	010	007	003	003	001																			
60-69	011	011	011	005	002	002																			
70-79	005	013	010	001	002	001	001																		
80-89	005	015	016	005	007	002	004																		
90-99	002	022	020	016	007	006	009	009	001	001															
100-109	003	030	022	034	024	017	010	006	018	004															
110-119	002	047	047	041	049	031	020	032	024	011	001														
120-129	004	023	054	040	032	046	070	044	023	021	007	001													
130-139	008	045	065	039	029	035	024	013	015	007	003	001													
140-149	003	039	055	030	014	004	004	003	001																
150-159	005	047	026	011	006	004	001																		
160-169	008	038	015	002	002																				
170-179	009	026	009	001	001																				
180-189	007	023	008		001																				
190-199	013	021	009	001																					
200-209	013	019	010	001																					
210-219	008	020	008	003																					
220-229	014	020	009	008																					
230-239	005	021	013	004	001																				
240-249	005	023	012	011	003																				
250-259	004	020	016	006	004	003																			
260-269	005	020	019	015	011	005	001	001																	
270-279	003	024	034	027	028	014	010	002	004	001															
280-289	005	018	044	043	040	063	032	030	017	011	011	013	014	013	001										
290-299	005	023	059	057	065	066	074	076	077	050	061	046	038	013	005	002									
300-309	003	035	047	065	075	057	071	043	039	034	026	013	002	001											
310-319	003	044	041	043	040	057	042	022	007																
320-329	005	020	031	024	025	022	013	003																	
330-339	003	025	020	015	011	004	010																		
340-349	003	020	011	010	001	006																			
350-359	004	015	013	002	001	002	001																		
	005	013	009	005	002	001																			
	853	791	573	491	390	287	147	112	74	54	27	6	0	0	0	0	0	0	0	0	0	0	0	0	0
	203	791	573	491	390	287	147	112	74	54	27	6	0	0	0	0	0	0	0	0	0	0	0	0	0

NUMBER OF ZERO RATES (NOT INCLUDED IN CROSS TOTALS) 0

STN 131	DEPTH 120	7000TC	START OF RECORD										45 MN	18 HR	26 DY	05 MO	75 YR	LENGTH OF RECORD= 49 DAYS										RATE OF OBSER.= 4 PER HOUR																								
			FREQUENCY DISTRIBUTION OF DIRECTION AND RATE										CM/SEC																																							
DIR	000	001	005	010	015	020	025	030	035	040	045	050	055	060	065	070	075	080	085	090	095	100	105	110	115	120																										
	TO	TO	TO	TO	TO	TO	TO	TO	TO	TO	TO	TO	TO	TO	TO	TO	TO	TO	TO	TO	TO	TO	TO	TO	TO	TO																										
0- 9	004	009	014	019	024	029	034	039	044	049	054	059	064	069	074	079	084	089	094	099	104	109	114	119	124																											
10- 19	004	012	009	005																						30																										
20- 29	002	008	007	002	002																					21																										
30- 39	001	011	006	004	002																					24																										
40- 49	002	007	013	011	003																					36																										
50- 59	002	010	003	009	006	001																				31																										
60- 69	002	009	014	006	008	002	003																			44																										
70- 79	001	008	006	011	013	003																				42																										
80- 89	003	010	008	018	013	008	002	001																		63																										
90- 99	002	006	015	013	018	009	010	006	004	005	004	006	003	002		002	001		001							107																										
100-109	008	021	022	036	025	032	031	022	028	030	032	022	015	019	011	015	018	016	007	006						453																										
110-119	001	012	018	026	034	047	035	049	044	040	037	040	023	034	029	028	032	034	037	028	026	010	004	001		701																										
120-129	001	011	020	022	030	056	046	034	020	017	017	013	017	011	008	008	008	003	004	003	001					350																										
130-139	019	026	028	030	020	024	013	014	009	010	006	009	001	008	004	003	001									225																										
140-149	001	017	030	031	029	014	011	010	005	004	003	001														156																										
150-159	002	014	024	026	024	015	004	001	005																	115																										
160-169	001	011	020	015	012	007	001	001																		68																										
170-179	005	018	019	012	007	001	001	001																		64																										
180-189	007	011	021	010	005	001																				55																										
190-199	001	020	018	008	006	001																				54																										
200-209	007	016	012	010	008	002																				55																										
210-219	004	019	010	007	002	001																				43																										
220-229	001	015	011	009	004	004																				44																										
230-239	003	014	009	003	007	003																				39																										
240-249	006	016	014	011	002	003																				52																										
250-259	012	005	012	014	001	001																				45																										
260-269	006	017	012	014	013	011	008	005	001																	88																										
270-279	002	017	010	011	022	025	034	025	015	009	006	003	001		005											185																										
280-289	003	013	023	027	030	028	034	041	055	032	042	032	019	017	012	001	003	001	001	001						415																										
290-299	002	016	022	017	040	028	037	050	051	036	049	033	028	045	035	029	030	033	028	018	010	001				639																										
300-309	003	017	028	023	022	017	018	010	009	010	007	009	009	008	009	002	008	008	009	006						232																										
310-319	003	010	020	005	011	006	001																			62																										
320-329	001	016	019	002	003																					47																										
330-339	001	012	010	004	001																					28																										
340-349	004	010	007	005																						25																										
350-359	003	012	005	001																						21																										
	001	009	005	002																						17																										
	453	452	457	457	457	279	300	279	246	191	206	175	132	134	125	85	100	96	83	34	55	16	4	4577		1																										

NUMBER OF ZERO RATES (NOT INCLUDED IN CROSS TOTALS) 0

STN 143 DEPTH 820 7000TC STAKI OF RECORD 30 NH 19 HR 27 DY 05 NO 75 YR
 LENGTH OF RECORD= 48 DAYS
 RATE OF OBSER.= 4 PER HOUR

FREQUENCY DISTRIBUTION OF DIRECTION AND RATE CM/SEC

DIR	000	001	010	020	030	040	050	060	070	080	090	100	110	120	130	140	150	160	170	180	190	200	210	220	230	240
0-9	TO	TO	TO	TO	TO	TO	TO	TO	TO	TO	TO	TO	TO	TO	TO	TO	TO	TO	TO	TO	TO	TO	TO	TO	TO	
10-19	009	019	029	039	049	059	069	079	089	099	109	119	129	139	149	159	169	179	189	199	209	219	229	239	249	
20-29	001	013	014	002	005	001	001	001	001	001	001	001	001	001	001	001	001	001	001	001	001	001	001	001	001	
30-39	002	014	011	006	001	001	001	001	001	001	001	001	001	001	001	001	001	001	001	001	001	001	001	001	001	
40-49	003	010	010	005	003	003	003	003	003	003	003	003	003	003	003	003	003	003	003	003	003	003	003	003	003	
50-59	001	012	007	004	001	001	001	001	001	001	001	001	001	001	001	001	001	001	001	001	001	001	001	001	001	
60-69	002	015	011	007	002	002	002	002	002	002	002	002	002	002	002	002	002	002	002	002	002	002	002	002	002	
70-79	002	020	006	012	003	002	002	002	002	002	002	002	002	002	002	002	002	002	002	002	002	002	002	002	002	
80-89	001	024	009	010	004	001	001	001	001	001	001	001	001	001	001	001	001	001	001	001	001	001	001	001	001	
90-99	001	024	015	008	008	007	001	019	010	011	012	004	004	004	004	004	004	004	004	004	004	004	004	004	004	
100-109	001	029	024	012	011	017	019	019	010	011	012	004	004	004	004	004	004	004	004	004	004	004	004	004	004	
110-119	001	025	024	012	017	019	041	065	039	014	007	007	007	007	007	007	007	007	007	007	007	007	007	007	007	
120-129	001	029	034	033	042	028	023	019	005	005	005	005	005	005	005	005	005	005	005	005	005	005	005	005	005	
130-139	001	024	038	038	022	019	013	002	002	002	002	002	002	002	002	002	002	002	002	002	002	002	002	002	002	
140-149	003	014	045	038	020	013	002	002	002	002	002	002	002	002	002	002	002	002	002	002	002	002	002	002	002	
150-159	001	032	041	029	014	002	002	002	002	002	002	002	002	002	002	002	002	002	002	002	002	002	002	002	002	
160-169	005	031	032	020	006	002	002	002	002	002	002	002	002	002	002	002	002	002	002	002	002	002	002	002	002	
170-179	029	009	011	004	002	002	002	002	002	002	002	002	002	002	002	002	002	002	002	002	002	002	002	002	002	
180-189	003	023	025	002	001	001	001	001	001	001	001	001	001	001	001	001	001	001	001	001	001	001	001	001	001	
190-199	003	025	022	005	004	004	004	004	004	004	004	004	004	004	004	004	004	004	004	004	004	004	004	004	004	
200-209	005	025	014	007	005	005	005	005	005	005	005	005	005	005	005	005	005	005	005	005	005	005	005	005	005	
210-219	002	020	013	011	002	002	002	002	002	002	002	002	002	002	002	002	002	002	002	002	002	002	002	002	002	
220-229	003	024	014	011	005	001	001	001	001	001	001	001	001	001	001	001	001	001	001	001	001	001	001	001	001	
230-239	003	031	026	027	007	002	002	002	002	002	002	002	002	002	002	002	002	002	002	002	002	002	002	002	002	
240-249	072	003	034	031	017	018	005	001	001	001	001	001	001	001	001	001	001	001	001	001	001	001	001	001	001	
250-259	001	021	035	026	033	018	007	001	001	001	001	001	001	001	001	001	001	001	001	001	001	001	001	001	001	
260-269	001	024	037	030	043	041	018	018	018	013	003	001	012	007	001	001	001	001	001	001	001	001	001	001	001	
270-279	004	023	041	040	059	044	035	046	027	024	024	024	045	058	046	020	002	002	002	002	002	002	002	002	002	
280-289	003	031	027	033	042	037	044	059	062	065	050	045	045	045	045	045	045	045	045	045	045	045	045	045	045	
290-299	001	029	025	030	034	037	042	051	061	069	038	042	027	007	007	007	007	007	007	007	007	007	007	007	007	
300-309	001	023	033	028	030	025	023	027	025	017	003	002	002	001	001	001	001	001	001	001	001	001	001	001	001	
310-319	001	018	017	024	025	021	008	012	008	001	001	001	001	001	001	001	001	001	001	001	001	001	001	001	001	
320-329	002	006	017	017	019	009	005	004	004	004	004	004	004	004	004	004	004	004	004	004	004	004	004	004	004	
330-339	004	014	019	016	007	007	003	002	002	002	002	002	002	002	002	002	002	002	002	002	002	002	002	002	002	
340-349	001	010	017	004	003	002	002	002	002	002	002	002	002	002	002	002	002	002	002	002	002	002	002	002	002	
350-359	001	013	008	007	002	002	002	002	002	002	002	002	002	002	002	002	002	002	002	002	002	002	002	002	002	
	774	763	589	589	589	589	589	589	589	589	589	589	589	589	589	589	589	589	589	589	589	589	589	589	589	
	65	763	763	763	763	763	763	763	763	763	763	763	763	763	763	763	763	763	763	763	763	763	763	763	763	

NUMBER OF ZERO RATES (NOT INCLUDED IN CROSS TOTALS) 72

STN 135	DEPTH 020	7000TC	FREQUENCY DISTRIBUTION OF DIRECTION AND RATE										START OF RECORD										RATE OF OBSER.= 4 PER HOUR									
			CM/SEC										75 YR										49 DAYS									
			CM/SEC										75 YR										49 DAYS									
			CM/SEC										75 YR										49 DAYS									
			CM/SEC										75 YR										49 DAYS									
			CM/SEC										75 YR										49 DAYS									
			CM/SEC										75 YR										49 DAYS									
			CM/SEC										75 YR										49 DAYS									
			CM/SEC										75 YR										49 DAYS									
			CM/SEC										75 YR										49 DAYS									
			CM/SEC										75 YR										49 DAYS									
			CM/SEC										75 YR										49 DAYS									
			CM/SEC										75 YR										49 DAYS									
			CM/SEC										75 YR										49 DAYS									
			CM/SEC										75 YR										49 DAYS									
			CM/SEC										75 YR										49 DAYS									
			CM/SEC										75 YR										49 DAYS									
			CM/SEC										75 YR										49 DAYS									
			CM/SEC										75 YR										49 DAYS									
			CM/SEC										75 YR										49 DAYS									
			CM/SEC										75 YR										49 DAYS									
			CM/SEC										75 YR										49 DAYS									
			CM/SEC										75 YR										49 DAYS									
			CM/SEC										75 YR										49 DAYS									
			CM/SEC										75 YR										49 DAYS									
			CM/SEC										75 YR										49 DAYS									
			CM/SEC										75 YR										49 DAYS									
			CM/SEC										75 YR										49 DAYS									
			CM/SEC										75 YR										49 DAYS									
			CM/SEC										75 YR										49 DAYS									
			CM/SEC										75 YR										49 DAYS									
			CM/SEC										75 YR										49 DAYS									
			CM/SEC										75 YR										49 DAYS									
			CM/SEC										75 YR										49 DAYS									
			CM/SEC										75 YR										49 DAYS									
			CM/SEC										75 YR										49 DAYS									
			CM/SEC										75 YR										49 DAYS									
			CM/SEC										75 YR										49 DAYS									
			CM/SEC										75 YR										49 DAYS									
			CM/SEC										75 YR										49 DAYS									
			CM/SEC										75 YR										49 DAYS									
			CM/SEC										75 YR										49 DAYS									
			CM/SEC										75 YR										49 DAYS									
			CM/SEC										75 YR										49 DAYS									
			CM/SEC										75 YR										49 DAYS									
			CM/SEC										75 YR										49 DAYS									
			CM/SEC										75 YR										49 DAYS									
			CM/SEC										75 YR										49 DAYS									
			CM/SEC										75 YR										49 DAYS									
			CM/SEC										75 YR										49 DAYS									
			CM/SEC										75 YR										49 DAYS									
			CM/SEC										75 YR										49 DAYS									
			CM/SEC										75 YR										49 DAYS									
			CM/SEC										75 YR										49 DAYS									
			CM/SEC										75 YR										49 DAYS									
			CM/SEC										75 YR										49 DAYS									
			CM/SEC										75 YR										49 DAYS									
			CM/SEC										75 YR										49 DAYS									
			CM/SEC										75 YR										49 DAYS									
			CM/SEC										75 YR										49 DAYS									
			CM/SEC										75 YR										49 DAYS									
			CM/SEC										75 YR										49 DAYS									
			CM/SEC										75 YR										49 DAYS									
			CM/SEC										75 YR										49 DAYS									
			CM/SEC										75 YR										49 DAYS									
			CM/SEC										75 YR										49 DAYS									
			CM/SEC										75 YR										49 DAYS									
			CM/SEC										75 YR										49 DAYS									
			CM/SEC										75 YR										49 DAYS									
			CM/SEC										75 YR										49 DAYS									
			CM/SEC										75 YR										49 DAYS									
			CM/SEC										75 YR										49 DAYS									
			CM/SEC										75 YR										49 DAYS									
			CM/SEC										75 YR										49 DAYS									
			CM/SEC										75 YR										49 DAYS									
			CM/SEC										75 YR										49 DAYS									
			CM/SEC										75 YR										49 DAYS									
			CM/SEC										75 YR										49 DAYS									
			CM/SEC										75 YR										49 DAYS									
			CM/SEC										75 YR										49 DAYS									
			CM/SEC										75 YR										49 DAYS									
			CM/SEC										75 YR										49 DAYS									
			CM/SEC										75 YR										49 DAYS									
			CM/SEC										75 YR										49 DAYS									
			CM/SEC										75 YR										49 DAYS									
			CM/SEC										75 YR										49 DAYS									
			CM/SEC										75 YR										49 DAYS									
			CM/SEC										75 YR										49 DAYS									
			CM/SEC										75 YR										49 DAYS									
			CM/SEC										75 YR										49 DAYS									
			CM/SEC										75 YR										49 DAYS									
			CM/SEC										75 YR										49 DAYS									
			CM/SEC										75 YR										49 DAYS									
			CM/SEC										75 YR										49 DAYS									
			CM/SEC										75 YR										49 DAYS									
			CM/SEC										75 YR										49 DAYS									
			CM/SEC										75 YR										49 DAYS									
			CM/SEC										75 YR										49 DAYS									
			CM/SEC										75 YR										49 DAYS									
			CM/SEC										75 YR										49 DAYS									
			CM/SEC										75 YR										49 DAYS									
			CM/SEC										75 YR										49 DAYS									
			CM/SEC										75 YR										49 DAYS									
			CM/SEC										75 YR										49 DAYS									
			CM/SEC										75 YR										49 DAYS									
			CM/SEC										75 YR										49 DAYS									
			CM/SEC										75 YR										49 DAYS									

NUMBER OF ZERO RATES (NOT INCLUDED IN CROSS TOTALS) 0

STN 136	DEPTH 020	7000TC	START OF RECORD	15 MN	09 HR	27 DY	05 MO	75 YR	LENGTH OF RECORD= 50 DAYS RATE OF OBSER.= 4 PER HOUR																		
FREQUENCY DISTRIBUTION OF DIRECTION AND RATE													CM/SEC														
DIR	000	001	010	020	030	040	050	060	070	080	090	100	110	120	130	140	150	160	170	180	190	200	210	220	230	240	
	TO	TO	TO	TO	TO	TO	TO	TO	TO	TO	TO	TO	TO	TO	TO	TO	TO	TO	TO	TO	TO	TO	TO	TO	TO	TO	
	009	019	029	039	049	059	069	079	089	099	109	119	129	139	149	159	169	179	189	199	209	219	229	239	249		
	023	022	001																								
	017	020																									
	023	021																									
	023	018	001																								
	017	018	002																								
	014	023	001																								
	023	027	004																								
	025	041	011	002	001																						
	021	027	015	007	003																						
	023	055	022	021	014	007																					
	016	055	047	039	033	028	022	007	001																		
	019	046	068	064	063	048	087	046	015	005	001																
	023	048	059	046	031	032	028	024	009	002	001																
	011	029	026	027	013	004	002	001	001																		
025	034	020	011	003	001																						
024	024	006	002																								
001	010	015	001																								
170-179		017	011																								
180-189		013	006	002																							
190-199		010	007																								
200-209		016	006																								
210-219		012	004																								
220-229		013	008																								
230-239		013	016	002																							
240-249		018	013	001																							
250-259		008	027	011																							
260-269		012	025	019	006																						
270-279		021	048	052	014	012	006	001	002																		
280-289		020	055	074	058	032	023	030	033	019	025	011	005	002													
290-299		024	082	104	115	104	102	109	103	089	065	056	044	018	002	002											
300-309		021	079	104	091	078	057	036	020	018	014	007		001	002	001											
310-319		019	058	063	030	014	002		001																		
320-329		015	043	022	004																						
330-339		021	032	010	001																						
340-349		019	023	005																							
350-359		017	022	002																							
		1088	538	320	237	151	113	49	21	4	3	0	0	0	0	0	0	0	0	0	0	0	0	0	0	0	
	646	755	401	315	237	151	76	21	3	0	0	0	0	0	0	0	0	0	0	0	0	0	0	0	0	0	

NUMBER OF ZERO RATES (NOT INCLUDED IN CROSS TOTALS) 1

STN 132	DEPTH 020	7000TC	FREQUENCY DISTRIBUTION OF DIRECTION AND RATE																				START OF RECORD		45 MN		16 HR		26 DY		05 MO		75 YR		LENGTH OF RECORD= 49 DAYS		RATE OF OBSER.= 4 PER HOUR	
			CN/SEC																																			
DIR	000	001	010	020	030	040	050	060	070	080	090	100	110	120	130	140	150	160	170	180	190	200	210	220	230	240												
	TO	TO	TO	TO	TO	TO	TO	TO	TO	TO	TO	TO	TO	TO	TO	TO	TO	TO	TO	TO	TO	TO	TO	TO	TO	TO												
0- 9	009	019	029	039	040	059	069	079	089	099	109	119	129	139	149	159	169	179	189	199	209	219	229	239	249													
10- 19	013	019	009	001																																		
20- 29	016	013	005	001																																		
30- 39	013	012	003																																			
40- 49	012	015	007	001																																		
50- 59	018	015	008	002																																		
60- 69	008	032	006	004																																		
70- 79	006	022	006	002																																		
80- 89	010	025	013	005																																		
90- 99	013	049	041	012	007	001																																
100-109	010	034	025	032	013	007	004	004	002			001																										
110-119	006	036	040	039	034	032	023	029	028	025	027	013	002																									
120-129	013	044	045	053	055	037	055	076	086	071	060	020	006																									
130-139	011	036	042	043	055	031	026	037	024	013	005	002																										
140-149	005	039	025	022	022	012	011	003																														
150-159	008	028	016	008	004	002																																
160-169	016	018	010	006	002																																	
170-179	011	021	005	001																																		
180-189	010	017	002	001																																		
190-199	015	019																																				
200-209	010	016	001																																			
210-219	009	015	001																																			
220-229	008	015																																				
230-239	010	018	003	001																																		
240-249	009	019	006																																			
250-259	008	030	009	002	001																																	
260-269	010	034	017	013	002	001	001																															
270-279	011	038	033	030	014	012	005	001	001																													
280-289	006	038	053	050	045	041	035	034	037	027	019	027	016	007	006																							
290-299	006	041	054	070	072	085	075	091	057	062	049	048	040	014	006																							
300-309	006	035	065	080	058	052	023	031	015			005	003	003																								
310-319	004	030	079	051	024	013	001	001																														
320-329	010	035	029	019	006	002																																
330-339	009	027	020	006	003																																	
340-349	011	020	006	004																																		
350-359	006	021	004	004																																		
	013	026	001	001																																		
	360	952	659	563	415	339	307	259	198	166	113	67	21	12	0	0	0	0	0	0	0	0	0	0	0													

NUMBER OF ZERO RATES (NOT INCLUDED IN CROSS TOTALS) 0

CA 1 EP 321
-76R07

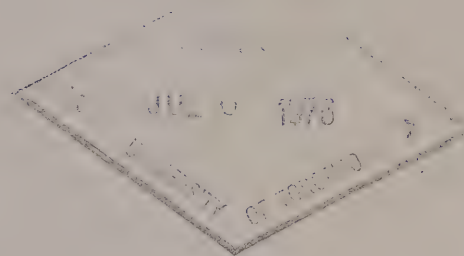
*Alaska
North American
Pacific Region*

Pacific Marine Science Report 76-7

Government
Publications

A FIELD TRANSLATION SYSTEM FOR AANDERAA DATA TAPES

by



W.H. Bell, D.M. Farmer and G.R. Kamitakahara

INSTITUTE OF OCEAN SCIENCES, PATRICIA BAY
Victoria, B.C.



For additional copies or further information, please write to:

Environment Canada
Institute of Ocean Sciences, Patricia Bay
512 - 1230 Government Street
Victoria, B.C.
V8W 1Y4

A FIELD TRANSLATION SYSTEM

• FOR

AANDERAA DATA TAPES

by

W.H. Bell, D.M. Farmer and G.R. Kamitakahara

Institute of Ocean Sciences, Patricia Bay
Victoria, B.C.

March 1976

This is a manuscript which has received only limited circulation. On citing this report in a bibliography, the title should be followed by the words "UNPUBLISHED MANUSCRIPT" which is in accordance with accepted bibliographic custom.

ABSTRACT

The use of moored arrays of recording current meters to obtain long time-series observations of various oceanographic parameters has generated a requirement for some data-processing capability in the field. This report describes a raw-data translation system which can reconstitute the data recorded on Aanderaa Data Logger magnetic tapes, perform various mathematical operations on it and plot it in time-series form on a strip chart recorder. A description is given of the various components of the translation system and of the software programs.

TABLE OF CONTENTS

	<u>Page</u>
ABSTRACT	i
TABLE OF CONTENTS	iii
LIST OF FIGURES	v
LIST OF TABLES	v
INTRODUCTION	1
DATA TAPE FORMAT	2
TRANSLATOR COMPONENTS	5
1. Tape Deck	5
2. Signal Conditioning	5
3. Oscilloscope	5
4. Read Interface	5
5. Processor	7
6. Write Interface and Digital-to-Analog Conversion	7
7. Strip Chart Recorder	7
8. Packaging	8
SOFTWARE	8
1. Format	8
2. Operations	8
3. Program Logic	10
APPENDIX A - SOFTWARE PROGRAM LOGIC	11
1. Background	11
2. Foreground	11

LIST OF FIGURES

Figure 1.	Data tape translation system	3
Figure 2.	Sample output trace from the translator	4
Figure 3.	Block diagram of data tape translator	6
Figure 4.	Software program: Background flowchart	15
Figure 5.	Software program: Foreground flowchart - input	16
Figure 6.	Software program: Foreground flowchart - output	17

LIST OF TABLES

Table 1.	General recording formats of Aanderaa Instruments	9
Table 2.	Data operations	12
Table 3.	Example of operations for a current meter data dump	14

INTRODUCTION

Long time series observations of oceanographic parameters taken with moored recording instruments have become a most important tool in oceanographic research. It is commonplace to acquire data records of two months or more from recording current meters, thermistor chains, anemometers and tide gauges. This new capability has generated a range of new problems in handling the large quantity of data produced. This report describes an attempt to resolve some of these problems by bringing part of the data-processing capability into the field, in particular, that part which translates the raw data into a more comprehensible form. The principle is not new, and shipboard computers are widely used for this purpose. The equipment described here differs from these larger scale systems principally in that it is self contained and portable (but does require a power source). It is thus especially useful in the study of inshore oceanography and lakes where smaller vessels or launches are used in place of large research ships.

The need for a portable field data translation system first became apparent during an operation in a fairly remote lake of northern B.C. There were more than twenty recording instruments in use at the time, each requiring a tape change every one or two months. The amount of data generated was substantial as was the data processing effort required to keep abreast of it.

The demand for immediate data translation arises for two quite different reasons:

1. There is a practical requirement of knowing whether or not an instrument is working. It is insufficient to know that the instrument works when it is recovered, for example, during a tape-change, since some of the faults that can occur are of a sporadic nature. Of course, the need to know immediately of instrument failures is less important when the field operation lasts only as long as the data-logger tape, or when enough instruments are available to permit their replacement with each tape-change. Servicing instruments in the field is greatly facilitated if a plot of the record is available.
2. Immediate data presentation is essential if the program is to be modified as a result of new information. This applies both to the modification of the instrument (dynamic range adjustments, sampling frequencies necessary to avoid aliasing, etc.) and also to modification of instrument deployment (depths, locations). Thus, a particular project might involve a brief pilot study in which very rapid sampling was used. Field analysis of the data from the pilot study would then be used to determine the most appropriate sampling frequency as well as instrument spacings, etc.

Additionally, there is the advantage of immediate data presentation. It permits the scientist to make a preliminary assessment of the data without having to wait through the delays in processing that are often unavoidable at computing centres. Moreover, the initial presentation is often good enough to permit the scientist to bypass the early stages of processing and plotting, and concentrate on more specific forms of analysis. Thus, the field translator described here has also been found equally useful in the laboratory whenever a quick plot is needed. Since the system is quite flexible and allows different expansions on each axis, it is especially convenient for

examining details of isolated phenomena that are too compressed to study on a plot of the full record.

The following criteria were established for designing the equipment:

1. The system must be portable. The operations often involve transporting equipment by small trucks and launches. Thus, the system must be reasonably invulnerable to vibration, dust or moisture. It must not be too heavy. Two people should be able to load it onto a truck. Its power requirements must also be reasonable (nominally 110 v, 60 hz, 10 amps).
2. It must also be flexible in the sense that different types of data are obtained which require different forms of presentation. Thus, it might be required to convert the incremental measurement of rotor counts into speed, or speed and direction might need to be resolved into components.
3. It would clearly have been impractical to have designed equipment to handle tapes from a very wide range of instruments. The system described here is set up to handle output from Aanderaa Data Loggers, but it could be modified to handle cassette tapes, or tapes with a different data format, if required.
4. A six pen chart recorder output was a useful compromise in that it allowed comparison of up to six channels simultaneously without being too bulky or producing too small a plot for easy analysis. For plotting data from those instruments that use more than six channels, the tape can be processed twice.

The interfaces between tape recorder and computer, and between computer and chart recorder, were designed and built under contract by MacDonald, Detweiler and Associates Ltd., Vancouver. The complete system is shown in Figure 1 and a sample output trace is presented in Figure 2.

DATA TAPE FORMAT

The tape translation system is designed to produce strip chart records of various time series information directly from the raw data recorded on magnetic tape in the Aanderaa Data Logger. The Data Logger records digital data on 1/4" tape, stored on 3" reels, in a pulse duration modulation code. Each data word consists of 10 bits, in serial form. The most significant bit is recorded first. Either 6 or 12 words comprise a complete measurement cycle or record. Each cycle is followed by a synchronizing (sync) pulse (except on some early tapes). A digital "1" is recorded as a short pulse occupying a physical length of 0.02 mm on the tape. A "0" is recorded as a pulse of length 0.06 mm. The distance between pulse or bit leading edges is 0.12 mm. Each data word is separated from the next word by a space. The length of a word plus space is 3 mm. The recording method is Return-to-Zero, i.e., the tape is magnetically saturated for pulses, otherwise it is unmagnetized. In addition to the desired coded data signal, there may be noise on the tape due to incomplete or improper degaussing of the tape prior to recording or to faulty mechanical or electronic components.



Figure 1. Data tape translation system.

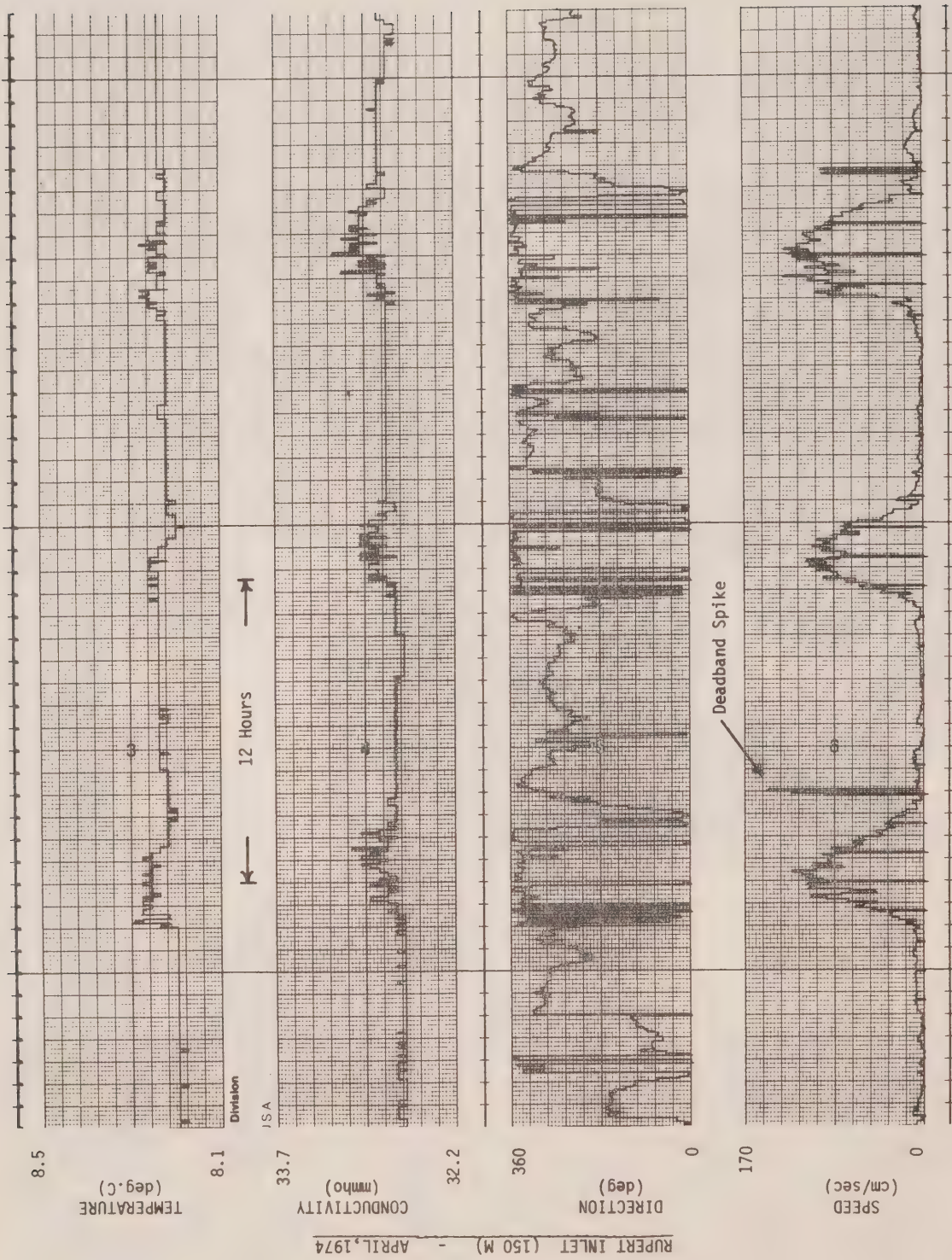


Figure 2. Sample output trace from the translator.

TRANSLATOR COMPONENTS

The tape translation system is shown in block diagram form in Figure 3. Pertinent details of each block are given below:

1. Tape Deck

The tape deck is an AKAI Model 4000DS. This is a standard reel-to-reel device for home audio systems. It weighs about 25 lbs. The power requirement is 115 v, 60 Hz at 35 watts. Tape playback speed is 7 1/2 ips, or 64 data words per second. The playback head is followed by a fixed-gain preamp with an output impedance of 100 K ohms. There are no controls which need to be manipulated on the tape deck except those controlling the tape drive.

2. Signal Conditioning

When the raw data tape is played back, the signal obtained from the play-back head is the derivative of the signal represented by the saturated portions of the magnetic tape, or by tape noise (because the output voltage is proportional to the rate-of-change of flux). Signal-conditioning circuitry must be employed to reconstitute the data pulses and to provide some degree of noise rejection.

The basic conditioning circuitry comprises a buffer amplifier, a high-pass filter, and two comparators, each followed by inverters. One comparator processes the positive-going signals and the other processes the negative-going ones. The filter bandwidth is adjustable, as are the comparator "slicing" level and hysteresis.

The inverter outputs are applied to a series of flip-flops, gates and timers. Some of these are used for simple error detection, such as the sequential occurrence of two pulses of like polarity. The remainder are used for regenerating the data signal, converting the pulse width modulations into binary bits and detecting the interword gap. The reconstructed data words are loaded into a 10-bit shift register, ready for transfer to the computer. Errors cause brief illumination of a light-emitting diode mounted on the front panel. Error bits can be "written" on one channel of the strip chart recording, if desired.

3. Oscilloscope

The oscilloscope permits an examination of the data waveforms and observation of the effect of adjustments to the signal conditioning controls. A Hewlett-Packard Model 1200 B oscilloscope was chosen for this application because of its versatility and rugged construction. Its power requirement is 115 v, 48-440 Hz at 50 watts. The weight is 23 lbs.

4. Read Interface

The read interface is designed around a Digital Equipment Corporation (DEC) M 1709 Omnibus Interface Foundation Module. This contains most of the required logic circuitry, including bus drivers/receivers, device selectors, interrupt/skip circuitry, etc. The interrupt system is used to inform the

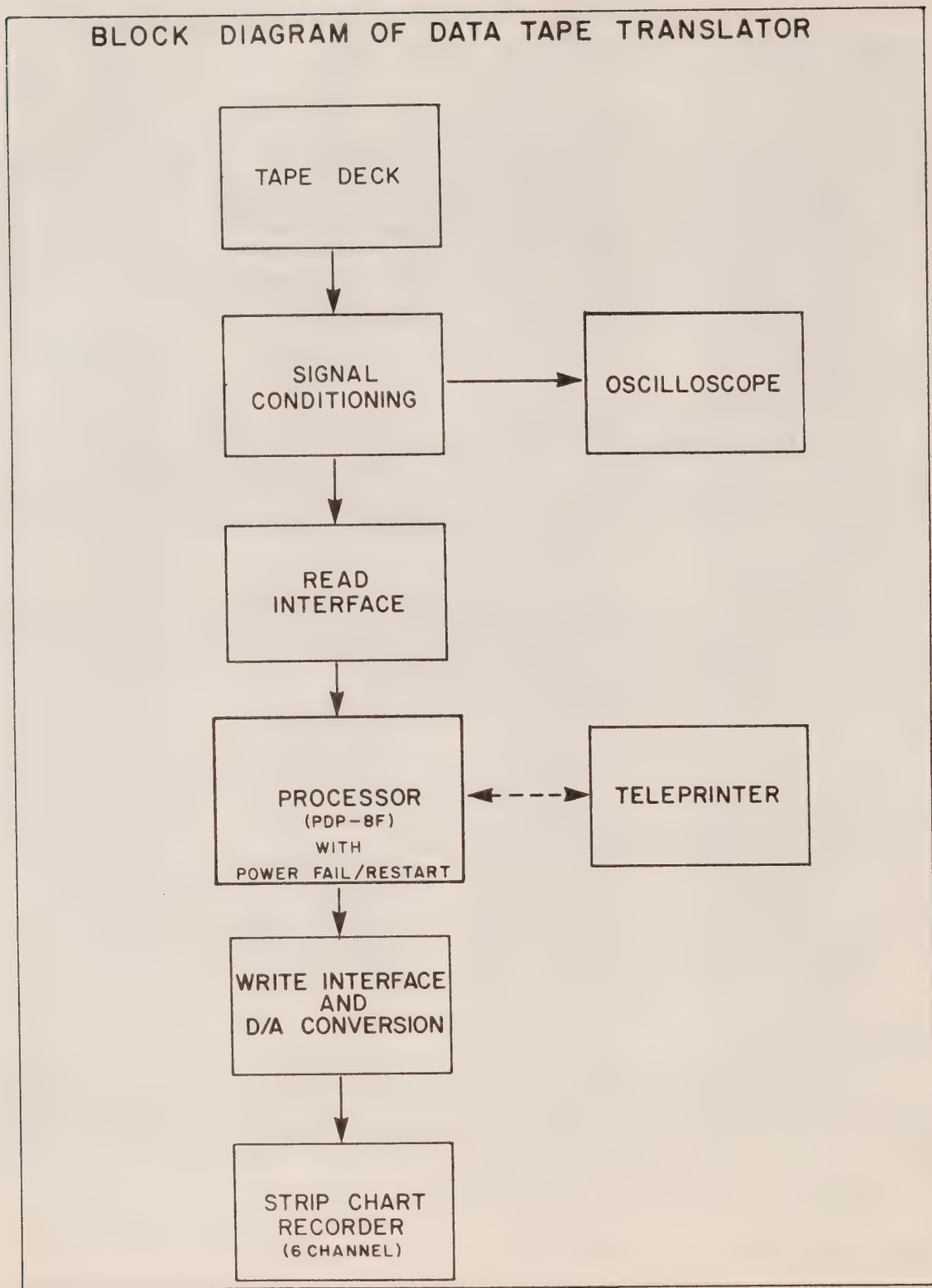


Figure 3.

central processor that a data word is ready to be read from the 10-bit shift register of the signal conditioning section, or that a sync pulse (indicating the end of a record) has been encountered.

5. Processor

Initially, a choice had to be made between hard-wired logic or a minicomputer for the central processor of the tape translation system. It was decided that the minicomputer approach provided much greater flexibility at little additional cost, since the hard-wired logic design costs would be greater, even though the component costs were lower, and system alterations would be more difficult to make. The duties of the central processor in this application are light, being principally to make decisions about the state of the data input and to provide appropriate control signals.

The DEC PDP-8F was chosen for its low cost and ready availability. It was obtained in a rack-mount version with 8 K memory, teletype interface, and power fail/restart option. Since it was intended to read programs into memory, via a teletype, before leaving headquarters for field operations, the restart option was a necessity. This requirement arose because for some proposed field operations, it would not be possible to cope with either the bulk of the teletype or its extremely stringent line frequency stability requirement ($60 \text{ Hz} \pm 0.45 \text{ Hz}$). The PDP-8F has a power requirement of 500 watts. It draws a maximum of 5.6 amps at 95-130 v, 47-63 Hz. The weight is about 90 lbs.

6. Write Interface and Digital-to-Analog Conversion

The write interface is similar to the read interface, it also being designed around the DEC M 1709 Interface Module. It generates timing pulses for the transfer of data from the PDP-8F accumulator to holding registers at the inputs to six digital-to-analog converters (DAC). The DAC's are Analog Devices Model DAC-10Z-1 with 10-bit resolution and 5 microseconds settling time. They are powered by an Analog Devices Model 920 power supply. The DAC's and their power supply (and the signal conditioning circuitry) are on printed circuit boards mounted in a DEC H 911-S backplane assembly, installed behind the tape deck in the mounting case. The DAC outputs are buffered by operational amplifiers. The digital words in the holding registers are converted to an analog signal and directed to a 6-channel recorder to provide a time series representation of the data.

7. Strip Chart Recorder

The Brush Model 15-6367-00 general purpose 6-channel strip chart recorder was chosen for this application. It uses pressurized ink writing, has a frequency response of 40 Hz, an input impedance of 10 megohms, and has proven itself to be reliable in field use. It weighs 65 lbs. and consumes 200 watts of power at $115 \text{ v} \pm 10\%$.

With a system input speed of 64 words/sec, and with 6 words/record, the writing rate to the recorder is about 10 records/sec. For a typical instrument sampling rate of 6 records/hr, with a phenomenon having a semi-diurnal period (about 12 hours), the writing time for one cycle is about 7 secs. A chart speed of 1 mm/sec provides a suitable display size without wasting paper. A raw data tape containing about 6000 records (6 weeks with a

10-min sample interval) requires a processing time of 10 minutes.

8. Packaging

All of the system components are permanently installed in two Hewlett-Packard Model 9211-1245 fiberglass Field Cases. They contain shock-mounted rack mounts, and have covers which provide an airtight seal. The system can be transported directly to its destination in the field cases, with no additional packaging. To put the translator into operation, it is only necessary to remove the field case covers, link the components together with cables and apply power.

The outside dimensions of the case are approximately 26 x 30 x 29 inches and the empty weight is 70 lbs. The nominal rack height is 21 inches. The rack mounts had to be lengthened slightly to accommodate the component pieces satisfactorily. The oscilloscope and chart recorder are installed in one case, and the computer, backplane and tape deck in the other.

SOFTWARE

The software program for the PDP-8 performs various operations on the data derived from Aanderaa instruments and plots the results on the six-channel brush recorder. The program was written in PDP-8 assembler language and compiled on the IBM 370 at the University of British Columbia. A binary paper tape was generated for input into the computer through a teletype. A brief description of the software design is given immediately below, while a more detailed examination is presented in Appendix A.

1. Format

The general recording formats of the three types of Aanderaa instruments used are shown in Table 1. Anemometers and current meters have 6 channels (5 of which record sensor readings and one which records a reference number characteristic of a particular instrument). The thermistor chains have 12 channels (11 of which record temperature readings and one which records the reference number).

2. Operations

Various operations may be done on each channel independently. These include routines to do the following:

- (1) Plot 6 channels of raw data. (Thermistor chain data requires two passes, dumping 6 channels per pass.)
- (2) Multiply a channel by any factor and add a constant value to a channel. These two operations can, in combination, be used to produce calibrated data from the raw data.
- (3) Differentiate the speed channel to give a recognizable speed quantity. (In raw data form it is given simply as the number of accumulated rotor counts.)

TABLE 1

GENERAL RECORDING FORMATS OF AANDERAA INSTRUMENTS

Anemometer:

Channel No.	1	2	3	4	5	6
Variable:	Reference number	Air temp	Water temp	Buoy direction	Wind direction	Integrated wind speed

Current Meter:

Channel No.	1	2	3	4	5	6
Variable:	Reference number	Water temp	Conductivity	Pressure	Current direction	Integrated current speed

Thermistor Chain:

Channel No.	1	2	3	4	5	6	7	8	9	10	11	12	
Variable:	Reference	Thermistor											
	number	number:	#1	#2	#3	#4	#5	#6	#7	#8	#9	#10	#11

- (4) Keep track of time, marking off days and hours.
- (5) Plot vector components computed from the direction and speed channel for both anemometers and current meters.
- (6) Remove "spikes" introduced into the data by instrument malfunction or anomalies. (For example, in older instruments spurious values could occur when the circular potentiometer driven by the rotor is in a small dead-band zone near the ends of the resistive element.)

The program is set up so any operation may be easily added to it as a separate subroutine.

3. Program Logic

The main program has two basic sections, a background and a foreground. The background section begins by initializing various parameters. It then enters a loop in which the information represented by the computer front-panel sense switch settings is read and stored. This information refers to the operations to be carried out on the data. The loop is continuously re-entered until sense switch number 11 is found to be set, indicating that the operator is ready to begin processing. The program then permits adjustments to be made to the zero and full-scale settings of the strip chart recorder, and it provides appropriate input voltages for this purpose. Next, another loop is entered which checks the condition of the digital-to-analog (D/A) conversion flag. It also causes the front panel lights to flash sequentially, indicating correct program operation. Exit from this loop, into the foreground routine, occurs when the D/A flag is set.

The foreground section is divided into input and output routines. The input portion reads a data word into an input buffer register when requested to do so by an interrupt signal. The interrupt signal is provided by the previously-mentioned read interface when the input shift register is full. Data words are tested to determine whether they are synchronizing pulses, inter-record gaps or genuine data. They are also tested for certain error conditions. When all of the words of the data set have been examined and stored (if appropriate), the D/A flag is set and control returns to the background program.

The foreground output routine is entered from the background program when the D/A flag is detected. This routine takes the stored input data, processes it through the operations requested by the sense switch settings, and directs it to the output registers. When all channels of the data set have been processed, they are then plotted out sequentially on the strip chart recorder via the D/A converters.

APPENDIX ASOFTWARE PROGRAM LOGIC

The program consists of two major sections, a background and a foreground, as described below and shown in flow chart form in Figures 4, 5 and 6.

1. Background

The background section begins by initializing various parameters. It then reads the front panel sense switches (SSW) and checks to see if SSW #11 is set. If it is set, it saves the sense switch information. If it is not set, the front panel is re-read until SSW #11 is set. The various operations to be done on the data are indicated at this point by setting particular combinations of SSW #2, #3, #4 and #5. Instructions to do these various operations are contained in several locations whose starting addresses are shown in Table 2. For example, the set of instructions to do a raw data dump of the last six channels of a thermistor chain is contained in locations starting at 5100 and indicated by setting SSW #2, #5 and #11. (Note that bit #11 should always be set.)

Next, the operator adjusts each pen to the zero position on the Brush recorder. The background section then allows the Brush recorder to be adjusted to full scale and then to zero again. It does this by loading 1024 in the output registers, whence the D/A converters provide appropriate voltages at the inputs to the Brush recorder channels. The computer halts and allows the operator to adjust each pen manually to coincide with the full scale line to the far left of each track on the strip chart. The operator then presses CONTINUE and a zero voltage is presented to each channel. Again the computer halts and allows the operator to adjust for the zero pen position to the far right of each track. By pressing CONTINUE, the background program proceeds to a continuous loop in which lights on the front panel are illuminated sequentially in rotation to the left. Continuous rotation of the lights on the front panel indicates that the program is running well. Each time the program progresses through the loop, it checks to see if the digital-to-analog (D/A) conversion flag is set. The D/A flag is set in the foreground section after one complete cycle of data has been read into the input buffer. When the background loop detects the set flag, the program is directed to the output routine where various operations are performed on the cycle of data.

2. Foreground

The foreground section can also be thought of as having two parts: an input and an output. The input part reads data from the tape recorder one word at a time and fills the input buffer with one complete cycle of data. It does so by means of an interrupt system. When the background loop detects an interrupt, the program is directed to a skip chain to determine which device is causing the interrupt. It first checks for a power failure flag. If a power failure is detected, the computer has 1 millisecond left in which to operate. In this time, the program counter, the restart instruction, the accumulator and the link are saved. When the power comes up again the program is automatically directed to location zero where the restart instruction is stored. The accumulator and link are restored and the program starts up where it left off. If the power failure flag is not set, the program checks for a

TABLE 2

DATA OPERATIONS

ADDRESS	OPERATION	FRONT PANEL SWITCH NOS.
4000	Six channel raw data dump	11
4100	Six channel raw data dump with speed differenced	5, 11
4200	Six channel tape with channels calibrated and speed differenced	4, 11
4300	Current meter with vector components	4, 5, 11
4400	Anemometer with vector components	3, 11
4500	Spike removal	3, 5, 11
5000	Raw data dump of first six channels of thermistor chain	2, 11
5100	Raw data dump of last six channels of thermistor chain	2, 5, 11
5200	First six channels of thermistor chain (calibrated)	2, 4, 11
5300	Last six channels of thermistor chain (calibrated)	2, 4, 5, 11

tape recorder interrupt. If this flag is set, it proceeds to the input section of the foreground program. The first word is read. If the accumulator is zero, as would be the case before data starts on the tape, the program returns to the background loop. If the accumulator is not zero, the data is tested for error conditions. If the data is negative an error has occurred. If it is positive and Bit 1 is set, then Bits 2-10 are checked to see if they are equal to zero. If they are not, a second type of error has occurred. The program then decides whether the word is a data value, a sync pulse or a gap. If it is either a gap or sync pulse, the count is recorded and the action returned to the background loop. If the word is data, it is stored in the first location of the input buffer. All channels of the data set are read in turn. The D/A flag is then set, and the channel count and input address pointers reset. The program returns then to the background loop.

When the D/A flag is detected in the background loop, the program is directed to the output section. Various counters and pointers are first initialized, then the address of a set of instructions is obtained. The locations for instruction sets contain various items concerning the operations to be done on each channel. The output section determines the initial location of the set of instructions from the information saved when the front panel was read. By incrementing a pointer, it determines the total number of channels involved, the number of the channel to be operated on, the number of operations and the address of the operation. Having done this, each operation which represents a separate subroutine is carried out one channel at a time. After each operation, the action is returned to the main program with the new data value. The program checks to see if any other operation is requested. If there is, it gets the address of the next operation and jumps to that particular subroutine. It returns again with another new value, having completed the second operation. It will continue to complete all operations on any particular channel before it continues on to the next channel. When all operations for one complete cycle of data are obtained, values are plotted out on the brush recorder. The D/A flag is cleared and the action returns to the background loop.

Table 3 illustrates a dump of a current meter record in which the following operations occur. The raw data of the reference channel (#1) and the direction channel (#5) are dumped. The temperature channel (#2), the conductivity channel (#3), and the pressure channel (#4) are all multiplied by a factor of 5 and then offset by a constant of 1000. The numbers in Table 3 are all given in octal; hence, an offset of 1000 corresponds to an offset of decimal 512 bits. The speed channel (#6) is differenced and then multiplied by a factor of 5.

TABLE 3

EXAMPLE OF OPERATIONS FOR A CURRENT METER DATA DUMP

LOCATION	CONTENTS OF LOCATION (OCTAL)	COMMENTS
4200	6	No. of channels in instrument
4201	1	Instrument channel no. to be output on brush recorder channel 1
4202	0	No. of operations to be done on channel 1
4203	2	Channel no. to be output on brush recorder channel 2
4204	7776	No. of operations to be done on channel 2
4205	1314	Address of 1st operation (multiply)
4206	5	Multiplicative factor
4207	1311	Address of 2nd operation (add)
4210	1000	Constant to be added
4211	3	Channel no. to be output on brush recorder channel 3
4212	7776	No. of operations to be done on channel 3
4213	1314	Address of 1st operation (multiply)
4214	5	Multiplicative factor
4215	1311	Address of 2nd operation (add)
4216	1000	Constant to be added
4217	4	Channel no. to be output on brush recorder channel 4
4220	7776	No. of operations to be done on channel 4
4221	1314	Address of first operation (multiply)
4222	5	Multiplicative factor
4223	1311	Address of second operation (add)
4224	1000	Constant to be added
4225	5	Channel no. to be output on brush recorder channel 5
4226	0	No operations on channel 5
4227	6	Channel no. to be output on brush recorder channel 6
4230	7776	No. of operations to be done on channel 6
4231	1257	Address of 1st operation (difference)
4232	1314	Address of 2nd operation (multiply)
4233	5	Multiplicative factor

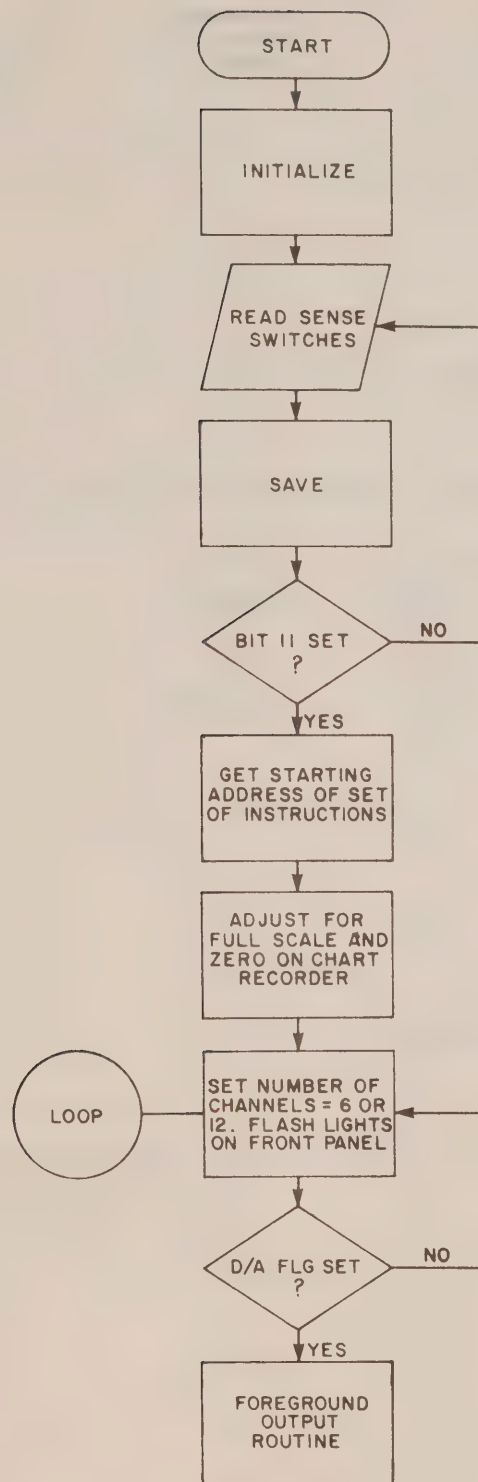
BACKGROUND
FLOWCHART

Figure 4.

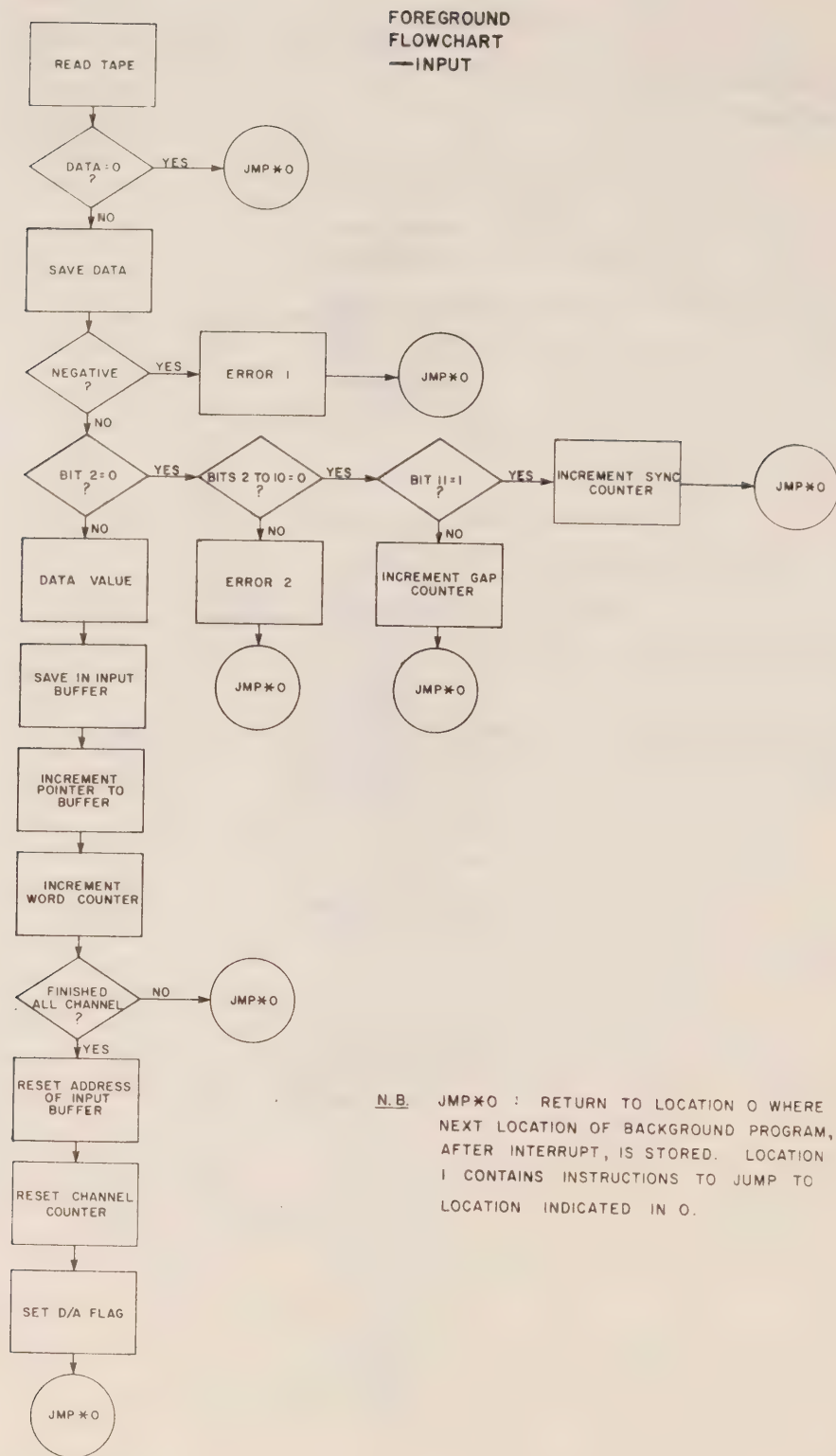


Figure 5.

FOREGROUND
 FLOWCHART
 —OUTPUT

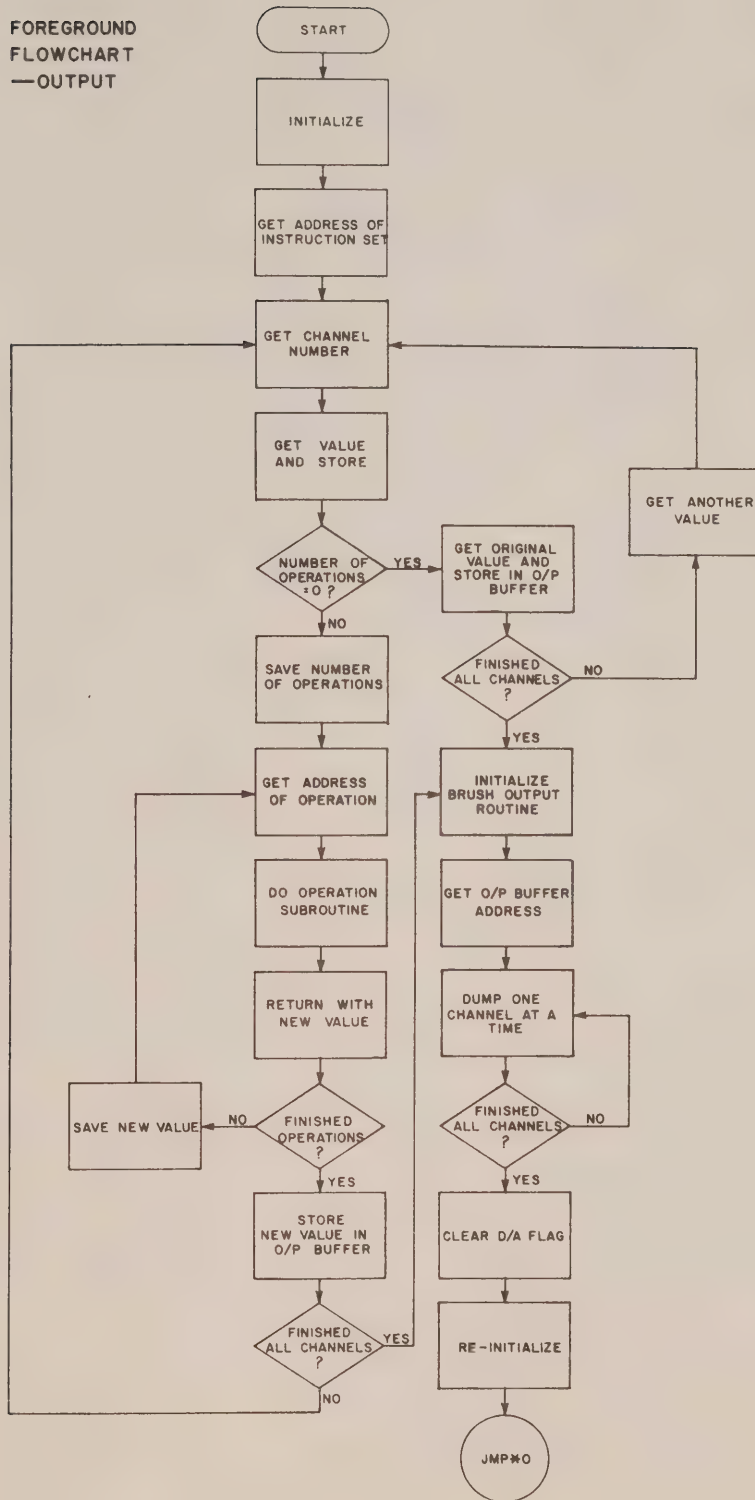


Figure 6.

CAI EP 321

-76R08

**RADAR TRACKING OF DRIFT DROGUES
IN
PENDRELL SOUND AND PORT MELLON**

June and September 1974

by L.P. Landry



**INSTITUTE OF OCEAN SCIENCES, PATRICIA BAY
Victoria, B.C.**



For additional copies or further information, please write to:

Environment Canada
Institute of Ocean Sciences, Patricia Bay
512 - 1230 Government Street
Victoria, B.C.
V8W 1Y4

Pacific Marine Science Report 76-8

RADAR TRACKING OF DRIFT DROGUES IN
PENDRELL SOUND AND PORT MELLON
JUNE AND SEPTEMBER 1974

by

L.P. Landry

Institute of Ocean Sciences, Patricia Bay
Victoria, B.C.

March 1976

This is a manuscript which has received only limited circulation. On citing this report in a bibliography, the title should be followed by the words "UNPUBLISHED MANUSCRIPT" which is in accordance with accepted bibliographic custom.

TABLE OF CONTENTS

	<u>Page</u>
TABLE OF CONTENTS	i
LIST OF FIGURES	ii
ABSTRACT	1
INTRODUCTION	2
INSTRUMENTATION	4
The Radar Set	4
The Cameras	4
The Drogues	5
Anemometers	5
FIELD PROCEDURE	5
DATA PROCESSING	6
Digitization	6
Droque Identification	6
Data Verification	6
DATA PRESENTATION	7
Pendrell Sound	7
Port Mellon	8
SUMMARY	9
ACKNOWLEDGEMENTS	9

LIST OF FIGURES

	<u>Page</u>
Figure 1. Radar screen displaying Port Mellon area	3
Figure 2. The drogue	10
Figure 3. Hourly averaged wind vectors from two anemometers in Pendrell Sound	11
Figure 4. Tides for Pendrell Sound (measured at Campbell River and adjusted to Redondo Bay)	12
Figure 5. Legend for Pendrell Sound vector average diagrams . . .	13
Figures 6-16. Six hour average vectors of drogue movement through $\frac{1}{4}$ mile squares	14-24
Figure 17. Current roses for two sides of Pendrell Sound	25
Figure 18. Hourly averaged wind vectors for Port Mellon and predicted tides at Point Atkinson	26
Figure 19. Legend for Port Mellon vector average diagrams	27
Figures 20-44. Three hour average vectors of drogue movement through $\frac{1}{4}$ mile squares	28-52

ABSTRACT

This report presents a summary of data derived from two studies of surface water movements in B.C. coastal waters. The measurements were made by continuously radar-tracking drifting drogues and photographing the radar screen at intervals. Using techniques developed at the Institute of Oceanography, University of British Columbia, the resulting photographs were processed by computer to produce a movie of the drift-drogue motions. We present here drawings of vector averages of the drogue motions which summarise the principal results displayed in the movie, along with relevant information on the wind and tide.

INTRODUCTION

This report summarises data collected by Coastal Zone Oceanography Section in two drift-drogue studies conducted in B.C. coastal waters. The drogues were tracked by radar and the data analysed using a set of techniques developed at the Institute of Oceanography, University of British Columbia. The final form of data analysis is a computer generated movie of the drifting drogues, shown in such a way that the speed and direction of each of the moving drogues is clearly visible, together with information on the state of the tide and the wind vectors.

The computer generated movie provides a detailed Lagrangian description of drogue motions for the experimental period. However, it is also useful to have a "hard-copy" summary of the data and it is this summary, together with a description of the technique, that forms the basis of this report.

The drogue tracking and data presentation system was developed at the Institute of Oceanography, University of British Columbia by Mr. J. Buckley under the supervision of Dr. S. Pond and was first used experimentally near the head of Howe Sound. Although some changes in equipment have since been made, the technique is basically the same as that devised by the Institute of Oceanography.

During the period 8-12 July 1974 a study of the surface (0-1 m) currents in Pendrell Sound was carried out by the Coastal Zone Oceanography Section of Ocean and Aquatic Sciences, Environment Canada. This study was part of a physical oceanographic programme which was to assist in the understanding of the features of Pendrell Sound relevant to the oyster seed collecting industry. The other parts of this programme included a heat budget to determine advection through the mouth of the Sound, and a search for major surface exchanges related to wind effects using recording thermistor chains. The base of operations was the Pacific Biological Station's barge VELELLA, anchored in a position facilitating maximum radar coverage of the head of the Sound and with taut fore and aft lines to prevent yawing as much as possible. A total of 14 people participated, including personnel from Coastal Zone Oceanography (CZO), Pacific Biological Station (PBS) and the Institute of Oceanography at UBC (IOUBC). Vessels used to place, identify, and recover drogues were CZO's launch SQUAMISH and PBS's vessels CALIGUS and QUATL QUACH.

From 23-26 September 1974 a second surface (0-1 m) current study was undertaken as a result of Canadian Forest Products' request that they be allowed to change the configuration of their present outfalls into Howe Sound from their pulp mill at Port Mellon. The field work was a cooperative venture between CZO, who supplied some personnel and the tracking equipment and expertise, the Pacific Environment Institute (PEI), who supplied some personnel, the vessels L. PACIFICA, ACTIVE LASS and COHO, and the Environmental Protection Service (EPS), who supplied some manpower. The field programme was carried out from PEI's barge L. PACIFICA anchored at the southwest tip of Woolridge Island across Thornbrough Channel from the pulp mill. Data reduction and the analysis included in this report were done by CZO with the data being forwarded to EPS for further analysis for their purposes.

The intent of the tracking system is twofold: (1) to produce a time lapse movie to enable an almost immediate visual inspection of the

overall surface water movement, and (2) to obtain a series of still photographs (Fig. 1) which can be easily digitized and subsequently used to produce current roses, velocity vs. time traces, current vectors averaged over specific areas for given times and other information, as well as a "cleaned-up" movie of digitized drogue positions, a digitized coastline, and wind speed and direction and tide height.

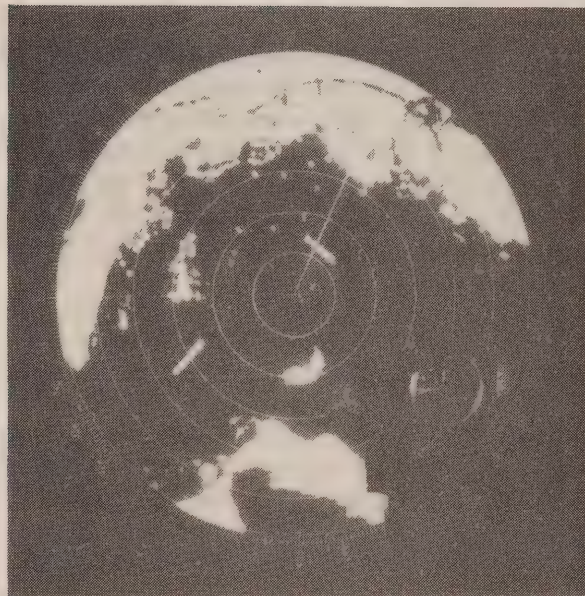


Figure 1

Radar Screen Displaying Port Mellon Area

INSTRUMENTATION

The Radar Set:

The radar set used was a Decca model RM916 with a 6-foot scanner and a CRT effective diameter of 7.5 inches operated on the 3 nm and 1.5 nm range scale having a 0.5 nm and 0.25 nm ring interval for Pendrell Sound and Port Mellon respectively and using the long pulse length (0.75 μ s). The power input was 115 V ac with a 250 W rectifier unit used to provide a 32 V dc supply for the transceiver and display units and a 110 dc supply for the turning unit.

Decca states that the range discrimination is 10 m on the 0.5 nm range scale. Although no tests have been done, the overall position resolution including radar error, optics error, and digitizing error is estimated to be in the order of ± 30 m on the 3 nm scale. Thus, in a one knot current with two pictures taken 10 minutes apart during which time a drogue would travel about 300 m, the velocity would be in error by $\pm 10\%$ - however, this error will be proportionately reduced by averaging over longer periods.

The scanner, turning unit and transceiver were mounted on an aluminum frame on the roof of the barge, giving the scanner an elevation of about 9 m above water. The display unit was mounted in an angle-iron frame rigidly connected to the camera platform to prevent relative movement between the cameras and the display screen. This was then set up in a darkroom to enable the radar-base operators to adjust settings of the cameras and display unit while still taking correctly exposed pictures and relaying instructions via VHF radio to the boat operators.

The Cameras:

The still pictures were taken with a motorized Hasselblad model 500 EL/M with a 70 frame back and a Zeiss Planar 1:3.5 $f = 100$ mm lens fitted with a proxar $f = 1$ m lens to enable focussing at the distance necessary to obtain the largest possible image of the screen. About 400 $2\frac{1}{4}'' \times 2\frac{1}{4}''$ negatives, approximately spaced 10 minutes apart throughout each study, were obtained on 15 foot strips of Kodak Plus-X Pan ASA 125 70 mm film with up to 70 frames per strip.

Since one scanner sweep occurred every two seconds, the shutter speed was fixed at 12 seconds to allow six sweeps per frame. The reason for this was twofold: distant drogues often do not give a return every sweep but invariably give at least one return in six sweeps; rain and sea clutter appear on the radar screen as a very large number of small echoes whose positions are random from scan to scan so that a drogue return will appear up to six times darker on the photographs and thus be more easily visible through clutter.

To ensure optimum exposure, a 12 frame test roll of film was taken and developed before beginning the operation and again a few times during the study, particularly after changing gain or brilliance settings in attempts to reduce rain and sea clutter. The usual aperture setting was f11 and it was never more than one stop up or down from this.

The movie was taken with a Super 8 Nizo model 800 which has a built-in intervalometer. The zoom lens was set to give the largest image possible and a close-up proxar was used to enable focussing at a convenient distance. About 350 feet of Kodak Ektachrome 160 Super 8 movie film was shot. The lens was left on the automatic aperture setting and correct exposure was obtained by advancing one frame every 12 seconds. Thus, when viewed at the normal speed of 18 frames per second, one hour of real time was seen every 17 seconds. However, because of very slow currents faster viewing speeds made image movements much more apparent and it thus became easier to visualize water movement.

The Drogues:

The drogues consisted of a 9" x 9" fluorescent orange aluminum radar reflector, drilled to reduce wind drag, mounted atop a 5 foot by 1 inch diameter aluminum pipe mast. Strapped to this mast was a white light run on two D-cells which flashed about 30 times per minute. The aluminum pipe extended through a 1 foot diameter plastic ball float to a depth of 1 metre. Clipped to the ball and the bottom of the pipe was a blind of woven polyethylene threads covered in plastic 3.1 m long by 1.0 m deep which was fastened to a 1" diameter concrete reinforcing rod acting as a weight and a 2" x 2" wooden bar acting as a float. The air to water surface area ratio of this drogue is approximately 1:60.

Anemometers:

Aanderaa anemometers with Lambrecht anemometers as back-up were placed on tripods above Geodyne buoys positioned as shown in Figure 5. For Port Mellon, wind data was from a Lambrecht anemometer atop the L. PACIFICA (see Fig. 19).

FIELD PROCEDURE

The boat personnel, operating 12 hours per shift, were expected to install, remove and identify drogues as instructed by the radar base operator. To assist in later drogue identification, log sheets of all operations were kept and rough positions plotted on copies of the chart that had been marked with range rings and bearing lines.

Having set the radar display to receive the optimum picture and having correctly adjusted the cameras, the radar base operator took a still picture every 10 minutes, changed film as necessary, timed the movie film advance periodically and adjusted the rain and sea clutter controls if conditions warranted. In addition to running the equipment, the radar base operator controlled all other phases of the operation. These included directing the boat operators to install drogues so as to keep a good pattern throughout the area, check on drogue numbers to assist in identification during subsequent computer processing of the pictures and retrieve drogues leaving the area of visibility or drifting ashore. The base operator also kept a log sheet of details concerning the drogues, such as the time of each operation, the identification number on each drogue, an approximate range and bearing to the boat during any operation, a running total of the number of drogues in the

water, and the time of every picture and frame.

DATA PROCESSING

Digitization:

All points appearing as drogues on the negatives were digitized using a "trilateral reader" designed and built at PBS in Nanaimo. This reader consisted of a Leitz Wetzlar Universal type projector, adapted slightly to accept 70 mm film strips, mounted on a rigid frame with an opaque screen on the opposite end. There is a potentiometer mounted on each top corner of the screen a known distance apart. Each has a spring loaded drum around which a string is wrapped and both strings are attached to a cursor which can be moved anywhere on the screen. The string lengths are determined by the potentiometers and the coordinates of the cursor are found by trilateration, the cursor and two potentiometer drums being the apices of a triangle. Output from the reader was put on paper tape via a teletype. Tests done in Nanaimo have shown the error between two points, including operating error, to be $\pm 1\%$ in the vertical direction - slightly more in others (K. Simpson, pers. comm.). In addition to a digitized trilateral coordinate for each point appearing as a drogue, for each photograph the radar site and two reference points were digitized and identification including roll and picture number, time and date were included on the paper tape output. A digitized coastline was also put on the tape.

Drogue Identification:

The paper tape output from the digitizing process was put onto a 9-track 800 BPI magnetic tape which was then run through a programme on the UBC IBM 370 which converts the trilaterated coordinates to rectangular ones and puts them in a format compatible with the PDP-12 where the information is then displayed on a cathode ray tube (CRT).

On the PDP-12 with the use of prints made on a 3M brand "400" micro-film reader-printer and the log sheets kept in the field, each digitized point on every photograph was assigned its proper drogue number or identified as an unwanted point (log, boat, etc.) and removed. This information was stored on a disc which was then used to generate a 9-track 800 BPI magnetic tape which was run through a program on the IBM 370 which removes unwanted points, sorts and assembles float track records, and interpolates the records to one minute intervals. This new edited data file thus contains each record which consists of one float track identified with times and rectangular coordinates for every drogue position along the track.

Data Verification:

Tracks of each drogue are interpolated (cubic spline interpolation with error allowed at each data point) to one minute intervals and displayed in two ways for data verification whereby errors can be easily identified and removed: (1) all data points at each particular time (i.e. every minute) are collected and displayed at a desired rate to present a "movie" on the CRT;

(2) displacements, velocities, and accelerations are displayed on a 6-channel analogue brush recorder and listed. After identifying and removing the most obvious errors by viewing the movie and examining the listed accelerations, the analogue output is used to identify the less obvious errors. At this point the data is in a form whereby the desired output listings and plots, depending on the objectives of the study, can easily be generated.

DATA PRESENTATION

Pendrell Sound:

(a) Wind - Two sets of wind records from Aanderaa anemometers (six instantaneous speed and direction readings per hour) were obtained and plotted (see Fig. 3 for summary of wind) as hourly averaged vectors.

(b) Tide - The tidal elevation used was derived from hourly measured values at Campbell River adjusted to the Redonda Bay secondary port (see Fig. 4 for summary of tide).

(c) Representation of Coast - The $\frac{1}{4}$ mile squared coastline is a representation of the real coastline used for summarising drogue movements. These squares divide the whole of the Sound into $\frac{1}{4}$ mile x $\frac{1}{4}$ mile areas which are the areas represented by the vector averages. A vector may start outside the squared coastline if a portion of water area through which a drogue passes lies outside the squared coastline.

(d) Vector Averages - The vector plots as seen in Figs. 6 to 16 represent the average movement of all drogues passing through each $\frac{1}{4}$ mile square for six hour periods. This period was chosen since it is half the semi-diurnal tidal cycle although, in this case, wind effects seem more important than tide. An important limitation of this averaging procedure is the misleading representation given by a vector average over a period of highly variable currents. Also, if the square is occupied by drogues for only a small part of the six hour averaging period, the averaged vector is unlikely to be a fair representation. However, examination of the variances has shown that a majority of the plotted vector averages does not show too significant a variance.

The choice of an averaging time over which to obtain a vector presentation is necessarily a compromise. If too short a period is used there will be insufficient data on which to base the vector average; if the period is too long the finer details will be lost. Thus, the choice must be made on the basis of local conditions, in particular the relative significance of wind and tide and its variability during the time of the study. For the Pendrell Sound data, we have chosen a six-hourly average whereas a three-hourly average has been used for Port Mellon. However, we must emphasize that these vector summaries are intended to be used in conjunction with the 16 mm film, and not simply on their own. The film will of course provide the details which are necessarily lost in the vector averaged summary.

It should be noted that the scale of the vectors is 0.2 m/sec/inch and there are no component velocities greater than 0.3 m/sec with a large majority being less than 0.1 m/sec.

For the Pendrell Sound data, an additional form of presentation is used in order to search for any net circulation around the upper reaches of the sound. The sound was further subdivided into two parts, A and B, as seen in Fig. 5. The averaged vectors in each section were contained by splitting the data into 45° segments for each six hour period; the result is shown in Fig. 17 with the length of each vector corresponding to the fraction of time that the current direction was in that particular segment. The scale is such that 0.5 cm corresponds to 0.1 of the six hour period.

Port Mellon:

(a) Wind - An analogue wind record from a Lambrecht anemometer was obtained and hourly averaged wind vectors were plotted from this (see Fig. 18 for summary of wind).

(b) Tide - Predicted tides at Point Atkinson were used (see Fig. 18 for summary of tide).

(c) Representation of Coast - As for Pendrell Sound.

(d) Vector Averages - The vector plots as seen in Figs. 20 to 44 represent the average movement of all drogues passing through each $\frac{1}{4}$ mile square for three hour periods. Three hour rather than six hour averages were computed as the current seemed more variable and the net circulation is probably produced by quite different effects than in a closed area like Pendrell Sound. The same limitations of the averaging procedure exist as for Pendrell Sound, although to a lesser degree due to the shorter averaging period.

The scale of the vectors is 0.2 m/sec/inch and there are no component velocities greater than 0.3 m/sec with a large majority being less than 0.1 m/sec.

SUMMARY

Use of this new technique of continuously tracking drifting drogues by photographing a radar screen has shown considerable value in obtaining a pictorial representation of surface flows.

Although the field work is manpower-intensive, the data processing is a rapid and simple procedure. Once the data is on magnetic tape in its final format, it is relatively easy to generate different forms of both listed and plotted data required for the desired analyses and objectives of a particular study.

ACKNOWLEDGEMENTS

The author wishes to acknowledge the assistance of Mr. Joe Buckley of IOUBC both for his help, together with Dr. S. Pond, in making us self-sufficient in the field use of the system developed by them, and for his computer programs and his invaluable assistance in running them.

For assistance with the Pendrell Sound field work, we would like to thank all the participating personnel from IOUBC and the Pacific Biological Station for their manpower and logistical assistance.

For assistance with the Port Mellon field work, we are indebted to Dr. John Davis for his logistical support and the use of the facilities aboard L. PACIFICA, and other personnel from the Pacific Environment Institute and Environmental Protection Service.

We are also grateful to Mr. Brian Stewart for digitizing approximately 400 photographs for each project. We are indebted to Mr. Andrew Lee for painstakingly redrafting and correcting most of the figures.

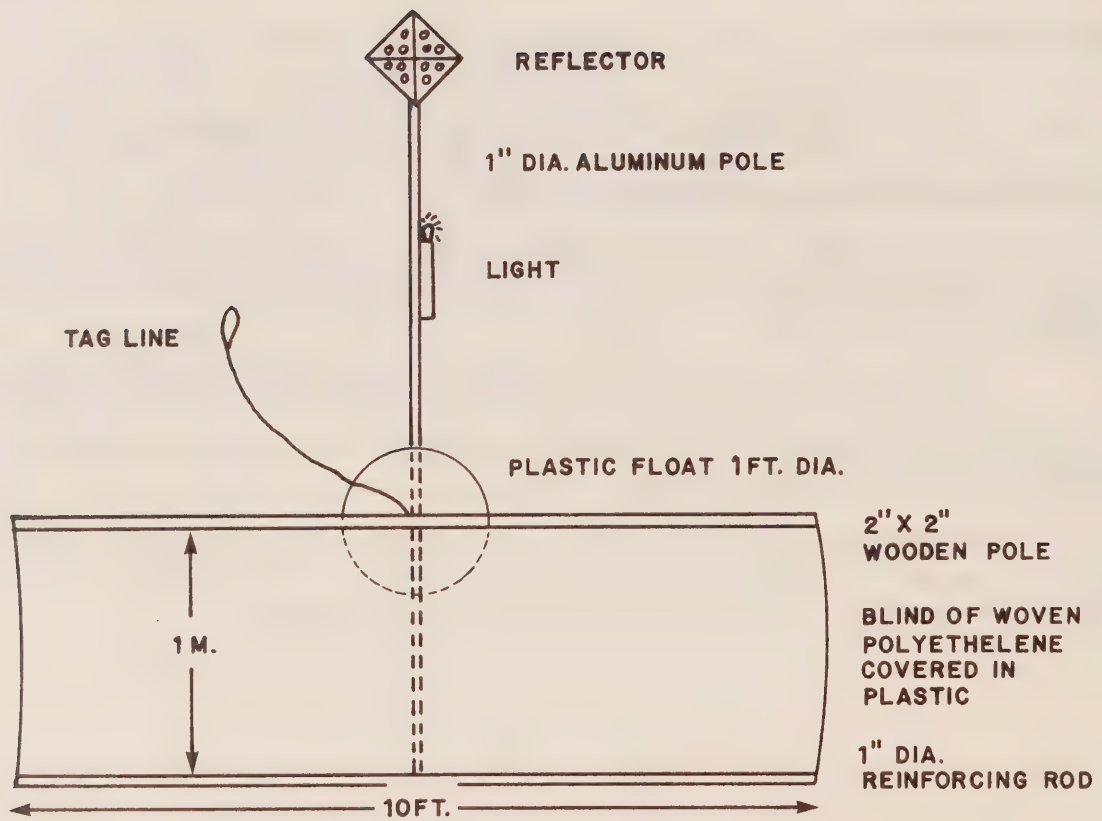


Figure 2.

WIND at Pendrell Sound

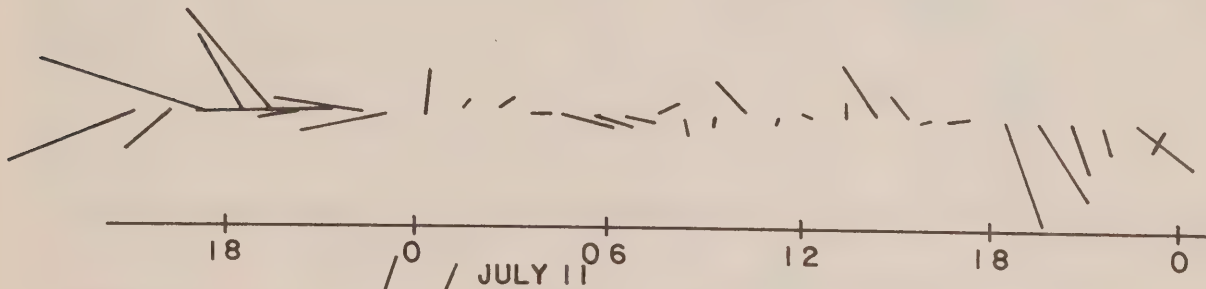
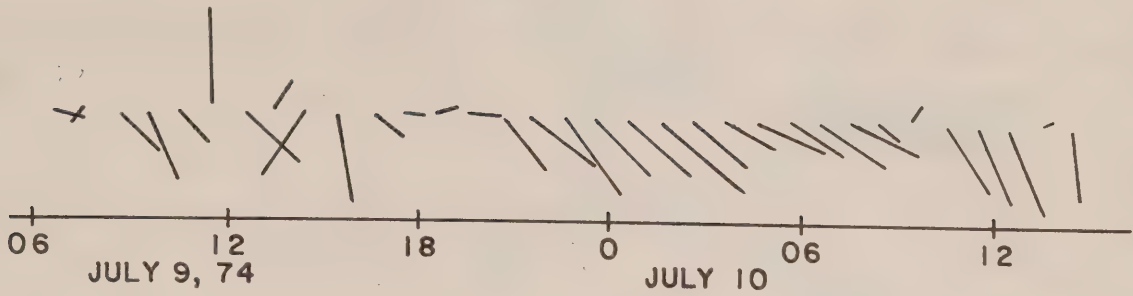
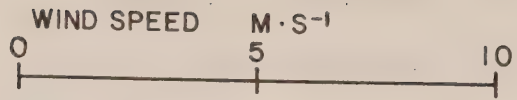
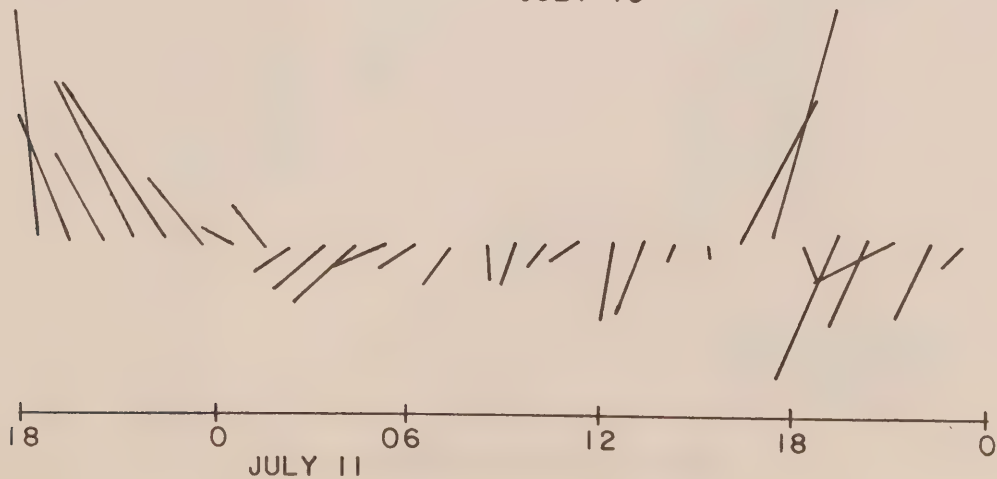
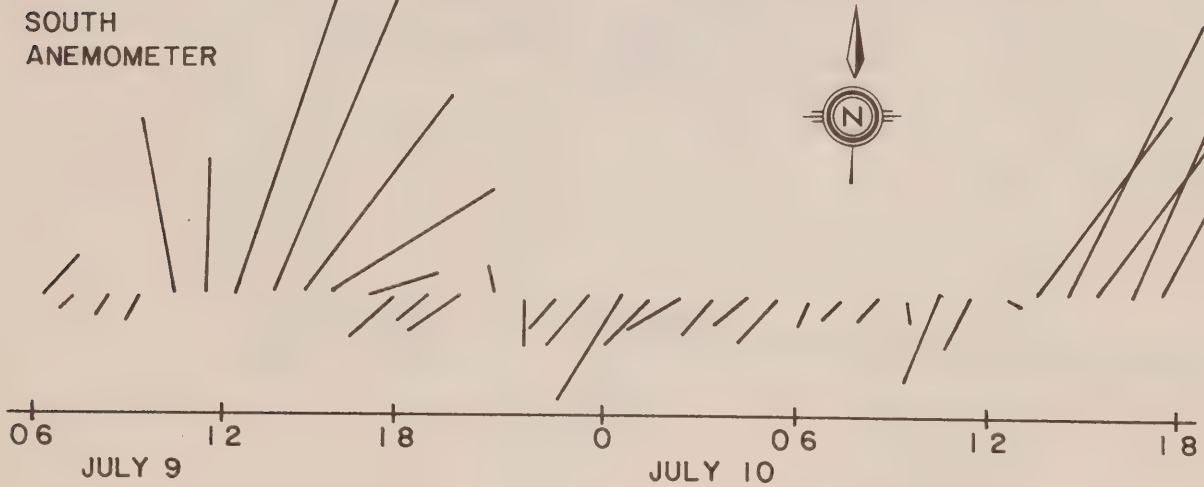
NORTH
ANEMOMETERSOUTH
ANEMOMETER

Figure 3

TIDE at Pendrell Sound

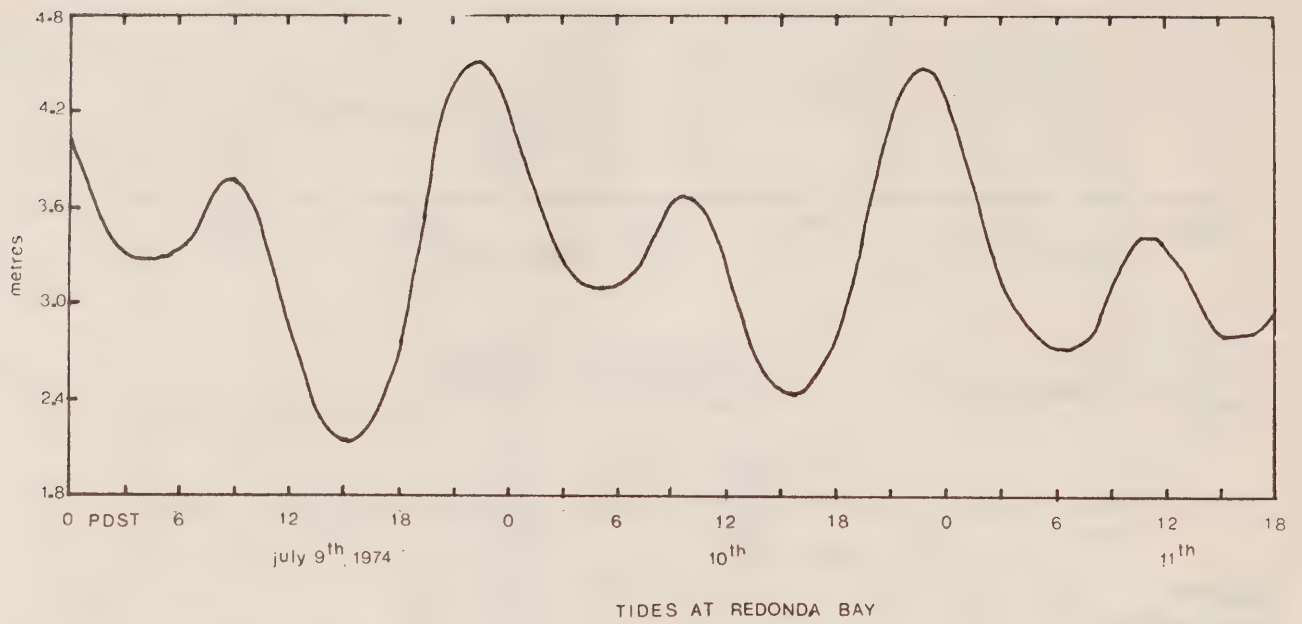


Figure 4

Legend: Pendrell Sound

approx. scale: 1 inch = 1/2 mile

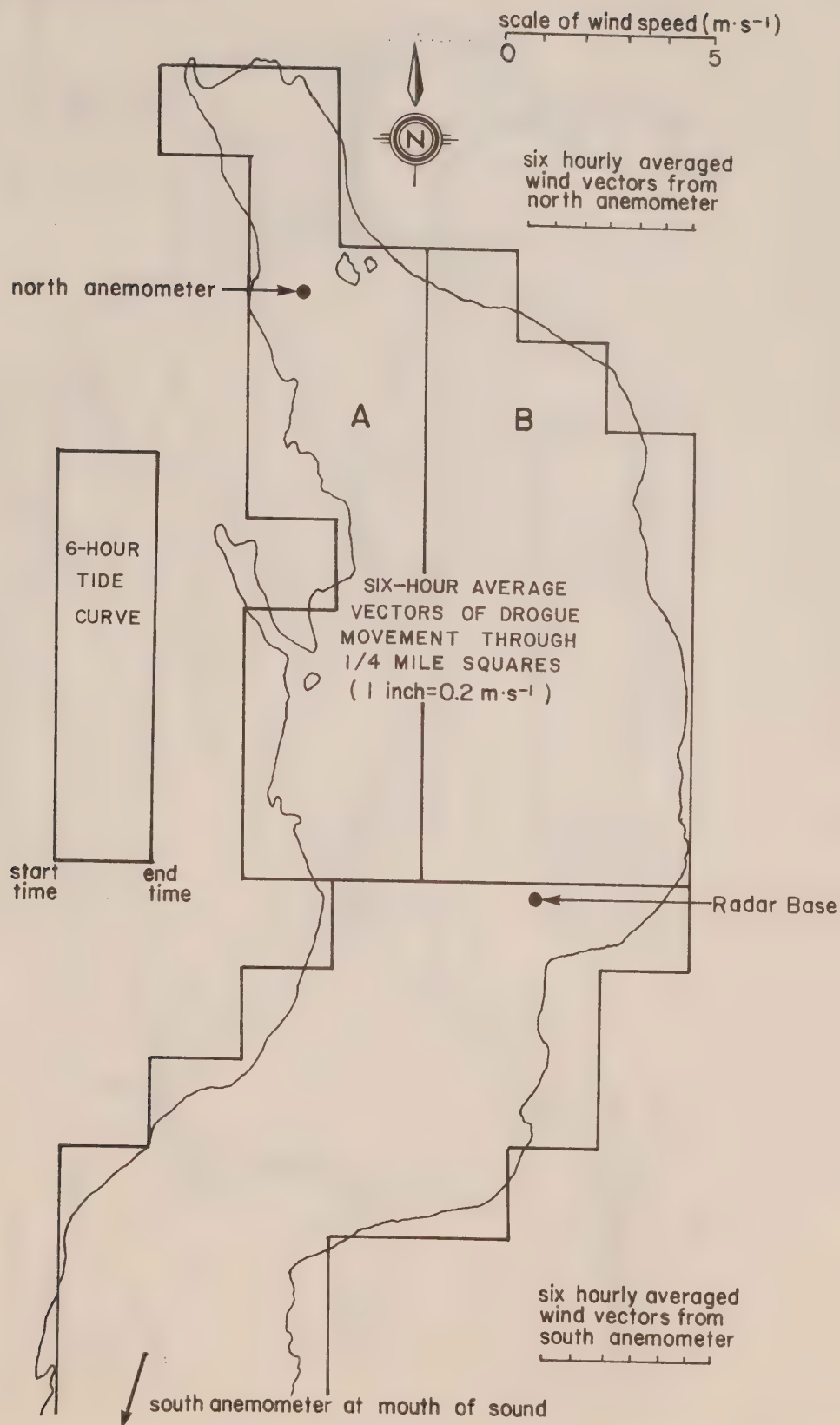


Figure 5.

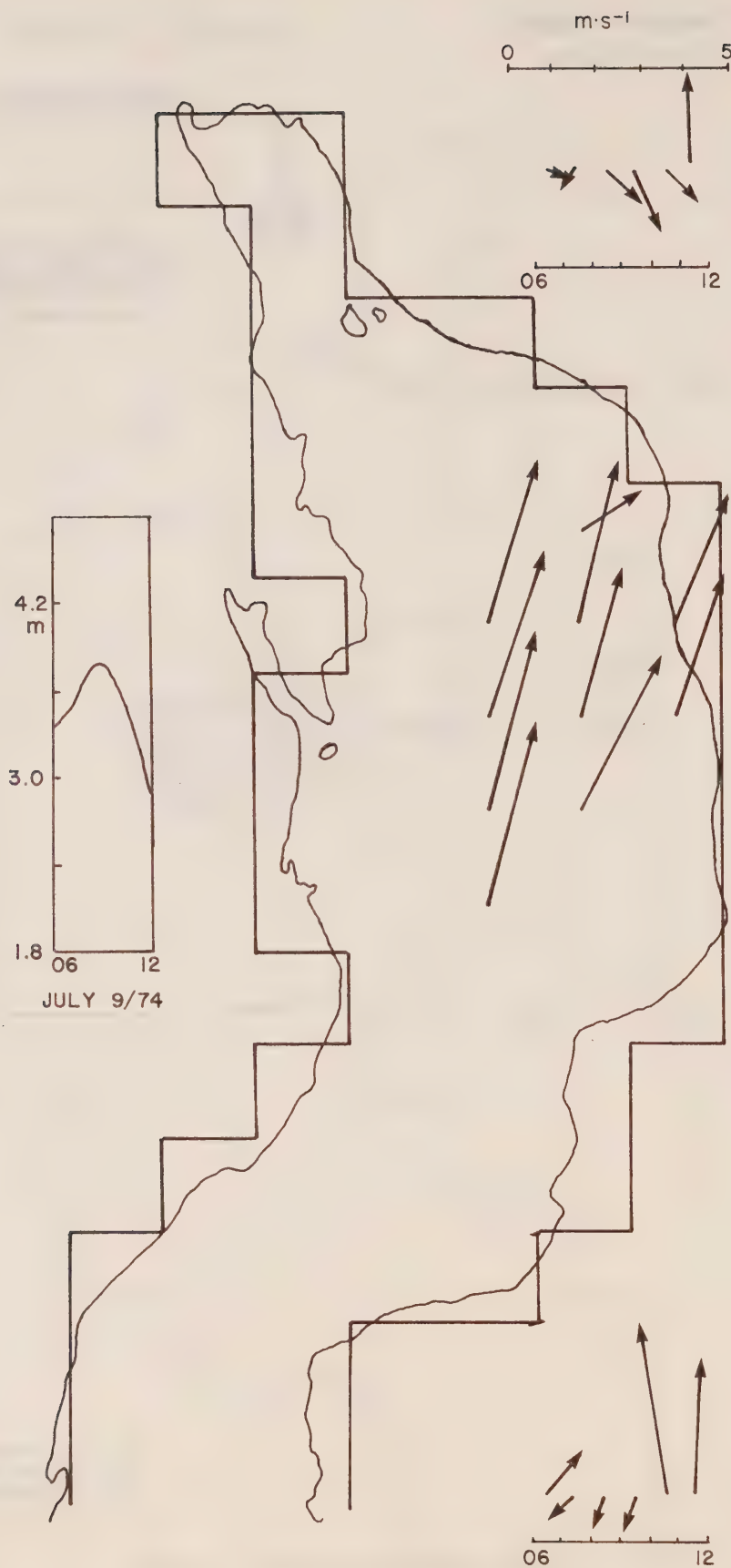


Figure 6. Pendrell Sound drogue motions: July 9/74 0600 hrs - 1200 hrs.

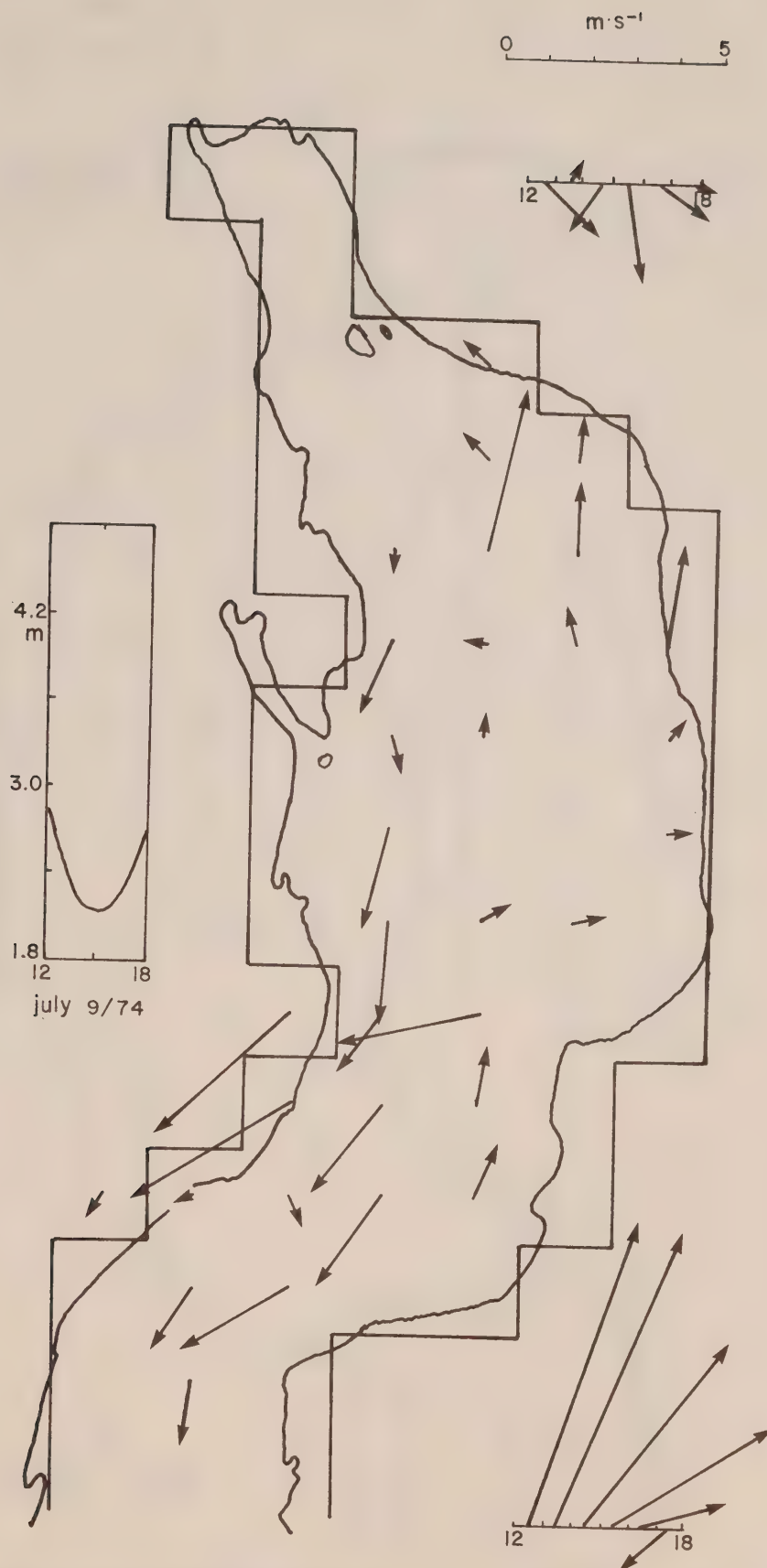


Figure 7. Pendrell Sound drogue motions: July 9/74 1200 hrs - 1800 hrs.

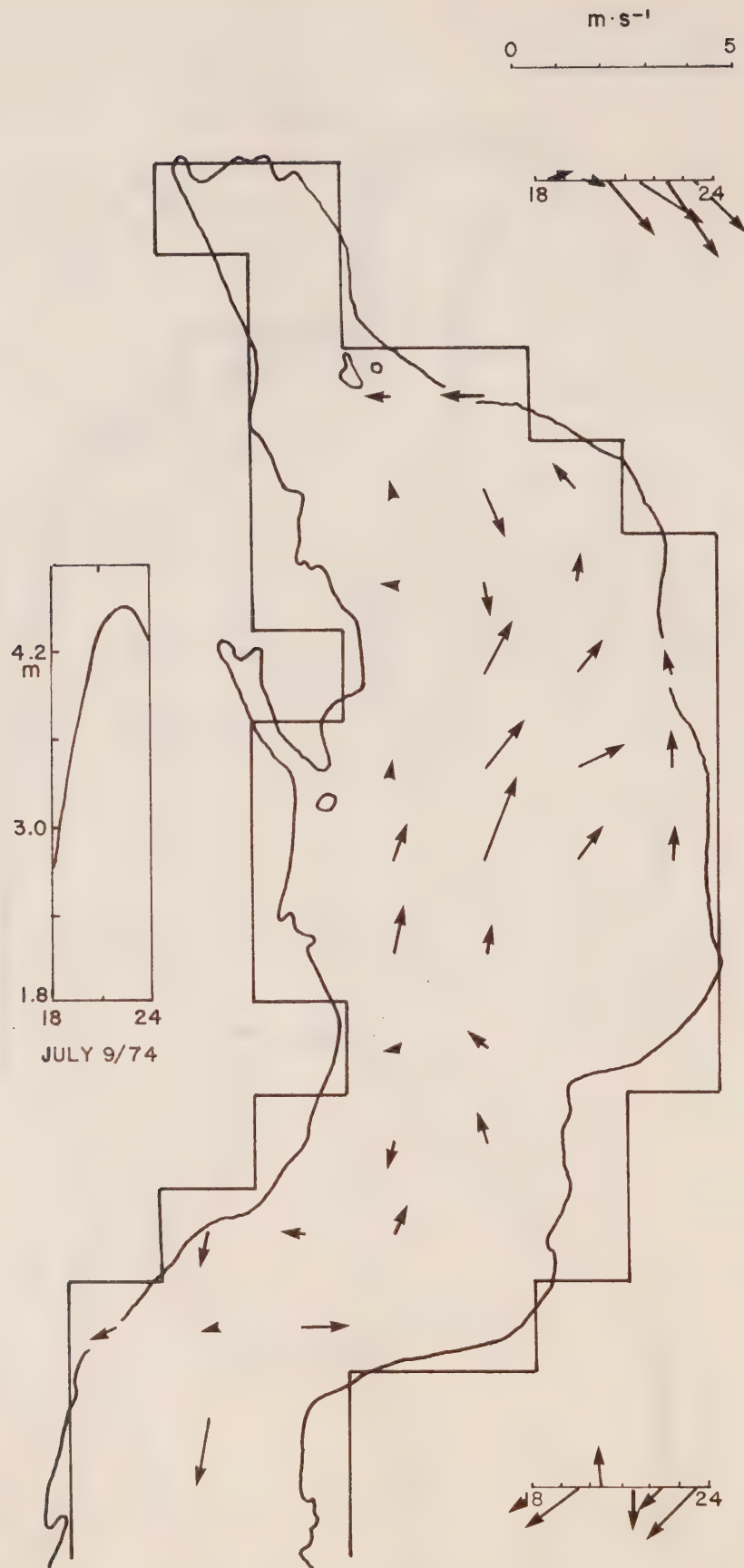


Figure 8. Pendrell Sound drogue motions: July 9/74 1800 hrs - 2400 hrs.

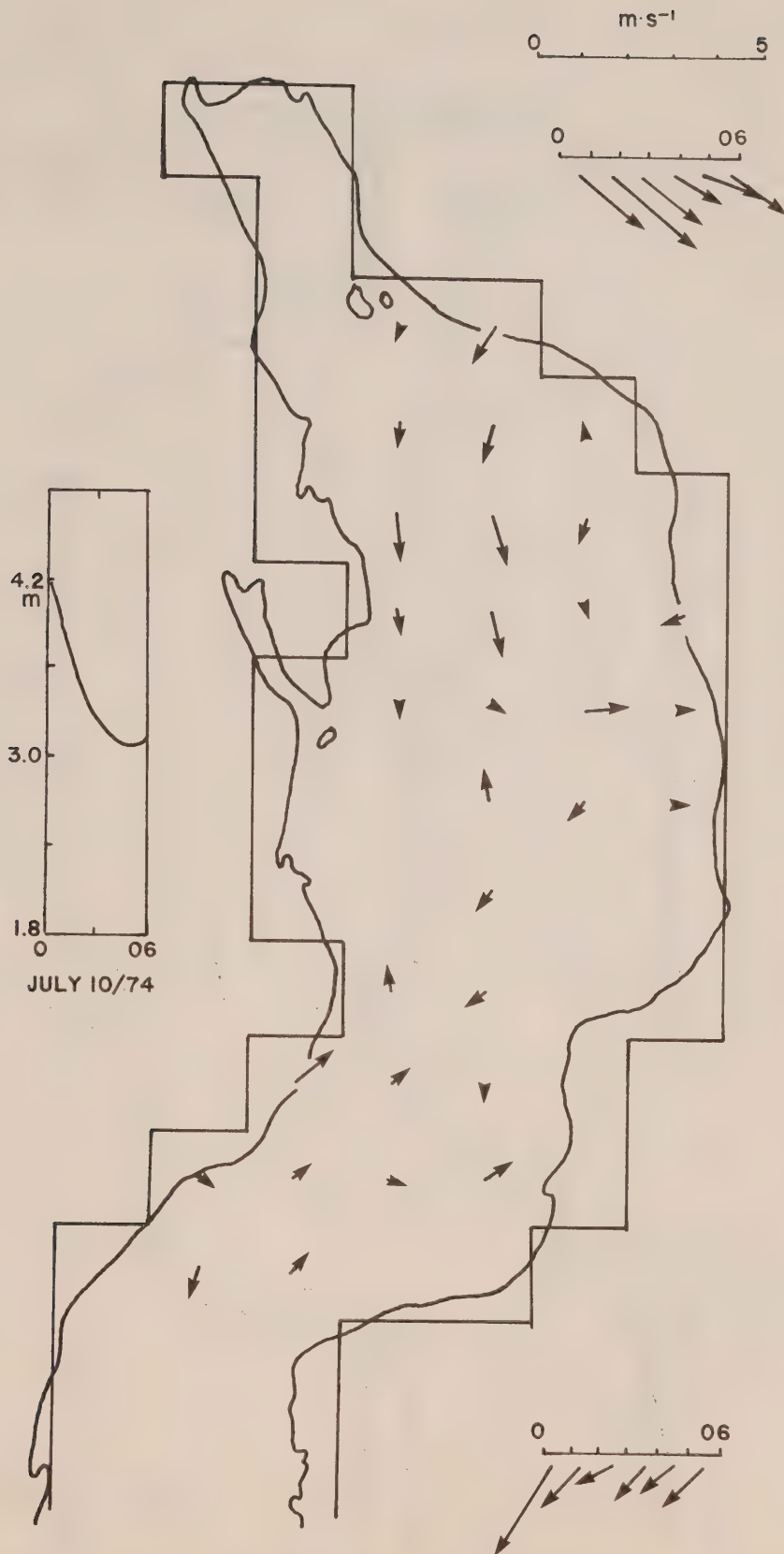


Figure 9. Pendrell Sound drogue motions: July 10/74 0000 hrs - 0600 hrs.

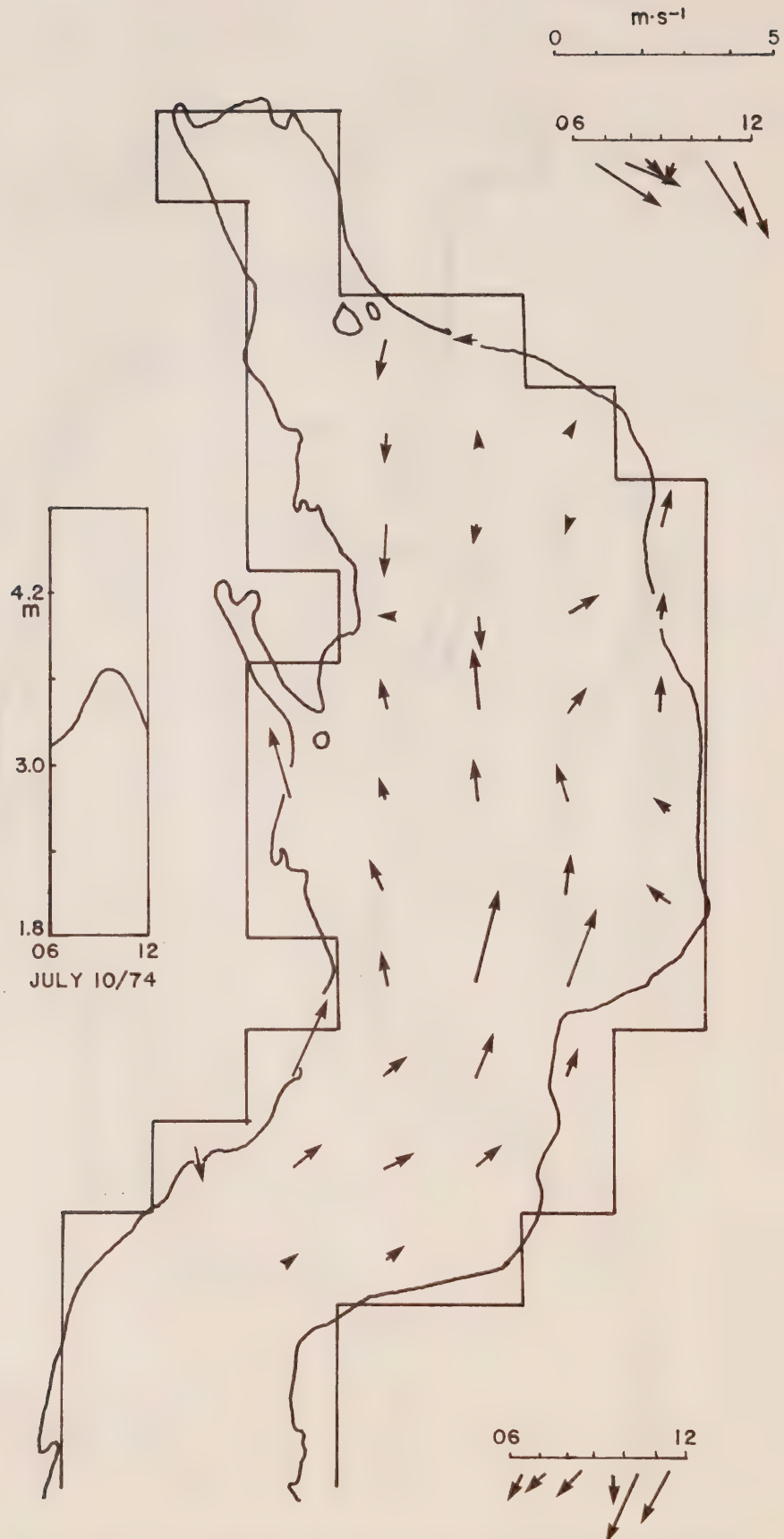


Figure 10. Pendrell Sound drogue motions: July 10/74 0600 hrs - 1200 hrs.

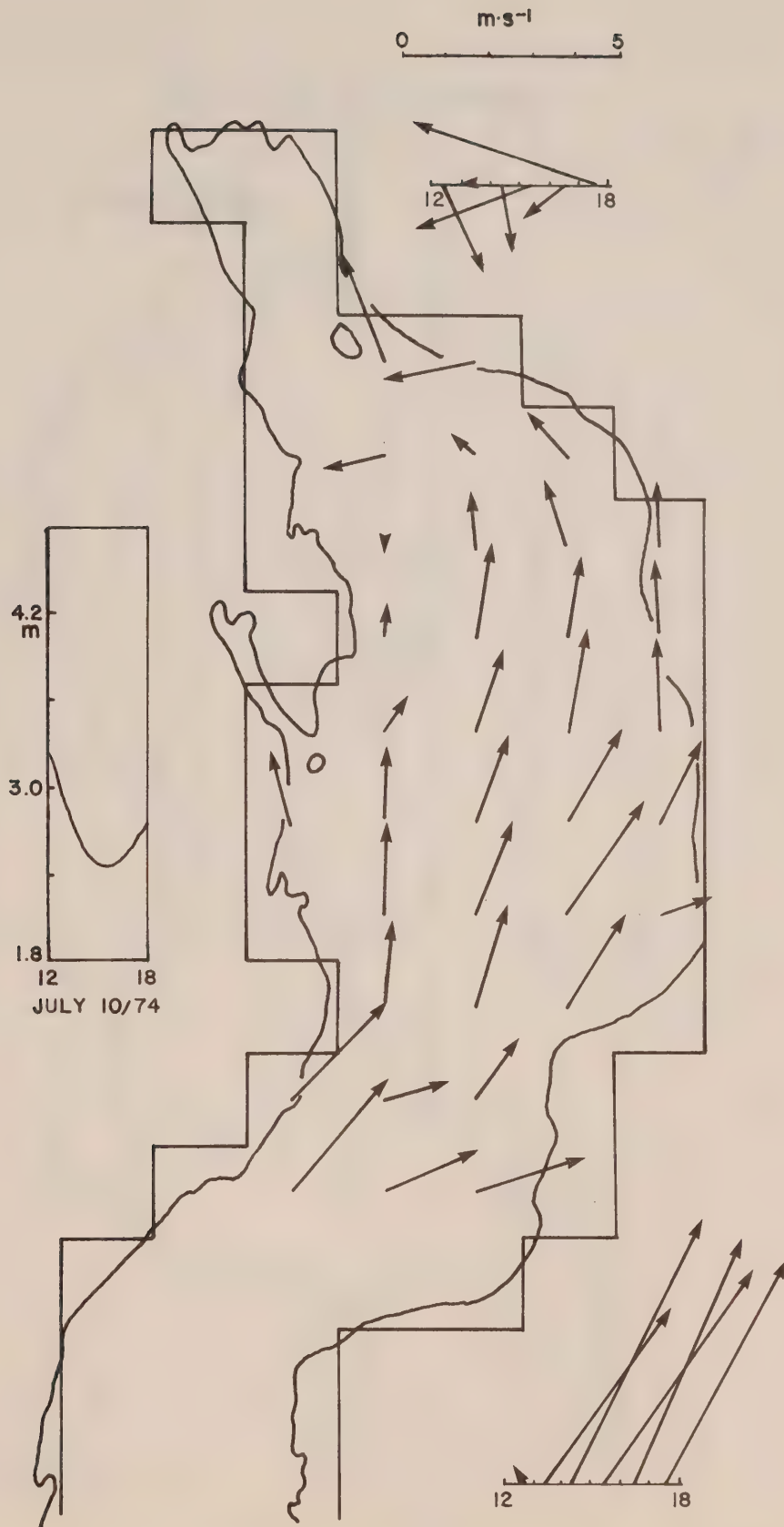


Figure 11. Pendrell Sound drogue motions: July 10/74 1200 hrs - 1800 hrs.

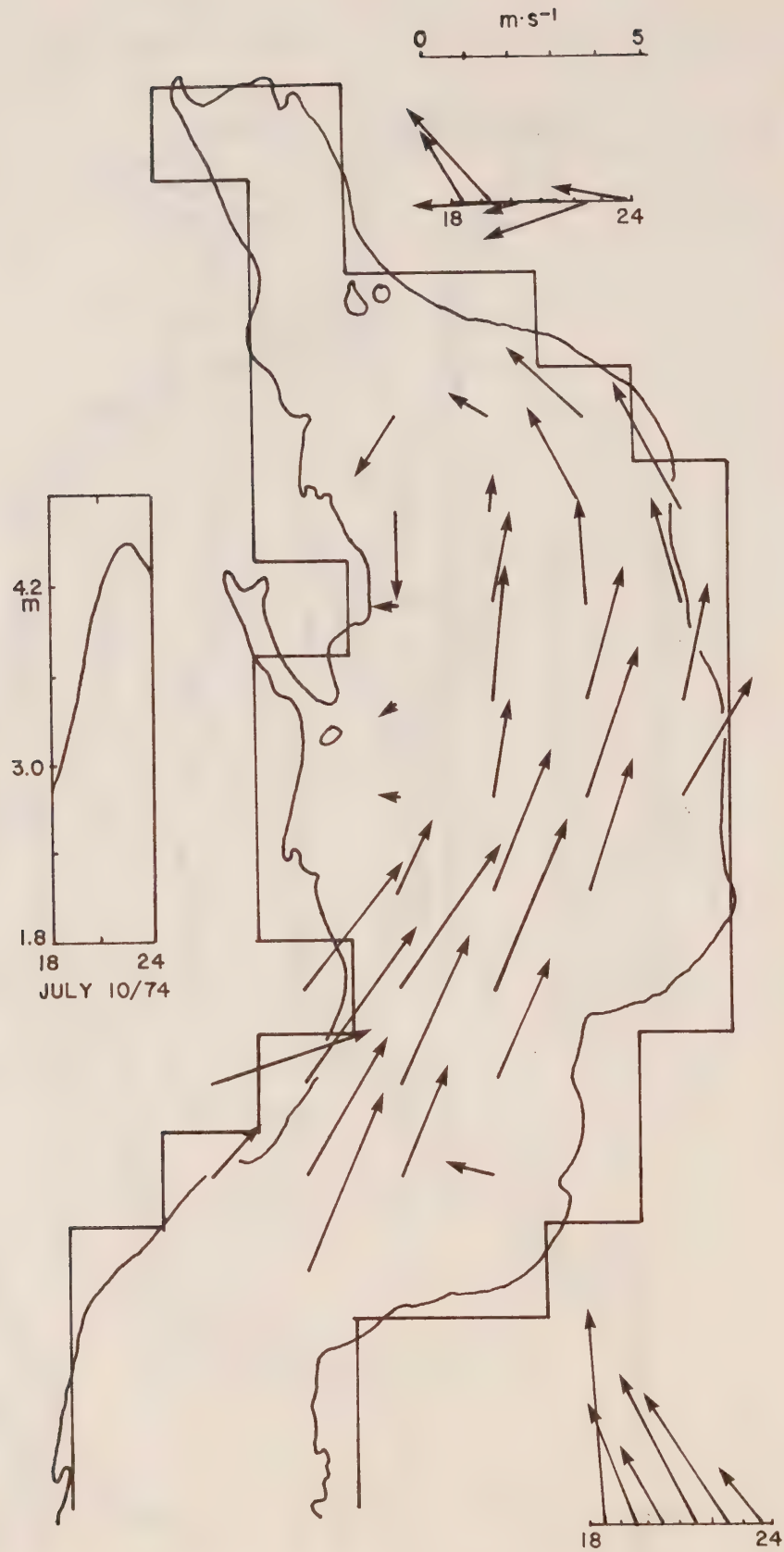


Figure 12. Pendrell Sound drogue motions: July 10/74 1800 hrs - 2400 hrs.

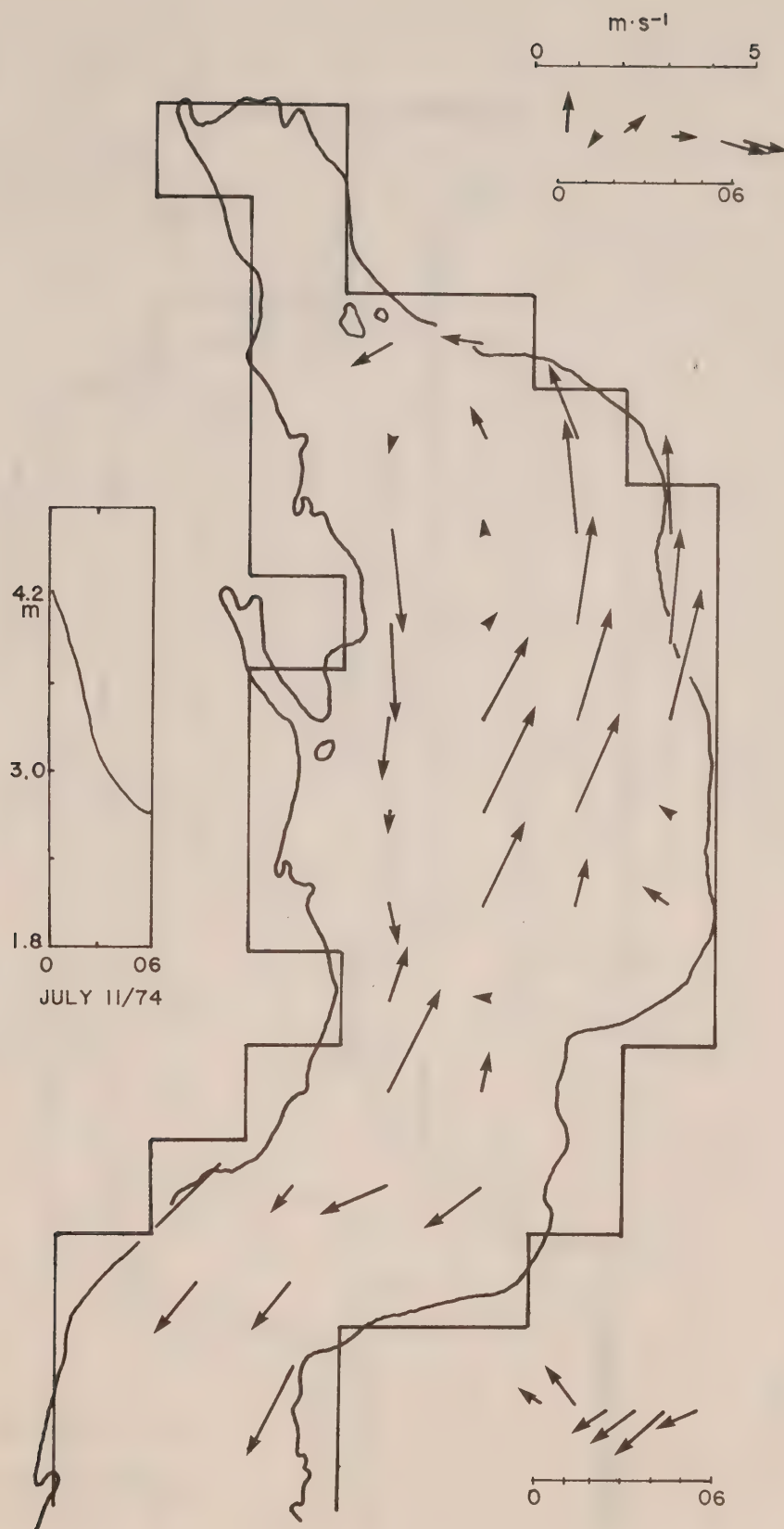


Figure 13. Pendrell Sound drogue motions: July 11/74 0000 hrs - 0600 hrs.

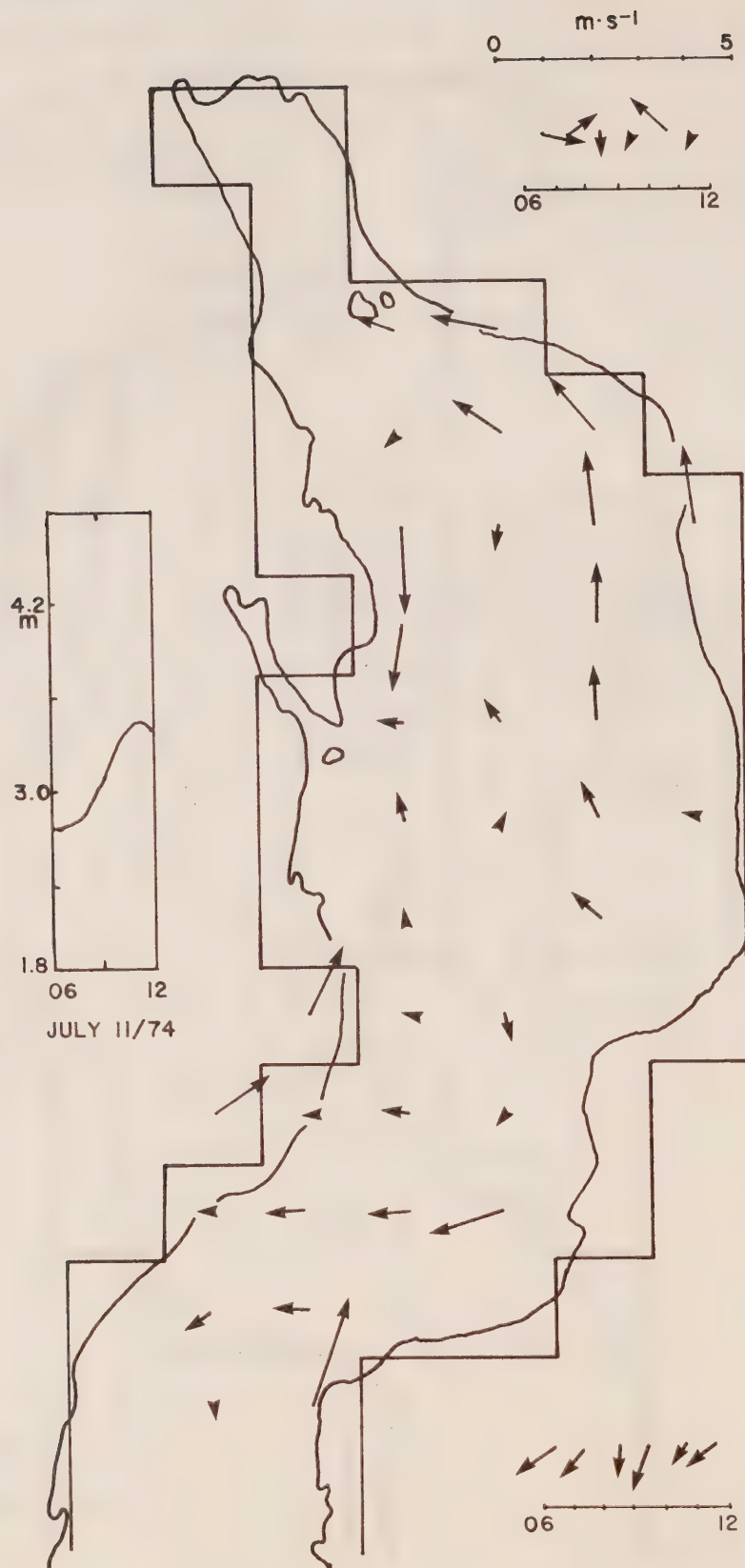


Figure 14. Pendrell Sound drogue motions: July 11/74 0600 hrs - 1200 hrs.

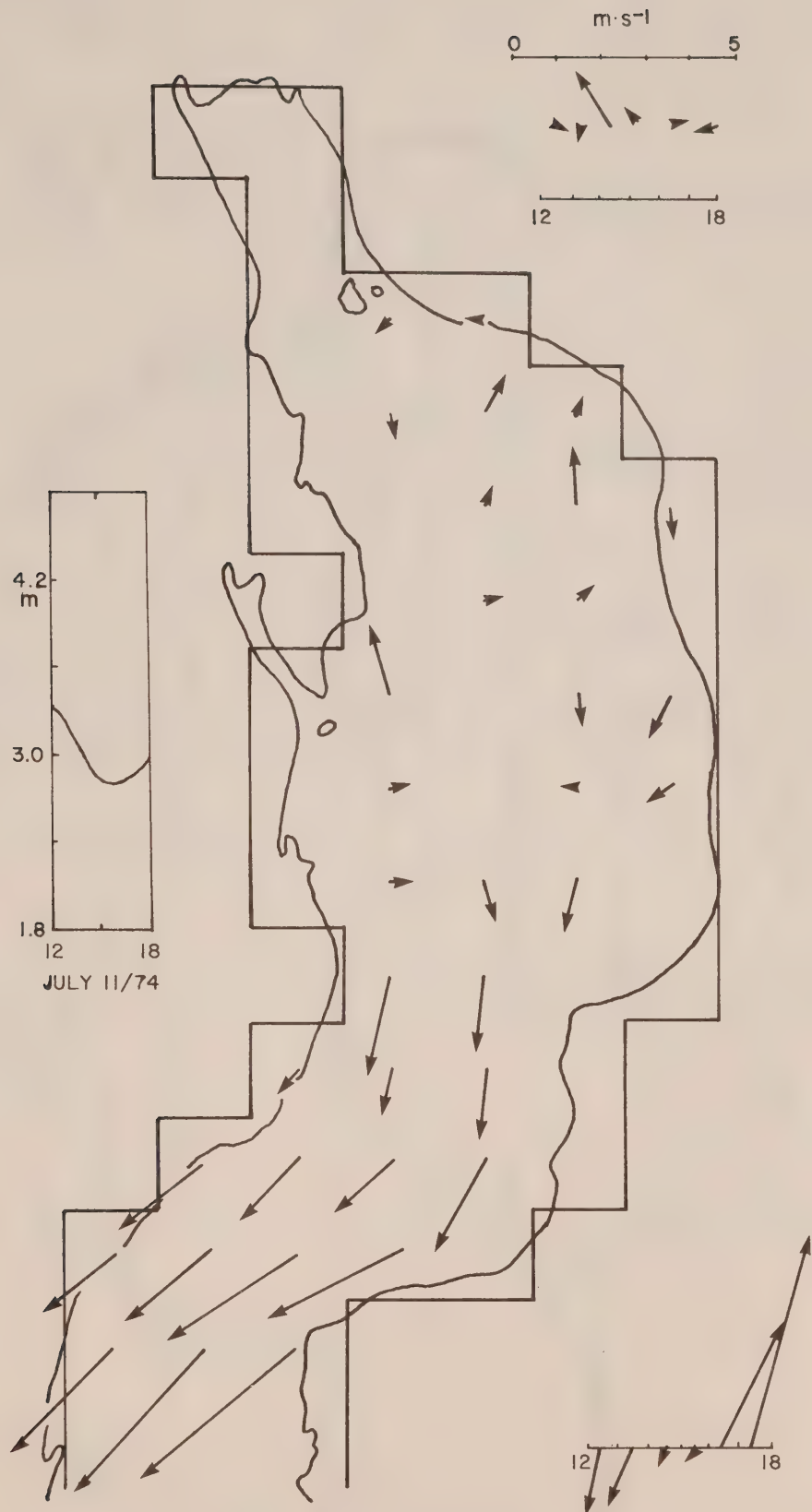


Figure 15. Pendrell Sound drogue motions: July 11/74 1200 hrs - 1800 hrs.

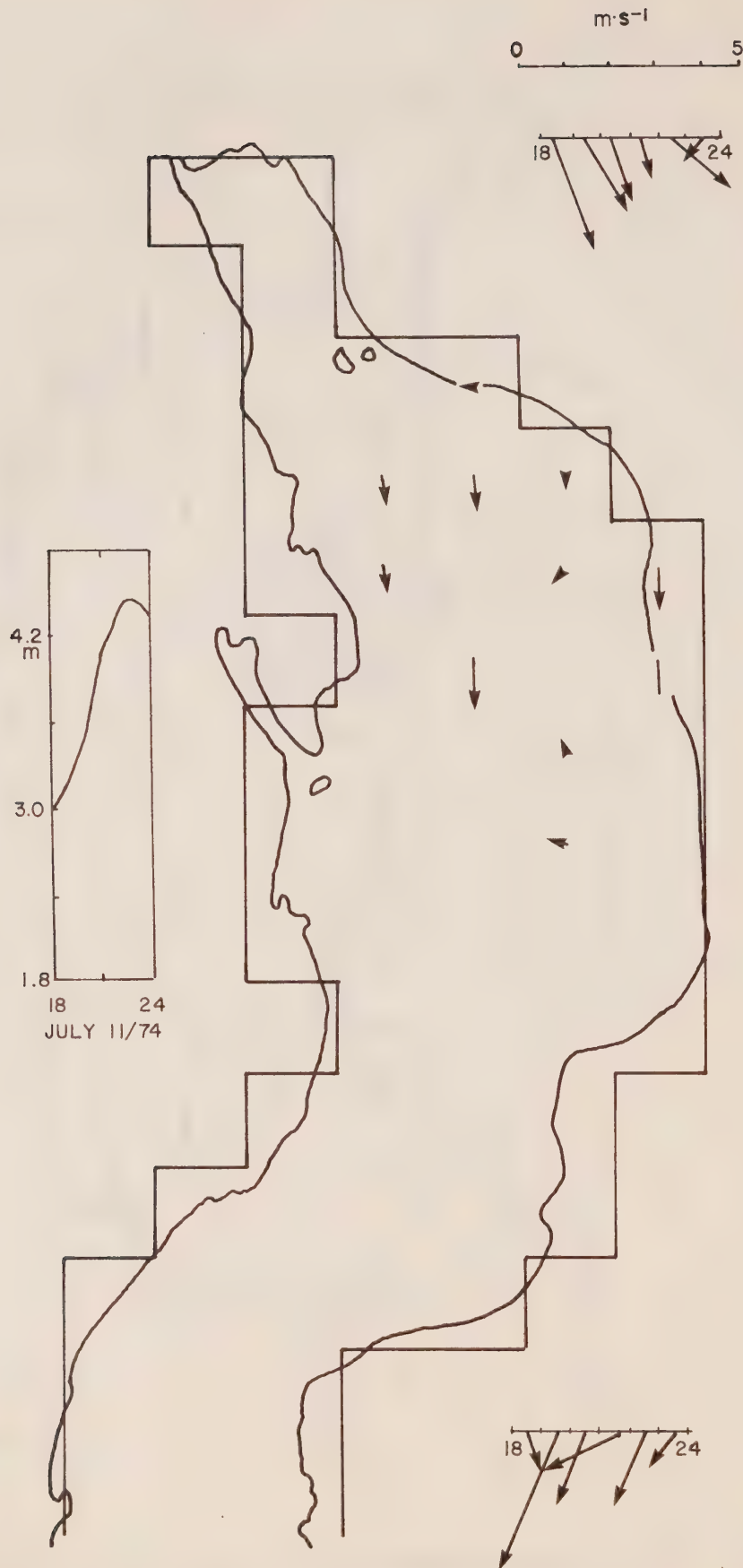


Figure 16. Pendrell Sound drogue motions: July 11/74 1800 hrs - 2400 hrs.

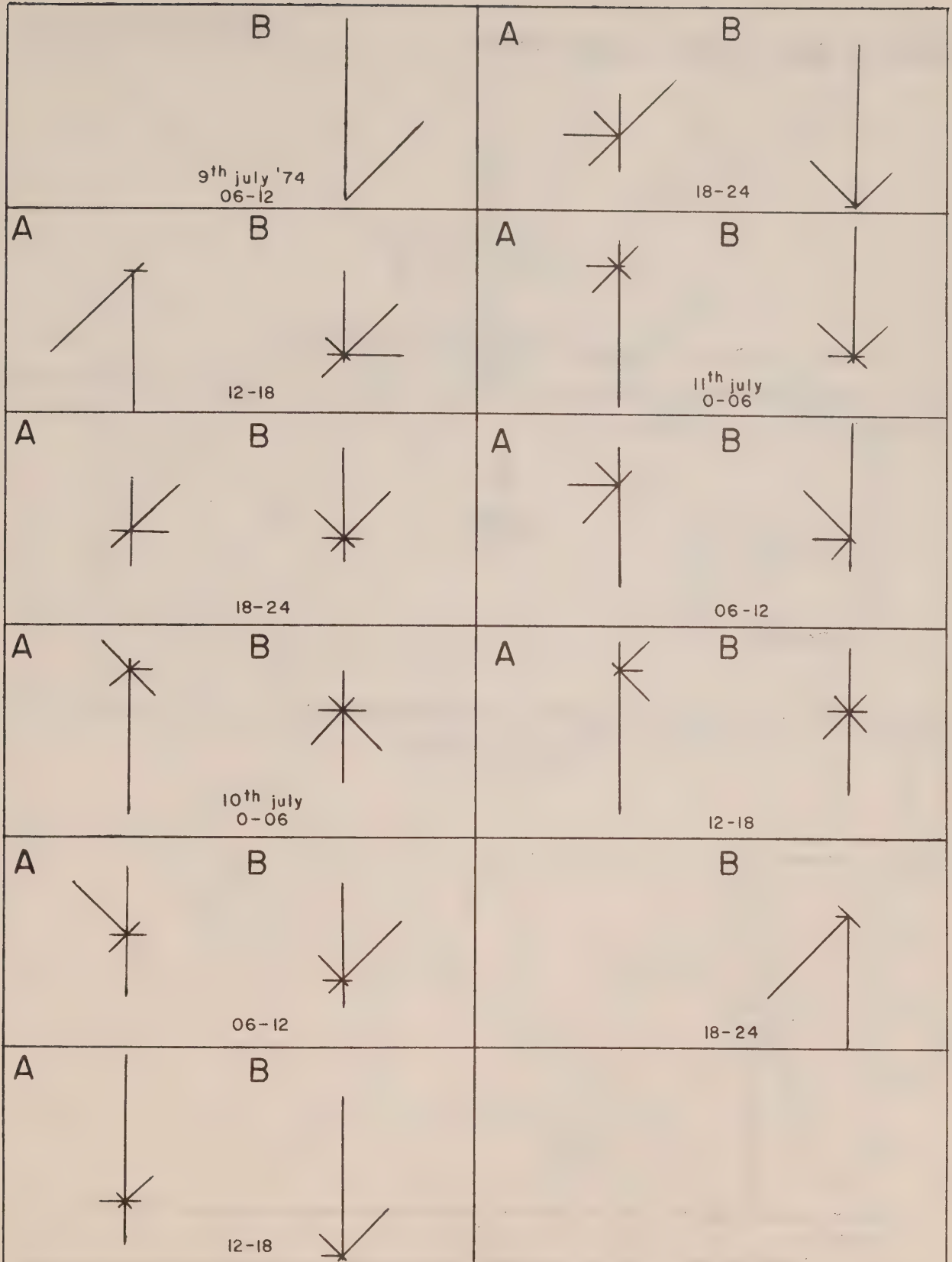


Fig. 17 Current Roses for two sides of Pendrell Sound (see Fig. 5) to show tendency toward anticlockwise circulation.

WIND and TIDE: Port Mellon

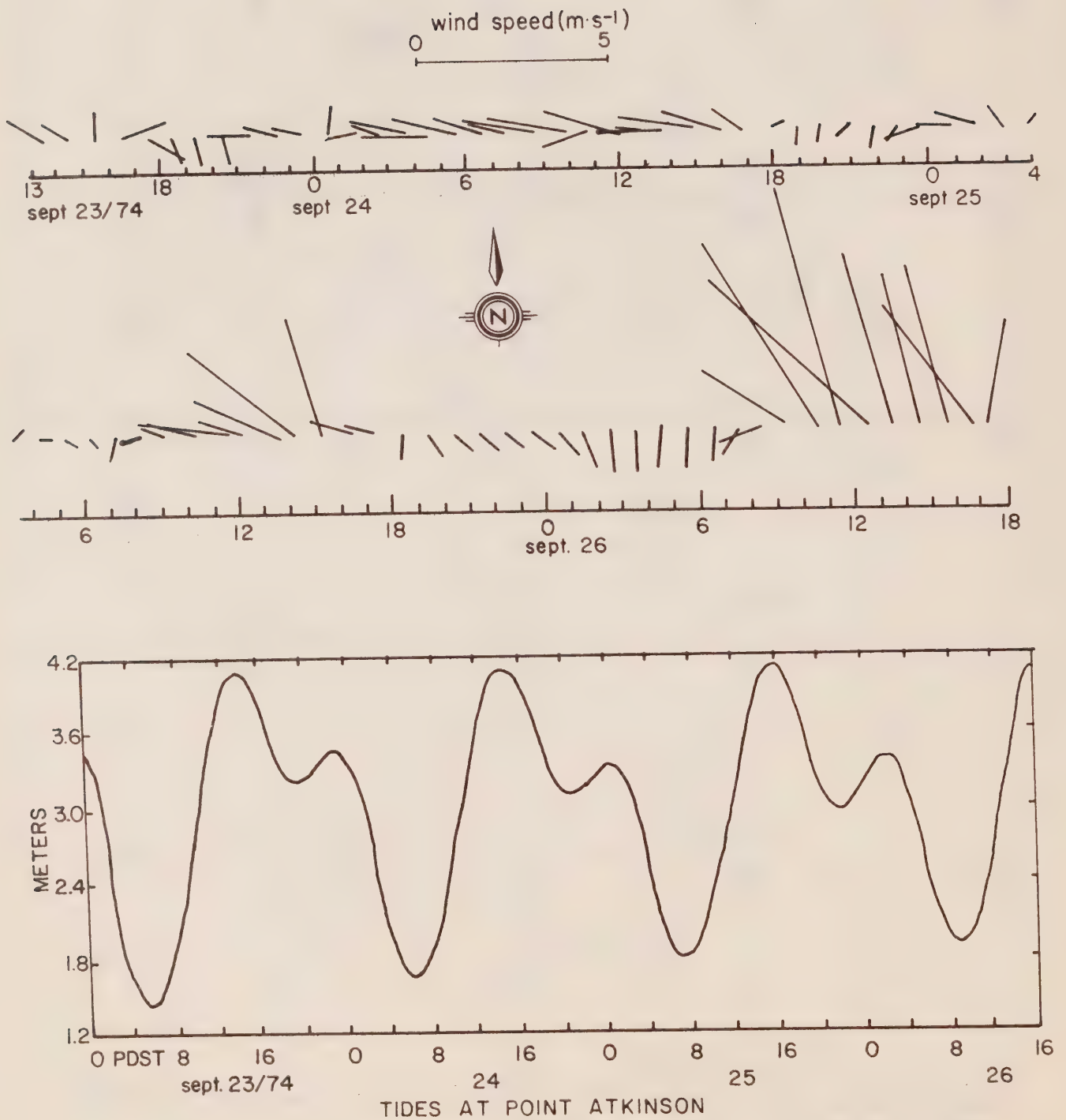


Figure 18.

Legend: Port Mellon
 approx. scale: 2.5 inches=1 mile

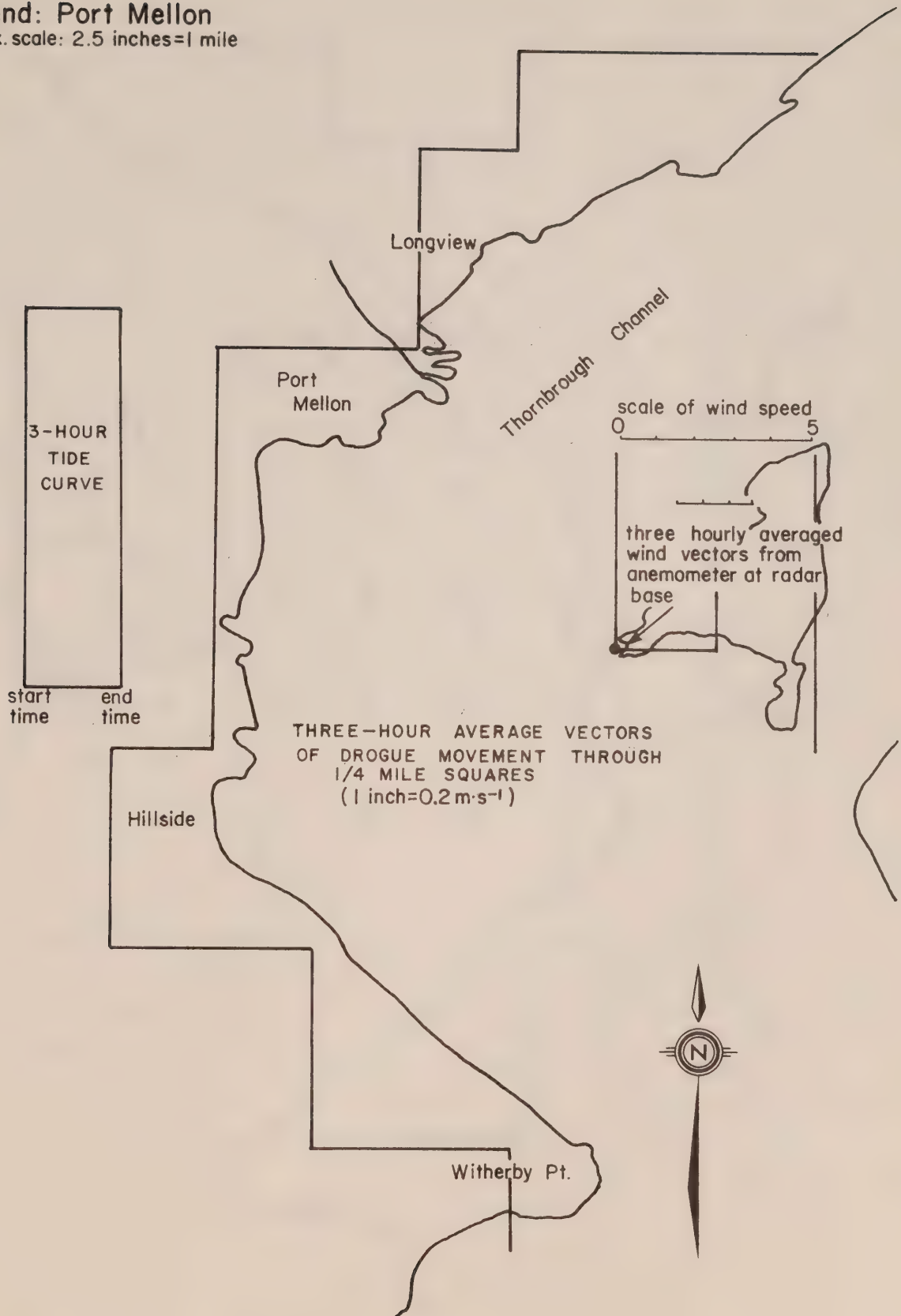


Figure 19.

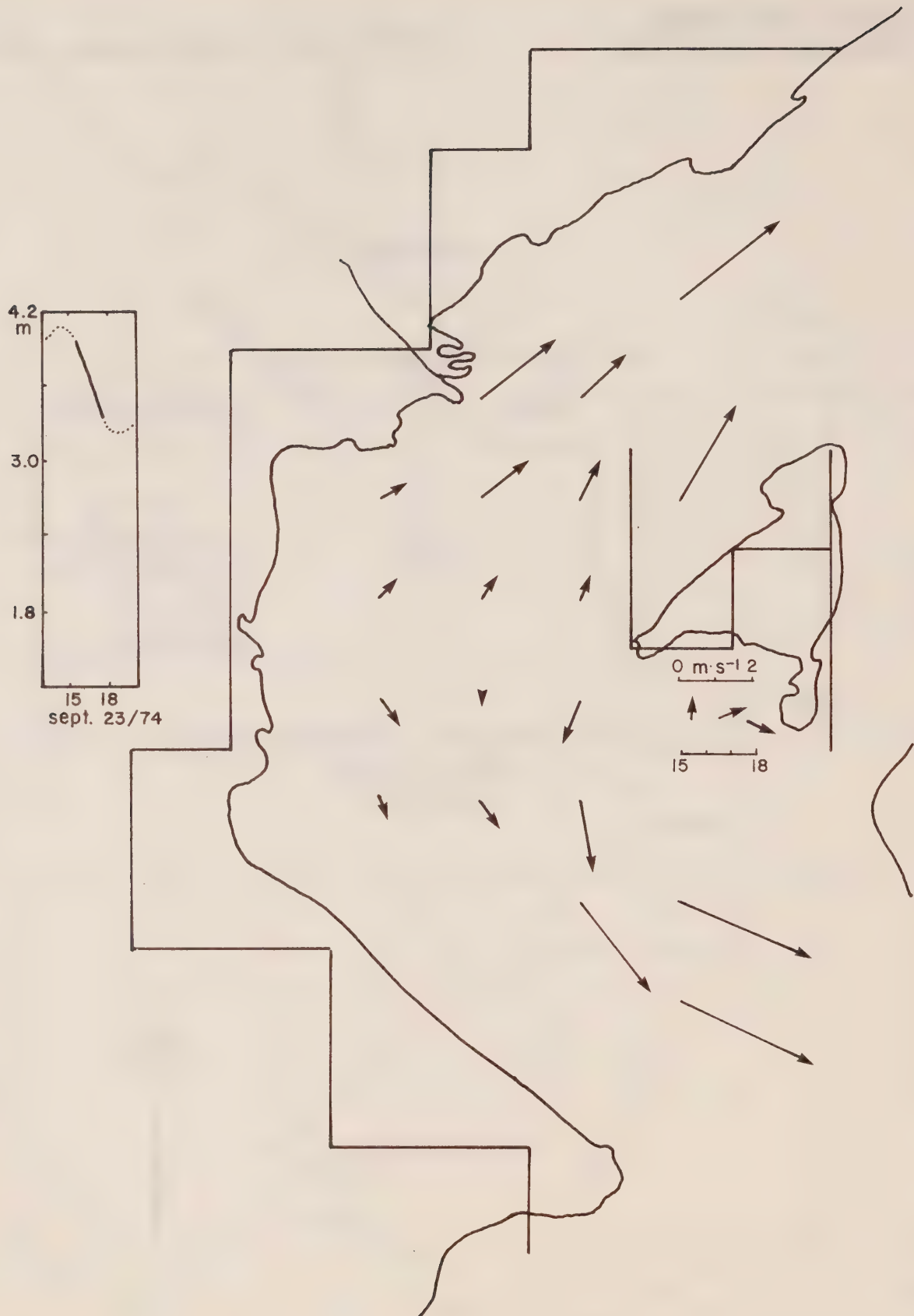


Figure 20. Port Mellon drogue motions: Sept. 23/74 1500 hrs - 1800 hrs.

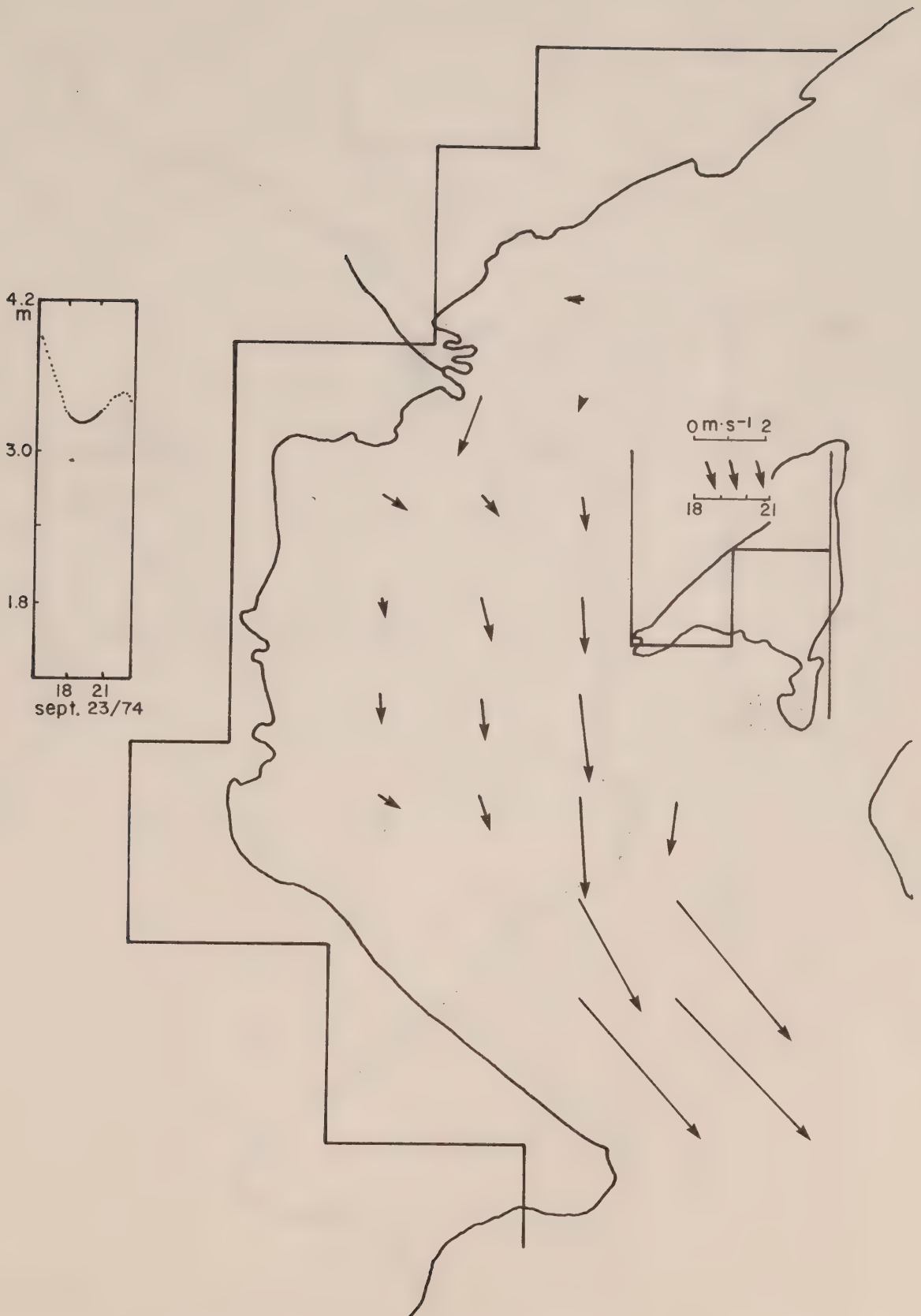


Figure 21. Port Mellon drogue motions: Sept. 23/74 1800 hrs - 2100 hrs.

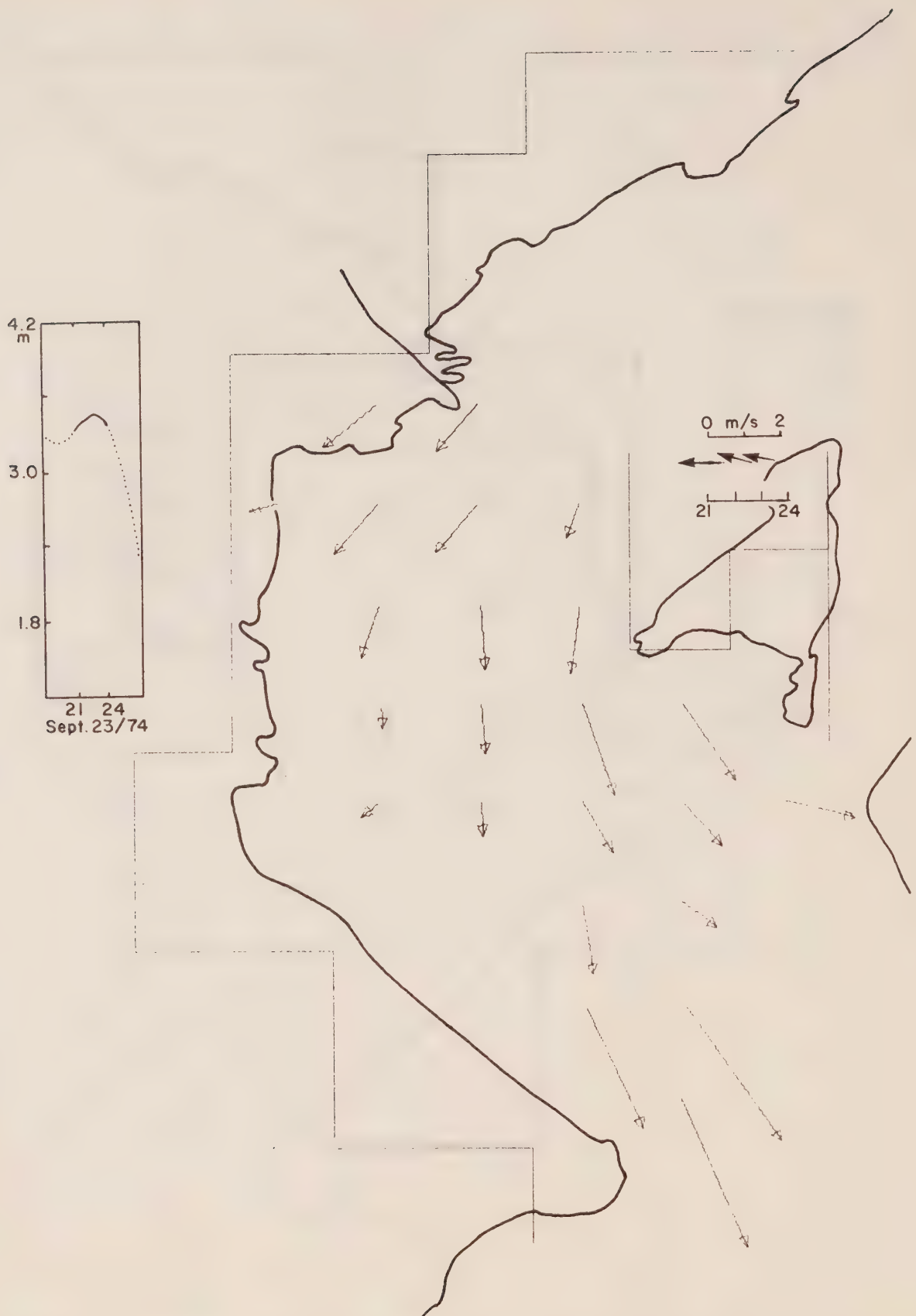


Figure 22. Port Mellon drogue motions: Sept. 23/74 2100 hrs - 2400 hrs.

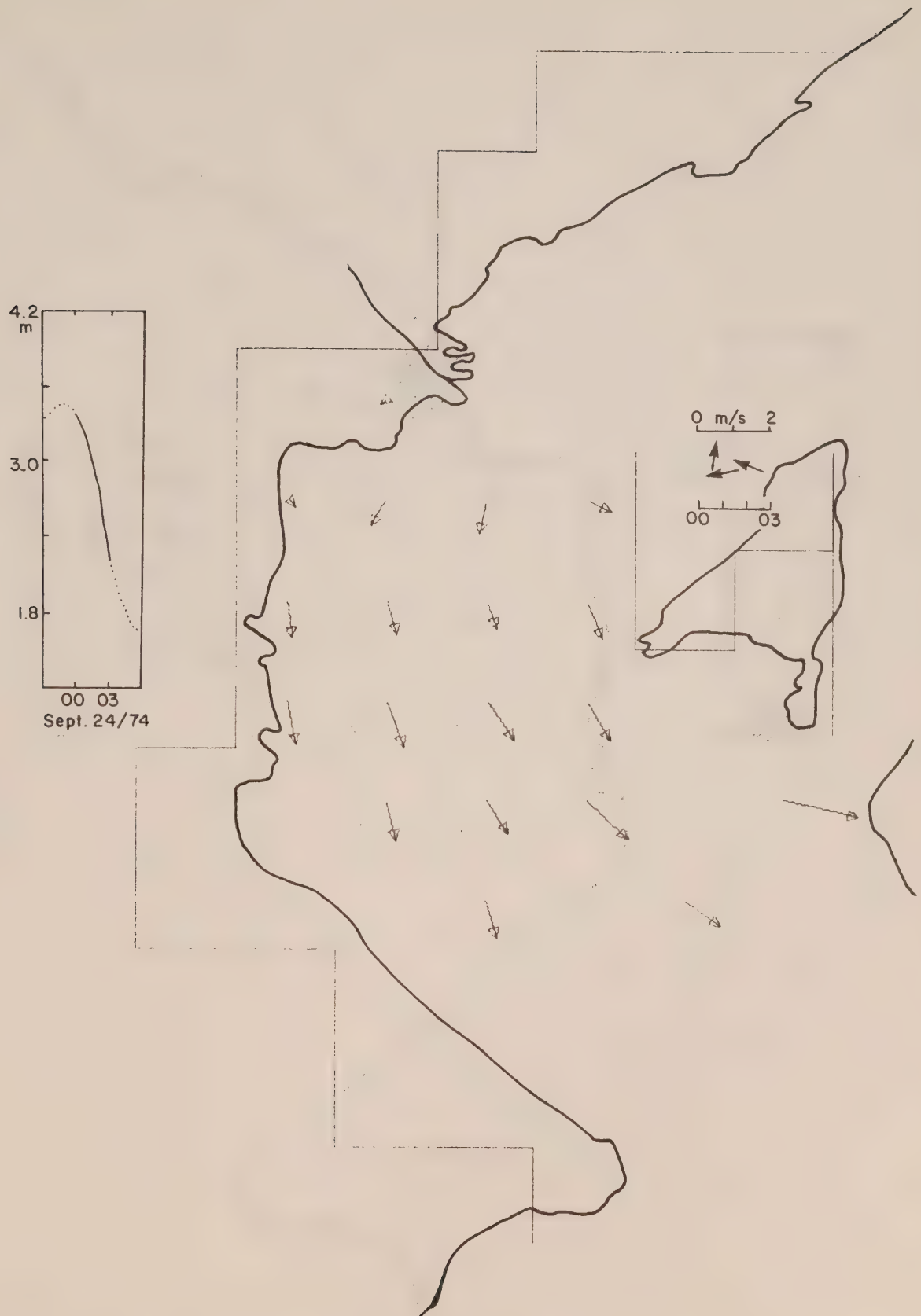


Figure 23. Port Mellon drogue motions: Sept. 24/74 0000 hrs - 0300 hrs.

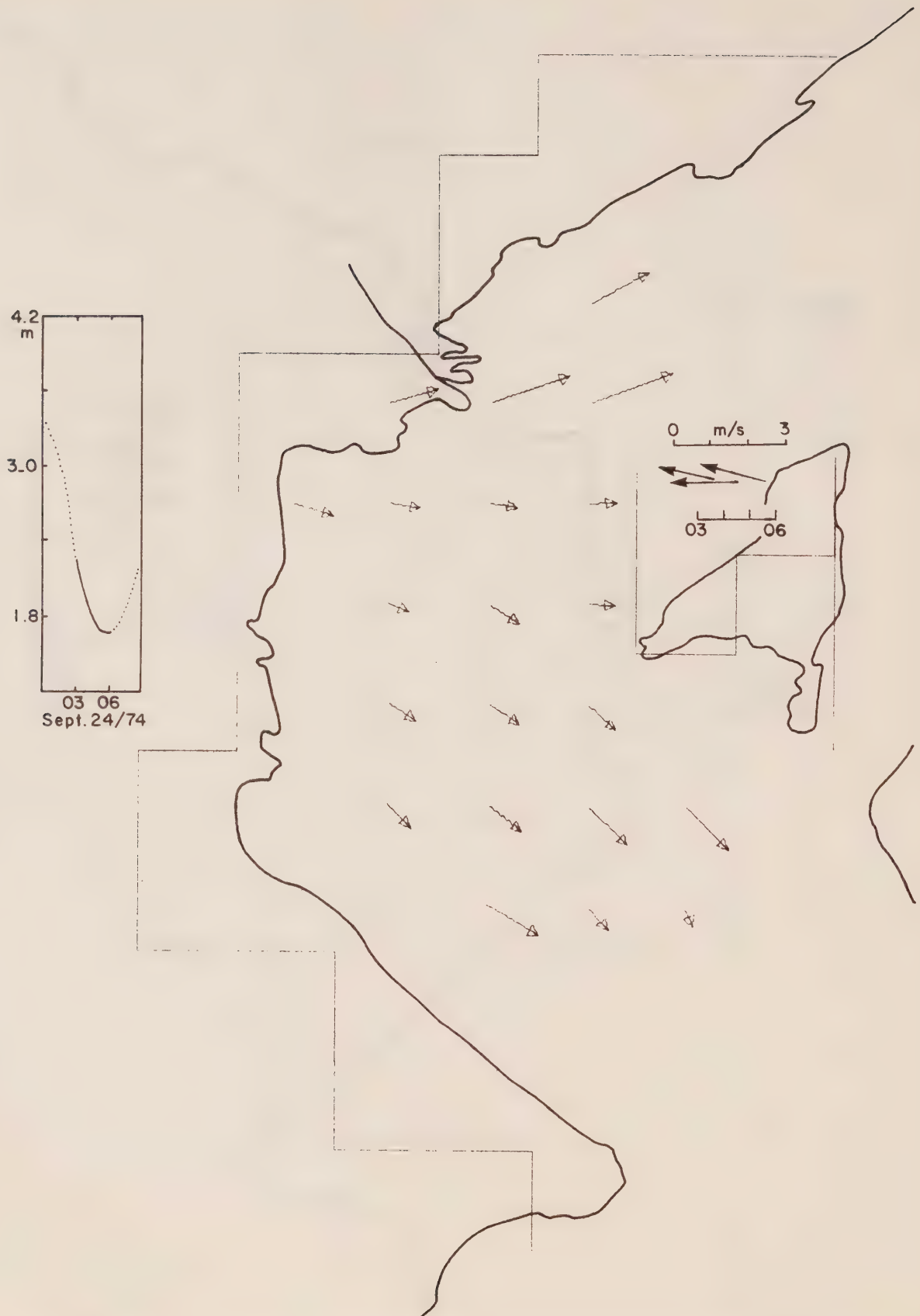


Figure 24. Port Mellon drogue motions: Sept. 24/74 0300 hrs - 0600 hrs.



Figure 25. Port Mellon drogue motions: Sept. 24/74 0600 hrs - 0900 hrs.

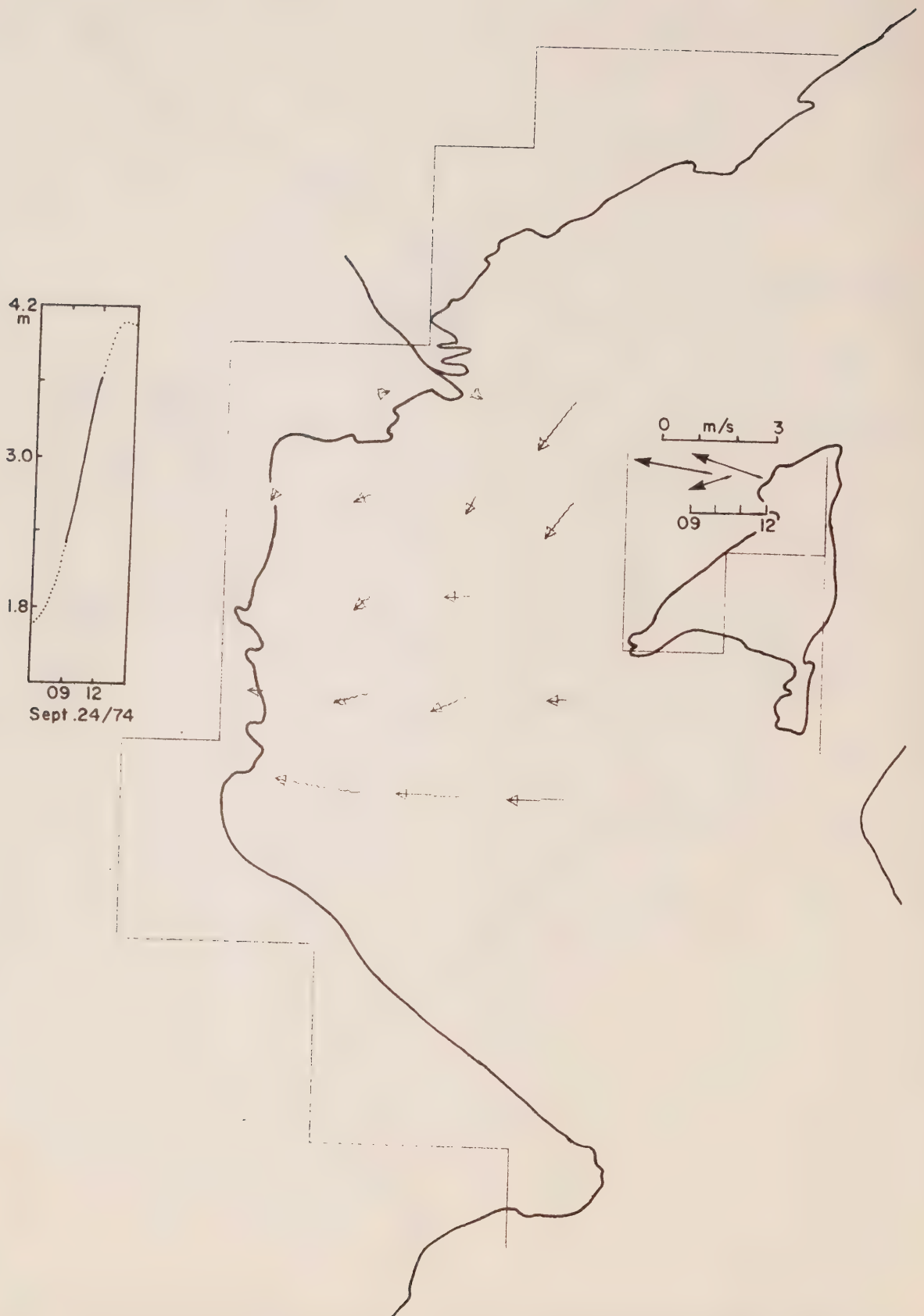


Figure 26. Port Mellon drogue motions: Sept. 24/74 0900 hrs - 1200 hrs.

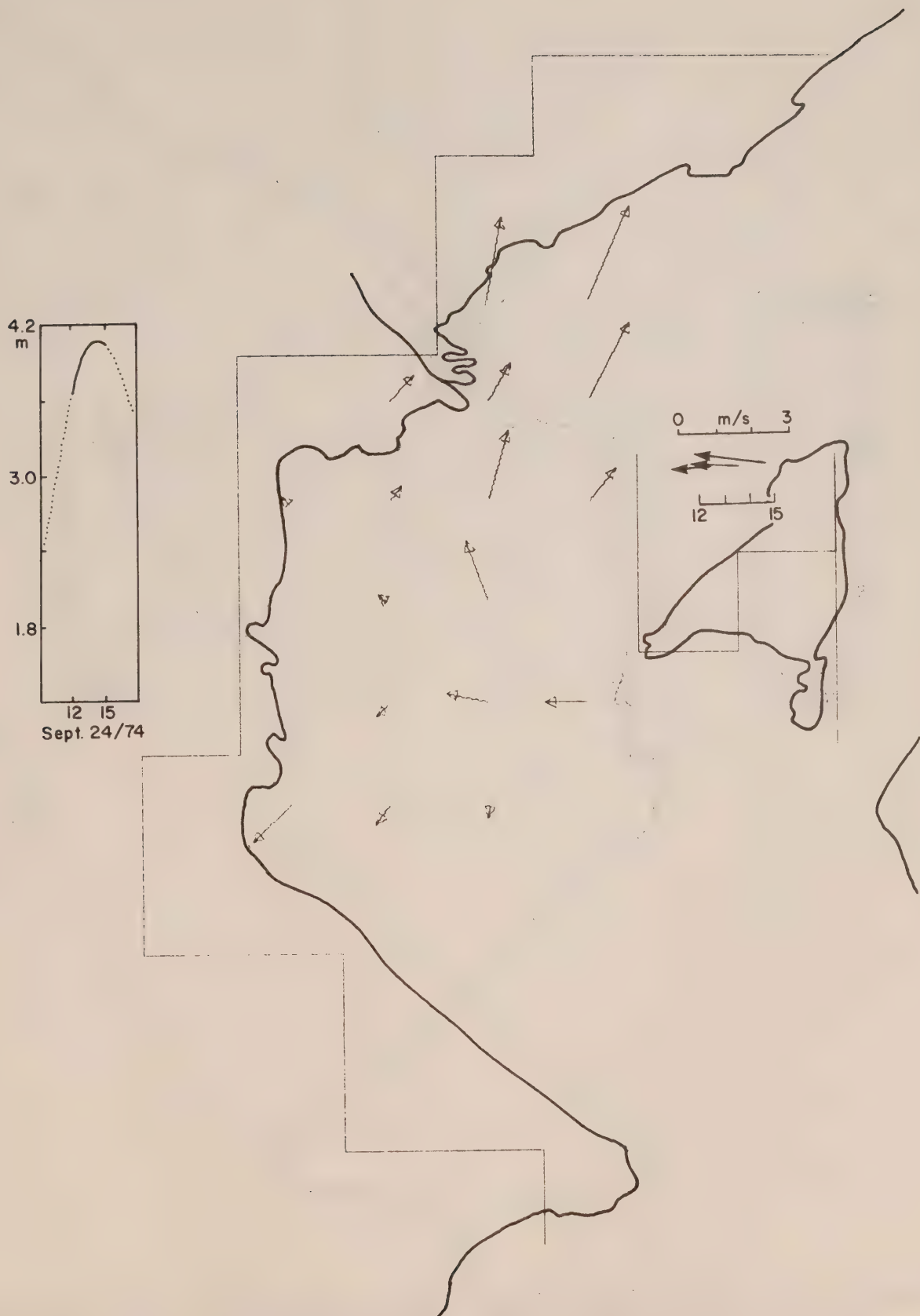


Figure 27. Port Mellon drogue motions: Sept. 24/74 1200 hrs - 1500 hrs.

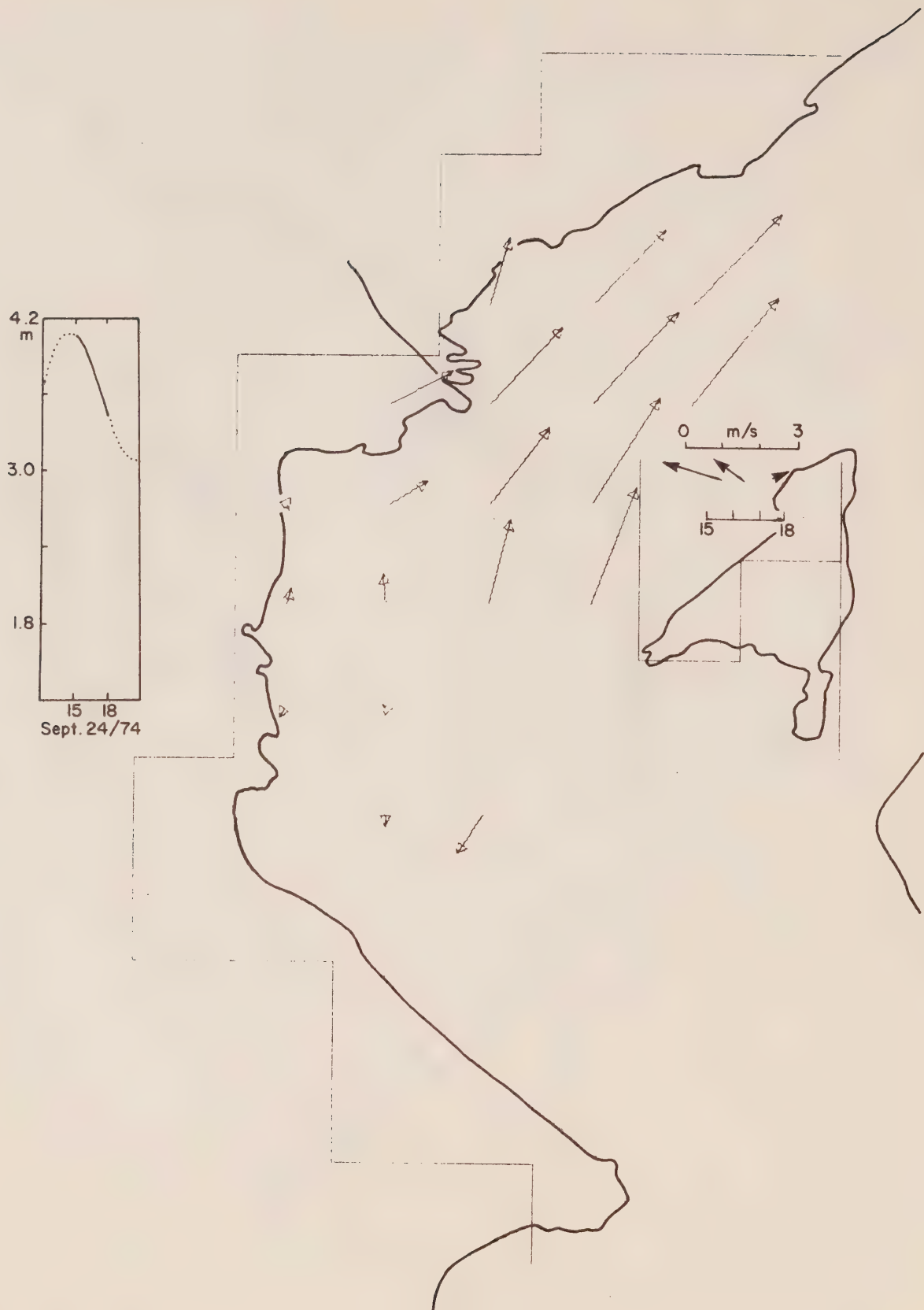


Figure 28. Port Mellon drogue motions: Sept. 24/74 1500 hrs - 1800 hrs.

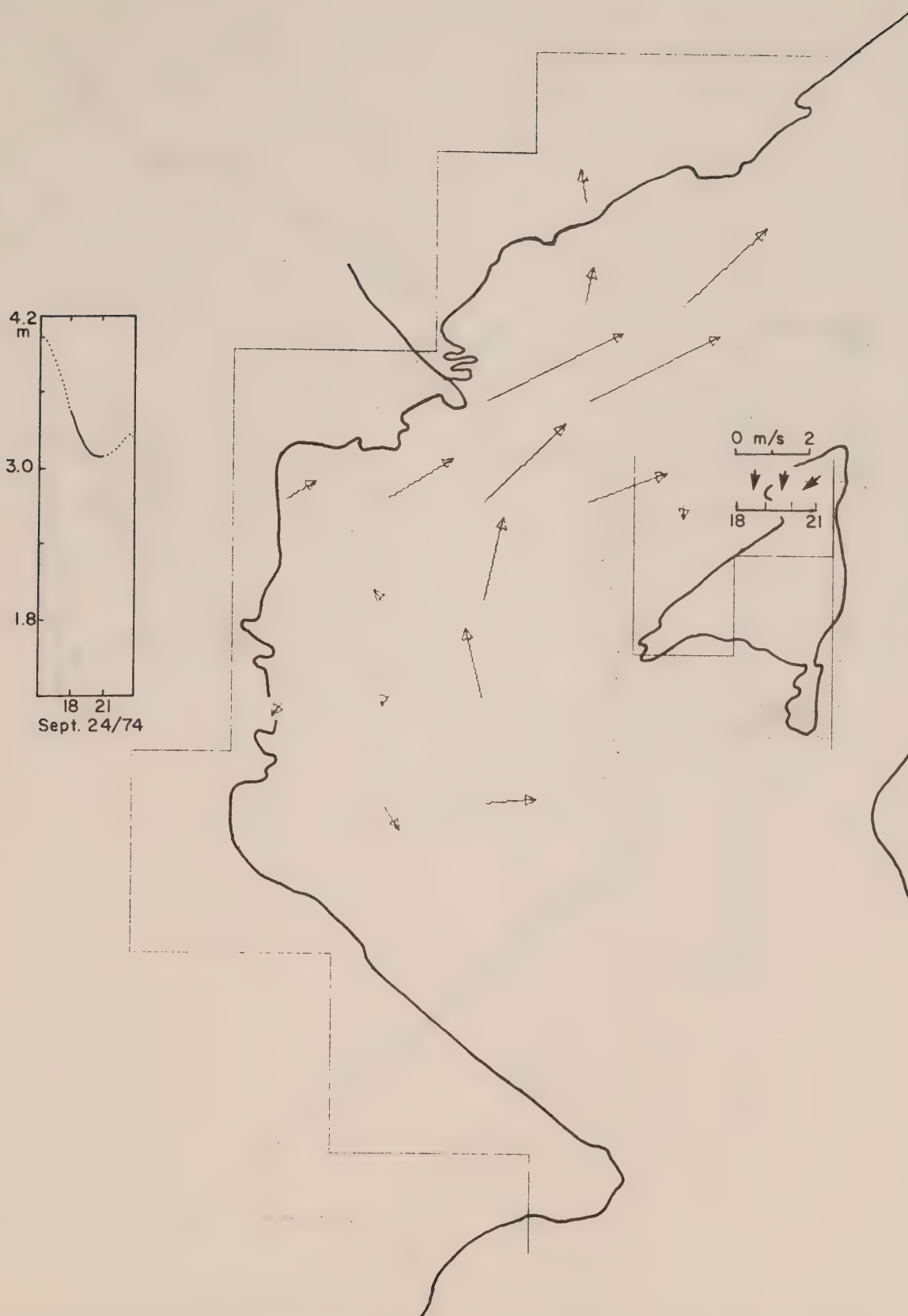


Figure 29. Port Mellon drogue motions: Sept. 24/74 1800 hrs - 2100 hrs.

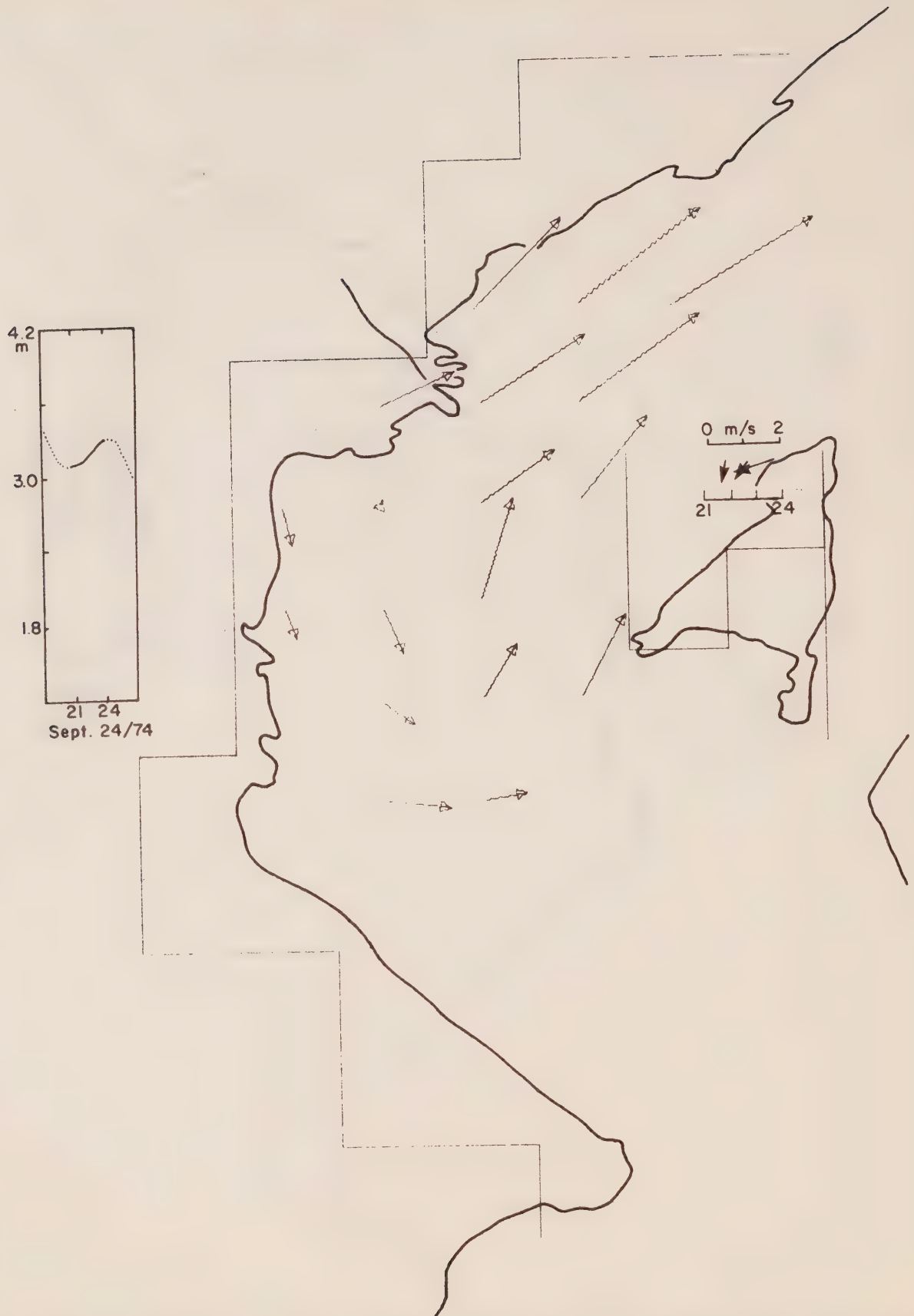


Figure 30. Port Mellon drogue motions: Sept. 24/74 2100 hrs - 2400 hrs.

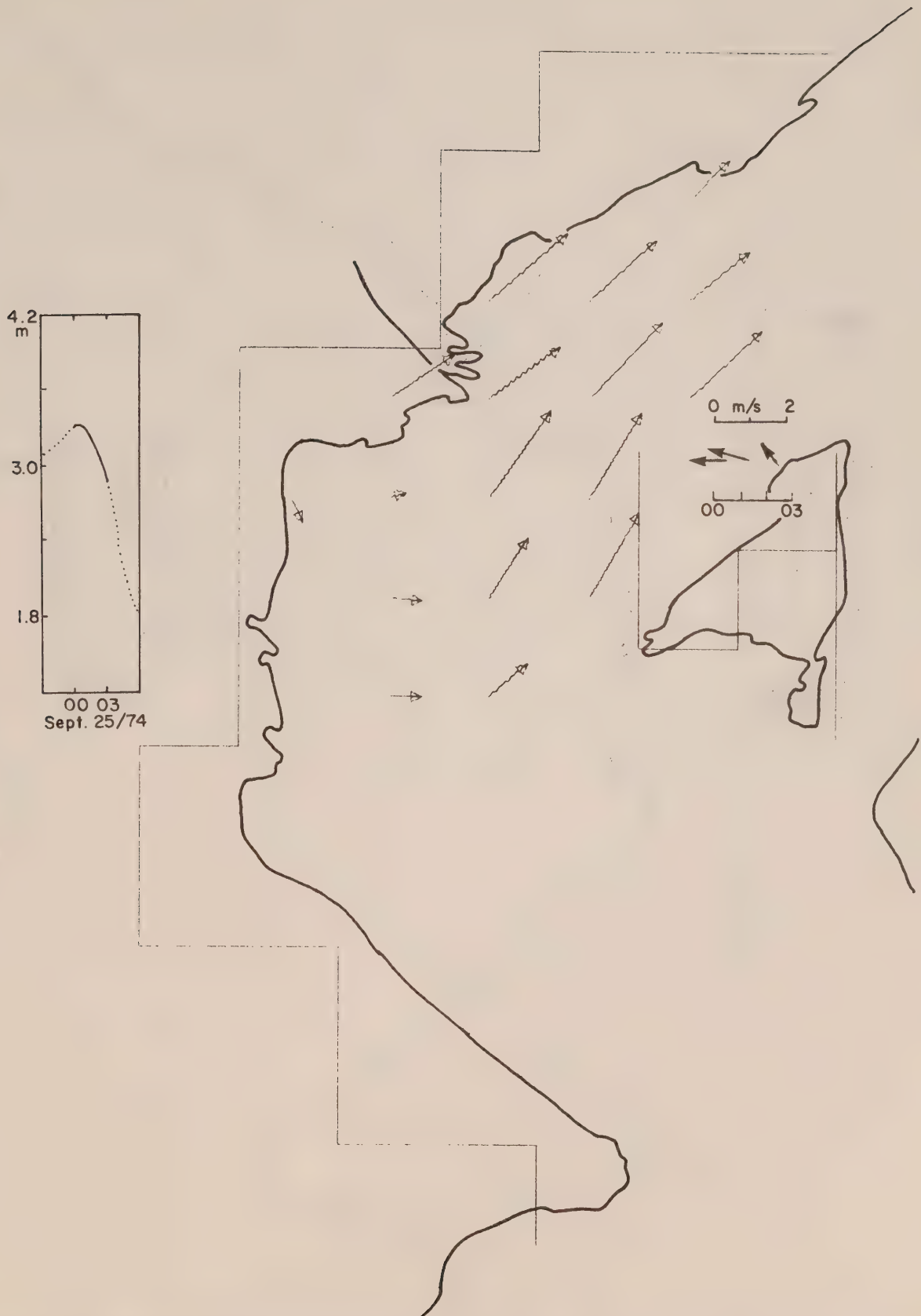


Figure 31. Port Mellon drogue motions: Sept. 25/74 0000 hrs - 0300 hrs.

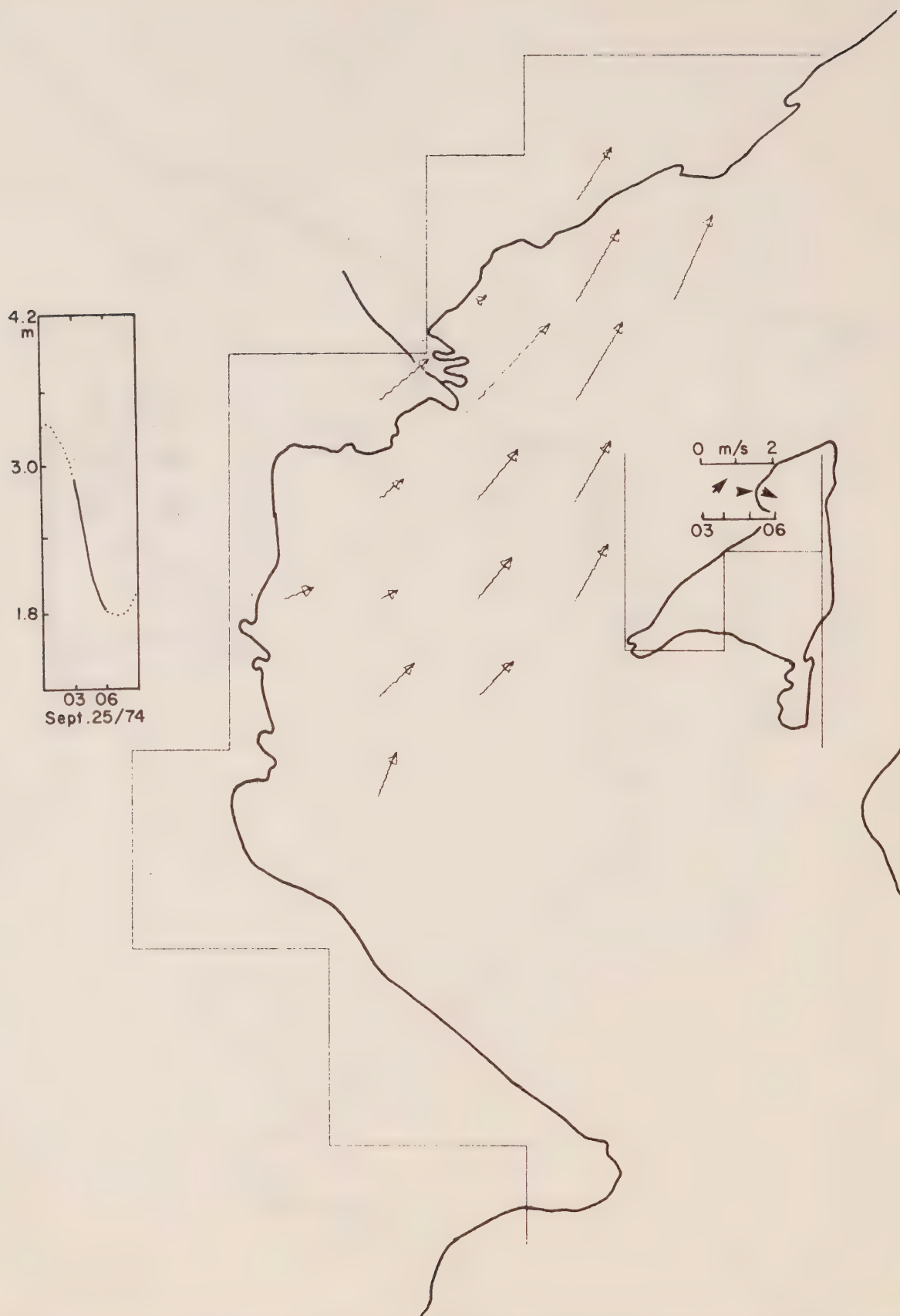


Figure 32. Port Mellon drogue motions: Sept. 25/74 0300 hrs - 0600 hrs.



Figure 33. Port Mellon drogue motions: Sept. 25/74 0600 hrs - 0900 hrs.



Figure 34. Port Mellon drogue motions: Sept. 25/74 0900 hrs - 1200 hrs.

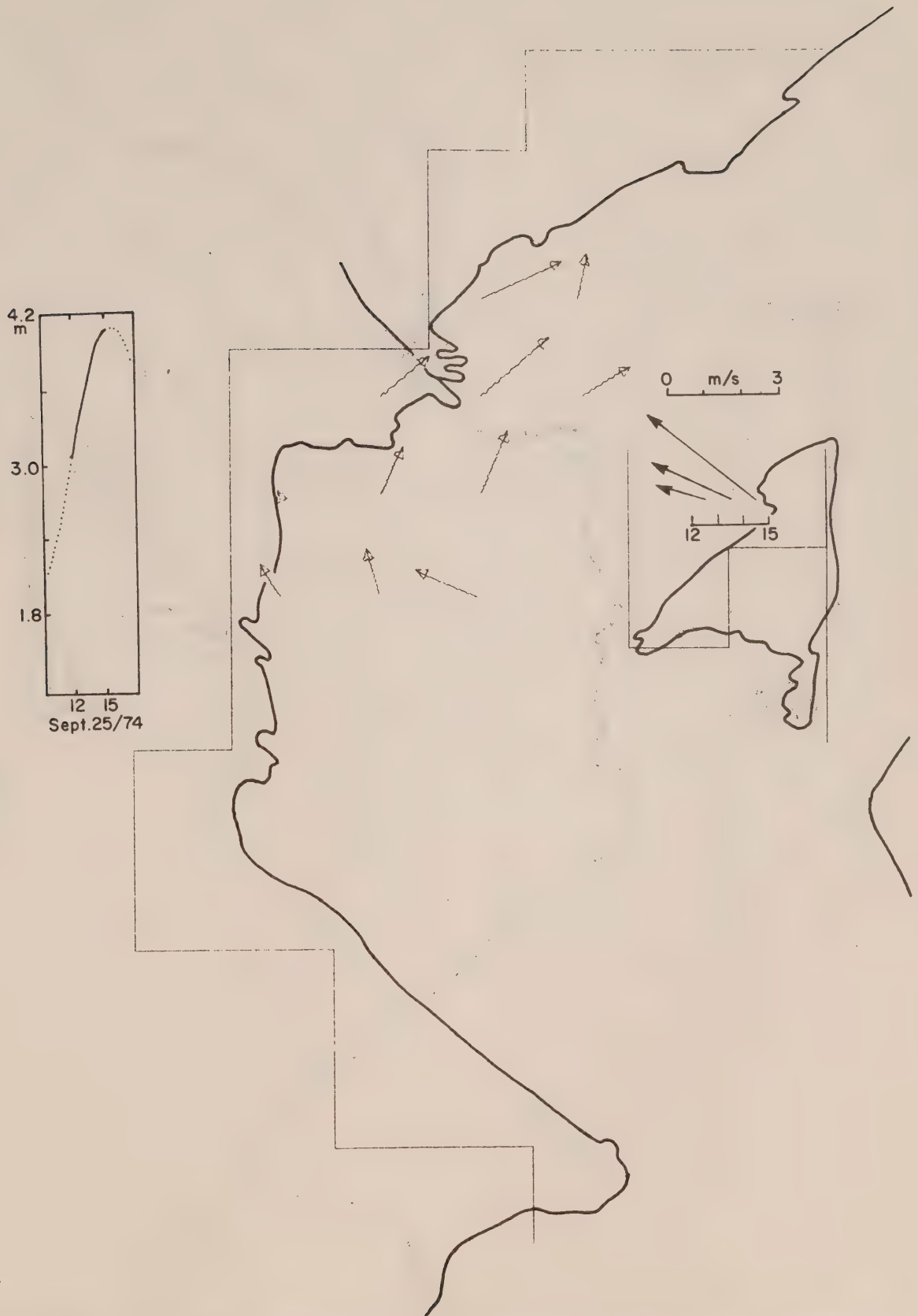


Figure 35. Port Mellon drogue motions: Sept. 25/74 1200 hrs - 1500 hrs.

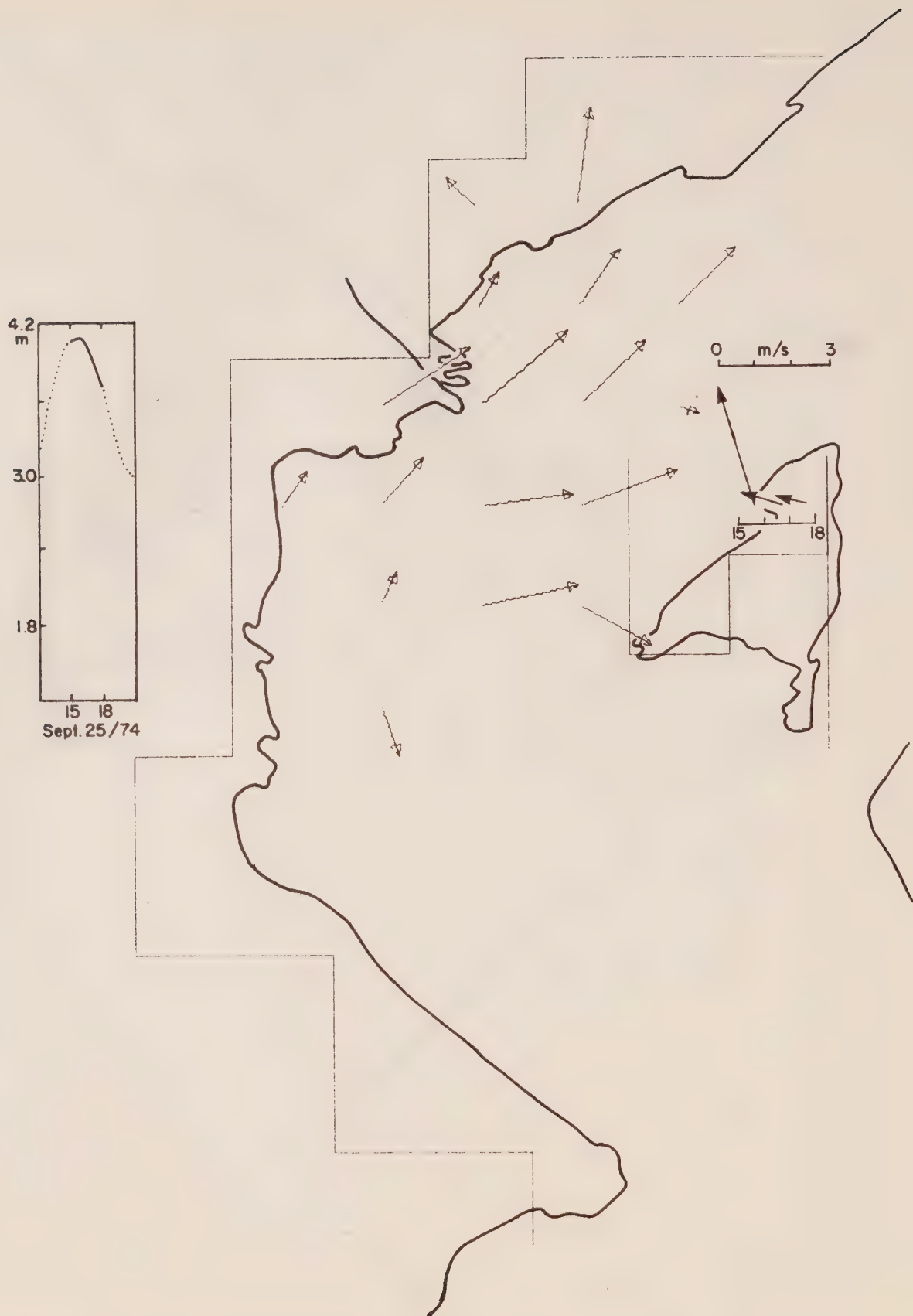


Figure 36. Port Mellon drogue motions: Sept. 25/74 1500 hrs - 1800 hrs.

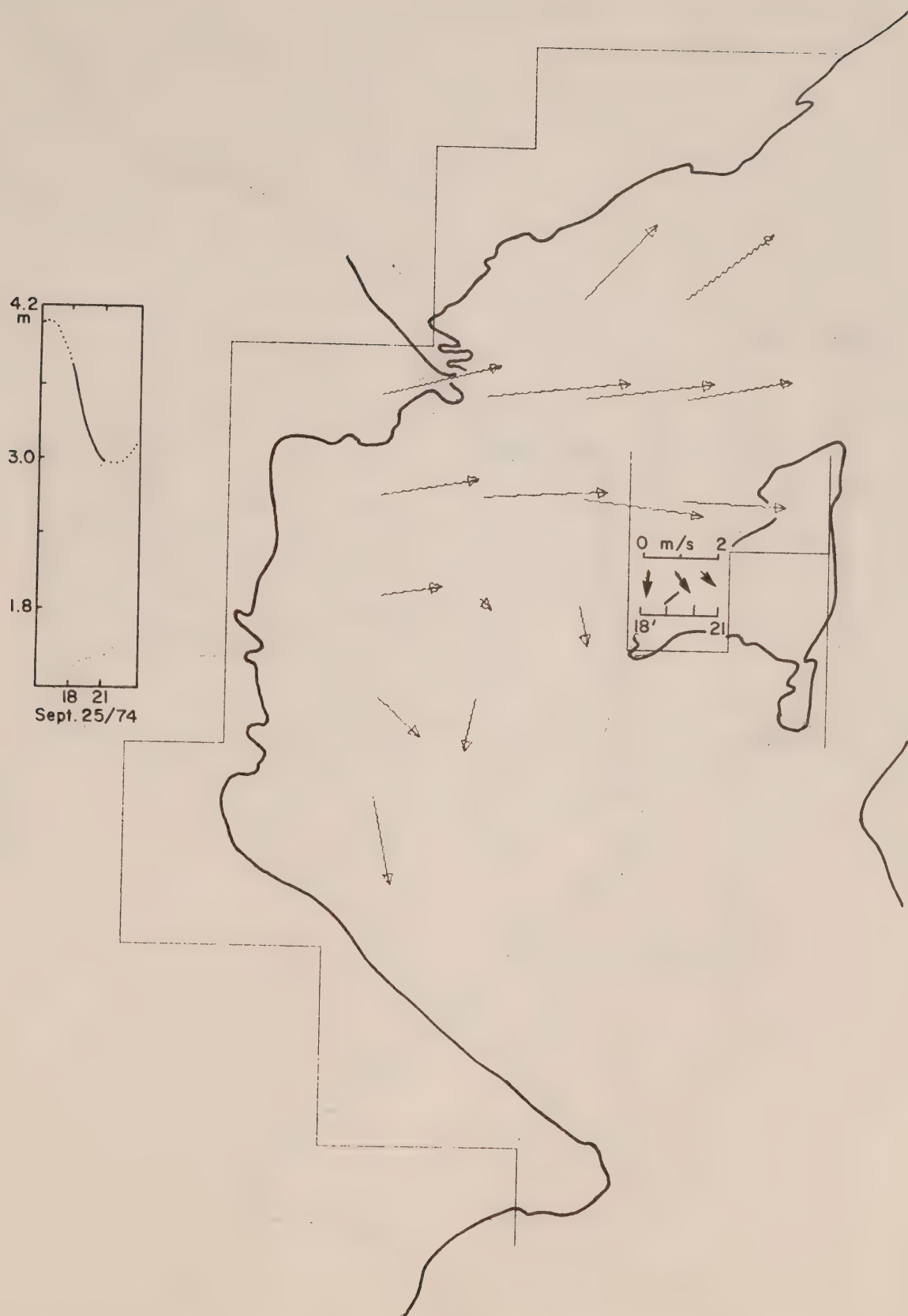


Figure 37. Port Mellon drogue motions: Sept. 25/74 1800 hrs - 2100 hrs.

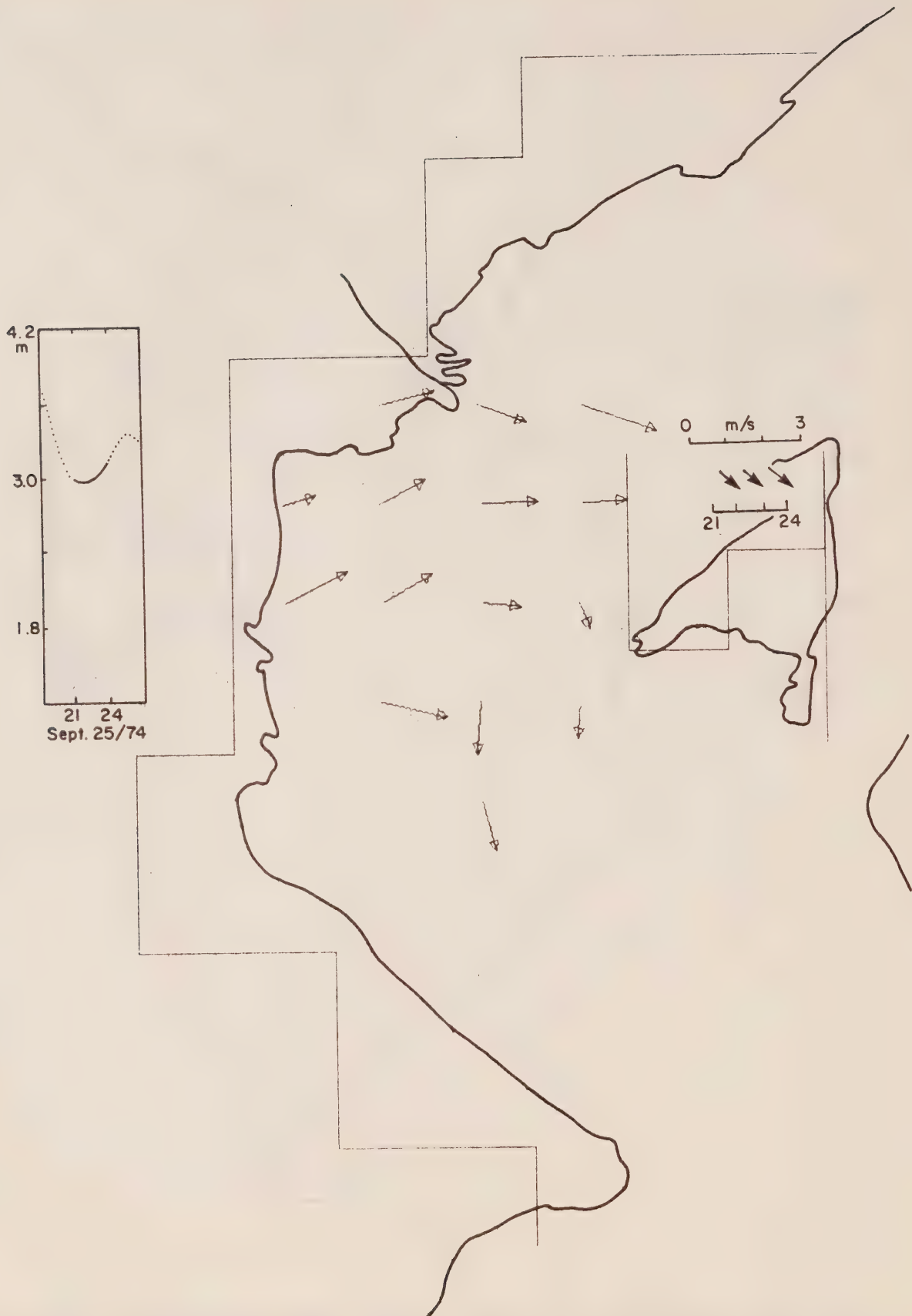


Figure 38. Port Mellon drogue motions: Sept. 25/74 2100 hrs - 2400 hrs.

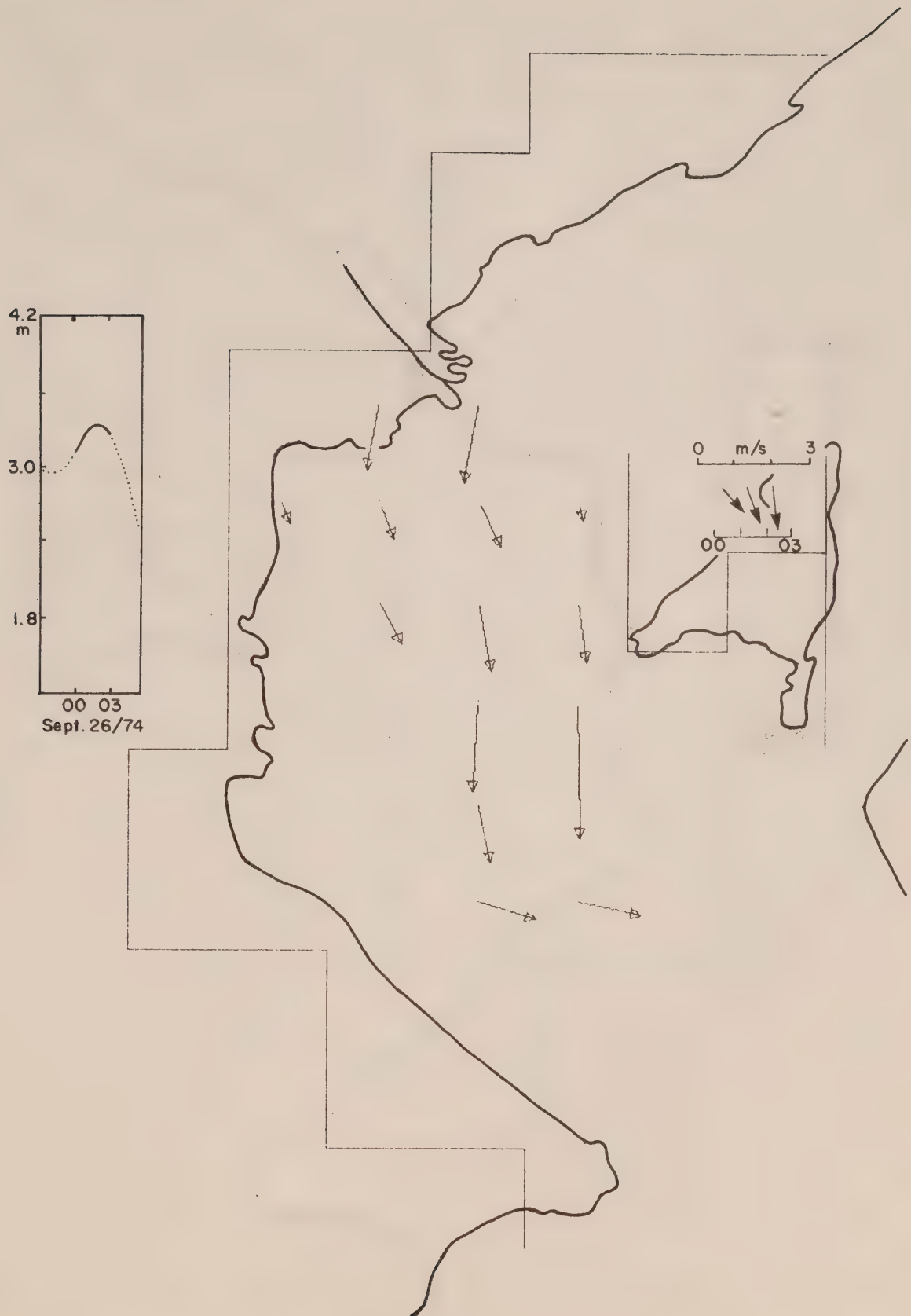


Figure 39. Port Mellon drogue motions: Sept. 26/74 0000 hrs - 0300 hrs.

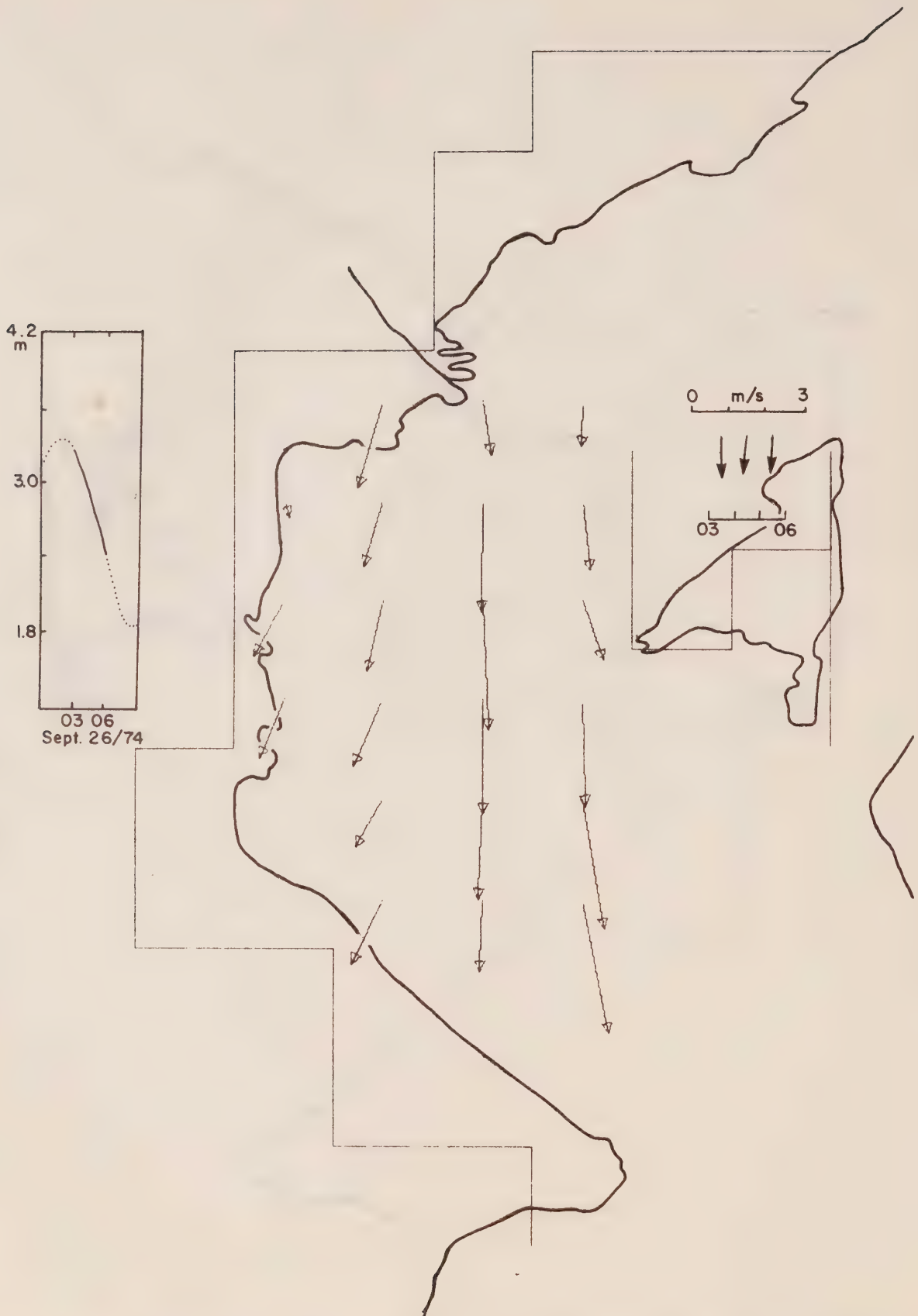


Figure 40. Port Mellon drogue motions: Sept. 26/74 0300 hrs - 0600 hrs.

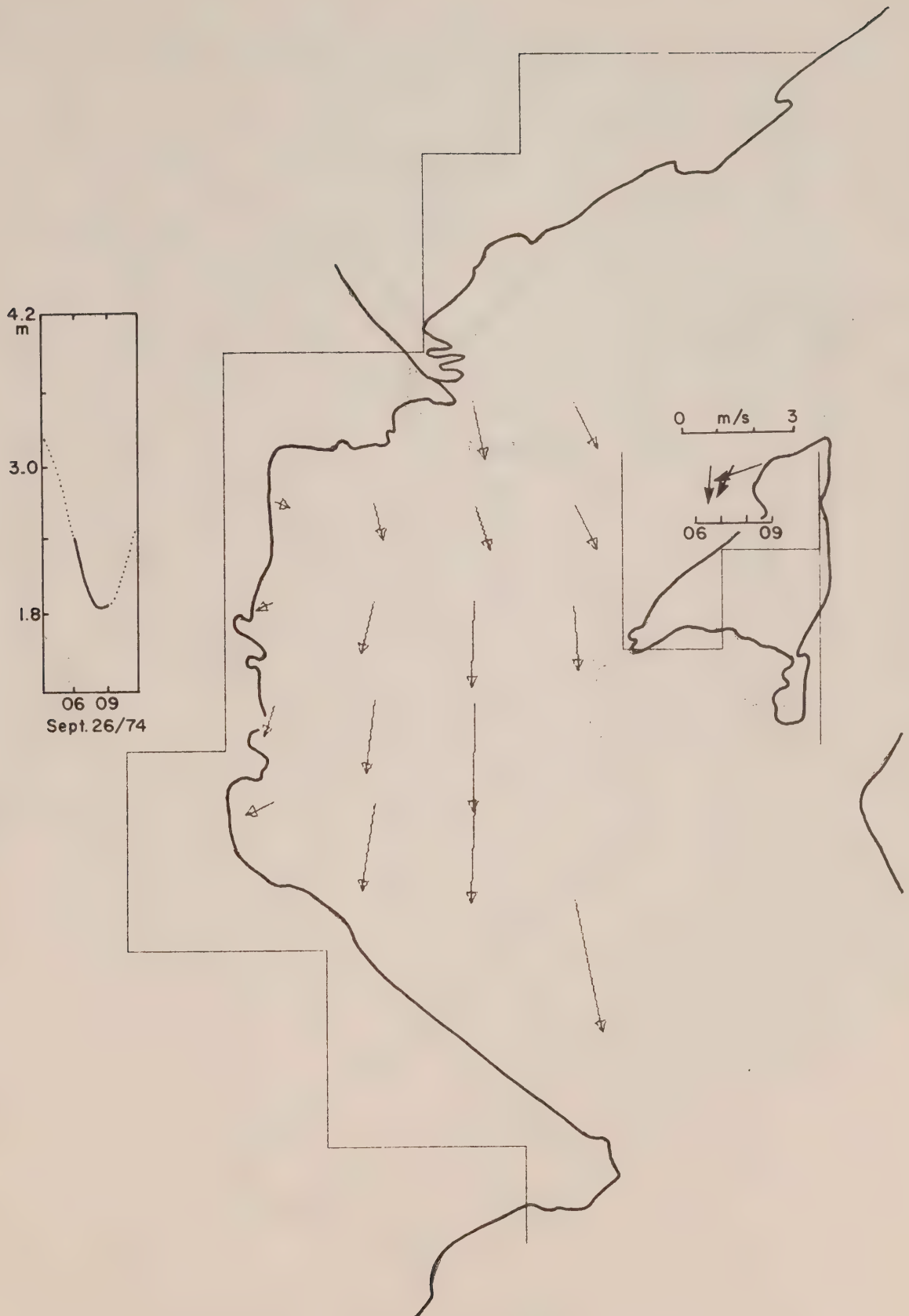


Figure 41. Port Mellon drogue motions: Sept. 26/74 0600 hrs - 0900 hrs.

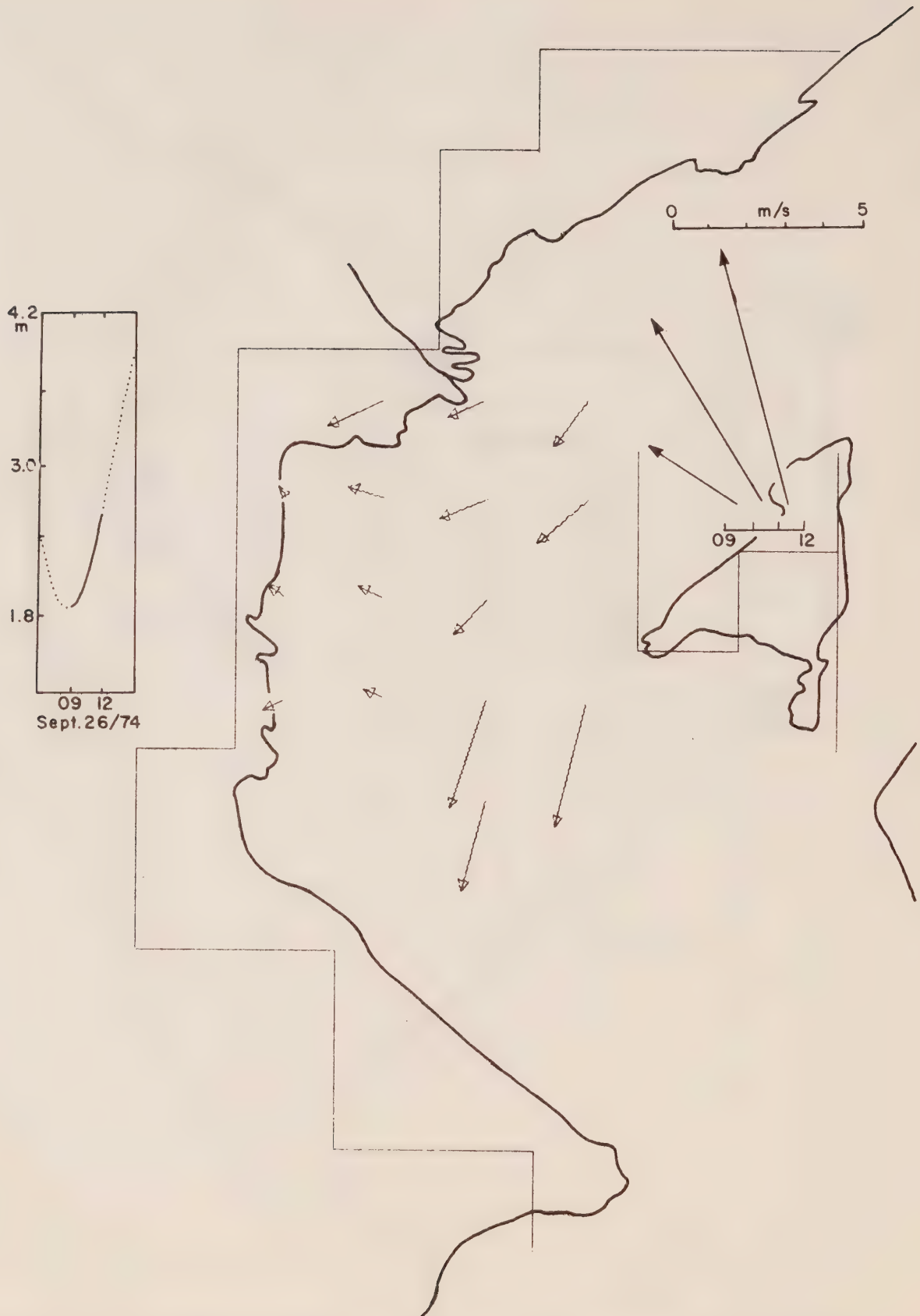


Figure 42. Port Mellon drogue motions: Sept. 26/74 0900 hrs - 1200 hrs.

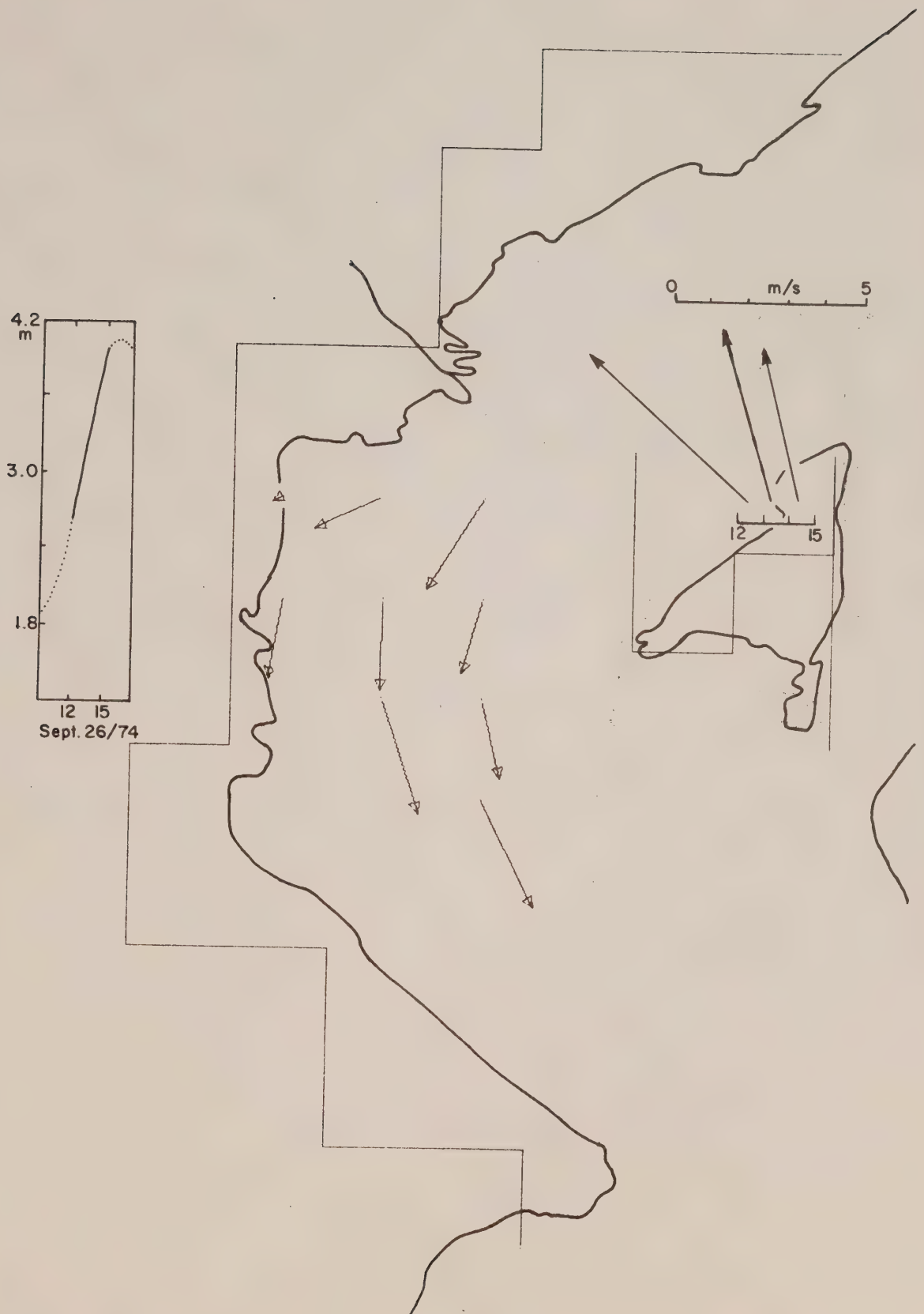


Figure 43. Port Mellon drogue motions: Sept. 26/74 1200 hrs - 1500 hrs.

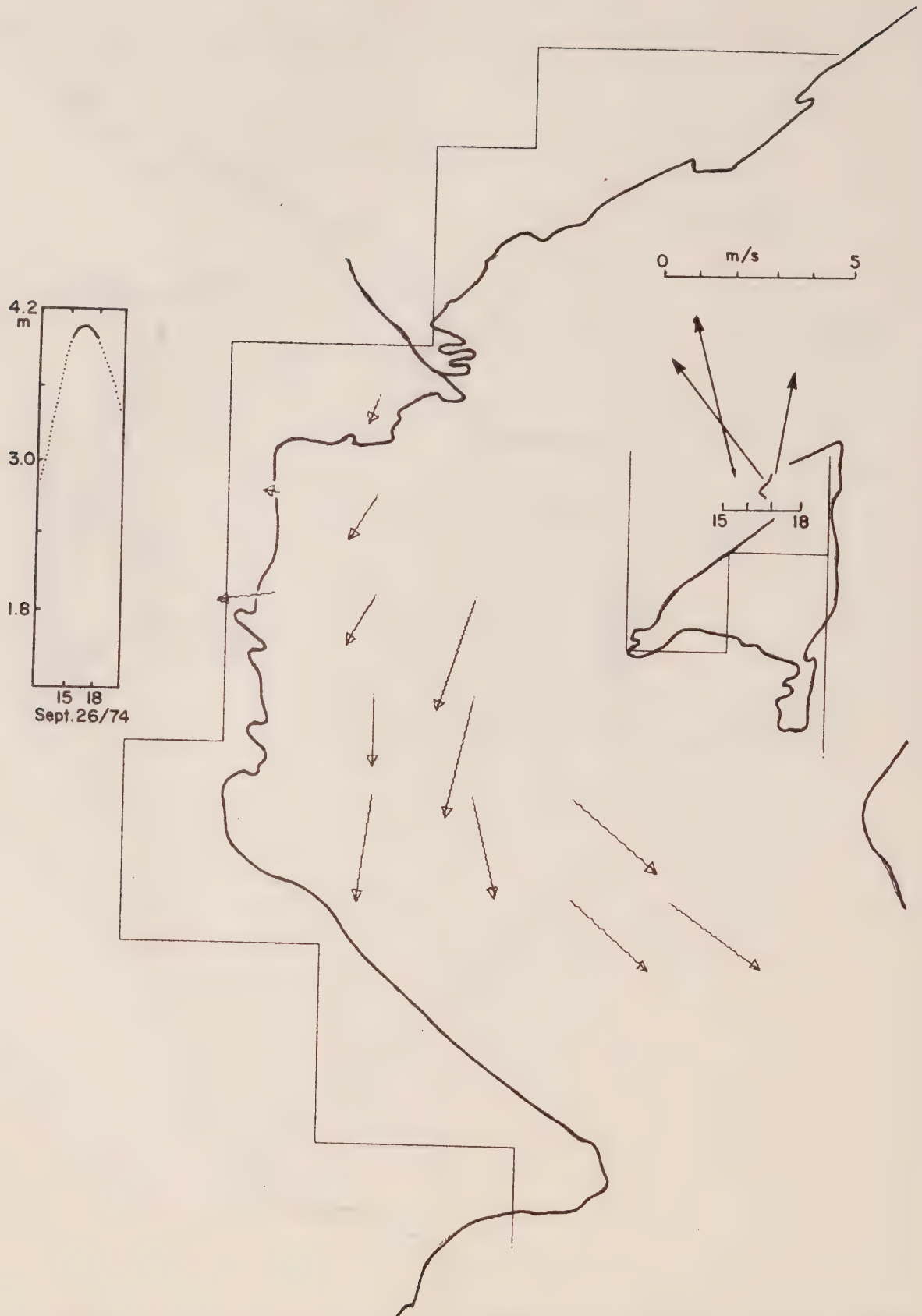


Figure 44. Port Mellon drogue motions: Sept. 26/74 1500 hrs - 1800 hrs.

*Canada Marine Science Directorate
Pacific Region*

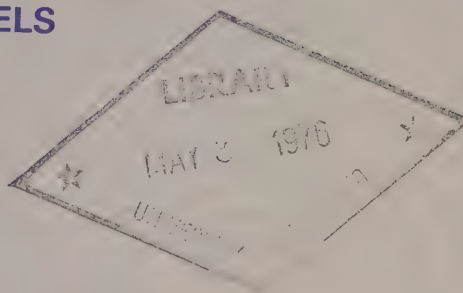
Pacific Marine Science Report 76-9

Government
Publications

CAI EP 321

-76R09

**TECHNIQUES FOR MOORING
OCEANOGRAPHIC INSTRUMENTS
FOR SMALL VESSELS**



by **J.A. STICKLAND and R.H. BIGHAM**

**INSTITUTE OF OCEAN SCIENCES, PATRICIA BAY
Victoria, B.C.**



For additional copies or further information, please write to:

Environment Canada
Institute of Ocean Sciences, Patricia Bay
512 - 1230 Government Street
Victoria, B.C.
V8W 1Y4

TECHNIQUES FOR MOORING
OCEANOGRAPHIC INSTRUMENTS FROM SMALL VESSELS

by

J.A. Stickland and R.H. Bigham

Institute of Ocean Sciences, Patricia Bay
Victoria, B.C.

March 1976

This is a manuscript which has received only limited circulation. On citing this report in a bibliography, the title should be followed by the words "UNPUBLISHED MANUSCRIPT" which is in accordance with accepted bibliographic custom.

ABSTRACT

This report includes a step-by-step account of the procedures that we have used when mooring and recovering oceanographic instrument arrays from small vessels. Two types of mooring are discussed: the taut-line system and the fore-and-aft mooring. In both cases the text is supported by a detailed set of diagrams. Other content of the report includes consideration of mooring arrangements, corrosion, procedures for documenting moorings and related aspects, and a bibliography of recommended reference books.

TABLE OF CONTENTS

	<u>Page</u>
ABSTRACT	i
TABLE OF CONTENTS	iii
CHAPTER I	
Introduction	1
CHAPTER II	
Choice of Mooring System	3
2.1 Current Meter Moorings	3
2.2 Anemometers, Thermistor Chains, etc.	4
CHAPTER III	
Taut-Line Moorings - Subsurface Buoy	5
3.1 Preparation for Launching	5
3.2 Launching Procedure	6
3.3 Preparation for Recovery	8
3.4 Recovery Procedure	8
3.5 Selection of Mooring Line	11
CHAPTER IV	
Fore-and-Aft Mooring System (Surface Buoy)	12
4.1 Preparation for Launching	12
4.2 Launching Procedure	13
4.3 Recovery Procedure	14
4.4 Selection of Materials	15
CHAPTER V	
Related Techniques and Practical Considerations	16
5.1 Taut-Line Moorings with Surface Buoys	16
5.2 Mooring from Medium-Sized Vessels	16

TABLE OF CONTENTS CONTINUED

	<u>Page</u>
5.3 <i>Leakage Fixing</i>	17
5.4 <i>Corrosion</i>	17
TABLE I	18
5.5 <i>Working Documentation</i>	19
RECOMMENDED READING	21
LIST OF FIGURES	23

CHAPTER I

Introduction

This report is designed for those whose job it is to moor oceanographic equipment in coastal waters from small vessels. From the practical point of view, the use of small vessels is important in that cost of mooring is enormously reduced (ship-time cost being one-fifth or less that of a full-sized oceanographic vessel); the flexibility of operation is correspondingly increased. For example, local fishing boats can often be used, whenever or wherever they may be needed, and it can become practical to undertake programs that would be prohibitively expensive using larger vessels.

The report does not pretend to be all-inclusive. Rather, it is an attempt to summarise, step by step, the procedures that we have found successful for two types of instrument mooring. The techniques are designed to be used with or without acoustic releases, although such releases are not specifically included in the text or drawings. If an acoustic release is used, the ground-line system provides essential redundancy in case of acoustic failure. Only in a few cases, such as in very rough terrain or in the presence of submerged cables, is the ground-line technique inappropriate; in such cases an acoustic release is essential. A bibliography on buoy technology is provided at the end of this manual and the reader is urged to consult it for further information.

By "small vessel" we refer to ships with a length of about 32-65'. This length range includes a very large proportion of the fishing boats used on the west coast of Canada, and the techniques described here apply primarily to this type of boat. For example, on such vessels the large anchor weights, such as concrete clumps and railway wheels, utilized on larger vessels, could be replaced by anchor chain - whose overall weight might be comparable but which is much easier to handle.

All of the techniques described here are the result of considerable experience, often gained under adverse conditions. They have proven extremely reliable. In the past seven years, we have undertaken 19 fore-and-aft moorings and approximately 90 taut-line moorings, both subsurface and surface. These were carried out in various coastal regions around southern B.C. and in Babine Lake, using boats ranging in size from 32' to 76'. Of these moorings, only one was lost. The ground-line recovery system has always been successful. On three occasions, fore-and-aft moorings were frozen into the ice at Babine Lake; one was dragged some distance by moving ice. However, all were successfully recovered.

Mooring from small vessels has some very real advantages in confined waters - in which manoeuverability is essential. By using the anchoring arrangements described in this manual, successful moorings have been undertaken in tidal currents of over 3 knots. However, for very strong currents a heavier anchoring system used with a medium-sized vessel, as briefly described in Chapter V, may be more appropriate. For current-meter operations, we have usually found that, for ease of handling, three instruments on a single mooring is a practical number. Larger numbers of instruments to be used in one location are best moored in multiple arrays.

We wish to acknowledge the encouragement and assistance of D.M. Farmer in preparing this report. All of the procedures described here have been in regular use with the Coastal Zone Oceanography Group, and we acknowledge the assistance of other members of this group in contributing to their practical testing. All of the illustrations were drafted by J.H. Meikle.

CHAPTER II

Choice of Mooring System

Before choosing an appropriate mooring system, it is important to consider certain practical aspects. These include the type of instruments to be used, the depths at which they are to be suspended, and the local water characteristics of current, bathymetry, tides and waves. Moreover, the vessel available will in general impose certain constraints.

2.1 Current Meter Moorings

In the usual case, taut-line moorings are essential. Unless near-surface currents are to be measured, subsurface moorings are usually preferable, since they are less likely to be damaged or dragged by passing vessels. However, to be safe from traffic, especially from the cables used in the towing of barges, the buoys must be at least 100 feet below the surface. Even this arrangement may be vulnerable to trawlers and draggers, so that, where possible, it is advisable to warn all fishermen who use the area.

Since temperatures often tend to be less at depth than near the surface, corrosion of the upper part of the mooring system is reduced in the case of subsurface arrays. Most important from the point of view of measurement, a subsurface mooring is relatively free from rapid surface motions which can seriously degrade the data.

Where current speeds are large, subsurface moorings can undergo substantial movement. Horizontal motions of, say, tidal period, will usually be unimportant; on the other hand, vertical motions, especially in stratified water, can be extremely serious and make interpretation of the data very difficult. In cases where appreciable vertical motion is suspected, instruments should always be fitted with a pressure sensor.

If strong currents are expected, some knowledge of the perturbation they will produce can be gained from mathematical models that include such effects as velocity profile, buoy shape and size, cable drag, instrument weights and anchor system details (chain or clump). Standard references include tables and diagrams which are hard to use and in many cases incomplete. A simple but comprehensive model is provided by Bell (1976). Figure 1 shows a particular example in which a uniform current acts on a simple subsurface mooring. It is seen that, for this case, a current in excess of about 2-3 knots causes substantial sinking of the buoy. The horizontal displacement also increases with current speed.

Near-surface current meter measurements are usually difficult to carry out because of the influence of surface-wave action on the buoy. These problems are particularly acute with instruments that do not average the separate components of the current vector over the recording interval. Nevertheless, surface taut-line mooring is a useful technique, especially in areas of limited fetch, where wave action is small, or in regions of strong vertical current shear, where a dense vertical array of instruments is the only practical means of examining the current structure. In such cases "plank-on-edge"

buoys, designed to impart minimum surface-wave energy to the mooring line, are, to our knowledge, the only satisfactory type in present use.

2.2 *Anemometers, Thermistor Chains, etc.*

Anemometers require a stable surface buoy, and in this respect an 8' or larger diameter "toroidal" float is satisfactory. Appropriate arrangements for attaching an anemometer are shown in Figure 2. If no instruments are to be suspended below the buoy, a taut line mooring is satisfactory and requires less line than a fore-and-aft system.

For thermistor chains suspended from the buoy, a fore-and-aft mooring is the most appropriate (Figure 3). The great advantage of this procedure is that, since the buoy does not have to be recovered and reset for each instrument servicing, a smaller boat or launch can often be used. Thermistor chains can easily be pulled up by hand and serviced within the launch, while still remaining attached to the surface buoy. An 8' diameter toroidal buoy is the smallest that should be used; a smaller buoy not only allows more movement of, for example, the anemometer, but can become an unstable and hazardous platform to work upon when servicing instruments.

Where heavy traffic occurs and a surface buoy is required, it is obviously advantageous to utilize as large and as rugged a buoy as can be obtained. Our experience has shown that the 8' toroid, properly painted and equipped with a flashing light, is readily seen by passing vessels.

CHAPTER III

Taut-Line Moorings - Subsurface Buoy

We have found taut-line subsurface mooring systems to be satisfactory for use in lakes and coastal waters; they have proven ideal for suspending current meters and thermistor chains under most conditions. In lakes, this type of system has been used extensively; it has been left entirely untouched for periods of up to eight months with little or no sign of wear or corrosion. In the ocean, the system has been satisfactorily used for continuous periods of up to six months.

3.1 Preparation for Launching

The following is the procedure we have found most satisfactory for launching the buoy and instrument-array system from a drum seiner. This vessel should be equipped with a boom, trawl winch, seine drum, hydraulically-operated vertical rollers and a horizontal roller (see Figure 4).

- (1) Wind 1/2" diameter 2 in. 1 nylon line on the trawl winch. This line will be used for lowering the secondary anchor from a davit located near the side of the vessel (Figure 10).
- (2) Wind 1" diameter braided polypropylene ground-line on to the seine drum. The length of the ground-line should be more than twice the water depth. Put this line on as tightly and evenly as possible to prevent the weight of the main anchoring system from causing the top wraps (layers) of line from biting into the lower wraps during the launching operation. After winding about 50 ft onto the drum, attach a small ribbon marker to the line. This marker will be required during the recovery operation.
- (3) Assemble the heavy-link-chain main anchor system as shown in Figure 5.
- (4) Shackle the ground-line to the main anchor system.
- (5) Coil pre-cut and thimbled main mooring line segments, in correct order and proper location, on the vessel deck, leaving both ends of all lines exposed. These lines are eventually connected to the anchor system at one end (Figure 5) and to the buoy system at the other end (Figure 6), and they support the instruments. If the suspended instruments are not of the type that actually form part of the cable, then the main mooring line will of course consist of a single segment only. The coiling must be carried out with care to permit convenient attachment of the instruments and to prevent tangling of the segments during the launching operation.
- (6) Attach the current meters to the main mooring-line segments which have been previously coiled on deck.
- (7) Attach the top end of main mooring line, which now is a single length composed of the various segments that are connected by instruments, to the subsurface buoy (Figure 6).

- (8) Attach a small float to the subsurface buoy with a double length of 1/4" polypropylene line looped through the lifting-eye (not tied) and doubled back to the float. This assembly will be required for final positioning of the subsurface buoy upon completion of launching.
- (9) Wind the heavy-link-chain anchor system on to the seine drum up to, but not including, the 5/8" diameter chain and Danforth anchor (see Figure 5).
- (10) Check the entire system to ensure that all shackles and instrument attachment points are cotter-keyed or seized.

The system is now ready for launching.

3.2 *Launching Procedure*

- (1) When the mooring location is reached, moor a small marker float as a position indicator.
- (2) The following steps (7-9) require the vessel to be under way to maintain a reasonable tension on the instrument mooring line to prevent tangles or kinks from occurring. Therefore, the vessel should proceed to a point about three times the water depth from the marker float and work its way slowly toward the proposed mooring location, thus providing sufficient time to launch the buoy, main mooring line and instruments, and to lower the main anchor system.
- (3) At this stage both the ground-line and the anchor-chain system are wound on the drum (see 3.1(9)). The next step involves lowering the anchor-chain system over the stern of the vessel until Point X (Figure 5) is resting on the horizontal stern roller.
- (4) Now connect the lower end of the main mooring line to the free end at Point Y (Figure 5).
- (5) Double check the entire system to ensure that all shackles and instrument attachment points are cotter-keyed or seized and that there are no tangles or cross-overs in the mooring line or the ground-line.
- (6) Slowly run out the remainder of the heavy-link-chain anchor system until it is clear of the horizontal stern roller. At this stage, only the ground-line is resting on the roller; it is supporting the weight of the entire anchor system.
- (7) Using the main boom, launch the subsurface buoy and have the vessel move slowly ahead. Then launch by hand the main mooring line and current meters which have been previously prepared and laid out in order on the vessel's deck. Handle the instruments with care to avoid damaging the instrument rotors, etc. on the ship's gunwale or side (Figure 7).
- (8) When the main line and instruments have all been launched, the subsurface buoy should be trailing directly astern of the vessel. The lowering of the main anchor system may now begin. It will be recalled that up to this time the main anchor system has been suspended over the stern of the vessel ((6) above).

- (9) With continued way on the vessel, slowly lower the main anchor system with the ground-line which is on the seine drum (Figure 8). Cease lowering the main anchor system as soon as the subsurface buoy begins to submerge. When the desired position has been reached (with reference to the marker float), again commence lowering the main anchor system with the ground-line until it strikes bottom. During the final lowering, the subsurface buoy will submerge. Continue keeping way on the vessel (with tension on the ground-line) to maintain a reasonable angle on the ground-line. This prevents any possibility of the ground-line tangling with the mooring line which is now vertical. The approximate position of the subsurface buoy will be evident by the small float which was previously attached (Figure 9 and Section 3.1(8)).

If, at any time during the above launching procedure, tension is not properly maintained on the mooring line, the launch should be aborted and the system retrieved to ensure that tangles or kinking of the line have not taken place. Such freedom from tangles or kinking is most important and we have found that a perfectionist's approach is mandatory.

- (10) With way on the vessel, continue to run out the ground-line under a reasonable amount of tension in the direction of the location chosen for the secondary (ground-line) anchor drop. When approximately 100 feet of ground-line is left on the drum, stop the vessel and lock off the ground-line on a cleat located near the stern of the vessel. Remove the remaining 100 feet of ground-line from the drum, coil it on deck and then shackle the end of the ground-line to the secondary anchor.
- (11) Lead the trawl winch line through the grab block which is attached to the davit. Shackle the release-hook to the trawl winch line. Attach the release hook to the ring on the secondary anchor and tie off the trip mechanism to prevent premature release of the hook. Using the main boom, lift the anchor over the vessel's side. Take up the weight of the anchor on the release-hook line and remove the boom hook from the anchor, so that the anchor is now suspended by the release hook line which is wound on the trawl winch (Figures 10 and 11).
- (12) Slip the ground-line from the cleat and proceed ahead until the ground-line slack is taken up.
- (13) Untie the release-hook trip mechanism and cock the release hook.
- (14) With way on the vessel, slowly lower the secondary anchor with the release-hook line (Figures 10 and 11). Run out a length of wire approximately $1\frac{1}{4}$ times the water depth. When the ground-line has been tightened up, run the vessel astern until the release-hook line is vertical. At this stage the anchor will settle to the bottom and the release hook will release the anchor. The hook may then be retrieved (Figure 12).
- (15) The purpose of tightening the ground-line (step 14) is to place the ground-line near the ocean floor so it cannot be easily snagged by commercial fishing vessels, such as trollers, operating in the area. In shallow water it is advisable to tie small weights at intervals along the ground-line as it is being fed off the seine drum.

- (16) Bring the vessel alongside the small float that was previously attached to the subsurface buoy for accurate position fixing - 3.1(8).
- (17) After the position of the buoy has been obtained, pull up the slack in the float line by hand and mark the line with plastic tape or a felt marker. Untie the line from the float and retrieve the line and float. The length of line that was below the water surface can now be measured and the exact depth of the subsurface buoy and instruments can be obtained. This information should be immediately recorded, together with the height of local tide.
- (18) Retrieve the moored position marker float that was used for a reference during the launching procedure.

The launching of the subsurface buoy current meter array system has now been completed.

3.3 *Preparation for Recovery*

- (1) Prepare the grapple assembly - complete with heavy-link anchor chain and swivel - as shown in Figure 13. The swivel is very important for preventing twists or tangles in the grappling line. The heavy-link anchor chain shackled to the front and back section of the grapple is needed to hold the grapple in a horizontal position so that it can hook the ground-line during the dragging operation. The heavy-link anchor chain at the back section of the grapple also serves to prevent the grapple from bouncing on rough terrain, a motion which could result in the grapple and its line become fouled with each other.
- (2) Lead the trawl winch line through the grab-block attached to the davit and attach the grapple assembly to it. It is necessary to use synthetic line, rather than wire, with the grappling hook in order to prevent any chance of the ground-line becoming nicked or chafed.
- (3) Tie about 6 feet of 1" polypropylene line to a cleat on the davit for use in operation 3.4(7) as described below.

3.4 *Recovery Procedure*

- (1) Bring the vessel as close as possible to the position of the subsurface buoy and moor a marker buoy to use for reference when the dragging operation for the ground-line commences.
- (2) Proceed to a position equidistant from both the marker float and the secondary anchor; this position should also be perpendicularly removed from the ground-line by about twice the water depth. The latter is to allow sufficient time for lowering the grapple assembly and the required length of line before the ground-line position is reached as the vessel will be under way.
- (3) When at the desired position, proceed slowly in the direction of the ground-line and slowly lower the grapple with the trawl-winch line. Run

out a length of line approximately $1 \frac{1}{4}$ times the water depth. Due to the necessity of using a length of line greater than the water depth it is very important to have sufficient way on the vessel to prevent any tangling or fouling of the grapple and line. If the bottom is known or suspected to be extremely rough and/or rocky, it would be wise to reduce the length of the grapple line, in order to reduce the scope and therefore prevent the grapple from permanently fouling on the bottom. In this case a length of line equal to the water depth plus approximately 10% should be used.

- (4) Attach a tensiometer to the grapple line. Continue slowly ahead in the direction of the ground-line (Figure 14). Hooking the ground-line will be evident by the reaction of the tensiometer, and can probably be further confirmed by taking visual sights on the marker buoy moored earlier to mark the subsurface buoy position.
- (5) During the operation involved in steps 6 to 11 inclusive, it may be necessary to manoeuvre the vessel to keep the ground-line clear of the propeller, rudder, etc.
- (6) When the ground-line has been hooked, stop the vessel, unhook the tensiometer and retrieve the grapple by means of the trawl winch.
- (7) When the grapple breaks the water surface, haul it up as close as possible to the block attached to the davit and tie off the ground-line securely with the 1" diameter tag line previously attached to a cleat on the davit, 3.3(3).
- (8) Lower the grapple with the seine winch and clear the grapple from the ground-line. Using the main boom, swing the grapple inboard and place it on the deck. The ground-line is now supported by the 1" diameter tag line secured to the davit cleat.
- (9) Unshackle the grapple from the trawl-winch line and replace with a grab-block. Attach the grab-block to the ground-line. Seize the block release with twine; this is to prevent any chance of the block opening and dropping the ground-line during the recovery operation.
- (10) Remove the 1" tag line secured to the davit cleat and clear the ground-line. At this stage, the ground-line is leading through the grab-block, which in turn is supported by the davit. The procedure for recovering the secondary anchor may now begin.
- (11) Manoeuvre the vessel ahead slowly in the direction of the secondary anchor. At this stage the ground-line will be running freely through the grab-block (Figure 15). When the section of the ground-line appears bearing the 50 foot marker (3.1(2)), reduce the speed of the vessel until the secondary anchor breaks the water surface. Manoeuvre the vessel until the anchor is against the grab-block hanging from the davit. Tie off the anchor with the tag line previously secured to a cleat on the davit. Run the vessel astern to obtain sufficient slack in the ground-line to permit unshackling of the ground-line from the secondary anchor and also to permit attachment of the ground-line to the seine drum.

- (12) Using the boom, swing the secondary anchor inboard. Unshackle the end of the ground-line from the secondary anchor and attach to the seine drum. The recovery of the ground-line and main anchor system may now begin.
- (13) Place the ground-line between the hydraulically-operated vertical rollers and retrieve it using the seine drum. Wind the ground-line on the seine drum using the vertical rollers as required. When retrieving the ground-line, it may be necessary to run the vessel astern to avoid putting any unnecessary strain on the seine drum and ground-line (Figure 16).
- (14) When the angle on the ground-line approaches near-vertical and the line tension increases, stop the seine drum and immediately put the vessel in forward at dead-slow-idle speed. This maintains a small angle on the ground-line and prevents this line from tangling with the main line, which is vertical. If it appears that excessive strain is being put on any part of the system, take the vessel out of gear for a moment.
- (15) Continue to idle the vessel ahead, and momentarily stop and start the seine drum to allow the anchor system to slowly ease out of the bottom. This step is very important in avoiding excessive strain on the seine drum and on the ground-line, especially if the area has a soft mud bottom.
- (16) After the anchor system is pulled free from the bottom, continue to run the vessel slowly ahead. This is necessary so that, as the main anchor system is hauled up, the subsurface buoy will come to the surface astern of the vessel and not underneath it (Figure 17).
- (17) Running the vessel ahead also serves to keep tension on the main mooring line, thus preventing any tangling of the line and instruments.
- (18) When the main anchor system breaks the water surface, stop the seine drum and remove the vertical rollers. Re-start the seine drum and continue to haul up the main anchor system over the horizontal stern roller until the bottom termination of the main mooring line is between the horizontal roller and the seine drum (i.e. Point Y in Figure 5).
- (19) Unshackle the main mooring line at the swivel and thimble connection. Tie off the end of the line with a tag line previously secured to a cleat located near the stern of the vessel.
- (20) Recover the remainder of the heavy-link anchor chain system by winding it on the seine drum until the shank of the anchor reaches the horizontal stern roller. At this stage the anchor can be recovered by means of the main boom and placed on deck.
- (21) Recover the main mooring line and instruments by hauling the line in by hand or winding it on the seine drum (Figure 18). The method used will depend on the length of mooring line and on the number and spacing of instruments (i.e. the weight involved). At this stage of the recovery, keeping way on the vessel to prevent tangling of the mooring line and instruments will probably not be necessary. As each instrument is retrieved, immediately check its serial number against the serial number recorded on the original launch sheet to ensure no confusion about location and depth of the instruments will arise at a later date.

- (22) Using the main boom, recover the subsurface buoy. The recovery of the entire moored instrument array has now been completed.
- (23) Carry out a thorough and detailed check of all components of the entire mooring system, i.e. instruments, mooring lines, shackles, swivels, anodes, etc. for wear and corrosion. If any of the components appear to warrant replacement, replace them. Any time and cost involved in replacing any doubtful components can be considered to be well spent.

We have found replacement of a component of the mooring system represents very low-cost insurance when one considers the following factors:

- (a) Overall cost of the entire operation;
- (b) Loss of data due to instrument malfunction; such loss would seriously limit the usefulness of any long-term observations;
- (c) Loss of the entire moored instrument array.

3.5 *Selection of Mooring Line*

Main Mooring Line:

1/4" diameter 6 x 19 galvanized improved plough steel cable. Breaking strain rated at 2.3 tons.

Ground-line:

1" diameter 2-in-1 braided polypropylene line.

CHAPTER IV

Fore-and-Aft Mooring System (Surface Buoy)

We have found fore-and-aft mooring systems ideal for suspending thermistor chains and as platforms for meteorological instruments, both in lakes and in coastal waters. The mooring lasts at least as long as a taut line system and has been used in fresh water for up to one year.

Our experience has been acquired principally with the Geodyne toroidal surface buoy and our comments are based on this experience. However, other surface buoys are available and, provided they are large and strong enough, should prove satisfactory.

4.1 Preparation for Launching

Following is the procedure we have found most successful for launching the system from a drum seiner. The vessel should be equipped with a boom, trawl winch, seine drum, hydraulically-operated vertical rollers and a horizontal roller. The general mooring plan is shown in Figures 19 to 22.

- (1) Wind 3/8" diameter release hook wire on the seine drum or plan to make use of the trawl winch if already equipped with a suitable length of wire. The former method is preferable.
- (2) Shackle the wire bridles, complete with rings, to the buoy. For convenience in handling the buoy, tie the loose ends of the bridle (the ends with rings) to the tower legs.
- (3) (a) Wind the first (hereafter referred to as No. 1) 5/8" diameter braided 2-in-1 nylon mooring line on the seine drum.
(b) Shackle the No. 1 anchor, complete with anchor chain, to the exposed end of the mooring line.
- (4) (a) Flake or coil the second (No. 2) 5/8" diameter braided 2-in-1 nylon mooring line on the deck of the vessel; leave both ends exposed.
(b) Shackle the top end of the No. 2 mooring line to the single bridle attached to the buoy.
(c) Shackle the other end of the No. 2 mooring line to the No. 2 anchor complete with anchor chain and release-hook ring.
- (5) Check the system to ensure that all shackles are tightened and seized. The system is now ready for launching.

4.2 *Launching Procedure*

- (1) When the mooring location is reached, moor a small marker float for position reference.
- (2) Proceed to a position upwind from the marker buoy to allow sufficient time for lowering the first anchor into position.
- (3) Using the main boom, lift the No. 1 anchor over the stern of vessel and take up the weight of the anchor on the No. 1 mooring line which is wound on the seine drum. (Refer to 4.1(3).) Clear the boom hook and, using the seine drum, lower the No. 1 anchor over the horizontal stern roller until the anchor strikes bottom. It will probably be necessary to manoeuver the vessel during the lowering, in order to position the anchor correctly (Figure 23).
- (4) With way on the vessel to avoid line tangling, continue to run out the No. 1 mooring line in the direction of the location planned for the No. 2 anchor drop. When approximately 100 feet of line is left on the drum, stop the vessel and lock off the line on a cleat located near the stern of the vessel. Remove the remaining 100 feet of line from the drum, coil it on deck and shackle the end of the line to the double bridle on the buoy.
- (5) Using the main boom, launch the buoy and lash it to the vessel's side near the stern.
- (6) Shackle the release hook to the release hook wire on the seine drum.
- (7) Attach the release hook to the ring on the No. 2 anchor (Figure 22) and tie off the trip mechanism to prevent the hook prematurely releasing. Using the main boom, lift the anchor over the vessel's stern. Take up the weight of the anchor on the release-hook wire and clear the boom hook from the anchor. The anchor is now suspended by the release-hook wire, which is on the seine drum.
- (8) Untie the buoy from the vessel's side and proceed slowly ahead, paying out all of the No. 2 mooring line by hand (Figure 24).
- (9) Keep a small amount of way on the vessel for approximately 20 minutes in order to stretch the mooring lines. If there is sufficient current or wind, keeping way on the vessel will probably not be necessary (Figure 25).
- (10) Untie the release-hook trip mechanism and cock the release hook.
- (11) With way on the vessel (in absence of sufficient current or wind), slowly lower the anchor with the release-hook wire (Figure 26). Run out a length of wire approximately $1 \frac{1}{4}$ times the water depth, still keeping way on the vessel. At this stage, a tensiometer should be attached to the release-hook wire to ensure that the safe working load (SWL) of the mooring lines is not exceeded. If it is evident that the No. 1 anchor is dragging or if it appears that the SWL of the lines may be exceeded, take the vessel out of gear momentarily until the excessive strain drops

off. After stretching the lines in the above manner for approximately 5 minutes, run the vessel astern until the No. 2 anchor settles to the bottom. At this stage, the release hook will release from the anchor. The hook is then retrieved (Figure 27).

If possible, the mooring should be undertaken at low tide to ensure that the lines remain tight.

4.3 *Recovery Procedure*

The following procedure should be followed for recovering the buoy and its components, such as mooring lines, anchors, etc.

- (1) Secure the recovery vessel alongside the buoy and prepare to recover the mooring line that leads down-wind or down-current (whichever has the greatest effect upon vessel set) from the buoy.
- (2) With a length of 5/8" diameter tag line previously secured to a cleat located amidships on the gunwale of the vessel, cinch up and securely tie off the buoy at the base of the tower leg nearest to the wire bridle that is to be worked upon. Place the main boom hook under the wire bridle of the buoy and hoist the wire bridle up to a height (Figure 28) such that the components shown in Figure 20 or 21, depending upon which line is being retrieved, are at a convenient level for subsequent operations carried out from the ship's deck. With another length of tag line, also previously secured to the same point as the first tag line, cinch up and securely tie off the nylon buoy mooring line at Point R (Figure 20).
- (3) Lower the boom hook and clear it from the wire bridle.
- (4) At this point, the desired slack in the wire bridle will have been attained. However, the mooring lines and tie-off lines will be under extreme tension; therefore, double-check that the tie off lines are well secured at all points before proceeding further with the recovery operation.
- (5) Unshackle the wire bridle at Point S (Figure 20) and, for convenience, shackle the bridle around the tower leg. One mooring line has now been separated from the buoy.
- (6) With caution (since both mooring lines are still under tension), slip free the No. 1 tag line securing the buoy. At this stage the buoy and vessel will drift free of each other (Figure 29).
- (7) The mooring line secured to the No. 2 tag line will now go slack and may be untied from the tag line.
- (8) Attach the mooring line to the seine drum and retrieve the line and anchor system. Detach the mooring line from the anchor system and proceed back to the buoy.

- (9) Bring the vessel alongside the buoy and, using the main boom, hoist the buoy aboard and place it on deck. Detach the No. 2 mooring line from the wire buoy bridle and shackle it to the No. 1 mooring line already on the seine drum. Retrieve the mooring line and anchor system, as in step 8. The recovery operation is now complete.

4.4 *Selection of Materials*

It is advisable to use galvanized-wire bridles on the buoy as they cannot easily be cut or damaged by accident or by tampering. The bridles should be 20 feet long, with mechanically-spliced eyes on each end, complete with extra heavy galvanized thimbles. The mooring lines should be 2-in-1 braided nylon with spliced eyes in each end, complete with thimbles. The length of each mooring line should be equal to at least twice the water depth. Three-strand twist nylon is not recommended due to its extreme elasticity. Its use can result in severe horizontal buoy motion in moderate and heavy sea states. Polypropylene line is not recommended because of its tendency to elongate continuously under load, resulting in slack buoy-mooring lines. Slack buoy-mooring lines will allow the buoy to rotate, resulting in damage or loss of the suspended instruments. A high drag-to-weight ratio anchor is required; we have found those of 200-400 lbs to be most satisfactory. To decrease the possibility of the anchors dragging, a 10 foot length of heavy anchor chain is used between the mooring line and the anchor shank. A 1" x 6" steel ring and chain are shackled to the crown of one anchor to permit attachment of the release hook (Figure 22).

CHAPTER V

Related Techniques and Practical Considerations5.1 *Taut-Line Moorings with Surface Buoys*

The techniques for taut-line surface moorings are identical to those used for subsurface moorings, except in choice of materials and line lengths.

Special care must be taken to allow for tidal movements, because of the great buoyancy of surface floats. For this reason, lengths of chain are used to maintain tension on the line. Nylon line (2-in-1 braided) is used since it can stretch and maintain tension. With medium or larger vessels, heavy anchors such as railway wheels (Figure 30) may be used, in which case all of the tidal excursion must be taken up by line stretch.

Generally, a line length of 90-95% of the water depth should be used. The exact choice depends on the ratio of tidal amplitude to water depth and type of anchor (chain or heavy clump) and reference should be made to the manufacturer's data on line characteristics.

In Canadian waters, surface buoys must be properly colour coded, with broad yellow and red vertical stripes. They are required to have a flashing white light, with a quick flash for 4 seconds followed by darkness for 16 seconds. They also require a radar reflector, or must be a good radar target themselves. In all cases, surface moorings should be reported to the Ministry of Transport so that notice to mariners can be given. As with all moored equipment, it is advisable to paint on names and telephone numbers, so ownership can be traced if necessary.

5.2 *Moorings from Medium-Sized Vessels*

Most larger fishing vessels such as 80-100 foot draggers and seiners are equipped with deck machinery such as winches, booms and davits, capable of handling heavy-weight anchor systems consisting of single clumps weighing up to 2,000 lbs (see Figure 30). This capability is required when mooring large-size toroid and Plank-on-edge (POE) buoys (3,000-5,000 lbs net buoyancy) and also when mooring subsurface buoys that require heavy anchors. It is especially needed for mooring operations in strong currents. The techniques involved for launching and recovering the heavier taut-line mooring systems are basically the same as for the light-weight chain systems. However, there are two major differences: (1) the main anchor system is lowered and recovered from the side of the vessel (see deck layout, Figure 31) and (2) during the recovery operation, the vessel is run *ahead*, instead of astern, to prevent any possibility of the groundline becoming entangled with the propeller.

5.3 Position Fixing

Accurate position fixing is essential when mooring instruments with subsurface buoys. The methods used will vary depending upon the vessel's position-fixing equipment and upon the area of operation. Methods usually used in inshore waters consist of one or more of the following: horizontal sextant angles, radar bearings and ranges, and precision depth sounding. In cases where it is difficult to obtain an accurate position fix, a surface marker buoy can be moored to the anchor on the free end of the ground-line. However, every attempt should be made to obtain as accurate a position as possible in case the surface marker buoy is lost and grappling for the ground-line becomes necessary.

Many coastal areas are covered by navigation systems such as Loran. However, it is questionable whether the accuracy of these will always be sufficient for locating ground-lines unless the work is undertaken in areas that are particularly well covered. Other systems, such as Minifix, allow very accurate positioning, but can normally only be set up on a temporary basis.

Mooring systems incorporating acoustic releases require less accurate position fixing since the releases may include a locating system and also can be triggered from a distance of up to eight miles.

5.4 Corrosion

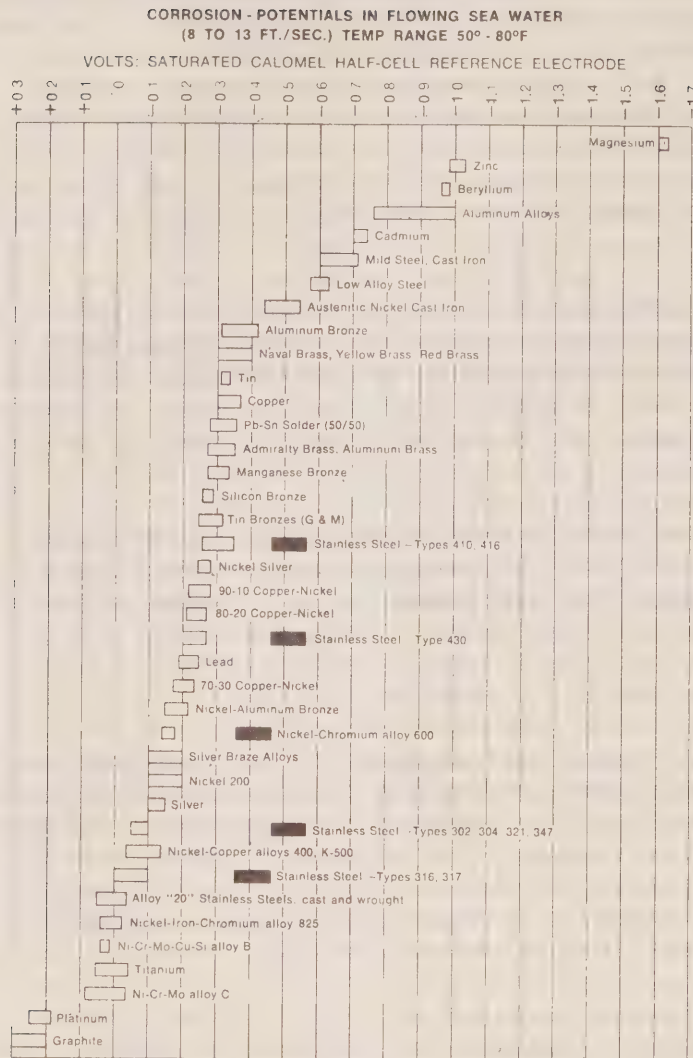
The problem of marine corrosion should be given serious consideration when planning or designing mooring systems for oceanographic instruments. It is easy to underestimate both the extent and intensity of the corrosion process in the marine environment. The effects of marine corrosion can vary from light rusting or pitting to the total destruction of metallic components. It is not possible to discuss this important problem in detail here; we suggest the reader consult the relevant references listed at the end of this manual.

However, it seems worthwhile to indicate one or two of the more important aspects. The most common cause of marine corrosion is the coupling of metals which have different electrical potentials in sea water. Metals are listed according to their electrical potentials in the "Galvanic Series", which we reproduce in Table I. If two dissimilar metals are connected together in sea water, the one with higher corrosion potential (the one furthest to the *right* in Table I) will act as the "anode" and corrode, whereas the metal with the lower corrosion potential (the "cathode") will be protected.

This fact enables a number of guidelines for the design of a mooring system:

- (1) Where possible, avoid using dissimilar metals together (electrically connected). The concept of 'relative areas' is useful here. If, for example, in the anchor system shown in Figure 2, the swivels are made of manganese bronze (corrosion potential \approx 0.3 volts) and the rest of the chain is of mild steel (\approx 0.6 to \approx 0.7 volts), the corrosion of the mild steel will be spread over so large an area that it will present no

TABLE I



Alloys are listed in the order of the potential they exhibit in flowing sea water. Certain alloys indicated by the symbol: ■ in low-velocity or poorly aerated water, and at shielded areas, may become active and exhibit a potential near -0.5 volts.

(Reproduced from InterOcean Catalogue 1975)

problem. Where possible, use anodic (more corrosion-prone) materials for the larger, thicker and less critical parts of the system.

- (2) Paint the more cathodic material. Don't paint the anodic material since severe pitting will occur wherever there are small holes in the paint covering.
- (3) Where possible, electrically isolate the dissimilar materials. For example, in Figure 3, nylon thimbles separate the manganese bronze swivel from the galvanised wire rope.
- (4) Use sacrificial anodes in key areas. These should invariably be used on moored instruments. When wire rope is used in warm, well-oxygenated water, it can be protected with anodes strapped on it at intervals. In our experience, excessive corrosion of galvanised wire line has only occurred in the upper few metres of the water column, although it might be more of a problem in warmer waters.

High-purity zinc anodes are recommended for instrument protection. Ensure good electrical connection between anode and instrument.

5.5 *Mooring Documentation*

Good mooring practice requires proper records of all moorings. Two basic types of information are required: instrument data and mooring data.

Data sheets regarding the instruments will, of course, depend on the type of instruments used. It is beyond the scope of this report to discuss in detail the necessary records; however, experience has shown that at least the following items are essential:

- (1) Instrument type, serial number, model, etc.
- (2) Location, depth, time of mooring/recovery dates.
- (3) Modification (i.e. sensor range changes, etc.).
- (4) Calibration parameters, date of last calibration (for each sensor).
- (5) Sampling interval and other optional adjustments.

The mooring operation itself requires records of at least the following:

- (1) Date of mooring and recovery.
- (2) Precise knowledge of location.
- (3) Instrument depths.
- (4) Type of buoy used, together with serial number.
- (5) Details of all accessories, including:

- bridle chain diameter and length
- bridle wire diameter and length
- navigation light type and serial number
- instrument brackets (for surface moorings)
- type of anchor and anchor-chain lengths
- mooring-line type and lengths of sections used
- ground-line type and length
- types and numbers of shackles, swivels and rings.

(6) Details of transport to or from the field location, if relevant.

The general mooring layout should be drawn up. Copies of the layout and all related records should be maintained in duplicate, with one set permanently on file.

During the field operation, a log book should be maintained with records of key operations in the mooring and recovery procedure. This is often useful when interpreting data collected just prior to recovery. For example, the exact time that the grapple picks up the ground-line is considered to be the time of the last useful record obtained, although the instrument itself may not be retrieved and switched off until as much as two or three hours later.

RECOMMENDED READINGBuoy Mooring

Handbook of Ocean and Underwater Engineering. McGraw-Hill, New York, 1969.

A comprehensive manual on all aspects of ocean engineering. Sec. 9, pp. 81-115 covers buoy operations. Sec. 9, p. 119 includes extensive list of additional references on buoy systems. Section 7 covers the problem of materials and corrosion.

Buoy Technology Symposium, Transactions. Marine Technology Society, Washington, D.C. March 1964.

Buoy Technology Symposium, Transactions, Supplement. Marine Technology Society, Washington, D.C. March 1964.

Buoy Technology Symposium, Transactions. Marine Technology Society, Washington, D.C. 1967.

The above transactions include a large number of papers on almost every aspect of mooring operations.

National Needs and Ocean Solutions. Transactions of the 10th Annual Conference. Marine Technology Society, Washington, D.C. September 1974.

Includes a section on buoy technology with useful papers on dynamical response of moored systems.

W.H. Bell, Static Analysis of Single-Point Moorings (in preparation).

A comprehensive computer model for determining the static response of a moored buoy system to a current.

W.S. Huggett, 1969. Technique for Mooring Underwater Instruments on the Continental Shelf. Canadian Hydrographic Service. Victoria, B.C. Technical Report.

Techniques developed for mooring buoys from the oceanographic vessel C.S.S. PARIZEAU.

Corrosion

A.H. Tuthill and C.M. Schillmoller. Guidelines for Selection of Marine Materials. The International Nickel Co. of Canada Ltd., Toronto, 1966.

A short, readable summary of essential aspects of salt-water corrosion problems and corrosion control.

L.L. Shreir, Corrosion, Wiley, New York, 1963. 2 volumes.

A comprehensive handbook on all aspects of corrosion and corrosion control.

T.H. Rogers, Marine Corrosion, Newnes, London, 1968.

One of the best books written on marine corrosion.

H.H. Uhlig, Corrosion Handbook, Wiley, New York, 1948.

LIST OF FIGURES

Note: Drawings are not to scale.

- Figure 1. Response of typical subsurface buoy system to a uniform current - see section 2.1.
- Figure 2. Fore-and-aft moored toroidal buoy.
- Figure 3. Fore-and-aft moored toroidal buoy with two thermistor chains suspended through the centre.
- Figure 4. Deck equipment layout on 34' fishing vessel.
- Figure 5. Main anchor assembly.
- Figure 6. Subsurface buoy with main mooring line attached.

Launching of Subsurface Current Meter Array

- Figure 7. Lowering current meters on main line by hand.
- Figure 8. Lowering main anchor with ground-line.
- Figure 9. Subsurface buoy and instruments in position, paying out ground-line.
- Figure 10. Lowering secondary anchor with release hook.
- Figure 11. Detail of secondary anchor with release hook attached.
- Figure 12. Buoy system moored in place, release hook being retrieved.

Recovery of Subsurface Current Meter Array

- Figure 13. Lightweight grapple assembly.
- Figure 14. Grappling for ground-line.
- Figure 15. Recovery of secondary anchor.
- Figure 16. Winding in ground-line on seine drum.
- Figure 17. Lifting main anchor.
- Figure 18. Pulling in current meters.

Fore-and-Aft Moored Toroidal Buoy

- Figure 19. Fore-and-aft moored toroidal buoy.
- Figure 20. Section A, detail of Figure 19.

Figure 21. Section B, detail of Figure 19.

Figure 22. Section C, detail of Figure 19.

Figure 23. Anchor on bottom, paying out No. 1 line.

Figure 24. Paying out No. 2 line by hand.

Figure 25. Stretching mooring lines.

Figure 26. Lowering No. 2 anchor with release hook.

Figure 27. No. 2 anchor set, release hook being recovered.

Recovery of Fore-and-Aft Moored Toroidal Buoy

Figure 28. Lifting one line and tying off to gain necessary slack for disconnecting.

Figure 29. Retrieving No. 1 anchor and line.

Figure 30. Heavyweight anchor system.

Figure 31. Deck equipment layout on medium-sized fishing vessel.

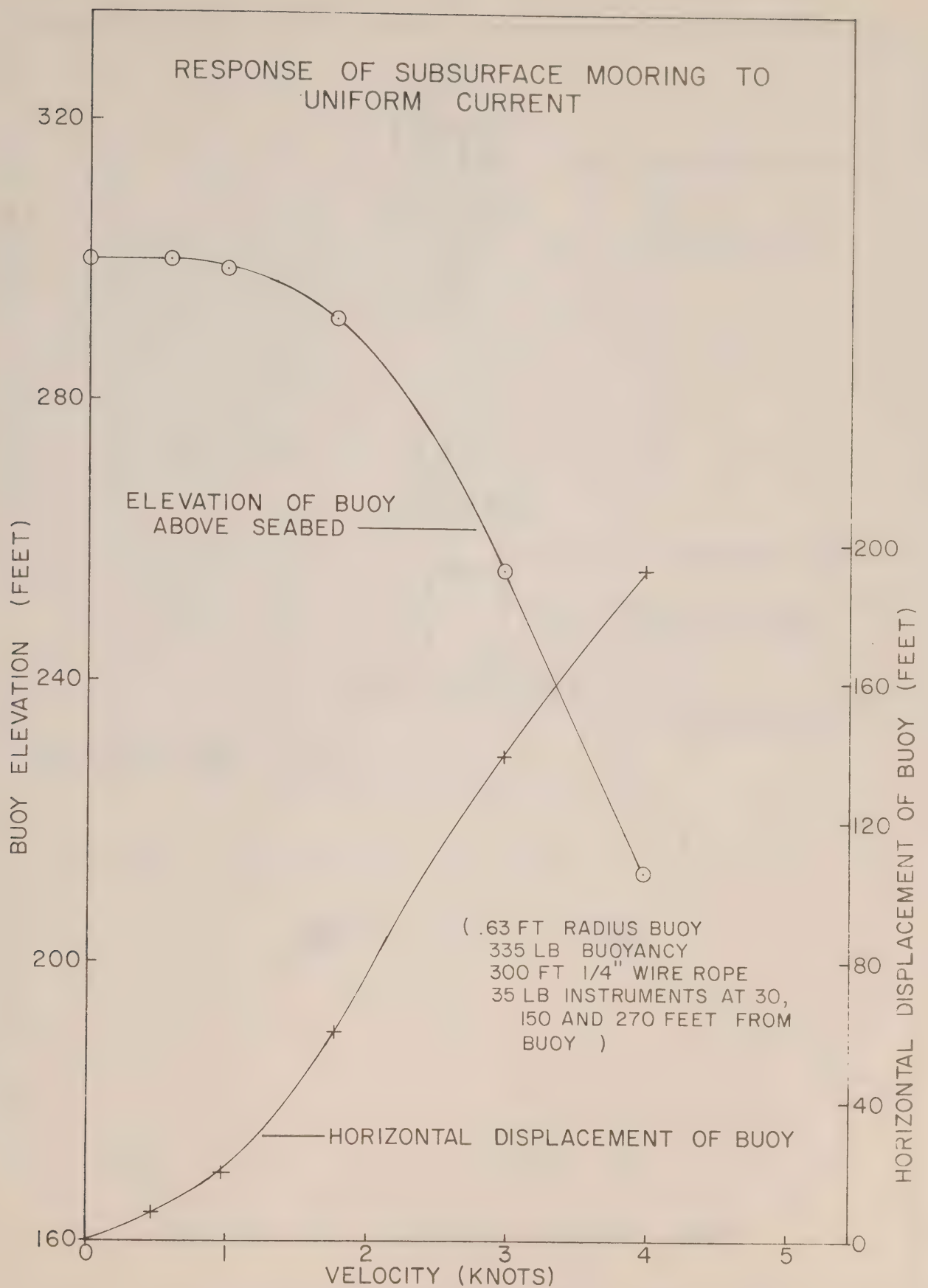


Figure 1

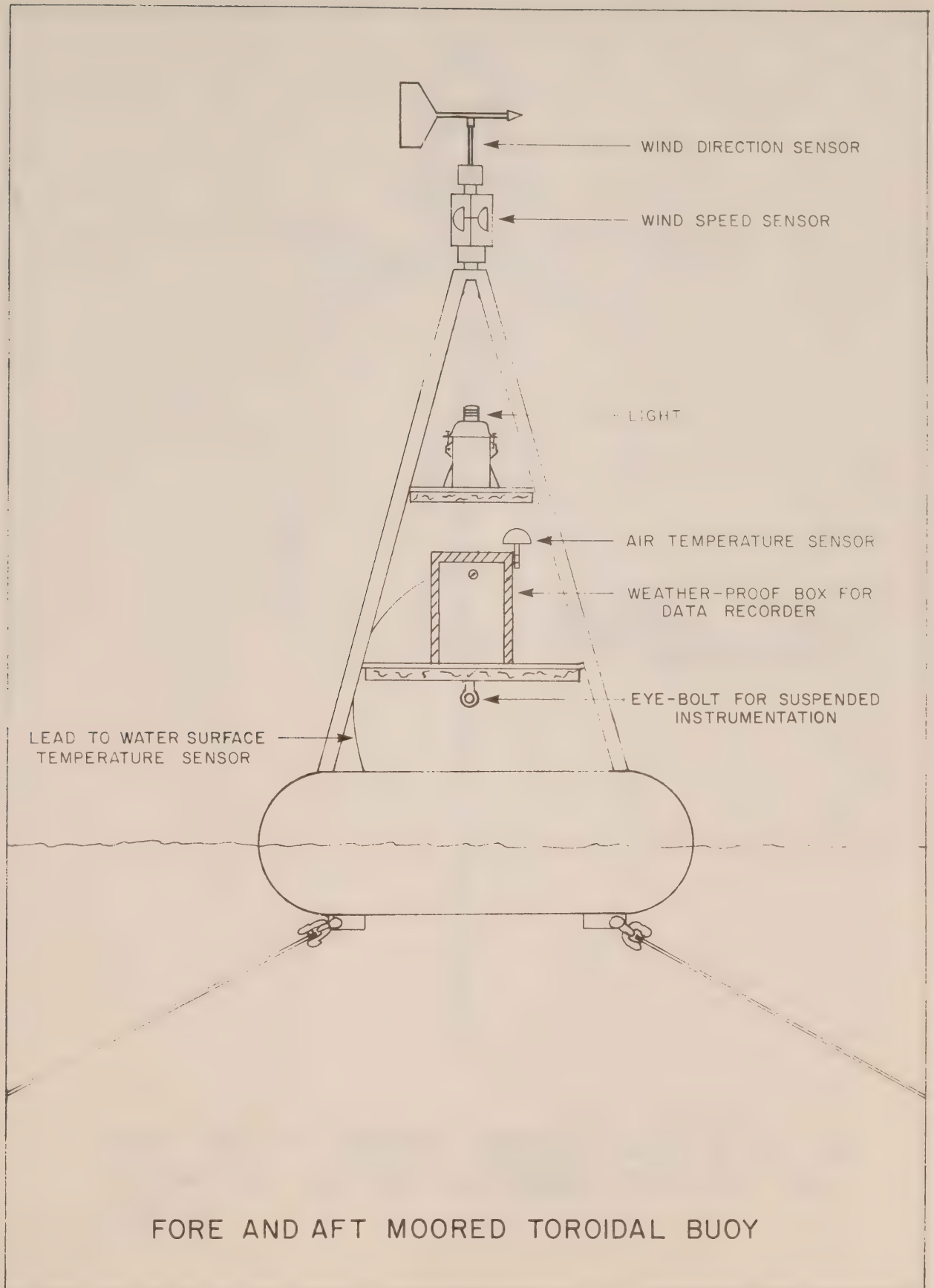
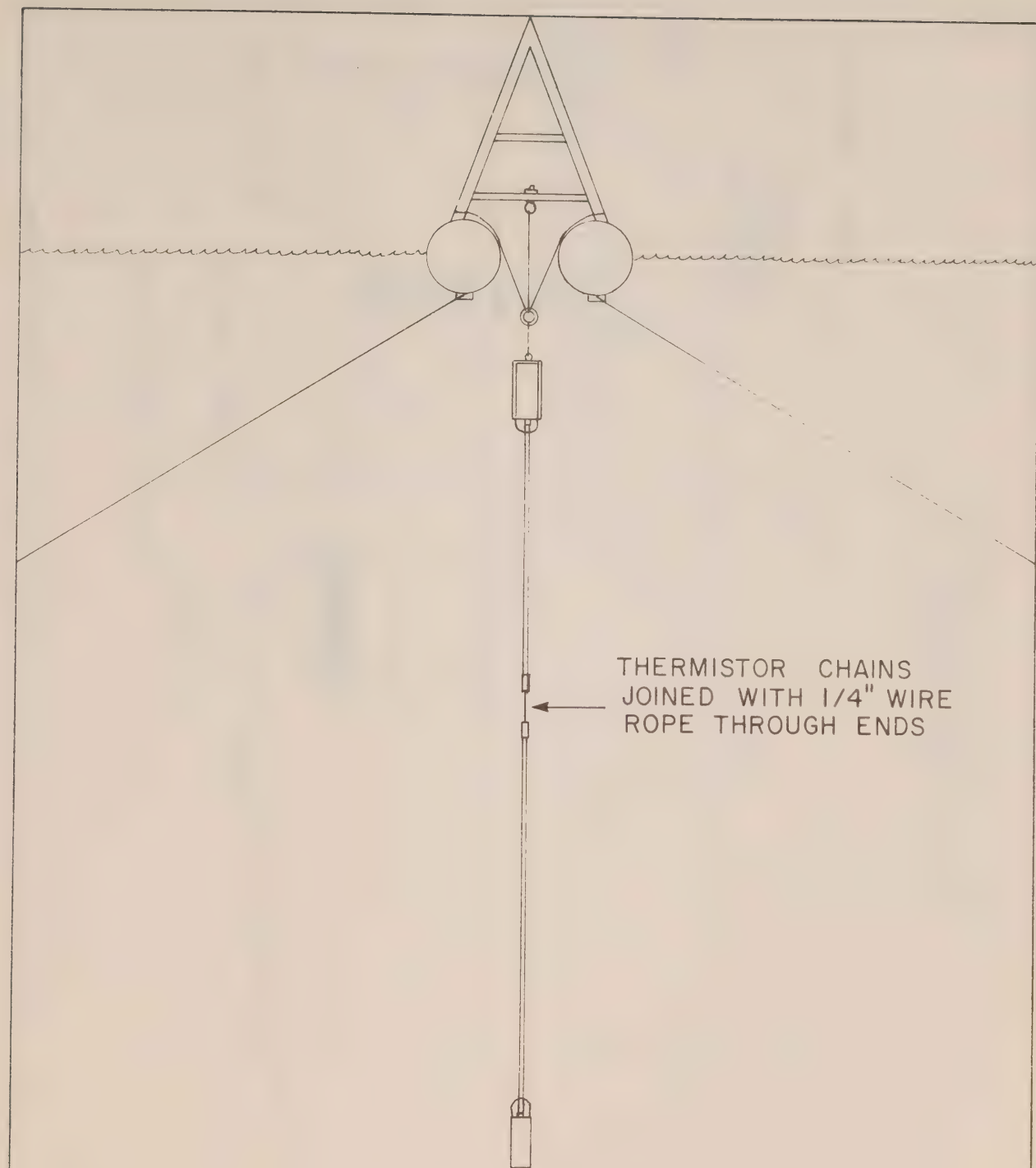


Figure 2



FORE AND AFT MOORED TOROIDAL BUOY WITH TWO
THERMISTOR CHAINS SUSPENDED THROUGH THE
CENTRE

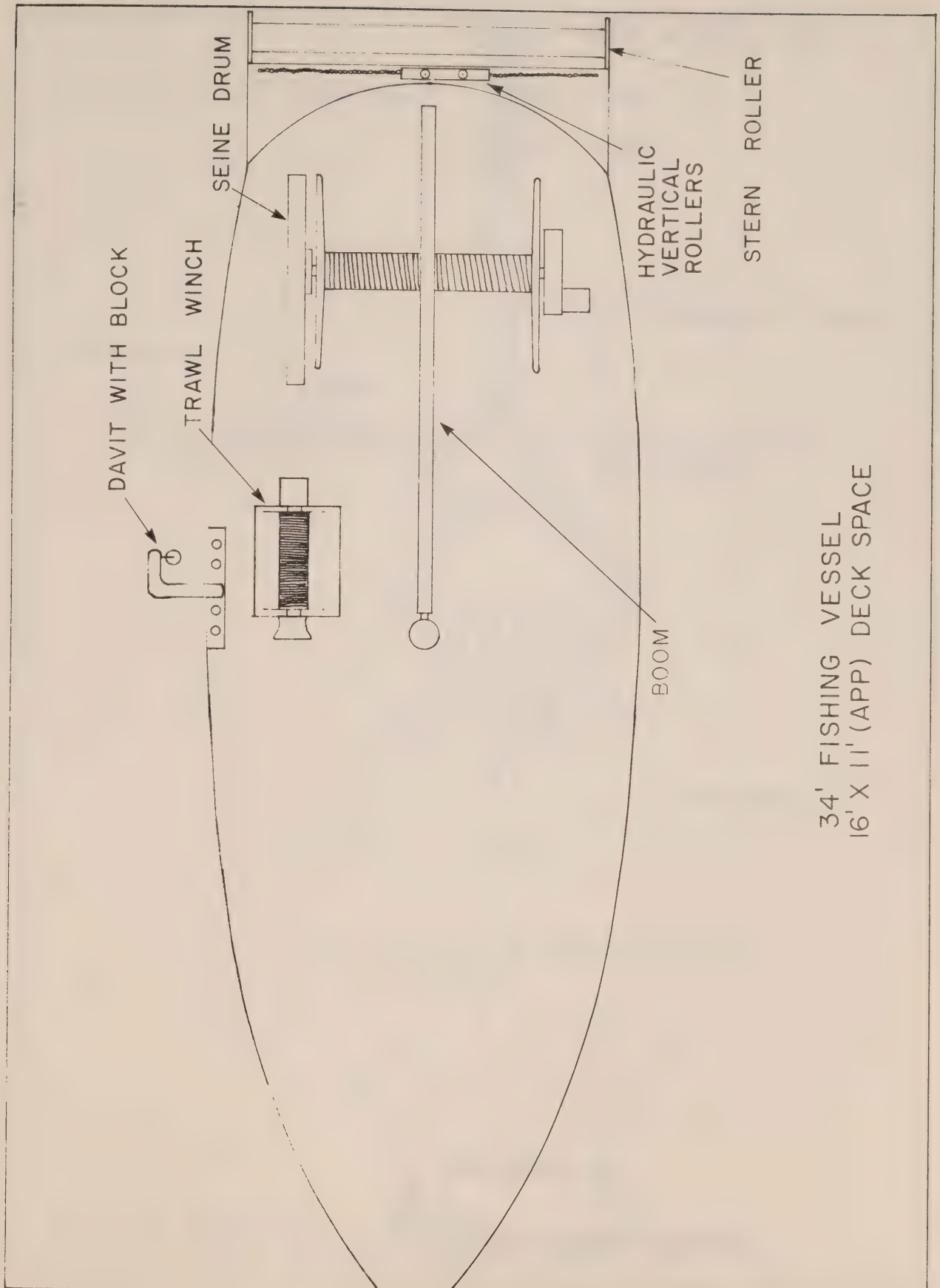


Figure 4

MAIN ANCHOR ASSEMBLY

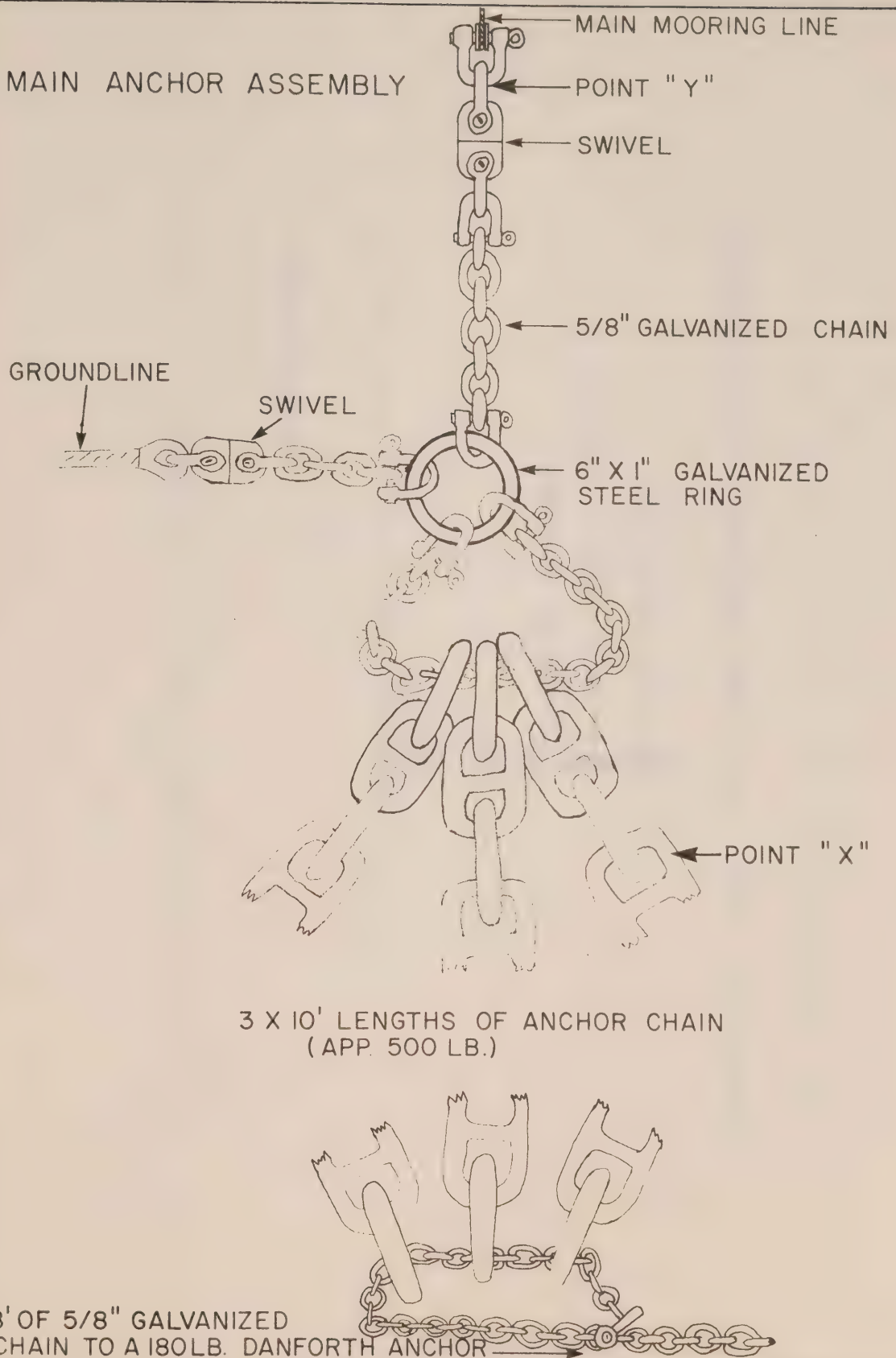
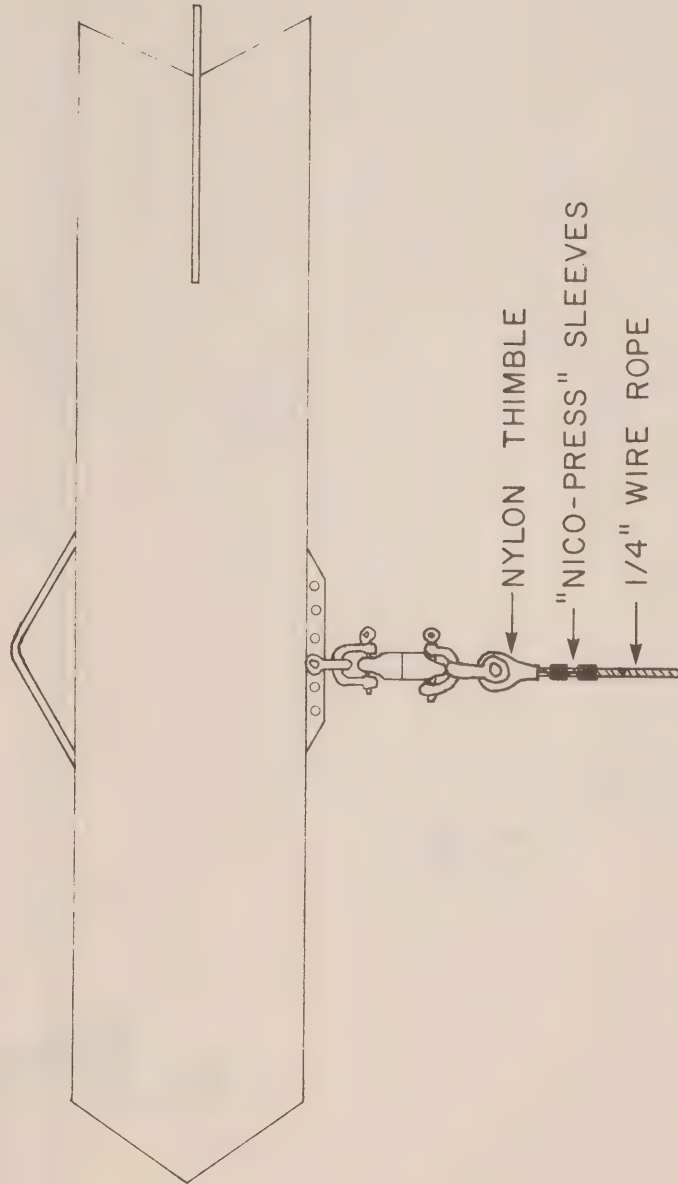
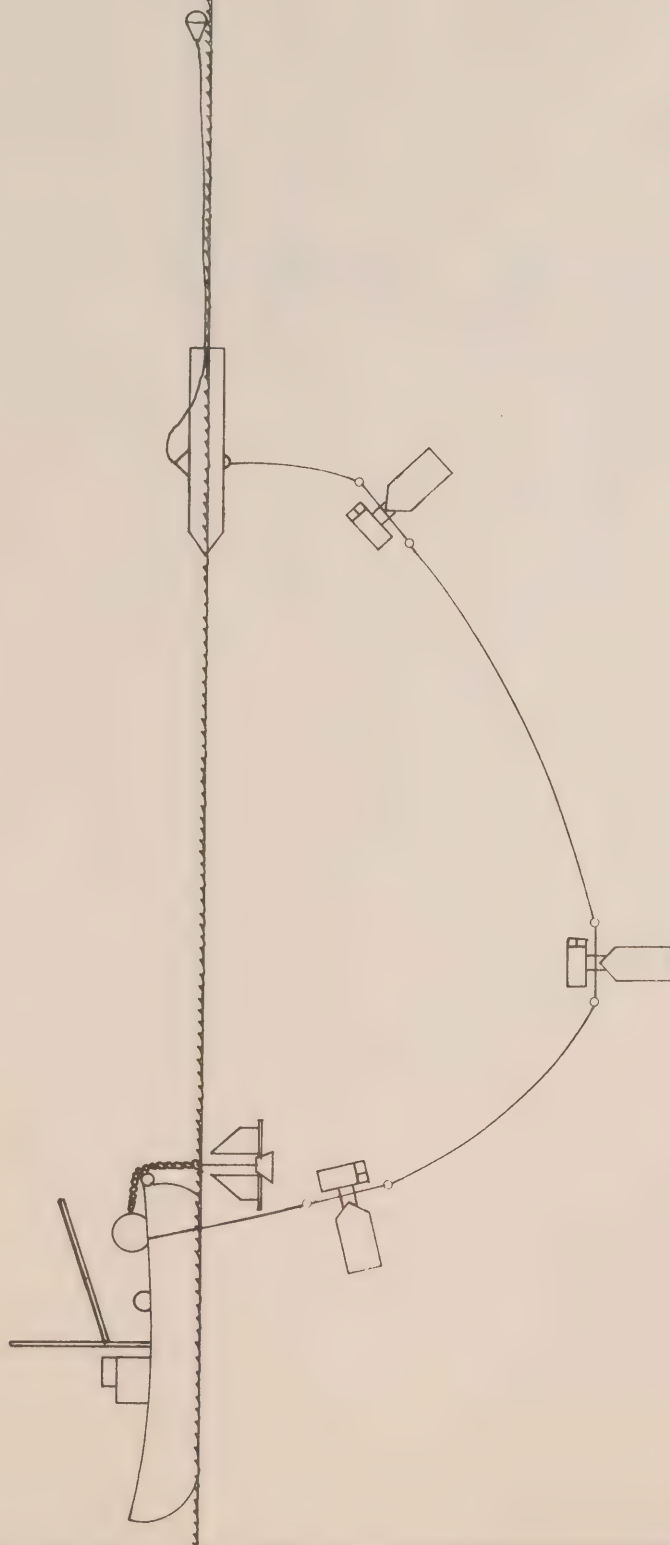


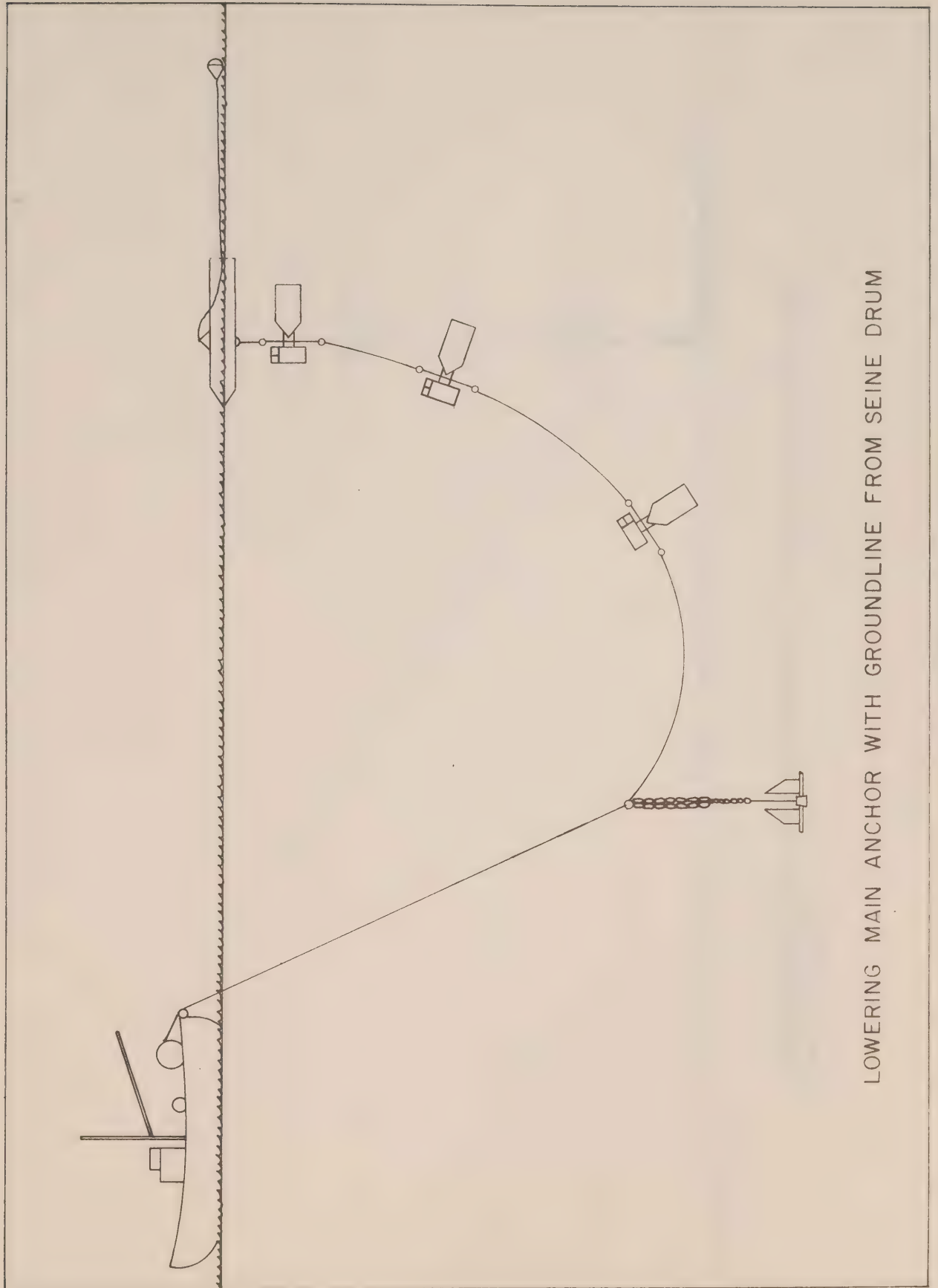
Figure 5



SUBSURFACE BUOY WITH MAIN MOORING LINE ATTACHED

LOWERING CURRENT METERS ON MAIN LINE, BY HAND, ANCHOR
SYSTEM IN PLACE, SUSPENDED OVER STERN ROLLER





LOWERING MAIN ANCHOR WITH GROUNDLINE FROM SEINE DRUM

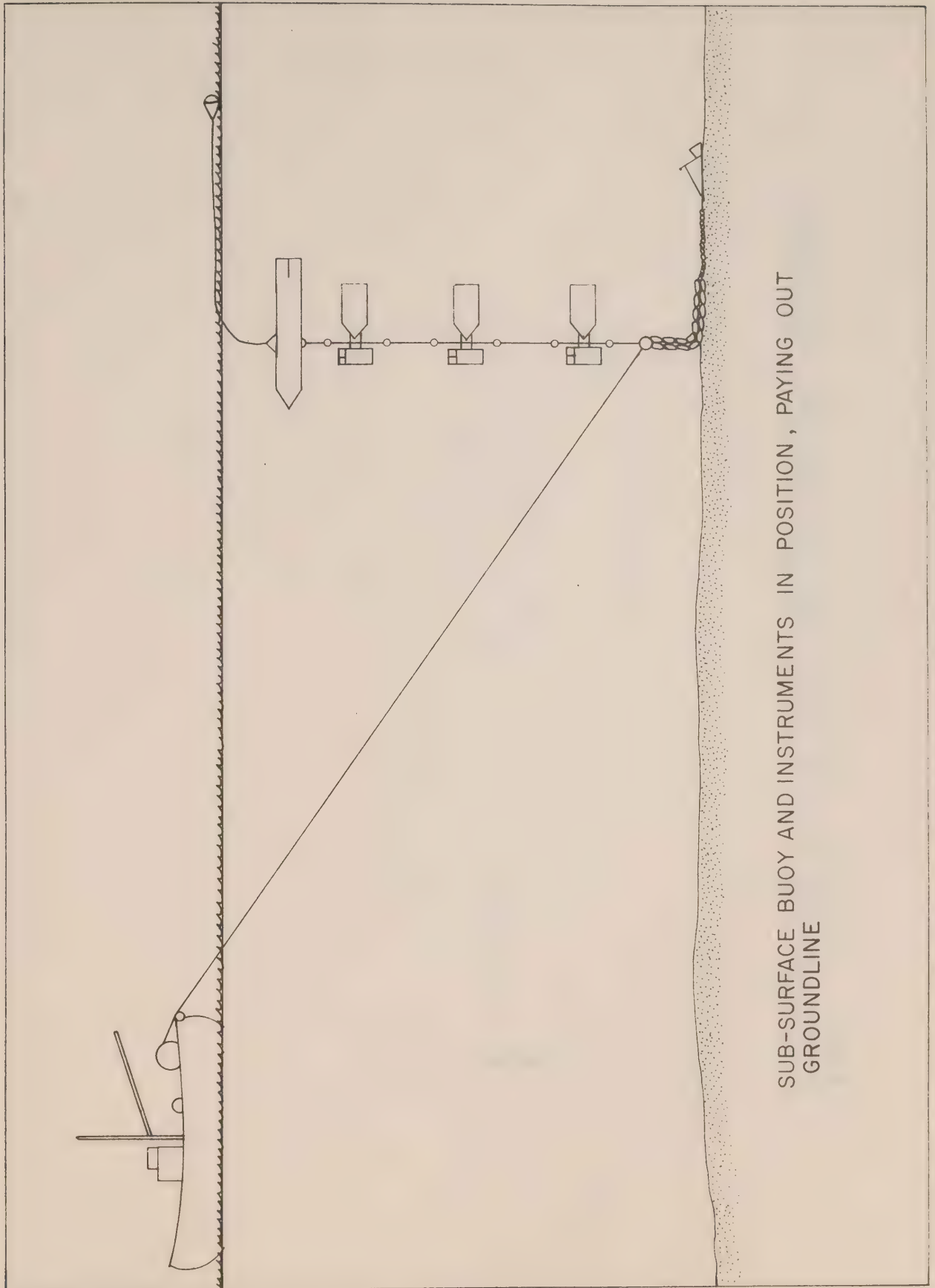


Figure 9

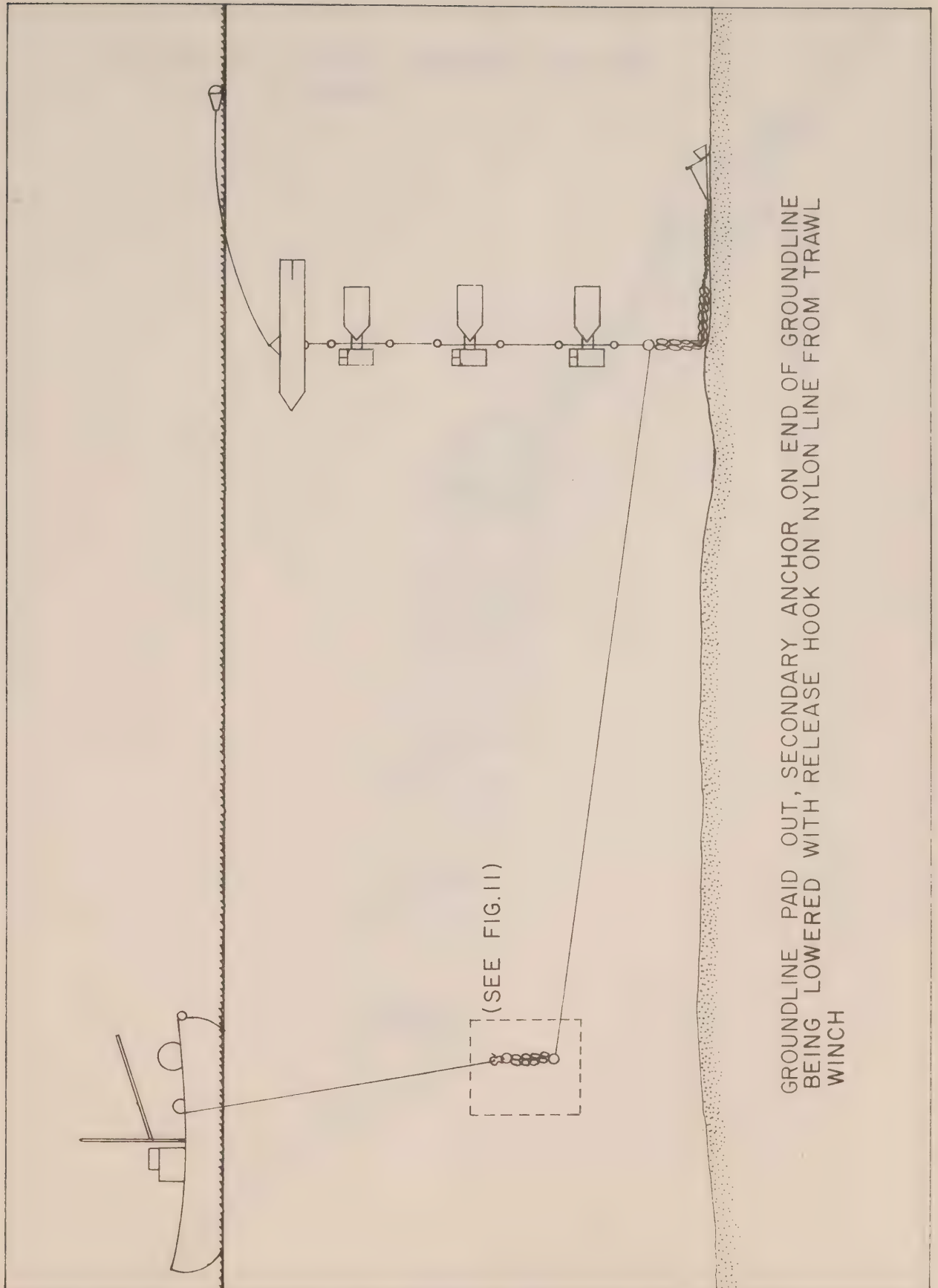


Figure 10

SECONDARY ANCHOR SHOWING RELEASE
HOOK ATTACHED

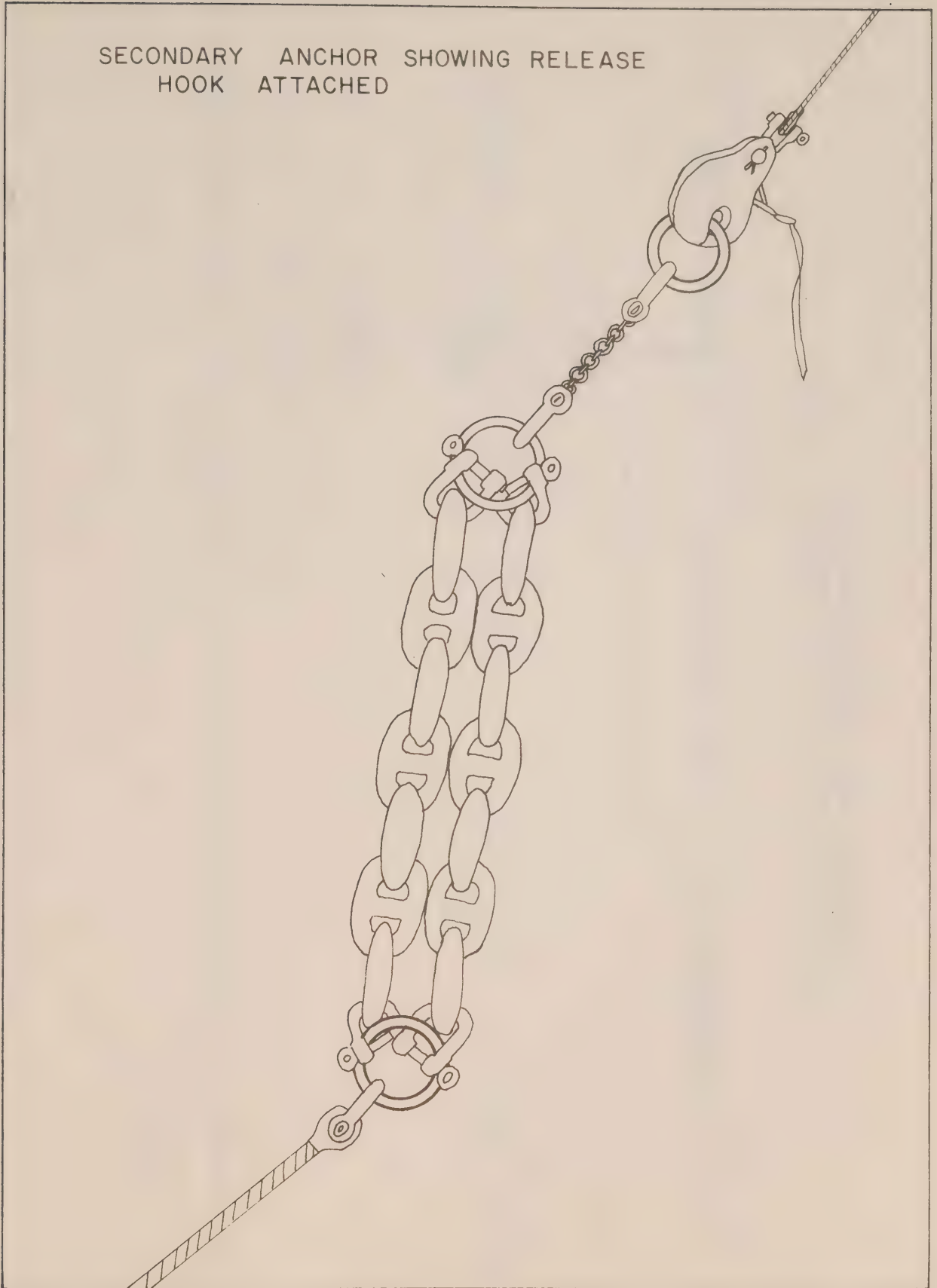


Figure 11

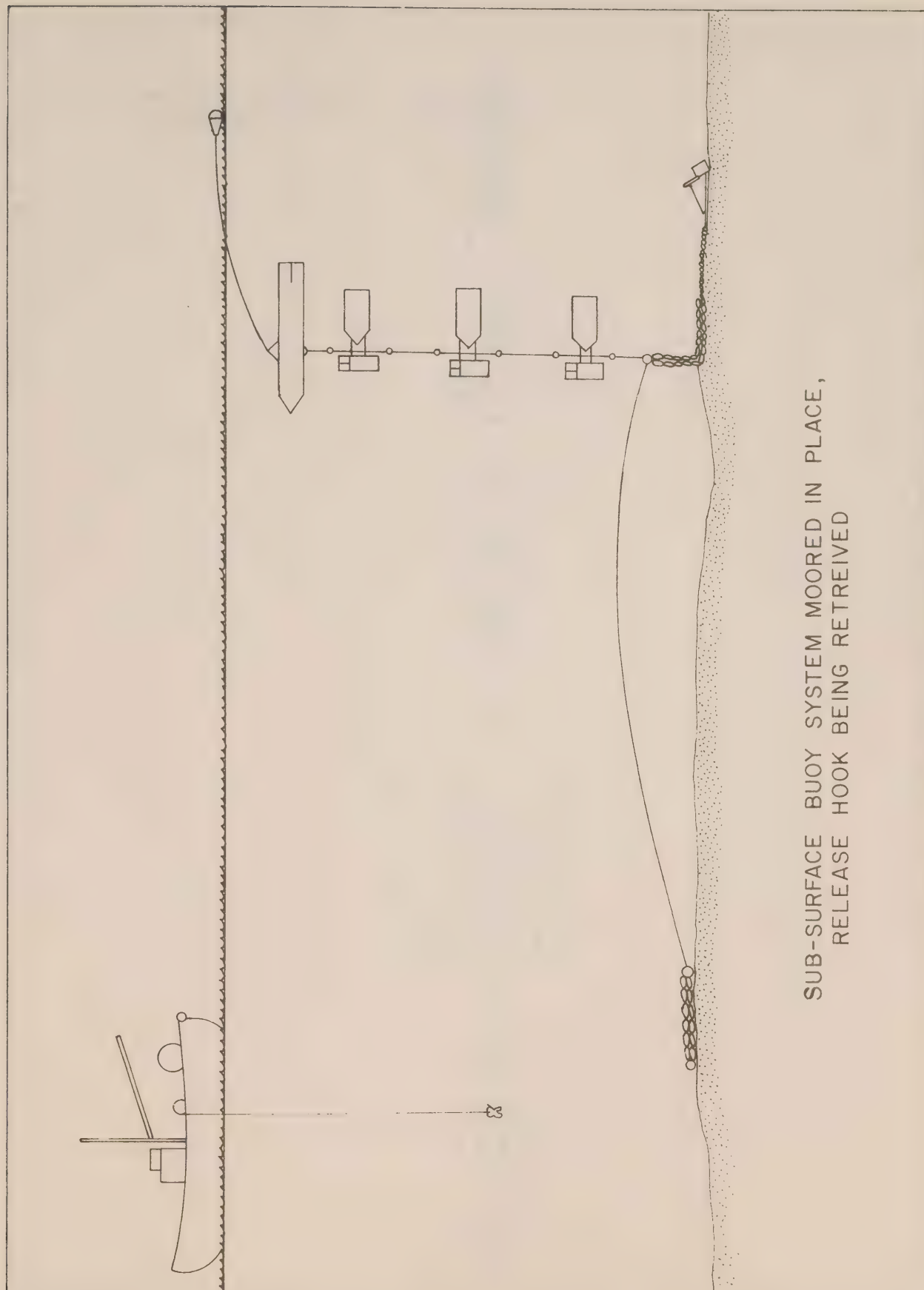


Figure 12

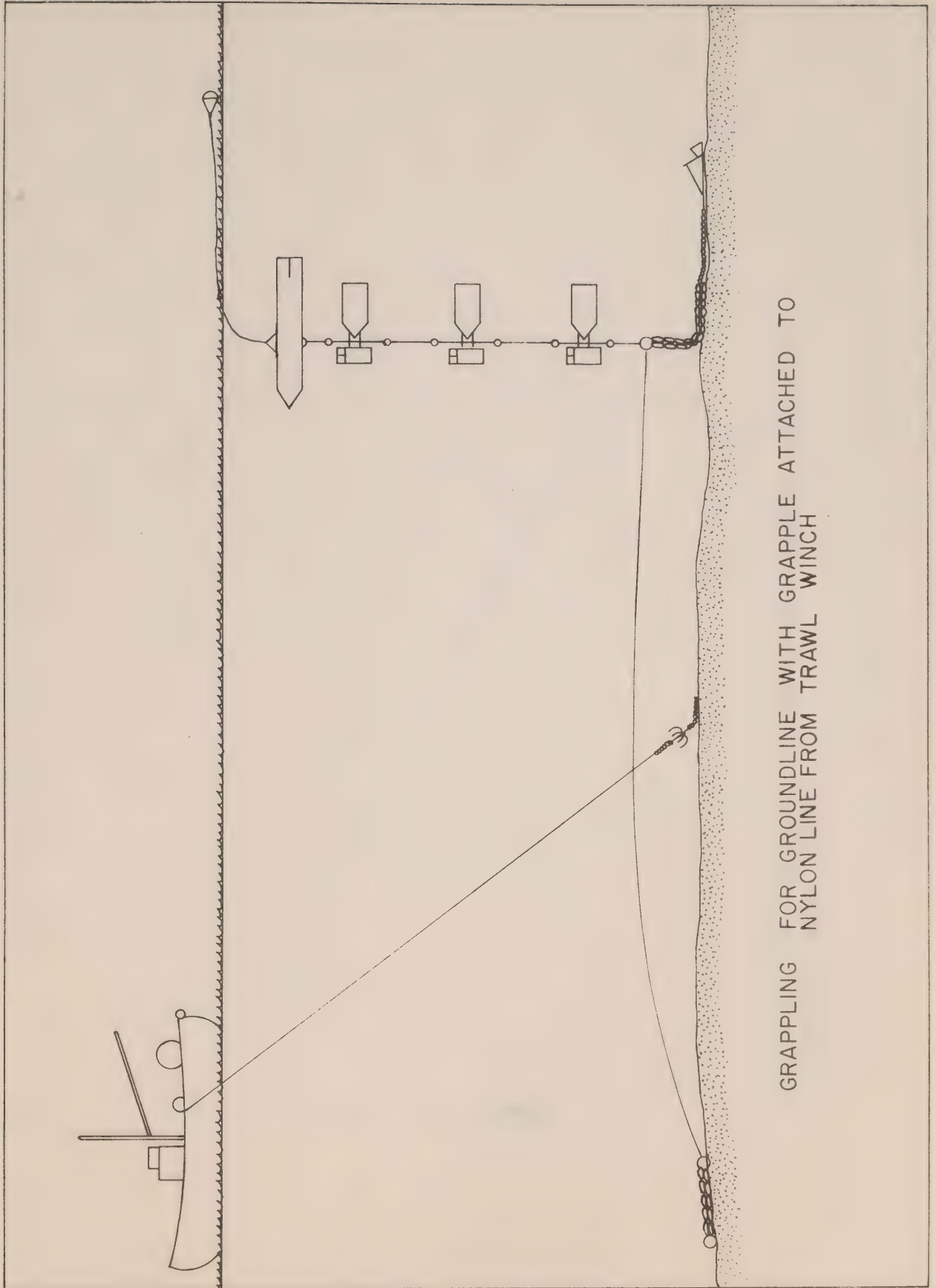


Figure 14

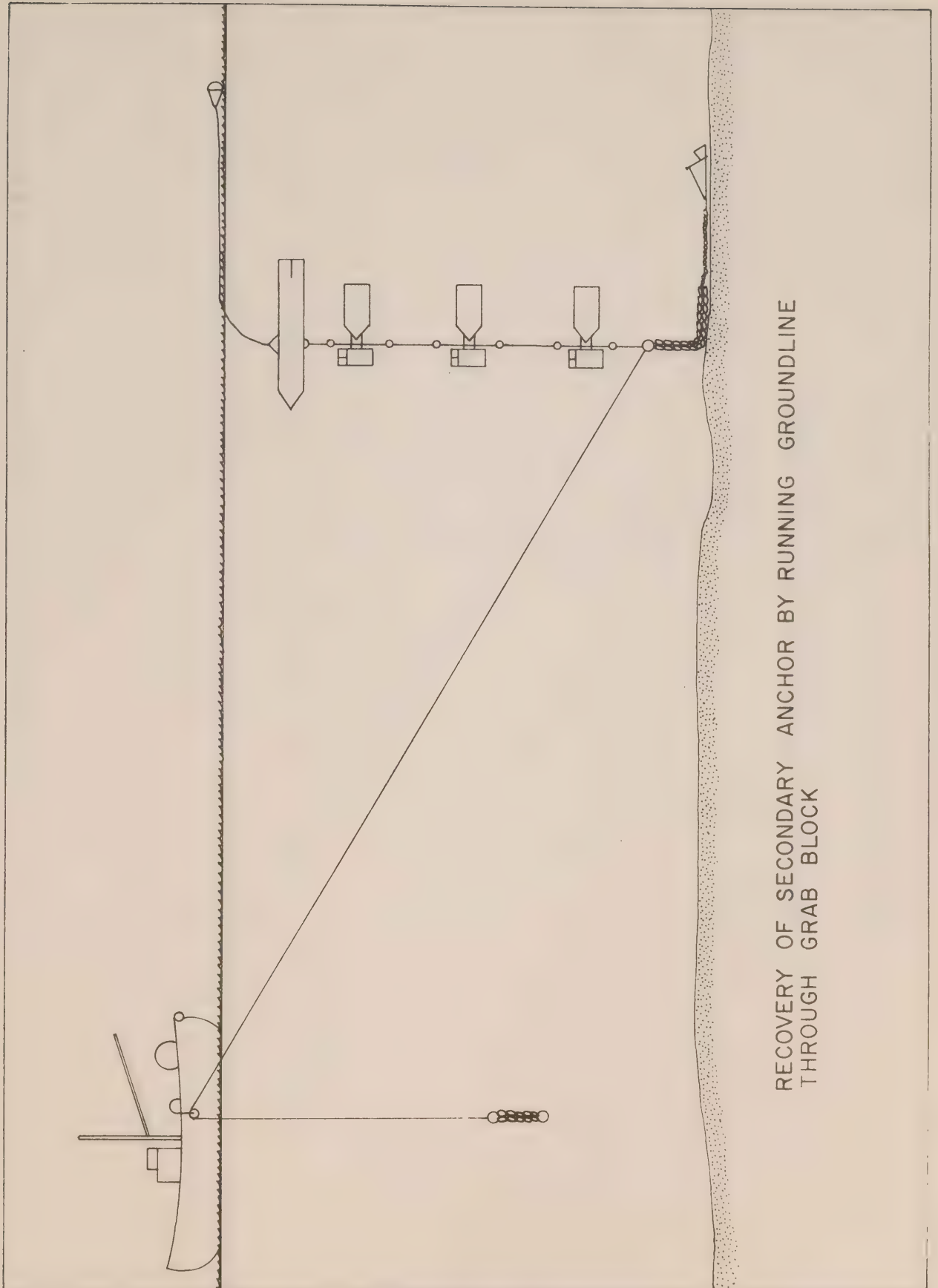


Figure 15

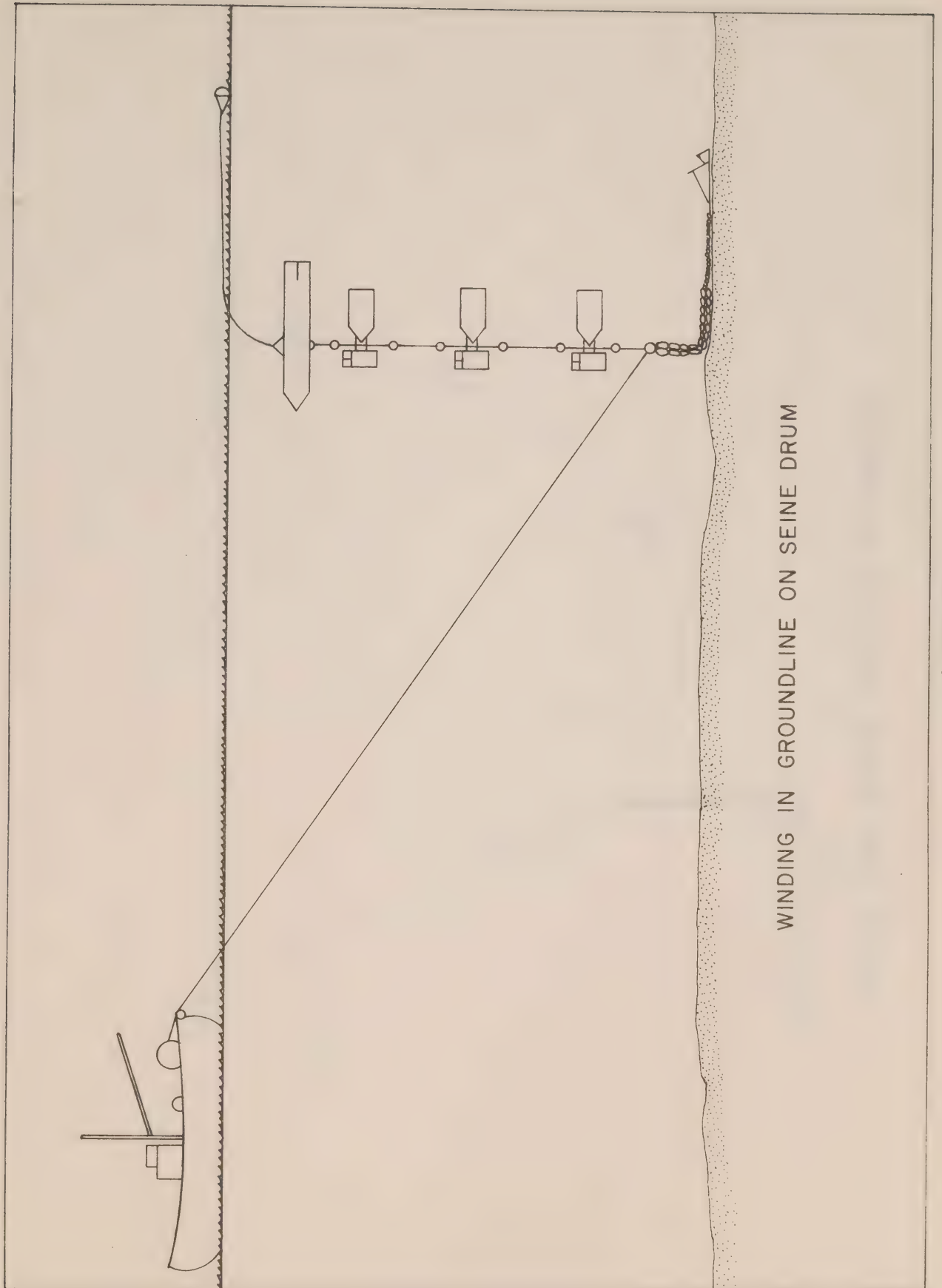
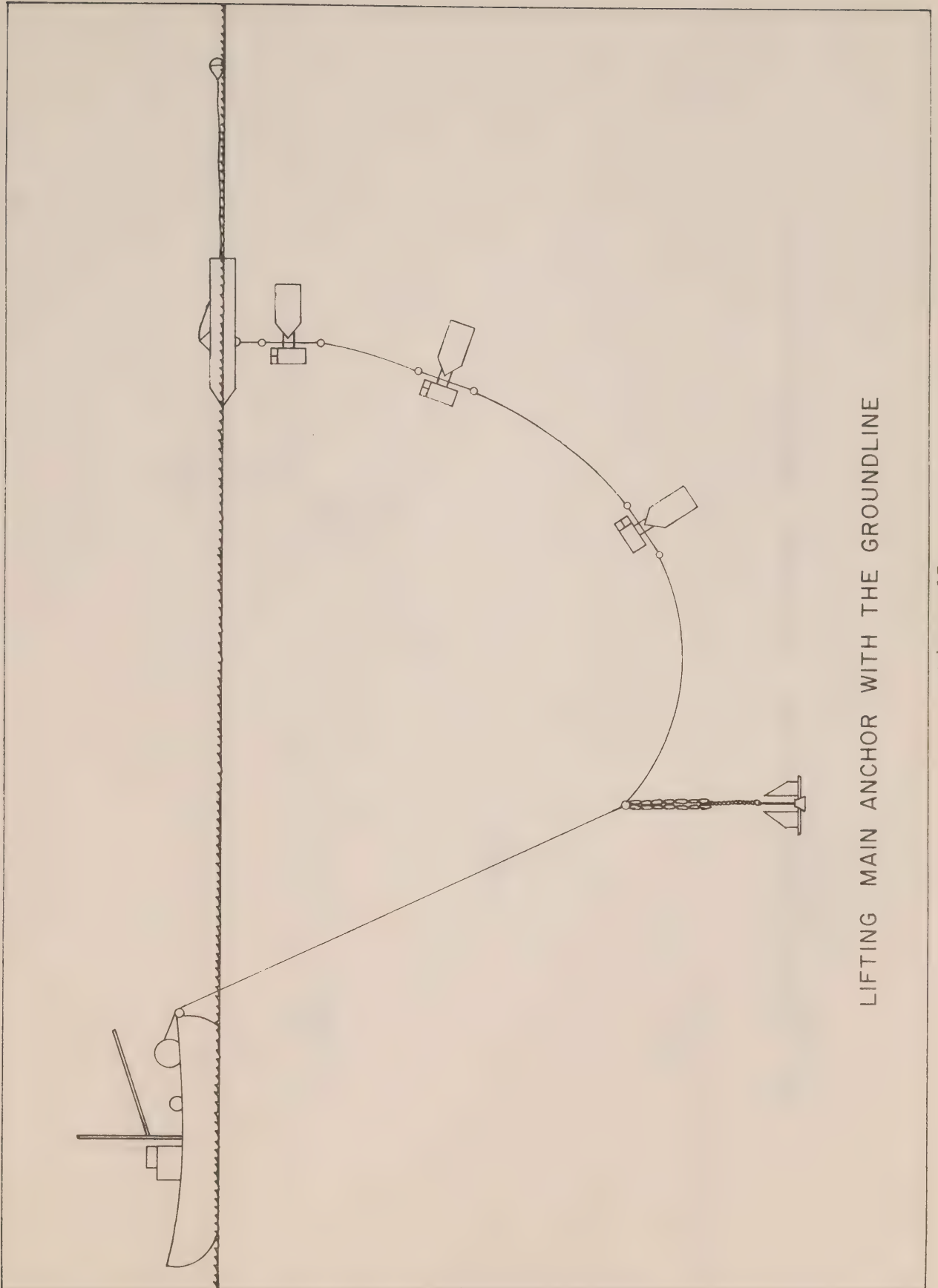
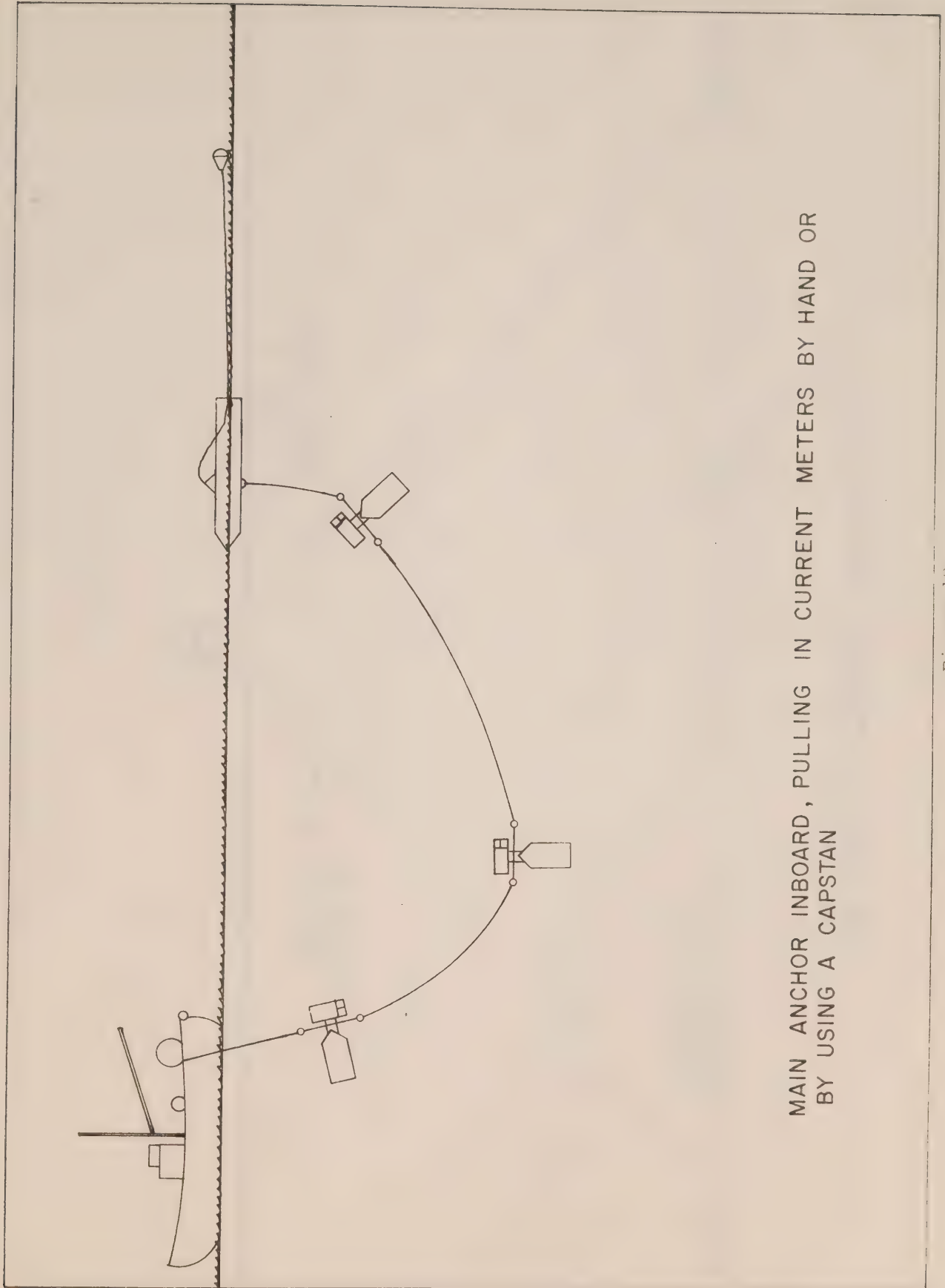


Figure 16



LIFTING MAIN ANCHOR WITH THE GROUNDLINE



MAIN ANCHOR INBOARD, PULLING IN CURRENT METERS BY HAND OR
BY USING A CAPSTAN

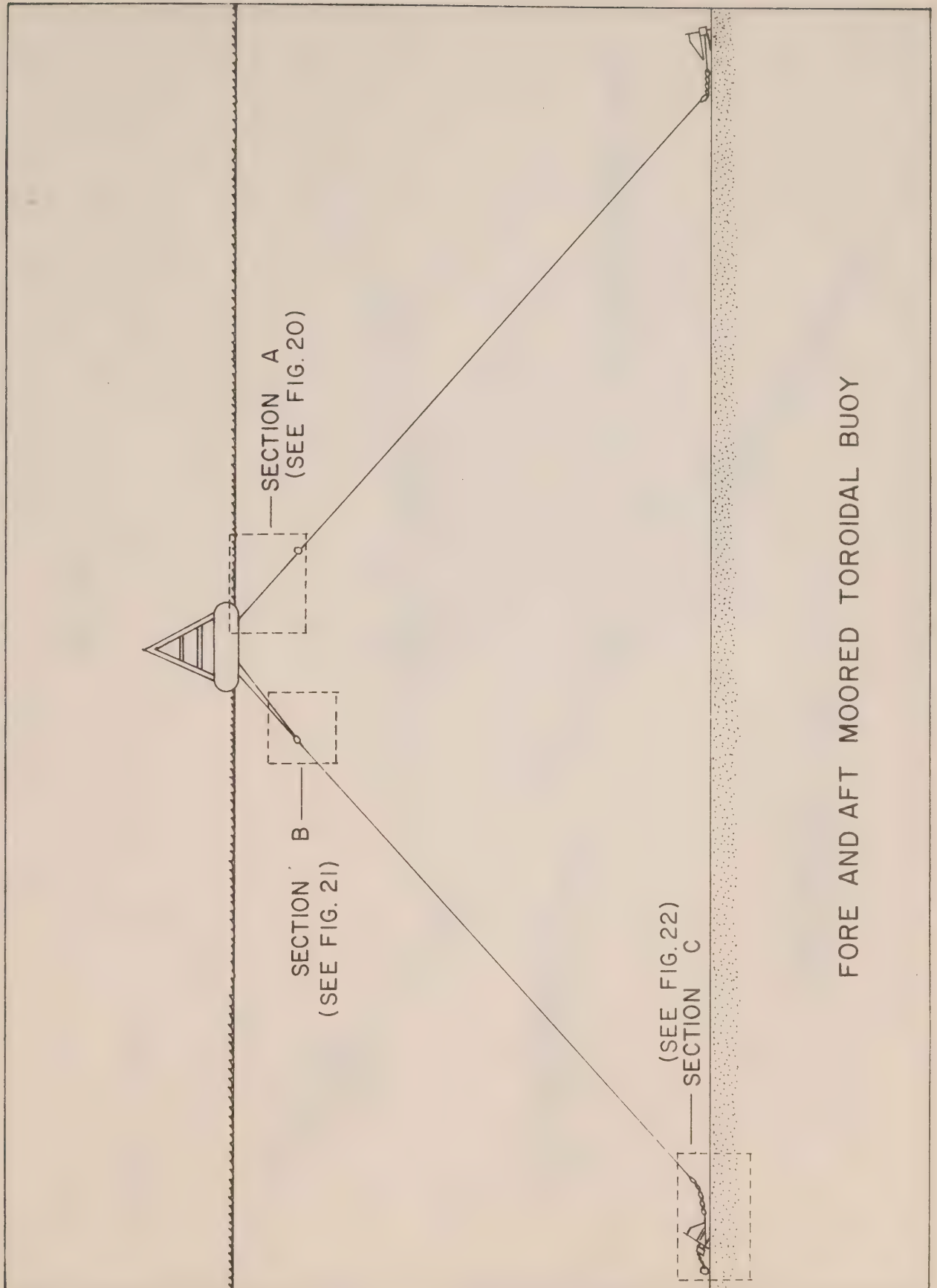


Figure 19

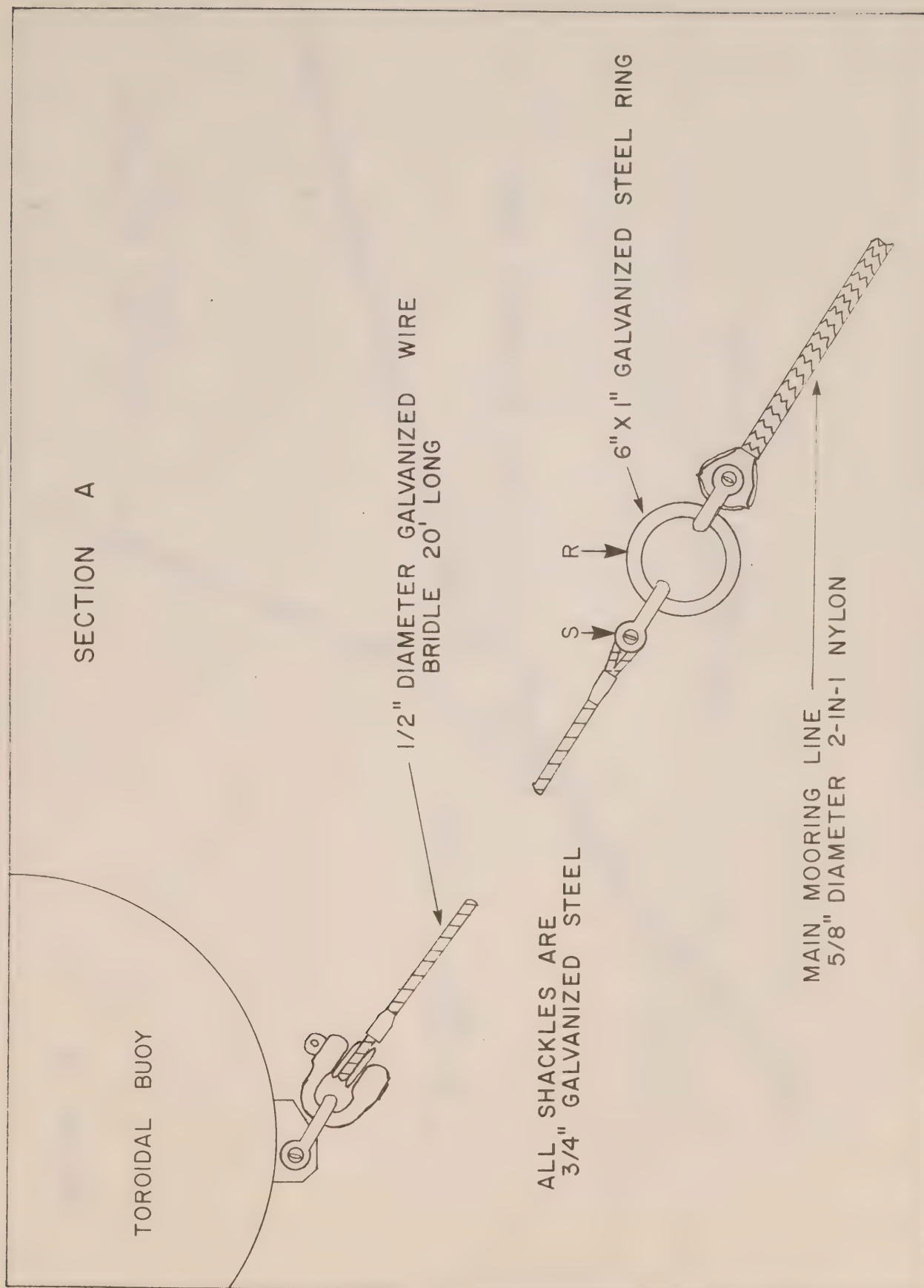


Figure 20

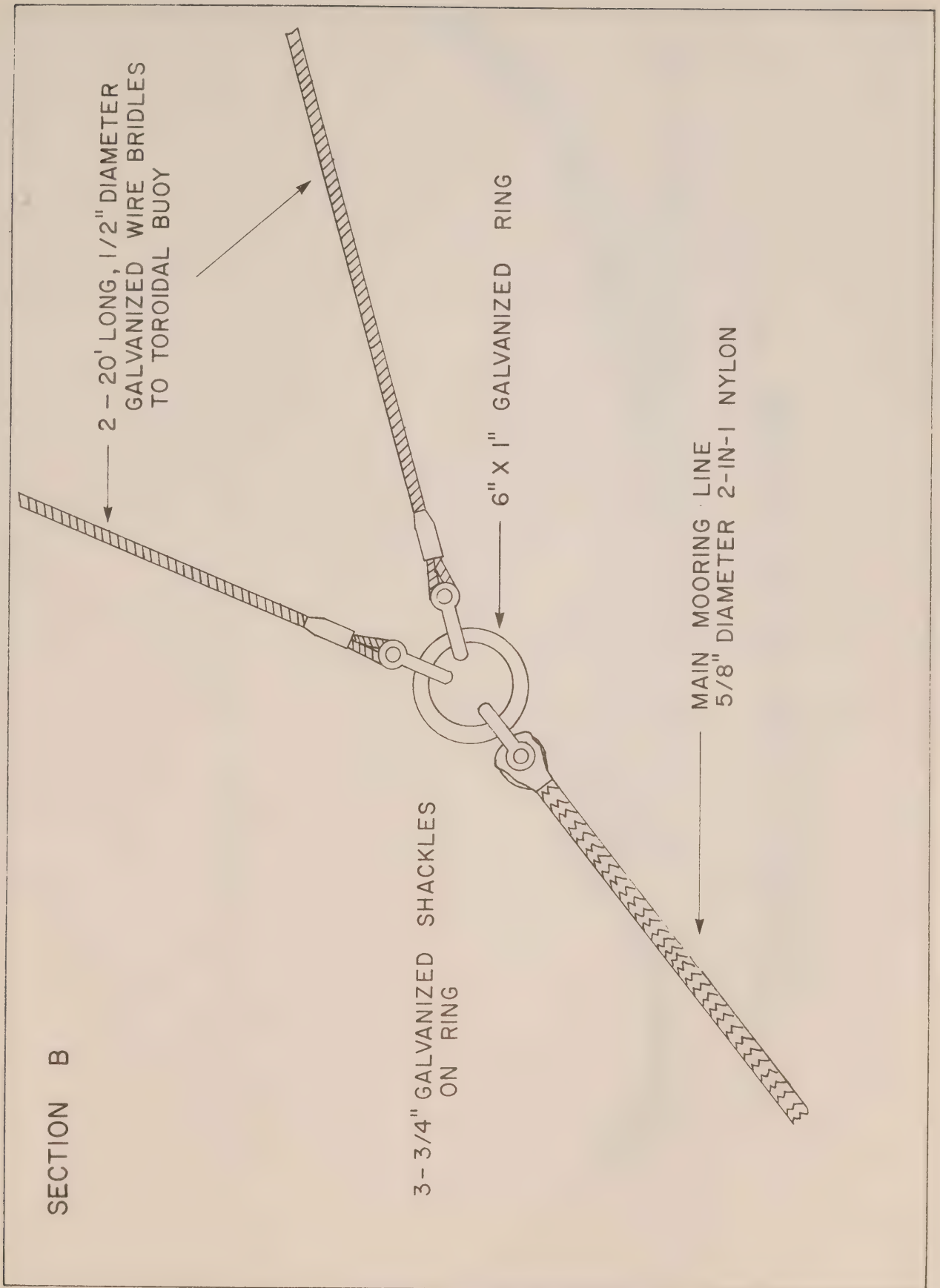


Figure 21

SECTION C



NO. 2 ANCHOR WITH DROP CHAIN AND RING AT ONE END AND 10' OF
1 7/16" DIAMETER ANCHOR CHAIN AT THE OTHER

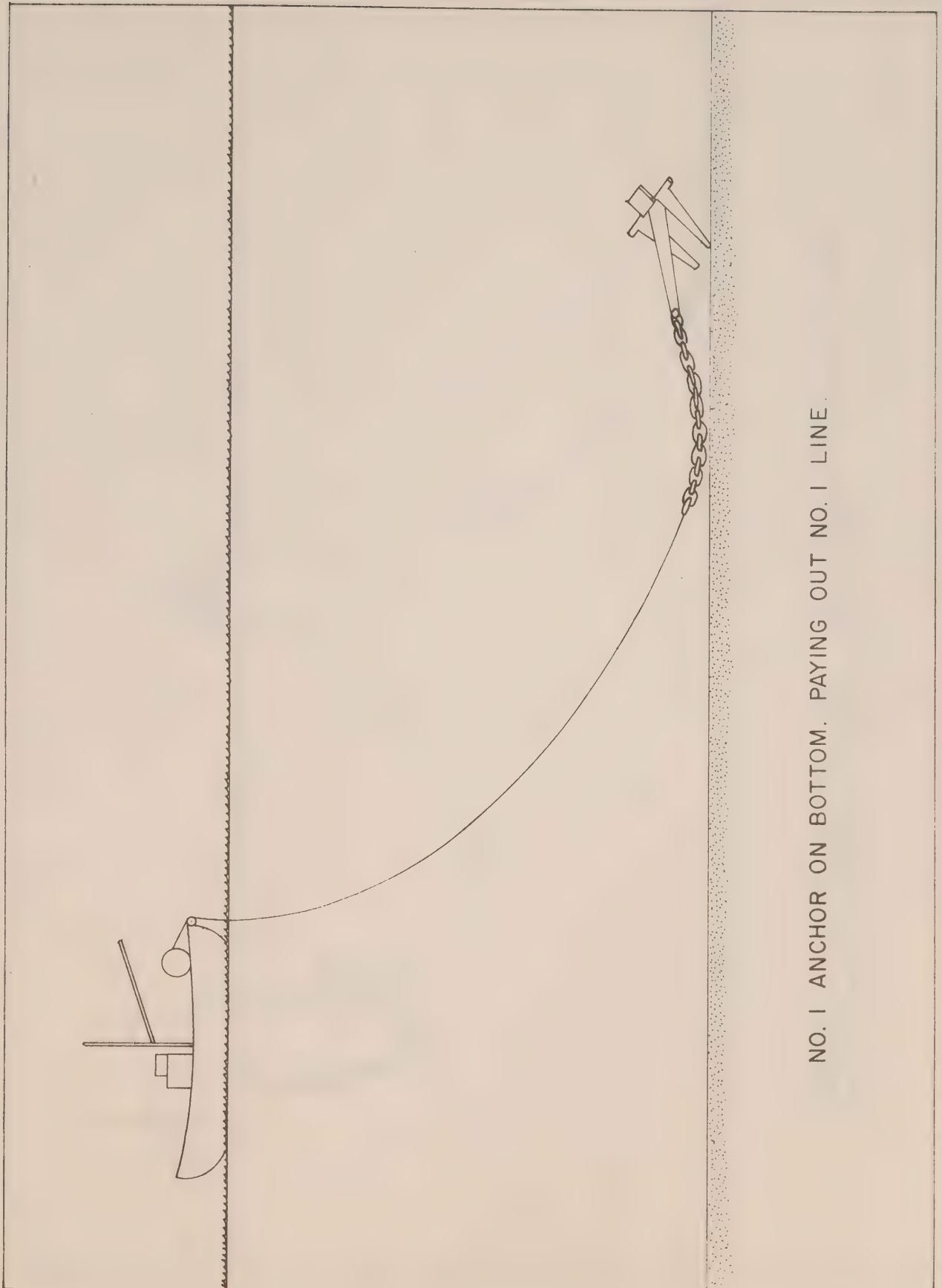
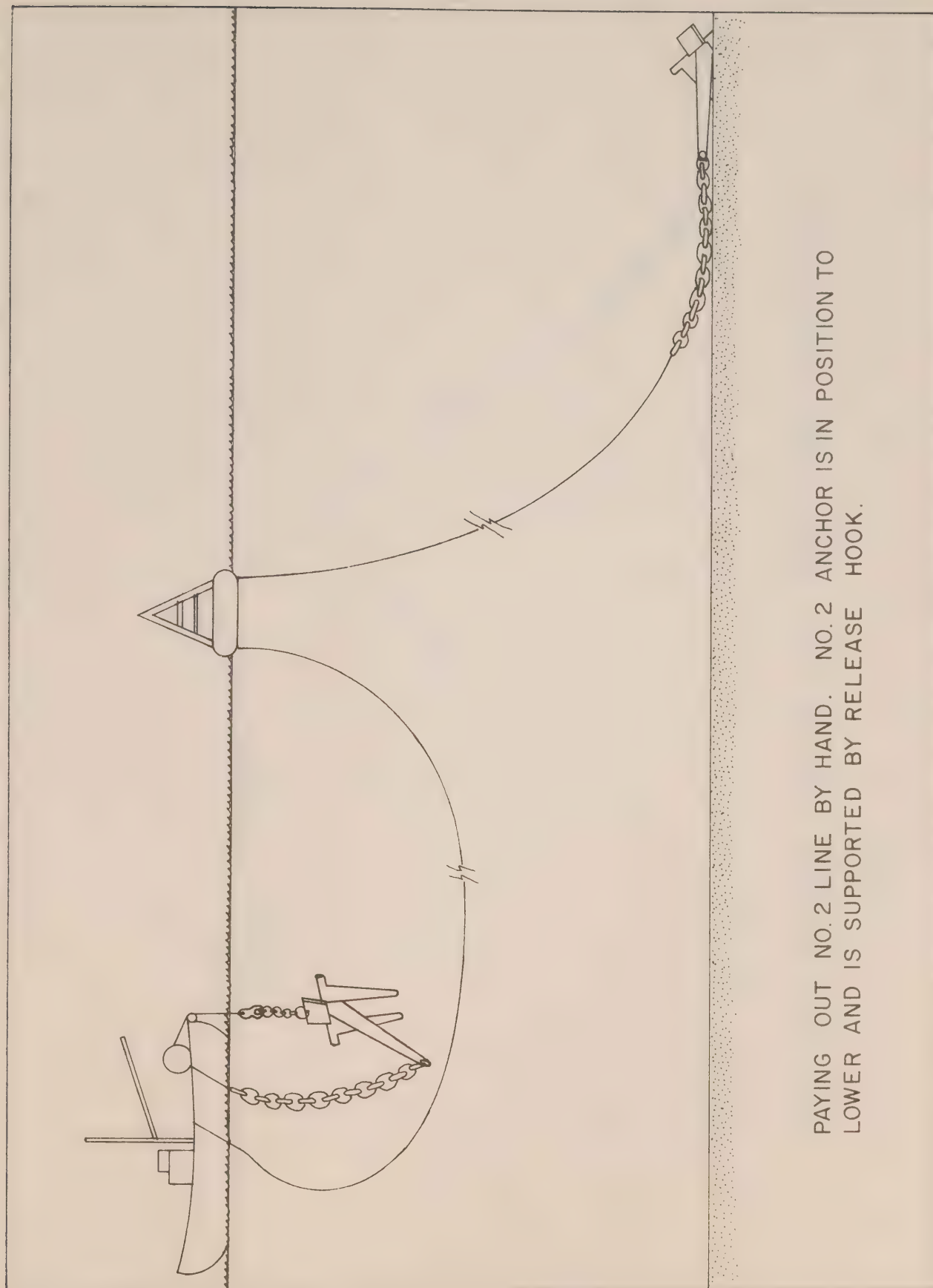


Figure 23



PAYING OUT NO. 2 LINE BY HAND. NO. 2 ANCHOR IS IN POSITION TO LOWER AND IS SUPPORTED BY RELEASE HOOK.

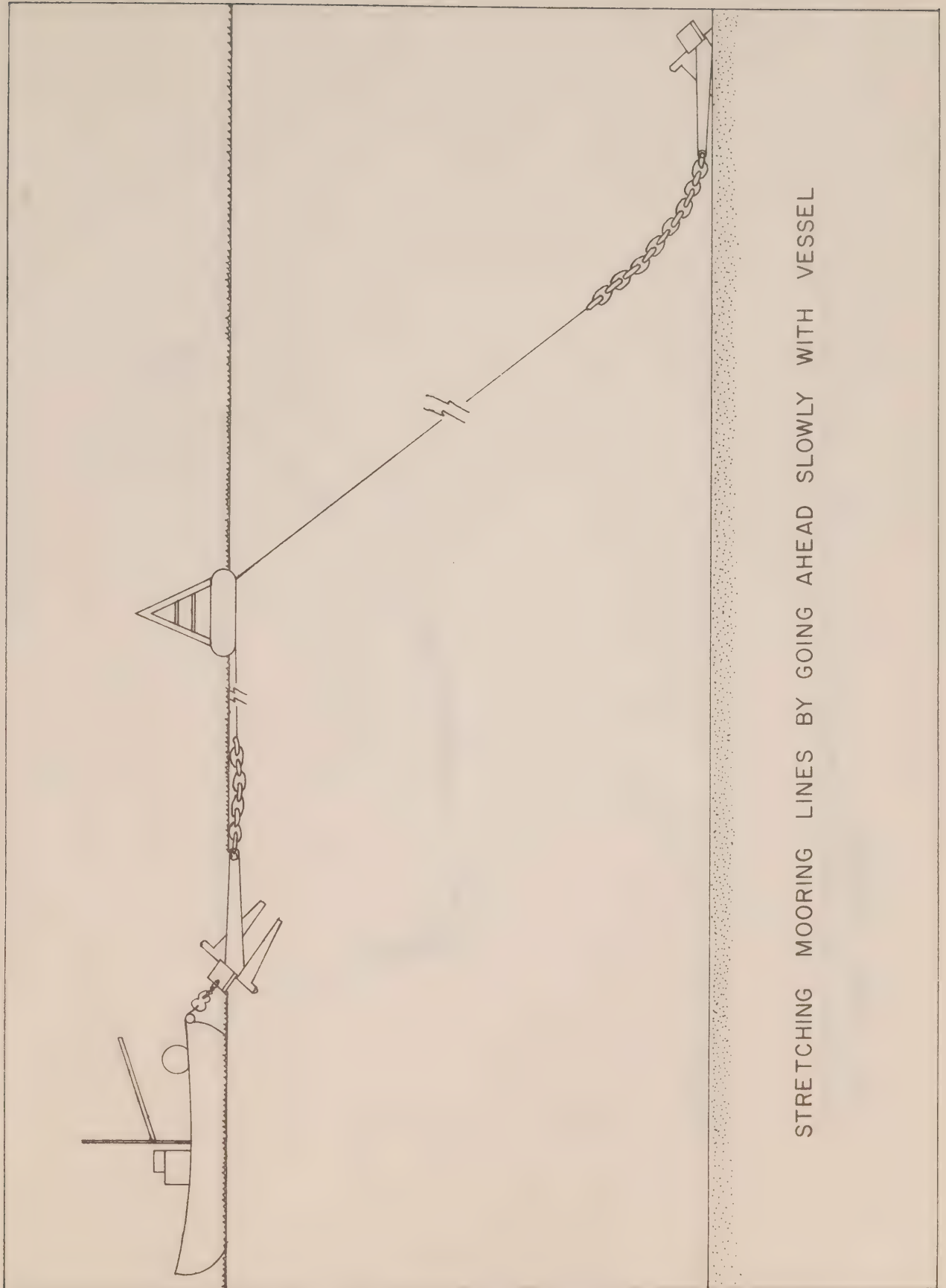


Figure 25

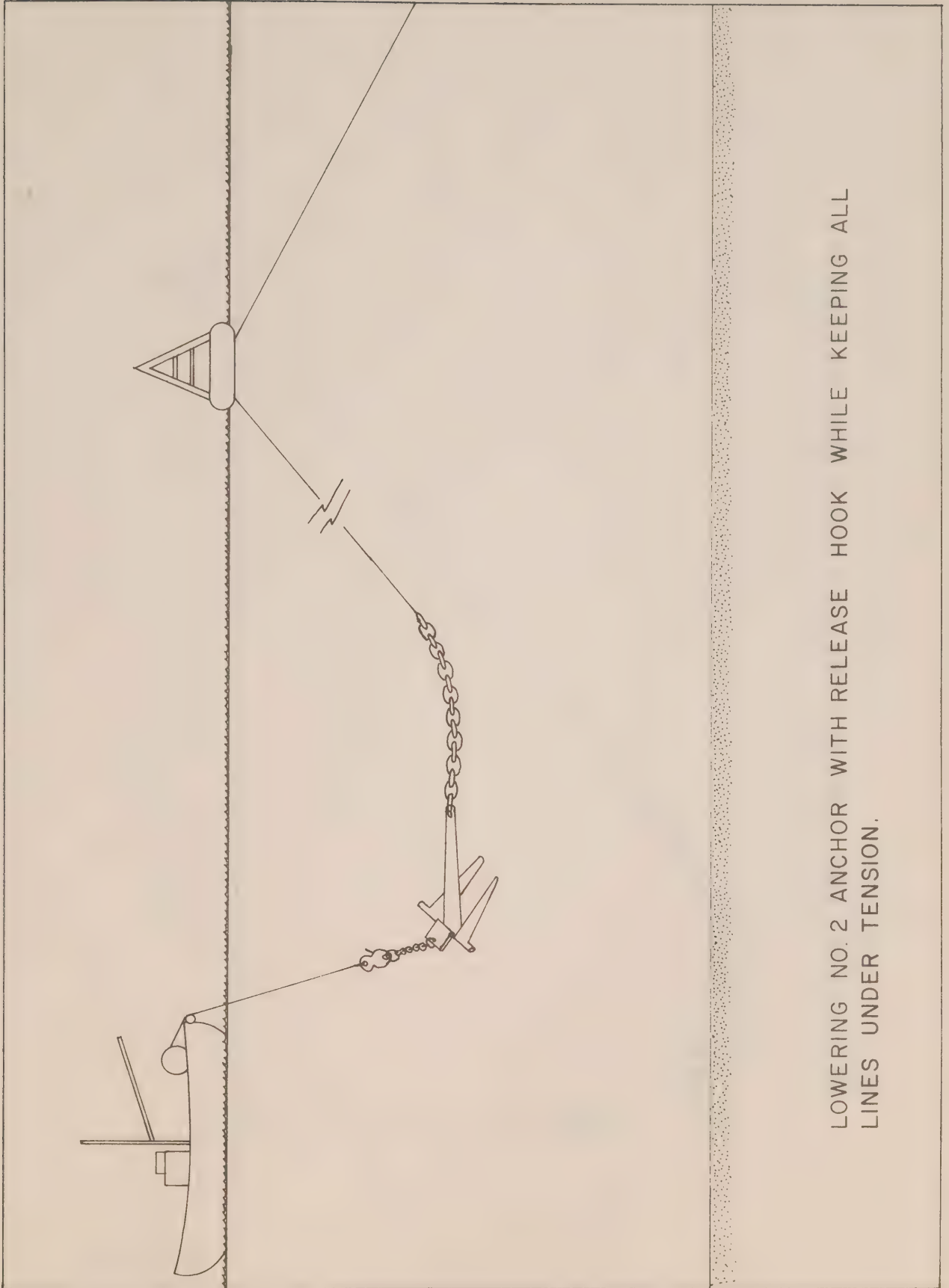
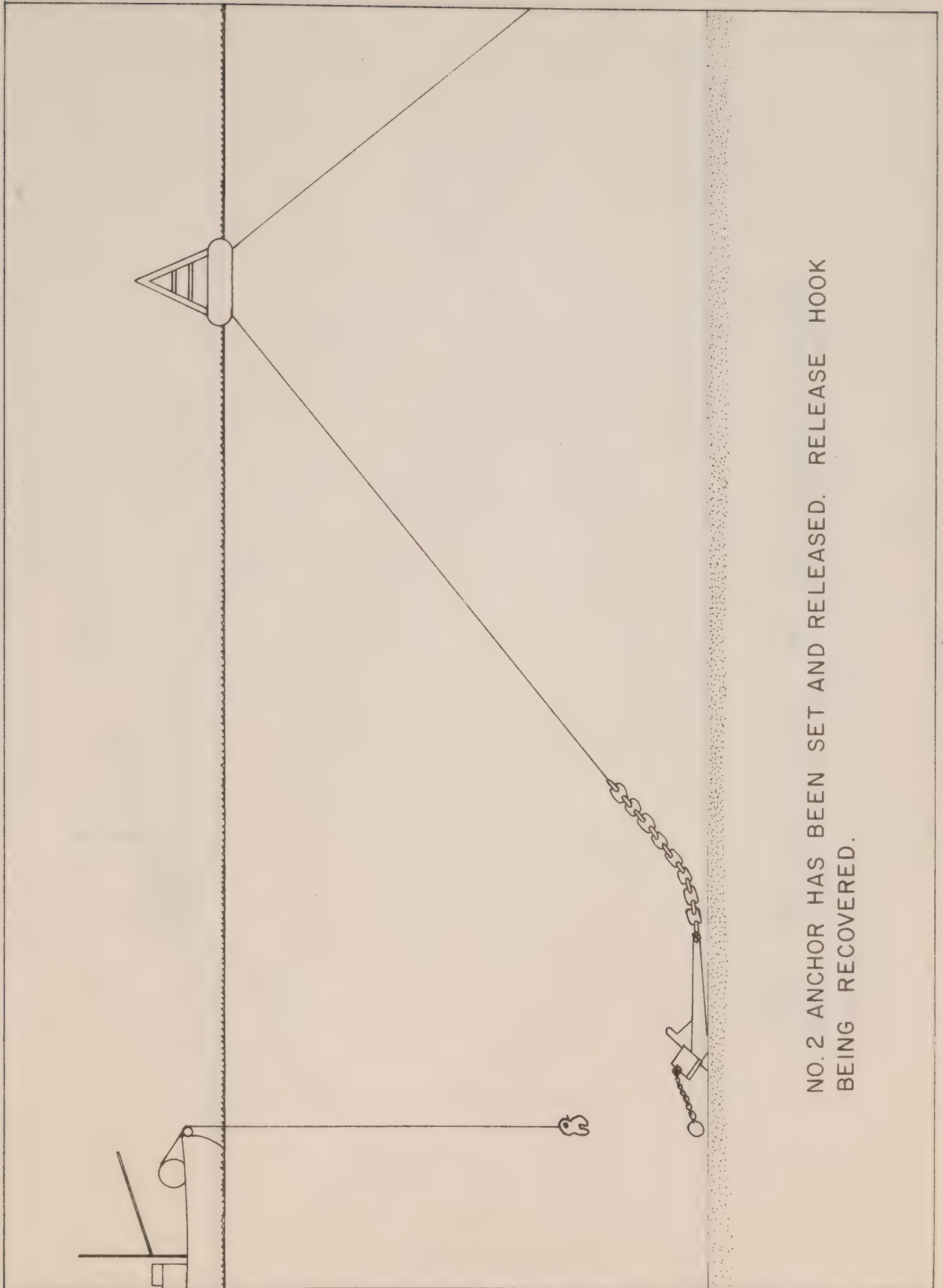
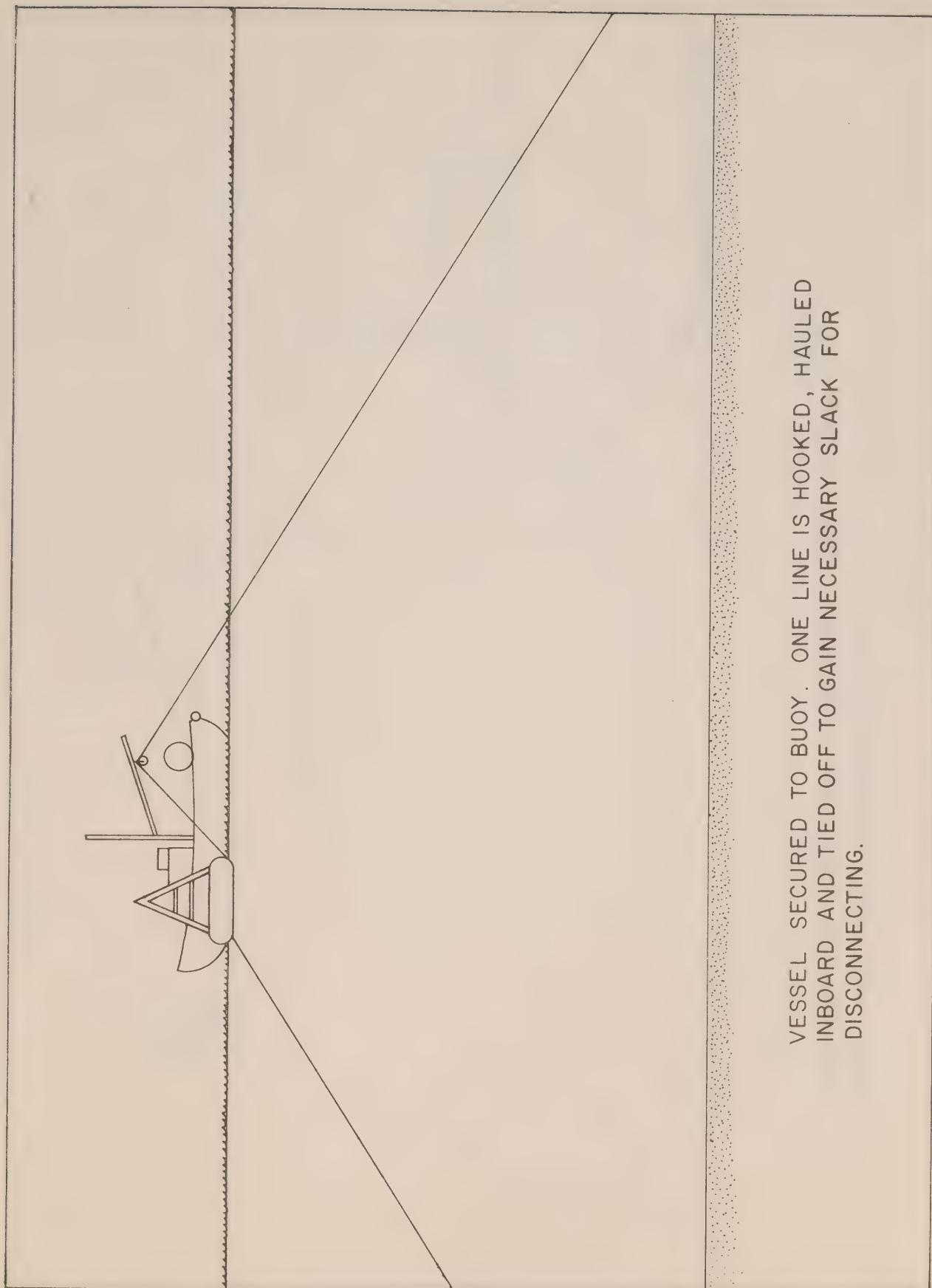


Figure 26



NO. 2 ANCHOR HAS BEEN SET AND RELEASED. RELEASE HOOK
BEING RECOVERED.



VESSEL SECURED TO BUOY. ONE LINE IS HOOKED, HAULED INBOARD AND TIED OFF TO GAIN NECESSARY SLACK FOR DISCONNECTING.

Figure 28

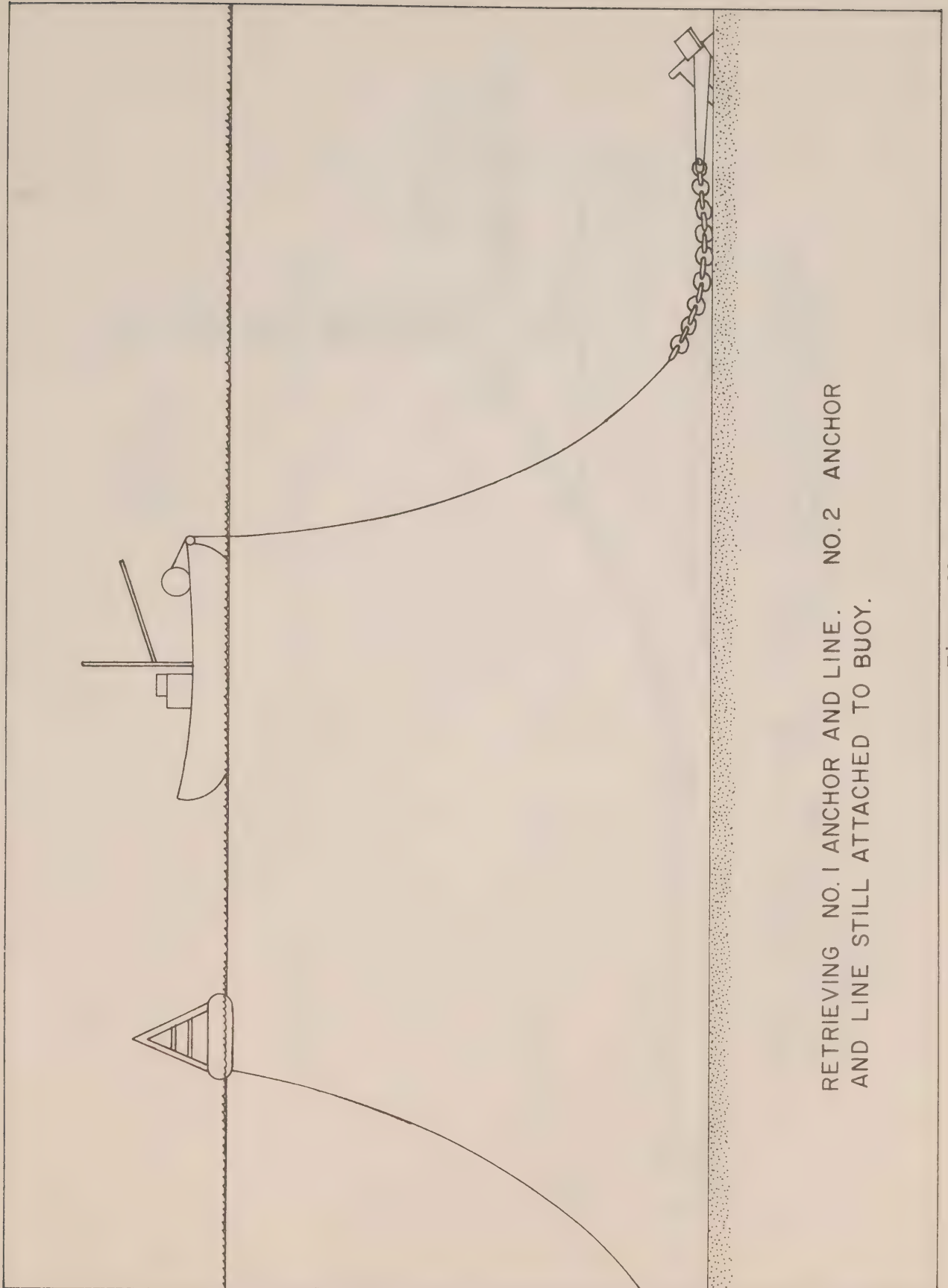
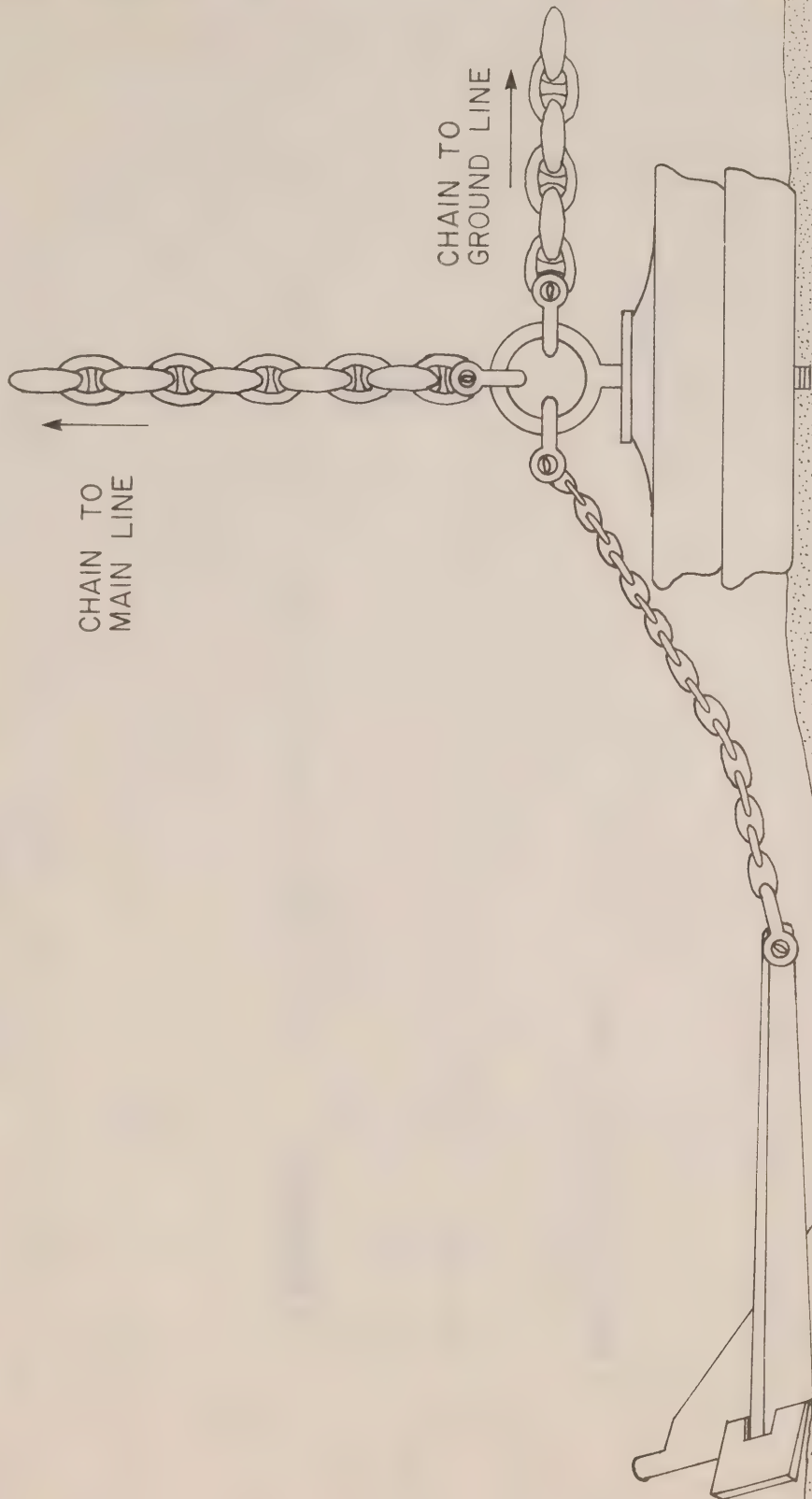
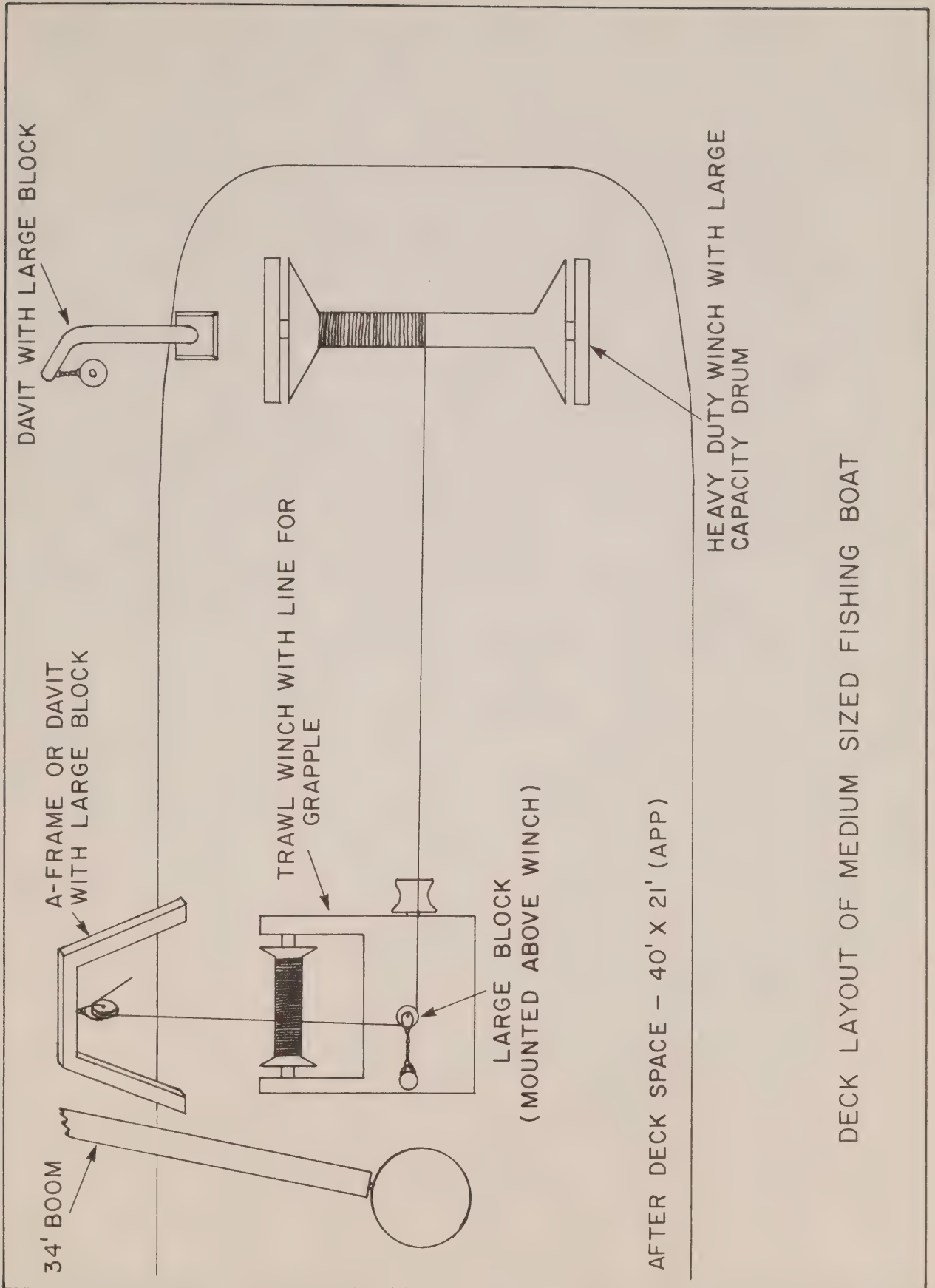


Figure 29



HEAVY-WEIGHT ANCHOR SYSTEM, TWO TRAIN WHEELS
BOLTED TOGETHER WITH A 180lb. DANFORTH ANCHOR
ATTACHED



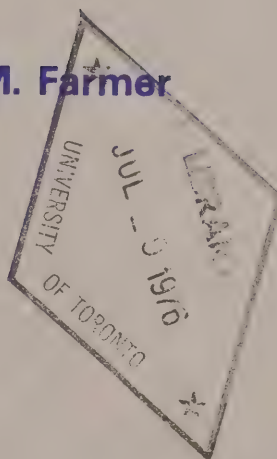
DECK LAYOUT OF MEDIUM SIZED FISHING BOAT

CH1 EP 321
- 76R10

DEEP WATER EXCHANGE IN RUPERT-HOLBERG INLET

by

D. Stucchi and D.M. Farmer



INSTITUTE OF OCEAN SCIENCES, PATRICIA BAY
Victoria, B.C.



For additional copies or further information, please write to:

Environment Canada

Institute of Ocean Sciences, Patricia Bay

512 - 1230 Government Street

Victoria, B.C.

V8W 1Y4

DEEP WATER EXCHANGE IN
RUPERT-HOLBERG INLET

by

D. Stucchi and D.M. Farmer

Institute of Ocean Sciences, Patricia Bay
Victoria, B.C.

May 1976

This is a manuscript which has received only limited circulation. On citing this report in a bibliography, the title should be followed by the words "UNPUBLISHED MANUSCRIPT" which is in accordance with accepted bibliographic custom.

TABLE OF CONTENTS

	<u>Page</u>
TABLE OF CONTENTS	i
ABSTRACT	ii
LIST OF FIGURES	iii
ACKNOWLEDGMENTS	iv
1. INTRODUCTION	1
1.1 Objective	1
1.2 Brief Review of Deep Water Exchange	1
1.3 Physical Description of Rupert-Holberg Inlet	2
1.4 Precipitation and Run-off	2
1.5 Tides	3
2. 1974 OBSERVATIONS OF DEEP WATER EXCHANGE	3
3. LONG TERM DATA	6
3.1 Background Temperature and Salinity Data	6
3.2 Models of Exchange Processes	7
3.3.1 1975 Long Term Data	8
3.3.2 Interpretation of 1975 Long Term Data	9
3.3.3 Parameterization of Exchange Processes	10
3.4 Further Details of Deep Water Exchange	12
4. SUMMARY AND CONCLUDING REMARKS	13
REFERENCES	15
FIGURES	

ABSTRACT

This report summarizes a series of oceanographic observations taken in the Quatsino Sound-Rupert-Holberg Inlet system on Vancouver Island. The observations included current meter records and salinity and temperature measurements. The water exchange occurring between Quatsino Sound and Rupert-Holberg Inlet is shown to be sensitively determined by the relative densities of water inside and outside Quatsino Narrows. During late spring and summer more saline water flows through the narrows forming a turbulent density current that runs along the floor of the Rupert-Holberg basin with speeds of up to 3 knots. The concept of deep water exchange and also the corresponding surface exchange occurring at other times of the year provides a framework for the interpretation of long term salinity and temperature time series taken with recording instruments. Descriptive models are proposed for the different types of exchange process. Attention is directed to the implications of suspended solids in the water namely, the effects upon salinity measurements, and the possible influence on the structure of the exchange process itself. These effects have important application to the disposal of mine tailings from the copper-molybdenum mine on Rupert Inlet.

LIST OF FIGURES

- Figure 1. Map of Quatsino Sound, Rupert-Holberg Inlet and Neroutsos Inlet.
- Figure 2. Map of inner Quatsino Sound and Rupert-Holberg Inlet showing locations of current meter and temperature, salinity stations.
- Figure 3. Sectional diagram from Hankin Point to Quatsino Narrows, showing 1974 current meter mooring.
- Figure 4. Mean ebb tide and mean flood tide current vectors of 1974 current meter data.
- Figure 5. A portion of the actual time series of current speed from 5, 70 and 155 metres.
- Figure 6. Mean ebb tide and mean flood tide salinities and temperatures from 1974 data.
- Figure 7. A portion of the current speed and salinity time series of the 1974 data from 5 and 155 metres.
- Figure 8. Representative background temperature and salinity data from Quatsino Sound. For location of Station D see Figure 2.
- Figure 9. Representative background temperature and salinity data from Rupert-Holberg Inlet. For location of Station H see Figure 2.
- Figure 10. Thirty-six year grand mean of daily sea surface temperature and salinity from Kains Island Lighthouse. Vertical bars represent standard deviation. For location of Kains Island see Figure 1.
- Figure 11. Representative temperature and salinity profiles from Quatsino Sound (Station D) and Rupert-Holberg Inlet (Station H).
- Figure 12. Balloon photograph of active region in front of Quatsino Narrows. Upwelling of turbid water is evident off Hankin Pt.
- Figure 13. Mean ebb tide and mean flood tide salinities and temperatures from the first set of long term data, 1975.
- Figure 14. Daily rate of change of salinity at H32 and temperature at H164, and temperature difference between Q10 and H164. (DWE = Deep Water Exchange, SWE = Surface Water Exchange)

ACKNOWLEDGMENTS

We thank Mr. C.A. Pelletier, Chief of Environmental Control for Utah Mines Ltd., for providing us with the background temperature and salinity data and the use of the mines' survey vessel Mac I.

1. INTRODUCTION

1.1 Objective

In this report we present and discuss some of the unique observations of deep water exchange made in Rupert-Holberg Inlet. In addition, the first set of long term observations from Quatsino Sound and Holberg Inlet will be interpreted in terms of simple models of exchange processes. The goal is to improve our understanding of the oceanography of Rupert-Holberg Inlet and other inlets with similar characteristics.

This study is particularly relevant to the practice of submarine tailings disposal. Utah Mines, a copper-molybdenum mine located on the north shore of Rupert Inlet, has been discharging mine tailings and waste rock into Rupert Inlet since 1971. The resulting turbidity field and the widespread dispersion of mine wastes are closely related to the physical oceanography of these inlets. An understanding of the oceanography of the receiving waters is essential to the proper assessment of environmental consequences of submarine tailings and rock disposal.

1.2 Brief Review of Deep Water Exchange

In many fjords and silled basins the circulation of the deep waters (water below sill depth) is restricted by the sill. The low dissolved oxygen content or anoxic conditions of the deep waters highlight the lack of exchange with surface waters or waters of comparable depth outside the sill. Conservative properties such as salinity and temperature tend to change slowly in the deep waters of many fjords. However, there are times when the deep waters experience comparatively rapid change in their properties. In these instances the density of the deep water increases, and frequently the dissolved oxygen content also increases. (Convective overturn resulting from gravitational instability of the surface waters is not considered in this report.)

The deep water is exchanged or renewed by more dense water which spills or intrudes over the sill. The intruding denser water spreads out along the basin bottom, filling the deeper portions and elevating the original deep water. The volume of water replaced can be determined from the observed elevation of the original waters and Gade (1970) has described a convenient method for making such estimates. Intruding waters of intermediate density will displace only the less dense deep waters. Thus, the deep waters of silled basins provide a temporary record of the high density extremes of the outside waters at sill depth. The record is temporary because the homogenizing effect of the vertical turbulent diffusion of heat and salt slowly reduce the density of the deep waters. Vertical turbulent diffusion is a controlling factor in the exchange process as it reduces the density threshold thus making deep water exchange more probable. The frequency, duration and form of deep water exchange are determined by several factors, namely the density characteristics of outside waters, the geometry of the basin and sill, local meteorology, run-off, tides and, as previously mentioned, vertical turbulent diffusion. The following brief review of deep water exchange in a number of local fjords shows the diversity of this process.

Saanich Inlet, located at the southern end of Vancouver Island, has a maximum basin depth of 236 m and a sill depth of 70 m through which it communicates with Haro Strait. Anderson and Devol (1973) have concluded that

the intermittently anoxic deep waters of this inlet are replaced annually in varying amounts. Deep water exchange occurs in late summer or early fall coincident with the presence of denser water in Haro Strait. The flushing waters are introduced in the form of short bursts (boluses) during the flood tide. The overall duration of a particular exchange in which there was 37% renewal was calculated to be about 12 days.

Nitinat Lake, a fjord located on the west coast of Vancouver Island, experiences sporadic renewals, as the shallow 4 m sill effectively isolates the fjord's permanently anoxic water from the Pacific Ocean (Ozretich, 1975). Ozretich concludes that deep water exchange occurs in response to reduced volumes of Fraser River water and to below average rainfall. The exchange takes place only during the flooding tide and is enhanced by high tides and wind stress.

During a two year study of Bute Inlet, a deep silled (350 m) fjord on the mainland coast of British Columbia, Lafond and Pickard (1975) observed five deep water exchanges. The deep waters of this fjord are renewed by the denser deep waters of the Strait of Georgia. The duration of inflows during the exchange varies between one and two months.

Howe Sound, a mainland fjord just north of Vancouver, has an inner basin with a 60 m sill. The upper deep waters of the inner basin undergo replacement frequently while the bottom waters are only renewed every three or four years (Bell, 1973). The occurrences of deep water exchange are related to large surface water outflow caused by either strong down channel winds or periods of high run-off.

In the Port Susan estuary, a silled basin within Puget Sound, Cannon (1975) reports current measurements of deep water exchange made on the 100 m sill. The current meter data obtained in August and September reveals four separate inflows of duration 4 to 7 days. Observed changes in dissolved oxygen and density are consistent with deep water exchange.

1.3 Physical Description of Rupert-Holberg Inlet

Rupert and Holberg Inlets are located near the northern end of Vancouver Island and they communicate with the Pacific Ocean via Quatsino Sound (see Figure 1). The geometrical properties of these two inlets are summarized in Table 1. Together, the two inlets form one basin — Rupert-Holberg Basin — 44 km in length. Quatsino Narrows, a long, shallow, slender channel, connects the basin to Quatsino Sound. The depth of Quatsino Narrows decreases from 38 m at its southern extremity to a minimum of 18 m at its northern end, where it opens into the basin (see Figures 2 and 3).

1.4 Precipitation and Run-off

The precipitation pattern typical of the west coast of Vancouver Island is one of high precipitation during late fall and winter months and minimum rainfall in the summer months (Pickard, 1963). The run-off pattern is similar with its peak in winter and late fall, and its minimum in summer. The Marble River is the only major river discharging into the Rupert-Holberg Basin. Its mouth is just east of Quatsino Narrows, on the south shore of Rupert Inlet (see Figure 1). This differs from the situation in most fjords and estuaries where the river is located at the head; consequently the classical model of

estuarine circulation will probably not be applicable. About 50% of the approximate drainage area surrounding Rupert and Holberg Inlets is drained by the Marble River (Drinkwater, 1973). Average and peak total freshwater inflows approximated by Drinkwater are listed in Table 1.

1.5 Tides

The tides along the west coast of Vancouver Island are mixed, mainly semi-diurnal. At Coal Harbour, in Holberg Inlet, the average tidal range is 2.8 m; 4.2 m is the maximum range (Canadian Hydrographic Service, 1974). The corresponding tidal prisms are included in Table 1. The average and maximum tidal exchanges constitute approximately 3% and 5% of the total Rupert-Holberg Basin volume. Tidal currents as large as 3 m/sec have been observed (Canadian Hydrographic Service, 1972) at the north end of Quatsino Narrows on both the ebb and flood tides. Strong currents, back eddies and other signs of turbulent stirring are evident throughout Quatsino Narrows. On the flood tide the area between Hankin Point and Quatsino Narrows is visibly turbulent with numerous patches of turbidity, boils of upwelling, eddies and strong currents. The vertical uniformity of the water column as well as the large annual variation in properties have been ascribed to tidal mixing in Quatsino Narrows and the active region in front of the Narrows (Drinkwater and Osborn, 1975).

2. 1974 OBSERVATIONS OF DEEP WATER EXCHANGE

During the period from 20 April to 7 May, a string of three Aanderaa current meters, equipped with conductivity and temperature sensors, was moored between Hankin Point and the northern end of Quatsino Narrows (see Figure 2). The current meters were positioned at depths of 5, 70 and 155 metres, as shown in Figure 3. Current velocity, temperature and conductivity were sampled at 5 minute intervals.

The vertical current structure throughout the period is readily seen from Figures 4 and 5 to be one of strong bottom currents during most of the time that the tide is flooding. Mean flood speeds of 40-45 cm/sec near the bottom (155 m) are appreciably higher than mean flood speeds at the surface (5 m, 20 cm/sec) and at mid-depth (70 m, 10-15 cm/sec). Peak current speeds of 154 cm/sec at 155 metres are considerably larger than the maximum flood speeds of 117 cm/sec and 80 cm/sec observed at 5 and 70 metres respectively. The prevailing direction for the flood currents, at all depths, is north, as shown in Figure 4. It is evident from Figure 5 that the bottom currents persist for approximately one hour after the predicted time of high water slack. The turn of the tide is based on the time of slack surface water in Quatsino Narrows even though drogue observations showed the deeper water to be still flooding at this stage of the tidal cycle (Canadian Hydrographic Service, 1972). Figure 4 shows that during the flood tide the bulk of the tidal exchange occurs near the bottom whereas during the ebb tide the exchange occurs near the surface. Ebb tide currents are smaller than the flood currents at 5 m and at 70 and 155 m they are non-existent. This is because of the shallow sill which restricts the outgoing flow to only the near surface waters, and also because the geometry of the junction of Quatsino Narrows with Rupert-Holberg Inlet is such that only on the flood tide is a jet produced. On the ebb tide, surface water flows towards the Narrows reaching large speeds only in the immediate vicinity of the entrance. Thus the tidal currents,

TABLE 1*

	<u>Rupert Inlet</u>	<u>Holberg Inlet</u>
Length	10 km	34 km
Mean Width	1.8 km	1.3 km
Mean Mid-Inlet Depth	110 m	80 m
Maximum Depth	165 m	170 m
Volume	$2.0 \times 10^9 \text{m}^3$	$3.4 \times 10^9 \text{m}^3$
Freshwater Inflow to Rupert-Holberg Basin	average	$12 \times 10^6 \text{m}^3/\text{day}$
	maximum	$40 \times 10^6 \text{m}^3/\text{day}$
Tidal Prism	average	$170 \times 10^6 \text{m}^3/\text{tidal cycle}$
	maximum	$260 \times 10^6 \text{m}^3/\text{tidal cycle}$

* from Pickard (1963) and Drinkwater (1973).

below sill depth, in front of the Narrows are rectified by the geometry of this junction.

The salinity and temperature data from these same instruments are presented in terms of averages over ebb and flood periods in Figure 6 and a portion of the actual salinity and current speed from 5 and 155 metres is presented in Figure 7. The salinity data in Figure 7 are representative of the entire time series. Figure 7 reveals that higher than average salinities are coincident with the high bottom currents. Since density is primarily determined by salinity (in this situation salinity is approximately 6 times more important than temperature) it is then evident that the water of the bottom current is more dense than the ambient water. The strong flow near the bottom appears to be a density current. A rough calculation reveals that a density difference of 0.25 Sigma-t, σ_T , units between the inflowing and ambient waters, is sufficient to cause the inflowing water to sink to the bottom by the time it reaches the current meter mooring. Using a reduced gravity ($g' = g \frac{\Delta \rho}{\rho}$) of 0.25 cm/sec², the time taken for the jet to sink from the surface to the bottom, a depth, D, of 155 metres is

$$\left(\frac{2 D}{g'}\right)^{\frac{1}{2}} = \left(\frac{2 \times 155 \times 10^2}{0.25}\right)^{\frac{1}{2}} = 352 \text{ seconds.}$$

The time taken for the jet to travel from the end of Quatsino Narrows to the current meter mooring is longer, approximately 450 sec if an average speed of 200 cm/sec is assumed.

A closer inspection of the vertical current structure reveals a phase lag with respect to depth during the flood tide. The flood current appears first at the surface then at mid-depth and finally at 155 metres. The time difference between the current at 155 m deep and the surface current is approximately two hours. This time difference in the flood currents may be explained in terms of density variations of the inflowing water over the flood period. The water in Quatsino Narrows at the turn to flood is Rupert-Holberg Inlet surface water that was drawn out on the preceding ebb tide. It is less saline than both the deeper water of Rupert and Holberg Inlets and the Quatsino Sound water which enters later in the flood. From the turn of the tide it takes approximately 1-1/2 hours for this water to pass through Quatsino Narrows. Later in the flood the more saline waters of Quatsino Sound are injected into Rupert-Holberg Inlet. The salinities observed during the flood tide support this hypothesis. Initially, at 5 metres, high currents are correlated with higher salinities, however, these higher salinities are still about 0.5‰ lower than salinities at 70 metres. Since the inflowing water is less dense than the deeper water the currents are confined to the upper portion of the water column. Later as the surface currents diminish, the bottom currents increase and so does the salinity associated with these currents.

The instruments were in the water for 17 days and during this period there was a net temperature increase of 0.3-0.4°C at 70 and 155 m, and ~ 0.5°C at 5 metres. More significantly, the salinity increased by ~ 1‰ at 5 m, 0.4‰ at 70 m and ~ 0.3‰ at 155 m. (At 155 metres there are periods when the salinity decreases, but these may be due to fouling of the conductivity sensor by mine tailings.) The density of the water column has

increased because of the salinity increase. Since salt, unlike heat, can only be exchanged through Quatsino Narrows, a net salt flux into Rupert-Holberg Inlet has occurred from Quatsino Sound during this period. The salt input has occurred during the flood tide in the form of a density current flowing from Quatsino Narrows down the side of Rupert and Holberg Inlets to the basin bottom. The density of the top 20 m (sill depth) of Quatsino Sound water injected into Rupert-Holberg Inlet on the flood tide is generally greater than that of the resident water.

The density current is certainly a turbulent flow as the Reynolds numbers associated with speeds of 100 cm/sec or more are high. The turbulent nature of the flow is evident from the significant amounts of high frequency variance in all of the measured variables. On the basis of the observed vertical current and density structure, and the long term increase in salinity, we conclude that a rectified deep water tidal exchange process was occurring from the 20th April to 7 May, 1974.

3. LONG TERM DATA

3.1 Background Temperature and Salinity Data

The seasonal temperature and salinity variations in Quatsino Sound and Rupert-Holberg Inlet have been monitored primarily by Utah Mines. Mine data representative of Quatsino Sound Station D and Rupert-Holberg Inlet Station H are displayed in Figures 8 and 9 respectively. In addition, daily sea surface (1 m) temperature and salinity data were taken near the mouth of Quatsino Sound at Kains Island Lighthouse from 1935 to 1970 (Hollister and Sandnes, 1972). The 36 year grand mean of monthly temperatures and salinities and standard deviation are plotted in Figure 10. In spite of the sparseness of the mine data, a similar seasonal trend is evident in the data from all three stations. The salinity increases during the late spring and summer to a maximum ($\sim 32\text{‰}$) in August-September and the declines quickly to a minimum ($28 \sim 29\text{‰}$) in winter or early spring. The temperature is at a maximum (11°C) in August-September and at a minimum (6°C) in March-April.

In Holberg Inlet the 167 m salinities are higher (0.2 to 1‰) than those at 30 m but otherwise similar in detail. The surface salinities in Quatsino Sound (Station D) are also very similar to the salinities of Rupert-Holberg Inlet but the resemblance diminishes in the deeper salinities in Quatsino Sound. The profiles of temperature, salinity and density in Rupert-Holberg Inlet are similar throughout the inlet and can be characterized as having very little stratification except for a thin surface layer. These contrast sharply with the very stratified Quatsino Sound profiles (see Figure 11).

The increasing salinity in Rupert and Holberg Inlets during the late spring and summer months is accomplished by deep water exchange. Salinity increases from Quatsino Sound are communicated to Rupert-Holberg Inlet by deep water exchange, as was observed in the 1974 data and described in Section 2 of this report. The increasing density of the surface Quatsino waters is in part a response to the reduction in precipitation and run-off during these months. Upwelled water from west of Quatsino Sound is believed to be the source for the maximum density waters observed in August and September (Pickard, 1963). There is also a suggestion from the mine data

that deep water exchange occurs for short periods during the fall and winter months. The variability in precipitation and run-off during the fall and winter months is probably responsible for these brief periods of deep water exchange. An examination of the Kains Island data reveals that the variability (indicated by the vertical bars in Figure 10) of the salinity is highest in the fall and winter months, i.e., the standard deviation is twice that in the summer months.

Except for the short periods of deep water exchange when the salinity increases, the salinity decreases during the fall and winter months. The exchange process acting at these times is able to extract salt from the entire water column of Rupert-Holberg Inlet. The salt extraction process is controlled by the reduced densities of the surface waters, which are in turn a response to the high precipitation and run-off that occurs at this time of year. This salt extraction process may also occur briefly during the spring and summer months as the mine data suggests.

Unlike deep water exchange, the salt extraction process requires that potential energy be supplied to the entire water column so that the denser, more saline water may be mixed upward. The uniformity of the water column and the large seasonal property changes of the deep waters in Rupert-Holberg Inlet are evidence for the presence of such a mixing process. The region of active mixing is the area between Hankin Point and the northern end of Quatsino Narrows, an area that is visibly active during each flood tide. Calculations of the available tidal mixing energy (Drinkwater and Osborn, 1975) appear to indicate that there is sufficient energy to mix a 10 m surface layer from Quatsino Sound into the water column of Rupert-Holberg Inlet. Furthermore, tidal mixing is certainly enhanced by the 'T'-shaped geometry of the junction of Quatsino Narrows and Rupert-Holberg Inlet, as portions of the tidal jet will be deflected vertically. During deep water exchange the density current is deflected upward by Hankin Point. Upwelling of the deep waters has been observed and it can be identified in the photograph (Figure 12) by the marked turbidity of the water just off Hankin Point.

3.2 Models of Exchange Processes

Two points have emerged from the examination of the background temperature and salinity data; first, the importance of the density of the inflowing surface water from Quatsino Sound, as indicated by its similarity to the waters of Rupert-Holberg Inlet, and second, the role of tidal mixing as evidenced by vertical homogeneity of the water column and the property changes at depth in Rupert-Holberg Inlet. These two points must be included in any realistic model of the exchange processes.

The 1974 data provides a base for a simple model of deep water exchange. The incoming jet of denser Quatsino Sound surface water flows down the side of Rupert-Holberg basin to the bottom, entraining resident water into the flow as it proceeds. A portion of this bottom flow is deflected upwards by Hankin Point and further mixing with the surrounding waters occurs. The remaining portion of the flow is diverted laterally along the basin bottom, displacing the less dense waters upwards. Horizontal density gradients created by the input of denser water at depth transport salt towards the head of Rupert and Holberg Inlets away from the active region. As a result, the temperature and salinity fluctuations of the deep waters resemble those of the incoming water. At higher levels in the water column the temperature and salinity fluctuations

are not as closely related to the incoming water. On the outgoing tide the less dense surface waters are drawn out through the Narrows. Thus, as the salt input process continues, the overall density of the water column increases.

Tidal mixing is an essential feature of the salt extraction model. Buoyancy forces act to confine the incoming jet of less dense water to the surface while the entrainment of resident waters into the flow acts to increase the vertical extent of the jet. The vertical penetration of the jet is, in part, governed by the relative density contrast and the speed of the inflowing jet. The 'T' shaped geometry of the junction may also affect the vertical penetration of the jet.

Two extreme configurations of the salt extraction process can be visualized; first, a neutrally buoyant inflow and second, a very fresh inflow. In the first extreme case the tidal jet spreads over the entire water column since there is no density stratification to limit the vertical penetration. In the second case large buoyancy forces confine the tidal mixing to the upper portions of the water column leading to the mechanism subsequently referred to as surface water exchange. Because of the more intense mixing near the surface, fluctuations in temperature and salinity occur first near the surface. The deep waters of the basin remain static and unaffected by the tidal jet. Regardless of the depth of penetration represented by these two extreme cases, during the flood tide salt is transported upwards, thus allowing its removal during the ebb tide. Horizontal density gradients created by the mixing of the tidal jet cause a lateral readjustment of the mass field. For the salt extraction process this implies a net horizontal flux of salt towards the active area in front of Quatsino Narrows.

3.3.1 1975 Long Term Data

In order to investigate the relationships between the surface waters of Quatsino Sound and the waters of Rupert-Holberg Inlet, a long term monitoring program for temperature and salinity was initiated in mid-March 1975. The program consisted of two moorings, each with two Aanderaa current meters with temperature and conductivity sensors. The Quatsino Sound mooring was located off the seaward side of Drake Island with current meters at 10 and 30 metres, hereafter referred to as Q10 and Q30. The Holberg Inlet mooring was located southeast of Coal Harbour, with current meters at 32 and 164 metres, hereafter called H32 and H164. The locations of these two moorings are shown in Figure 2, denoted Q and H respectively.

Except for data from Q30, the first set of temperature and salinity data from March 14 to May 13 is presented in Figure 13 as ebb tide averages and flood tide averages. No salinity data was obtained from the deep instrument on the Holberg mooring because of a sensor failure.

The increasing long-term temperature trend is similar at all four depths. Superimposed on the trend are temperature variations of length 3 to 10 days and varying amplitude. In particular, one of these temperature variations - a temperature dip of 5 to 10 day duration - can be traced at all 4 depths. The chronology of the temperature dip is: March 17 at Q30, March 20 at Q10, March 22 at H32 and March 25 at H164. The averaged temperature time series at Q10 has the largest variance, especially in the latter half of the time series. In contrast, the temperature at H164 is very smooth.

All three time series of salinity show a net increase in salinity of approximately $1^{\circ}/_{\infty}$. The long term trend is similar on all three time series, however, they are different in detail. The Q30 salinity is markedly different from the other two series in that it exhibits a strong 14 day periodicity of amplitude as large as $0.5^{\circ}/_{\infty}$. The H32 m time series is smooth, exhibiting little difference between ebb and flood averages, a sharp contrast to the Q10 time series which exhibits a large difference ($<0.5^{\circ}/_{\infty}$) between ebb and flood averages. These large differences are to be expected in the very stratified surface waters.

3.3.2 Interpretation of 1975 Long Term Data

During the first 6 or 7 days, ending on March 20, deep water exchange appears to be occurring as the salinity at H32 rises slightly. Unfortunately, there are insufficient temperature data available at H164 during this initial period to support this argument. Between March 21 and March 25 the salinity at H32 has dropped about $0.1^{\circ}/_{\infty}$, indicating that the salt extraction process is occurring. This hypothesis is further supported by the chronology of the temperature dip mentioned earlier. The temperature dip observed at Q10 appears a few days later at H32, while the temperature at H164 remains relatively static. This is consistent with surface water exchange, i.e., the salt extraction mechanism. An upper bound for the vertical eddy diffusivity, K_z , associated with the salt extraction process can be estimated from this data by using an appropriate length scale, L and time scale, T . For at least two days surface water exchange was observed to be occurring while the deep waters were static. Using a time scale of 2 days and the vertical separation between H32 and H164 as a length scale,

$$K_z \leq \frac{L^2}{T} \sim \left(\frac{132 \times 10^2}{2 \times 24 \times 3600} \right)^2 \sim 10^3 \text{ cm}^2/\text{sec.}$$

The time scale used may be inappropriately short since the water property changes at H164 are a result of a switch in the exchange process not a result of the vertical eddy diffusivity. Thus, this calculation must be considered as only providing an upper bound. The temperature dip shows up at H164 only after the salinity begins to increase, around March 25. The rise in salinity begins first at Q10 and then at H32. Moreover, the salinity increase at Q10 is steeper (about $0.7^{\circ}/_{\infty}$ between March 26 and April 10 vs. about $0.5^{\circ}/_{\infty}$ at H32). After the salinity at Q10 reaches a value of about $31.1^{\circ}/_{\infty}$ it remains fairly stable, the salinity at H32, however, increases steadily until April 25 and only gradually until the end of the record, by which time it has reached $31^{\circ}/_{\infty}$. Salinity is a better indicator of exchange than heat since salt can only be exchanged through Quatsino Narrows, whereas heat can also be exchanged through the air-sea interface. Nevertheless, comparison of temperatures at Q10 and H164 reveals that those at H164 closely follow those at Q10, except for some scattered points around April 18, May 5 and 13. The departures at these times are almost certainly due to a thicker warm layer in Quatsino Sound. This similarity in temperature at H164 and Q10 and the increasing salinity at H32 are both consistent with our model of deep water exchange. The above discussion of the long term data in terms of the exchange processes is summarized in the following table.

DATES

STATIONS		UP TO MAR 20	MARCH 20-25	MAR 25-APR 25	APRIL 25 TO END
Q10	θ	Steady	Decreasing	Increasing	Increasing
	S	Steady	Slight Decrease	Increasing	Steady (Slight Drop)
H164	θ	_____	Steady	Increasing	Increasing
H32	θ	Steady	Decreasing	Increasing	Increasing
	S	Increasing	Decreasing	Increasing	Slight Increase
Exchange		Deep Water	Salt Extraction	Deep Water	Deep Water
Process		Exchange	Process	Exchange	Exchange

3.3.3 Parameterization of Exchange Processes

A more quantitative explanation of the long term data may be achieved if the rates of change of salinity and temperature are considered. In the absence of salinity data from H164, the rate of change of H32 salinity, $\frac{\Delta S}{\Delta T}_{H32}$ is interpreted as determining the particular type of exchange process in effect, i.e., a positive slope for deep water exchange and a negative slope for the salt extraction process. The rate of change of H164 temperature (i.e., $\frac{\Delta \theta}{\Delta T}_{H164}$) coupled with the temperature difference between Q10 and H164 (i.e., $\theta_{Q10} - \theta_{H164}$) may reveal whether or not deep water exchange is occurring. If deep water exchange is in progress then the rate of change of deep water temperature, $\frac{\Delta \theta}{\Delta T}_{H164}$, should be non-zero providing there is an appreciable temperature difference between the resident deep waters and the intruding waters. When the deep waters are quiescent, we would expect $\frac{\Delta \theta}{\Delta T}_{H164} \sim 0$, and surface water exchange would be occurring. The following table summarizes the above discussion.

	$\frac{\Delta S}{\Delta T}_{H32}$	$\theta_{Q10} - \theta_{H164}$	$\frac{\Delta \theta}{\Delta T}_{H164}$
Deep		+	+
Water	+	0	0
Exchange		-	-
Surface		+	0
Water	-	0	0
Exchange		-	0

The validity of the above method of analysis depends upon several points. First, it is assumed that the temperature at Q10 is representative of the water entering Rupert-Holberg Inlet on the flood tide. This assumption is weak, in light of the observed stratification of the surface waters of Quatsino Sound. On the other hand the long term trends occurring in the Quatsino surface water are more likely to be faithfully represented by the time series at Q10. Second, it is possible that during the flood tide both types of exchange process occur in series as the 1974 data show. Thus, in periods when deep water exchange is dominant, fresher water may be mixed down to 30 m by surface water exchange which occurs for only a short period at the beginning of the flood tide. This may affect the salinities at, say H32 so as to mask the deep water exchange. Also, in a neutral situation in which the tidal jet is spread over the entire water column, properties of the entire water may be changing, thus providing ambiguous data. This latter situation may only occur as a transitional phase between the two exchange processes.

From daily averaged time series of temperature at H164 and Q10 and salinity at H32, daily rates of change of salinity at H32 and temperature at H164 were computed. The temperature difference between Q10 and H164 was also computed. These computed quantities are plotted in Figure 14 and in addition the type of exchange process believed to have been occurring is indicated. The data are dominated by the deep water exchange process especially from March 25 to April 26. There are several instances during this period when surface water exchange may be occurring. In these three instances

$\frac{\Delta S}{\Delta T}_{H32}$ is near zero and $\frac{\Delta \theta}{\Delta T}_{H164}$ is correspondingly small. On April 4, $\frac{\Delta S}{\Delta T}_{H32}$ is zero, yet $\frac{\Delta \theta}{\Delta T}_{H164}$ is appreciable; this may be due either to both exchange processes acting in series or to the existence of a neutral condition. A similar situation occurs on May 10, in this case $\frac{\Delta S}{\Delta T}_{H32}$ is definitely negative

yet $\frac{\Delta\theta}{\Delta T}_{H164}$ is appreciable. The temperature difference between Q10 and H164 is not always consistent with $\frac{\Delta\theta}{\Delta T}_{H164}$ but the trends in $\theta_{Q10} - \theta_{H164}$ usually are. For example, during April 20-25, a time of deep water exchange, $\frac{\Delta\theta}{\Delta T}_{H164}$ is negative even though $\theta_{Q10} - \theta_{H164}$ is positive. However, it is apparent that $\theta_{Q10} - \theta_{H164}$ is decreasing rapidly during this period. The Quatsino surface water have cooled considerably during this period but the temperature at Q10 is not representative of the inflowing waters.

This first attempt at parameterizing the exchange processes has achieved some measure of success. Better results may be achieved if salinity data from H164 are available and if a better description of the inflowing waters is obtained. Ultimate success depends upon improved modelling of the exchange mechanism.

3.4 Further Details of Deep Water Exchange

A closer examination of the 1974 data reveals several subtle details not considered in our model. The effect of the fortnightly amplitude variation of the tides can be seen in the mean flood currents at 155 metres (see Figure 4). The magnitudes of the mean flood currents are appreciably reduced between April 27 and May 2, a period of neap tides. The mean flood currents at 5m and 70 m do not exhibit this tidal modulation. The salinity and temperature data from all three depths shows no appreciable tidal modulation.

Cross-spectral analysis of salinity and speed at 155 m reveals that at frequencies higher than 8 cycles/day the time lag between salinity and speed is less than 10 minutes although coherence squared is less than 0.4. This suggests that the more saline parcels of water are usually passing at higher speeds.

An important detail not discussed earlier is the apparently anomalous low salinity at 155 m during the initial stages of deep water exchange. The salinity initially drops below ebb tide levels and then increases to a maximum in the latter portion of the flood tide, whereas the bottom currents initially rise rapidly to maximum and then generally decrease in the latter portion of the flood tide. This decrease in salinity during the early flood tide appears to be inconsistent with concepts of a salinity induced density current. The explanation may lie in the effect of mine tailings suspended within the sinking jet. If tailings settle out on the Quatsino Narrows side of the Rupert-Holberg basin during the ebb tide, they may be resuspended by the more vigorous action of the inflowing jet, thus changing the density of the jet sufficiently to cause it to sink to the bottom of the basin, even though it is initially less saline than the surrounding fluid. As the tide progresses the salinity of the jet rises above that of the surrounding water, although suspended tailings would continue to influence the jet's density.

A second possibility, which is consistent with the above hypothesis, is that the operation of the sensors is affected by suspended tailings. Calculations based on the proportion of suspended particles necessary to

produce the observed conductivity change, show that the density effect of the suspension above would correspond to the effect of almost doubling the salinity. The concentration of suspended particles necessary to maintain a marginally denser initial flow are only 0.2-0.3 gm/litre which would produce no noticeable effect on the conductivity of the water. Thus whether or not we allow for effects of tailings on the sensor operation, it seems likely that they play an important role in determining the density of the jet and may influence its location in the water column during the early part of the flood tide.

There are two major implications of this last argument; first, the density can no longer be adequately described by only temperature and salinity as the amount of suspended solids significantly affects the water density. Second, the presence of mine tailings adds an interactive aspect to the deep water exchange process. The resuspension of mine tailings by the flood currents increases the density of the water thereby promoting a density flow.

The observed lower salinities at 70 m during the flood tide may be due to the downward mixing of fresher water by the currents in the upper half of the water column.

4. SUMMARY AND CONCLUDING REMARKS

Models of the deep water exchange and the salt extraction process in Rupert-Holberg Inlet have been developed from existing temperature, salinity and current velocity data. The area where the exchange processes act is at the junction of Rupert-Holberg Inlet with Quatsino Narrows, the general area between Hankin Pt. and the north end of Quatsino Narrows. Tidal mixing and the density of the incoming tidal jet are the two main features considered.

In the model of deep water exchange the tidal jet is negatively buoyant; consequently it flows down the side of Rupert-Holberg Inlet to the bottom as a density current. A portion of this flow is deflected vertically by the far shore at Hankin Pt. Driven by the horizontal density gradients the denser waters flow along the basin floor displacing the less dense waters upward in the water column. As the input of denser water of depth continues the density of the water column increases. Temperature, salinity and current velocity measurements made in the spring of 1974 provide good evidence of deep water exchange.

In the salt extraction process the incoming tidal jet is buoyant; consequently its activity is concentrated in the upper portions of the water column. Strong vertical mixing, deriving its energy from the tidal exchange then works to decrease the resulting salinity stratification, thus the salinity of the surface waters is increased at the expense of the deeper waters. The salt that is mixed upwards is then drawn out of Rupert-Holberg Inlet on the ebb tide. As the salt extraction process continues the salinity of the water column decreases. The flux of salt towards the active area is driven by horizontal density gradients created by tidal mixing in front of the Narrows.

In both these models the vertical extent of the tidal jet is determined by the density difference between the resident waters and the inflowing jet and also by the speed of the tidal jet from which the mixing mechanism derives its energy. In addition the 'T' shaped geometry of the junction increases the

vertical penetration of the jet.

Deep water exchange is dominant during the spring and summer months when low precipitation and run-off and the presence of upwelled water in Quatsino Sound are responsible for the increased density of the inflowing water. The salt extraction process occurs in the fall and winter months when the density of the inflowing waters is reduced by high precipitation and run-off.

The first set of long term data has been successfully interpreted in terms of these exchange models, and an attempt at a more quantitative interpretation has also had some measure of success. Better results can be achieved with more representative and reliable long term data. Refinements have been made to the ongoing long term monitoring program and future analysis of these data will provide a better basis for modelling the exchange processes.

The widespread dispersion of mine tailings in Rupert-Holberg Inlet (Goyette, 1975) has added another dimension to the oceanography of this inlet. The active region in front of the Narrows is a turbidity source during times of deep water exchange when strong currents scour the bottom. The resuspension of mine tailings may modify the flow by increasing the density of the water. This raises the possibility of a feedback loop that could serve to extend the time of scouring action beyond the periods during which deep water exchange might be expected solely on the basis of temperature and salinity conditions.

This study has raised several interesting questions about the flushing of Rupert and Holberg Inlets. We still do not understand the significance of the T-junction geometry in front of the Narrows. Is this an essential feature determining the vertical extent of stirring and mixing during the salt extraction phase as suggested by Drinkwater (1973), or can such a process occur solely as a result of intense turbulence near the inflowing jet? It would be useful to understand the effect on efficiency of the salt extraction mechanism of small changes in salinity of the inflowing water; does a more saline jet, which penetrates deeper, remove salt more effectively than a fresher inflow? What effect will density stratification, within the jet itself, have on the exchange? There is also a real need to verify our hypothesis for turbidity effects on the density of the jet. It is not inconceivable that the structure of the exchange process could be altered by man, either unintentionally through the resuspension of mine tailings, or perhaps intentionally by changing surface salinities through the control of river discharge.

REFERENCES

- Anderson, J.J. and A.H. Devol. 1973. Deep water renewal in Saanich Inlet, an intermittently anoxic basin. Estuarine and Coastal Marine Science 1, 1-10.
- Bell, W.H. 1973. The exchange of deep water in Howe Sound Basin. Marine Sciences Directorate, Pacific Region, Victoria, B.C. Pacific Marine Science Report 73-13.
- Canadian Hydrographic Service. 1972. Tidal currents, Quatsino Narrows, British Columbia. Queen's Printer, Ottawa.
- Canadian Hydrographic Service. 1974. Canadian tide and current tables. Volume 6. Queen's Printer, Ottawa.
- Cannon, G.A. 1975. Observations of bottom-water flushing in a fjord-like estuary. Estuarine and Coastal Marine Science 3, 95-102.
- Drinkwater, K.F. 1973. The role of tidal mixing in Rupert and Holberg Inlets. M.Sc. Thesis, University of British Columbia, Vancouver, B.C.
- Drinkwater, K.F. and T.R. Osborn. 1975. The role of tidal mixing in Rupert and Holberg Inlets, Vancouver Island. Limnology and Oceanography 20(4): 518-529.
- Gade, H.G. 1970. Hydrographic investigations in the Oslofjord, a study of water circulation and exchange processes. University of Bergen, Geophysics Institute, Report 24.
- Goyette, D.E. 1975. Marine tailings disposal - case studies. Presented at: Mining Effluent Regulations/Guidelines and Effluent Treatment Seminar, Banff, Alberta.
- Hollister, H.J. and A.M. Sandnes. 1972. Sea surface temperatures and salinities at shore stations on the British Columbia coast 1914-1970. Marine Sciences Directorate, Pacific Region, Victoria, B.C. Pacific Marine Science Report No. 72-13.
- Lafond, C.A. and G.L. Pickard. 1975. Deep water exchanges in Bute Inlet, British Columbia. J. Fish. Res. Bd. Canada 32(11): 2075-2089.
- Ozretich, R.S. 1975. Mechanism for deep water renewal in Lake Nitinat, a permanently anoxic fjord. Estuarine and Coastal Marine Science 3: 189-200.
- Pickard, G.L. 1963. Oceanographic characteristics of inlets of Vancouver Island, British Columbia. J. Fish. Res. Bd. Canada 20(5): 1109-1144.

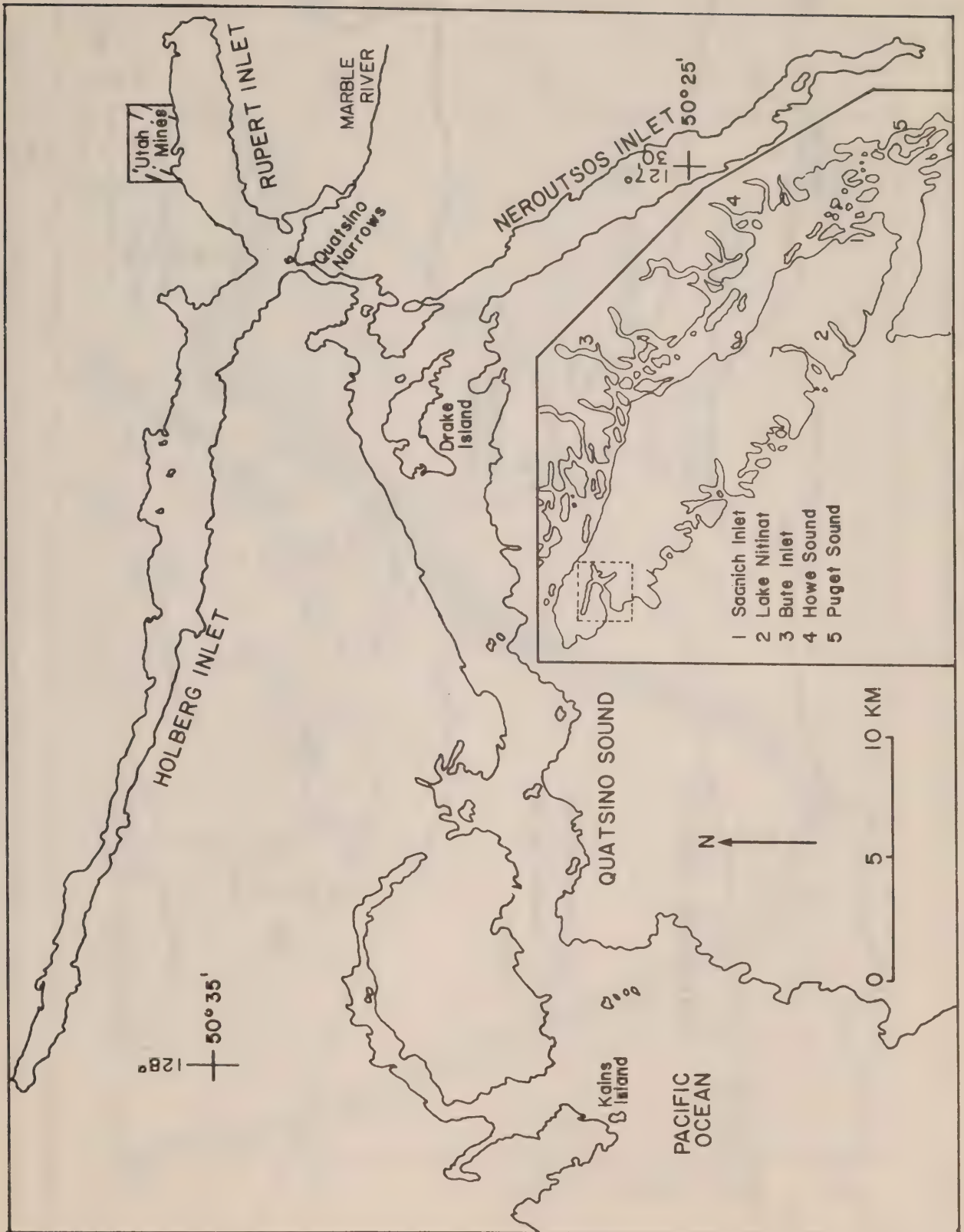


Figure 1. Map of Quatsino Sound, Rupert-Holberg Inlet and Neroutsos Inlet.

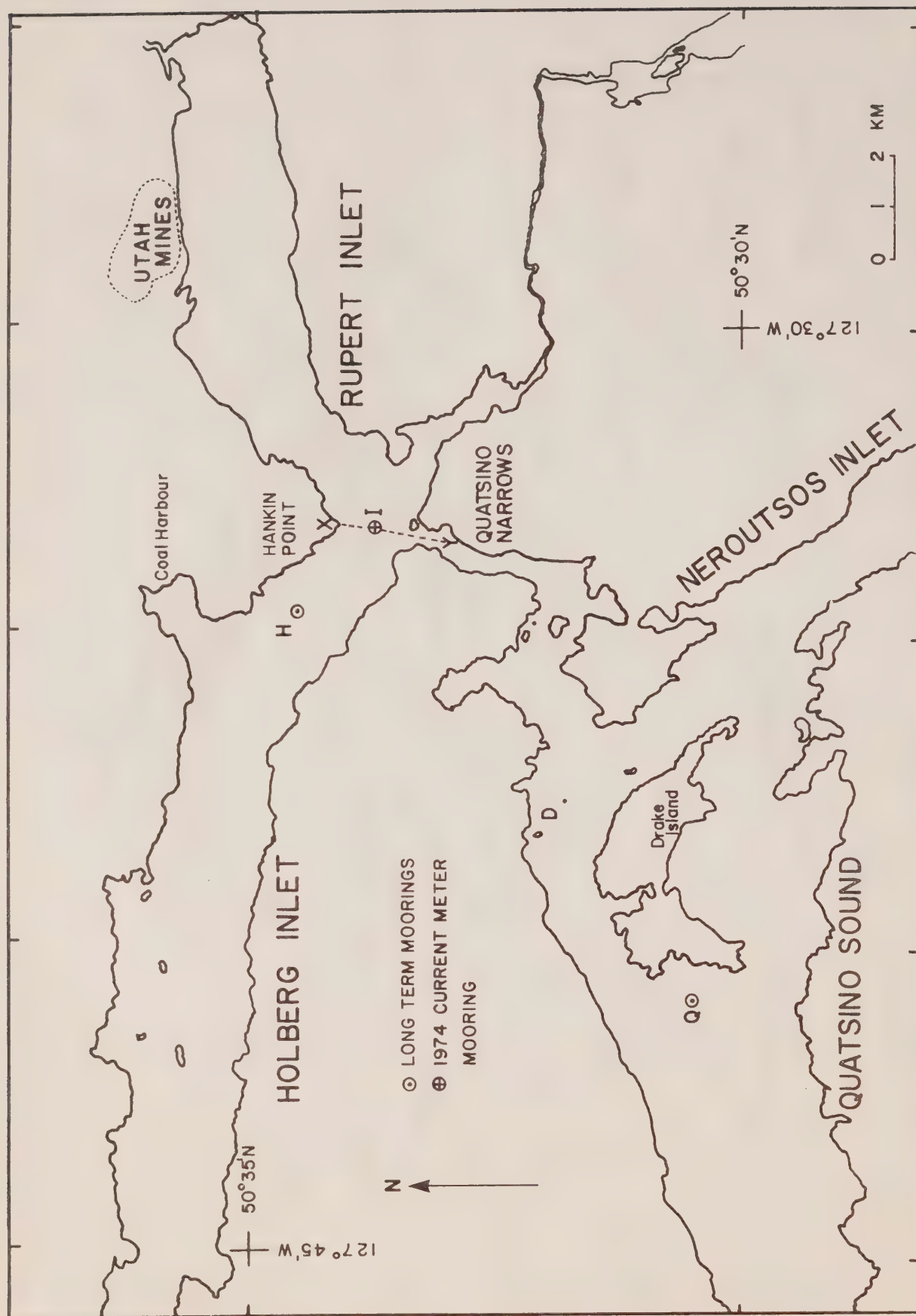


Figure 2. Map of inner Quatsino Sound and Rupert-Holberg Inlet showing locations of current meter and temperature, salinity stations.

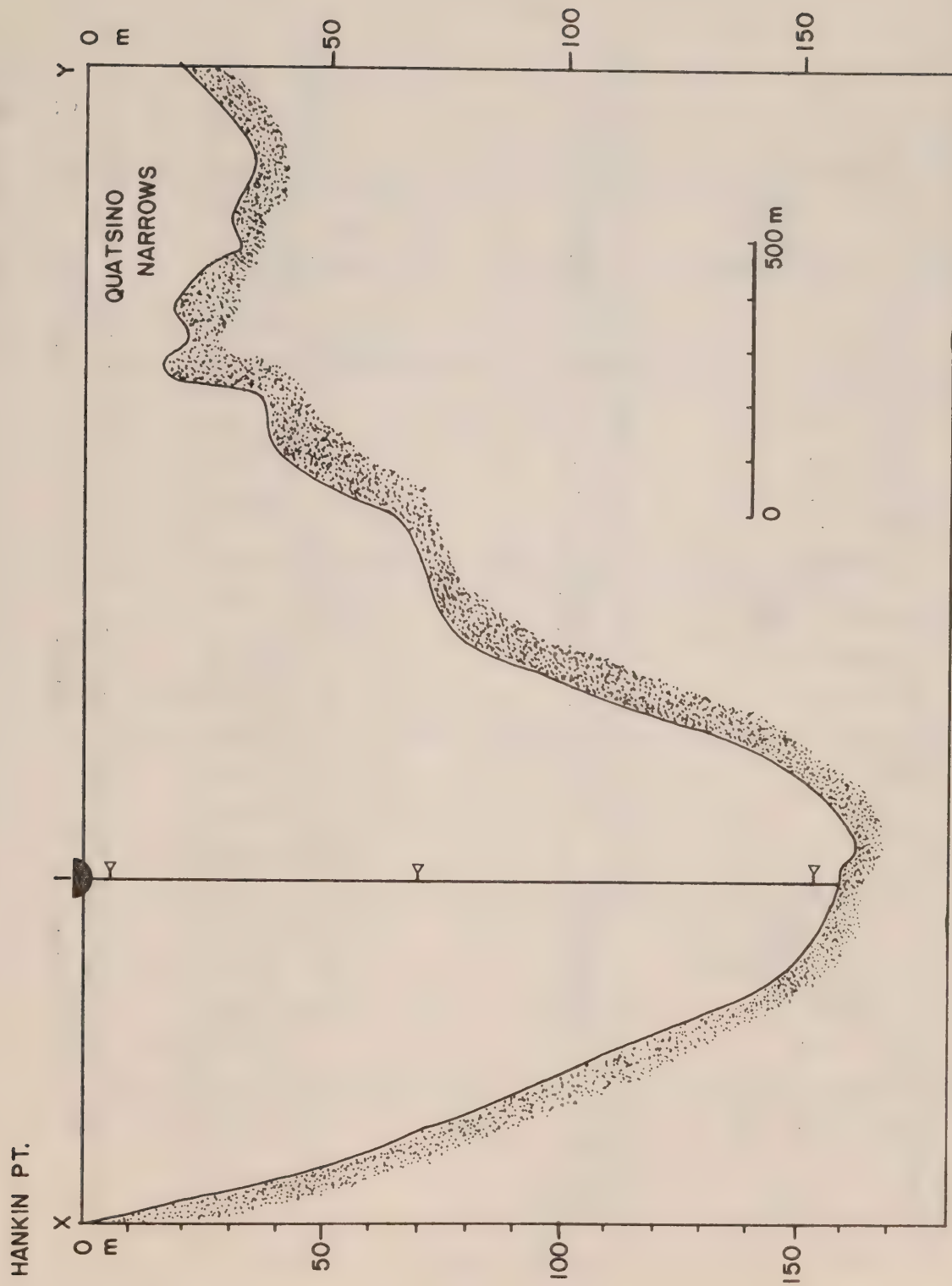


Figure 3. Sectional diagram, from Hankin Pt. to Quatsino Narrows, showing 1974 current meter mooring

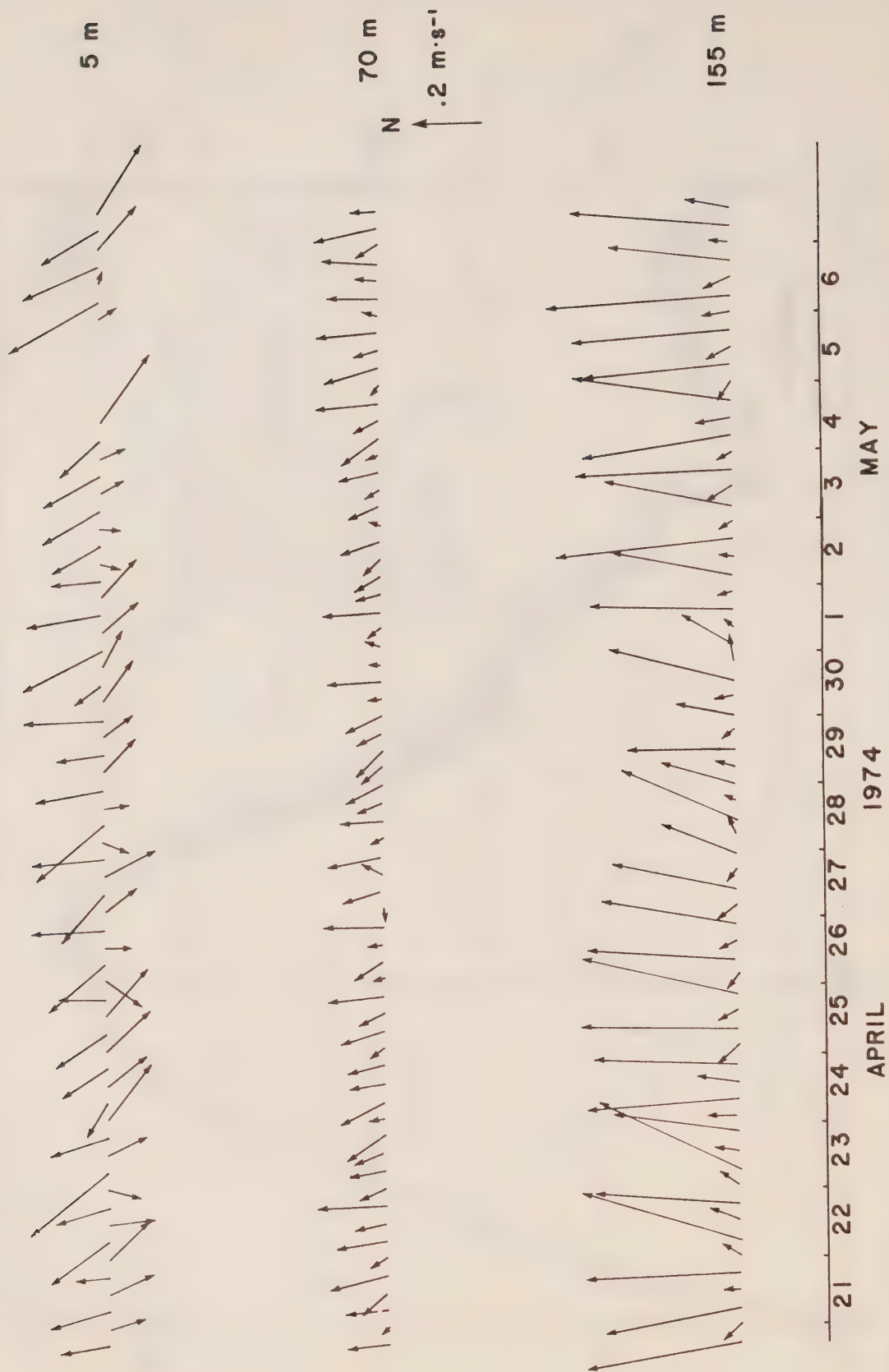


Figure 4. Mean ebb tide and mean flood tide current vectors of the 1974 current meter data.

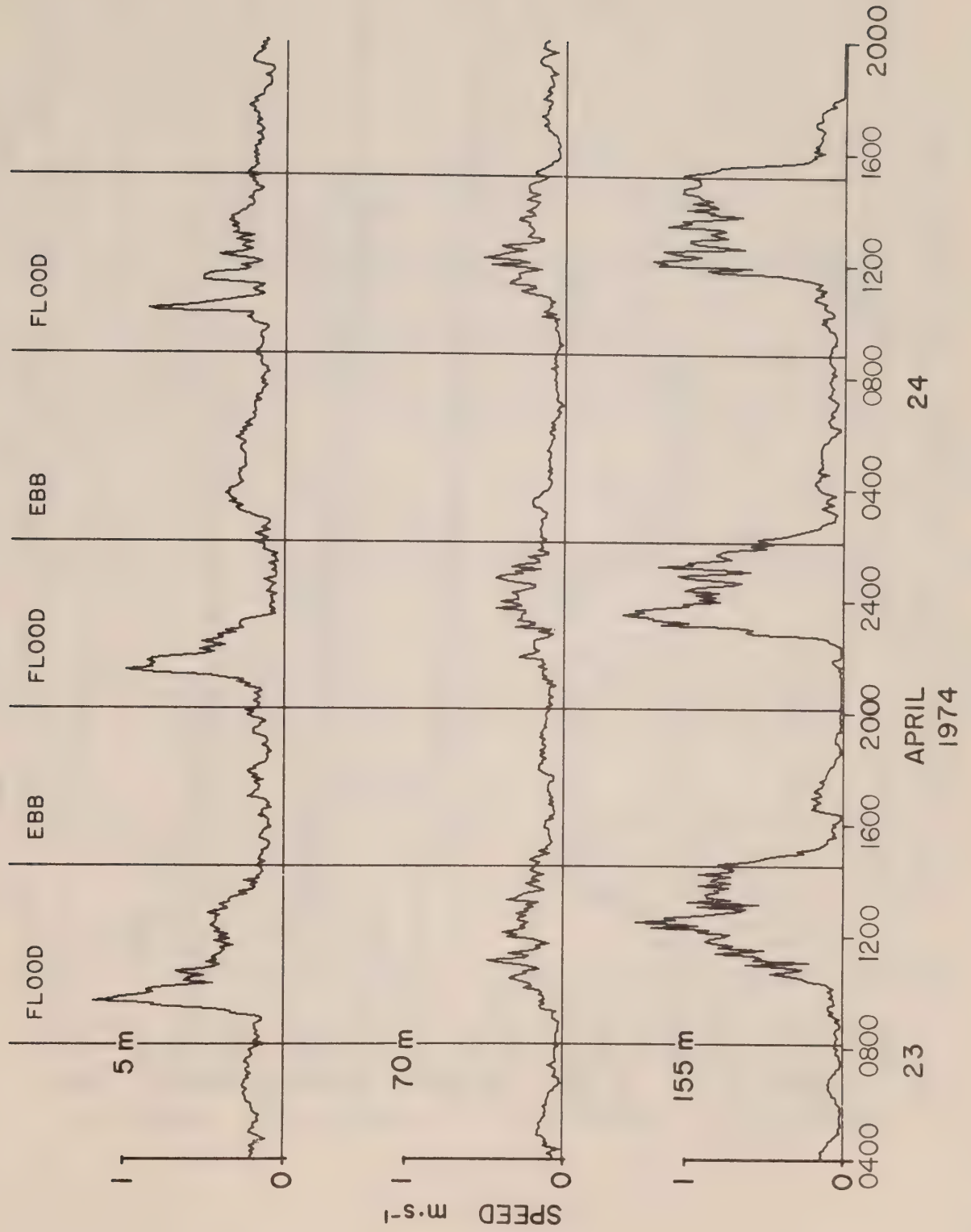


Figure 5. A portion of the actual time series of current speed from 5, 70 and 155 metres.



Figure 6. Mean ebb tide and mean flood tide salinities and temperatures from 1974 data.

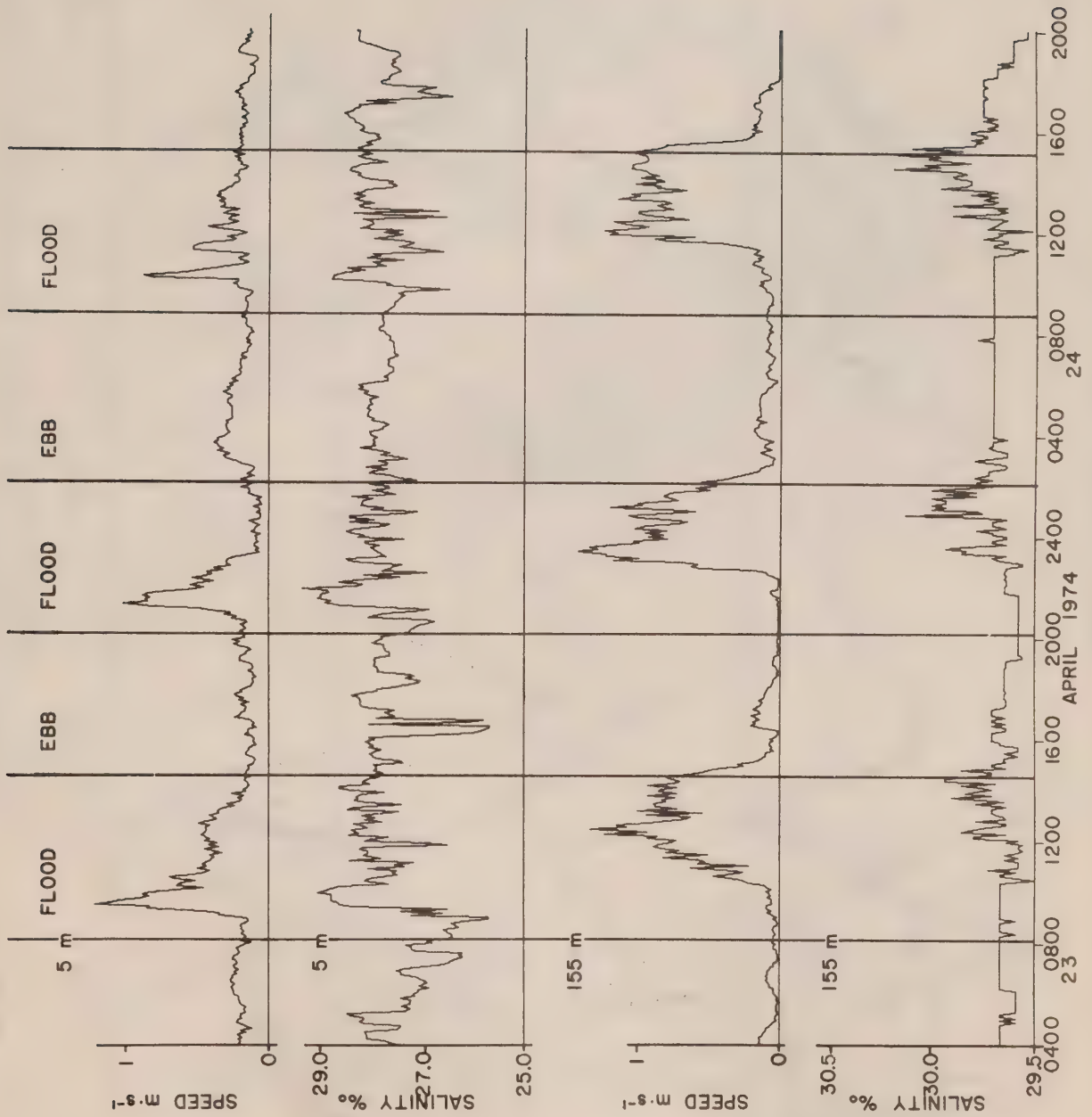


Figure 7. A portion of the current speed and salinity time series of the 1974 data from 5 and 155 metres.

QUATSINO SOUND ST D

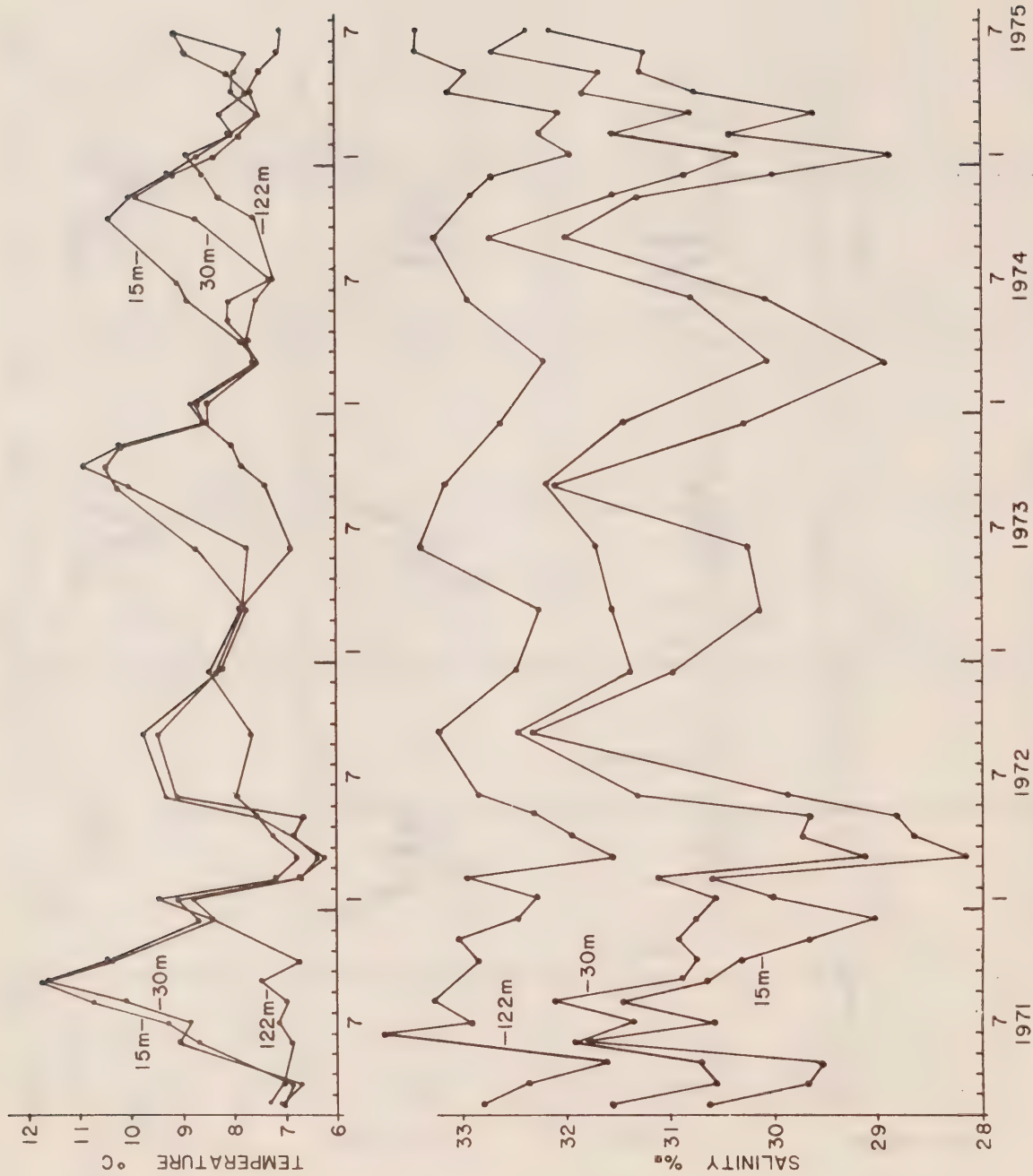


Figure 8. Representative background temperature and salinity data from Quatsino Sound. For location of Station D see Figure 2.

HOLBERG INLET ST H

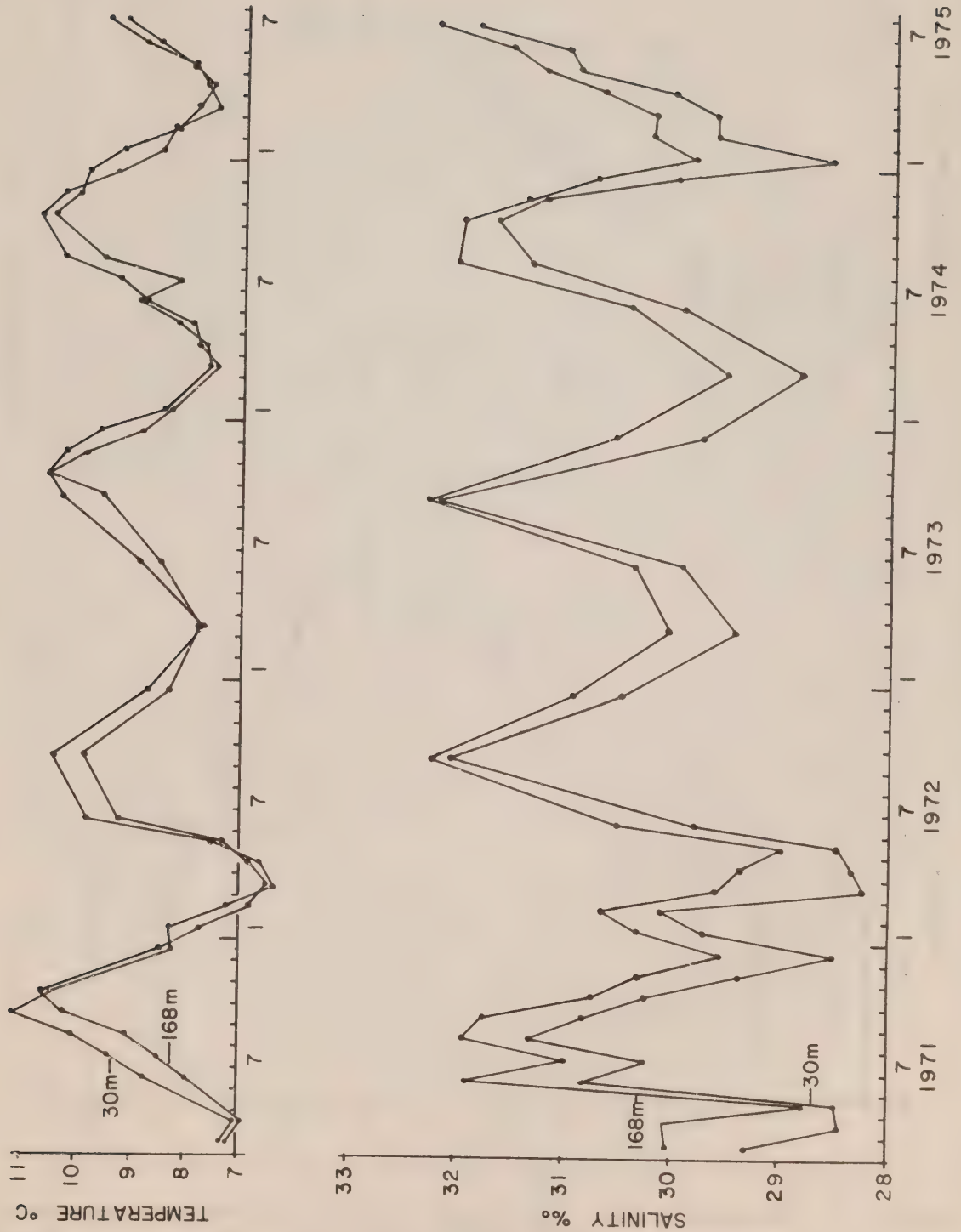


Figure 9. Representative background temperature and salinity data from Rupert-Holberg Inlet. For location of Station H see Figure 2.

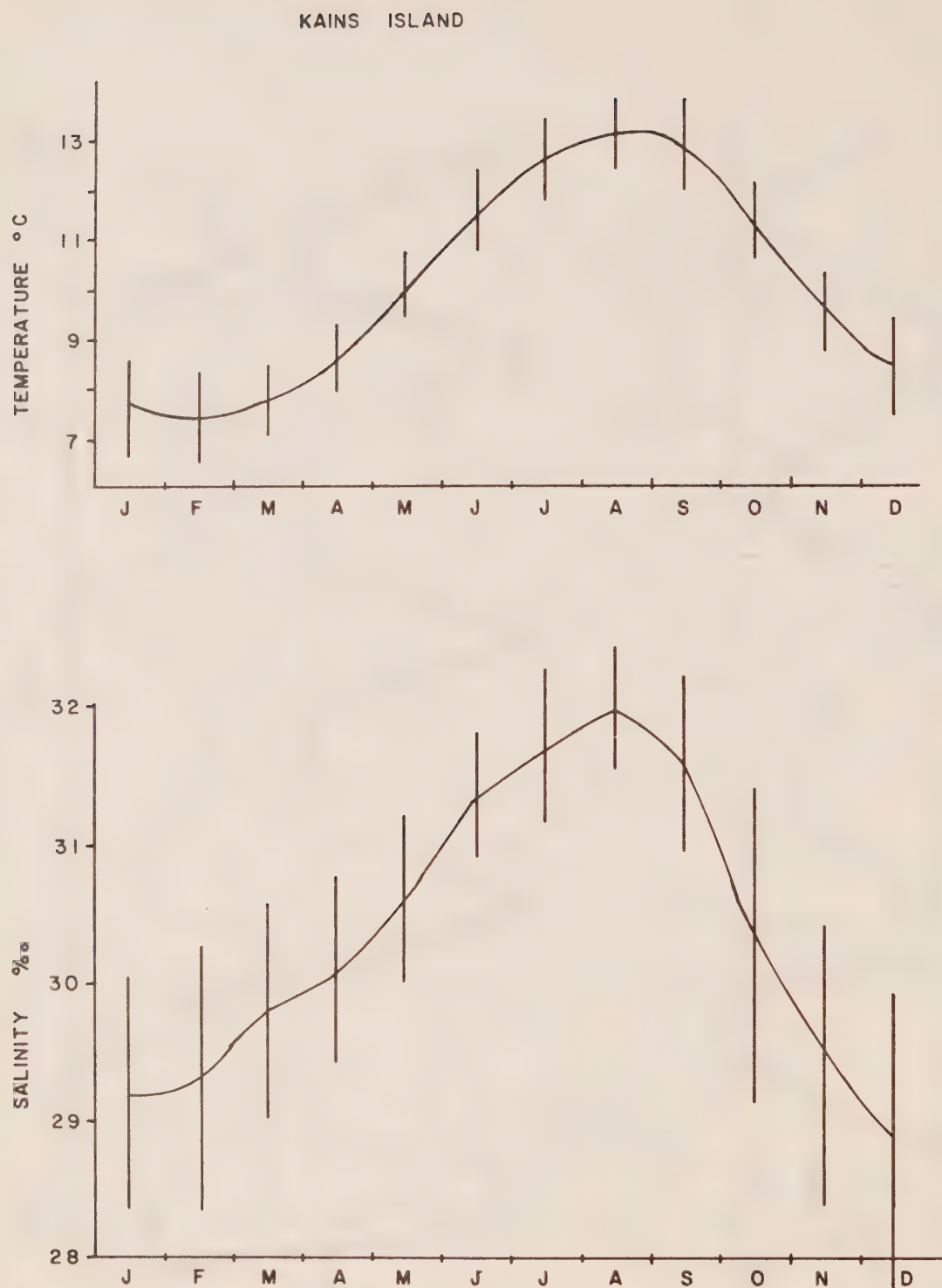


Figure 10. Thirty-six year grand mean of daily sea surface temperature and salinity from Kains Island Lighthouse. Vertical bars represent standard deviation. For location of Kains Island see Figure 1.

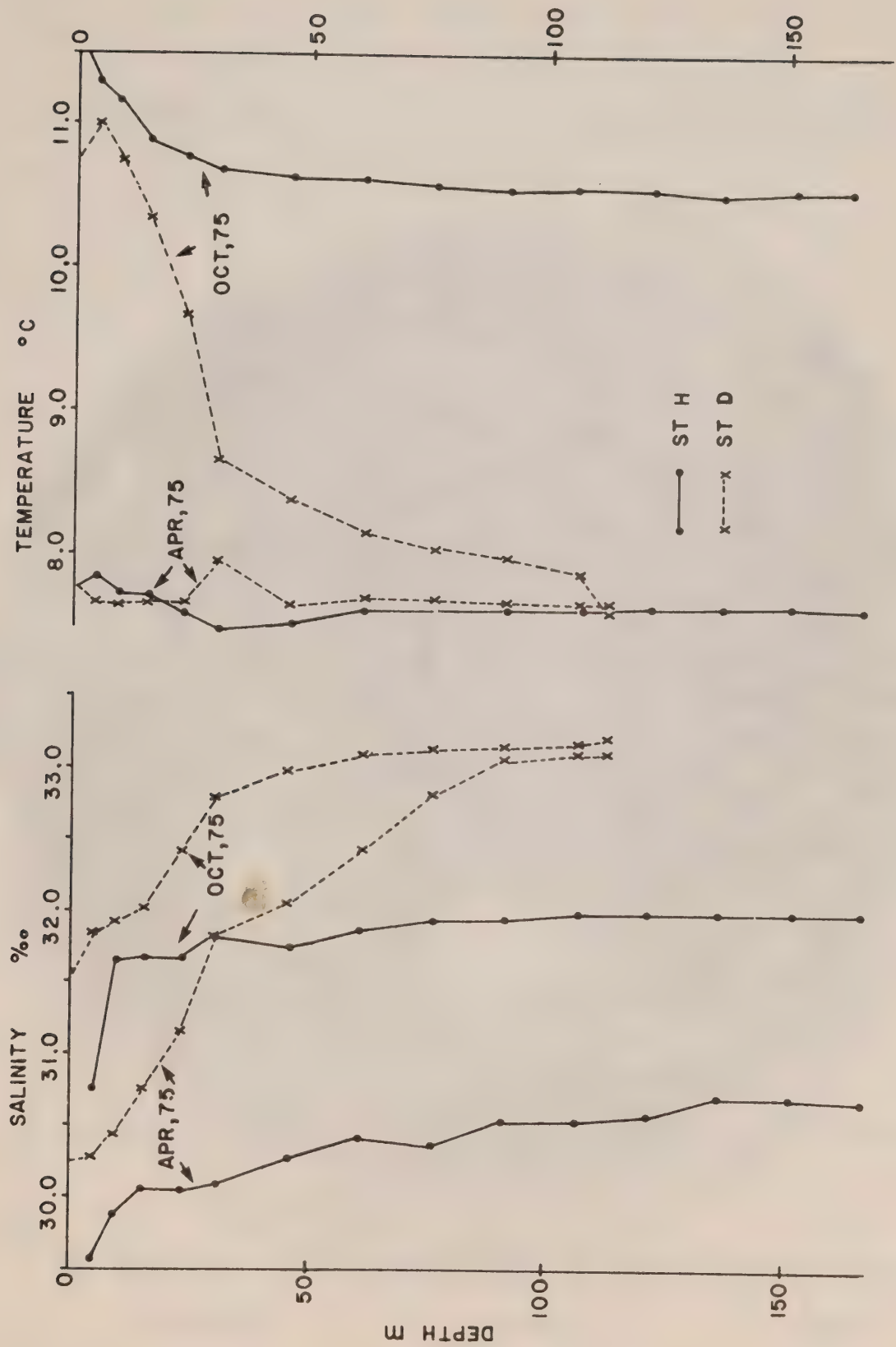


Figure 11. Representative temperature and salinity profiles from Quatsino Sound (St. D) and Rupert-Holberg Inlet (St. H).



Figure 12. Balloon photograph of active region in front of Quatsino Narrows.

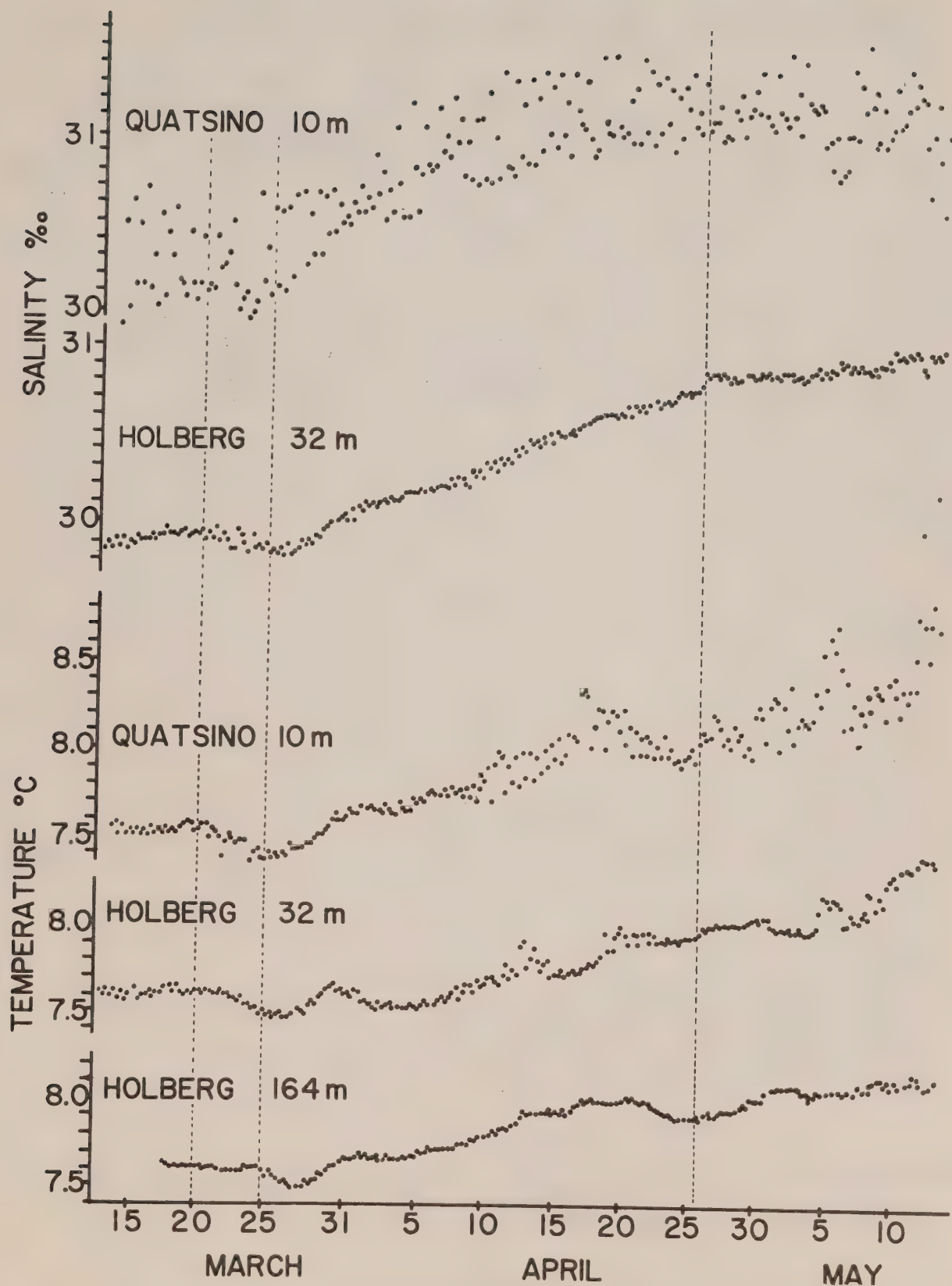


Figure 13. Mean ebb tide and mean flood tide salinities and temperatures from the first set of long term data, 1975.

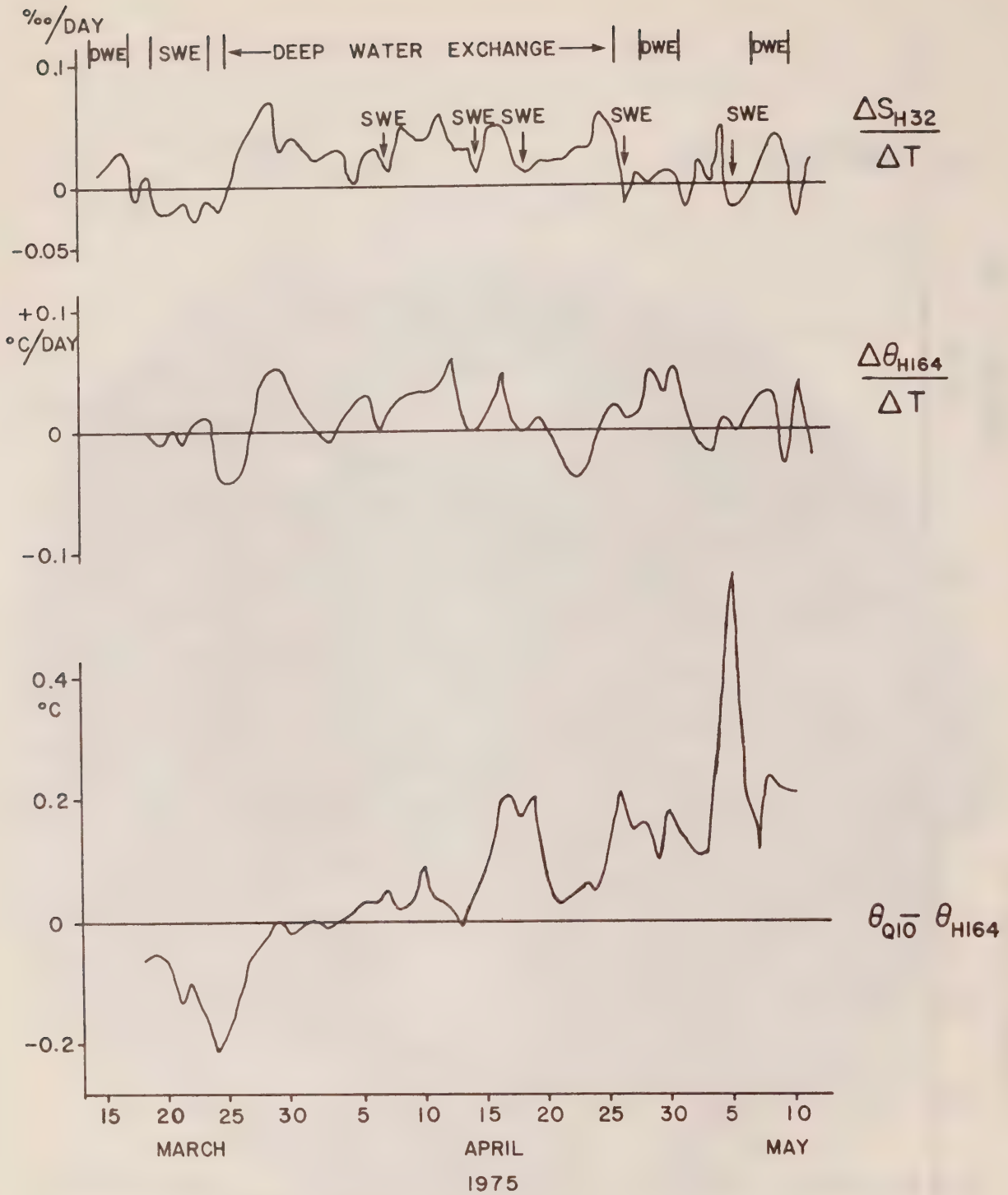


Figure 14. Daily rate of change of salinity at H32 and temperature at H164, and temperature difference between Q10 and H164. (DWE = Deep Water Exchange, SWE = Surface Water Exchange).

CAI EP 321
-76R11

Pacific Marine Science Report 76-11

Government
Publications

**ANALYSIS OF SALINITY AND TEMPERATURE RECORDS
TAKEN AT THREE LIGHTHOUSE STATIONS ON THE B.C. COAST**

by

Ian Webster and David M. Farmer

**INSTITUTE OF OCEAN SCIENCES, PATRICIA BAY
Victoria, B.C.**



For additional copies or further information, please write to:

Environment Canada
Institute of Ocean Sciences, Patricia Bay
512 - 1230 Government Street
Victoria, B.C.
V8W 1Y4

71 SEP 321
76 R11

Pacific Marine Science Report 76-11

ANALYSIS OF SALINITY AND TEMPERATURE RECORDS
TAKEN AT THREE LIGHTHOUSE STATIONS ON THE B.C. COAST

by

Ian Webster and David M. Farmer

Institute of Ocean Sciences, Patricia Bay
Victoria, B.C.

March 1976

This is a manuscript which has received only limited circulation. On citing this report in a bibliography, the title should be followed by the words "UNPUBLISHED MANUSCRIPT" which is in accordance with accepted bibliographic custom.

ABSTRACT

Daily sea surface temperature and salinity observations have been made at numerous locations along the B.C. coast for varying lengths of time. This report examines 35 years of data collected from 3 of these light stations at Langara Island, Kains Island and Amphitrite Point. Its primary purpose is to develop techniques which could be applied to the analysis of the data from the other light stations. The interdependencies of temperature, salinity and local rainfall data are examined as well as the relationships between data from separate stations. Techniques applied are simple annual and monthly averaging procedures and the relatively modern technique of spectral analysis.

TABLE OF CONTENTS

	<u>Page</u>
ABSTRACT	i
TABLE OF CONTENTS	iii
PREFACE	1
I. INTRODUCTION	2
II. DATA SOURCES	3
A. Stations	3
TABLE I	3
B. Procedures and Equipment	3
1. Temperature and Salinity Data	3
2. Rainfall Data	4
C. Summary of Available Data	4
III. DATA ANALYSIS	6
A. Data Preparation	6
1. Temperature and Salinity Data	6
TABLE II	6
2. Rainfall Data	7
B. Analysis Method	7
1. Low Frequency Analysis	7
2. Spectral Analysis	7
a) Choice of Block Size	7
b) Spectral Filters	8
c) Fast Fourier Transform	9
d) Spectra, Coherences and Phases	10
e) Plotting of Spectra	11
3. Seasonal Variations	13

TABLE OF CONTENTS, CONTINUED

	<u>Page</u>
IV. DISCUSSION OF RESULTS	14
A. Low Frequency Analysis	14
1. Temperature	14
2. Salinity	14
3. Rainfall	14
B. Spectral Analysis Results	15
TABLE III	15
1. Temperature	15
a) Power Spectra	15
b) Coherences and Phases	16
2. Salinity	16
a) Power Spectra	16
b) Coherences and Phases	17
3. Rainfall Power Spectra	17
4. Kains Island: Temperature-Salinity and Rainfall-Salinity Coherences and Phases	18
5. Amphitrite Point: Temperature-Salinity and Rainfall- Salinity Coherences and Phases	18
6. Langara Island: Temperature-Salinity and Rainfall- Salinity Coherences and Phases	19
C. Monthly Means	19
1. Temperature, Salinity and Rainfall	19
2. Standard Deviations of Salinity and Temperature; T,S Correlation	20
V. SUMMARY AND CONCLUSIONS	21
REFERENCES	23
LIST OF FIGURES	25

PREFACE

This report represents the first stage of a critical analysis of the lighthouse salinity and temperature data collection programme. Daily observations of temperature and salinity have been collected at various lighthouse stations along the British Columbia coast for over forty years. The quality of data has changed considerably with perhaps the most significant alteration resulting from the switch to hydrometer determination of salinity in 1969. Nevertheless, the length of the data records permits some interesting analyses using modern spectral techniques and in this first report some of these are developed and applied to three time series obtained at relatively exposed stations on Vancouver Island and the Queen Charlotte Islands.

The intention of this report therefore is to present certain interesting features of the data together with an account of the techniques used in the presentation. This will serve both as a guide to future analysis of lighthouse station data and as an indication of the type of information that may be derived in this way. We hope eventually to be able to extend this form of analysis and presentation to data derived from the remaining stations.

Our final goal will be to carry out a careful analysis of the relative importance of each station in providing new information, not available from data collected at other stations and also to determine the significance to the data quality of changes in observational technique. We shall then be in a position to rationalise the data collection programme and ensure that the particular needs of users are met in the most economical and effective manner.

I. INTRODUCTION

Daily sea surface temperature and salinity observations have been made at numerous locations along the British Columbia coast for varying lengths of time. Most of the stations are at Ministry of Transport lighthouses where the lightkeepers voluntarily collect the observations. The daily oceanographic data to 1970 have been published in 30 annual record volumes (listed under Data Records) and the results summarized in Pacific Marine Science Report 72-13 (Hollister and Sandnes, 1972).

The purpose of this report is primarily to develop techniques for presentation of certain important features of the data. The report attempts to present an account of long and short term variations, the relationships between their variations and possible relationships between the data of different stations. Initially it was decided to concentrate the analysis on 3 light stations on the outer coast of British Columbia at Langara Island, Kains Island and Amphitrite Point. For Langara Island and Kains Island daily precipitation records exist for most of the period of temperature and salinity observations whereas for Amphitrite Point they exist for 10 years of that period. A detailed analysis of the relationship of daily precipitation to salinities is carried out to determine possible causes of salinity variation.

As each data series consists of approximately 35 years of daily samples it was considered that the analysis should be split into a low frequency section and a high frequency section. The low frequency analysis examines variations of period 1 year or longer such as long term trends. The high frequency analysis is dealt with statistically using the technique of spectral analysis. Using this technique variations of period down to 2 days are examined. Other aspects of the data such as mean seasonal variations are looked at using monthly averaging procedures.

Each of the stations, Langara Island, Kains Island and Amphitrite Point, commenced observations within a year or two of 1935. Observations have been made more or less continuously on a daily basis up to the present. Over the years temperatures have been measured with various types of thermometers with accuracy 0.5°F (0.3°C) or better. Salinities were determined in the laboratory on samples collected in the field by a modified Mohr titration until 1959 then by a conductive salinometer. Towards the end of 1969 collection of salinity samples was replaced by measurement of salinity by hydrometers. The estimated accuracy of the salinity determination fell from better than 0.06 PPT for the titration and salinometer methods to 0.3 PPT for the hydrometer. Because of the reduced accuracy of the salinity data after 1969 the data considered in this report runs to the end of 1969.

NOTE: Throughout this report PPT means Parts Per Thousand.

II. DATA SOURCES

A. Stations

The locations of the 3 light stations Langara Island, Kains Island, and Amphitrite Point are shown in Figure 1. Daily precipitations are observed at the Langara Island and Amphitrite Point light stations whereas the closest precipitation measurements to Kains Island are made 20 miles to the east at Quatsino situated on the north side of Quatsino Inlet. The station locations and the data record lengths for precipitation, temperature, and salinity observations are tabulated below:

TABLE I
Summary of Station Locations

<u>Station</u>	<u>Observed Parameters</u>	<u>Latitude N</u>	<u>Longitude W</u>	<u>Data Duration</u>
Langara Is.	T, S	54° 15'	133° 03'	Nov. 1936-Aug. 1937 March 1940-present
" "	R	"	"	July 1936-present
Kains Is.	T, S	50° 27'	128° 02'	Jan. 1935-present
Quatsino	R	50° 32'	127° 37'	June 1895-present
Amphritrite Pt.	T, S	48° 55'	125° 32'	Sept. 1934-present
" "	R	"	"	Jan. 1958-present

T - Temperature
S - Salinity
R - rainfall

B. Procedures and Equipment

1. Temperature and Salinity Data

The observational procedures are summarized from descriptions given in Pacific Marine Science Report 72-13 (Hollister and Sandnes, 1972). The daily observation is made within 1 hour before the time of high tide, light schedules and other duties permitting. From 1934 the standard procedure included the collection of a sea water sample in a glass bottle and a temperature measurement both taken from a depth of 3 feet below the surface. In 1961 the style of sample bottle changed when a new plastic lined screw cap was introduced to replace the original waxed cork method of sealing. Tests on the new bottles showed salinity increases of up to 0.02 PPT for sea water samples stored over a period of 180 days.

The salinities prior to 1959 were measured using a modified Mohr titration method with an estimated accuracy of 0.06 PPT. Early in 1959 conductive salinometers were used for this purpose, a method which has an estimated accuracy of 0.03 PPT. From late 1969 salinity determinations have been done using a hydrometer in a 25 oz. water sample. An accuracy of 0.3 PPT is estimated for salinities collected by this method.

Temperature has been measured by a thermometer mounted inside a protective case on the end of a sampling rod. During the period since 1935 a number of varieties of thermometer have been used to measure the sea water temperature. Indications are that the earliest thermometers were of the mercury filled type which had an estimated accuracy of something like 0.5°F. (0.3°C). A red liquid filled thermometer reading Fahrenheit degrees with an estimated accuracy of 0.5°F (0.3°C) was in use between 1937 and 1939. This was replaced by a Celsius reading mercury thermometer which in turn was replaced in mid 1949 by a similar type with a Fahrenheit scale. Both thermometers in use after 1939 were compared with a laboratory thermometer and had a maximum allowable scale error of 0.3°F (0.2°C).

The daily temperature and salinity observations used in this study were taken from a magnetic tape supplied by the Marine Environmental Data Service of Environment Canada. Data was available for 17 light stations starting in 1914 and continuing until the end of 1973. Because temperature was written on the tape as degrees Fahrenheit and salinity as parts per thousand (PPT) these will be the units used in this report. The corresponding Celsius temperature is included also in brackets.

2. Rainfall Data

Daily rainfall data was made available for the 3 stations on a magnetic tape supplied by the Climatology Division of the Meteorological Branch of the Department of Transport. This data is the estimated rainfall in inches for consecutive 24 hour climatological days. The commencement time of the climatological day has been changed in the period since 1935. From January 1, 1933 to December 31, 1940 precipitation was measured at 0630 Local Standard Time (LST) on the day following the calendar day to which the precipitation was accredited. In the period January 1, 1941 to December 31, 1954 this measurement time was changed to 0730 Eastern Standard Time, that is to 0430 LST on the B.C. coast. On June 1, 1957 the observation time was advanced 1/2 hour to 0400 LST. From July 1, 1961 to the present the climatological day begins at 0600 GMT or at 2200 LST on the previous evening.

C. Summary of Available Data

The bar graphs shown in Figure 2 illustrate the essential features of data availability for rainfall, temperature and salinity at each station. Also indicated are the periods for which different measurement techniques apply.

Temperature and salinity have been measured continuously at Kains Island and Amphitrite Point at least from January 1, 1935 to the present whereas this continuous data is only available at Langara Island from mid 1940 to the present. It was therefore decided that January 1, 1935 would make a convenient starting point for the analysis. After the introduction of hydrometers for

salinity determinations in late 1969 the accuracy of the salinity measurement would be expected to be an order of magnitude less than before so that some time near the end of 1969 would be a desirable termination point for the analysis. For reasons which will be discussed the spectral analysis was carried out on 5 data blocks of 2560 days each which makes the analyzed section of data a total of 12800 days long. Thus the actual date for the termination of analysis is January 16, 1970.

III. DATA ANALYSIS

A. Data Preparation

As the temperature and salinity data were available from a source separate from the rainfall data the initial preparation of the 2 types of data was carried out differently. A block diagram of the data analysis scheme is seen in Figure 3.

1. Temperature and Salinity Data

Each record on the magnetic tape supplied by the Marine Environmental Data Service contained a daily temperature value and a daily salinity value. Hence, as far as the analysis procedures go temperatures and salinities are considered identically.

For all 3 stations there was a proportion of the data missing for one reason or another. The occurrence of missing data appeared to be random and varied in length from 1 day at a time to almost half a year of consecutive days on one occasion at Amphitrite Point. These missing data were merely filled in by a linear interpolation between the end points of the data gap. Also, the data were checked for any spikes. These were replaced by the arithmetic average of the 2 data points on either side of the spike. A single point was considered a spike if its value was more than 5.0°F (2.8°C) for temperature or 5.0 PPT for salinity different from the data points on either side of it. On examination of the data it was decided that any differences larger than 5.0 were probably due to error. Because of the large amount of missing data up to mid 1940 for Langara Island it was decided to omit analysis on the first block of data and to analyze the last 4 blocks of data only. The amounts of data either missing or occurring as spikes are given in the following table for the sections of data analyzed.

TABLE II

Summary of Data Either Missing or Occurring as Spikes

<u>Station</u>	<u>Total Points</u>	<u>T missing</u>	<u>S missing</u>	<u>T spike</u>	<u>S spike</u>
Kains Island	12800	338	432	6	7
Amphitrite Pt.	12800	926	1082	3	89
Langara Is.	10240	1375	1478	5	4

Kains Island appears to have the cleanest record with less than 4% of its data having to be filled in. Langara Island is the worst station whereas Amphitrite Point lies between it and Kains Island. The 13% of temperature data and 14% of salinity data missing for Langara Island would be expected to result in similar percentage losses in the variance at high frequencies. As the longest data stretch missing for Langara Island

is 105 consecutive days variations of period greater than about 1/3 of a year should be very little affected by missing data. Kains Island and Amphitrite Pointe will suffer smaller percentage losses in high frequency variance than will Langara Island, but the half year missing for Amphitrite Point will affect variances up to about that period to a certain extent.

2. Rainfall Data

The rainfall data supplied from magnetic tape had to be edited before it was analyzed. Each rainfall record was supplied with its date, which was checked to ensure that the records were exactly sequential. The only piece of missing data found in this fashion was an entire September in the data for Langara Island. Since September has a relatively low rainfall anyway it was felt that the replacement of that month's data by zeros should have little effect. Next, all rainfall data which was either trace or unknown was replaced by zero as were any data which had a precipitation magnitude greater than 10 inches for the day. Only over a period of several years in the data series for Langara Island did a few values over 10 inches appear. These values were so high they were obviously incorrect.

B. Analysis Method

Once the initial data preparation had been accomplished temperature, salinity and rainfall were analyzed in fairly parallel fashion. In order to examine different time scales the data analysis was divided into 3 sections; low frequency analysis, spectral analysis and an analysis of seasonal variations.

1. Low Frequency Analysis

The low frequency analysis is concerned with trends and variations of time scales greater than 1 year. To examine these scales the data for a given parameter at a given station have simply been averaged over a year and these yearly averages then plotted.

2. Spectral Analysis

The spectral analysis is carried out on a block size of 7 years with a sampling frequency of 1 value per day. Using such a sampling procedure the technique is capable of examining variations of period 7 years down to the Nyquist period of 2 days. Not much reliance can be placed on the lower frequency harmonics so that the results will be interpreted primarily for periods of 1 year and less. The computation of the spectra involves several steps. In order to reduce the leakage of energy from the harmonic of period 1 year into neighbouring harmonics the data are first passed through filters before they are Fourier transformed. The Fourier coefficients are then combined and averaged over bandwidth and over blocks to produce smoothed power spectra, coherences and phases.

a) Choice of Block Size

An inevitable consequence of the spectral analysis procedure is that energy present at a frequency not equal to a harmonic frequency will contribute to the computed energy at all the other harmonics. A

visual examination of the time series for temperature, salinity and rainfall indicates that most of the energy generally lies in the variation of period 1 year. To minimize the energy leaking from the annual variation into the other harmonics it was necessary to construct the block size such that one of its harmonics would have a period as close as possible to 1 year. This can be accomplished by choosing a block size close to an integral number of years in length. Also, the Fast Fourier Transform used to compute the Fourier coefficients operates much more efficiently if the number of points in the block is factorable into small prime numbers. Based on the preceding considerations a block size of 2560 days was chosen. For the complete 35 years of data it was thus possible to analyze 5 blocks of duration 7 years 3 days each. Furthermore 2560 can be factored into small prime numbers as $2560 = 5 \times 2^9$.

b) Spectral Filters

A preliminary spectral analysis of the temperature and salinity data indicated that the energy density at period 1 year was about 100 times that at higher frequencies. To minimize the effects of energy leakage from this harmonic, the data were run through digital filters in order to reduce the yearly energy before the Fourier transform. The low frequency Fourier coefficients were computed from data which had been passed through a low pass filter whereas those for frequencies above the annual frequency were computed from high pass filtered data.

The low pass digital filter consisted of a moving "box car" average of length 300 days. In constructing the filter a problem arose because the first and last averages ran off the ends of the data block. This problem was circumvented by taking a section from the end of the data block and fastening it to the beginning and vice versa. The transplanted sections were then matched to the ends of the data by adding a DC level to ensure there were no sudden jumps in the augmented record. In general a moving average of length Δ is easily shown to cause energy density at frequency f to be attenuated by the factor $G(f)$.

$$G(f) = \left[\frac{\sin(\pi f \Delta)}{\pi f \Delta} \right]^2$$

A filter length of 300 days was chosen so that this gain factor would be approximately 10^{-2} for the yearly harmonic.

Data with the low frequency components removed can be constructed by subtracting the signal passed by a low pass filter from the original data. The data used in the high frequency analysis was synthesized by first filtering the data by a moving box car average of length 75 days followed by subtraction from the original time series. This filter, which has a gain factor of:

$$G(f) = \left[1 - \frac{\sin(\pi f \Delta)}{\pi f \Delta} \right]^2$$

results in an attenuation of 10^{-2} at the yearly harmonic. The gain functions of both the high and low pass filters used prior to the Fourier transform are plotted in Figure 4.

c) Fast Fourier Transform

Fourier coefficients were computed from each block for both the high frequency and low frequency data using a Fast Fourier Transform (FFT) subroutine compiled by P. Chang of the Institute of Oceanography at the University of British Columbia. This subroutine is based on an algorithm by R.C. Singleton (1969). The FFT computes coefficients which satisfy the relation:

$$x(t_i) = A_0 + \sum_{n=1}^{N/2} A_n \cos 2\pi f_n t_i + \sum_{n=1}^{N/2} B_n \sin 2\pi f_n t_i$$

where:

$x(t_i)$ is the value of the data point at time t_i

A_n, B_n are the n 'th cosine and sine coefficients respectively.

N is the number of points in the data record.

f_n is the positive n 'th frequency harmonic.

If T is the time duration of the data record then $f_n = \frac{n}{T}$

The cosine and sine coefficients are computed by the FFT as:

$$A_n = \frac{2}{N} \sum_{i=1}^{N/2} x(t_i) \cos 2\pi f_n t_i$$

and

$$B_n = \frac{2}{N} \sum_{i=1}^{N/2} x(t_i) \sin 2\pi f_n t_i$$

d) Spectra, Coherences and Phases

From the Fourier coefficients power spectra, coherences and phases were computed. One can construct a power spectrum by considering the energy in the n 'th harmonic of a Fourier series which is $\frac{A_n^2 + B_n^2}{2}$ to be made up primarily of energy contributions in the frequency band $f_n - \frac{1}{2T}$ to $f_n + \frac{1}{2T}$. Since each harmonic has a bandwidth $\frac{1}{T}$ the energy per unit bandwidth or equivalently the power at frequency f_n is given by:

$$P(f_n) = \frac{T}{2} (A_n^2 + B_n^2)$$

The cospectrum between 2 data series is a measure of their 'in phase' power. The cospectrum at a particular frequency f_n can be constructed from the Fourier coefficients of the 2 series. Let the coefficients from the first series be unprimed and those of the second be primed then the cospectrum is defined as:

$$C(f_n) = \frac{T}{2} (A_n A_n' + B_n B_n')$$

Likewise a measure of the '90° out of phase' power is the quadrature spectrum given as:

$$Q(f_n) = \frac{T}{2} (A_n' B_n - A_n B_n')$$

In order to obtain reliable spectra it is usually recommended that spectral estimates be averaged in some fashion. In this study the spectra are 'smoothed' in 2 ways. First, the individual spectral estimates were averaged over frequency bands of width δf such that

$$\frac{\delta f}{f_c} = 0.1, f_c \text{ being the center frequency in the band. The band}$$

averaged power spectrum is thus:

$$\overline{P(f_c)} = \frac{1}{m} \sum_{n=c-m/2}^{c+m/2} P(f_n)$$

Where m is the number of harmonics in the band. The first 6 harmonics (after 0) were too far apart to be averaged with this bandwidth.

The smoothed spectra for each block were then averaged over the number of blocks B to produce a doubly smoothed spectrum.

$$\overline{\overline{P(f_c)}} = \frac{1}{B} \sum \overline{P(f_c)} \quad 1)$$

The double smoothing of co- and quad- spectral estimates was carried out in analogous fashion. The smoothed co-, quad- and power spectra can be combined to compute a coherence spectrum. This coherence is just a measure of the proportion of power coherent between 2 data series. At frequency f_c it is defined as:

$$K(f_c) = \left[\frac{\overline{\overline{C(f_c)}}^2 + \overline{\overline{Q(f_c)}}^2}{\overline{\overline{P(f_c)}} \cdot \overline{\overline{P'(f_c)}}} \right]^{\frac{1}{2}} \quad 2)$$

The phase of the coherent power can also be computed:

$$\phi(f_c) = \tan^{-1} \left[\frac{\overline{\overline{Q(f_c)}}}{\overline{\overline{C(f_c)}}} \right] \quad 3)$$

A measure of the reliability of a smoothed spectral estimate can be obtained by computing its standard deviation. The standard deviation of the band averaged spectral estimates from their block averaged mean is thus:

$$\sigma(f_c) = \left[\frac{\sum \overline{\overline{P}}^2 - B \overline{\overline{P}}^2}{B - 1} \right]^{\frac{1}{2}} \quad 4)$$

Each coherence, phase and power spectrum is actually a composite. Those spectral estimates of period 1 year or more were computed from the analysis of low frequency data whereas the higher frequency estimates were computed from data passed through the high pass filter. Before they were plotted all the spectral estimates and standard deviations were corrected for filter attenuation by multiplying them by the inverse of the filter gain functions.

e) Plotting of Spectra

The power spectra are plotted as $\log(f P(f))$ vs. $\log f$. By plotting frequency on a logarithmic scale the lower end of the frequency scale is suitably expanded to permit the observation of details in that part of the spectrum. Let δE be the energy contained in the frequency band δf . The relationship of δE and δf to the power

$P(f)$ is just:

$$\delta E \approx P(f) \delta f$$

since:
$$\delta(\log f) \approx \frac{\delta f}{2.3f}$$

$$\delta f = 2.3f \delta(\log f)$$

and:
$$\delta E \approx 2.3f P(f) \delta(\log f)$$

Thus $f P(f)$ is proportional to the energy contribution in the logarithmic frequency band $\delta(\log f)$.

The vertical bars on each smoothed spectral estimate define the limits $\overline{P(f_c)} \pm \sigma(f_c)$ where $\sigma(f_c)$ is the standard deviation of the block averages computed from 4).

Coherences and phases are both plotted on a linear scale versus $\log f$. A problem arises in determining what are significant coherences. If one were to compute coherences using equation 2) between 2 noise sources the expected coherence will decrease as the amount of smoothing increases. In fact the coherence will be 1.0 if it is computed from unsmoothed co-, quad-, and power spectral values. Jenkins and Watts (1968) derive the expected coherence between 2

noise sources as $h^{-1/2}$ where h is the product of the number of blocks and the number of frequency harmonics averaged in each block for a given coherence calculation. The variance of smoothed coherence for noise is approximated by Jenkins and Watts (1968) as:

$$\sigma^2 = \frac{1}{2h} (1 - K^2)^2$$

from which one can compute the standard deviation of noise coherence as:

$$\sigma = \left(\frac{1}{2h}\right)^{1/2} \left(1 - \frac{1}{h}\right)$$

In Figure 5 are plotted expected noise coherences together with their standard deviations for analysis of 1, 4 and 5 blocks of data. The upper standard deviation will be regarded as a 'level of significance' for the actual coherence spectra. The level appropriate to this number of blocks analyzed is indicated on each plot.

3. Seasonal Variations

Examination of the data records indicated that many important features were dependent on the seasonal cycle. Details of these features were difficult to see using the spectral analysis technique which tends to average them out. In order to look at seasonal variations average monthly salinities, temperatures and rainfall are computed for the section of record for which spectral analysis was done. Two cycles of these monthly averages were plotted.

Also examined was the seasonal variability in the high frequency fluctuations of salinity and temperature. A high frequency temperature fluctuation, T' , was obtained by subtracting data passed through a 7 day moving block average filter from the original data. This high pass digital filter has a 50% power attenuation at a period of about 10 days. The attenuation factors of the filter are plotted in Figure 4. The standard deviation of the temperature fluctuations will be defined as:

$$\sigma_{T'} = \frac{1}{Y} \sum_Y \left(\frac{1}{D-1} \sum_D T'^2 \right)^{\frac{1}{2}}$$

where: Y is the number of years of analysis

D is the number of days in the particular month.

Salinity standard deviations are determined in analogous fashion.

Also computed from the high frequency data are the monthly temperature, salinity correlations defined as:

$$\sigma_{TS} = \frac{1}{Y} \sum_Y \left(\frac{1}{D-1} \sum_D T' \cdot S' \right)$$

where S' is the salinity fluctuation.

IV. DISCUSSION OF RESULTS

A. Low Frequency Analysis

Plots of the yearly averages of temperature, salinity, and rainfall are shown in Figure 6.

1. Temperature

The yearly temperatures are best correlated between Amphitrite Point and Kains Island. Over the 35 years of analysis Amphitrite Point had an average temperature of 50.48°F (10.27°C) versus an average of 50.25°F (10.14°C) at Kains Island. The shape of the trend and the magnitude of the yearly temperature fluctuations are similar at Langara Island, the most northern station, but its average temperature of 47.59°F (8.66°C) is some 2.5°F (1.4°C) lower. The order of magnitude of the yearly temperature fluctuations at all 3 stations is 1°F (0.6°C).

2. Salinity

Salinity variations at Kains Island and Amphitrite Point show a good similarity in shape but Kains Island is somewhat more saline having an average salinity of 30.32 PPT against Amphitrite's 29.72 PPT. The annual salinity variations of these 2 stations which are of order 0.5 PPT contrast with the much smoother salinity curve at Langara Island which has a yearly fluctuation of order 0.1 PPT. Also Langara Island has the highest average salinity of 32.13 PPT. This behaviour likely reflects the greater distance of Langara Island from large fresh water sources. A very striking feature of the salinity at all 3 stations is its downward trend. The reference slope on each graph represents a drop in salinity of 0.4 PPT in 35 years. The rate of decrease of salinity does not seem to be too different at any of the 3 stations so it would appear that it is a phenomenon characteristic of the entire coast. There is no obvious correlation between average salinities and average temperatures. The temperature shows no trend corresponding to the general decrease in salinity nor are temperature fluctuations reflected in salinity fluctuations.

3. Rainfall

Average annual precipitations vary wildly from year to year. Only 1 block of data is plotted for Amphitrite Point but presumably its rainfall pattern is similar to that at Kains Island in other years. However, Kains Island seems to have the highest rainfall of all 3. Variations in rainfall correlate to some extent with temperature fluctuations. The rainfall peaks in 1950 and 1955 and falls on the 2 periods of lowest temperature at all 3 stations. Furthermore, the year 1940 and the period 1958 to 1963, years of low rainfall, are also periods of relatively high temperature. Presumably the weather conditions which prevail during years of high rainfall cause a cooling of the sea surface. Rainfall and salinity seem to be little correlated. It is true that the high rainfall of 1950 coincides with the lowest salinities, but on the other hand the rainfall maximum of 1955 appears to be associated with a relatively high salinity. Furthermore, the period of low rainfall from 1958 to 1963 corresponds to a period of relatively low salinity.

B. Spectral Analysis Results

The following table is a summary of the number of blocks of data analyzed for each spectral analysis. A 'P' in brackets indicates a power spectrum was done whereas a 'C' indicates that coherence and phase were computed. The number of blocks analyzed, which was limited by the available data, is also indicated in each square. In the plots of phase to follow a positive angle will mean that the parameter defined along the top of the table below will lead that parameter defined along the side.

TABLE III

Summary of Spectral Analysis Results

		Kains Island			Amphitrite Point			Langara Island		
		T	S	R	T	S	R	T	S	R
Kains Island	T	5(P)	5(C)		5(C)			4(C)		
	S		5(P)			5(C)			4(C)	
	R		5(C)	5(P)						
Amphitrite Point	T				5(P)	5(C)				
	S					5(P)				
	R					1(P)	1(P)			
Langara Island	T							4(P)	4(C)	
	S								4(P)	
	R								4(c)	4(P)

1. Temperature

a) Power Spectra

In Figure 7 are shown the temperature power spectra and standard deviations for Kains Island. Also plotted are the temperature power spectra for Amphitrite Point and Langara Island. All 3 spectra appear to be qualitatively and quantitatively similar. The most predominant feature is the annual temperature peak which rises 2 decades above the rest of the spectrum. This peak, representing the seasonal heating and cooling of the sea surface, contains about 90% of the total energy in the spectrum. At periods greater than 1 year frequency•power is roughly proportional to frequency, that is the power is approximately constant. For periods greater than a year the spectral estimates should be less certain. The power is approximately proportional to the inverse of frequency for periods between 1 year and 14 days. However, at the frequencies of the second and third harmonics of the annual frequency the power is somewhat lifted above the general level. Also at a period of 2 weeks the power is higher than in neighbouring estimates. This is likely due to the fact that the sample was collect-

ed near high tide every day. As the cycle of the tides progressed so would the time of day at which the observations were made. Thus any diurnal effects such as solar heating or movements of water bodies in response to diurnal winds would appear in the data at tidally related frequencies. At periods shorter than 2 weeks the power begins to fall off at a rate higher than the inverse of frequency. The high frequency 'tail' of the spectrum begins to curl up but this is almost certainly due to the aliasing of energy above the Nyquist frequency of 0.5 days^{-1} .

b) Coherences and Phases

Figure 8 shows the coherences and phases between temperatures at Kains Island, the middle light station, and the other 2 stations. Also shown in Figure 8a are 'levels of significance' appropriate to the number of blocks analyzed in each case.

Amphitrite Point and Langara Island are significantly coherent with Kains Island for all frequencies with period down to about 7 days. For periods less than 1 year the coherences lie between 0.8 and 1.0 for both pairs of light stations. That the coherence should be so high is no doubt partly due to the analysis technique but the plots of the annual temperature averages indicate that there are good correlations at low frequencies. Also borne out by the annual averages is the higher low frequency coherence between Amphitrite Point and Kains Island than between the latter and Langara Island. Kains Island is much closer geographically to Amphitrite Point than to Langara Island. At frequencies above the yearly harmonic which has coherences of almost exactly 1.0 the coherences drop sharply yet are still greater than the levels of significance. Generally coherences in this middle frequency range are similar for the 2 pairs of stations if allowance is made for their different levels of significance. The coherences for periods shorter than 7 days drop below the levels of significance. Seven days is approximately the natural period for weather systems which may be the shortest period phenomenon, aside from daily solar heating, capable of affecting all 3 light stations similarly.

The phases for both pairs of stations are all within 45° of 0° for periods longer than about 14 days. The phases of Amphitrite Point with respect to Kains Island for the first, second and third annual harmonics are 1° , -28° and 27° respectively whereas for Langara Island with respect to Kains Island these phases are -8° , -32° and -24° . The different phases reflect the mechanisms by which solar energy is transformed into the heating of the sea surface. At periods shorter than 14 days both Langara Island and Amphitrite Point lag Kains Island. In fact, the ever increasing phase lag between Amphitrite Point and Kains Island is approximately that which would be produced by a constant time lag of 1.5 days between the 2 stations. A constant time lag of 1.5 days is plotted as a dotted line on Figure 8b.

2. Salinity

a) Power Spectra

In contrast to the temperature spectra the salinity spectra which are plotted in Figure 9 are distinct for the 3 stations. At all

frequencies the power at Langara Island is of the order of a decade lower than that at Kains Island and Amphitrite Point. This is probably due to the fact that Langara Island is the farthest removed from the salinity-changing effects of river runoff. All 3 light stations have a salinity spectral maximum at the annual frequency although at Langara Island the energy in this harmonic is only 7% of the total energy whereas at Kains Island and Langara Island it is 60% and 44% of the total respectively. At lower frequencies frequency power falls off. However, frequency-power for the 3 stations is approximately constant from the annual period down to periods of about 20 days after which this quantity increases for Langara Island. Thus at higher frequencies Amphitrite Point has somewhat more energy in its salinity spectrum than does Kains Island. There is no tendency for any of the salinity spectra to 'tail off' at their high frequency ends as do the temperature spectra. Local maxima are attained in the salinity spectra for the $1/2$ yearly harmonic and the 14 day harmonic for both Kains Island and Langara Island, but curiously these are not evident in the spectrum for Amphitrite Point.

b) Coherences and Phases

Figure 10 shows plots of the salinity coherence and phase between the 2 pairs of light stations Kains Island-Amphitrite Point and Kains Island-Langara Island.

Energy at Kains Island and Amphitrite Point is significantly coherent up to frequencies corresponding to a period of about 14 days. The coherences at frequencies less than the annual frequency are below those for temperature whereas for periods between 1 year and 14 days they are higher. The coherence at the annual frequency is close to 1.0. The coherence at the annual frequency between Kains Island and Langara Island on the other hand is only about 0.8. Coherences with Langara Island are significantly lower than those with Amphitrite Point at most other frequencies, too. Generally, the Kains Island-Langara Island coherences lie below the level of significance for periods less than one year.

For shorter periods than 14 days the phases between the 2 pairs of light stations are relatively scattered reflecting the loss of coherence evident at higher frequencies. At lower frequencies Amphitrite Point tends to lead Kains Island, but the relative phase is less than 30° . The phases between Langara Island and Kains Island on the other hand are more scattered at the same frequencies and in this case Langara Island shows a tendency to lag Kains Island. However, the energy at the annual frequency of Langara Island leads that of Kains Island by 62° .

3. Rainfall Power Spectra

Rainfall power spectra for all 3 stations are shown plotted in Figure 11. The rainfall spectrum for Kains Island and that for Langara Island are similar both quantitatively and in shape whereas that for Amphitrite Point is similar in shape to the other 2 but is of lower level. This may be because the analysis for Amphitrite Point was carried out on

only 1 block of rainfall data. The years of the Amphitrite Point analysis seem to have had a below average rainfall judging by the more complete record for Kains Island (see Figure 6). At frequencies below the annual frequency the spectrum falls off rapidly. However, the power in the yearly harmonic is of the order of a decade above that in the rest of the spectrum. Frequency-power gradually increases at higher and higher frequencies. Local maxima in the 3 rainfall spectra are pronounced at a period of 1/2 year but not at a period of 1/3 year.

4. Kains Island: Temperature-Salinity and Rainfall-Salinity Coherences and Phases

Salinity-temperature (T,S) and salinity-rainfall (R,S) coherences are plotted together in Figure 12a for Kains Island. The T,S coherences behave quite differently from the R,S coherences. Aside from the good coherence at the annual frequency one could not say there was really significant T,S coherence for any frequency lower than that of period 7 days. During a period in which there is vertical mixing in a body of water which is stratified both in salinity and thermally, one might expect temperature and salinity to show a significant correlation. Following such a period of mixing the temperature of the surface water will approach an equilibrium with the atmosphere through the processes of conduction and radiation. That the coherence between temperature and salinity becomes less significant at periods longer than a week indicates that perhaps this is the time required for the temperature readjustment. Conversely rainfall and salinity show significant coherence at most frequencies of period shorter than 1/3 of a year and less significant coherences at longer periods.

The T,S and R,S phase relationships for Kains Island are plotted in Figure 12b. Although the T,S phase varies between 180° and -180° the phases for those periods at which significant coherences were observed, that is for less than 7 days, are clustered near 0° . This indicates that the mixing is predominantly a winter phenomenon which occurs when the higher salinities are associated with warmer temperatures. The phase relationships between rainfall and salinity are peculiar. In keeping with the expectation that high rainfall be associated with low salinity, salinity lags rainfall by 175° at a period of 1 year. At periods about 1/3 of a year, though, the R,S phases are clustered about 0° . Salinity lags rainfall more and more at higher frequencies until at a frequency corresponding to a period of about 4 days the lag is around 120° . It would thus seem that on the shorter term meteorological conditions which move the surface water and which are associated with rainy periods may have as much of an effect on the salinity as does the influence of the rain itself.

5. Amphitrite Point: Temperature-Salinity and Rainfall-Salinity Coherences and Phases

T,S and R,S coherences and phases are plotted for Amphitrite Point in Figure 13. T,S coherences are generally not dissimilar from those of Kains Island although coherences are somewhat higher at Amphitrite Point for periods between 40 and 120 days. The coherence between rainfall and salinity at Amphitrite Point could not be said to be significant at any frequency. This R,S analysis, however, is based on only 1 block of data

whereas the analysis at Kains Island included the whole 35 years of data.

The phase plot for Amphitrite Point shows that temperature and salinity tend to be 180° out of phase for periods between 250 days and 20 days. At higher frequencies this phase approaches 0° as do the T,S phases for Kains Island. The phases between rainfall and salinity at Amphitrite Point do not show any pattern, which is probably a reflection on the low R,S coherences.

6. Langara Island: Temperature-Salinity and Rainfall-Salinity Coherences and Phases

Figure 14 shows T,S and R,S coherences and phases for Langara Island. For periods less than a year the T,S coherences are significantly higher than they are for either Kains Island or Amphitrite Point. In fact the majority of these higher frequency coherences are above the level of significance. On the other hand the R,S coherence is below the level of significance for most frequencies.

Almost all the phases between temperature and salinity cluster near either 180° or -180° , that is temperature and salinity are of opposite phase. At the annual frequency salinity leads temperature by 97° in contrast to leads of 24° at Kains Island and 22° at Amphitrite Point. Rainfall, although not particularly coherent with salinity, tends to have a phase within 90° of salinity for periods longer than about 10 days.

It seems that the surface water characteristics at Langara Island are governed much more by the periodic vertical mixing of cooler, more saline, deeper water into the surface than by the direct or indirect effects of rainfall. In contrast the R,S relationship is stronger than the T,S relationship at the other 2 stations for periods longer than a week or so. This suggests that for lower frequencies at least the surface water characteristics at Amphitrite Point and at Kains Island are affected appreciably by the local movements of horizontally stratified water bodies of varying salinities.

C. Monthly Means

1. Temperature, Salinity and Rainfall

Shown plotted in Figure 15 are 2 cycles of the monthly means for temperature, salinity and rainfall. The salinity cycles for Amphitrite Point and Kains Island are similar in shape and range but vary in average level. These 2 stations both reach their maxima in August and their minima in December. Langara Island being situated further from any major fresh water sources exhibits a much smaller annual salinity range of the order of 0.5 PPT versus 4 PPT for the other 2 stations. This station has a salinity maximum in June and a minimum in November but a secondary maximum also appears in August.

Rainfall is small at all 3 stations during the summer months June to August. It begins a sharp increase in November to reach a maximum in January. The average salinities begin to drop before the rainfall starts to rise appreciably so it would appear that it is more than precipitation which causes the annual salinity variations. Pickard and McLeod (1953)

have suggested that changes in the seasonal evaporation rates and in upwelling caused by the long shore seasonal winds are partly responsible.

The mean annual range in temperature is approximately 10°F (6°C) at all 3 stations. Monthly temperatures at Kains Island and Amphitrite Point are virtually identical but those at Langara Island are 2.5°F (1.4°C) lower. Also, the temperature cycles of the 2 southerly stations precede that of Langara Island. From results computed using spectral analysis the phase lag of the annual frequency harmonic is 8° which represents a time lag of 8 days.

2. Standard Deviations of Salinity and Temperature; T,S Correlation

Standard deviations of salinity and temperature and the T,S correlation are shown plotted in Figure 16. The standard deviation of temperature is a maximum for Kains Island and Amphitrite in July and for Langara Island a month later whereas the minima occur for the 3 stations in March or April. That this seasonal variation occurs is not surprising since the surface water is more strongly thermally stratified during the summer months. Any disturbance causing vertical mixing will thus cause larger temperature variations at that time.

The standard deviations of salinity display an inverse cycle to that of temperature for Kains Island and Amphitrite Point. They are minima in late summer and maxima around November or so. This is not surprising as the salinity stratification is expected to be a minimum during the period of minimum rainfall. For these 2 southern stations the peak in the salinity standard deviations occurs a couple of months ahead of the peak in precipitation. It would seem that later on in the winter, storms could markedly erode the high salinity stratification. One also notes that the standard deviations of salinity are everywhere higher for Amphitrite Point than they are for Kains Island. On the other hand the temperature standard deviations are higher at their peaks for Kains Island than for Amphitrite Point. It would seem that Amphitrite Point achieves the greater salinity stratification whereas Kains Island achieves the greater temperature stratification. The standard deviations of salinity at Langara Island show a smaller average and much less variation than at the other 2 stations.

The T,S correlation curves are much as expected. At Kains Island and Amphitrite Point during the months May to September, the T,S correlation is negative as the fresher surface layer is heated by the summer sun and negative for the months October to March. Langara Island shows different behaviour. Its T,S correlation is negative from June to November and is near zero for the rest of the year.

V. SUMMARY AND CONCLUSIONS

It is evident that each of the analysis techniques used in this study point up different features of the data. The relatively modern technique of spectral analysis is useful in examining the time scales at which variations and co-variations in parameters such as salinity, temperature and rainfall occur. However, yearly and seasonal variations are better examined using simple averaging procedures.

Despite the geographical separations of the 3 light stations examined in this report their temperature records show a good statistical similarity. Although average temperatures at Langara Island are 2.5°F (1.6°C) lower than they are at the 2 southern stations the magnitudes and shapes of the yearly fluctuations correspond to one another. Also, these variations in yearly averaged temperatures seem to be related to changes in the annual precipitations. Presumably the meteorological conditions associated with higher rainfall such as greater cloud cover and particular atmospheric circulation patterns are the cause.

All 3 stations exhibit a seasonal maximum in surface temperature in late summer and a minimum in February. The average seasonal range in temperature is in each case near 10°F (6°C). Indications are that the water columns are most thermally stratified in summer and least stratified in early spring.

The temperature power spectra at Kains Island, Langara Island and Amphitrite Point are quite similar to one another. In each case approximately 90% of the energy is represented at the annual frequency. At higher frequencies the energy per unit bandwidth decreases. For periods longer than about a week the temperature energy at Amphitrite Point and at Langara Island is significantly coherent with that at Kains Island.

In contrast to temperatures the salinity records at the 3 stations differ considerably. The variation of the yearly salinity averages at Kains Island and Amphitrite Point show a correspondence which is not as good as that of temperature. The fluctuations of the yearly averages at these stations are of order 0.5 PPT. The pronounced seasonal variation in salinity has an average range of 4.0 PPT on the other hand. At all times of the year Kains Island is 0.5 PPT salinity higher than Amphitrite Point.

Compared to the 2 Vancouver Island stations, Langara Island shows much less yearly and seasonal salinity variation. The magnitudes of the fluctuations are approximately 0.1 PPT and 0.5 PPT for the yearly and seasonal variations respectively. This behaviour and the fact that Langara Island has the highest average salinity are likely due to the absence of any large sources of fresh water in the vicinity of the station.

Salinities from all 3 stations show a decrease over the 35 years of the study of about 0.4 PPT. The fluctuations of the annual averages bear little obvious relationship to either changes in precipitation or in temperature.

Salinities at the 2 southern stations are highest in August, a month of low precipitation. They have fallen appreciably by October yet the rainfall does not begin to rise until November. Lowest salinities occur in December although the highest rainfalls occur in January. Both the standard deviations of the salinity and the temperature-salinity correlation are high

in November to December indicating a high salinity stratification, the more saline water being associated with warmer temperatures. The standard deviations of salinity are small for all times of the year at Langara Island, however.

The salinity spectra indicate that something like 50% of the energy is concentrated in the annual frequency for Kains Island and Amphitrite Point against less than 10% for Langara Island. The coherence of salinity energy is naturally best between the 2 southern stations and is only marginal with Langara Island. For periods less than 14 days this coherence becomes insignificant. The coherences of temperature with salinity at Kains Island and at Amphitrite Point are most significant for periods less than 7 days, but are more coherent at Langara Island to longer periods. On the other hand, rainfall and salinity at Langara Island are less coherent than they are at the other 2 stations.

REFERENCES

- Hollister, H.J., and A.M. Sandnes. 1972. Sea surface temperatures and salinities at shore stations on the British Columbia coast 1914-1970. Environment Canada. Marine Sciences Directorate, Pacific Region. Pacific marine science report 72-13.
- Jenkins, G.M., and D.G. Watts. 1968. Spectral analysis and its applications. Holden Day, San Francisco; 525 pps.
- Pickard, G.L., and D.C. McLeod. 1953. Seasonal variation of temperature and salinity of surface waters of the British Columbia coast. J. Fish. Res. Board Can. 10: 125-145.
- Singleton, R.C. 1969. An algorithm for computing the mixed Radix Fast Fourier Transform. IEEE Transactions on Audio and Electroacoustics, Vol. AU-17: 93-103.

Data Records

- Canada Pacific Oceanographic Group. MS 1947-1951. Observations of seawater temperature, salinity and density on the Pacific Coast of Canada. Vol. I, 1914-1934 to Vol. X, 1950. Fish. Res. Board Can., Nanaimo, B.C.
- MS 1952-1957. Observations of seawater temperature and salinity on the Pacific Coast of Canada. Vol. XI, 1951 to Vol. XVI, 1956. Fish. Res. Board Can., Nanaimo, B.C.
- MS 1958-1959. Observations of seawater temperature and salinity on the Pacific Coast of Canada. Vol. XVII, 1957 and Vol. XVIII, 1958. Fish. Res. Board Can., MS. Rep. (Oceanogr. and Limnol.) 23 and 48.
- Canadian Oceanographic Data Centre. 1968. Observations of seawater temperature and salinity on the Pacific Coast of Canada, 1966. 1968 Data Record Series, No. 8. Dept. of Energy, Mines and Resources, Ottawa. Cat. No. M58-1/1968-8.
- Hollister, H.J. MS 1960-1964. Observations of seawater temperature and salinity on the Pacific Coast of Canada. Vol. XIX, 1959 to Vol. XXIII, 1963. Fish. Res. Board Can. Ms. Rep. (Oceanogr. and Limnol.) 67, 104, 131, 161, 160.
- MS 1965. Graphs of seawater temperature and salinity observations at British Columbia coast stations, 1964. Fish. Res. Board Can. Ms. Rep. (Oceanogr. and Limnol.) 195.
- MS 1966a. Seawater temperature and salinity observations at British Columbia coastal stations in 1965. Fish. Res. Board Can. Ms. Rep. (Oceanogr. and Limnol.) 215.
- MS 1966b. Observations of seawater temperature and salinity at British Columbia coastal stations in 1964 and 1965. Fish. Res. Board Can. Ms. Rep. (Oceanogr. and Limnol.) 226.

Hollister, H.J. MS 1971. Observations of seawater temperature and salinity at British Columbia shore stations, 1967, 1968, 1969, 1970. Fish. Res. Board Can. Ms. Rep. 1133, 1144, 1154, 1156.

LIST OF FIGURES

1. Map of British Columbia's coast showing locations of sampling stations Langara Island, Kains Island and Amphitrite Point. (all underlined)
2. Schematic diagram of data availability for Langara Island, Kains Island and Amphitrite Point. Vertical dashed lines mark changes in the analysis procedure. The extents of the blocks used in the spectral analysis are indicated at bottom.
3. Schematic diagram of the analysis procedure.
4. Gain functions for filters used in spectral analysis and in computation of temperature, salinity standard deviations and correlations.
5. Expected noise coherences for 1, 4 and 5 blocks of analysis. The vertical bars represent the + and - standard deviations of the expected noise coherence.
6. Annual averages of salinity, temperature and rainfall for Langara Island, Kains Island and Amphitrite Point.
7. Power spectra of temperatures for Langara Island, Kains Island and Amphitrite Point. Vertical bars indicate the standard deviations between blocks for Kains Island.
8. Coherences (Figure 8a) and Phases (Figure 8b) of temperatures between the two pairs of stations Kains Island, Langara Island and Kains Island, Amphitrite Point. The dotted line in Figure 7a is the 'level of significance' for coherences appropriate to the number of blocks analyzed.
9. Power spectra of salinities for Langara Island, Kains Island and Amphitrite Point.
10. Coherences (Figure 10a) and Phases (Figure 10b) of salinities between the two pairs of stations Kains Island, Langara Island and Kains Island, Amphitrite Point.
11. Power spectra of rainfall for Langara Island, Kains Island and Amphitrite Point.
12. Coherences (Figure 12a) and Phases (Figure 12b) of temperature and rainfall with salinity for Kains Island.
13. Coherences (Figure 12a) and Phases (Figure 13b) of temperature and rainfall with salinity for Amphitrite Point.
14. Coherences (Figure 14a) and Phases (Figure 14b) of temperature and rainfall with salinity for Langara Island.
15. Average monthly salinities, temperatures and rainfall at Langara Island, Kains Island and Amphitrite Point.

List of Figures continued

16. Average monthly temperature, salinity correlations and standard deviations of salinity and temperature for Langara Island, Kains Island and Amphitrite Point.



Figure 1. Map of British Columbia's coast showing locations of sampling stations Langara Island, Kains Island and Amphitrite Point. (all underlined)

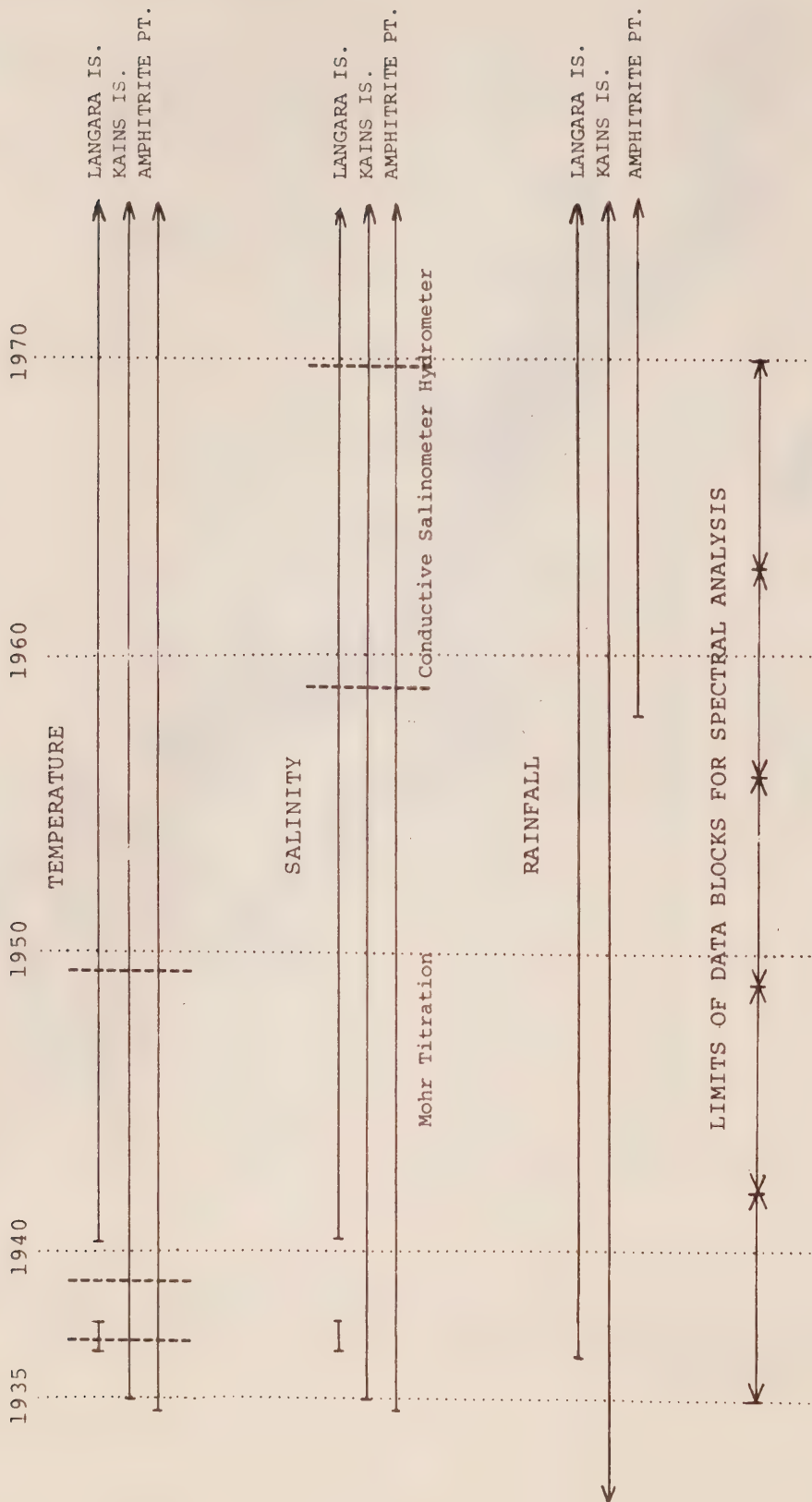


Figure 2. Schematic diagram of data availability for Langara Island, Kains Island and Amphitrite Point. Vertical dashed lines mark changes in the analysis procedure. The extents of the blocks used in the spectral analysis are indicated at bottom.

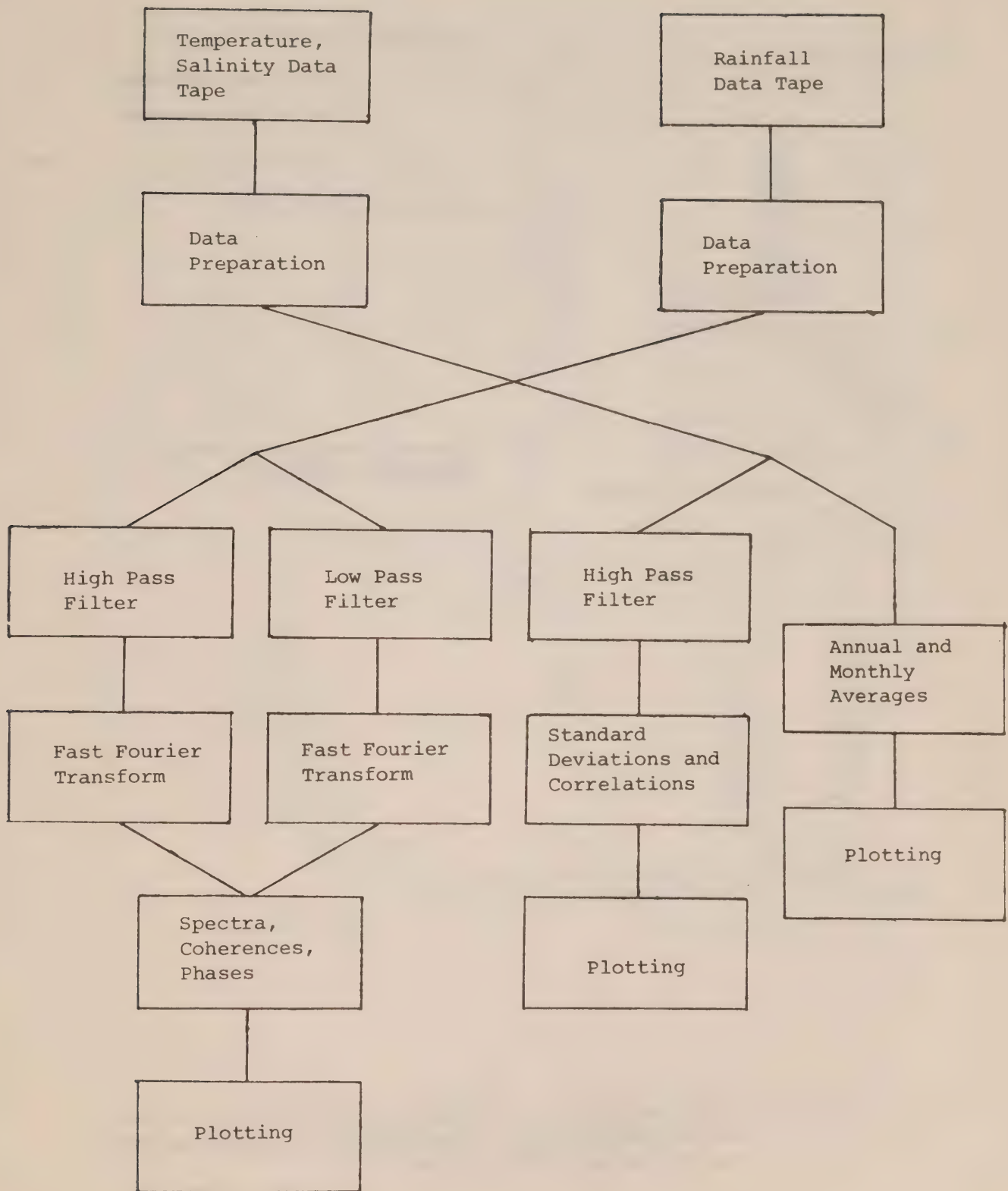


Figure 3. Schematic diagram of the analysis procedure.

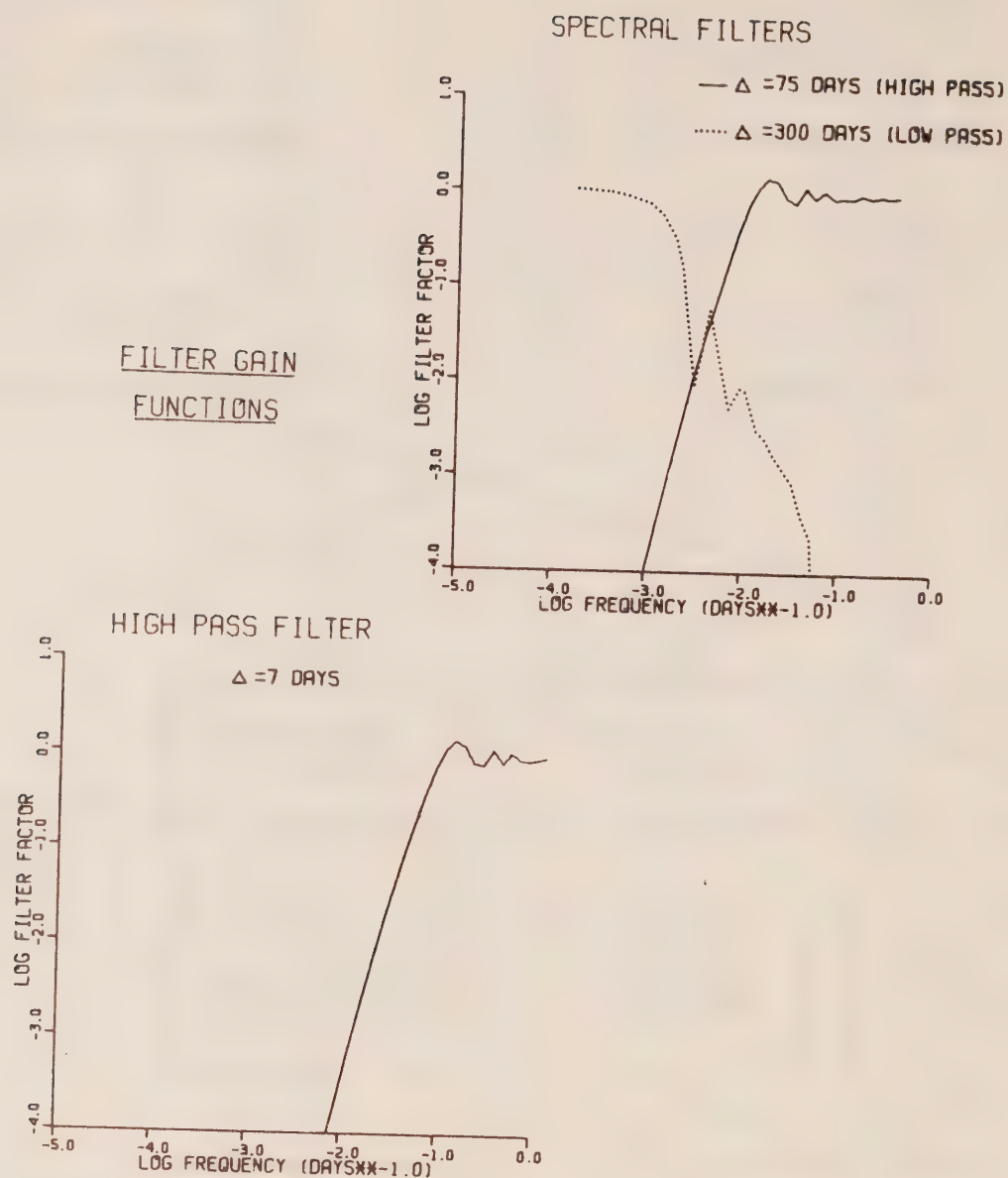


Figure 4. Gain functions for filters used in spectral analysis and in computation of temperature, salinity standard deviations and correlations.

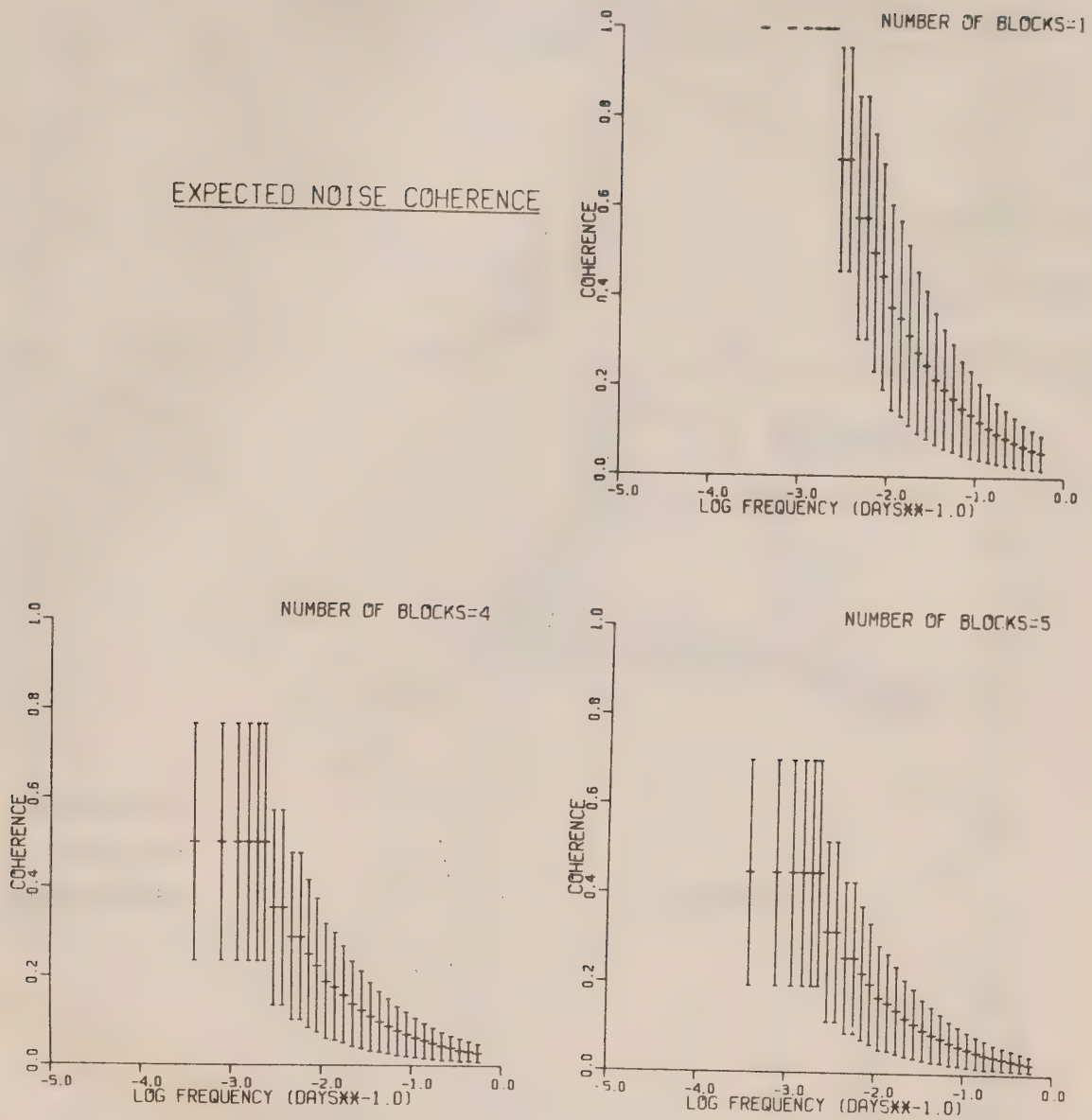


Figure 5. Expected noise coherences for 1, 4 and 5 blocks of analysis. The vertical bars represent the + and - standard deviations of the expected noise coherence.

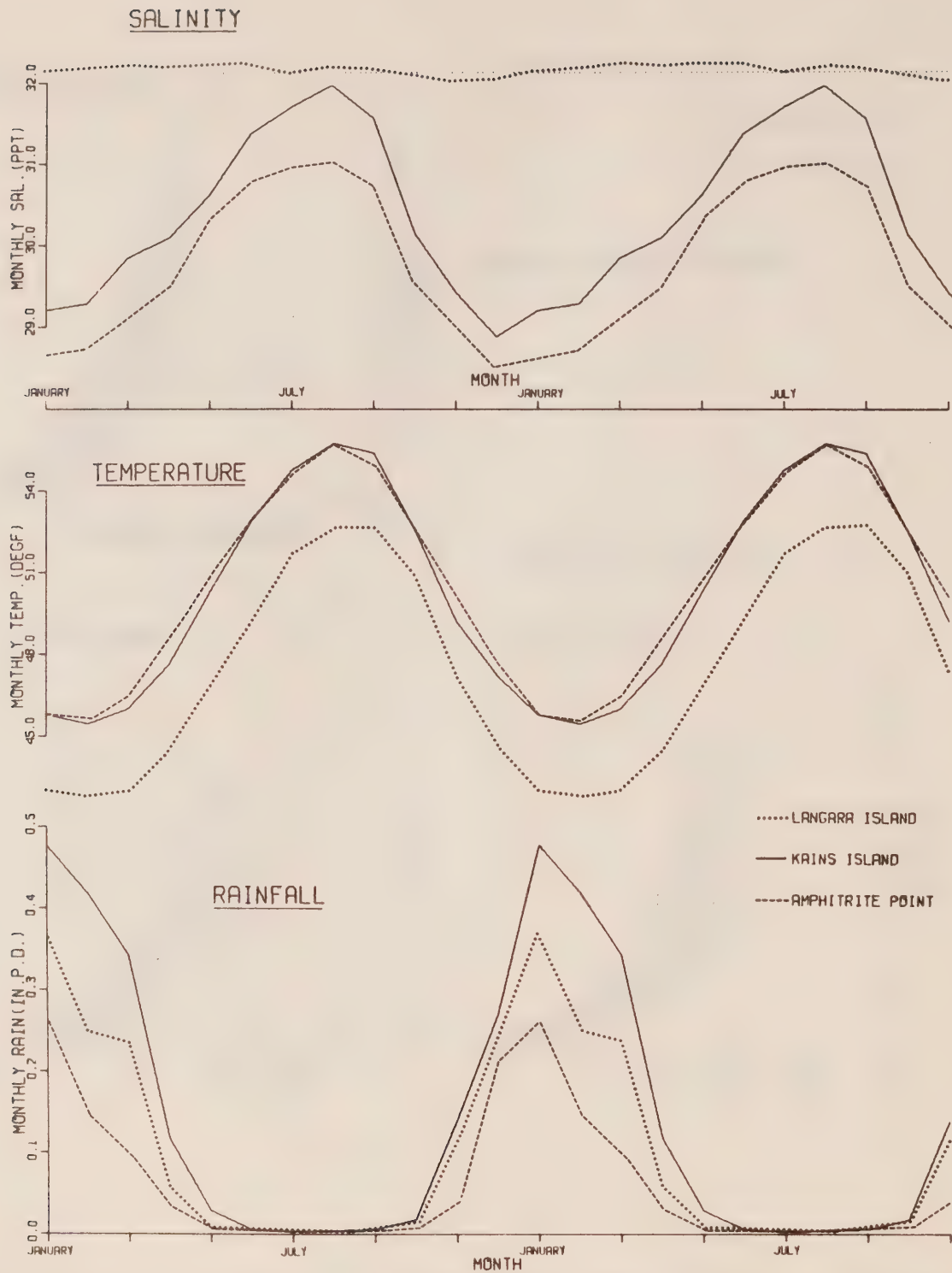


Figure 6. Annual averages of salinity, temperature and rainfall for Langara Island, Kains Island and Amphitrite Point.

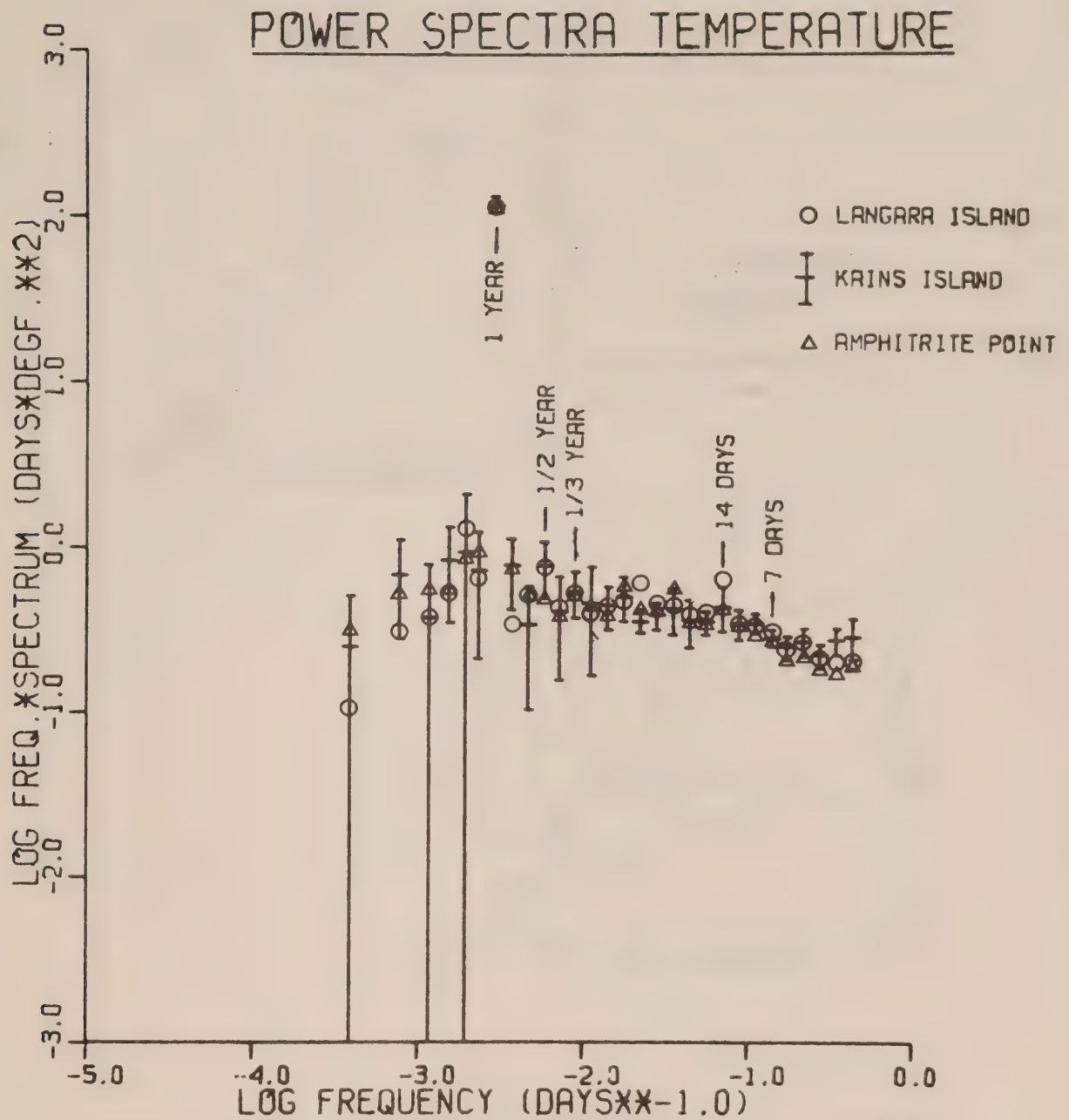


Figure 7. Power spectra of temperatures for Langara Island, Kains Island and Amphitrite Point. Vertical bars indicate the standard deviations between blocks for Kains Island.

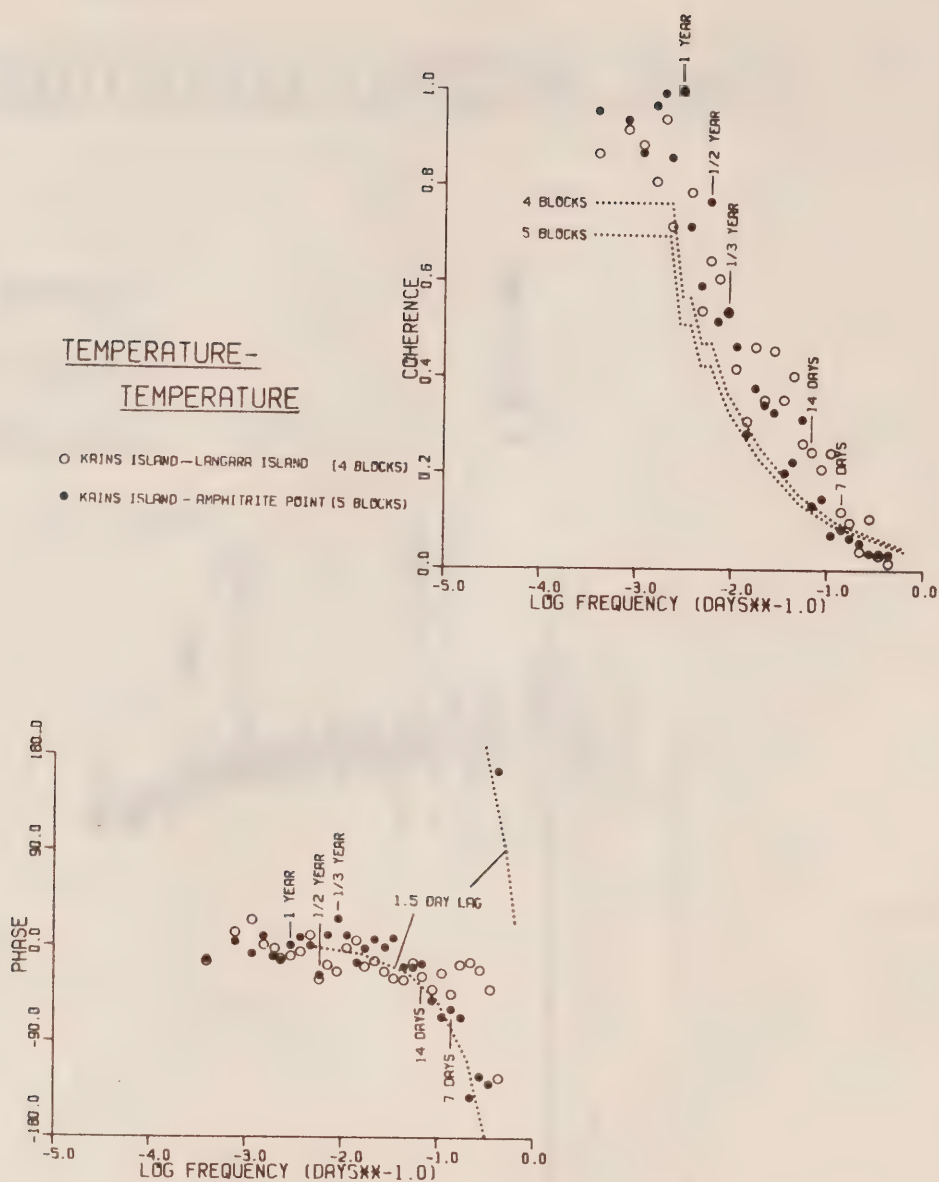


Figure 8. Coherences (Figure 8a) and Phases (Figure 8b) of temperatures between the two pairs of stations Kains Island, Langara Island and Kains Island, Amphitrite Point. The dotted line in Figure 7a is the 'level of significance' for coherences appropriate to the number of blocks analyzed.

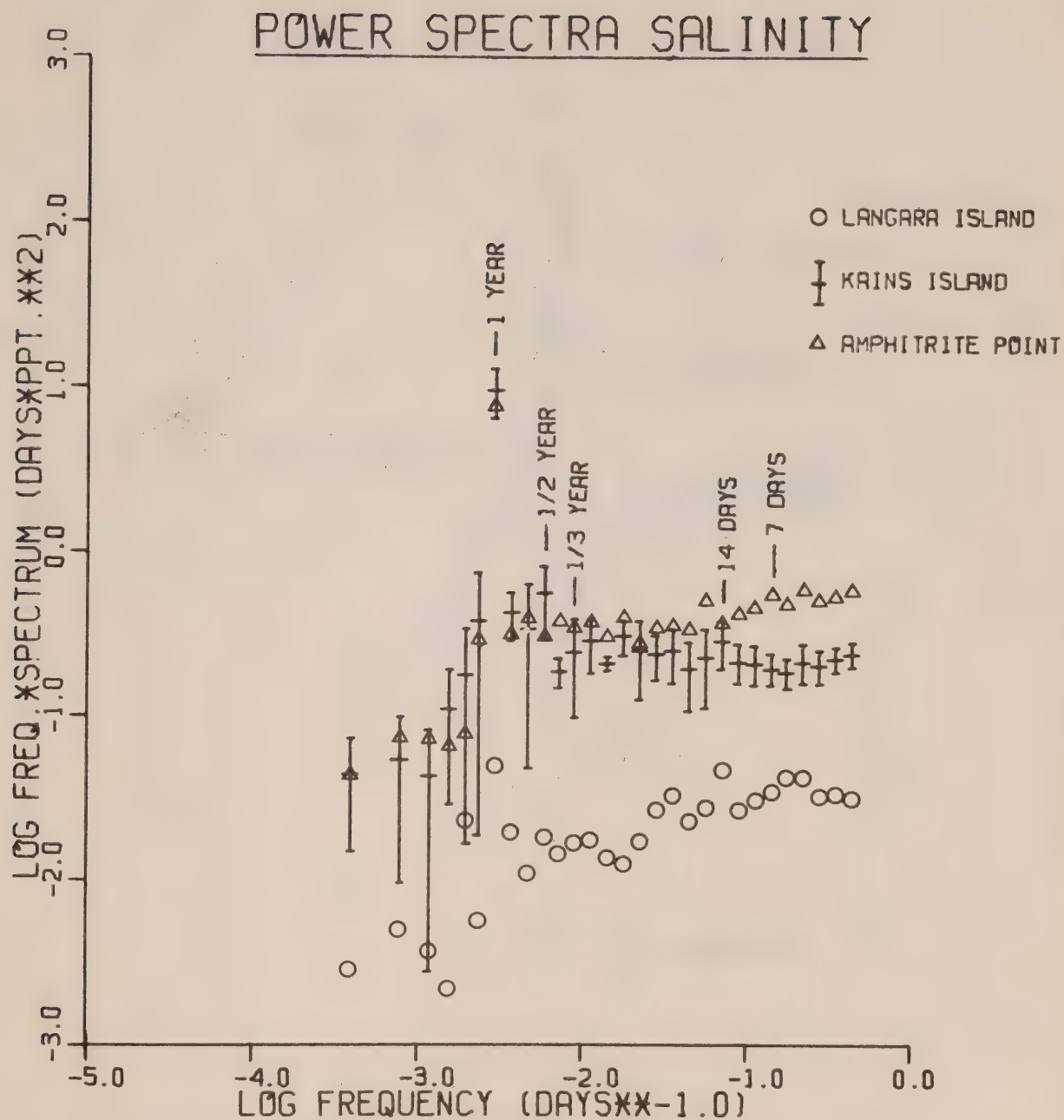


Figure 9. Power spectra of salinities for Langara Island, Kains Island and Amphitrite Point.

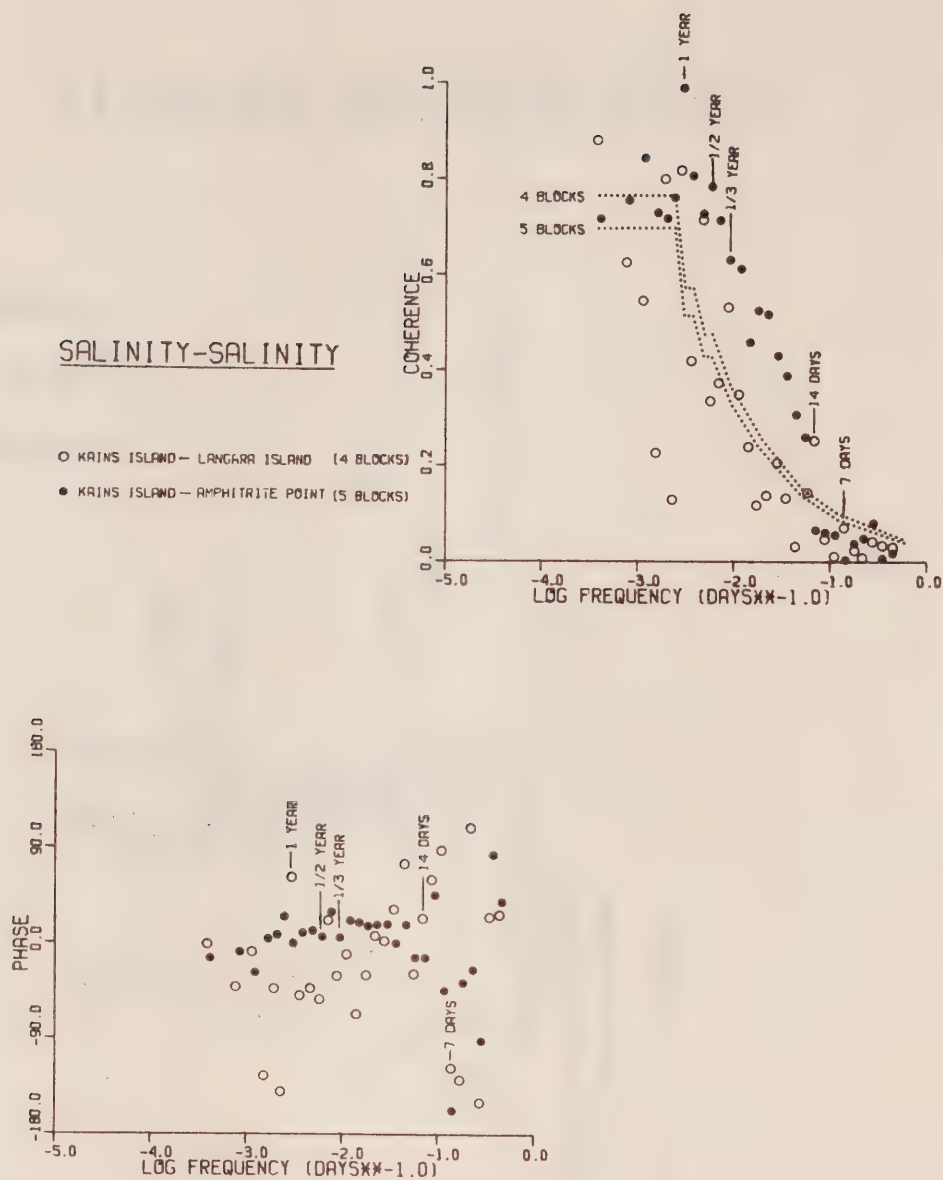


Figure 10. Coherences (Figure 10a) and Phases (Figure 10b) of salinities between the two pairs of stations Kains Island, Langara Island and Kains Island, Amphitrite Point.

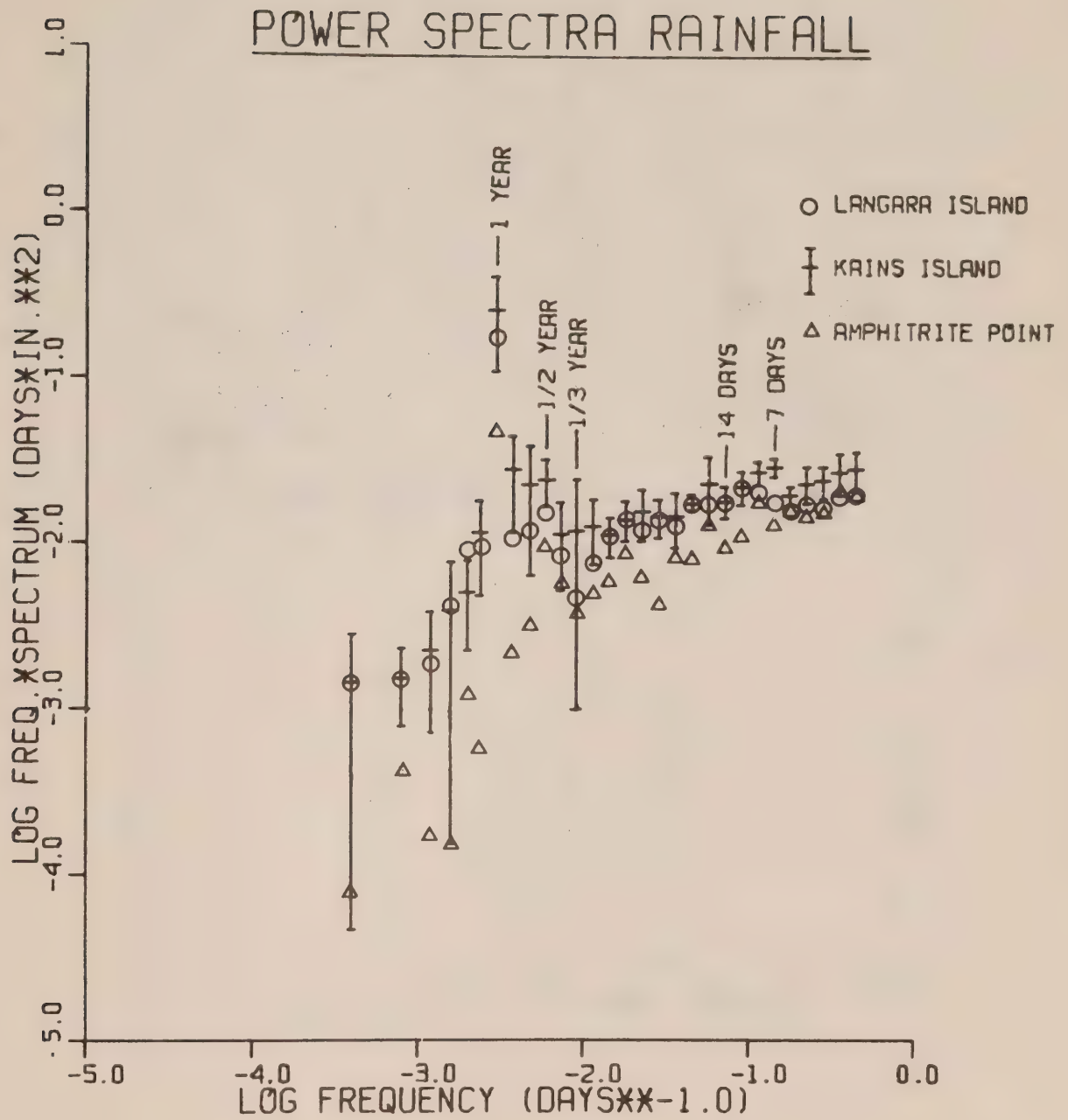


Figure 11. Power spectra of rainfall for Langara Island, Kains Island and Amphitrite Point.

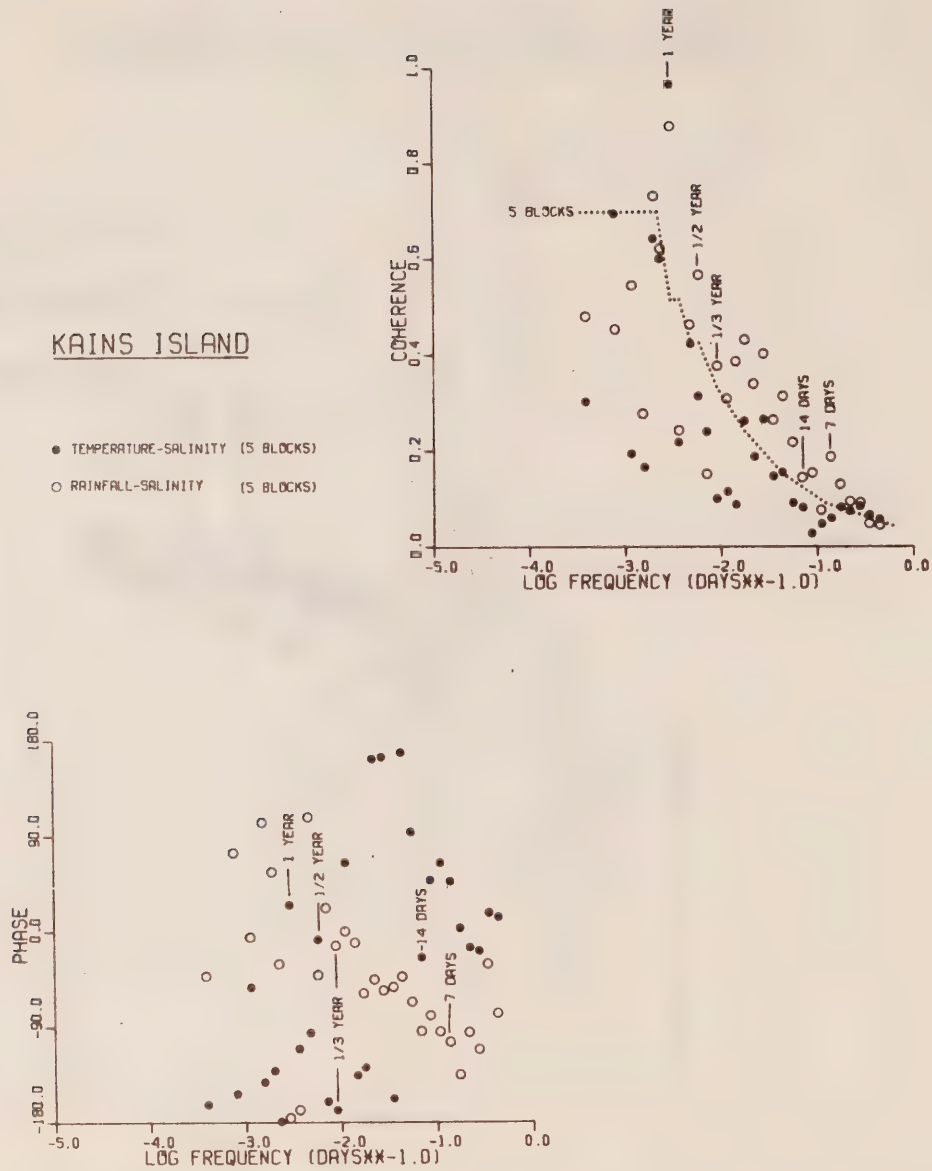


Figure 12. Coherences (Figure 12a) and Phases (Figure 12b) of temperature and rainfall with salinity for Kains Island.

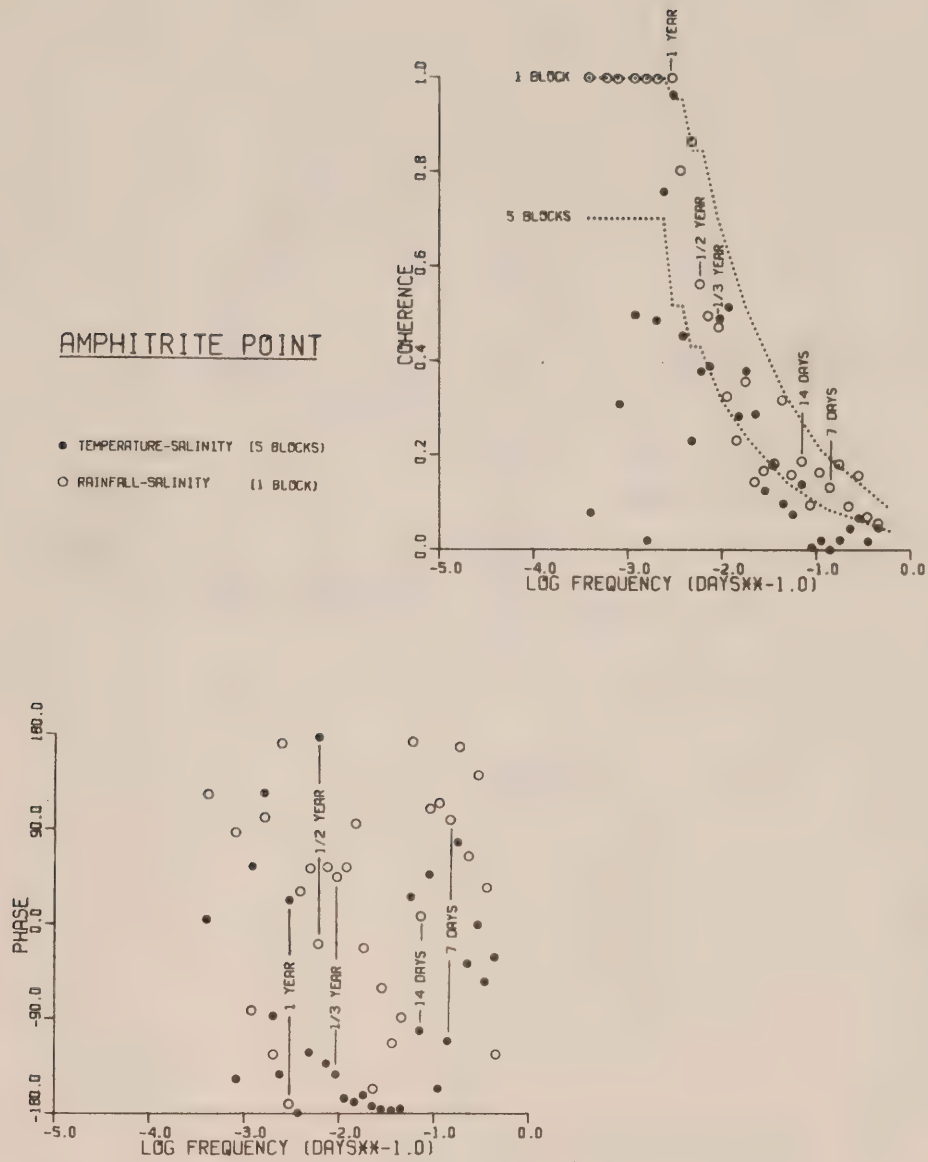


Figure 13. Coherences (Figure 13a) and Phases (Figure 13b) of temperature and rainfall with salinity for Amphitrite Point.

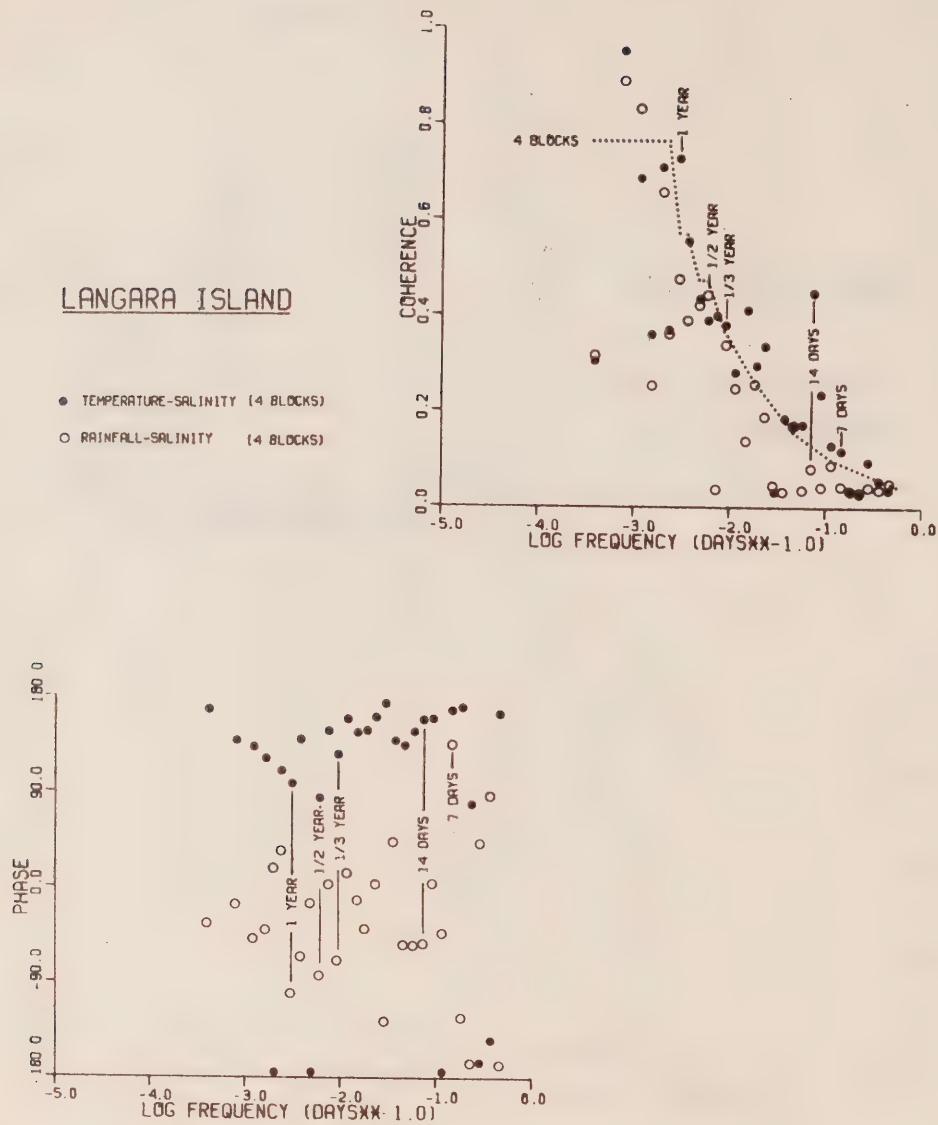


Figure 14. Coherences (Figure 14a) and Phases (Figure 14b) of temperature and rainfall with salinity for Langara Island.

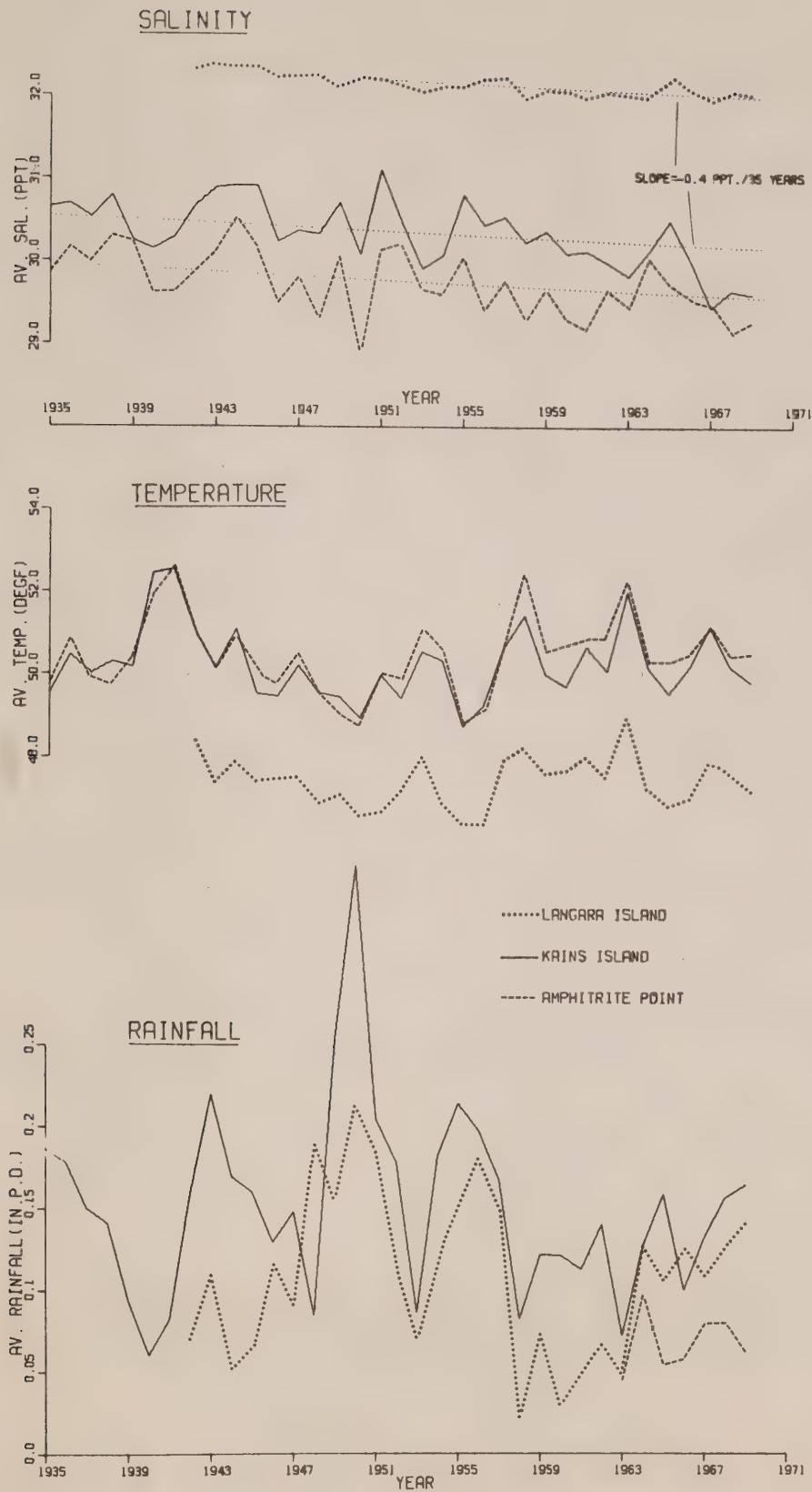


Figure 15. Average monthly salinities, temperatures and rainfall at Langara Island, Kains Island and Amphitrite Point.

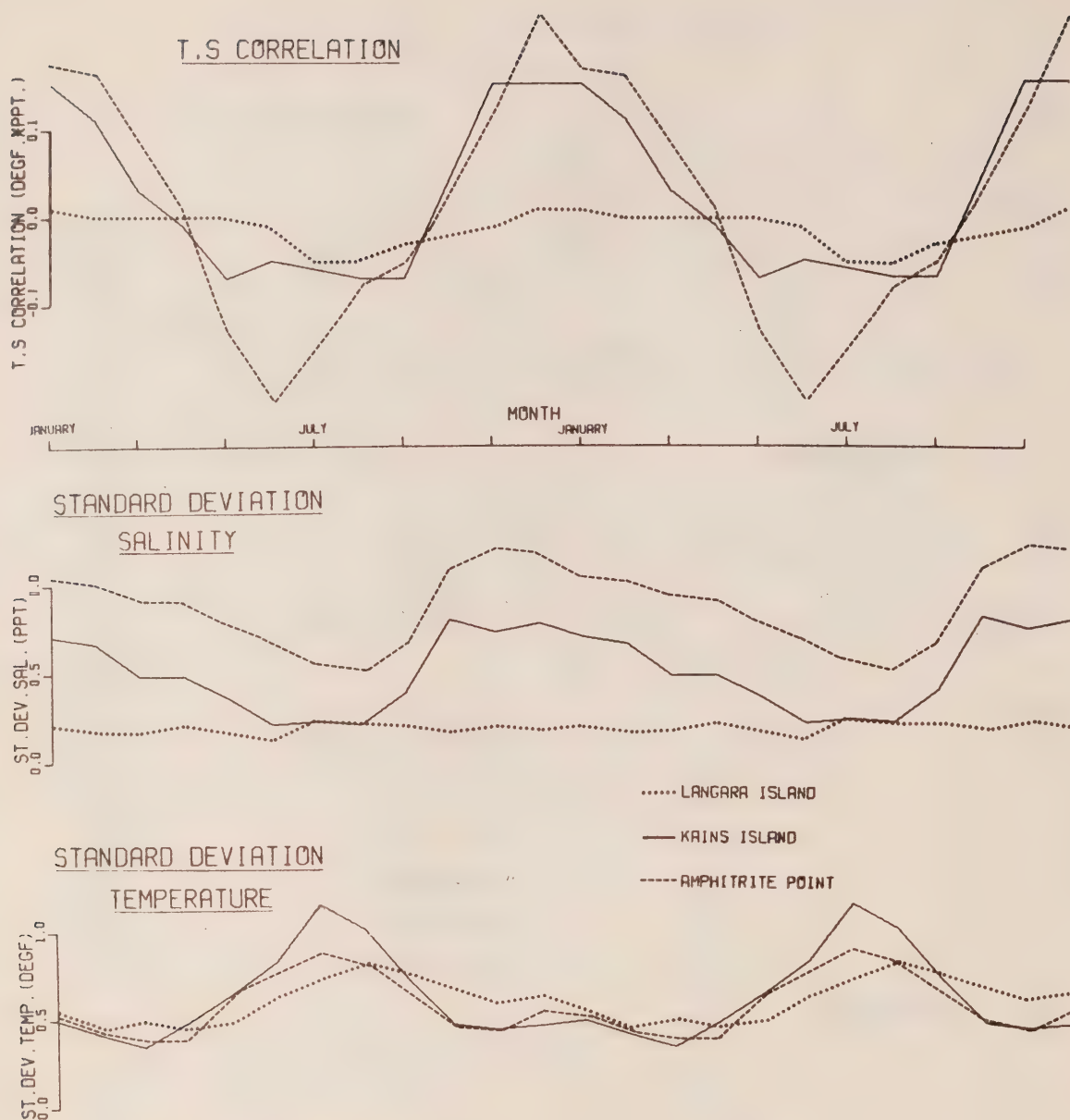


Figure 16. Average monthly temperature, salinity correlations and standard deviations of salinity and temperature for Langara Island, Kains Island and Amphitrite Point.

